CR-184029

TWR-17371

Rev A

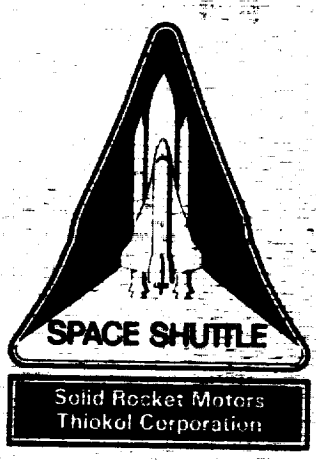

Space Shuttle Development Motor No. 9 (DM-9) Final Test Report

Volume 1

September 1990

Prepared for

National Aeronautics and Space Administration
George C. Marshall Space Flight Center
Marshall Space Flight Center, Alabama 35812

Contract No.	**NAS8-30490**
DR No.	**5-3**
WBS No.	**HQ301-10-10**
ECS No.	**1001**

Thiokol CORPORATION

SPACE OPERATIONS

P.O. Box 707, Brigham City, UT 84302-0707 (801) 863-3511

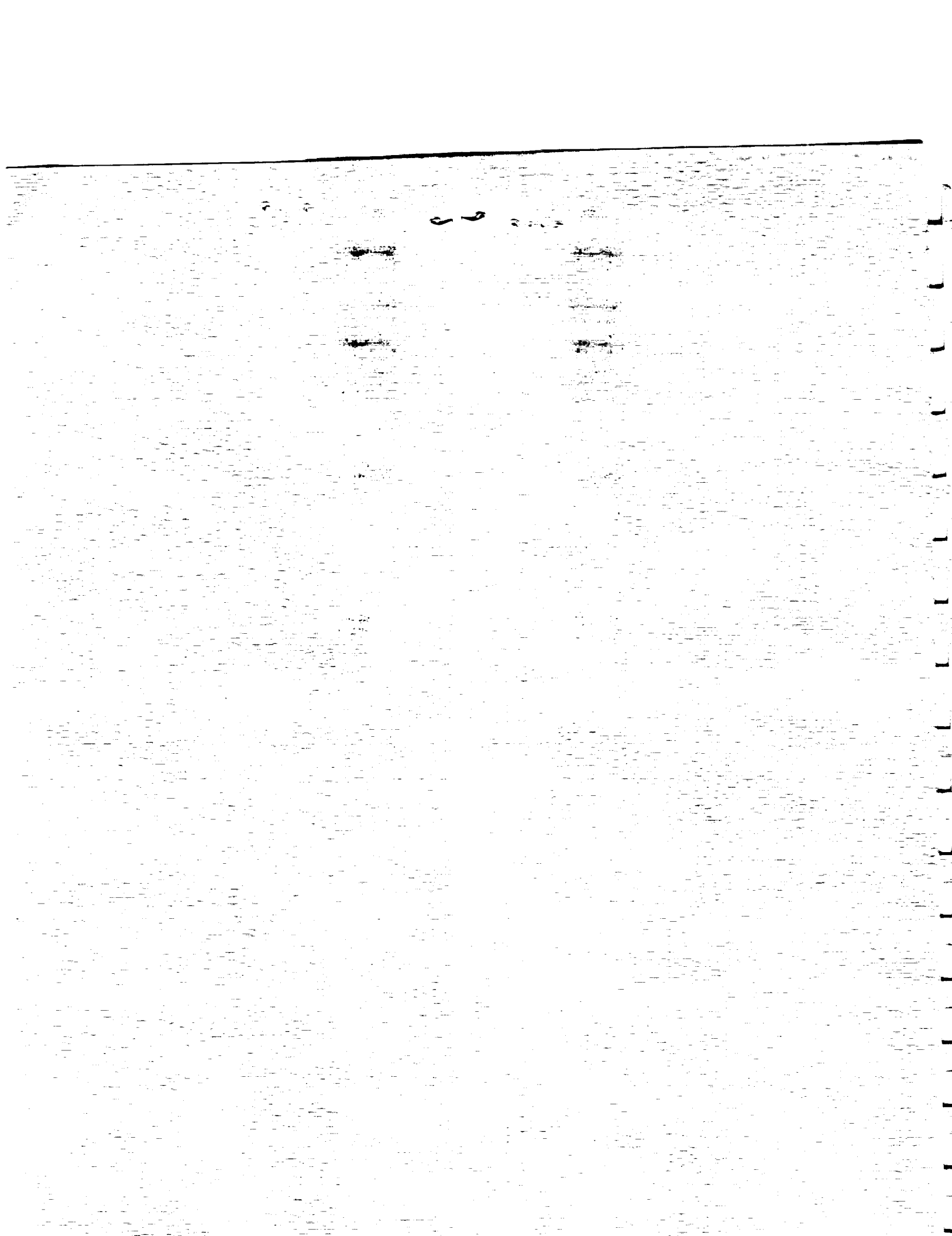

N101135-8

DM-9 Static Test (23 Dec 1988)--Fired Under Extreme Environmental Conditions

Space Shuttle Development
Motor No. 9 (DM-9)
Final Test Report

Prepared by:

Diane Garrett

Test Planning and Reports
Systems Engineer

Approved by:

Requirements
Manager

Program Manager

Project Engineer

Systems Safety

Reliability

P C Tydeck 9-10-90

Data Management
ECS No. 1001

Major contributors to the final test report are:

Ballistic/Mass Properties	K. Speas
Aero/Thermo	R. Buttars
Dynamics	C. Chang
Igniter	D. Bullard
Insulation	S. Manz
Nozzle	R. George
Nozzle/Flex Bearing	J. Donat
Nozzle/Thrust Vecotr Control System	F. Weiler
Structural Applications	L. Nelsen
Structural Design	K. Sperry
Field Joint Protection System	E. Hale
Instrumentation	R. Bell
Systems Tunnel	~~C. Prokop~~ R. Kirby

REVISION DESCRIPTION

REV LTR	DATE	DESCRIPTION
Basic	11 Mar 88	
A	10 Sep 90	TWR-17371 is revised and marked in the right hand margin by a vertical bar. The following is a summary of changes made in TWR-17371, Revision A. 3.1.5 Nozzle Performance Nozzle TVC Was: Evaluation of the TVC systems is underway. Now: The TVC performed nominally and. . . . 3.1.7 Seals Performance Factory Joints Was: Disassembly and evaluation is incomplete Now: For factory joint evaluation see TWR-18135, Rev A, Section 5.1. 3.1.9 Joint Protection System/Systems Tunnel Performance Systems Tunnel Was: Initial observations indicate. . . . Now: Observations indicate. . . . 4.0 CEI SPECIFICATIONS Replaced Column 3 with the following: AE The nozzle is compatible with systems performance requirements AO The nozzle performance MS were positive

REV LTR	DATE	DESCRIPTION
		AQ The maximum radial displacement was 0.0264 in. and the angular. . . . AR Dynamic thrust vector alignment requirements were met. AS The nozzle null offset angle was +0.8 deg at 0 psi nozzle stagnation. . . . AW No evidence of blowby, erosion, or heat effect. . . . AY Factory joints show no visual damage. . . . AZ More than one virgin ply of insulation. . . . BA The flex bearing remained sealed. . . . BB The flex bearing was capable. . . . BC Sealing verification did not degrade. . . . BD There were no gas paths of leaks. . . . 5.4 INSTRUMENTATION DISCUSSION Was: DM-8 instrumentation included. . . . Now: DM-9 instrumentation included. . . . Table 7.1-3 Was: 0.1680 77.00 0.1670 234,001. . . . Now: 0.1680 77.00 0.1760 257,272. . . . 7.4.3 Conclusions/Recommendations Factory Joints Was: Disassembly and evaluation are incomplete. Now: No problems were found after the factory joints were disassembled.

REV LTR	DATE	DESCRIPTION

7.4.4.1 Field Joint Insulation

Forward Field Joint

Was: No evidence of foreign material. . . .
Now: No evidence of foreign material, ply separations or tang edge unbonds were indentified. Fourteen clevis edge unbonds were found. . . .

Was: This region will be evaluated. . . .
Now: The insulation in these regions showed slightly more. . . .

Center Field Joint

Was: No evidence of foreign material. . . .
Now: No evidence of foreign material, ply separations, or tang or clevis. . . .

Aft Field Joint

Was: No evidence of foreign material. . . .
Now: No evidence of foreign material, ply separations, or tang edge unbonds. . . .

7.4.4.2 Factory Joint.

Was: Disassembly and evaluation are incomplete.
Now: All seven factory joints were disassembled and inspected. . . .

7.4.4.3 Nozzle-to-Case Joint.

Was: An extensive evaluation. . . .
Now: Four edge unbonds at the nozzle. . . .

REV LTR	DATE	DESCRIPTION
		7.5.3 Conclusions/Recommendations Nozzle Assembly Delete: Sectioning of the ablative liner is required to complete inspections and to verify erosion margins of safety. Replace b. with: The CPW1-3600 specification (paragraph 3.2.1.4.13b) in effect when DM-9 was fired. . . . Replace c. with: Positive performance margins of safety were obtained on the intact portion of the OBR, on the cowl ring aft end, and on the remainder. . . . Was: g. Evaluation of postfired hardware is currently. . . . Now: g. Evaluation of postfired hardware is documented in TWR-17269. . . . 7.5.4.1 Nose Inlet Assembly. Was: Char and erosion analysis. . . .is underway. Now: Char and erosion analysis. . . .showed positive performance MS. Throat Inlet Assembly Was: Char and erosion analysis. . . .is underway. Now: Char and erosion analysis. . . .showed positive performance MS.

REV LTR	DATE	DESCRIPTION
		Cowl Ring Was: Char and erosion analysis. . . .is underway. Now: Char and erosion analysis. . . .showed positive performance MS. Fixed Housing Insulation Was: Char and erosion analysis. . . .is underway. Now: Char and erosion analysis. . . .showed positive performance MS. Forward Exit Cone Assembly Was: Char and erosion analysis. . . .is underway. Now: Char and erosion analysis. . . .except at station locations 20 (90 and 270 deg) and 24 (270 deg). Aft Exit Cone Assembly Delete: Sectioning of the area is required for further analysis. Was: Char and erosion analysis. . . .is underway. Now: Char and erosion analysis. . . .except at station location 95.77 (90 deg). 7.5.4.2 Delete Torque Analysis 7.5.4.4 TVC System. Was: Evaluation. . . .is underway. Now: Section on TVC has been added.

REV LTR	DATE	DESCRIPTION
		7.7.3 Conclusions/Recommendations Factory Joints Was: Disassembly. . . .not complete. Now: For factory joint evaluation, see TWR-18135, Rev A, Section 5.1. 7.7.4.2 Factory Joints. Was: Disassembly. . . .incomplete. Now: For factory joint evaluation, see TWR-18135, Rev A, Section 5.1. 7.7.4.4 Internal Nozzle Fixed Housing-to-Aft End Ring (Joint No. 5) Was: The cause is under investigation at this time. Now: It is determined that they were caused by disassembly. 7.9.4 Results/Discussion Was: c. Systems Tunnel. . . .Initial observations indicate. . . . Now: c. Systems Tunnel. . . .Observations indicate. . . . Table 7.10.1 DM-9 Leak Test Results. Correct two typographical errors. Add as note to bottom of page: *Equivalent of one bubble per second--test for packing with retainers only

ABSTRACT

This report presents the results obtained during the 23 Dec 1987 static firing of the DM-9 test article. The DM-9 full-scale static test article employed RSRM field joint capture feature hardware with J-seal insulation configuration, and nozzle-to-case joint radial bolt design with bonded insulation configuration. The nozzle incorporated RSRM components, including a thicker cowl with involute outer boot ring. The nozzle employed redundant and verifiable seals in all five joints, and room temperature vulcanization backfill in three joints. With very few exceptions, the DM-9 test article was flight configuration.

The test was conducted under extreme weather conditions: temperature of 25°F and wind at 15 to 20 mph. Ballistics performance values were within specification requirements. The RSRM field joint (J-seal) insulation configuration functioned as predicted with no indication of hot gases reaching the capture feature O-rings. There was a blowhole in the polysulfide adhesive in the nozzle-to-case joint, but no evidence of hot gases past the wiper O-ring. Nozzle design changes appeared to perform nominally, with exception of the outer boot ring, which suffered partial structural breakup late in the test. Field joint heaters maintained the controlling resistance temperature device temperature within the specified requirements during heater operation. The thrust vector control system operated properly. The redesigned water deluge system, temperature conditioning equipment, and other test support equipment performed as planned.

CONTENTS

CONTENTS (cont)

CONTENTS (cont)

CONTENTS (cont)

APPENDIX

Appendix

Appendixes are in Volume II--TWR-17371

FIGURES

FIGURES (cont)

FIGURES (cont)

FIGURES (cont)

FIGURES (cont)

FIGURES (cont)

FIGURES (cont)

FIGURES (cont)

FIGURES (cont)

FIGURES (cont)

FIGURES (cont)

TABLES

TABLES (cont)

ABBREVIATIONS AND ACRONYMS

μin.	microinch
1-D	one-dimensional
1-L	one-longitudinal
2-D	two-dimensional
2-L	two-longitudinal
3-D	three-dimensional
ac	alternating current
ANSYS	general structural analysis (computer program)
AP	ammonium perchlorate
APU	auxiliary power unit
B-B	barrier-booster
B-KNO_3	boron-potassium nitrate
Btu	British thermal unit
CCP	carbon-cloth phenolic
CEI	contract end item
CF	carbon-fiber-filled
cg	center of gravity
CO_2	carbon dioxide
CP	cylindrical perforated
CV	coefficient of variation
deg	degree
dia	diameter
DM	demonstration motor
DR	discrepancy report
EDS	energy dispersive spectrometry
EPDM	ethylene-propylene-diene monomer
ETA	external tank attach
ETM	engineering test motor
FEP	fluoroethylene polymer
FJAF	field joint assembly fixture
FJPS	field joint protection system
FSM	fuel supply module
ft	foot

ABBREVIATIONS AND ACRONYMS (cont)

ft^2	square foot
FWC	filament wound case
g	gram
GCP	glass-cloth phenolic
Hg	mercury
HPM	high performance motor
hr	hour
Hz	Hertz
ICD	interface control document
ID	inside diameter
in.	inch
$in.^2$	square inch
ips	inches per second
I_{sp}	specific impulse
JES	joint environment simulator
JPS	joint protection system
kip	thousand pounds
klb	thousand pounds
LAT	lot acceptance test
lb	pound
lbf	pounds force
LH	left hand
lbm	pounds mass
LSC	linear shaped charge
max	maximum
MDD	material decomposition depth
MEOP	maximum expected operating pressure
mil	0.001 inch
min	minute
Mlbf	million pounds force
MOP	maximum operating pressure
mph	mile per hour
ms	millisecond

ABBREVIATIONS AND ACRONYMS (cont)

MS	margin of safety
MSFC	Marshall Space Flight Center
NA	not applicable
NASA	National Aeronautic and Space Administration
NBR	nitrile butadiene rubber
NJES	nozzle joint environment simulator
OBR	outer boot ring
OD	outside diameter
PAA	phosphoric acid anodization
PBAN	polybutadiene acrylonitrile/acrylic acid copolymer
PIRN	preliminary interface revision notice
PMBT	propellant mean bulk temperature
PMD	perimeter measuring device
pps	photos per second
PSD	power spectral density
psi	pounds per square inch
psia	pounds per square inch absolute
psig	pounds per square inch gage
QM	qualification motor
RH	right hand
RSRM	redesigned solid rocket motor
RTD	resistance temperature device
RTV	room temperature vulcanization
S&A	safe and arm (device)
SBRE	surface burn rate error
sccs	standard cubic centimeters per second
SCN	specification change number
sec	second
SII	SRM igniter initiator
SRB	solid rocket booster
SRM	solid rocket motor
Sta	station
TASS	Thiokol Automated Stress System

ABBREVIATIONS AND ACRONYMS (cont)

TPTA	transient pressure test article
TVC	thrust vector control
TWR	Thiokol Wasatch report
USBI	United Space Boosters, Inc.
V	volts
W	watts
wt	weight
°F	degree Fahrenheit

1

INTRODUCTION

The solid rocket motor (SRM), used in pairs, is the primary Space Shuttle propulsive element, providing impulse and thrust vector control (TVC) from SRM ignition to solid rocket booster (SRB) separation. The Space Shuttle Development Motor No. 9 (DM-9) static firing was a full-scale redesigned solid rocket motor (RSRM) static test. This test report includes a detailed presentation and discussion of DM-9 performance, and of test results concurrence with the RSRM development and certification test program. The major focus of this report is placed on the test objectives, anomalies, and motor performance.

DM-9 was successfully fired on 23 Dec 1987 at Thiokol Test Bay T-24. The test was conducted in accordance with the requirements of CTP-0019, "Space Shuttle Development Motor No. 9 (DM-9) Static Fire Test Plan." Postfire inspection procedures followed TWR-16472, Vol. I through IX. Postfire engineering evaluation limits are found in TWR-17198, Vol. 1 through 9.

1.1 TEST ARRANGEMENT AND FACILITIES

The DM-9 static test arrangement was in accordance with Drawing 2U65034, and is shown in Figure 1.1-1. Figures 1.1-2 and 1.1-3 show isometric views of the T-24 test bay. A redesigned water deluge system (Figure 1.1-4) was employed during the test. The aft skirt and the igniter area was conditioned by separate external heating sources (Figure 1.1-5).

1.2 TEST ITEM DESCRIPTION

The DM-9 static test article was a full-scale RSRM with the case consisting of 11 individual, weld-free, high performance motor (HPM) segments preassembled into four casting segments. The assembled case was approximately 116 ft in length and 12 ft in diameter. Factory joints were configured with RSRM case segments and RSRM

N101080-1

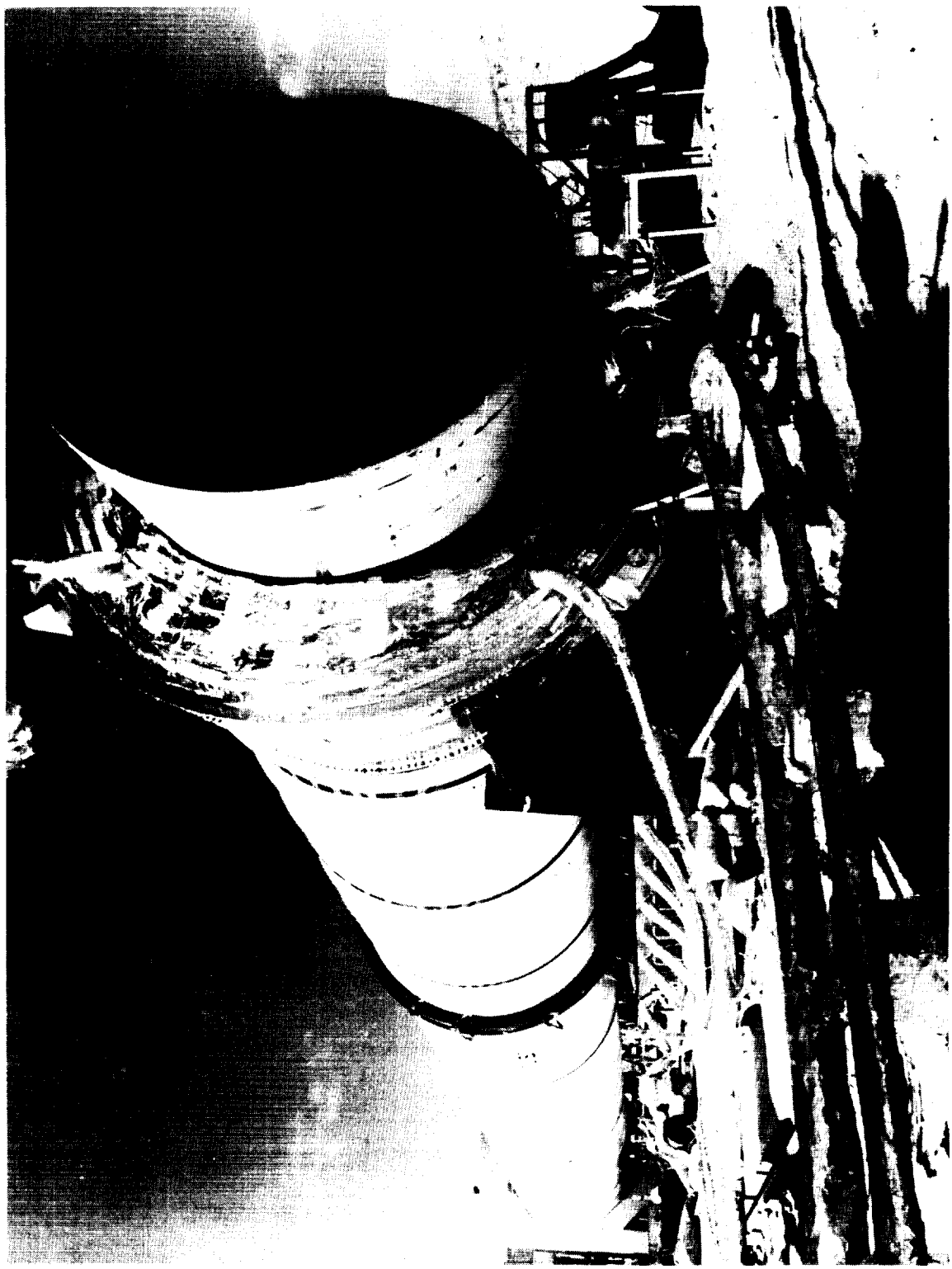

Figure 1.1-1. DM-9 Static Test Motor at T-24 Test Bay

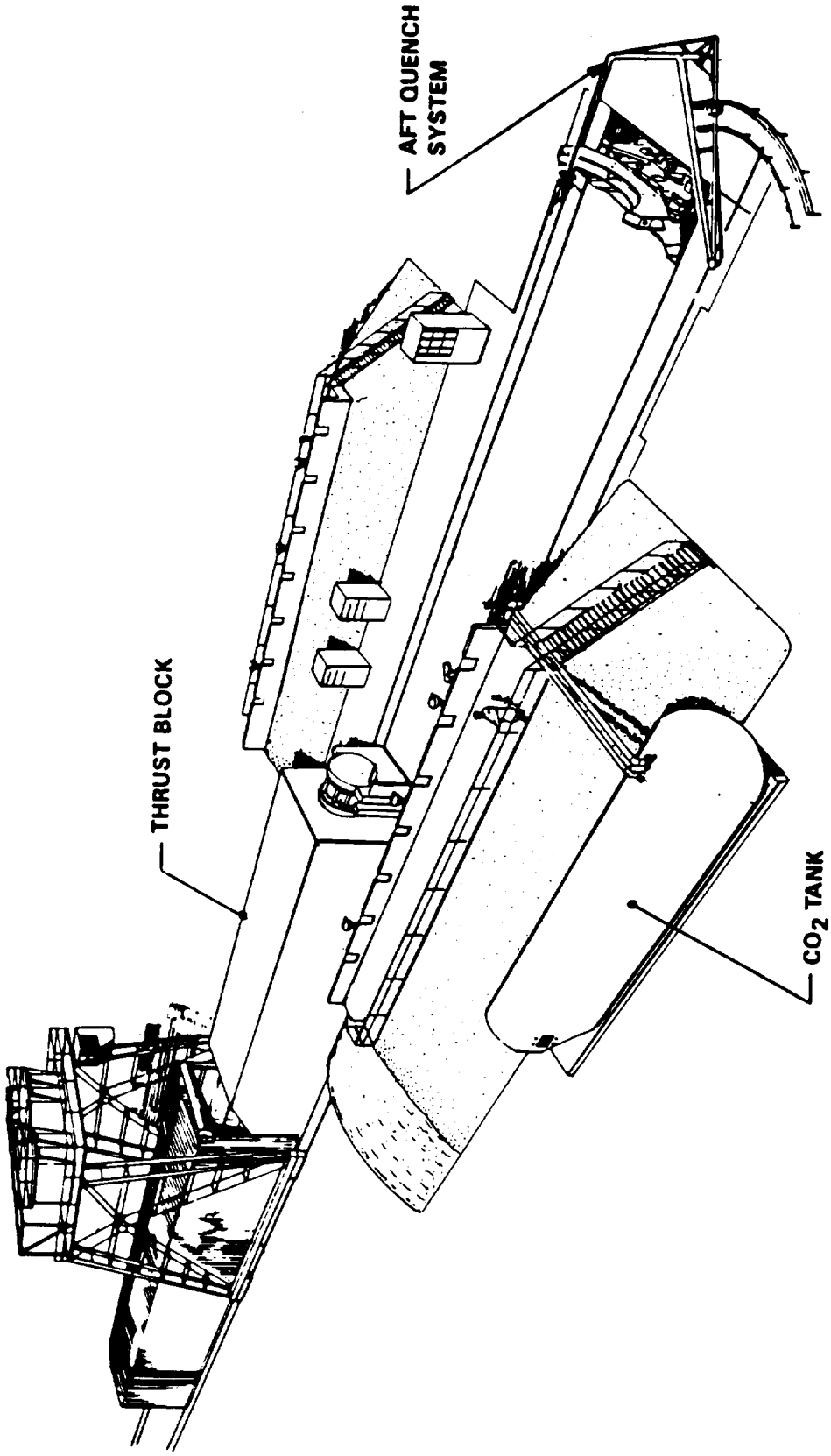

Figure 1.1-2. T-24 Isometric View

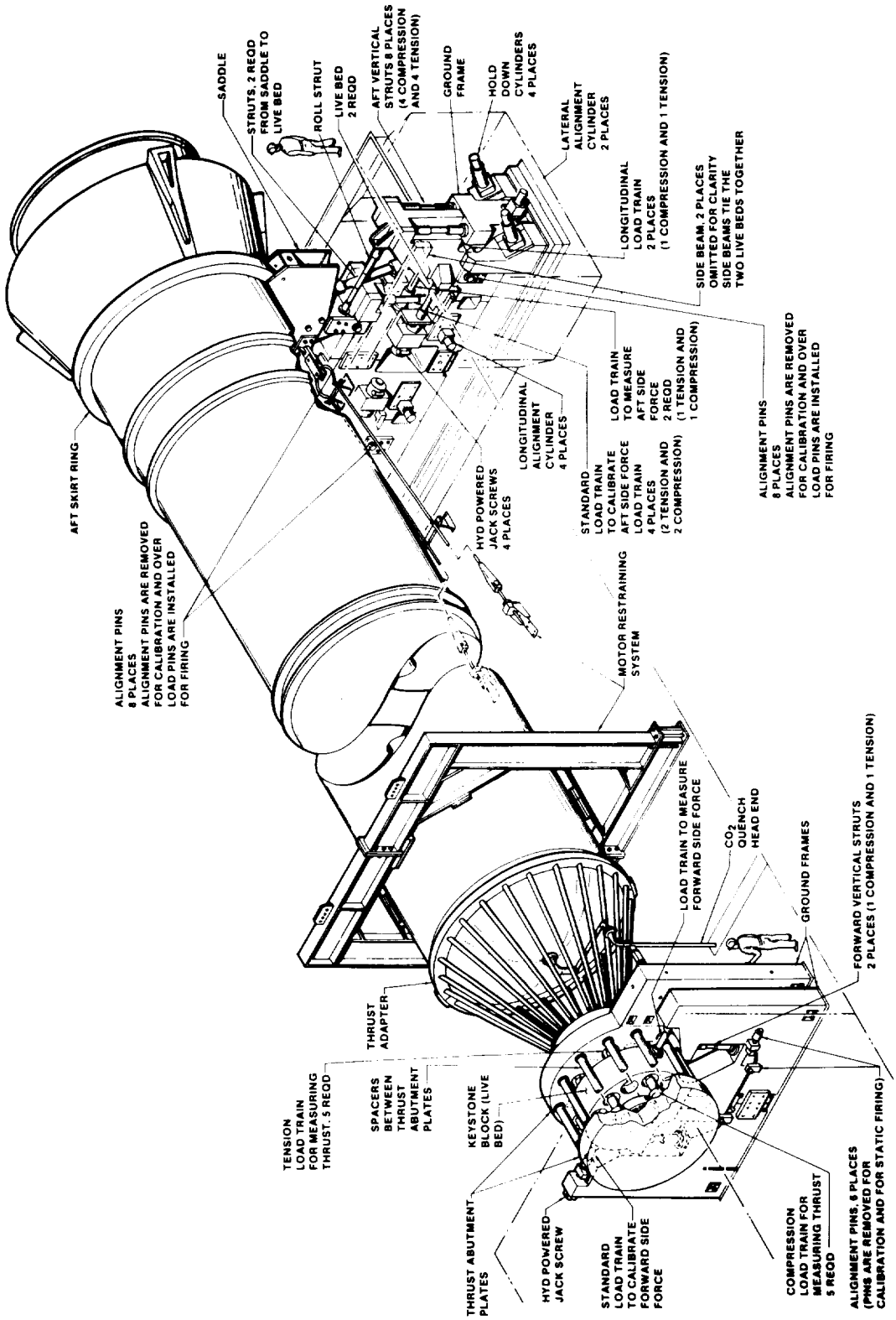

Figure 1.1-3. SRM Static Test Stand (full-duration tests)

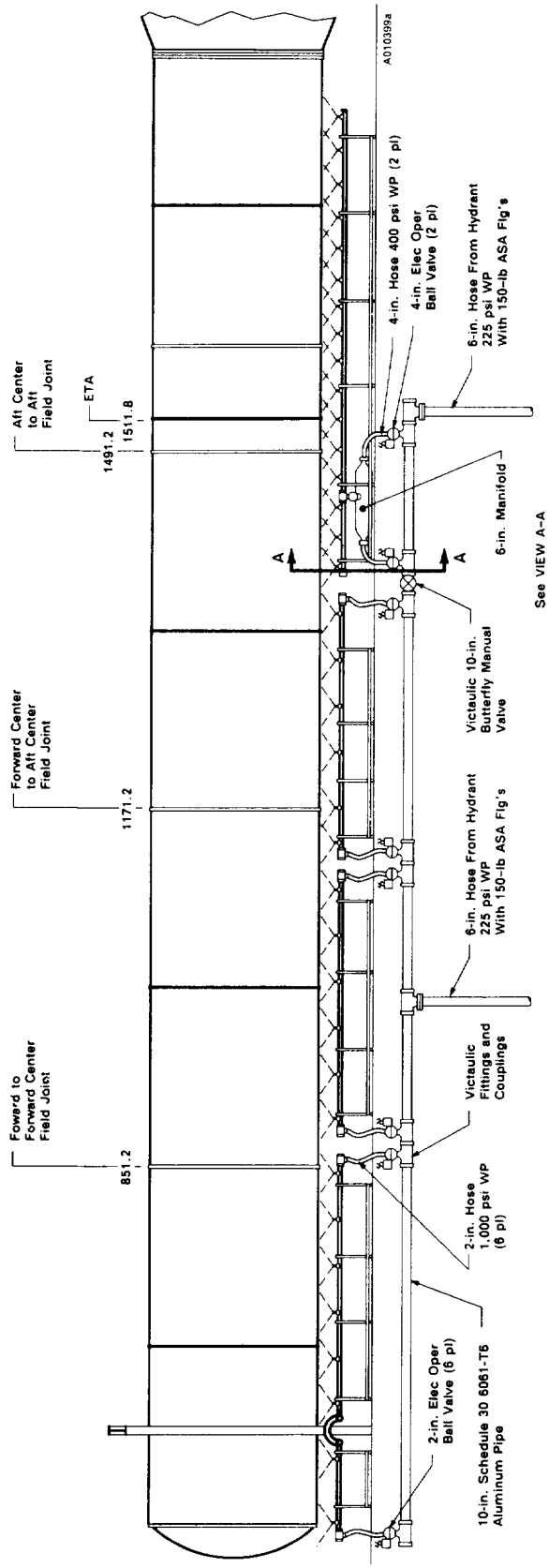

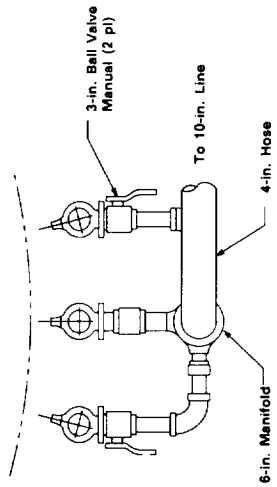

Figure 1.1-4. DM-9 Water Deluge System

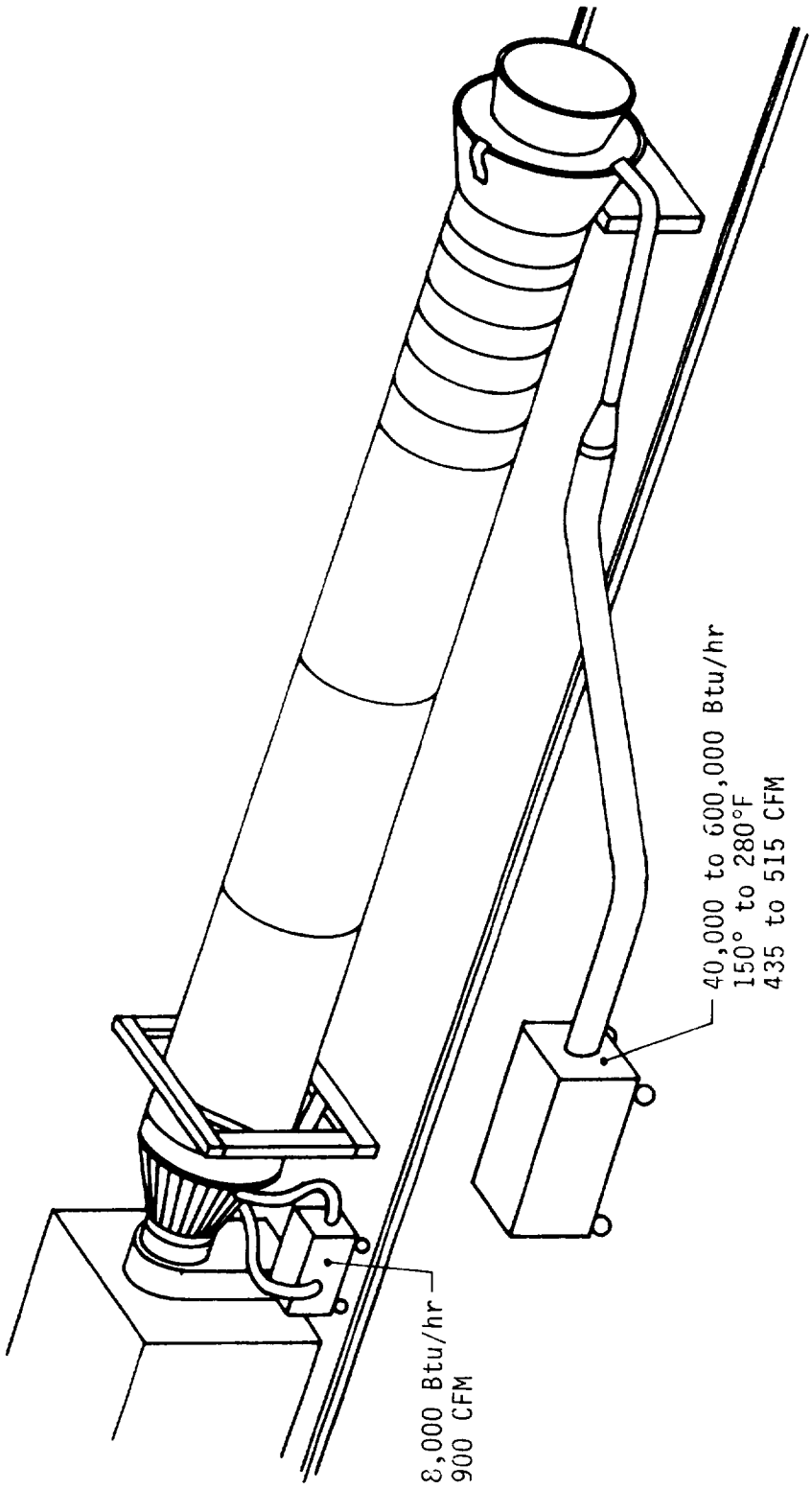

Figure 1.1-5. Aft Skirt/Igniter Conditioning

insulation configuration (thicker than DM-8 with added seal ply). The three field joints were configured with interference fit, capture feature joint hardware, and bonded RSRM (flight configuration) J-seal insulation configuration. The clevis-to-capture feature void (V_2) was filled with fluorocarbon joint filler. Case joints were assembled using long pins, hat retainer band, and custom shims. The nozzle-to-case joint incorporated an RSRM fixed housing with 100 (0.875 in.-dia) radial bolts and an RSRM interference fit bonded insulation configuration. Fluorocarbon (V747-75) O-rings were employed for all primary and secondary seals, the field joint capture feature, and the nozzle-to-case joint wiper. The flight configuration joint protection system was installed on all three field joints. A vulcanized weatherseal was installed on the factory joints.

The nozzle assembly incorporated the following:

- RSRM forward exit cone assembly
- RSRM fixed housing
- RSRM nose inlet assembly (phosphoric acid anodization (PAA) and primer on nose inlet housing)
- RSRM throat inlet assembly
- Thicker cowl with involute outer boot ring
- Flex bearing and added O-ring groove on aft end ring (RSRM configuration)
- RSRM aft exit cone
- RTV backfill in Joints 1, 3, and 4
- Redundant and verifiable seals in all five joints
- RSRM nozzle plug

An SRB aft skirt with TVC systems, actuators, and thermal curtain assembly was attached to the aft segment. An RSRM igniter assembly with an HPM, safe and arm (S&A) device, and a 360-deg external tank attach (ETA) ring completed the motor assembly.

The DM-9 motor configuration and joint details are shown in Figure 1.2-1. The nozzle configuration is shown in Figure 1.2-2.

The DM-9 drawing tree is included in Appendix A. More detailed descriptions and components can be found in Section 7.

The major DM-9 deviations from flight configuration are listed in Table 1.2-1.

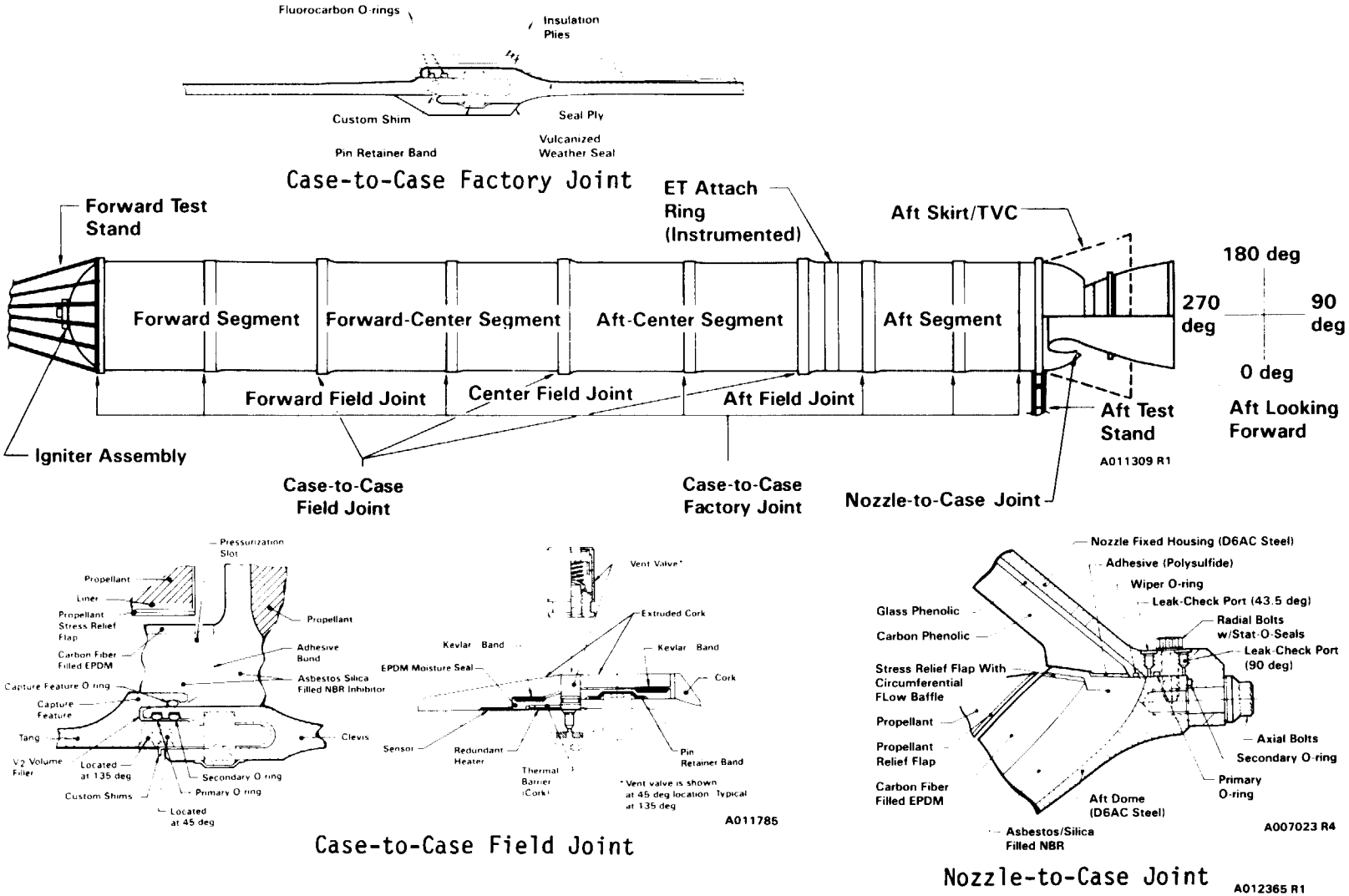

Figure 1.2-1. DM-9 Motor Configuration

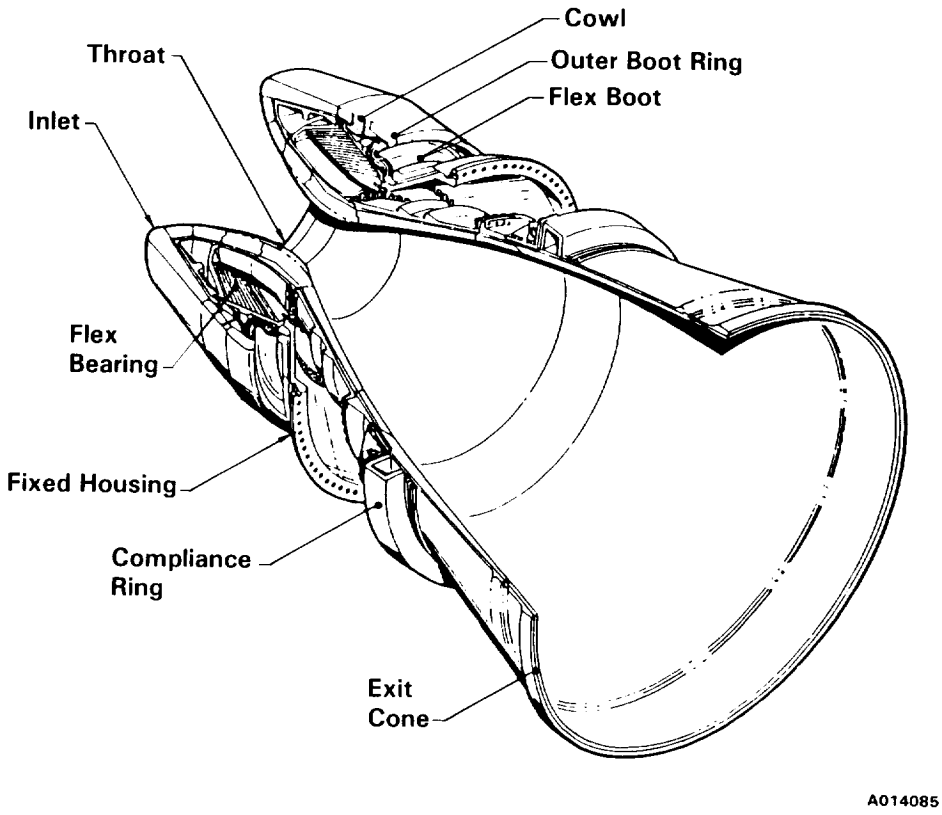

Figure 1.2-2. DM-9 Motor Nozzle Configuration

1.3 TEST PREREQUISITES

All of the DM-9 test prerequisites were met before the test firing. Prerequisite tests for DM-9 are shown in Figure 1.3-1, along with their associated final test report numbers.

Table 1.2-1. DM-9 Test Motor Differences From Flight Configuration

Igniter

Modified igniter adapter for CO_2 quench

Propellant/Liner

X-ray on DM-9 aft segment only (X-ray on all flight segments)

Field Joint

O-rings

- 7U O-rings - 1U O-rings certified by full inspection
- O-rings have cryogenic deflashing - concern is cryogenic effects on long-term resiliency characteristics

Case measurements by pi tape. Post-test measurements taken by perimeter measuring device (PMD)

Factory Joint

O-rings

- 7U O-rings - 1U O-rings certified by full inspection
- O-rings have cryogenic deflashing - concern is cryogenic effects on long-term resiliency characteristics

Teflon stress release tape at center segments only

Joint Protection System (Field Joint)

Vent valves installed on forward field joint only
Connectors different (DM-9 versus flight)
Potting compound (DM-9 versus flight) is different
Welding of heater elements is the same, but flight inspection will be different
Crimp tensile test was not performed

Table 1.2-1. DM-9 Test Motor Differences From Flight Configuration (cont)

Nozzle-to-Case Joint

O-rings

- 7U O-rings - 1U O-rings certified by full inspection
- O-rings have cryogenic deflashing - concern is cryogenic effects on long-term resiliency characteristics

Ambient cure on polysulfide adhesive (accelerated cure used for flight)

Ultrasonics used on all radial and 20 axial bolts to verify proper loading (all bolts on flight)

Four radial strainserts and two axial strainserts in place of flight configuration bolts

Nozzle Assembly

PAA and primer coating on nose inlet housing
Shear pins on the forward and aft exit cones vented, but do not have positive stop
0.875-in. radial bolts do not have locking feature
No linear shaped charge (LSC) for exit cone cutoff
No snubber installed
No paint on aft exit cone insulation

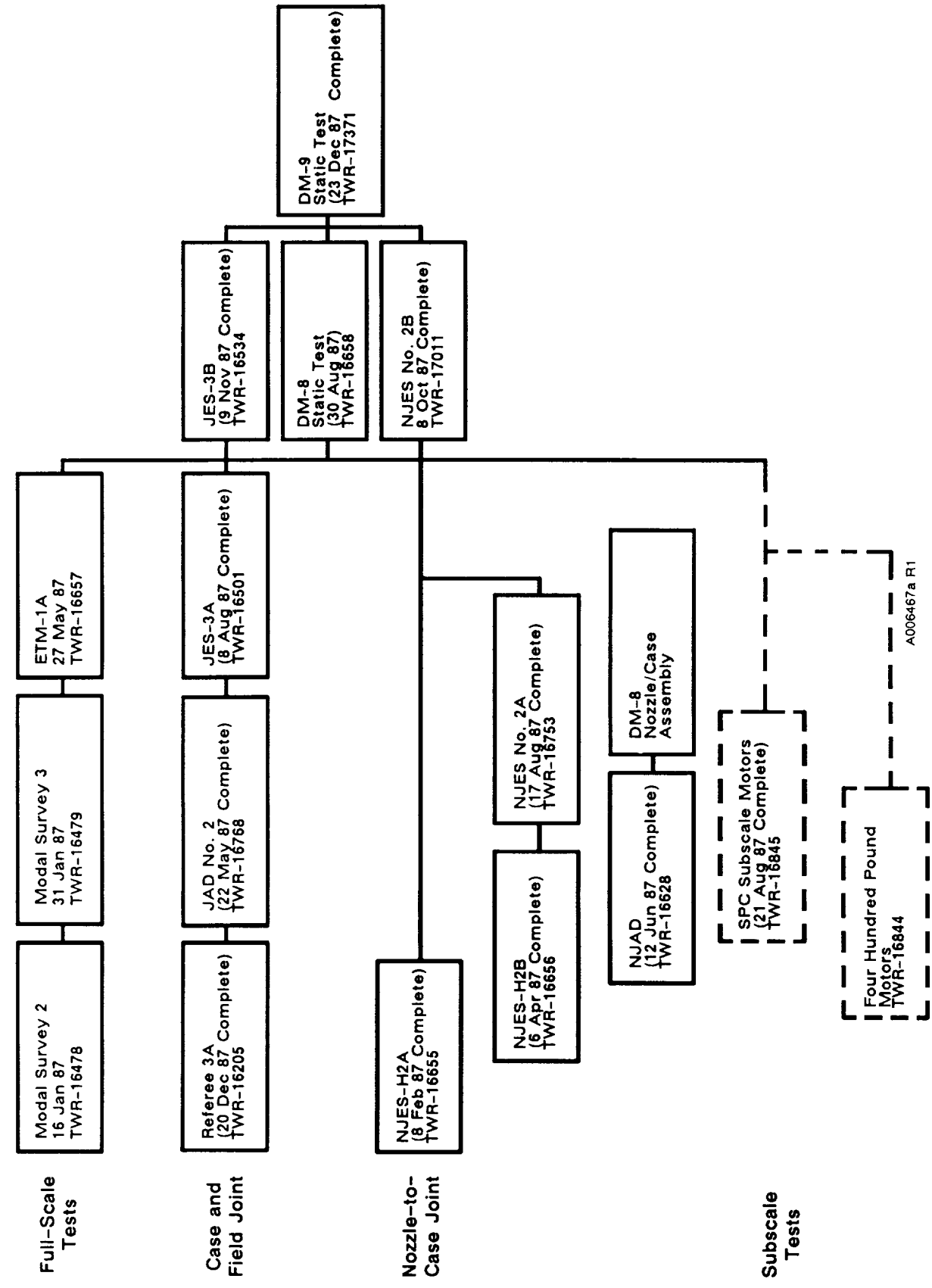

Figure 1.3-1. DM-9 Prerequisite Test Summary

2

TEST OBJECTIVES

The DM-9 test objectives were derived from objectives in TWR-15723 to satisfy the requirements of specification CPW1-3600A, dated 3 Aug 1987.

	Qualification	CEI Paragraph
A	Certify that the sealing of the case field joints is not affected by static test structural deflections.	3.2.1.2.1.a
B	Certify the case field joint seal performance at ambient temperature.	3.2.1.2.1.b
C	Certify that the case field joint seal verification does not degrade the performance or integrity of the joint system.	3.2.1.2.1.c
D	Certify that the case structural and sealing integrity is not degraded.	3.2.1.8.1.1.a
E	Certify that the leak test method is compatible with the joint insulation.	3.2.1.8.1.1.b
F	Certify that the insulation ensures system performance and structural integrity are maintained during the assembly process and operation.	3.2.1.8.1.1.c
G	Certify that the insulation protects the primary and secondary seals from visible degradation from motor combustion gas.	3.2.1.8.1.1.d
H	Certify the ability of the insulation to protect case joints from thermal degradation during a full-duration (ambient temperature) burn.	3.2.1.8.1.1.e
I	Certify that the insulation does not shed fibrous or particulate matter during assembly which could prevent sealing.	3.2.1.8.1.1.f
J	Certify that the field joint insulation withstands slag accumulation during motor operation.	3.2.1.8.1.1.g

	Qualification	CEI Paragraph
K	Certify that the field joint insulation does not induce changes to the propellant grain design which could invalidate the existing ballistic performance database.	3.2.1.8.1.1.i
L	Certify that the nozzle-to-case joint insulation withstands slag accumulation during motor operation.	3.2.1.8.1.1.g
M	Certify that the nozzle-to-case joint insulation does not induce changes to the propellant grain design which could invalidate the existing ballistic performance.	3.2.1.8.1.1.i
N	Certify that the sealing of the nozzle-to-case joint is not affected by static test structural deflections.	3.2.1.2.1.a
O	Certify the nozzle-to-case joint seal performance with the joint conditioned between 75° and 120°F.	3.2.1.2.1.b
P	Certify that the nozzle-to-case joint seal verification does not degrade the performance or integrity of the joint system.	3.2.1.2.1.c
Q	Certify that the nozzle-to-case joint O-ring is maintained within the temperature range specified in ICD 2-0A002 (75° ±25°F). A PIRN (BI-0718) will change this to 75° to 120°F when approved.	3.2.1.2.1.f
R	Certify backfill of internal nozzle joints (flight configuration).	
S	Certify aluminum systems tunnel bondline integrity after exposure to motor pressurization loads.	3.2.1.10.4
T	Certify the ability of the field joint protection system to prevent rain entry.	3.2.1.3.h
U	Certify the ability of the field joint heater assembly to maintain the joint temperature between 75° and 120°F.	3.2.1.11.a
V	Certify the ability of the field joint protection system to prevent the accumulation of water in the joint.	3.2.1.11.b

	Qualification	CEI Paragraph
W	Certify the operation of the field joint heater with a power supply meeting the requirements of ICD 3-44005.	3.2.1.11.1.2
X	Determine pressure distribution within the motor during ignition and main burn.	3.2.1.3.k
Y	Certify the motor performance at ambient temperature.	3.2.1
Z	Certify that the ignition interval is between 202 and 262 ms.	3.2.1.1.1.1
AA	Certify that the rate of pressure buildup is between 70.9 and 115.9 psi for any 10 ms interval.	3.2.1.1.1.2
AB	Certify that the nominal thrust-time curve falls within the upper and lower bounds identified in CPW1-3600A, Table I.	3.2.1.1.2.1
AC	Certify that the performance tolerances and limits do not exceed those allowed in CPW1-3600A, Table II.	3.2.1.1.2.2
AD	Certify that the impulse gates specified in CPW1-3600A are achieved when corrected to 60°F.	3.2.1.1.2.4
AE	Certify that the nozzle assembly and exit cone design are compatible with the performance requirement specified in CPW1-3600A.	3.2.1.4
AF	Certify that the loaded RSRM center of gravity (cg) falls between 1,179 and 1,165 on the longitudinal (X) axis.	3.2.2.2.3
AG	Certify that the case is capable of containing the static test internal pressure.	3.2.1.3.a
AH	Certify that the case segment mating joints have a pin retention device.	3.2.1.3.g
AI	Certify that the ignitions system precludes the leakage of hot gas during and subsequent to motor ignition.	3.2.1.5.a

	Qualification	CEI Paragraph
AJ	Verify that the case segment mating joints incorporate provisions to ensure proper segment orientation and alignment to facilitate joining, stacking, disassembly, and refurbishment.	3.2.1.3.f
AK	Verify that the RSRM segments are capable of horizontal assembly and disassembly.	3.2.5.1
AL	Certify that the seal verification does not degrade the performance or integrity of the factory joint system.	3.2.1.2.2.c
AM	Certify that the nozzle liner design prevents the formation of pockets, wedge outs, and anomalies as defined.	3.2.1.4.13
AN	Certify that nozzle assembly primary ablatives meet the design safety factors.	3.3.6.1.2.7
AO	Certify that the nozzle performance margins of safety (MS) are zero or greater.	3.3.6.1.2.8
AP	Certify that the nozzle meets vectoring requirements.	3.2.1.4.1
AQ	Certify that the nozzle radial offset does not exceed the limits.	3.2.1.4.2
AR	Certify that the nozzle meets dynamic thrust vector requirements.	3.2.1.4.3-a, -b
AS	Certify that the nozzle meets null offset angle requirements.	3.2.1.4.4-a, -b, -c
AT	Certify that the nozzle plug can be expelled without damage to other components or an adverse effect on RSRM performance.	3.2.1.4.7.c
AU	Certify by demonstration that the TVC actuator attach points meet the requirements of ICD 3-44003.	3.2.1.4.8
AV	Certify that the flex bearing is capable of vectoring a total of 85 cumulative degrees during each flight duty cycle.	3.2.1.4.11.1

	Qualification	CEI Paragraph
AW	Certify that the factory joint insulation can accommodate static test motor structural deflection and erosion.	3.2.1.2.2.a
AX	Certify that the factory joint insulation is capable of sealing after normal manufacturing processes and during static test at ambient conditions.	3.2.1.2.2.b
AY	Certify that the seal verification does not degrade the performance or integrity of the factory joint system.	3.2.1.2.2.c
AZ	Certify that at least one virgin ply of insulation remains over the factory joint after the motor is fired.	3.2.1.2.2.d
BA	Certify that the flex bearing will remain sealed throughout the TVC duty cycle during static testing.	3.2.1.2.3.a
BB	Certify proper flex bearing sealing capability at ambient conditions after processing in a normal manufacturing environment.	3.2.1.2.3.b
BC	Certify that the flex bearing seal verification does not degrade the performance or integrity of the system.	3.2.1.2.3.c
BD	Certify that there are no gas leaks between the flex bearing internal components.	3.2.1.2.3.d
BE	Certify that the nozzle internal seals and the aft exit cone joint can accommodate static test motor-induced structural deflections.	3.2.1.2.5.a
BF	Certify that seal verification does not degrade the performance or integrity of the nozzle internal joints or the aft exit cone joint.	3.2.1.2.5.c
BG	Certify that bore seals are verifiable in the proper direction.	3.2.1.2.5.e
BH	Certify electrical bonding per MIL-B-5087B.	3.2.1.6.f

Development

BI Evaluate the structural integrity of ETA ring under pressurization loads (MSFC test objective).

BJ Acquire engineering data for validation of joint models.

BK Obtain data to verify finite element models.

BL Determine the effects of dither/TVC performance at elevated hydraulic oil temperatures (MSFC test objective).

BM Evaluate the performance of the nozzle-to-case and field joint adhesive.

Table 2-1, Test Objective Compliance Matrix, shows the type, method of compliance, and instrumentation type applicable to the test objectives.

Table 2-1. Test Objective Compliance Matrix--DM-9 Test Article

Test Plan Objective Summary (CEI Specification Cross Reference Index)	Type of Objective		Method of Compliance With Objective			Instrumentation Type Applicable to Test Objective	Evaluation Criteria
	Development	Flight Cert	Direct Measurement	Analytical Model Verification	Post-Test Inspection		
1. Certify sealing performance of capture feature hardware (3.2.1.2.1.a, 3.2.1.2.1.b, 3.2.1.2.1.c)*		X	X		X	Strain	*
2. Certify performance of unvented J-seal (flight configuration) insulation joint (3.2.1.8.1.1.a, 3.2.1.8.1.1.b, 3.2.1.8.1.1.c, 3.2.1.8.1.1.d, 3.2.1.8.1.1.e, 3.2.1.8.1.1.f, 3.2.1.8.1.1.g, 3.2.1.8.1.1.i)		X			X		*
3. Certify performance of unvented nozzle-to-case joint insulation (3.2.1.8.1.1.a, 3.2.1.8.1.1.b, 3.2.1.8.1.1.c, 3.2.1.8.1.1.d, 3.2.1.8.1.1.e, 3.2.1.8.1.1.g, 3.2.1.8.1.1.i)*		X			X		*
4. Certify sealing performance of radially bolted nozzle-to-case joint hardware (3.2.1.2.1.a, 3.2.1.2.1.b, 3.2.1.2.1.c, 3.2.1.2.1.f)		X	X		X	Strain	*

*The criteria for flight certification objectives will be based on the requirements of the referenced CEI specification cross-reference index

Table 2-1. Test Objective Compliance Matrix--DM-9 Test Article (cont)

Test Plan Objective Summary (CEI Specification Cross-Reference Index)	Type of Objective		Method of Compliance With Objective			Instrumentation Type Applicable to Test Objective	Evaluation Criteria
	Development	Flight Cert	Direct Measurement	Analytical Model Verification	Post-Test Inspection		
5. Certify backfill of internal nozzle joints. (Flight configuration)		X			X		*
6. Certify aluminum systems tunnel bondline integrity (3.2.1.10.4)		X			X		*
7. Evaluate structural integrity of 360-deg ETA ring under pressurization loads (MSFC test objective)	X		X			Strain	ETA ring and attachment hardware retain structural integrity during test, allowing detailed measurement of stress distribution in ring
8. Acquire engineering data for validation of joint models	X		X	X		Pressure temperature, strain, deflection	Data are collected for validation of joint models
9. Certify joint protection system (3.2.1.11.a, 3.2.1.11.b, 3.2.1.11.1.2, 3.2.1.3.h)		X			X		*
10. Certify pressure distribution within the motor during ignition and main burn meets specification requirements (3.2.1.3.k)		X	X	X		Pressure, thrust acceleration, strain	*

*The criteria for flight certification objectives will be based on the requirements of the referenced CEI specification cross-reference index

Table 2-1. Test Objective Compliance Matrix--DM-9 Test Article (cont)

Test Plan Objective Summary (CEI Specification Cross-Reference Index)	Type of Objective		Method of Compliance With Objective			Instrumentation Type Applicable to Test Objective	Evaluation Criteria
	Development	Flight Cert	Direct Measurement	Analytical Model Verification	Post-Test Inspection		
11. Certify that thrust and pressure performance meets specification requirements (3.2.1, 3.2.1.1.1.1, 3.2.1.1.1.2, 3.2.1.1.2.1, 3.2.1.1.2.2, 3.2.1.4 (MTI), 3.2.1.1.2.4, 3.2.2.2.3)		X	X	X		Pressure, thrust	*
12. Certify performance of redesigned propellant forward segment smooth bore to fin cavity transition (3.2.1, 3.2.1.1.1.1, 3.2.1.1.1.2, 3.2.1.1.2.1, 3.2.1.1.2.2)		X	X	X		Pressure, thrust	*
13. Certify structural integrity of the case, ignition system and nozzle (3.2.1.3.a, 3.2.1.3.g, 3.2.1.3.i, 3.2.1.4 (MTI), 3.2.1.5)		X	X	X	X	Pressure, temperature, strain, deflection, acceleration	*
14. Certify combustion stability (3.2.1.1.1.1, 3.2.1.1.1.2, 3.2.1.1.2.1)		X	X	X		Pressure, thrust, strain, acceleration	*
15. Verify the assembly/disassembly of the unvented J-seal insulation field joint design in the horizontal position (3.2.1.3.f, 3.2.5.1)	X				X		Horizontal assembly and disassembly of field joints are accomplished without damage to the field joint insulation or hardware

*The criteria for flight certification objectives will be based on the requirements of the referenced CEI specification cross-reference index

Table 2-1. Test Objective Compliance Matrix--DM-9 Test Article (cont)

Test Plan Objective Summary (CEI Specification Cross-Reference Index)	Type of Objective		Method of Compliance With Objective			Instrumentation Type Applicable to Test Objective	Evaluation Criteria
	Development	Flight Cert	Direct Measurement	Analytical Model Verification	Post-Test Inspection		
16. Certify effectiveness of all seals (3.2.1.2.2.c, 3.2.1.2.1.c)*		X			X		*
17. Certify nozzle design changes (3.2.1.4.13, 3.3.6.1.2.7, 3.3.6.1.2.8)		X	X	X	X	Temperature, strain	*
18. Certify nozzle operation and performance (3.2.1.4 (MTI), 3.2.1.4.1, 3.2.1.4.2, 3.2.1.4.3, 3.2.1.4.3.a, 3.2.1.4.3.b, 3.2.1.4.4.a, 3.2.1.4.4.b, 3.2.1.4.4.c, 3.2.1.4.7.c, 3.2.1.4.8, 3.2.1.4.11.1)		X	X		X	Temperature, strain, proximity	*
19. Certify the joint heater's ability to maintain the field joints within specified limits (3.2.1.11.a)		X	X			Temperature	*
20. Obtain data to verify finite element models	X		X	X		Pressure, temperature, strain, deflection	Data are collected to verify finite element models
21. Certify leak check procedures on all field joint seals (3.2.1.2.1.c, 3.2.1.8.1.1.b,)		X			X		*

*The criteria for flight certification objectives will be based on the requirements of the referenced CEI specification cross-reference index

910335-15.4

Table 2-1. Test Objective Compliance Matrix--DM-9 Test Article (cont)

Test Plan Objective Summary (CEI Specification Cross-Reference Index)	Type of Objective		Method of Compliance With Objective			Instrumentation Type Applicable to Test Objective	Evaluation Criteria
	Development	Flight Cert	Direct Measurement	Analytical Model Verification	Post-Test Inspection		
22. Evaluate the performance of the nozzle-to-case joint adhesive		X			X		*
23. Certify the performance of factory joint insulation (3.2.1.2.2.a, 3.2.1.2.2.b, 3.2.1.2.2.c, 3.2.1.2.2.d)		X			X		*
24. Certify flex bearing sealing characteristics during motor operation (3.2.1.2.3.a, 3.2.1.2.3.b, 3.2.1.2.3.c, 3.2.1.2.3.d)		X			X		*
25. Certify performance of nozzle internal seals (3.2.1.2.5.a, 3.2.1.2.5.c, 3.2.1.2.5.e)		X			X		*
26. Certify electrical bonding characteristics (3.2.1.6.f)		X	X			Resistance	*
27. Determine the effects of dither/TVC performance at elevated hydraulic oil temperatures (MSFC test objective)	X		X			Temperature, accelerometers, pressures, deflection	Evaluate TVC data. Verify if dither is induced by elevated hydraulic oil temperature and nozzle exit cone resonance frequencies

*The criteria for flight certification objectives will be based on the requirements of the referenced CEI specification cross-reference index

PAGE 24 INTENTIONALLY BLANK

3

EXECUTIVE SUMMARY

3.1 SUMMARY

The DM-9 static test was successfully conducted under extreme weather conditions: a temperature of 25°F, and wind 15 to 20 mph with gusts to 30 mph. Data were gathered at instrumented locations during pretest, test, and post-test operations. Dimensional measurements were taken before and after static testing to document insulation performance. The information assembled from the test procedure has supplied valuable knowledge about the performance of the RSRM design components used in DM-9.

3.1.1 Propellant/Ballistics/Mass Properties Performance

The DM-9 ballistic performance was typical and within expected limits. The new forward segment transition block could not be linked with abnormal gas flow or pressure disturbances. Ignition interval and pressure rise rate limits were met. Impulse gates were met. The DM-9 ballistic performance compared closely with DM-8 performance and HPM historical data. DM-9 slag weight was 2,270 lb. The cause of the excessive slag is suspected of being associated with the ammonium perchlorate (AP) particle size distribution.

The DM-9 motor exhibited chamber pressure oscillations similar to previously tested Space Shuttle SRMs. The oscillations experienced by DM-9 were higher than the average of the last six static tests, though still within previously observed limits.

The modified igniter performed successfully as predicted. The pressure distribution in the motor was well below the design requirements. A summary of DM-9 performance values is listed in Table 3.1-1.

Section 7.1 contains a detailed description of the propellant, ballistics, and mass properties performance test results.

Table 3.1-1. DM-9 Performance Summary With CPW1-3600 CEI Specification Limits

	Vacuum Spec Limits (60°F)	DM-9 Predicted (60°F)	DM-9 Delivered (60°F)
Web Time (sec)	106.1 - 117.2	111.4	110.6
Action Time (sec)	115.4 - 131.4	122.8	122.4
MOP Headend (psia)	858.7 - 978.1	920	913
Max Sea Level Thrust (Mlbf)	2.87 - 3.25	3.054	3.290
Web Time Avg Headend Pressure (psia)	625.8 - 695.8	662	668
Web Time Avg Vacuum Thrust (Mlbf)	2.45 - 2.72	2.610	2.615
Web Time Total Impulse (Mlbf-sec)	286.1 - 291.8	289.81	289.35
Action Time Impulse (Mlbf-sec)	293.3 - 299.2	296.89	296.97
I_{sp} Avg Delivered (lbf-sec/lbm)	265.3 - 269.0	268.6	268.6
Ignition Interval (sec), Time 563.5 psia	0.202 - 0.262	0.232	0.244
Maximum Pressure Rise Rate (psi/10 ms)	X < 115.9	92.0	81.0

Loaded Propellant Weight of 1,106,184 lb

3.1.2 Aero/Thermal

Slag

A large amount of slag collected in the aft segment during the firing. The total slag weight (2,270 lbm) was similar to that experienced on DM-8 (2,381 lbm), as expected, but less than on ETM-1A (3,377 lbm), and higher than that found on most static motors.

Temperature Data

Temperature data were nominal. The maximum temperature of the case at the slag-affected areas was 195.6°F.

Section 7.2 contains a detailed description of the aero/thermal test results.

3.1.3 Dynamics

The numerous transducers used to monitor DM-9 during static firing gathered valuable data for assessing and analyzing the dynamic behavior of the RSRM. The first bending frequency noted in the data is 1.8 Hz.

Section 7.3 contains a detailed description of the motor's dynamic response.

3.1.4 Insulation Performance

Field Joints

The insulation performance in all three of the redesigned case field joints was excellent. The joint bondline for all three case field joints appeared to have contact for the full circumference as evidenced by a postfire witness line of adhesive contact. There was no evidence of circumferential flow or hot gas penetration (i.e., sooting, charring) into the joint beyond the nominal expected char and erosion.

Nozzle-to-Case Joint

The nozzle-to-case joint had a gas path to the wiper O-ring, but not past it, at 46.8 deg. There was no blowby, erosion, or heat effect to the wiper O-ring. This shows that the new joint design is tolerant to this type of defect condition. One large

void was noted in the adhesive bondline forward of the insulation step from 74 to 109 deg, but it did not create a through path to the wiper O-ring. There was also less erosion in the joint region than had been analytically predicted, but it was similar to DM-8.

Case

There were no hot spots on the external case, unlike DM-8 and ETM-1A, which both had hot spots on the aft segment. The slag weight in the aft and aft center segment of DM-9 was 2,270 lbm total, which was slightly less than that measured on DM-8 (2,381 lbm). The deluge system operated correctly on DM-9.

No critical, major, or minor potential anomalies were identified by the Insulation Component Program Team. Three potential anomalies that remained observations were identified.

Section 7.4 contains a detailed description of the insulation test results.

3.1.5 Nozzle Performance

Nozzle Assembly

Erosion of the DM-9 forward nozzle assembly, aft exit cone, and fixed housing was smooth and uniform. All regions of the DM-9 nose inlet assembly eroded smoothly, with no visible pockets or wash areas. The aft inlet ring (-504), forward nose ring (-503), and nose cap showed minimal post-test surface delaminations. Erosion of the throat and throat inlet rings was smooth and uniform. The DM-9 forward exit cone liner erosion was nominal, showing no major washing or pocketing.

The DM-9 cowl ring showed irregular erosion patterns intermittently around the part circumference and cross-ply cracks extending axially through the part vent and shear pinholes. Axial cracks were also observed spaced between vent holes.

Visual examination showed that the majority of the DM-9 cowl vent holes were plugged with slag.

Charred carbon-cloth phenolic (CCP) plies wedged out on the nose cap aft end intermittently around the nozzle circumference. There was evidence that the CCP material wedged out after motor burn. Charred plies on the nose cap aft end have wedged out on the majority of static test and flight nozzles.

The DM-9 bearing protector performed nominally with light soot and char appearing on the outside diameter (OD) surface. A minimum of three nitrile butadiene rubber (NBR) plies of the DM-9 flex boot remained around the circumference following the test. The cavity side of the flex boot showed no evidence of flow or erosion.

The nozzle metal hardware showed no damage and performed nominally. The DM-9 nozzle plug burst into multiple pieces at motor ignition.

Overall performance of the nozzle assembly appeared typical of past flight and static test motors, with the exception of the new involute outer boot ring (OBR).

OBR

The DM-9 involute OBR separated from the nozzle over a 150-deg arc. The remainder was intact and bonded to the nozzle. Six pieces of the OBR were found on the floor of the aft segment, making up all but a small portion of the separated ring.

Joint Backfill

The backfilled nozzle internal joints showed RTV extending below the char line 360 deg circumferentially except for the throat/forward exit cone joint. The backfill extending below the joint char line is a design goal. This is not a certification issue and will not affect flight. There was no evidence of blowby, erosion, or heat effect to any of the backfilled joint O-rings.

Flex Bearing

Overall flex bearing performance during static test was acceptable. The bearing was in excellent condition and showed no indictions of exposure to heating or of

any damage. This was the fifth usage of this assembly, and there were no detectable anomalies in function or performance throughout the test.

Nozzle - Composite Structures

The review of instrumentation data has verified the structural integrity of the nozzle in all locations measured. In general, predicted strains compared well with measured strains and nozzle strains were small. Hoop strains tend to follow the pressure trace. Although no strain gages could be located on or near the OBR, other nozzle gages aided in determining the time of failure.

Measured strain due to TVC actuation during firing are generally less than 170 in./in. in the hoop direction and 150 in./in. in the meridional direction. However, the magnitude of these included strains at critical joint regions, including the aft nose inlet housing joint and the fixed housing-aft dome joint could be significant.

Differences in prefire and static test strains due to vectoring require further study to understand the effects of pressure, temperature, and erosion.

Nozzle TVC

The TVC performed nominally and followed the specified duty cycle well.

Section 7.5 contains a detailed description of the TVC system results.

3.1.6 Case Performance

The DM-9 static test was conducted successfully with no anomalies associated with the case or joint metal hardware. Assembly procedures proved adequate, and valuable data were gathered on the structural response of the motor during testing. Chamber pressure was contained and data indicate that joint gap openings were restrained well under the maximum allowable values. No local yielding was measured.

The measured radial growth for the DM-9 field joints and nozzle-to-case joint is in close agreement with pretest predictions and radial growth data measured from subscale testing (JES-3A, JES-3B, NJES-2A, NJES-2B, and TPTA 1.1). The O-ring gap opening was not measured directly for the DM-9 field and nozzle-to-case joints.

However, these measurements were taken on the JES, NJES, and TPTA tests. The largest field joint O-ring gap measured in subscale tests (flawed or unflawed) was 0.006 in. (JES-3A and TPTA-1.1); analysis predicts 0.004 inch. The maximum measured primary gap opening for the nozzle-to-case joint was 0.007 in. (NJES-2A); analysis predicts 0.006 inch.

Since the DM-9 maximum joint pressures did not exceed the maximum subscale test pressures, it is a good assumption that the DM-9 O-ring gap openings did not exceed those measured in subscale tests.

There was no damage to the case resulting from slag accumulation in the aft segment. The redesigned water deluge system functioned properly.

Section 7.6 contains a detailed description of the case test results.

3.1.7 Seals Performance

Field Joints

There was no evidence of gas reaching the O-rings due to the effectiveness of the J-seal insulation. Therefore, the performance of the field joint O-rings cannot be fully evaluated. No evidence of damage was found to the field joint O-rings from the static test, assembly procedures, or new 1,000 psi leak check test.

Factory Joints

For factory joint evaluation, see TWR-18135, Rev A, Section 5.1.

Nozzle-to-Case Joint

There was no evidence of hot gas past the wiper O-ring of the nozzle-to-case joint insulation configuration. Therefore, the performance of the nozzle-to-case joint O-rings cannot be fully evaluated. There was a blowhole through the polysulfide adhesive, but no evidence of erosion, blowby, or heat damage to the wiper O-ring. The nozzle-to-case joint primary/ secondary O-rings successfully passed the 920 psig leak test.

A jagged cut in the secondary O-ring is suspected to be caused by handling damage. Gouges found in the wiper O-ring occurred during disassembly. No disassembly damage occurred to the primary O-ring.

Internal Nozzle Joints

Disassembly inspection showed that the seal components performed as expected. Gas reached the primary O-ring at four of the five nozzle internal joints. There was no evidence of blowby, erosion, or heat effect to any of the primary/secondary O-rings.

Igniter Joints

Inner and S&A gaskets performed as expected with no signs of erosion, heat effect, or sooting past the primary seals. A depression was found on the crown of the primary seal of the igniter gaskets. It was concluded that the depression was a manufacturing defect. All sealing surfaces were free of soot.

The depression found on the crown of the primary seal at 144 deg on the igniter gaskets was identified as a major anomaly. No critical or minor potential anomalies were identified by the Seals Component Team, but five observations were identified. These observations and the major anomaly are summarized in Section 7.7.4.6.

Section 7.7 contains a detailed description of the seals test results.

3.1.8 Igniter Performance

The igniter functioned as predicted providing adequate combustion to ignite the static motor at the specified rate and time.

The general condition of the ignition system and CO_2 injector was good. All of the igniter hardware performed in a satisfactory manner and performance was within specification limits. The refurbishable hardware, i.e., igniter chamber, adapter gaskets, and the S&A device were adequately protected from heat damage. There was no evidence of hot gas leakage through any of the seals. The nozzle insert performed

its function in a satisfactory manner. The barrier-booster (B-B) assembly experienced no anomalies in the motor firing and thus demonstrated its reuse capability.

Section 7.8 contains a detailed description of the igniter test results.

3.1.9 Joint Protection System (JPS)/Systems Tunnel Performance

JPS

A moisture seal integrity test was performed on the forward field joint and forward factory joint after the static test. The field joint test revealed water in the moisture seal, but no moisture was found within the factory joint moisture seal. The source of the moisture intrusion in the field joint was identified at the point where the moisture seal passes over the pin retainer band take-up mechanism. This mechanism is approximately 0.75 in. high; it lifted the sealing edge of the moisture seal off the case.

Systems Tunnel

Observations indicate no evidence of debonding of the systems tunnel and that structural integrity was maintained during the test.

Section 7.9 contains a detailed description of the JPS/systems tunnel test results.

3.1.10 Leak Check Performance

All leak rates were within allowable limits. Post-test disassembly inspection revealed no damage to the seals, insulation, adhesives, or the hardware attributable to the leak test procedures.

Section 7.10 contains a description of the leak check procedure test results.

3.1.11 ETA Ring Performance

The ETA ring was intact and on the case after the test. No anomalous conditions of the ETA ring have been documented.

Section 7.11 contains information about the ETA ring test results.

3.1.12 Ground Test Support Equipment

Igniter/Aft Skirt Conditioning

Conditioning requirements were met; however, many problems encountered stem directly from ambient conditions at the test bay on the static test date. Subfreezing temperatures, along with high winds, required maximum heat output of the aft skirt conditioning cart. The cart was located approximately 80 ft forward of the skirt to preclude damage during the static test. The distance also hampered the effectiveness of the system, and the hydraulic oil temperatures were not at the expected elevated temperature at T-0.

Arming operations were slightly different due to the addition of the igniter conditioning shroud, but it was a workable situation.

Water Deluge System

Severe cold temperature also affected the water deluge system and required the use of thermal blankets and a portable conditioning unit in order to keep water lines from freezing. The forward deluge was cycled off at approximately T+20 min and then cycled on and off intermittently to prevent system freeze-up. Final shutdown of the water deluge system occurred at approximately 1700 hr. Water system pressure was more than adequate for operation of the deluge system and all components operated satisfactorily.

CO_2 Quench

The CO_2 quench system functioned properly.

Section 7.12 contains information about the ground test support equipment test results.

3.2 RECOMMENDATIONS

Nozzle Boot Loads

Assumptions used in the thermostructural analyses of the involute outer boot ring have to be reevaluated. A more appropriate model with the boot loads will have to be studied. The boot loads test will provide valuable data that can be used in the analytical model to simulate loads due to TVC actuation.

Field Joint Protection System (FJPS)

The temperature data available to the test conductor at T-22 did not accurately provide the temperature of the field joints. As a result, it is recommended that the temperature of the sensor of the FJPS be made available on a real-time basis to the test conductor at Building T-22 for test commit criteria.

Weatherseal

The new, low-profile take-up mechanism designed for the pin retainer band will need to be installed on one of the qualification motors and the moisture seal test repeated.

Aft Skirt Conditioning

Test Engineering recommends that future conditioning requirements be determined well in advance and adhered to by all parties involved. It may also be necessary to replace the aft skirt conditioning unit with a steam type in order to reach specified temperatures without requiring maximum output of the unit.

Water Deluge System

To ensure against any slag-related damage to the case under a worst-case scenario, two additional water nozzles should be added to the deluge system at the instrumentation box.

4

CEI SPECIFICATIONS

This section shows DM-9 static test compliance with Specification CPW1-3600a, dated 3 Aug 1987. The following comments are drawn from the test with a one-to-one correlation to the test objectives listed in Section 2.

Qualification Objectives

	Test Objective/ CEI Specification Paragraph	Planned Verification Effort	Results
A	Certify that the sealing of the case field joints is not affected by static test structural deflection. (3.2.1.2.1.a)	Evaluate all (field joint) seals during a full-duration static test at ambient temperature for evidence of blowby or erosion.	No evidence of blowby, erosion, or heat effect to field joint primary/secondary O-ring seals (no evidence of hot gas past J-seal). Girth gage measurements indicate maximum field joint O-ring gap opening less than 0.006 inch.
B	Certify the case field joint seal performance at ambient temperature. (3.2.1.2.1.b)	Evaluate all (field joint) seals during a full-duration static test at ambient temperature for evidence of blowby or erosion.	Data indicate minimum field joint O-ring seal temperature at T-0 was 78.4°F. No evidence of blowby, erosion, or heat effect to field joint primary/secondary O-ring seals (no evidence of hot gas past J-seal).
C	Certify that the case field joint seal verification does not degrade the performance or integrity of the joint system. (3.2.1.2.1.c)	Post-test inspection to determine seal integrity.	Field joints show no visual damage to J-seal, adhesive, or primary/secondary O-ring seals attributable to the leak test procedure. Primary-to-secondary cavity was pressure tested to 1,000 psig.

D	Certify that the case structural and sealing integrity is not degraded. (3.2.1.8.1.1.a)	Evaluate the ability of the field and nozzle-to-case joint and acreage insulation to thermally protect case and seal components.	No evidence of hot gas past field joint J-seal, nozzle-to-case joint wiper O-ring, or to factory joint or case hardware (no evidence of hot gas to primary/secondary O-rings).
E	Certify that leak test method is compatible with the joint insulation. (3.2.1.8.1.1.b)	Demonstrate compatibility of the seal leak test with joint insulation design.	No leak test-related anomalous conditions found at field joint J-seal, nozzle-to-case joint, or igniter-to-case joint insulation.
F	Certify that the insulation ensures that system performance and structural integrity are maintained during the assembly process and operation. (3.2.1.8.1.1.c)		No assembly-related anomalous conditions found at field joint J-seal, nozzle-to-case joint, or igniter-to-case joint insulation.
G	Certify that the insulation protects the primary and secondary seals from visible degradation from motor combustion gas. (3.2.1.8.1.1.d)	Conduct a post-test inspection for evidence of seal degradation. Evaluate the ability of field and nozzle-to-case joint insulation to protect seals from motor combustion gases.	No evidence of hot gas past field joint J-seal, nozzle-to-case joint wiper O-ring, or to factory joint or case hardware (no evidence of hot gas to primary/secondary O-rings.
H	Certify the ability of the insulation to protect case joints from thermal degradation during a full-duration (ambient temperature) burn. (3.2.1.8.1.1.e)	Evaluate insulation performance throughout motor operation compared to worst manufacturing tolerances.	No evidence of hot gas past field joint J-seal, nozzle-to-case joint wiper O-ring, or to factory joint or case hardware (no evidence of hot gas to primary/secondary O-rings; no intentional flaws).

I	Certify that the insulation does not shed fibrous or particulate matter during assembly which could prevent sealing. (3.2.1.8.1.1.f)	Inspect insulation surfaces during dry fit for fibers or particulate matter.	No fibrous or particulate matter attributable to the insulation materials were found just prior to assembly or disassembly procedures.
J	Certify that the field joint insulation withstands slag accumulation during motor operation. (3.2.1.8.1.1.g)	Post-test inspection of joint insulation for slag effects.	No evidence of measurable slag damage to field joint insulation occurring during motor burn.
K	Certify that the field joint insulation does not induce changes to the propellant grain design which could invalidate the existing ballistic performance database. (3.2.1.8.1.1.i)	Evaluate the ballistic performance for compliance with existing database.	Changes in insulation design do not measurable alter motor operations.
L	Certify that the nozzle-to-case joint insulation withstands slag accumulation during motor operation. (3.2.1.8.1.1.g)	Post-test inspection of insulation for slag effects.	No evidence of measurable slag damage to nozzle-to-case joint insulation occurring during motor burn.
M	Certify that the nozzle-to-case joint insulation does not induce changes to the propellant grain design which could invalidate the existing ballistic performance database. (3.2.1.8.1.1.i)	Evaluate the ballistic performance for compliance with existing database.	Changes in insulation design do not measurable alter motor operations.

N	Certify that the sealing of the nozzle-to-case joint is not affected by static test structural deflections. (3.2.1.2.1.a)	Evaluate all (nozzle-to-case joint) seals during a full-duration static test at ambient temperature for evidence of blowby or erosion.	No evidence of blowby, erosion, or heat effect to nozzle-to-case joint primary/secondary O-ring seals (no evidence of hot gas past wiper O-ring). Girth gage measurements indicate maximum nozzle-to-case joint O-ring gap opening less than 0.007 inch.
O	Certify that the nozzle-to-case joint seal performance with the joint conditioned between 75° and 120°F. (3.2.1.2.1.b)	Evaluate all (nozzle-to-case joint) seals during a full-duration static test at ambient temperature for evidence of blowby or erosion.	Minimum measured temperature at nozzle-to-case joint thermocouples at T-0 was 80°F. No evidence of blowby, erosion, or heat effect to nozzle-to-case joint primary/secondary O-ring seals (no evidence of hot gas wiper O-ring).
P	Certify that the nozzle-to-case joint seal verification does not degrade the performance or integrity of the joint system. (3.2.1.2.1.c)	Post-test inspection to determine seal integrity.	No leak test-related anomalous conditions found at nozzle-to-case joint insulation, wiper O-ring joint insulation, wiper O-ring, adhesive, or primary/secondary O-ring seals. Primary-to-secondary cavity was pressure tested to 920 psig.
Q	Certify that the nozzle-to-case joint O-ring is maintained within the temperature range specified in ICD 2-0A002 (75° ±25°F). A PIRN (BI-0718) will change this to 75° to 120°F when approved. (3.2.1.2.1.f)	Conduct static test.	Temperature at nozzle-to-case joint thermocouples at T-0 ranged from 80° to 110°F.

R	Certify backfill of internal nozzle joints (flight configuration).		RTV backfill extended below joint char line in two of three backfilled nozzle joints. Hot gas reached the primary O-ring in all three joints. No evidence of blowby, erosion, or heat effect to joint primary/secondary O-ring seals.
S	Certify aluminum systems tunnel bondline integrity after exposure to motor pressurization loads. (3.2.1.10.4)		Tunnel bondline remained intact during static firing. No loose, missing, damaged, or abnormal conditions observed.
T	Certify the ability of the field joint protection system to prevent the entry of rain. (3.2.1.3.h)		Moisture found in field joint weather seal during post-test testing procedures.
U	Certify the ability of the field joint heater assembly to maintain the joint temperature between 75° and 120°F. (3.2.1.11.a)	Certify that the field joint temperature is maintained by the field joint heater assembly.	Data indicate minimum field joint O-ring seal temperature was T-0 was 78.4°F.
V	Certify the ability of the field joint protection system to prevent the accumulation of water in the joint. (3.2.1.11.b)		Moisture found in field joint weather seal during post-test testing procedures.
W	Certify the operation of the field joint heater with a power supply meeting the requirements of ICD 3-44005. (3.2.1.11.1.2)		Not applicable to DM-9 static test.

X	Determine pressure distribution within the motor during ignition and main burn. (3.2.1.3.k)	Certify the internal pressure in the forward segment and the pressure drop to the aft segment.	Pressure distribution within the motor during ignition and main burn was calculated and met specification requirements.
Y	Certify the motor performance at ambient temperature. (3.2.1)	Full-scale static test to be fired at ambient conditions. PMBT to be calculated and performance extrapolated to environmental extremes (modified forward segment grain).	Static test conducted at 25°F environmental temperature and 64°F PMBT. Ignition characteristics tabulated at 40°, 60°, and 90°F. Performance limits and tolerances were met.
Z	Certify the ignition interval is between 202 and 262 ms. (3.2.1.1.1.1)	Ignition characteristics to be measured at ambient firing conditions, reported at 60°F.	Ignition characteristics measured and tabulated at 60°F. Performance limits and tolerances were met.
AA	Certify that the rate of pressure buildup is between 70.9 and 115.9 psi for any 10-ms interval. (3.2.1.1.1.2)	Pressure rise rate will be measured during full static firing.	Maximum pressure rise rate was 81.0 psi/10 ms.
AB	Certify that the (nominal) thrust-time curve fails within the upper and lower bounds identified in CPW1-3600A, Table I. (3.2.1.1.2.1)	Evaluation of nominal thrust-time results with burn rate corrected to 60°F propellant mean bulk temperature (PMBT).	Thrust-time curve fell within thrust-time curve.
AC	Certify that the performance tolerances and limits do not exceed those allowed in CPW1-3600A, Table II. (3.2.1.1.2.2)	Evaluation of motor performance limits for individual motor and matched pairs.	The tolerances and performances did not exceed the limits specified in CPW1-3600A, Table II.

AD	Certify that the impulse gates specified in CPW1-3600A are achieved when corrected to 60°F. (3.2.1.1.2.4)	Evaluation of impulse attained during static firing.	Specified impulse gates corrected to 60°F were achieved.
AE	Certify that the nozzle assembly and exit cone design are compatible with the performance requirement specified in CPW1-3600A. (3.2.1.4)	Static test to evaluate nozzle compatibility with system performance requirements.	The nozzle is compatible with systems performance requirements.
AF	Certify that the load RSRM center of gravity (cg) falls between 1,179 and 1,165 in. on the longitudinal (X) axis. (3.2.2.2.3)	Loaded segments will be weighted and mass properties measured to establish motor cg.	The cg was determined.
AG	Certify that the case is capable of containing the static test internal pressure. (3.2.1.3.a)	These tests will provide data which will corroborate the case is capable of containing maximum expected operating pressure (MEOP).	No evidence that the case allowed leakage of internal pressures or local yielding.
AH	Certify that the case segment mating joints have a pin retention device. (3.2.1.3.g)	Postfire inspection to certify the function of the pin band retainer.	Pin retainer Drawings 1U82699 and 1U52570 were incorporated on DM-9. No anomalies were noted.
AI	Certify that the ignitions system precludes the leakage of hot gas during and subsequent to motor ignition. (3.2.1.5.a)	Inspection of hot gas leakage. Test for hot gas leakage.	No evidence of hot gas leakage from the igniter during motor operation.

AJ	Verify the case segment mating joints incorporate provisions to ensure proper segment orientation and alignment to facilitate joining, stacking, disassembly, and refurbishment. (3.2.1.3.f)	Demonstrate effectiveness of alignment tooling during mating.	Alignment tooling was successfully used during mating.
AK	Verify that the RSRM segments are capable of horizontal assembly and disassembly. (3.2.5.1)	Assembly and disassembly will be demonstrated horizontally.	DM-9 segments were successfully assembled in the horizontal position.
AL	Certify that the seal verification does not degrade the performance or integrity of the factory joint system. (3.2.1.2.2.c)	Noncompliance. No verification approach exists.	
AM	Certify that the nozzle liner design prevents formation of pockets, wedge outs, and anomalies as defined. (3.2.1.4.13)	Post-test inspection to evaluate the nozzle liner design. Static tests to evaluate nozzle liner design.	No wedge outs of the nozzle liner that violated performance MS occurred during motor operation with exception of the fracturing and separation of the OBR.
AN	Certify that nozzle assembly primary ablatives meet the design safety factors. (3.3.6.1.2.7)	Certify the nozzle design safety factors.	Design safety factors for nozzle primary ablatives were met on all intact parts with the exception of three stations on the forward exit cone and one station on the aft exit cone.

AO	Certify that the nozzle performance MS are zero or greater. (3.3.6.1.2.8)		The nozzle performance MS were positive for all parts except at three stations on the forward exit cone and one station on the aft exit cone.
AP	Certify that the nozzle meets vectoring requirements. (3.2.1.4.1)		Vectoring requirements were met.
AQ	Certify that the nozzle radial offset does not exceed the limits. (3.2.1.4.2)	Evaluation of geometric thrust vector radial and angular displacement during nozzle alignment.	The maximum radial displacement was 0.0264 in. and the maximum angular displacement was 0.019 deg. Both were within specified tolerances.
AR	Certify that the nozzle meets dynamic thrust vector requirements. (3.2.1.4.3-a,-b)	Evaluation of dynamic thrust vector, dynamic thrust vector misalignment, and dynamic thrust vector radial offset during static test.	Dynamic thrust vector alignment requirements were met.
AS	Certify the nozzle meets null offset angle requirements. (3.2.1.4.4-a,-b,-c)	Certify the null offset angle at 0, 615, and 915 psia nozzle stagnation pressure.	The nozzle null offset angle was +0.8 deg at 0 psi nozzle stagnation pressure, 0 deg at 615 psi nozzle stagnation pressure, and -0.055 deg at 915 psi nozzle stagnation pressure which is well within the requirement.
AT	Certify the nozzle plug can be expelled without damage to other components or adversely affecting RSRM performance. (3.2.1.4.7.c)	Static test to demonstrate that the plug can be expelled without damaging any part of the Shuttle System or adversely affecting the SRM performance.	Nozzle plug performed nominally. Plug burst into multiple pieces at motor ignition.

AU	Certify by demonstration that the TVC actuator attach points meet the requirements of ICD 3-44003. (3.2.1.4.8)	Demonstration of actuator attach points compatibility with TVC actuators.	Actuator attach points were compatible with TVC actuators.
AV	Certify the flex bearing is capable of vectoring a total of 85 cumulative degrees during each flight duty cycle. (3.2.1.4.11.1)	STW7-2740 testing of flex bearing total deflection capability.	Not applicable to DM-9 static test.
AW	Certify that the factory joint insulation can accommodate static test motor structural deflections and erosion. (3.2.1.2.2.a)	Certify that factory joint insulation provides a pressure seal with the specified safety factors after a full-scale (ambient temperature) motor burn.	No evidence of blowby, erosion, or heat effect to factory joint primary/secondary O-ring seals. Disassembly and inspection of factory joints showed no evidence of hot gas past internal insulation. All safety factors were above the 2.0 requirement.
AX	Certify that the factory joint insulation is capable of sealing after normal manufacturing processes and during static test at ambient conditions. (3.2.1.2.2.b)	Conduct static test to evaluate seal operation.	No evidence of blowby, erosion, or heat effect to factory joint primary/secondary seals. Disassembly and inspection of factory joints showed no evidence of hot gas past internal insulation.

AY	Certify that the seal verification does not degrade the performance or integrity of the factory joint system. (3.2.1.2.2.c)	Noncompliance. No verification approach exists.	Factory joints show no visual damage to insulation or primary/secondary O-ring seals attributable to leak test procedures. Disassembly and inspection of factory joints showed no evidence of hot gas past internal insulation and no damage to the insulation layup.
AZ	Certify that at least one virgin ply of insulation remains over the factory joint after motor is fired. (3.2.1.2.2.d)	Postfire factory joint insulation inspection. Conduct static test.	More than one virgin ply of insulation remained on all factory joints after disassembly and inspection.
BA	Certify that the flex bearing will remain sealed throughout TVC duty cycle during static test. (3.2.1.2.3.a)	Flex bearing sealing will be evaluated.	The flex bearing remained sealed throughout the static test.
BB	Certify proper flex bearing sealing capability at ambient conditions after processing in a normal manufacturing environment. (3.2.1.2.3.b)	Evaluation of flex bearing sealing characteristics.	The flex bearing was capable of sealing at ambient conditions.
BC	Certify that the flex bearing seal verification does not degrade the performance or integrity of the system. (3.2.1.2.3.c)	Certify that the flex bearing seal verification does not degrade the performance or integrity of the sealing system.	Sealing verification did not degrade the performance or integrity of the system. The flex bearing performance was nominal.

BD	Certify that there are no gas leaks between the flex bearing internal components. (3.2.1.2.3.d)	Post-test visual inspection to determine that a positive gas seal was maintained between flex bearing internal components.	There were no gas paths or leaks observed between the flex bearing internal components.
BE	Certify that the nozzle internal seals and the aft exit cone joint can accommodate static test motor-induced structural deflections. (3.2.1.2.5.a)	Qualification tests to verify that sealing accommodates structural deflections.	No evidence of blowby, erosion or heat effect to field joint primary/secondary O-ring seals (no evidence of hot gas past J-seal).
BF	Certify that seal verification does not degrade the performance or integrity of the nozzle internal joints or the aft exit cone joint. (3.2.1.2.5.c)	Post-test visual inspection to determine effects of leak checks on nozzle internal seals.	Nozzle internal joints show no visual damage to J-seal, adhesive, or primary/secondary O-ring seals attributable to the leak test procedure.
BG	Certify that bore seals are verifiable in the proper direction. (3.2.1.2.5.e)	Leak check to qualify bore seals are verifiable in the proper direction.	Bore seals were verified during pretest leak tests.
BH	Certify electrical bonding per MIL-B-5087B. (3.2.1.6.f)	Electrical bonding will be evaluated.	Electrical bonding was not tested on DM-9.
		Development Objectives	
BI	Evaluate structural integrity of ETA ring under pressurization loads (MSFC test objective).		No anomalous conditions of the ETA rings have been documented.
BJ	Acquire engineering data for validation of joint models.		Comparisons show that models and actual data fall within expected tolerances.

BK	Obtain data to verify finite element models.	Comparisons show that models and actual data fall within expected tolerances.
BL	Determine the effects of dither/TVC performance at elevated hydraulic oil temperatures (MSFC test objective).	There was no evidence of dither apparent in the test data.
BM	Evaluate the performance of the nozzle-to-case and field joint adhesive.	Post-test inspection revealed continuous adhesion circumferentially on field joints. There was a void and a gas path through the nozzle-to-case adhesive to the wiper O-ring.

PAGE 50 INTENTIONALLY BLANK

5

INSTRUMENTATION

5.1 INTRODUCTION

The DM-9 test article included instrumentation similar to that used on previous static motors and subscale test articles. Instrumentation was installed on the test article per Drawing 7U75851. Figures 5.1-1 through 5.1-6 illustrate instrument locations. Appendix B contains an instrumentation list and Appendix C contains data plots.

5.2 OBJECTIVES

DM-9 was instrumented to collect the engineering and motor performance data necessary to evaluate the following:

- Compliance with the test objectives (Section 2)
- Correlation with analytical models and predictions

5.3 CONCLUSIONS/RECOMMENDATIONS

All instrumentation objectives were met. Valuable data were collected on the static test article performance and, in general, the instrumentation performed very well.

A post-test inspection revealed that the P003 pressure transducer was loose (TWR-17937). No evidence of leakage was apparent. Had a leak at the pressure transducer occurred during the firing, it might have resulted in a catastrophic failure. The investigation is unable to determine the time at which the pressure transducer was loosened. To ensure that this event does not happen on future tests, all transducers will have a positive means of retention.

5.4 INSTRUMENTATION DISCUSSION

DM-9 instrumentation included 46 FM channels and 300 digital channels to be recorded during motor firing. In addition, there were 32 channels to determine

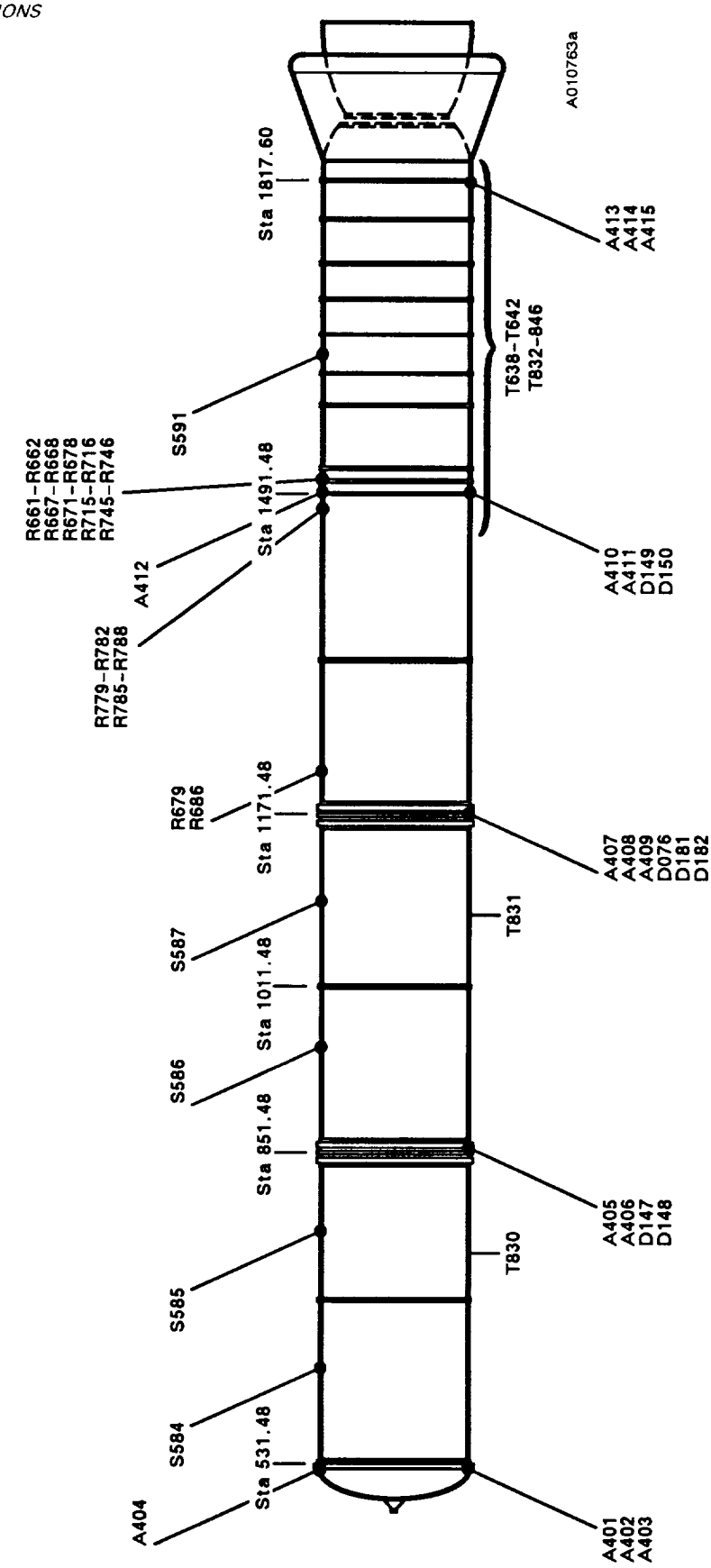

Figure 5.1–1. DM–9 Case Growth Instrumentation

A008559a

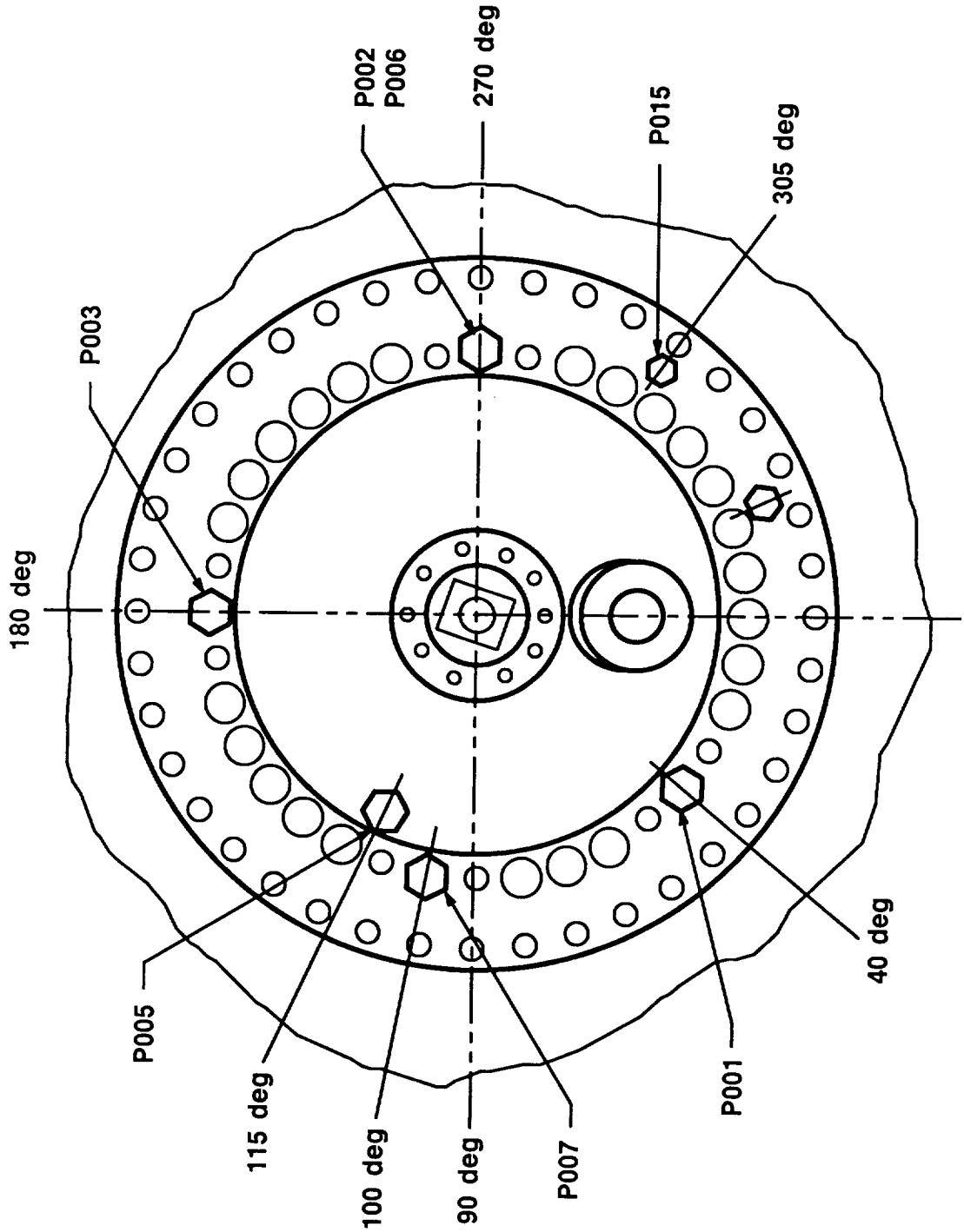

Figure 5.1-2. DM-9 Headend Pressure Transducer Locations

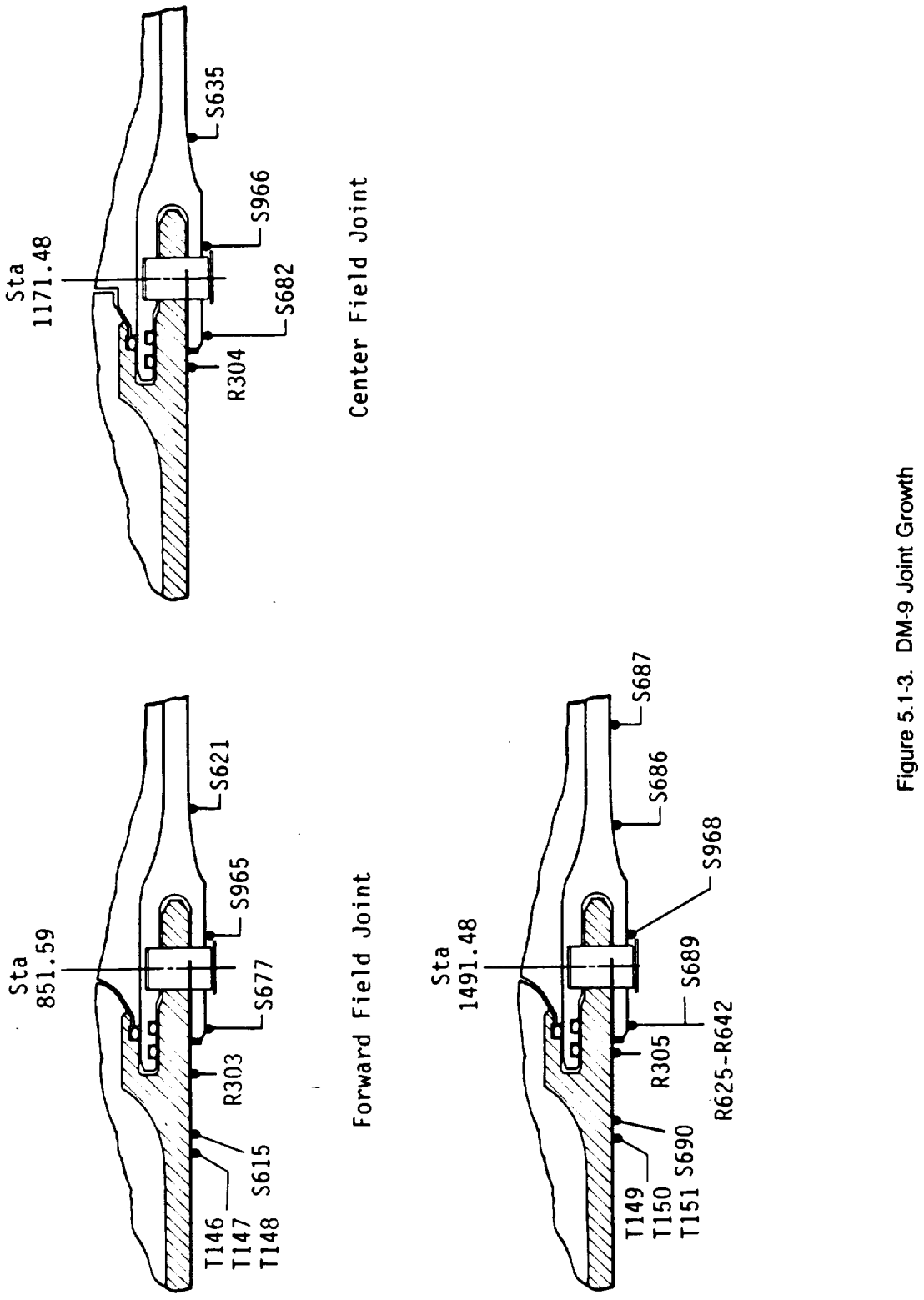

Figure 5.1-3. DM-9 Joint Growth

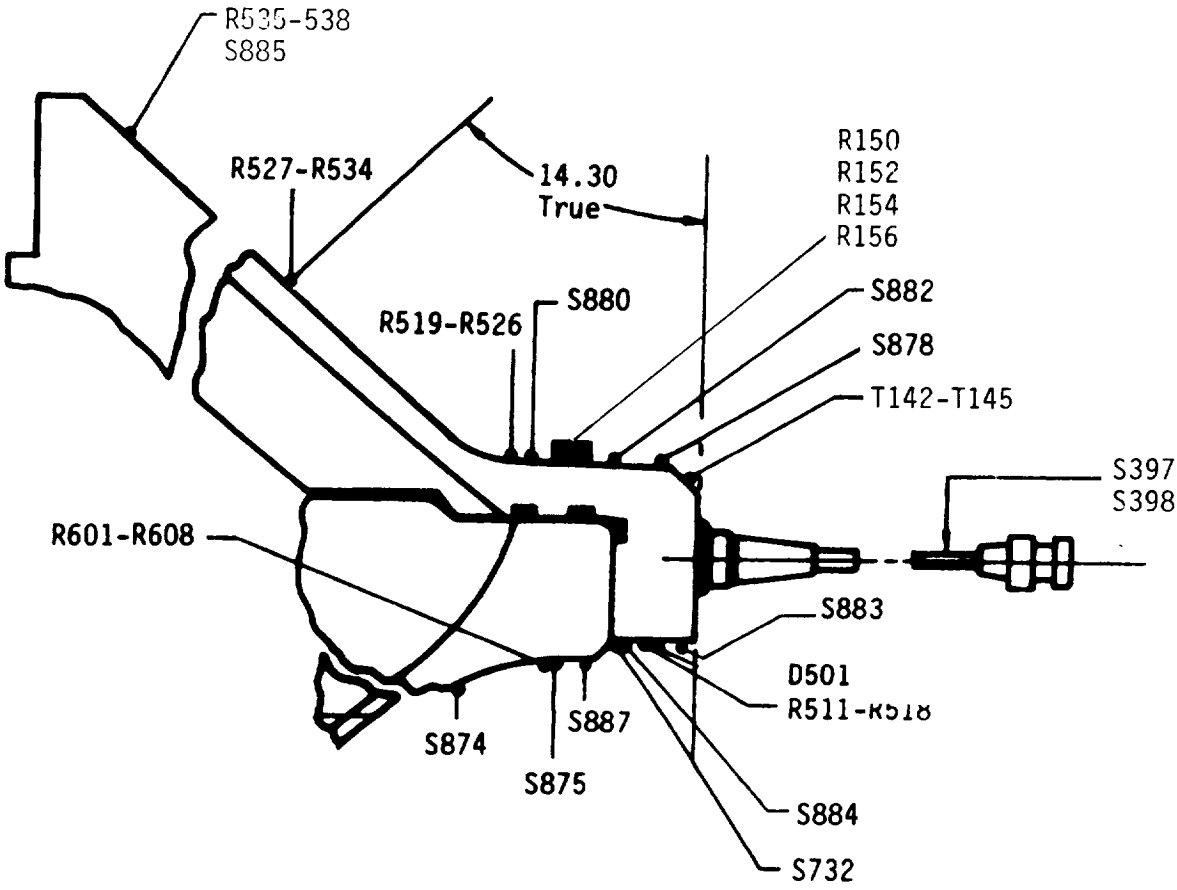

Figure 5.1-4. DM-9 Nozzle-to-Case Joint Instrumentation

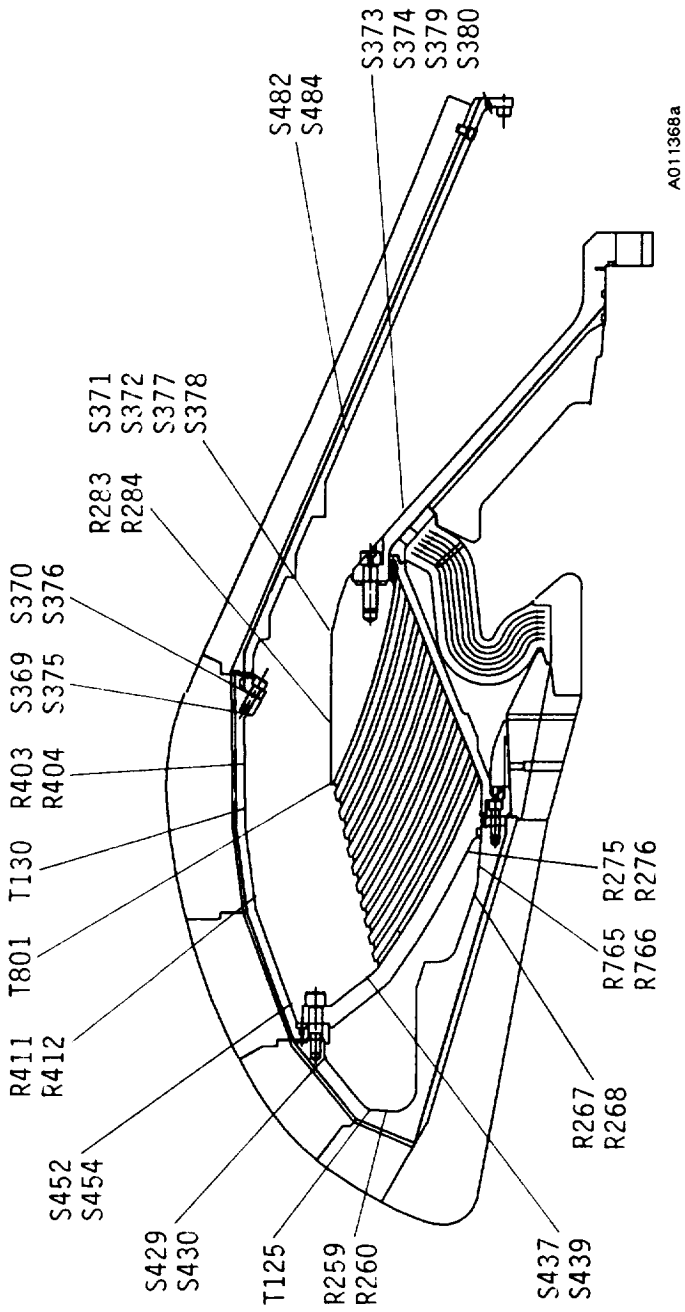

Figure 5.1-5. DM-9 Nozzle Instrumentation

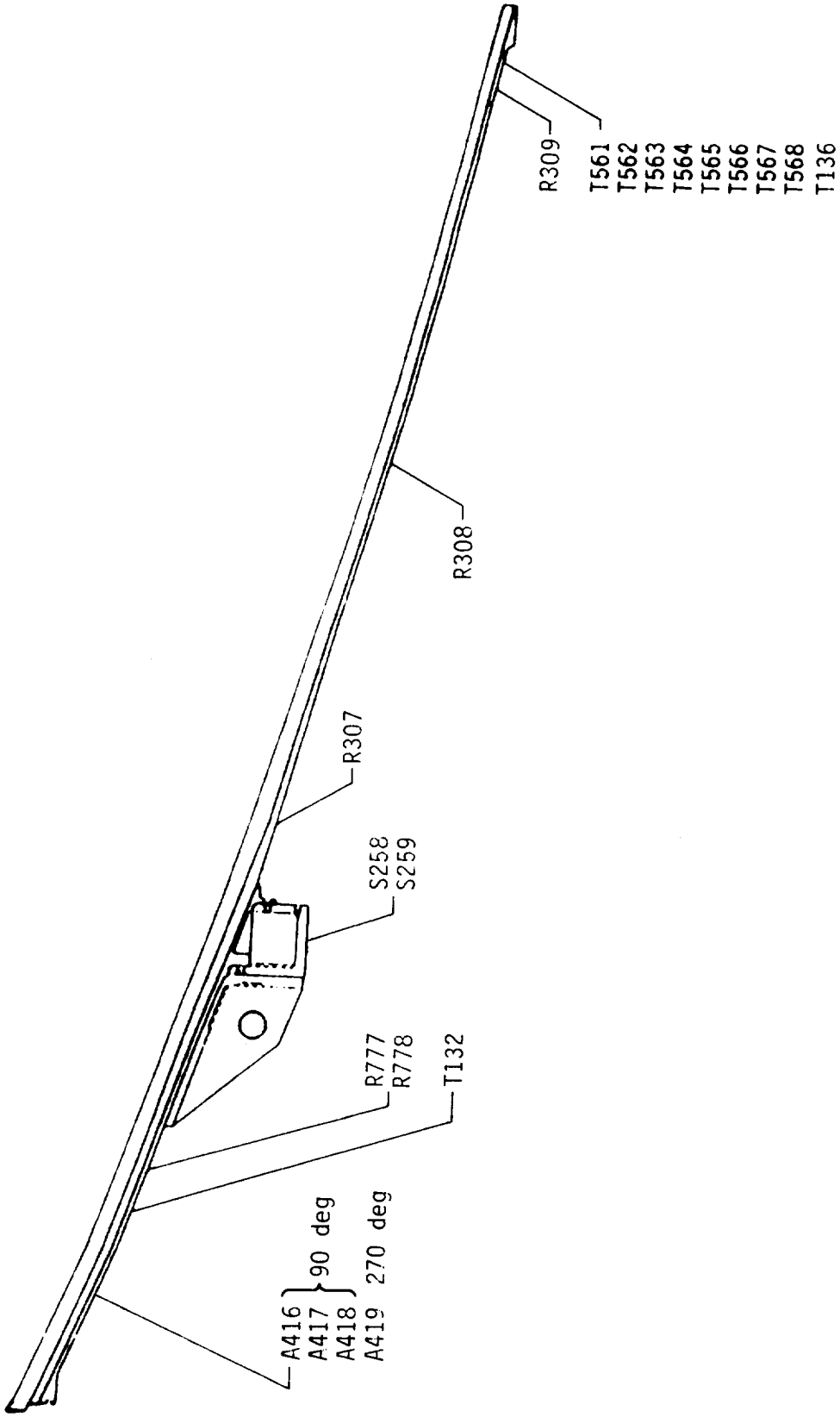

Figure 5.1-6. DM-9 Aft Exit Cone Instrumentation

propellant temperature and 1 channel for test bay temperature. Total motor instrumentation encompassed 379 channels, including pressure, force, acceleration, displacement, strain, and temperature gages.

Table 5.4-1 summarizes the instrument types used on DM-9. Barometric pressure and ambient temperature were measured and recorded manually and are listed in Table 5.4-2 for T-2 to T-0 hr. Instruments that failed to function properly are listed in Table 5.4-3 with comments.

Table 5.4-1. Instrumentation Summary

Type of Instrumentation	Area of Investigation	Number of Recording Channels
Accelerometer (A)	Nozzle vibration Case vibration Actuator flutter	31
Extensometers (D)	Motor sag measurement Nozzle position	19
Proximity (D)	Nozzle-to-case joint slip	1
Pressure Transducer (P)	Chamber pressure Internal dynamic environment Igniter chamber TVC system	22
Strain Gage (S&R)	Case line loads Radial bolt hole ETA ring effects Nozzle component stress Aft dome/fixed housing stress	118
Girth (S)	Pressure drop in bore Joint radial growth Aft exit cone growth Aft dome/fixed housing movement	29
Strainserts (S)	Nozzle-to-case joint bolt loads	6
Temperature (T)	External joint temperature TVC system Slag Exit cone temperature	61
	Total	287*

*Remaining measurements consist of command, voltage, current, and event measurements or prefire measurements

Table 5.4-2. Environmental Conditions

	Time (hr)	Condition	Temperature (°F)	Pressure (in. Hg)	Humidity (%)
T-2 hr	1230	100	24	25.06	76
T-1 hr 45 min	1245	100	24	25.06	79
T-1 hr 30 min	1300	100	24	25.04	80
T-1 hr 15 min	1315	100	24	25.04	81
T-1 hr	1330	100	25	25.04	82
T-45 min	1345	100	25	25.04	82
T-30 min	1400	100	25	25.04	81
T-15 min	1415	100	25	25.06	81
T-0	1430	100	25	25.07	82

Table 5.4-3. Instrumentation Discrepancies

Instrument	Sympton	Remark
D076	No data	Cable/discontinuity
T834	Hooked up backwards	Hooked up backwards
P505	Possible wrong range	Ranged at 600, should be 1,500
P506	Possible wrong range	Ranged at 600, should be 1,500
R150	Low data 434, 548, 661	Mode card bad
R152		Delta data only - zeros lost
R154		Delta data only - zeros lost
R156		Delta data only - zeros lost
R260	Twice the amplitude	Probably reasonable
R603M	Extremely noisy (bad)	Noise level compromised data
R626	Bad data at T+118	Lost probably due to deluge
R685	Dead at ignition	Intermittent cable
R741	Should be 742	Switched with 742
R742	Should be 741	Switched with 741
S373	Open on ignition	Gage bad
S379	Bad after ignition	Gage bad
X025	Bad	Incorrectly patched
A560		Underranged
A561		Underranged
P311	Excessive noise	Not able to repeat noise
A417	Range	Check range
A410	Bad cable, loose connector	Block fell off at ignition
A414	No data	Probably not hooked up

PAGE 62 INTENTIONALLY BLANK

6

PHOTOGRAPHY

Photographic coverage was required to document the test, test configuration, instrumentation, and anomalous conditions which may have occurred. The DM-9 photographs/video tapes are available from the Thiokol Photo Lab.

6.1 STILL PHOTOGRAPHY

Still color photographs of the test configuration were taken before, during, and after the test. Photographs were taken of joints at each 45-deg minimum and at anomalous conditions. A number of photographs were taken of the nozzle.

6.2 MOTION PICTURES

Color motion pictures were taken with 2 video, 12 documentary, and 15 highspeed cameras to cover the DM-9 test article. Camera No. 8 was not functioning prior to the test and was dropped. Camera No. 8A experienced mechanical problems during the test and the film was not archived. Documentary motion pictures are recorded on Roll No. 7454, and high-speed motion pictures on roll No. 7355 (camera number). Cameras are listed in Tables 6.2-1 and 6.2-2 and shown set up in Figures 6.2-1 through 6.2-3.

Table 6.2-1. Photography and Video Coverage, Development Motor

Camera	Station	Location	Type	Coverage
1	1	Gantry	HS	Motor and Plume
2	1	Gantry	Sq	Motor and Plume
3	1	Gantry	Doc	Motor and Plume
4	2	N. Road	Doc	Motor and Plume
5	3	N. Wall	Doc	North Side - Motor Joints
6	3	N. Wall	HS	North Side - Center Fwd Joint
6A	3	N. Wall	HS	North Side - Center Joint
7	4	S. Wall	Doc	South Side - Motor Joints
8	4	S. Wall	HS	South Side - Center Fwd Joint
8A	4	S. Wall	HS	South Side - Center Joint
9	5	N. Field	HS	North Side - Aft Joint
10	5	N. Field	Doc	Aft Joint - Nozzle and Plume
11	6	N. Field	HS	Aft Case
11A	6	N. Field	HS	Nozzle and Thermal Curtain
12	6	N. Field	HS	North Side of Case - All Joints
12A	6	N. Field	HS	Nozzle Plug Expulsion
13	6	N. Field	Doc	Motor and Plume
13A	6	N. Field	Doc	NASA Designation
13B	6	N. Field	SQ	Motor and Plume
14	7	N. Tower	Doc	North Side of Motor
15	8	S. Field	HS	South Side - Aft Joint
15A	8	S. Field	HS	Aft Case, Nozzle, and Plume
15B	9	S. Side	HS	South Side of Case - All Joints
15C	6	N. Field	HS	Nozzle Plug Expulsion
16	8	S. Field	Doc	Aft Case, Nozzle, and Plume
16A	8	S. Field	Vid	Overall of Motor
16B	9	S. Side	Doc	Overall of Motor/NASA Designation
17	10	S. Tower	HS	Case Nozzle and Plume
18	10	S. Tower	Doc	Case Nozzle and Plume
19	11	T-Block	Doc	Overall of Motor and Plume
19A	11	T-Block	Vid	Overall of Motor and Plume
20	11	Bay Floor	HS	Bottom of Case

CODE: HS - High speed at 300 pps
Doc - Documentary at 24 pps
Sq - Sequence at 1 pps
Vid - Video at real-time

Table 6.2-2. Camera Control and Priority Requirements, Development Motor

Camera	Station	Start Time (sec)	Stop Time (sec)	Priority
1	1	T-5	T+150	M
2	1	T-2	T+150	R
3	1	T-15	T+180	R
4	2	T-15	T+180	R
5	3	T-15	T+180	R
6	3	T-5	T+150	M
6A	3	T-5	T+150	M
7	4	T-15	T+180	R
8	4	T-5	T+150	M
8A	4	T-5	T+150	M
9	5	T-5	T+150	M
10*	5	T-15	T+555	M
11	6	T-5	T+150	M
11A	6	T-5	T+150	M
12	6	T-5	T+150	M
12A	6	T-5	T+150	M
13	6	T-25	T+180	R
13A	6	T-25	T+180	R
13B	6	T-2	T+180	R
14	7	T-25	T+180	R
15	8	T-5	T+150	M
15A	8	T-5	T+150	M
15B	9	T-5	T+150	M
15C***	9	T-5	T+150	M
16*	8	T-15	T+600	R
16A*	8	T-15	T+600	R
16B	9	T-15	T+600	R
17	10	T-5	T+150	M
18	10	T-15	T+180	R
19	11	T-15	T+180	R
19A**	11	T-15	T+180	M
20	11	T-5	T+150	M

Station	Location	Station	Location
1	Top of gantry crane	7	North tower
2	Northwest of bay	8	South of nozzle
3	North of bay	9	South and aft of nozzle
4	South wall	10	South tower
5	North of nozzle	11	Top of thrust
6	North of aft of nozzle		

*Covers test from north and south of aft quench system
**Video coverage of static test and aft quench system
***Nozzle plug cameras added since 1 May 1987

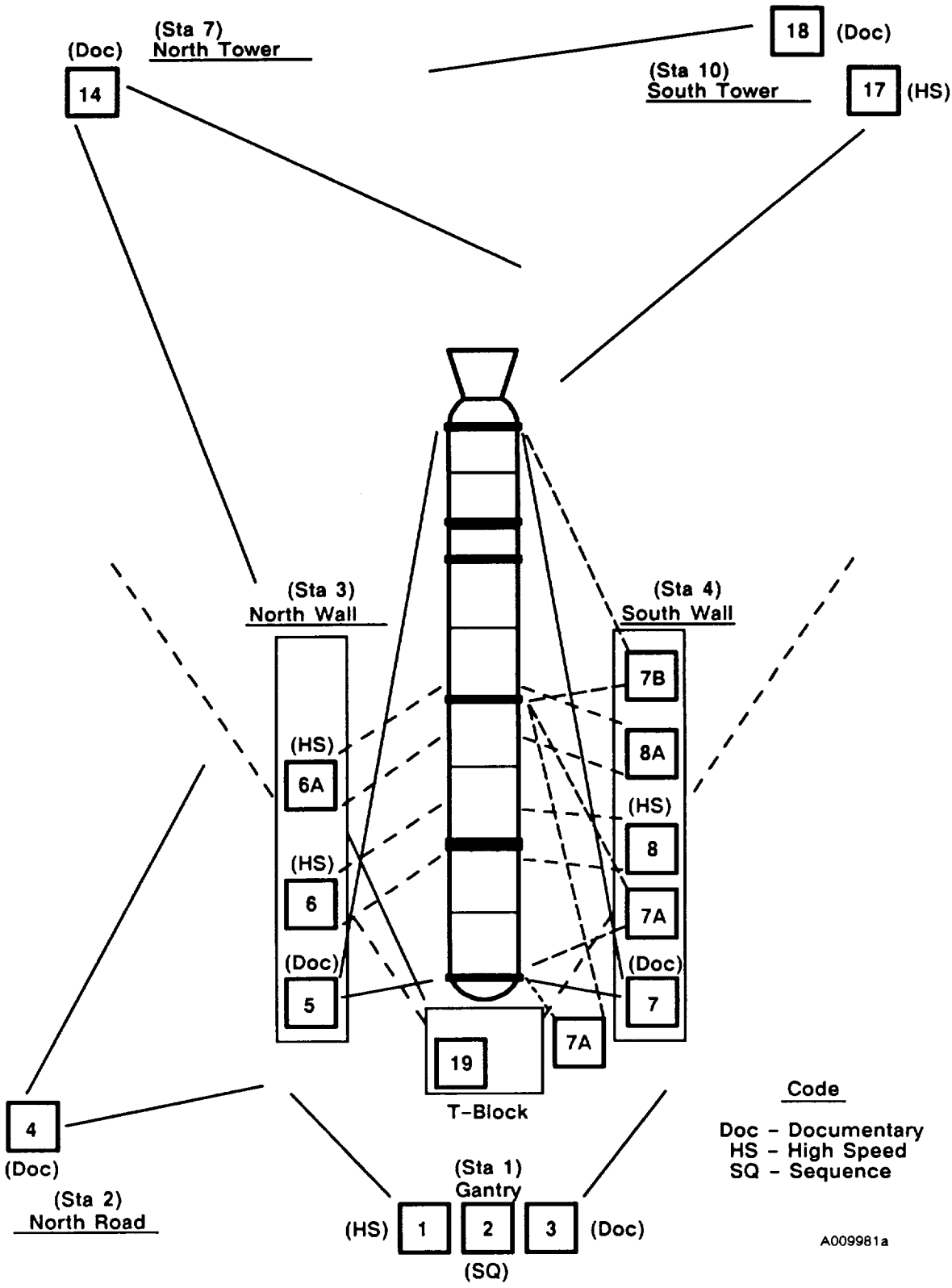

Figure 6.2-1. Photography Coverage, Development Motor

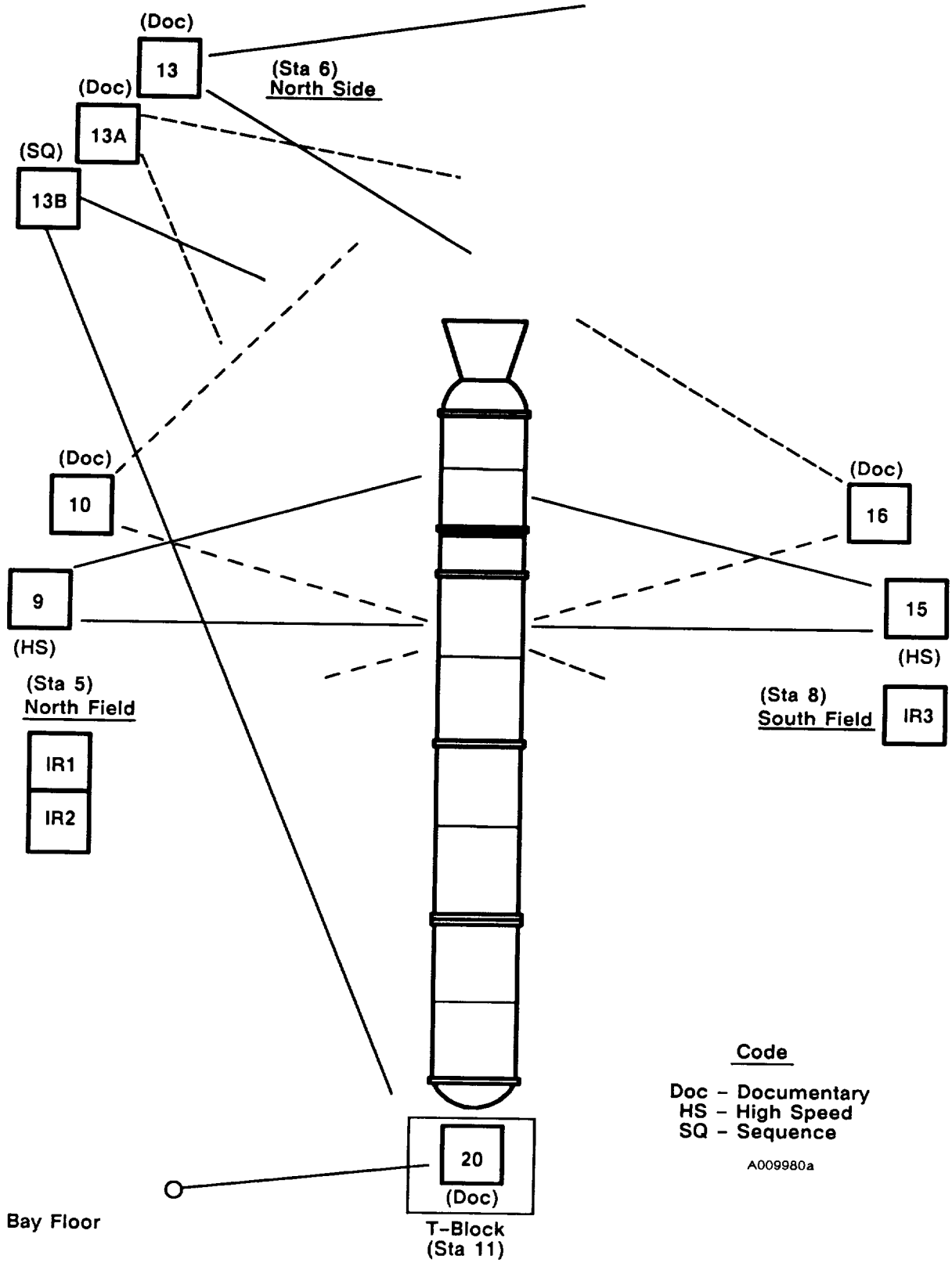

Figure 6.2-2. Photography Coverage, Development Motor

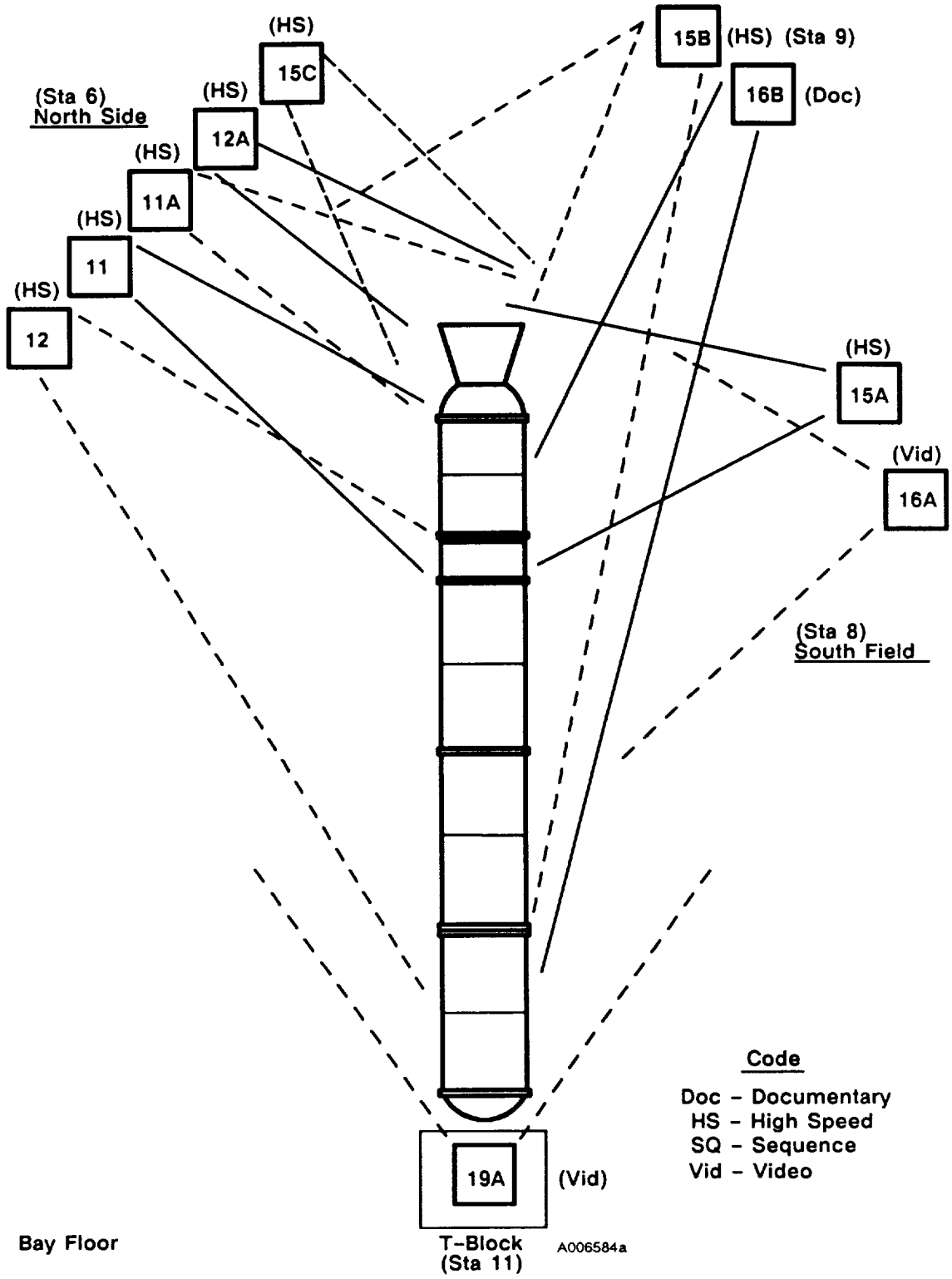

Figure 6.2-3. Photography and Video Coverage, Development Motor

7

TEST RESULTS AND DISCUSSION

7.1 BALLISTICS/MASS PROPERTIES

7.1.1 Introduction

The SRM propellant, TP-H1148, was a composite-type solid propellant, formulated of polybutadiene acrylonitrile/acrylic acid copolymer (PBAN), epoxy curing agent, AP oxidizer, and aluminum powder fuel. A small amount of burning rate catalyst (iron oxide) was added to achieve the desired propellant burn rate.

Grain

The propellant grain design consists of a forward segment with an 11-point star redesigned to a tapered, cylindrically perforated (CP) configuration, two center segments that are double-tapered CP configurations, an aft segment with a triple-tapered CP configuration, and a cutout for the partially submerged nozzle (Figures 7.1-1 and 7.1-2).

7.1.2 Objectives

The test objectives from Section 2 with regard to ballistics were:

- X Determine pressure distribution within the motor during ignition and main burn.
- Y Certify the motor performance at ambient temperature.
- Z Certify that the ignition interval is between 202 and 262 ms.
- AA Certify that the rate of pressure buildup is between 70.9 and 115.9 psi for any 10-ms interval.
- AB Certify that the nominal thrust-time curve falls within specified limits.
- AC Certify that the performance tolerances and limits do not exceed requirements.
- AD Certify that the impulse gates are achieved when corrected to 60°F.

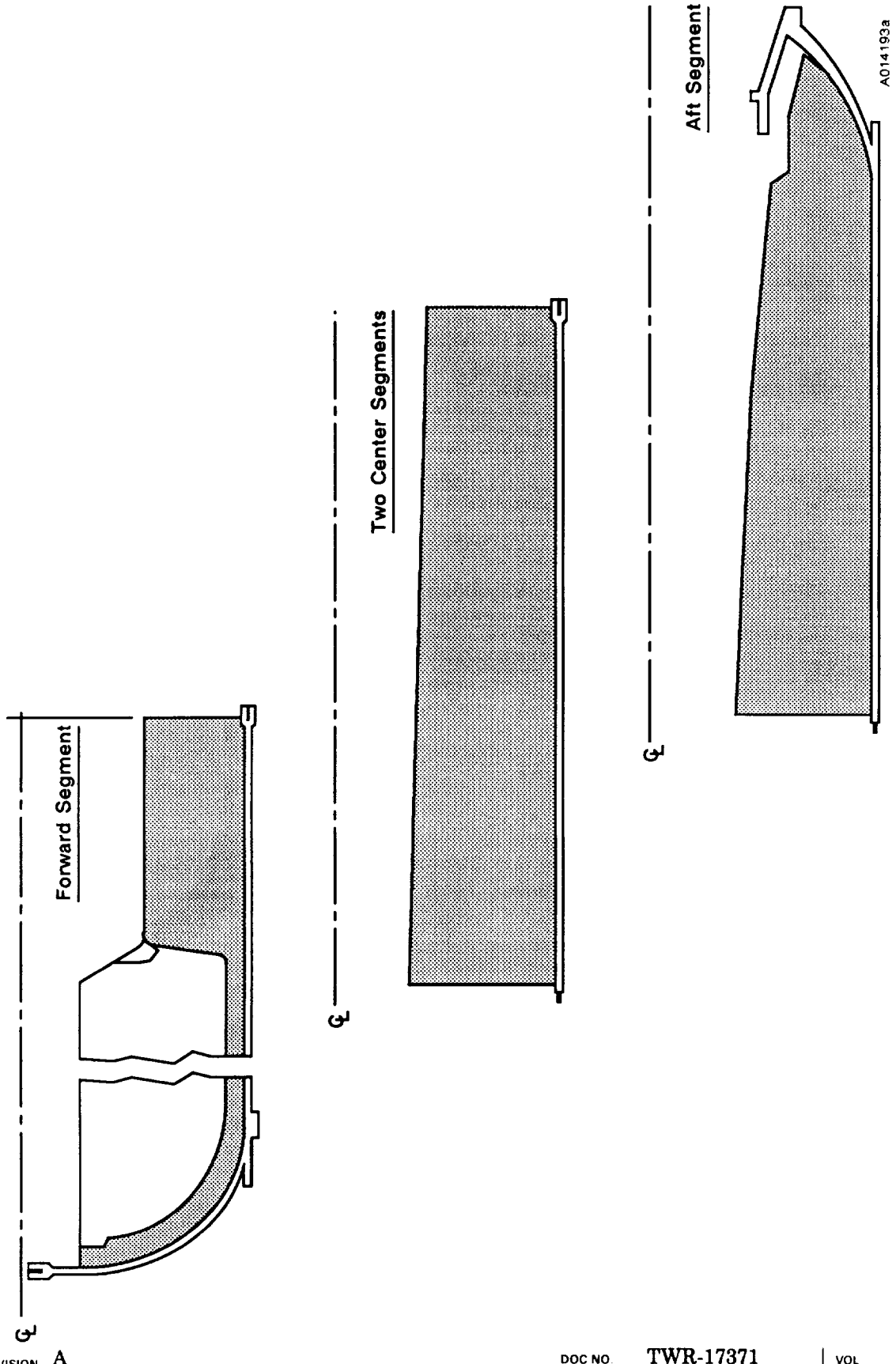

Figure 7.1-1. RSRM Propellant Grain Design Configuration

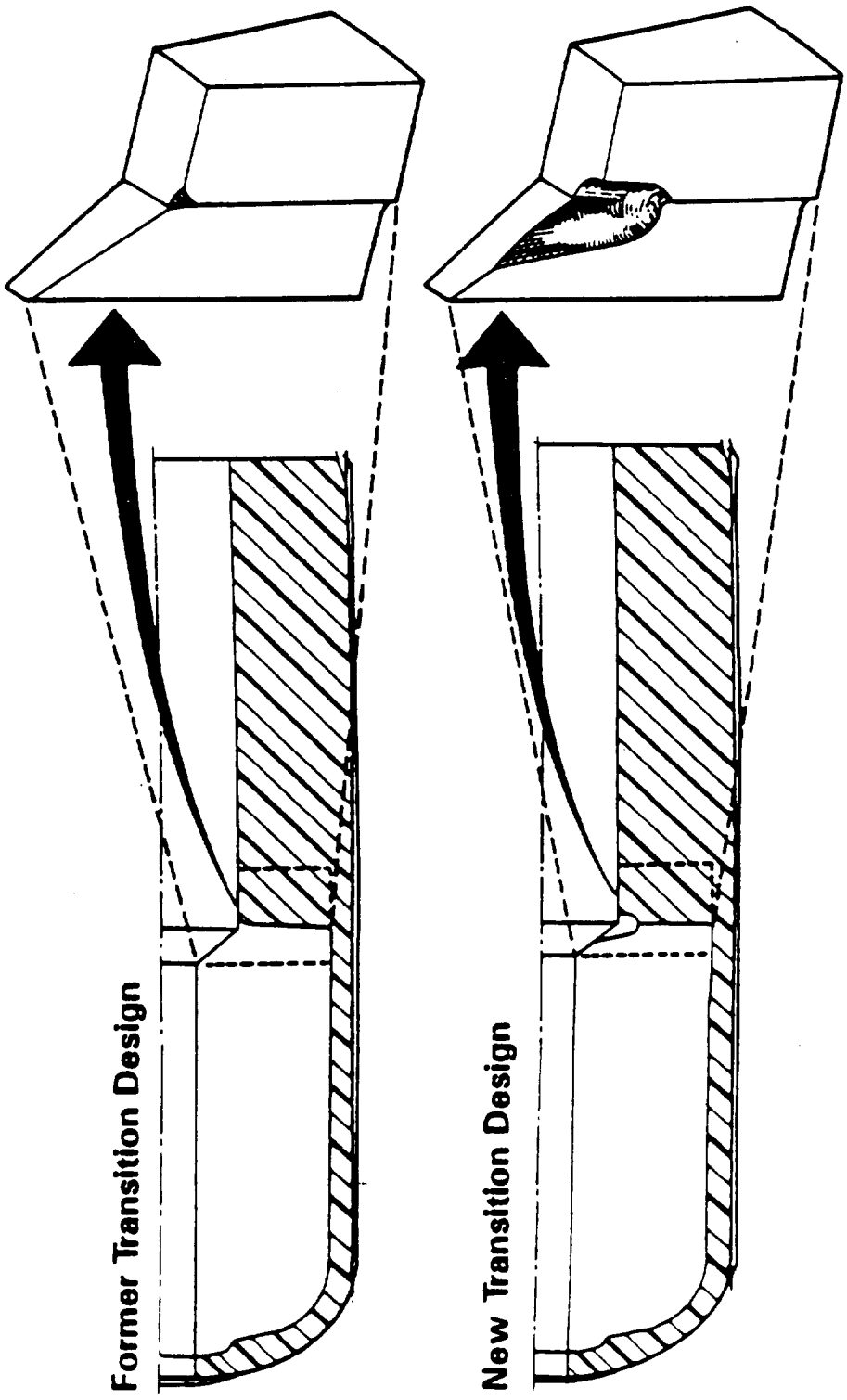

Figure 7.1-2. RSRM Redesigned Transition Region (forward segment)

AF Certify that the loaded RSRM cg falls between 1,179 and 1,165 on the longitudinal (X) axis.

7.1.3 Conclusions/Recommendations

The DM-9 ballistic performance was typical and within expected limits. The new forward segment transition block could not be linked with abnormal gas flow or pressure disturbances. Ignition interval and pressure rise rate limits were met. Impulse gates were met. The DM-9 ballistic performance compared closely with DM-8 performance and HPM historical data. DM-9 slag weight was 2,270 lb. The cause of the excessive slag is considered to be associated with the AP particle size distribution. The modified igniter performed successfully as predicted. The pressure distribution in the motor was well below the design requirements.

The DM-9 motor exhibited chamber pressure oscillations very similar to previously tested Space Shuttle SRMs. The oscillations experienced by DM-9 were higher than the average of the last six static tests, although still within previously observed limits.

7.1.4 Results/Discussion

A comparison of DM-9 performance with predicted values and with the performance of DM-8 revealed few differences. The predicted burn rate for DM-9 was 0.368 ips at 625 psia and 60°F; the target burn rate was 0.368 ips. The delivered burn rate was 0.369 ips. This higher burn rate caused the parameters to be slightly different than predicted, but the variation was within the current HPM population variation. Table 7.1-1 is a summary of the measured ballistic and nozzle performance data.

The predicted PMBT was 67°F. The PMBT for DM-9 at the time of the test was 64°F, which is midway between the allowed temperature range limits of 40° to 90°F. Table 7.1-1 contains the performance parameters adjusted to the minimum, nominal, and maximum allowed temperature ranges. All performance parameters were within the allowed envelopes. Figure 7.1-3 is a comparison of measured and predicted pressure-time histories, and Figure 7.1-4 is a comparison of measured and

Table 7.1-1. Summary of Measured Ballistic and Nozzle Performance Data

Thiokol Space Shuttle Test DM-9, 23 Dec 1987

A. Ambient Conditions	
Date and Time at Fire Pulse (12-23-87)	1450 hr
Ambient Temperature	25°F
Measured Mean Bulk Temperature	64°F
Measured Ambient Pressure	12.25 psia
B. Weight Data	
Total Loaded Propellant Weight	1,106,184 lbf
Total Expended Weight	1,109,820 lbf
Unexpended Propellant Residue (slag)	2,270 lbf
Expended Inert Weight	
1. Forward Segment	732.0 lbf
2. Forward Center Segment	645.0 lbf
3. Aft Center Segment	922.0 lbf
4. Aft Segment (including nozzle less aft exit cone)	3,607.0 lbf
5. Total Expended Inerts	5,906.0 lbf
Total Expended Propellant Weight	1,103,914 lbf
C. Nozzle Data	
Initial Throat Area	2,278.5 $in.^2$
Final Throat Area	2,444.3 $in.^2$
Web Time Average Throat Area	2,365.0 $in.^2$
Action Time Average Throat Area	2,372.5 $in.^2$
Total Time Average Throat Area	2,372.8 $in.^2$
Initial Exit Area	17,588 $in.^2$
Final Exit Area	17,691 $in.^2$
Total Time Average Exit Area	17,640 $in.^2$
Web Time Average Throat Radial Erosion Rate	0.00845 ips
Action Time Average Throat Radial Erosion Rate	0.00789 ips
Total Time Average Throat Radial Erosion Rate	0.00783 ips
Initial Expansion Ratio	7.7230
Web Time Average Expansion Ratio	7.4244
Action Time Average Expansion Ratio	7.4009
Action Time Average Nozzle Efficiency	0.98680
Total Time Average Nozzle Efficiency	0.98800

Table 7.1-1. Summary of Measured Ballistic and Nozzle Performance Data (cont)

Thiokol Space Shuttle Test DM-9, 23 Dec 1987

D. Time and Ballistic Data

Time at First Indication of Headend Pressure	0.032 sec
Ignition Delay Time	-0.027 sec
Time at 90% Maximum Igniter Pressure	0.059 sec
Ignition Interval Time	0.243 sec
Ignition Rise Time	0.211 sec
Time When Headend Chamber Pressure Achieves 563.5 psia During Ignition	0.243 sec
Time at Last Indication of Headend Pressure	122.9 sec
Time at Web Bisector	110.3 sec
Web Time	110.0 sec
Action Time	121.9 sec
Total Time	122.9 sec
Tailoff Thrust Decay Time	0.781 sec
Maximum Pressure Rise Rate	81.0 psi/10 ms
Maximum Thrust Rise Rate	256,500 lbf/10 ms
Maximum Igniter Pressure	1,885 psia
Maximum Measured Headend Pressure	918 psia
Time at Maximum Headend Pressure	0.640 sec
Maximum Thrust	3,167,000 lbf
Time at Maximum Thrust	17.5 sec
Maximum Thrust Corrected to Vacuum	3,382,000 lbf
Maximum Thrust Corrected to Sea Level	3,124,000 lbf
Maximum Nozzle Stagnation Pressure	858 psia
Web Time Average Headend Chamber Pressure	670.8 psia
Action Time Average Headend Chamber Pressure	621.4 psia
Web Time Average Nozzle Stagnation Pressure	653.6 psia
Initial Thrust	3,016,000 lbf
Initial Thrust Corrected to Vacuum	3,231,000 lbf
Initial Thrust Corrected to Sea Level	2,973,000 lbf
Web Time Average Thrust	2,414,000 lbf
Web Time Average Thrust Corrected to Vacuum	2,630,000 lbf
Action Time Average Thrust	2,228,000 lbf
Action Time Average Thrust Corrected to Vacuum	2,438,000 lbf
Characteristic Exhaust Velocity	5,047 ft/sec

Table 7.1-1. Summary of Measured Ballistic and Nozzle Performance Data (cont)

Thiokol Space Shuttle Test DM-9, 23 Dec 1987

E. Impulse Data	
Measured Total Impulse	271.69 Mlbf-sec
Total Impulse Corrected to Vacuum	297.35 Mlbf-sec
Measured Impulse at 20 sec	61.37 Mlbf-sec
20 sec Impulse Corrected to Vacuum	65.66 Mlbf-sec
Measured Impulse at 60 sec	161.61 Mlbf-sec
60 sec Impulse Corrected to Vacuum	174.51 Mlbf-sec
Web Time Impulse	265.63 Mlbf-sec
Web Time Impulse Corrected to Vacuum	289.29 Mlbf-sec
Action Time Impulse	271.55 Mlbf-sec
Action Time Impulse Corrected to Vacuum	297.13 Mlbf-sec
I_{sp}	244.66 sec
I_{sp} Corrected to Vacuum	267.70 sec
Web Time I_{sp}	246.00 sec
Web Time I_{sp} Corrected to Vacuum	267.93 sec
Action Time I_{sp}	244.74 sec
Action Time I_{sp} Corrected to Vacuum	267.79 sec
Propellant I_{sp}	246.11 sec
Propellant I_{sp} Corrected to Vacuum	269.37 sec
F. Pressure Integral Data	
Total Time Pressure Integral	75,784 psia-sec
Web Time Pressure Integral	73,802 psia-sec
Action Time Pressure Integral	75,742 psia-sec

Table 7.1-1. Summary of Measured Ballistic and Nozzle Performance Data (cont)

Thiokol Space Shuttle Test DM-9, 23 Dec 1987
Corrected to 40°F

D. Time and Ballistic Data	
Time at First Indication of Headend Pressure	0.034 sec
Time When Headend Chamber Pressure Achieves 563.5 psia During Ignition	0.254 sec
Time at Last Indication of Headend Pressure	126.1 sec
Time at Web Bisector	113.3 sec
Web Time	113.0 sec
Action Time	125.1 sec
Maximum Measured Headend Pressure	892 psia
Time at Maximum Headend Pressure	0.657 sec
Maximum Thrust Corrected to Vacuum	3,288,000 lbf
Maximum Nozzle Stagnation Pressure	834 psia
Web Time Average Headend Chamber Pressure	652 psia
Action Time Average Headend Chamber Pressure	604 psia
Web Time Average Nozzle Stagnation Pressure	635 psia
Action Time Average Nozzle Stagnation Pressure	589 psia
Web Time Average Thrust Corrected to Vacuum	2,558,000 lbf
Action Time Average Thrust Corrected to Vacuum	2,371,000 lbf
E. Impulse Data	
Total Impulse Corrected to Vacuum	296.90 Mlbf-sec
20 sec Impulse Corrected to Vacuum	63.78 Mlbf-sec
60 sec Impulse Corrected to Vacuum	110.32 Mlbf-sec
Web Time Impulse Corrected to Vacuum	288.91 Mlbf-sec
Action Time Impulse Corrected to Vacuum	296.68 Mlbf-sec
I_{sp} Corrected to Vacuum	267.37 sec
Web Time I_{sp} Corrected to Vacuum	267.53 sec
Action Time I_{sp} Corrected to Vacuum	267.39 sec
Propellant I_{sp} Corrected to Vacuum	268.95 sec

Table 7.1-1. Summary of Measured Ballistic and Nozzle Performance Data (cont)

Thiokol Space Shuttle Test DM-9, 23 Dec 1987
Corrected to 60°F

D. Time and Ballistic Data	
Time at First Indication of Headend Pressure	0.032 sec
Time When Headend Chamber Pressure Achieves 563.5 psia During Ignition	0.245 sec
Time at Last Indication of Headend Pressure	123.4 sec
Time at Web Bisector	110.7 sec
Web Time	110.5 sec
Action Time	122.4 sec
Maximum Measured Headend Pressure	913 psia
Time at Maximum Headend Pressure	0.643 sec
Maximum Thrust Corrected to Vacuum	3,367,000 lbf
Maximum Nozzle Stagnation Pressure	854 psia
Web Time Average Headend Chamber Pressure	668 psia
Action Time Average Headend Chamber Pressure	618 psia
Web Time Average Nozzle Stagnation Pressure	651 psia
Action Time Average Nozzle Stagnation Pressure	603 psia
Web Time Average Thrust Corrected to Vacuum	2,617,000 lbf
Action Time Average Thrust Corrected to Vacuum	2,427,000 lbf
E. Impulse Data	
Total Impulse Corrected to Vacuum	297.27 Mlbf-sec
20 sec Impulse Corrected to Vacuum	65.34 Mlbf-sec
60 sec Impulse Corrected to Vacuum	173.80 Mlbf-sec
Web Time Impulse Corrected to Vacuum	289.19 Mlbf-sec
Action Time Impulse Corrected to Vacuum	297.06 Mlbf-sec
I_{sp} Corrected to Vacuum	267.70 sec
Web Time I_{sp} Corrected to Vacuum	267.86 sec
Action Time I_{sp} Corrected to Vacuum	267.72 sec
Propellant I_{sp} Corrected to Vacuum	269.29 sec

Table 7.1-1. Summary of Measured Ballistic and Nozzle Performance Data (cont)

Thiokol Space Shuttle Test DM-9, 23 December 1987
Corrected to 90°F

D. Time and Ballistic Data	
Time at First Indication of Headend Pressure	0.030 sec
Time When Headend Chamber Pressure Achieves 563.5 psia During Ignition	0.232 sec
Time at Last Indication of Headend Pressure	119.5 sec
Time at Web Bisector	107.1 sec
Action Time	118.4 sec
Maximum Measured Headend Pressure	946 psia
Time at Maximum Headend Pressure	0.622 sec
Maximum Thrust Corrected to Vacuum	3,488,000 lbf
Maximum Nozzle Stagnation Pressure	885 psia
Web Time Average Headend Chamber Pressure	692 psia
Action Time Average Headend Chamber Pressure	640 psia
Web Time Average Nozzle Stagnation Pressure	674 psia
Action Time Average Nozzle Stagnation Pressure	624 psia
Web Time Average Thrust Corrected to Vacuum	2,711,000 lbf
Action Time Average Thrust Corrected to Vacuum	2,513,000 lbf
E. Impulse Data	
Total Impulse Corrected to Vacuum	297.82 Mlbf-sec
20 sec Impulse Corrected to Vacuum	67.76 Mlbf-sec
60 sec Impulse Corrected to Vacuum	179.21 Mlbf-sec
Web Time Impulse Corrected to Vacuum	289.83 Mlbf-sec
Action Time Impulse Corrected to Vacuum	297.62 Mlbf-sec
I_{sp} Corrected to Vacuum	268.20 sec
Web Time I_{sp} Corrected to Vacuum	268.35 sec
Action Time I_{sp} Corrected to Vacuum	268.22 sec
Propellant I_{sp} Corrected to Vacuum	269.79 sec

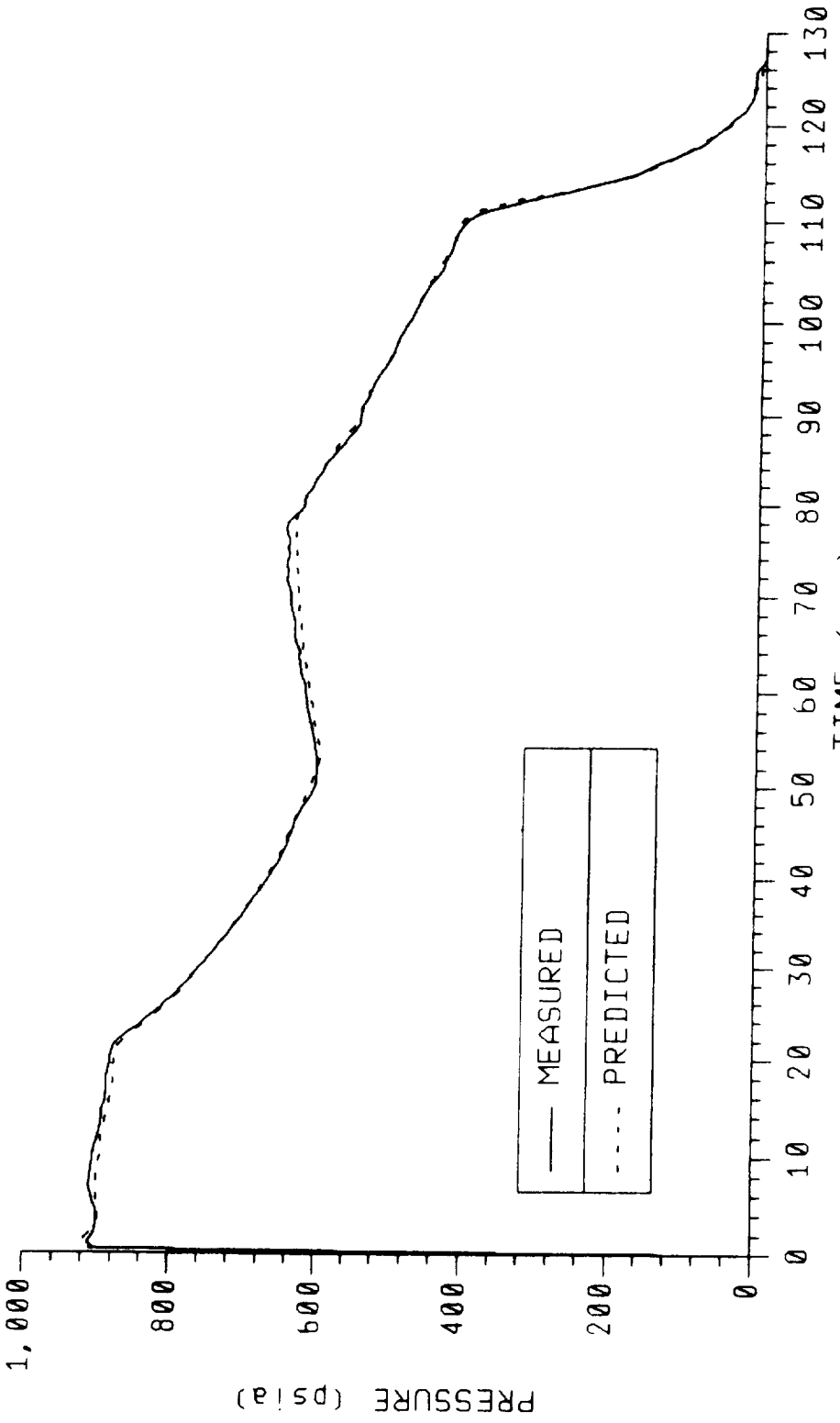

Figure 7.1-3. DM-9 Predicted and Measured Pressure Data

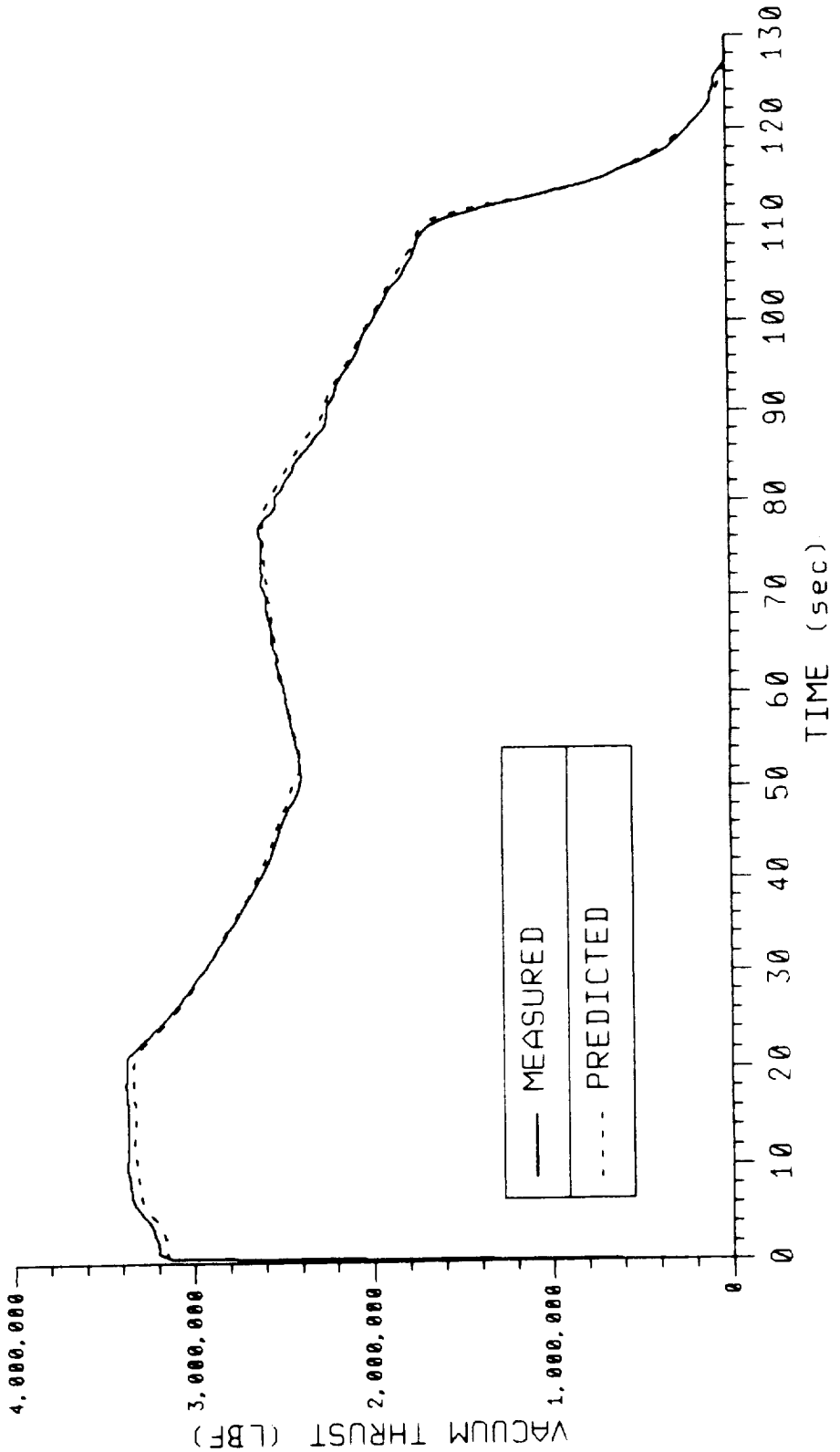

Figure 7.1-4. DM-9 Predicted and Measured Vacuum Thrust Data

predicted vacuum thrust-time histories. The pressure and thrust curves differed from the predicted curve, because of the difference in burn rate and PMBT. Trace shapes were very close to the predicted curve, which were based on nominal HPM performance and RSRM propellant design changes.

Figures 7.1-5 and 7.1-6 contain plots of the analytical reconstruction of the DM-9 performance. The analytical model calculated the motor burn rate and surface burn rate error (SBRE) factor. The calculated burn rate of 0.369 ips at 625 psia and 60°F was approximately 0.3 percent higher than the predicted value of 0.368 ips. The calculated SBRE table compared closely with the nominal HPM table as expected, since the propellant grain geometry was very similar. The only changes in propellant grain geometry were the modified stress relief transition block in the forward segment and propellant-to-insulation interfaces.

The motor average subscale burn rates, full-scale motor burn rates (determined from post-test curve matching), and resulting scale factors for SRM-15 to SRM-24 used to predict the DM-9 burn rate are listed in Table 7.1.2. The full-scale motor burn rates were determined from post-test curve matching in which the analytical model was forced to match the measured motor performance. The mean scale factor was 1.0175 with a sigma 0.00440 and a coefficient of variation (CV) of 0.432 percent. The scale factor for DM-9 firing was 1.0196.

A comparison of the thrust to headend chamber pressure ratios for DM-9 and DM-8 is shown in Figure 7.1-7. The two traces are similar. A similar thrust-to-pressure ratio is an indication that the throat erosion profiles were similar. The modified stress relief transition block in the forward segment did not noticeably change DM-9 performance as predicted. The influence of the new transition block on the pressure was predicted to be less than 2 psi, ranging between 2 and 50 sec. This pressure variation is impossible to separate from the normal SRM pressure variation. No abnormal pressure or gas flow variation could be traced to this change.

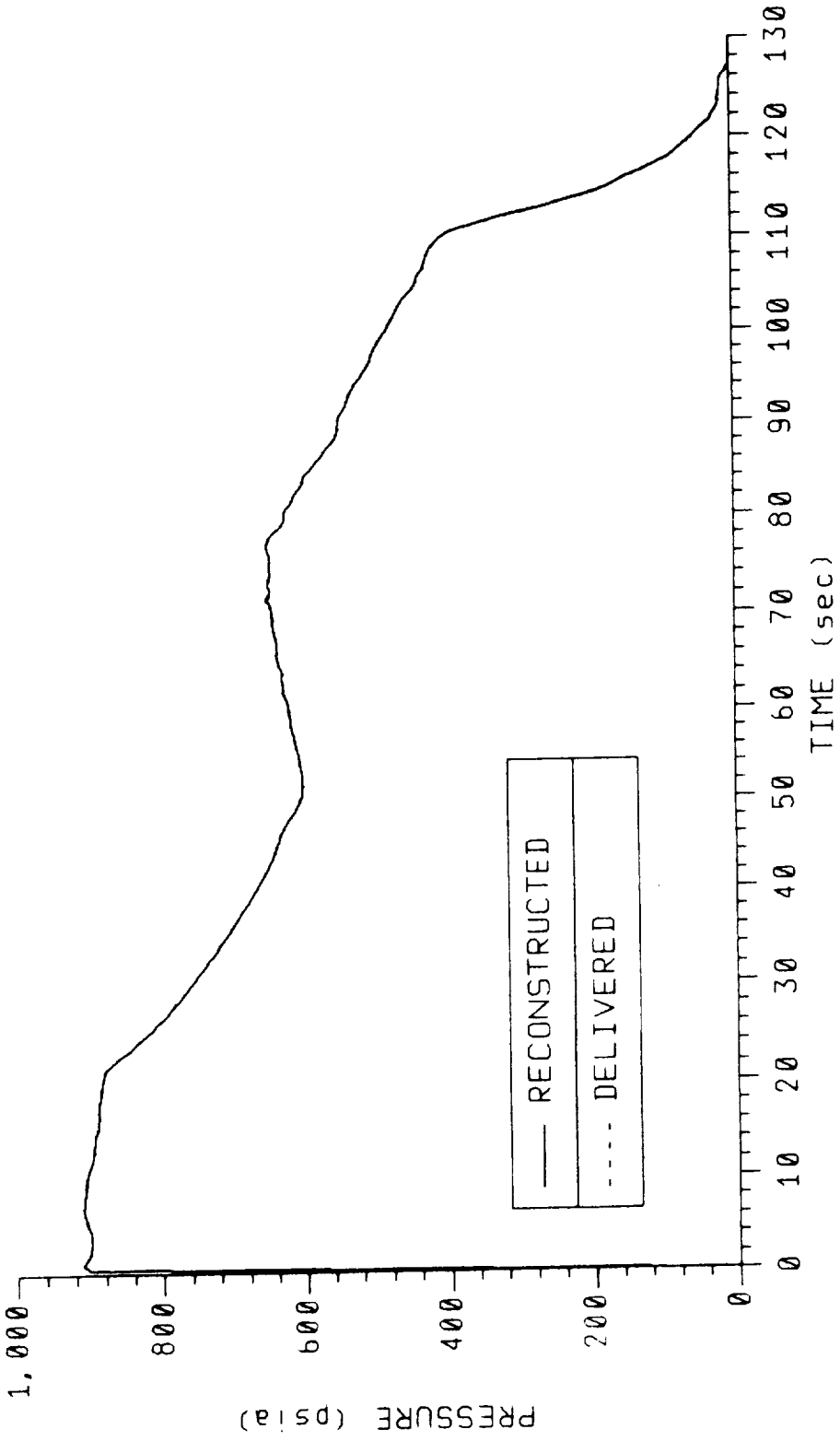

Figure 7.1-5. Reconstructed Headend Pressure Versus Time Superimposed Over Delivered DM-9 Headend Pressure

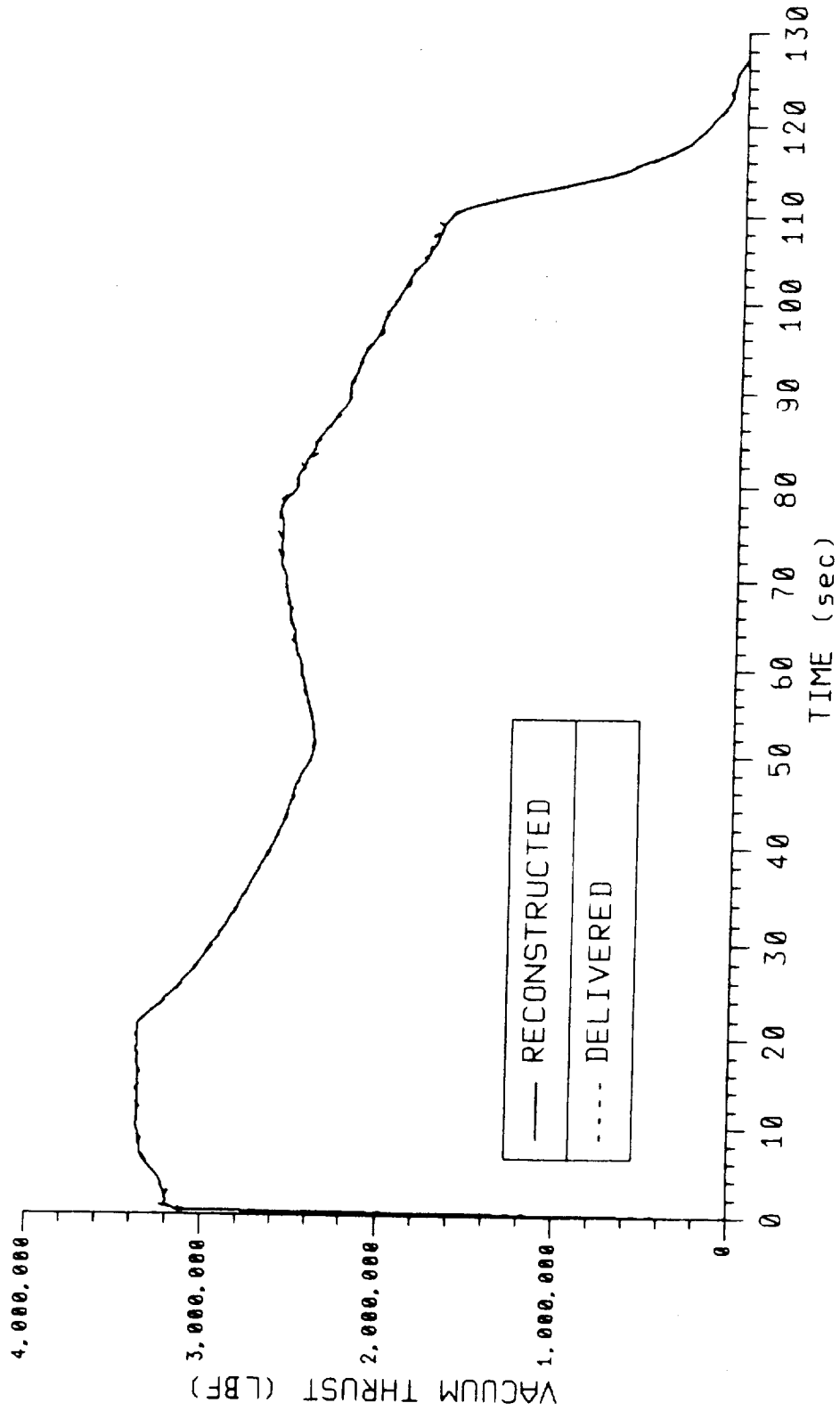

Figure 7.1-6. Reconstructed Vacuum Thrust Versus Time Superimposed Over Delivered DM-9 Thrust Corrected to Vacuum

Table 7.1-2. Burn Rate Data Comparison Subscale to Full-Scale

	Burn Rate				Scale Factor
Motor	SRM Target	5-in. CP Std	SRM Pred	SRM Del	5-in. CP Std
SRM-15A	0.368	0.366	0.370	0.3701	1.0112
SRM-15B	0.368	0.366	0.370	0.3709	1.0134
SRM-16A	0.368	0.365	0.369	0.3684	1.0093
SRM-16B	0.368	0.365	0.369	0.3688	0.1040
SRM-17A	0.368	0.363	0.367	0.3680	1.0138
SRM-17B	0.368	0.362	0.366	0.3694	1.0204
SRM-18A	0.368	0.362	0.367	0.3693	1.0202
SRM-18B	0.368	0.363	0.368	0.3690	1.0165
SRM-19A	0.368	0.364	0.369	0.3703	1.0173
SRM-19B	0.368	0.364	0.369	0.3704	1.0176
SRM-20A	0.368	0.368	0.373	0.3742	1.0168
SRM-20B	0.368	0.366	0.371	0.3744	1.0230
SRM-21A	0.368	0.367	0.370	0.3737	1.0183
SRM-21B	0.368	0.365	0.368	0.3744	1.0258
SRM-22A	0.368	0.362	0.365	0.3675	1.0152
SRM-22B	0.368	0.362	0.365	0.3697	1.0213
SRM-23A	0.368	0.364	0.367	0.3713	1.0201
SRM-23B	0.368	0.364	0.367	0.3721	1.0223
SRM-24A	0.368	0.360	0.365	0.3678	1.0217
SRM-24B	0.368	0.361	0.366	0.3674	1.0177
ETM-1A	0.368	0.365	0.372	0.3681	1.0085
DM-8	0.368	0.360	0.366	0.3677	1.0214
DM-9	0.368	0.362	0.368	0.3691	1.0196

Average Scale Factor = 1.0175 Sigma = 0.00440 CV (%) = 0.432

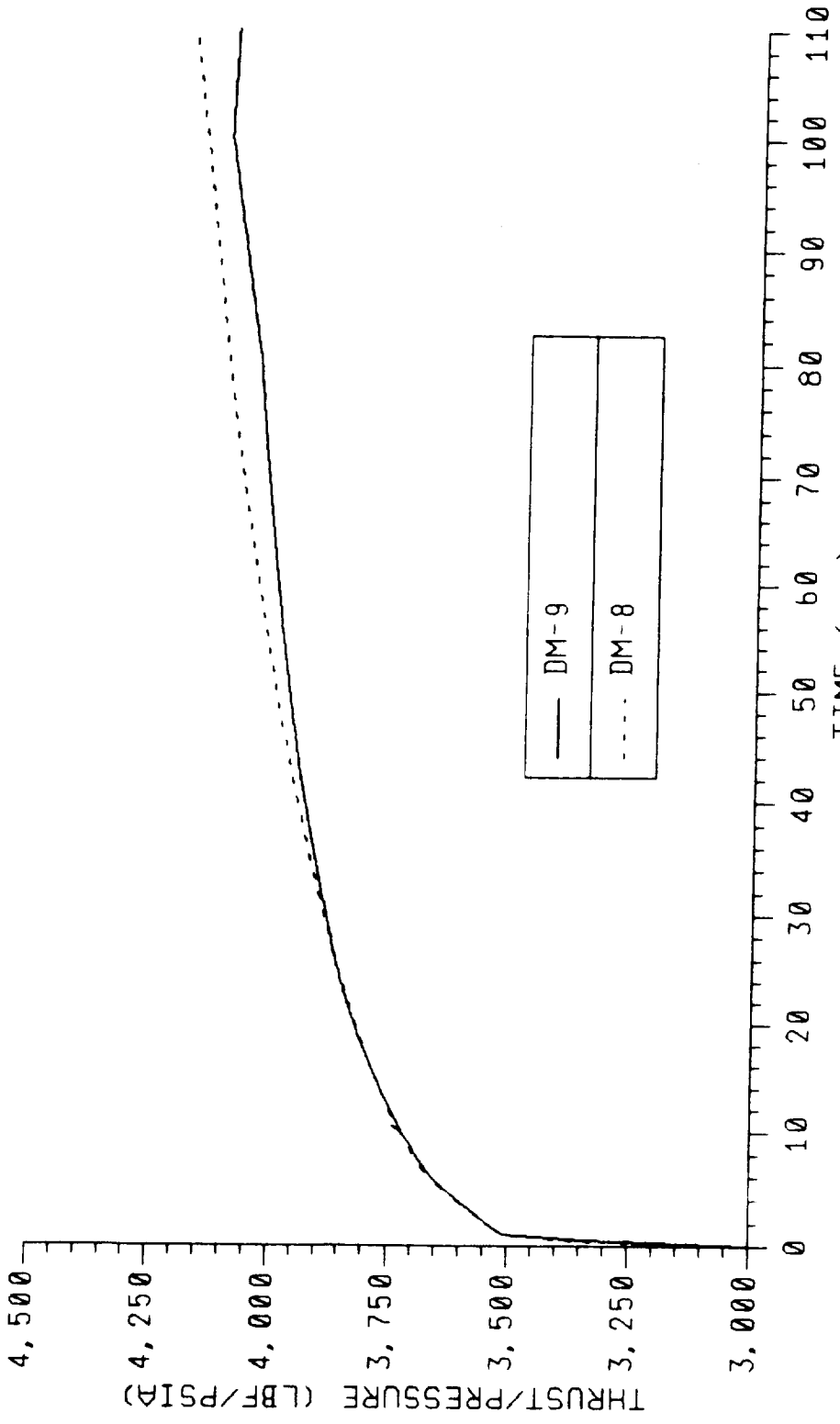

Figure 7.1-7. Comparison of Vacuum Thrust Versus Headend Chamber Pressure Ratio From DM-9 and DM-8

A plot of the measured data comparing the ignition transients of DM-9 and DM-8 is shown in Figure 7.1-8. The DM-9 transient was similar to DM-8. The DM-9 ignition interval was 244 ms, well within the specification limits of 202 and 262 ms. The DM-9 maximum pressure rise rate was 81.0 psi/10 ms. The mean historical three-point average pressure rise rate is 91.9 psi/10 ms with a variation of 5.31 psi/ 10 ms. A summary table showing the historical pressure rise rate, thrust rise rate, and ignition interval values are shown in Table 7.1-3. A summary of the DM-9 ignition events is shown in Table 7.1-4.

A comparison of DM-9 thrust data corrected to 60°F and a burn rate of 0.368 ips with the contract end item (CEI) specification CPW1-3600 is shown on Figure 7.1-9. The DM-9 performance was completely within limits during motor operation. Note that the limits are for the average of the RSRM motor population, not for an individual motor. These limits are the same ones used for the historical HPM population.

None of the individual motor performance tolerances and limit parameters was exceeded. A DM-9 performance summary with the CEI specification tolerance limits is shown in Table 7.1-5.

The DM-9 performance must be adjusted to a 0.368 ips burn rate at a 60°F PMBT and 625 psia average web time pressure to be compared with the CEI specification impulse gates. DM-9 had a 65.2 Mlbf-sec impulse at 20 sec, a 173.4 Mlbf-sec impulse at 60 sec, and a 297.0 Mlbf-sec impulse at action time. The required impulse gates are a minimum of 63.1 Mlbf-sec at 20 sec, a minimum of 171.2 Mlbf-sec to a maximum of 178.1 Mlbf-sec at 60 sec, and a minimum of 293.8 Mlbf-sec at action time. The DM-9 static test met all impulse gates.

DM-9 slag accumulation was 2,270 lbf. This is more than the historical average of 1,064 lbf, but less than predicted slag weight of 2,400 lbf. The cause of the excessive slag is considered to be associated with the AP particle size distribution.

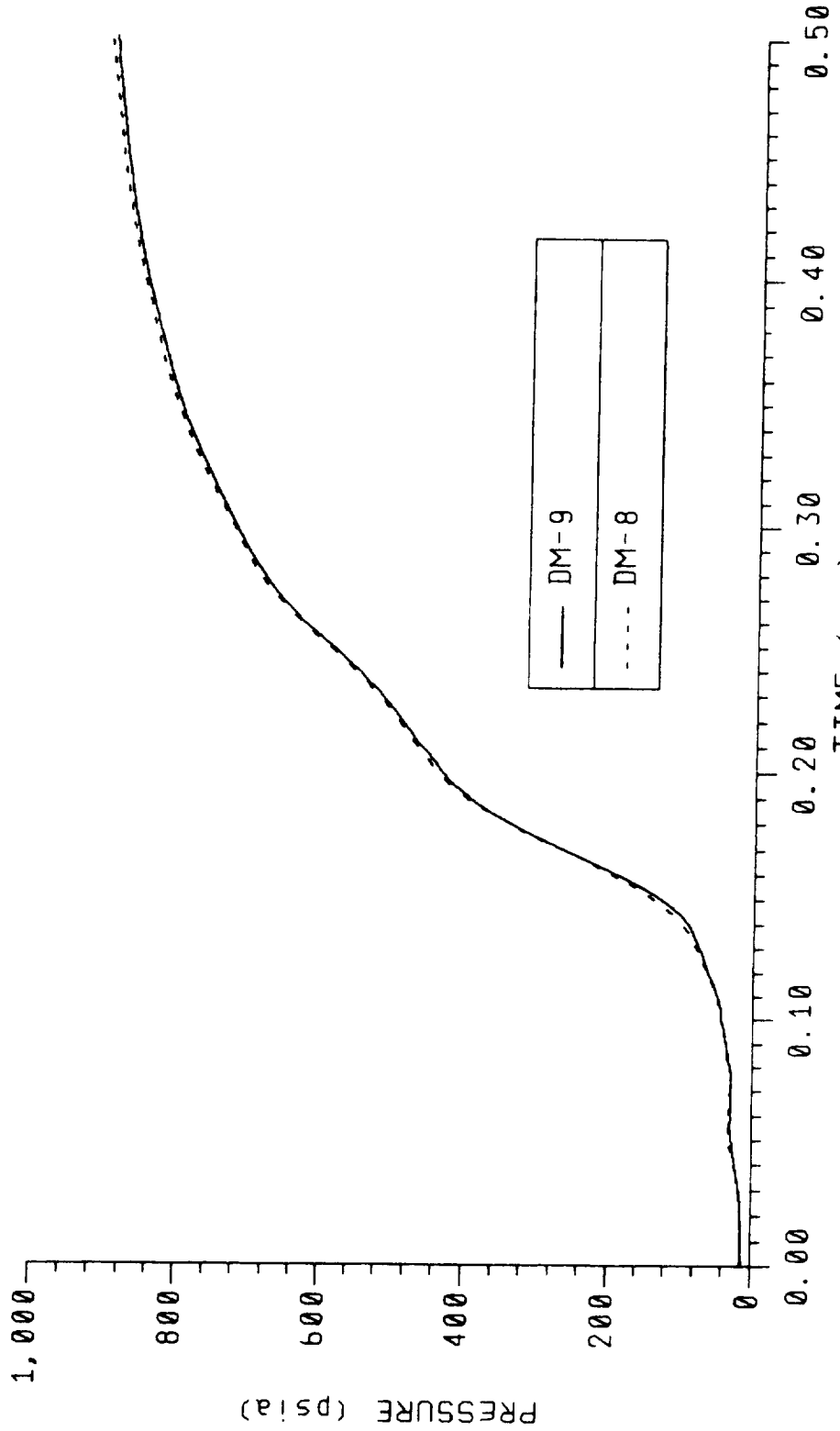

Figure 7.1-8. Measured Headend Pressure Ignition Transients

Table 7.1-3. Historical Three-Point Average Thrust and Pressure Rise Rate Data

Motor	Occurrence Time	Pressure Rise Rate	Occurrence Time	Thrust Rise Rate	Ignition Interval
Static Test					
DM-2	0.1480	85.30	0.1480	245380	0.2330
QM-1	0.1560	86.38	0.1560	246128	0.2362
QM-2	0.1640	93.58	0.1720	234950	0.2391
QM-3	0.1560	94.45	0.1520	245615	0.2287
QM-4	0.1505	91.96	0.2225	234438	0.2192
ETM-1A	0.1520	86.72	0.1560	230023	0.2279
Flight Motors					
SRM-1A	0.1530	87.58			0.2373
SRM-1B	0.1500	91.57			0.2358
SRM-2A	0.1530	90.74			0.2348
SRM-2B	0.1660	90.27			0.2345
SRM-3A	0.1500	91.05			0.2308
SRM-3B	0.1500	89.68			0.2271
SRM-5A	0.1530	95.10			0.2361
SRM-5B	0.1660	84.43			0.2380
SRM-6A	0.1530	92.72			0.2342
SRM-6B	0.1470	88.22			0.2329
SRM-7A	0.1500	99.90			0.2282
SRM-7B	0.1500	99.32			0.2276
SRM-8A	0.1530	106.29			0.2224
SRM-8B	0.1500	91.06			0.2196
SRM-9A	0.1530	92.31			0.2303
SRM-10A	0.1530	92.89			0.2373
SRM-10B	0.1500	84.56			0.2342
SRM-13B	0.1410	98.85			0.2115
Number		24		6	24
Average		91.87		236,357	0.2307
Standard Deviation		5.31		11,977	0.0069
CV (%)		5.78		5.07	2.99
DM-8	0.1680	77.00	0.1760	257,272	0.2424
DM-9	0.1640	81.00	0.1720	275,525	0.2436

Table 7.1-4. Measured SRM Ignition Performance Data

Parameter	DM-9	Specification Requirement
Maximum Igniter Mass Flow Rate (lbm/sec)	337.4	NA
Ignition Transient (sec) (0 to 563.5 psia)	0.244	0.202 - 0.262
Maximum Pressure Rise Rate (psi/10 ms)	81.0	115.9
Pressure Level at Start of Maximum Rise Rate (psia)	219	NA
Time Span of Maximum Pressure Rise (ms)	164.0 - 174.0	NA
Equilibrium Pressure 0.6 sec (ignition end) (psia)	917	NA
Time to First Ignition (sec) (begin pressure rise)	0.032	NA

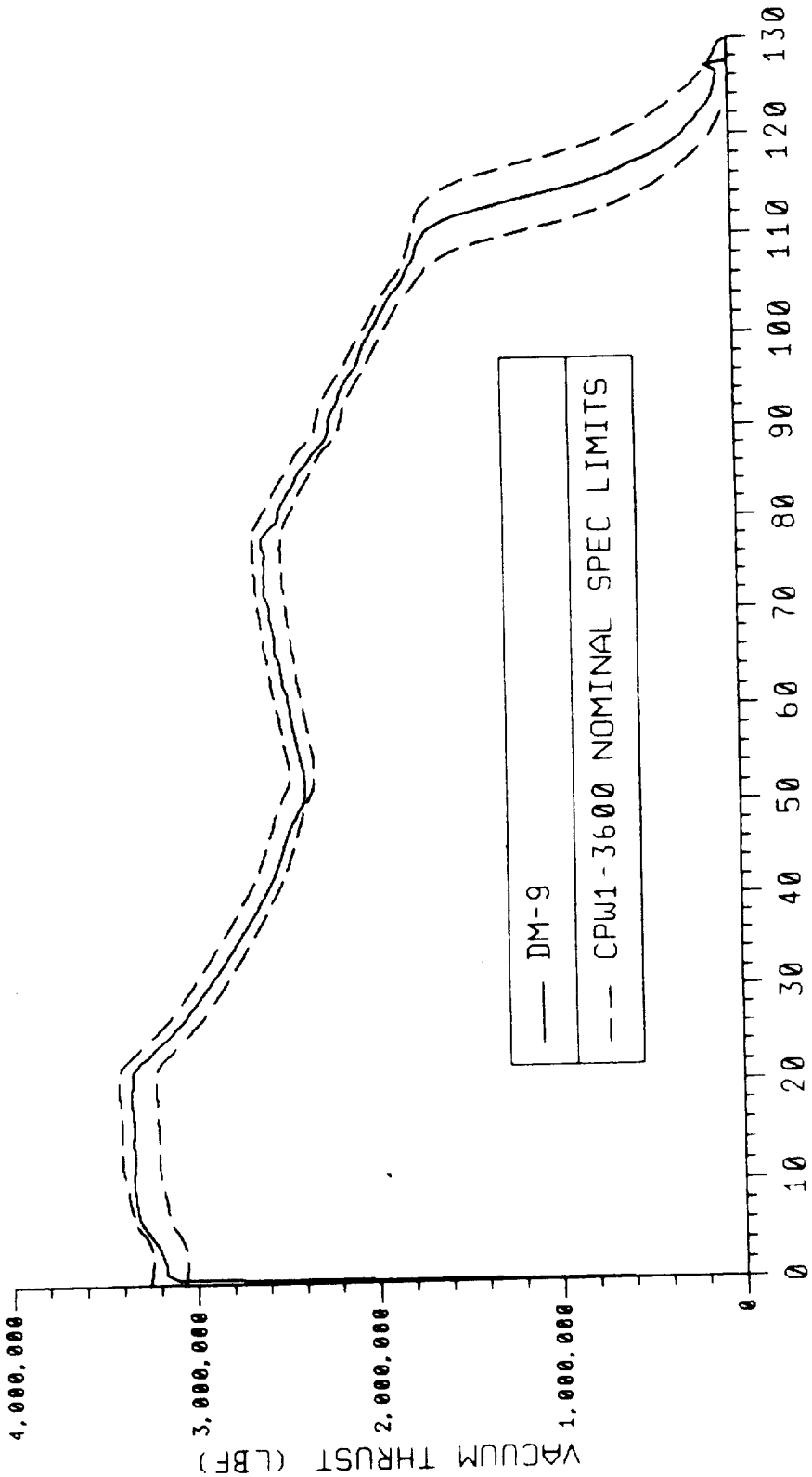

Figure 7.1-9. Comparison of DM-9 Thrust Data at 0.368 ips Burn Rate and 60°F

Table 7.1-5. DM-9 Performance Summary With CPW1-3600 CEI Specification Limits

	Vacuum Spec Limits (60°F)	DM-9 Predicted (60°F)	DM-9 Delivered (60°F)
Web Time (sec)	106.1 - 117.2	111.4	110.6
Action Time (sec)	115.4 - 131.4	122.8	122.4
MOP Headend (psia)	858.7 - 978.1	920	913
Max Sea Level Thrust (Mlbf)	2.87 - 3.25	3.054	3.290
Web Time Avg Headend Pressure (psia)	625.8 - 695.8	662	668
Web Time Avg Vacuum Thrust (Mlbf)	2.45 - 2.72	2.610	2.615
Web Time Total Impulse (Mlbf-sec)	286.1 - 291.8	289.81	289.35
Action Time Impulse (Mlbf-sec)	293.3 - 299.2	296.89	296.97
I_{sp} Avg Delivered (lbf-sec/lbm)	265.3 - 269.0	268.6	268.6
Ignition Interval (sec), Time 563.5 psia	0.202 - 0.262	0.232	0.244
Maximum Pressure Rise Rate (psi/10 ms)	X < 115.9	92.0	81.0

Loaded Propellant Weight of 1,106,184 lb

The igniter was cast from Propellant Batch No. E990005 using TP-H1178 propellant. The DM-9 igniter was the first modified igniter configuration (1U75163) to be fired in a full-scale motor. The configuration was very similar to the earlier HPM flight and static test igniter design (1U51882). A discussion on the difference between the two designs is contained in TWR-16265, Revision A. The DM-9 igniter maximum mass flow rate was 337.4 lbm/sec at 64°F, which compared well with the LAT-37 maximum mass flow rate of 331.8 lbm/sec at 64°F. The DM-9 igniter performance characteristics were within the expected ranges. Comparison of the DM-9 igniter performance with LAT-37 (the lot acceptance igniter for Propellant Mix No. E990005) at 64°F is shown in Figure 7.1-10. The DM-9 and LAT-37 igniter performance traces show close correlation up to the time the DM-9 igniter becomes unchoked because of motor chamber pressure.

A comparison of the igniter pressure versus motor headend and nozzle stagnation pressure for the first 1.4 sec of motor operation is shown in Figure 7.1-11. A plot of headend and nozzle stagnation pressure for the full duration of the static test is shown on Figure 7.1-12. These curves are characteristic of the ratio of the headend-to-nozzle stagnation pressures from previous SRM static test motors.

Tables 7.1-6 and 7.1-7 show DM-9 reconstructed pressure distribution during ignition and steady state at a PMBT of 64°F and adjusted PMBT temperature of 60°F, respectively. Figure 7.1-13 shows the location points referenced in the pressure distribution tables. The pressure distribution was reconstructed theoretically, since no internal pressures are assured other than headend pressure. The pressures were reconstructed using Caveny-Kuo ignition transient program, the SCB04 steady state one-dimensional (1-D) mass addition, and the SCA08 SRM modeling program.

The DM-9 static test motor was instrumented with a dynamic (ac coupled) pressure gage to provide oscillatory chamber pressure data. The gage (P006) was located at the headend of the motor, and data acquired from this gage are displayed in Figure 7.1-14. The first longitudinal (1-L) and second longitudinal (2-L) modes can be observed at 15 and 30 Hz, respectively.

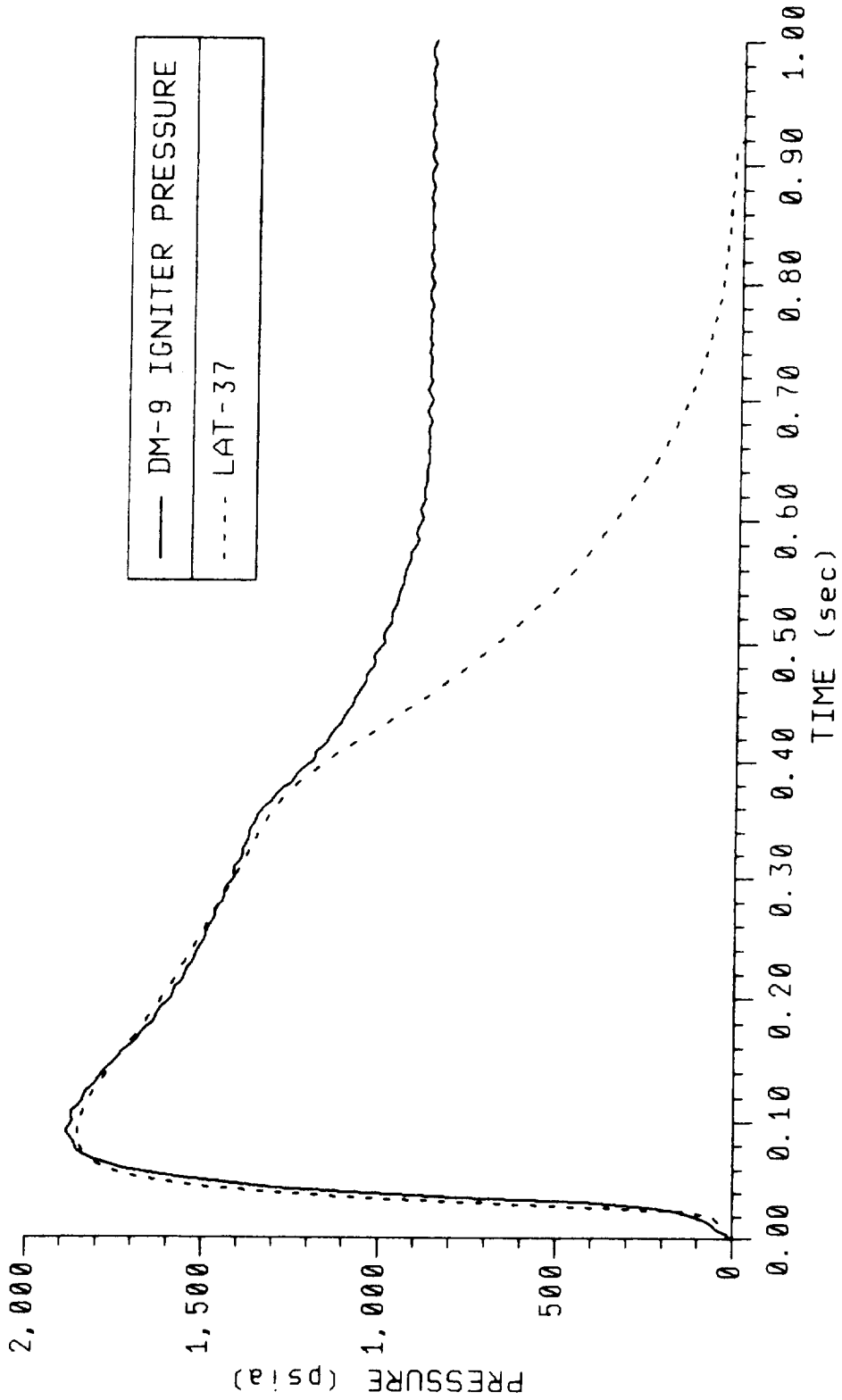

Figure 7.1-10. DM-9 Igniter Pressure Comparison With LAT-37 Pressure Time Trace at 64°F

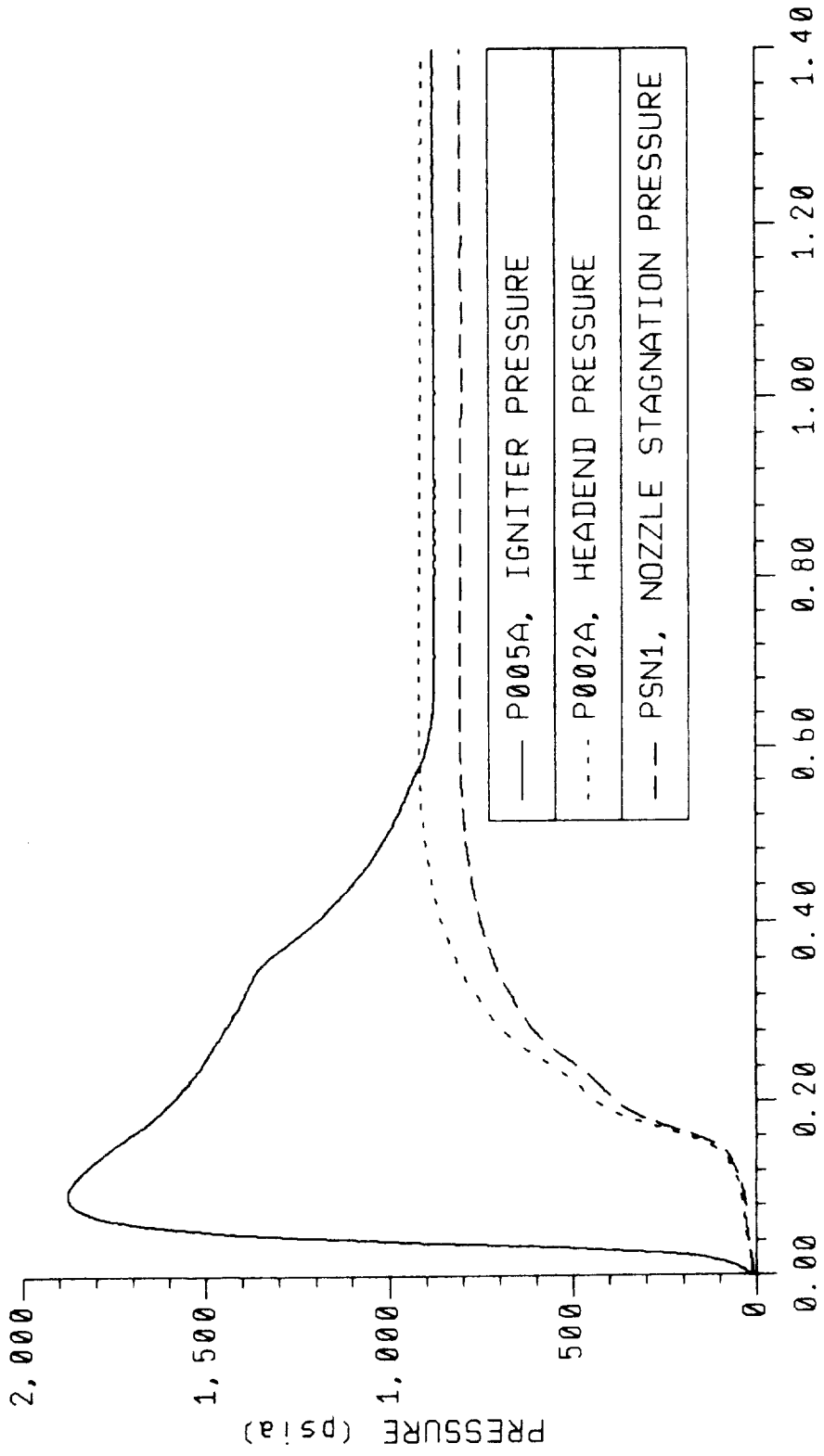

Figure 7.1-11. DM-9 Igniter, Headend, and Nozzle Stagnation Pressure Comparison

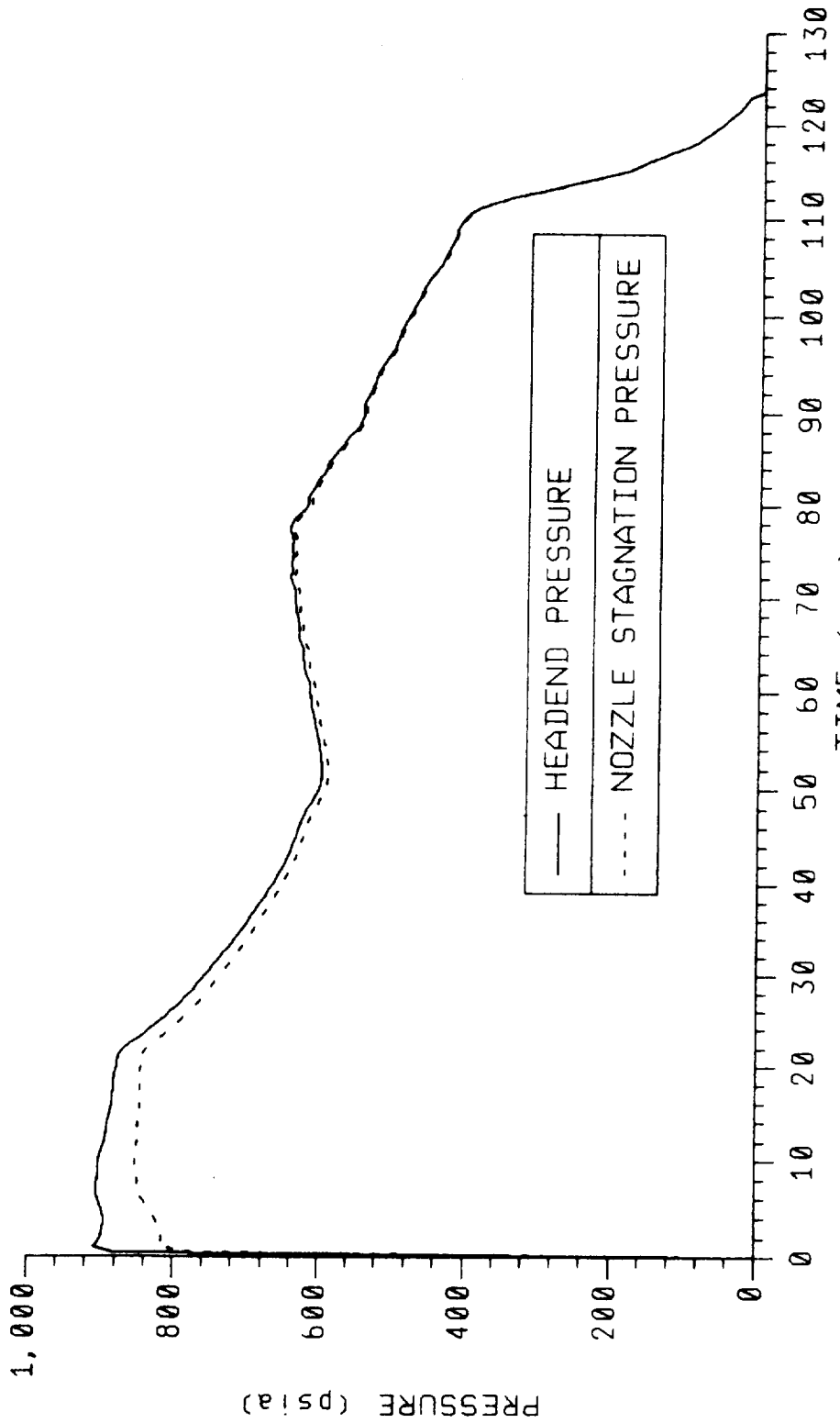

Figure 7.1-12. Headend and Nozzle Stagnation Pressure Time Histories

Table 7.1-6. DM-9 Pressure Distribution Summary at Test Condition (64°F)
Ignition: Caveny Kuo

TIME	HEAD-END PRESSURE (489.9)	X LOCATIONS (INCHES) 530.0	689.3	851.2	1012.1	1171.2	1332.1	1491.2	1511.0	1577.5	1697.5	1816.7	NOZZLE STAGNATION PRESSURE
0.000	11.6	11.5	11.5	11.5	11.5	11.6	11.5	11.5		11.4	11.5	11.5	11.5
0.000	11.7	11.6	11.6	11.6	11.6	11.7	11.6	11.6		11.5	11.6	11.6	11.6
0.002	12.8	12.5	12.3	12.3	12.3	12.4	12.3	12.3		12.2	12.3	12.3	12.3
0.004	14.1	13.7	13.3	13.3	13.3	13.4	13.3	13.4		13.2	13.3	13.3	13.3
0.006	13.9	13.6	13.2	13.1	13.1	13.2	13.1	13.2		13.0	13.1	13.1	13.1
0.008	13.8	13.5	13.0	12.9	12.9	13.0	12.9	12.9		12.8	12.9	12.9	12.9
0.010	13.3	13.1	12.6	12.4	12.4	12.5	12.4	12.3		12.2	12.3	12.4	12.4
0.012	12.8	12.6	12.2	11.9	11.8	11.9	11.8	11.8		11.7	11.8	11.8	11.8
0.014	12.6	12.4	12.0	11.6	11.6	11.7	11.5	11.5		11.4	11.5	11.6	11.6
0.016	12.3	12.1	11.8	11.4	11.2	11.3	11.2	11.2		11.1	11.2	11.2	11.2
0.018	12.6	12.4	12.1	11.6	11.4	11.5	11.4	11.4		11.3	11.4	11.4	11.4
0.020	12.9	12.6	12.4	11.8	11.5	11.6	11.5	11.5		11.5	11.4	11.5	11.5
0.022	13.7	13.4	13.1	12.4	12.1	12.2	12.0	12.0		11.9	12.0	12.1	12.1
0.024	14.4	14.1	13.7	12.9	12.6	12.6	12.4	12.4		12.3	12.4	12.4	12.4
0.026	15.5	15.2	14.7	13.8	13.3	13.3	13.1	13.2		13.0	13.1	13.2	13.2
0.028	16.6	16.3	15.7	14.6	14.0	13.9	13.7	13.8		13.6	13.7	13.7	13.7
0.030	17.9	17.6	17.0	15.6	14.8	14.7	14.5	14.6		14.4	14.5	14.5	14.5
0.032	19.1	18.8	18.2	16.6	15.6	15.4	15.2	15.3		15.1	15.2	15.2	15.2
0.034	20.3	20.1	19.7	17.8	16.5	16.3	15.9	16.0		15.8	15.9	15.9	16.0
0.036	21.5	21.3	21.2	19.1	17.5	17.1	16.7	16.8		16.5	16.6	16.7	16.8
0.038	22.6	22.5	22.6	20.4	18.4	17.8	17.4	17.4		17.2	17.3	17.3	17.4
0.040	23.7	23.7	24.2	21.9	19.5	18.7	18.1	18.1		17.9	18.0	18.0	18.1
0.042	24.5	24.6	25.6	23.4	20.5	19.4	18.7	18.7		18.5	18.6	18.6	18.7
0.044	25.4	25.7	27.1	25.1	21.9	20.3	19.5	19.5		19.3	19.3	19.2	19.4
0.046	26.0	26.4	28.3	26.6	23.2	21.1	20.1	20.0		19.8	19.7	19.8	20.0
0.048	26.6	27.2	29.5	28.2	24.8	22.1	20.8	20.6		20.4	20.4	20.4	20.6
0.063	28.3	29.0	31.7	30.7	27.5	24.3	22.6	22.3		22.0	22.0	22.0	22.2
0.065	28.4	29.5	32.5	31.8	29.2	25.3	23.1	22.7		22.4	22.4	22.3	22.5
0.067	28.5	29.8	32.8	32.3	30.5	26.1	23.3	22.7		22.4	22.3	22.3	22.5
0.069	28.6	30.2	33.0	32.7	31.6	27.1	23.6	22.8		22.4	22.3	22.3	22.5
0.071	28.8	30.6	33.2	32.9	32.5	28.3	23.9	22.8		22.3	22.2	22.2	22.4
0.073	29.2	31.0	33.4	33.2	33.1	29.8	24.4	22.9		22.4	22.2	22.1	22.3
0.075	29.6	31.3	33.6	33.4	33.5	31.2	25.1	23.0		22.4	22.1	22.1	22.3
0.077	30.0	31.7	33.9	33.8	33.9	32.8	26.2	23.3		22.6	22.3	22.2	22.4
0.079	30.6	32.1	34.3	34.3	34.3	34.1	27.7	23.8		22.9	22.5	22.3	22.5
0.081	31.3	32.7	35.0	34.9	35.0	35.3	29.6	24.7		23.5	22.9	22.8	23.0
0.083	32.1	33.4	35.7	35.6	35.8	36.3	31.7	25.8		24.3	23.5	23.3	23.5
0.086	33.1	33.3	35.1	35.0	35.3	35.8	32.5	25.9		23.9	22.8	22.5	22.7
0.087	34.1	31.4	31.9	31.7	32.0	32.6	30.3	23.6		21.0	19.6	19.1	19.3
0.089	35.2	31.1	31.0	30.6	30.8	31.5	29.8	23.6		20.4	18.5	17.8	17.9
0.091	36.5	32.0	31.5	30.6	30.7	31.3	30.0	24.8		21.1	18.5	17.6	17.7
0.093	37.8	33.4	31.8	30.1	30.0	30.5	29.3	25.4		21.3	17.9	16.7	16.8
0.095	39.2	34.8	32.6	30.4	29.8	30.0	28.8	26.2		22.0	17.8	16.1	16.2
0.097	40.7	36.2	33.5	31.2	30.0	29.8	28.4	26.8		23.0	18.1	15.9	16.0
0.100	42.2	37.8	34.2	32.3	30.7	29.7	28.2	27.2		24.0	18.7	15.9	16.0
0.101	43.8	39.4	34.8	33.3	31.9	30.1	28.1	27.4		24.9	19.5	16.1	16.2
0.103	45.4	41.0	35.9	34.0	33.0	30.8	28.2	27.3		25.3	20.3	16.6	16.7
0.105	47.1	42.6	36.6	34.3	33.6	31.4	28.0	26.6		24.9	20.6	16.9	17.0

Table 7.1-6. DM-9 Pressure Distribution Summary at Test Condition (64°F)
Ignition: Caveny Kuo (cont)

TIME	X LOCATIONS (INCHES)											
	HEAD-END PRESSURE (489.9)	530.0	689.3	851.2	1012.1	1171.2	1332.1	1491.2	1511.0	1577.5	1697.5	1816.7	NOZZLE STAGNATION PRESSURE
0.107	48.8	44.4	36.1	34.3	33.1	31.4	27.7	25.5		23.6	20.1	17.0	17.1
0.109	50.5	46.2	35.5	33.9	32.5	31.1	27.5	24.2		22.0	19.3	17.4	17.5
0.111	52.2	47.9	35.0	33.1	32.0	30.5	27.4	23.2		20.4	18.1	18.0	18.1
0.113	53.9	49.8	34.7	32.5	31.4	30.1	27.2	22.8		19.2	16.8	18.8	18.9
0.115	55.6	51.6	34.4	32.1	30.8	29.8	26.9	22.8		18.5	15.7	19.5	19.8
0.117	57.4	53.5	34.2	31.6	30.4	29.5	26.5	22.9		18.4	15.0	20.3	20.5
0.119	59.2	55.5	34.0	31.2	30.1	29.2	26.1	22.9		18.5	14.9	21.0	21.2
0.121	61.1	57.6	33.9	30.6	29.7	29.0	25.6	22.5		18.6	15.3	21.9	22.1
0.123	63.0	59.8	33.8	30.1	29.3	28.9	25.2	22.0		18.4	16.3	23.4	23.6
0.125	65.1	62.1	33.8	29.5	28.9	28.7	24.7	21.4		17.9	17.5	26.0	26.2
0.127	67.4	64.6	34.0	29.0	28.5	28.5	24.3	20.9		17.4	18.7	30.0	30.4
0.129	69.9	67.3	34.3	28.6	28.2	28.3	23.8	20.4		16.8	19.6	35.4	35.8
0.131	72.6	70.3	34.9	28.4	28.1	28.3	23.4	19.9		16.4	21.2	41.4	41.9
0.133	75.6	73.6	35.6	28.3	28.0	28.4	23.0	19.5		15.9	23.6	46.6	47.2
0.135	79.1	77.4	36.9	28.6	28.3	28.9	22.9	19.3		15.9	27.8	50.4	51.0
0.137	82.8	81.6	38.5	29.1	28.8	29.6	23.0	19.3		16.2	33.6	52.4	53.0
0.139	87.5	86.5	41.4	30.3	29.9	30.9	23.7	20.0		17.5	41.4	53.9	54.5
0.141	92.4	92.0	45.6	33.0	31.4	32.5	24.5	20.8		19.8	49.8	55.2	55.8
0.143	98.4	98.6	52.8	36.8	33.9	35.0	25.9	22.3		24.4	57.5	57.4	58.1
0.146	104.9	105.8	59.9	40.6	36.4	37.4	27.0	23.5		31.8	62.0	59.8	60.6
0.147	112.8	114.4	67.6	47.4	40.4	41.8	28.0	25.3		42.8	63.7	62.4	63.2
0.149	121.1	123.5	74.8	53.7	44.8	48.1	28.1	27.3		53.7	63.3	64.1	64.8
0.151	131.1	134.0	82.8	59.9	48.7	53.4	28.9	30.5		62.7	63.4	66.0	66.8
0.153	141.4	145.2	90.6	65.4	52.3	57.7	28.9	33.2		67.8	63.7	67.3	68.2
0.155	153.4	158.0	99.5	71.2	56.8	62.1	29.2	37.0		69.9	65.6	69.2	70.1
0.157	165.8	170.9	108.4	76.5	61.1	66.1	29.3	41.5		69.2	67.5	71.0	72.0
0.160	179.5	185.0	118.6	82.9	66.8	71.1	30.7	47.0		68.3	70.3	74.7	75.7
0.161	193.7	199.3	129.1	89.7	73.4	76.2	32.7	54.4		67.5	72.9	79.1	80.3
0.163	208.8	214.8	140.5	97.0	81.0	82.2	35.8	65.9		67.1	75.8	84.1	85.4
0.165	224.1	230.3	151.6	103.9	88.8	87.9	38.9	74.4		67.0	78.5	88.5	90.0
0.167	239.8	246.3	161.7	110.7	96.7	94.0	42.2	81.4		67.2	81.7	92.8	94.5
0.169	255.6	261.8	171.0	117.4	104.8	100.5	46.4	87.6		68.6	85.7	97.7	99.6
0.171	271.5	277.5	181.0	125.4	113.9	108.6	52.9	94.0		72.3	92.0	104.8	107.0
0.174	287.1	293.0	192.4	135.0	124.5	118.8	62.3	101.6		78.2	101.0	115.1	117.5
0.175	302.3	308.2	204.6	145.9	136.0	130.2	74.1	110.4		85.8	112.0	128.4	131.1
0.177	317.0	323.0	216.8	157.6	148.4	142.4	87.7	120.2		94.6	124.6	143.0	146.3
0.179	330.9	336.9	228.4	168.8	160.3	154.4	101.7	129.4		103.8	138.1	157.8	161.6
0.181	344.4	350.0	240.0	180.5	172.6	166.7	116.6	139.1		113.9	153.2	173.4	177.8
0.183	356.6	361.6	252.6	193.7	186.2	180.5	133.2	150.7		126.7	170.4	190.8	195.6
0.185	368.5	373.2	266.0	208.4	201.4	196.0	151.4	164.2		142.3	189.7	209.9	215.5
0.188	379.0	383.5	277.6	221.8	215.6	210.6	168.5	177.5		158.3	208.4	228.5	234.7
0.189	389.0	393.2	288.3	234.8	229.3	225.0	185.0	191.2		175.5	226.7	246.9	253.7
0.191	398.0	401.8	298.4	246.9	242.2	238.6	200.6	205.2		193.6	244.4	264.8	272.3
0.193	406.5	410.3	308.7	259.5	255.1	252.4	216.0	220.6		213.2	262.4	282.8	291.2
0.195	414.1	417.9	318.5	271.5	267.6	265.5	230.4	236.5		232.8	279.9	300.2	309.2
0.197	421.6	425.3	328.3	283.3	279.9	277.9	244.2	253.0		252.2	296.8	316.9	326.6
0.199	428.3	431.9	337.2	294.5	291.4	289.4	257.0	269.2		270.5	312.6	332.0	342.4
0.201	434.9	438.5	345.7	305.3	302.7	300.4	269.7	285.8		288.0	327.6	346.0	357.1

Table 7.1-6. DM-9 Pressure Distribution Summary at Test Condition (64°F)
Ignition: Caveny Kuo (cont)

TIME	HEAD-END PRESSURE (489.9)	X LOCATIONS (INCHES) 530.0	689.3	851.2	1012.1	1171.2	1332.1	1491.2	1511.0	1577.5	1697.5	1816.7	NOZZLE STAGNATION PRESSURE
0.203	440.8	444.4	353.5	315.5	313.3	310.8	282.5	302.1		304.3	341.1	358.3	370.0
0.205	446.7	450.2	361.5	325.9	323.8	321.0	296.0	318.4		319.9	353.8	369.7	382.0
0.207	452.2	455.7	369.3	335.9	334.0	331.1	310.4	334.4		334.5	365.5	380.0	392.9
0.209	457.8	461.1	377.2	346.0	343.9	341.4	325.6	349.5		348.2	376.0	389.7	403.0
0.211	463.1	466.4	384.9	355.6	353.5	351.8	341.3	363.6		360.3	385.5	398.4	412.4
0.213	468.4	471.7	392.7	365.2	362.9	362.8	357.4	375.9		371.1	394.3	406.5	420.9
0.215	473.7	476.9	400.2	374.3	372.3	374.3	373.2	386.7		380.4	402.3	413.9	428.8
0.217	478.9	481.9	407.9	383.2	382.0	386.5	388.2	396.3		388.9	409.9	421.0	436.3
0.219	484.2	487.0	415.7	392.5	392.4	399.8	402.1	405.2		397.1	417.4	428.0	443.8
0.221	489.6	492.2	423.7	402.0	403.7	413.7	414.3	413.6		405.0	424.8	434.7	451.0
0.223	495.2	497.6	431.5	411.7	416.0	427.4	425.1	421.3		412.6	432.0	441.3	458.0
0.225	500.9	503.1	439.3	421.6	429.0	440.5	434.4	428.5		419.7	438.8	447.6	464.6
0.227	506.7	508.7	447.5	432.5	442.8	452.8	442.8	435.6		426.7	445.5	453.8	471.2
0.229	512.8	514.6	456.0	444.2	456.8	463.8	450.8	442.6		433.7	451.9	460.0	477.9
0.231	519.0	520.7	465.3	457.0	470.5	473.8	458.7	449.7		440.8	458.5	466.3	484.5
0.234	525.4	527.1	474.9	470.3	483.0	482.3	466.0	456.4		447.5	464.7	472.1	490.7
0.235	532.2	533.7	485.0	483.5	493.8	489.8	472.8	462.9		453.7	470.7	477.7	496.7
0.237	539.0	540.5	495.3	495.8	502.8	496.3	478.9	468.5		459.2	475.9	482.7	501.9
0.239	546.1	547.5	505.9	506.7	510.1	501.9	484.3	473.5		464.2	480.7	487.2	506.8
0.241	553.4	554.5	516.1	515.7	515.8	506.6	489.0	477.5		468.3	484.5	490.9	510.8
0.243	560.8	561.8	525.3	523.1	520.6	510.7	492.9	481.0		471.8	487.8	494.1	514.3
0.245	568.3	569.1	533.7	529.0	524.9	514.3	496.4	483.9		474.7	490.6	496.9	517.4
0.248	576.1	576.5	541.5	534.3	529.0	518.0	499.8	487.0		477.7	493.5	499.7	520.4
0.249	583.8	584.0	548.5	539.2	533.0	521.5	503.1	489.9		480.7	496.4	502.5	523.4
0.251	591.7	591.4	555.2	544.3	537.4	525.4	506.8	493.2		484.1	499.7	505.7	526.8
0.253	599.4	598.9	562.1	550.3	542.7	530.0	511.3	497.4		488.3	503.8	509.5	531.0
0.255	607.0	606.7	569.3	556.8	548.5	535.2	516.2	502.0		493.0	508.3	513.9	535.7
0.257	614.7	614.4	576.1	563.1	554.2	540.4	521.0	506.5		497.4	512.6	518.2	540.1
0.259	622.1	621.8	582.4	569.2	559.9	545.4	525.6	510.8		501.7	516.8	522.2	544.4
0.262	629.5	629.1	589.2	575.5	565.8	550.9	530.7	515.6		506.4	521.3	526.7	549.0
0.263	636.5	636.3	595.8	581.7	571.7	556.3	535.8	520.2		510.9	525.8	531.1	553.6
0.265	643.3	643.1	602.5	587.6	577.3	561.4	540.6	524.7		515.2	530.0	535.3	558.0
0.267	649.8	649.4	608.4	593.1	582.2	565.9	544.9	528.6		519.1	533.7	539.0	561.9
0.269	656.2	655.7	613.9	598.3	587.0	570.2	548.9	532.4		522.8	537.3	542.6	565.8
0.271	662.0	661.5	618.8	602.9	591.3	573.9	552.4	535.6		526.1	540.5	545.8	569.3
0.273	667.9	667.3	623.6	607.3	595.5	577.8	555.7	538.9		529.2	543.8	549.2	572.9
0.275	673.2	672.6	628.1	611.4	599.4	581.4	559.0	541.8		532.2	547.0	552.6	576.5
0.277	678.4	677.8	632.8	615.6	603.3	585.0	562.4	544.9		535.1	550.4	556.2	580.3
0.279	683.3	682.7	637.1	619.6	607.0	588.5	565.6	547.9		538.2	553.8	559.7	584.1
0.281	688.2	687.4	641.3	623.6	610.8	591.9	568.8	550.9		541.4	557.4	563.4	588.0
0.283	692.7	691.9	645.2	627.4	614.4	595.1	571.8	553.9		544.5	561.0	567.0	591.9
0.285	697.2	696.3	649.1	631.0	618.0	598.5	574.8	556.9		547.8	564.7	570.9	596.1
0.287	701.4	700.6	652.7	634.6	621.4	601.6	577.7	559.9		551.1	568.3	574.8	600.3
0.289	705.6	704.7	656.4	638.0	624.7	604.7	580.8	563.0		554.4	572.2	578.9	604.7
0.291	709.6	708.7	659.8	641.3	627.8	607.7	583.8	566.3		557.8	576.1	582.9	609.0
0.293	713.6	712.7	663.3	644.4	630.8	610.7	586.8	569.5		561.2	580.0	586.9	613.3
0.295	717.4	716.6	666.3	647.1	633.6	613.3	589.4	572.4		564.4	583.7	590.7	617.4
0.297	721.1	720.5	669.2	649.7	636.0	615.7	591.9	575.2		567.6	587.3	594.4	621.3

Table 7.1-6. DM-9 Pressure Distribution Summary at Test Condition (64°F)
Ignition: Caveny Kuo (cont)

TIME	HEAD-END PRESSURE (489.9)	X LOCATIONS (INCHES) 530.0	689.3	851.2	1012.1	1171.2	1332.1	1491.2	1511.0	1577.5	1697.5	1816.7	NOZZLE STAGNATION PRESSURE
0.299	724.9	724.2	672.1	652.1	638.3	617.9	594.3	577.8		570.5	590.7	597.9	625.2
0.301	728.5	727.9	674.9	654.5	640.6	620.2	596.6	580.4		573.4	594.1	601.4	629.0
0.303	732.1	731.7	677.7	657.0	642.8	622.3	598.8	582.9		576.1	597.4	604.7	632.6
0.305	735.6	735.3	680.5	659.5	645.3	624.5	601.1	585.4		578.9	600.6	608.0	636.2
0.308	739.0	738.7	683.3	662.0	647.7	626.8	603.4	587.9		581.7	603.8	611.1	639.6
0.309	742.4	742.0	686.2	664.8	650.4	629.4	606.0	590.7		584.7	606.9	614.4	643.1
0.311	745.9	745.2	689.1	667.6	653.2	632.1	608.7	593.5		587.7	610.1	617.5	646.5
0.313	749.2	748.3	691.8	670.6	656.1	634.9	611.6	596.4		590.7	613.2	620.6	649.9
0.323	765.0	766.7	709.9	687.7	675.1	656.7	633.3	619.7		613.1	635.0	643.1	673.9
0.333	779.6	780.7	724.7	702.1	689.2	669.2	645.9	631.9		626.6	651.0	660.0	692.5
0.343	793.3	793.4	738.6	717.7	706.0	686.1	662.7	648.5		643.0	666.0	673.5	707.2
0.353	806.0	805.1	753.2	733.3	721.5	701.4	678.8	663.2		657.2	681.8	690.5	725.8
0.363	817.4	815.4	766.5	748.4	737.3	716.5	692.7	676.9		671.7	696.2	704.0	740.6
0.373	828.2	825.5	780.0	763.2	751.5	729.9	706.7	690.4		684.9	709.4	717.3	755.1
0.383	837.8	834.9	791.3	775.2	763.5	741.8	718.5	701.3		695.9	720.2	727.5	766.2
0.393	846.9	843.9	801.7	786.4	774.4	751.9	728.7	710.5		704.7	728.7	735.5	775.0
0.403	854.9	851.9	810.8	796.3	784.1	761.0	737.4	717.8		711.5	734.8	741.2	781.1
0.413	862.5	859.3	818.5	804.3	791.6	767.6	743.3	722.7		715.9	738.9	745.1	785.4
0.423	869.1	865.8	825.2	810.8	797.2	772.1	747.3	726.1		719.1	741.9	748.0	788.6
0.433	875.2	872.6	830.2	815.1	800.9	775.2	750.2	728.5		721.3	743.9	749.8	790.7
0.443	880.8	878.5	835.1	819.8	805.4	779.0	753.6	731.5		724.3	746.9	752.8	794.0
0.453	885.7	883.9	840.1	824.9	810.8	784.3	758.9	736.7		729.5	752.1	757.9	799.5
0.463	890.1	888.4	844.3	829.2	815.4	789.2	764.0	742.0		735.0	757.9	763.9	805.9
0.473	894.1	892.5	847.7	832.6	818.8	792.6	767.9	746.1		739.3	762.3	768.2	810.6
0.484	897.7	895.8	851.0	835.9	822.3	796.3	771.8	749.9		742.8	765.4	771.3	814.0
0.493	900.9	898.8	854.0	839.3	826.0	800.1	775.6	753.5		746.3	768.8	774.6	817.5
0.503	903.6	901.4	856.5	841.9	828.5	802.5	778.1	755.9		748.8	771.5	777.4	820.5
0.513	906.0	903.6	858.6	843.6	830.1	803.9	779.5	757.3		750.4	772.9	778.7	821.9
0.523	908.1	905.5	860.2	845.1	831.5	805.2	780.9	758.5		751.4	773.8	779.6	823.0
0.533	910.0	907.2	862.0	846.7	833.3	807.1	782.7	760.0		753.0	775.4	781.3	824.8
0.543	911.5	908.6	863.3	848.1	834.8	808.5	784.2	761.6		754.7	777.3	783.2	826.8
0.553	912.9	909.9	864.6	849.4	836.1	809.9	785.8	763.3		756.4	779.2	785.1	828.9
0.563	914.0	911.0	865.8	850.6	837.5	811.4	787.5	765.0		758.1	780.9	786.7	830.6
0.573	915.0	911.9	866.8	851.7	838.7	812.6	788.9	766.3		759.4	782.2	788.0	832.0
0.583	915.8	912.6	867.7	852.5	839.5	813.3	789.6	767.0		760.1	782.9	788.6	832.6
0.593	916.4	913.2	868.3	853.0	840.0	813.8	790.0	767.3		760.4	783.1	788.8	832.8

Table 7.1-6. DM-9 Pressure Distribution Summary at Test Condition (64°F)
Steady State: SCB04 1-D Mass Addition (cont)

	X LOCATIONS (INCHES)											
TIME	HEAD-END PRESSURE (489.9)	530.0	689.3	851.2	1012.1	1171.2	1332.1	1491.2	1511.0	1577.5	1697.5	1816.7	NOZZLE STAGNATION PRESSURE
0.6	916.8	915.5	868.6	853.2	840.1	813.9	790.1	767.4	760.8	760.5	783.1	789.8	832.9
0.8	914.4	913.3	870.0	855.4	842.7	818.4	794.8	774.0	767.1	766.8	788.5	794.8	828.3
1.0	912.0	910.9	869.5	855.4	843.1	820.0	796.8	777.0	770.1	769.7	790.6	796.7	820.6
2.0	903.0	902.1	865.2	851.8	840.0	819.4	796.2	778.0	770.8	770.2	789.6	795.2	819.9
3.0	899.2	898.4	864.9	852.2	840.8	821.2	799.1	782.0	774.8	774.2	792.2	797.4	823.0
4.0	898.5	897.8	867.2	855.0	844.0	824.4	803.9	787.8	780.6	779.8	796.8	801.8	828.3
5.0	901.6	901.0	872.6	860.7	850.1	830.7	811.6	796.0	789.1	788.2	804.2	809.0	836.6
6.0	906.7	906.1	879.8	868.3	858.1	838.7	820.8	805.7	799.0	798.1	813.3	817.7	846.5
7.0	909.3	908.8	884.6	873.5	863.7	844.8	828.0	813.7	807.1	806.1	820.2	824.3	852.1
8.0	907.7	907.3	885.1	874.6	865.2	846.8	831.2	817.3	811.0	810.0	823.1	826.9	853.4
9.0	906.0	905.6	885.2	875.2	866.2	848.4	833.6	820.3	814.4	813.2	825.2	828.8	854.4
10.0	905.2	904.8	886.2	876.5	867.8	850.9	836.8	823.9	818.3	817.0	828.2	831.6	856.0
12.0	897.6	897.3	881.6	872.8	864.8	849.2	836.6	824.6	819.7	818.3	827.9	830.6	852.8
14.0	893.5	893.2	879.8	871.8	864.3	849.9	838.5	827.4	823.1	821.6	829.8	832.1	852.2
16.0	888.2	888.0	876.3	869.0	862.1	848.9	838.5	828.1	824.3	822.7	829.8	831.7	850.0
18.0	886.2	886.0	876.0	869.3	862.8	850.7	841.2	831.4	827.9	826.3	832.5	834.0	850.4
20.0	881.9	881.8	873.0	866.9	860.9	849.9	841.0	831.8	828.7	827.1	832.4	833.7	848.3
22.0	870.2	870.1	863.2	857.8	852.1	842.1	833.9	825.2	822.5	820.9	825.0	825.9	838.8
24.0	836.1	836.0	830.7	826.0	820.9	812.1	804.6	796.5	794.2	792.4	795.8	796.3	808.0
26.0	806.5	806.4	802.3	798.2	793.7	785.8	778.9	771.5	769.5	767.7	770.3	770.5	781.1
28.0	781.5	781.4	778.3	774.7	770.6	763.5	757.3	750.3	748.5	746.8	748.8	748.8	758.5
30.0	759.4	759.4	757.0	753.9	750.1	743.9	738.0	731.5	730.0	728.3	729.6	729.5	738.5
32.0	738.5	738.5	736.8	734.0	730.7	725.0	719.7	713.5	712.2	710.5	711.4	711.2	719.6
34.0	719.4	719.4	718.1	715.6	712.5	707.5	702.6	696.9	695.7	693.9	694.6	694.2	701.9
36.0	701.6	701.6	700.6	698.6	695.8	691.2	686.6	681.3	680.2	678.6	678.9	678.4	685.6
38.0	684.0	684.0	683.4	681.6	679.2	675.1	670.7	665.7	664.7	663.2	663.3	662.7	669.4
40.0	667.0	667.0	666.6	665.1	663.0	659.3	655.3	650.7	649.8	648.2	648.1	647.4	653.7
42.0	652.5	652.5	652.3	651.0	649.0	645.7	642.0	637.6	636.8	635.4	635.2	634.4	640.2
44.0	641.2	641.2	641.1	640.0	638.2	635.2	631.7	627.6	626.9	625.4	625.1	624.3	629.9
46.0	631.9	631.9	631.8	630.9	629.3	626.5	623.1	619.3	618.6	617.2	616.8	616.0	621.3
48.0	619.2	619.2	619.2	618.5	617.0	614.5	611.4	607.7	607.1	605.7	605.2	604.3	609.4
50.0	604.4	604.4	604.4	603.7	602.3	599.9	596.9	593.5	592.9	591.6	591.1	590.3	595.1
52.0	601.9	601.9	601.8	601.2	599.9	597.7	594.9	591.6	591.0	589.8	589.2	588.4	593.0
54.0	604.7	604.7	604.6	604.1	602.7	600.5	597.9	594.7	594.2	593.1	592.5	591.7	596.1
56.0	610.1	610.1	610.0	609.5	608.3	606.2	603.7	600.6	600.1	599.0	598.4	597.6	601.9
58.0	615.7	615.7	615.6	615.1	614.0	612.0	609.6	606.7	606.3	605.2	604.6	603.7	607.9
60.0	619.7	619.7	619.6	619.1	618.0	616.2	613.8	611.1	610.7	609.6	609.0	608.2	612.2
62.0	627.4	627.4	627.4	626.9	625.7	624.0	621.7	619.1	618.7	617.6	617.0	616.2	620.2
64.0	628.4	628.4	628.4	628.0	627.0	625.2	623.0	620.5	620.2	619.1	618.5	617.8	621.5
66.0	635.3	635.3	635.3	634.9	633.9	632.3	630.2	627.8	627.5	626.5	625.8	625.0	628.8
68.0	638.9	639.0	638.9	638.5	637.6	636.1	634.0	631.8	631.5	630.5	629.9	629.1	632.7
70.0	641.6	641.6	641.6	641.2	640.3	638.8	636.9	634.7	634.4	633.5	632.8	632.1	635.6
72.0	646.5	646.5	646.5	646.1	645.3	643.9	642.0	639.9	639.6	638.7	638.0	637.4	640.7
74.0	645.2	645.2	645.2	644.9	644.0	642.8	640.9	639.0	638.7	637.9	637.2	636.5	639.7
76.0	645.0	645.0	645.0	644.7	643.9	642.6	640.9	639.0	638.7	637.9	637.2	636.6	639.7
78.0	643.9	643.9	643.9	643.6	642.8	641.6	639.9	638.0	637.8	637.0	636.3	635.8	638.8
80.0	623.7	623.7	623.7	623.4	622.6	621.5	619.8	618.0	617.8	617.1	616.3	616.0	618.9
82.0	611.4	611.4	611.4	611.1	610.3	609.2	607.6	605.9	605.7	604.9	604.2	604.0	606.8

Table 7.1-6. DM-9 Pressure Distribution Summary at Test Condition (64°F)
Steady State: SCB04 1-D Mass Addition (cont)

TIME	HEAD-END PRESSURE (489.9)	X LOCATIONS (INCHES) 530.0	689.3	851.2	1012.1	1171.2	1332.1	1491.2	1511.0	1577.1	1697.5	1816.7	NOZZLE STAGNATION PRESSURE
84.0	597.4	597.5	597.4	597.2	596.4	595.4	593.8	592.1	591.9	591.2	590.5	590.3	593.1
86.0	576.1	576.1	576.1	575.8	575.1	574.1	572.6	571.0	570.8	570.1	569.4	569.3	572.1
88.0	554.9	554.9	554.9	554.7	554.0	553.0	551.6	550.0	549.9	549.2	548.5	548.5	551.1
90.0	546.7	546.7	546.7	546.5	545.8	544.9	543.5	542.0	541.8	541.1	540.5	540.5	543.1
92.0	535.6	535.6	535.6	535.2	534.6	533.7	532.3	530.9	530.8	530.1	529.5	529.5	532.0
94.0	525.2	525.2	525.2	525.0	524.4	523.5	522.1	520.8	520.6	519.9	519.5	519.5	522.0
96.0	506.7	506.7	506.7	506.5	505.9	505.1	503.8	502.5	502.3	501.7	501.3	501.3	503.7
98.0	496.2	496.2	496.2	496.0	495.4	494.7	493.3	492.1	491.9	491.4	491.0	491.0	493.3
100.0	480.8	480.8	480.8	480.6	480.1	479.3	478.0	476.8	476.7	476.1	475.8	475.8	478.1
100.4	478.0	478.0	478.0	477.8	477.2	476.5	475.2	474.0	473.9	473.3	473.1	473.1	475.3
100.8	475.1	475.1	475.1	474.9	474.3	473.6	472.3	471.2	471.1	470.4	470.2	470.2	472.4
101.2	471.9	471.9	471.9	471.8	471.2	470.5	469.2	468.0	467.9	467.3	467.1	467.1	469.3
101.6	468.9	468.9	468.9	468.7	468.1	467.4	466.1	464.9	464.8	464.2	464.0	464.0	466.2
102.0	466.0	466.0	466.0	465.8	465.3	464.6	463.3	462.2	462.1	461.5	461.3	461.3	463.4
102.4	463.6	463.6	463.6	463.4	462.8	462.1	460.9	459.7	459.7	459.0	458.9	458.9	461.0
102.8	461.1	461.1	461.1	460.9	460.4	459.7	458.5	457.3	457.2	456.6	456.5	456.5	458.6
103.2	458.0	458.0	458.0	457.9	457.3	456.6	455.4	454.2	454.2	453.5	453.4	453.4	455.5
103.6	453.9	453.9	453.9	453.7	453.2	452.5	451.3	450.1	450.1	449.5	449.4	449.4	451.5
104.0	449.0	449.0	449.0	448.8	448.3	447.6	446.4	445.3	445.2	444.6	444.5	444.5	446.6
104.4	444.2	444.2	444.2	444.0	443.4	442.8	441.6	440.4	440.4	439.8	439.7	439.7	441.8
104.8	440.2	440.2	440.2	440.1	439.5	438.9	437.7	436.5	436.5	435.9	435.8	435.8	437.9
105.2	437.7	437.7	437.7	437.5	437.0	436.3	435.1	434.0	434.0	433.4	433.3	433.3	435.4
105.6	435.7	435.7	435.7	435.5	435.0	434.3	433.1	432.0	432.0	431.4	431.4	431.4	433.4
106.0	433.2	433.2	433.2	433.1	432.5	431.9	430.7	429.6	429.6	428.9	428.9	428.9	431.0
106.4	429.9	429.9	429.9	429.8	429.2	428.6	427.4	426.3	426.3	425.6	425.6	425.6	427.7
106.8	426.5	426.5	426.5	426.4	425.8	425.2	424.0	422.9	422.8	422.2	422.2	422.2	424.3
107.2	424.0	424.0	424.0	423.8	423.3	422.6	421.4	420.3	420.2	419.7	419.7	419.7	421.7
107.6	422.5	422.5	422.5	422.3	421.7	421.0	419.9	418.8	418.7	418.2	418.2	418.2	420.2
108.0	421.2	421.2	421.2	420.9	420.4	419.7	418.6	417.5	417.4	416.9	416.9	416.9	418.9
108.4	419.1	419.1	419.1	419.0	418.4	417.8	416.6	415.6	415.5	415.0	415.0	415.0	417.0
108.8	416.2	416.2	416.2	416.1	415.6	414.9	413.8	412.8	412.7	412.2	412.2	412.2	414.2
109.2	412.8	412.8	412.8	412.6	412.1	411.5	410.3	409.3	409.2	408.8	408.8	408.8	410.7
109.6	409.0	409.0	409.0	408.8	408.3	407.7	406.5	405.4	405.4	405.0	405.0	405.0	407.0
110.0	403.4	403.4	403.4	403.3	402.8	402.1	400.9	399.8	399.8	399.5	399.5	399.5	401.5
110.4	394.0	394.0	394.0	393.8	393.3	392.6	391.5	390.4	390.4	390.2	390.2	390.2	392.0
110.8	380.5	380.5	380.5	380.4	379.8	379.2	378.1	377.0	377.0	376.9	376.9	376.9	378.7
111.2	363.5	363.5	363.5	363.4	362.8	362.3	361.2	360.2	360.2	360.1	360.1	360.1	361.8
111.6	343.5	343.5	343.5	343.4	342.9	342.4	341.3	340.3	340.3	340.3	340.3	340.3	341.9
112.0	321.0	321.0	321.0	320.9	320.4	319.9	318.9	318.0	318.0	318.0	318.0	318.0	319.6
112.4	297.3	297.3	297.3	297.1	296.6	296.2	295.2	294.5	294.5	294.5	294.5	294.5	295.9
112.8	273.9	273.9	273.9	273.7	273.3	273.0	272.0	271.3	271.3	271.3	271.3	271.3	272.6
113.2	251.3	251.3	251.3	251.2	250.7	250.5	249.6	249.1	249.1	249.1	249.1	249.1	250.2
113.6	229.4	229.5	229.5	229.3	228.8	228.7	227.8	227.4	227.4	227.4	227.4	227.4	228.4
114.0	208.9	208.9	208.9	208.7	208.2	208.1	207.2	206.9	206.9	206.9	206.9	206.9	207.9
114.4	190.5	190.5	190.5	190.4	189.9	189.9	188.9	188.7	188.7	188.7	188.7	188.7	189.7
114.8	175.4	175.4	175.4	175.3	174.8	174.8	173.9	173.8	173.8	173.8	173.8	173.8	174.6
115.2	163.4	163.4	163.4	163.3	162.8	162.8	162.0	161.9	161.9	161.9	161.9	161.9	162.7
115.6	152.8	152.8	152.8	152.7	152.3	152.3	151.4	151.4	151.4	151.4	151.4	151.4	152.1

Table 7.1-6. DM-9 Pressure Distribution Summary at Test Condition (64°F)
Steady State: SCB04 1-D Mass Addition (cont)

TIME	X LOCATIONS (INCHES)												
	HEAD-END PRESSURE (489.9)	530.0	689.3	851.2	1012.1	1171.2	1332.1	1491.2	1511.0	1577.5	1697.5	1816.7	NOZZLE STAGNATION PRESSURE
116.0	141.0	141.0	141.0	140.9	140.5	140.5	139.6	139.7	139.7	139.7	139.7	139.7	140.3
116.4	127.3	127.3	127.3	127.2	126.9	126.9	126.2	126.2	126.2	126.2	126.2	126.2	126.8
116.8	113.7	113.7	113.7	113.6	113.3	113.3	112.7	112.7	112.7	112.7	112.7	112.7	113.2
117.2	101.6	101.6	101.6	101.5	101.3	101.2	100.7	100.7	100.7	100.7	100.7	100.7	101.2
117.6	91.5	91.5	91.5	91.4	91.2	91.2	90.7	90.7	90.7	90.7	90.7	90.7	91.1
118.0	83.1	83.1	83.1	83.0	82.8	82.8	82.3	82.3	82.3	82.3	82.3	82.3	82.7
118.4	75.6	75.6	75.6	75.5	75.3	75.3	74.9	74.9	74.9	74.9	74.9	74.9	75.2
118.8	68.7	68.7	68.7	68.6	68.4	68.4	68.1	68.1	68.1	68.1	68.1	68.1	68.4
119.2	62.1	62.1	62.1	62.0	61.9	61.9	61.5	61.5	61.5	61.5	61.5	61.5	61.8
119.6	55.6	55.6	55.6	55.4	55.3	55.3	55.0	55.0	55.0	55.0	55.0	55.0	55.3
120.0	49.2	49.2	49.2	49.1	49.0	49.0	48.7	48.7	48.7	48.7	48.7	48.7	49.0

Table 7.1-7. DM-9 Pressure Distribution Summary (60°F)
Ignition: Caveny Kuo

TIME	HEAD-END PRESSURE (489.9)	X LOCATIONS (INCHES) 530.0	689.3	851.2	1012.1	1171.2	1332.1	1491.2	1511.0	1577.5	1697.5	1816.7	NOZZLE STAGNATION PRESSURE
0.000	11.5	11.5	11.5	11.5	11.5	11.6	11.4	11.5		11.4	11.4	11.4	11.5
0.000	11.6	11.6	11.6	11.6	11.6	11.7	11.5	11.6		11.5	11.5	11.5	11.6
0.002	12.7	12.5	12.3	12.3	12.3	12.4	12.2	12.3		12.2	12.2	12.2	12.3
0.004	14.0	13.7	13.3	13.3	13.3	13.4	13.2	13.3		13.2	13.2	13.2	13.3
0.006	13.8	13.6	13.2	13.1	13.1	13.2	13.0	13.1		13.0	13.0	13.0	13.1
0.008	13.7	13.5	13.0	12.9	12.9	13.0	12.8	12.9		12.8	12.8	12.8	12.9
0.010	13.2	13.1	12.6	12.4	12.4	12.5	12.3	12.3		12.2	12.2	12.3	12.4
0.012	12.7	12.6	12.2	11.9	11.8	11.9	11.7	11.8		11.7	11.7	11.7	11.8
0.014	12.5	12.4	12.0	11.6	11.6	11.7	11.4	11.5		11.4	11.4	11.5	11.6
0.016	12.2	12.1	11.8	11.4	11.2	11.3	11.1	11.2		11.1	11.1	11.1	11.2
0.018	12.5	12.4	12.1	11.6	11.4	11.5	11.3	11.4		11.3	11.3	11.3	11.4
0.020	12.8	12.6	12.4	11.8	11.5	11.6	11.4	11.5		11.3	11.3	11.4	11.5
0.022	13.6	13.4	13.1	12.4	12.1	12.2	11.9	12.0		11.9	11.9	12.0	12.1
0.024	14.3	14.1	13.7	12.9	12.6	12.6	12.3	12.4		12.3	12.3	12.3	12.4
0.026	15.4	15.2	14.7	13.8	13.3	13.3	13.0	13.1		13.0	13.0	13.1	13.2
0.028	16.5	16.2	15.6	14.6	14.0	13.9	13.6	13.7		13.6	13.6	13.6	13.7
0.030	17.8	17.5	16.9	15.6	14.8	14.7	14.4	14.5		14.4	14.4	14.4	14.5
0.032	19.0	18.7	18.1	16.6	15.6	15.4	15.1	15.2		15.1	15.1	15.1	15.2
0.034	20.2	20.0	19.6	17.7	16.5	16.2	15.8	15.9		15.8	15.8	15.8	15.9
0.036	21.4	21.2	21.1	19.0	17.4	17.0	16.6	16.7		16.4	16.5	16.6	16.7
0.038	22.5	22.4	22.5	20.3	18.3	17.7	17.3	17.3		17.1	17.2	17.2	17.3
0.040	23.6	23.6	24.1	21.8	19.4	18.6	18.0	18.0		17.8	17.9	17.9	18.0
0.042	24.4	24.5	25.5	23.3	20.4	19.3	18.6	18.6		18.4	18.5	18.5	18.6
0.044	25.3	25.6	27.0	25.0	21.8	20.2	19.4	19.4		19.1	19.2	19.2	19.3
0.046	25.9	26.3	28.2	26.5	23.1	21.0	20.0	19.9		19.7	19.7	19.8	19.9
0.048	26.5	27.1	29.4	28.1	24.7	22.0	20.7	20.5		20.3	20.4	20.4	20.5
0.063	28.2	28.9	31.6	30.6	27.4	24.2	22.5	22.2		21.9	21.9	22.0	22.1
0.065	28.3	29.4	32.4	31.7	29.1	25.2	23.0	22.6		22.3	22.3	22.3	22.4
0.067	28.4	29.7	32.7	32.2	30.4	25.9	23.2	22.6		22.3	22.2	22.3	22.4
0.069	28.5	30.1	32.9	32.6	31.5	26.9	23.5	22.7		22.3	22.2	22.3	22.4
0.071	28.7	30.5	33.1	32.8	32.4	28.1	23.8	22.7		22.2	22.1	22.2	22.3
0.073	29.0	30.9	33.3	33.1	33.0	29.7	24.3	22.8		22.3	22.1	22.1	22.2
0.075	29.4	31.2	33.5	33.3	33.5	31.1	25.0	22.9		22.3	22.0	22.1	22.2
0.077	29.8	31.6	33.8	33.7	33.7	32.7	26.0	23.2		22.5	22.2	22.2	22.3
0.079	30.4	32.0	34.2	34.2	34.1	34.0	27.5	23.7		22.8	22.4	22.3	22.4
0.081	31.1	32.6	34.9	34.8	34.8	35.2	29.4	24.6		23.4	22.8	22.8	22.9
0.083	31.9	33.3	35.6	35.4	35.6	36.2	31.5	25.7		24.2	23.4	23.3	23.4
0.086	32.9	33.2	35.0	34.9	35.1	35.7	32.3	25.8		23.8	22.7	22.5	22.6
0.087	33.9	31.3	31.8	31.6	31.9	32.5	30.1	23.5		20.9	19.5	19.1	19.2
0.089	35.0	31.0	30.9	30.5	30.7	31.4	29.6	23.5		20.3	18.4	17.7	17.8
0.091	36.3	31.9	31.4	30.5	30.6	31.2	29.8	24.7		21.0	18.4	17.5	17.6
0.093	37.6	33.3	31.7	30.0	29.9	30.4	29.1	25.3		21.2	17.8	16.6	16.7
0.095	39.0	34.7	32.5	30.3	29.7	29.9	28.6	26.1		21.9	17.7	16.0	16.1
0.097	40.5	36.1	33.4	31.1	29.9	29.7	28.2	26.7		22.9	18.0	15.8	15.9
0.100	42.0	37.7	34.1	32.2	30.6	29.6	28.0	27.1		23.9	18.6	15.8	15.9
0.101	43.6	39.3	34.7	33.2	31.8	30.0	27.9	27.3		24.8	19.4	16.0	16.1
0.103	45.2	40.9	35.8	33.9	32.9	30.7	28.0	27.2		25.2	20.3	16.5	16.6
0.105	46.9	42.5	36.5	34.2	33.4	31.3	27.8	26.5		24.8	20.6	16.8	16.9

Table 7.1-7. DM-9 Pressure Distribution Summary (60°F)
Ignition: Caveny Kuo (cont)

TIME	HEAD-END PRESSURE (489.9)	X LOCATIONS (INCHES) 530.0	689.3	851.2	1012.1	1171.2	1332.1	1491.2	1511.0	1577.5	1697.5	1816.7	NOZZLE STAGNATION PRESSURE
0.107	48.5	44.3	36.0	34.2	33.0	31.3	27.5	25.4		23.5	20.1	16.9	17.0
0.109	50.2	46.1	35.4	33.8	32.4	31.0	27.3	24.1		21.9	19.2	17.3	17.4
0.111	51.9	47.8	34.9	33.0	31.9	30.4	27.2	23.1		20.3	18.0	17.9	18.0
0.113	53.6	49.6	34.6	32.4	31.3	30.0	27.0	22.7		19.1	16.7	18.7	18.8
0.115	55.3	51.4	34.3	32.0	30.7	29.7	26.7	22.7		18.4	15.6	19.5	19.7
0.117	57.1	53.3	34.1	31.5	30.3	29.3	26.3	22.8		18.3	14.9	20.3	20.4
0.119	58.9	55.3	33.9	31.1	30.0	29.0	25.9	22.8		18.4	14.8	21.0	21.1
0.121	60.8	57.5	33.8	30.5	29.6	28.8	25.4	22.4		18.5	15.2	21.9	22.0
0.123	62.8	59.7	33.7	30.0	29.2	28.7	25.1	21.9		[illegible]	16.2	23.4	23.5
0.125	64.9	62.0	33.7	29.4	28.8	28.5	24.6	21.3		[illegible]	17.4	25.9	26.1
0.127	67.2	64.5	33.9	28.9	28.4	28.3	24.2	20.8		[illegible]	18.6	29.9	30.3
0.129	69.6	67.2	34.2	28.5	28.1	28.1	23.7	20.3		[illegible]	19.6	35.3	35.7
0.131	72.3	70.2	34.8	28.3	28.0	28.1	23.3	19.8		[illegible]	21.2	41.3	41.8
0.133	75.3	73.5	35.5	28.2	27.9	28.2	22.9	19.4		[illegible]	23.5	46.4	47.0
0.135	78.8	77.3	36.8	28.5	28.2	28.7	22.8	19.2		[illegible]	27.7	50.2	50.7
0.137	82.5	81.4	38.4	29.0	28.7	29.5	22.9	19.2		[illegible]	33.5	52.2	52.7
0.139	87.1	86.3	41.3	30.2	29.8	30.8	23.6	19.9		[illegible]	41.2	53.7	54.2
0.141	92.0	91.8	45.4	32.9	31.8	32.4	24.4	20.7		[illegible]	49.6	55.0	55.5
0.143	98.0	98.4	52.5	36.6	33.7	34.9	25.7	22.2		[illegible]	57.2	57.3	57.8
0.146	104.5	105.6	59.6	40.4	36.3	37.2	26.8	23.4		[illegible]	61.8	59.6	60.3
0.147	112.3	114.1	67.3	47.2	40.2	41.6	27.8	25.2		[illegible]	63.5	62.2	62.9
0.149	120.6	123.2	74.5	53.4	44.6	47.8	27.9	27.2		[illegible]	63.1	63.9	64.5
0.151	130.5	133.7	82.4	59.6	48.5	53.2	28.7	30.4		[illegible]	63.2	65.8	66.5
0.153	140.8	144.9	90.2	65.1	52.0	57.4	28.7	33.1		[illegible]	63.5	67.1	67.9
0.155	152.7	157.6	99.1	70.9	56.5	61.8	29.0	36.9		[illegible]	65.3	69.0	69.8
0.157	165.0	170.6	107.9	76.2	60.8	65.8	29.1	41.3		[illegible]	67.2	70.8	71.7
0.160	178.7	184.6	118.1	82.6	66.5	70.8	30.5	46.8		[illegible]	70.0	74.5	75.4
0.161	192.9	198.9	128.6	89.3	73.1	75.9	32.5	54.2		[illegible]	72.6	78.8	79.9
0.163	207.9	214.3	139.8	96.6	80.7	81.8	35.6	65.6		[illegible]	75.5	83.8	85.0
0.165	223.1	229.8	150.9	103.5	88.4	87.5	38.8	74.0		[illegible]	78.1	88.2	89.6
0.167	238.8	245.7	161.0	110.2	96.3	93.6	42.1	81.0		[illegible]	81.3	92.4	94.1
0.169	254.5	261.2	170.2	116.9	104.3	100.0	46.2	87.2		[illegible]	85.3	97.4	99.2
0.171	270.3	276.8	180.2	124.8	113.4	108.2	52.7	93.5		[illegible]	91.6	104.5	106.5
0.174	285.8	292.4	191.6	134.4	123.9	118.3	62.0	101.1		[illegible]	100.6	114.7	117.0
0.175	300.9	307.5	203.7	145.3	135.4	129.6	73.8	109.9		[illegible]	111.5	127.9	130.6
0.177	315.7	322.3	215.9	156.9	147.8	141.7	87.3	119.6		[illegible]	124.0	142.5	145.6
0.179	329.5	336.2	227.4	168.1	159.6	153.7	101.2	128.8		[illegible]	137.5	157.3	160.9
0.181	342.9	349.2	238.9	179.7	171.8	165.9	116.1	138.5		[illegible]	152.5	172.9	177.0
0.183	355.1	360.8	251.5	192.8	185.4	179.7	132.6	150.0		[illegible]	169.6	190.2	194.8
0.185	366.9	372.3	264.8	207.5	200.5	195.1	150.7	163.5		[illegible]	188.9	209.2	214.6
0.188	377.3	382.6	276.4	220.9	214.7	209.7	167.7	176.7		[illegible]	207.4	227.7	233.7
0.189	387.3	392.4	287.1	233.8	228.3	223.9	184.2	190.4		[illegible]	225.7	246.1	252.6
0.191	396.2	401.0	297.1	245.8	241.1	237.5	199.7	204.2		[illegible]	243.3	263.9	271.1
0.193	404.7	409.4	307.4	258.3	254.0	251.3	215.0	219.6		[illegible]	261.3	281.9	289.9
0.195	412.3	417.0	317.1	270.3	266.4	264.2	229.3	235.4		[illegible]	278.6	299.2	307.9
0.197	419.7	424.4	326.8	282.1	278.7	276.6	243.1	251.8		[illegible]	295.5	315.8	325.2
0.199	426.5	431.0	335.7	293.2	290.2	288.1	255.8	268.0		[illegible]	311.2	330.9	340.9
0.201	433.0	437.5	344.2	304.0	301.3	299.0	268.5	284.5		[illegible]	326.1	344.8	355.5

Table 7.1-7. DM-9 Pressure Distribution Summary (60°F)
Ignition: Caveny Kuo (cont)

TIME	HEAD-END PRESSURE (489.9)	X LOCATIONS (INCHES) 530.0	689.3	851.2	1012.1	1171.2	1332.1	1491.2	1511.0	1577.5	1697.5	1816.7	NOZZLE STAGNATION PRESSURE
0.203	438.9	443.4	352.0	314.2	311.9	309.4	281.2	300.7		302.9	339.6	357.2	368.4
0.205	444.8	449.2	359.9	324.4	322.4	319.5	294.7	317.0		318.5	352.2	368.5	380.3
0.207	450.3	454.7	367.7	334.4	332.5	329.6	309.0	332.9		333.0	363.8	378.7	391.2
0.209	455.8	460.1	375.6	344.5	342.4	339.8	324.1	347.9		346.6	374.4	388.4	401.3
0.211	461.1	465.4	383.3	354.1	352.0	350.2	339.8	361.9		358.7	383.8	397.1	410.6
0.213	466.4	470.6	391.0	363.6	361.3	361.1	355.8	374.2		369.4	392.5	405.2	419.1
0.215	471.6	475.8	398.4	372.7	370.6	372.6	371.5	384.9		378.7	400.5	412.5	427.0
0.217	476.8	480.8	406.1	381.6	380.3	384.8	386.4	394.5		387.1	408.0	419.6	434.4
0.219	482.1	485.9	413.9	390.8	390.7	398.0	400.2	403.4		395.4	415.6	426.6	441.8
0.221	487.5	491.1	421.8	400.2	401.9	411.8	412.5	411.7		403.2	422.9	433.3	449.0
0.223	493.0	496.5	429.6	409.9	414.2	425.5	423.2	419.4		410.7	430.1	439.9	456.0
0.225	498.7	502.0	437.4	419.8	427.2	438.5	432.4	426.6		417.8	436.8	446.1	462.6
0.227	504.5	507.6	445.5	430.6	440.8	450.7	440.8	433.6		424.8	443.5	452.3	469.2
0.229	510.5	513.5	454.0	442.3	454.8	461.7	448.7	440.6		431.8	449.9	458.5	475.8
0.231	516.7	519.6	463.3	455.1	468.4	471.6	456.6	447.7		438.8	456.5	464.7	482.4
0.234	523.1	526.0	472.9	468.2	480.9	480.1	463.8	454.4		445.5	462.6	470.6	488.6
0.235	529.8	532.6	482.9	481.4	491.7	487.6	470.6	460.8		451.6	468.6	476.2	494.6
0.237	536.6	539.3	493.1	493.7	500.5	494.0	476.7	466.4		457.2	473.8	481.1	499.8
0.239	543.7	546.3	503.7	504.5	507.8	499.6	482.1	471.3		462.1	478.5	485.6	504.6
0.241	551.0	553.3	513.8	513.5	513.5	504.3	486.8	475.3		466.2	482.3	489.3	508.6
0.243	558.4	560.6	523.0	520.9	518.3	508.4	490.7	478.8		469.7	485.6	492.5	512.1
0.245	565.9	567.8	531.4	526.7	522.6	512.0	494.2	481.7		472.6	488.5	495.2	515.2
0.248	573.6	575.2	539.1	531.9	526.7	515.6	497.5	484.7		475.6	491.3	498.0	518.2
0.249	581.3	582.7	546.1	536.8	530.7	519.1	500.8	487.6		478.6	494.2	500.8	521.2
0.251	589.1	590.1	552.8	541.9	535.0	523.0	504.5	490.9		481.9	497.5	504.0	524.5
0.253	596.8	597.6	559.7	547.9	540.3	527.6	509.0	495.1		486.1	501.6	507.9	528.7
0.255	604.4	605.3	566.9	554.4	546.1	532.8	513.8	499.7		490.8	506.0	512.2	533.3
0.257	612.0	613.1	573.6	560.7	551.8	537.9	518.6	504.2		495.2	510.3	516.5	537.7
0.259	619.4	620.5	579.8	566.7	557.5	543.0	523.2	508.5		499.5	514.5	520.5	542.0
0.262	626.7	627.8	586.6	573.0	563.4	548.4	528.3	513.2		504.1	518.9	525.0	546.6
0.263	633.7	634.9	593.2	579.2	569.1	553.7	533.3	517.8		508.6	523.4	529.3	551.2
0.265	640.5	641.7	599.8	585.1	574.7	558.8	538.1	522.3		512.9	527.7	533.5	555.6
0.267	646.9	648.0	605.7	590.6	579.6	563.4	542.4	526.2		516.8	531.4	537.2	559.5
0.269	653.3	654.3	611.2	595.8	584.4	567.6	546.4	530.0		520.5	534.9	540.8	563.3
0.271	659.1	660.1	616.1	600.2	588.7	571.3	549.8	533.2		523.7	538.1	544.0	566.8
0.273	664.9	665.8	620.9	604.6	592.9	575.1	553.2	536.4		526.8	541.4	547.4	570.4
0.275	670.3	671.1	625.4	608.7	596.8	578.7	556.5	539.3		529.8	544.6	550.8	574.0
0.277	675.5	676.3	630.0	612.9	600.6	582.4	559.9	542.4		532.8	547.9	554.4	577.8
0.279	680.4	681.2	634.3	616.9	604.3	585.8	563.1	545.4		535.8	551.3	557.9	581.6
0.281	685.2	685.9	638.5	620.9	608.1	589.2	566.2	548.4		539.0	554.9	561.5	585.5
0.283	689.7	690.4	642.4	624.7	611.7	592.4	569.2	551.4		542.1	558.5	565.1	589.4
0.285	694.2	694.8	646.3	628.3	615.3	595.7	572.2	554.4		545.3	562.1	569.0	593.5
0.287	698.4	699.0	649.9	631.8	618.7	598.9	575.1	557.4		548.6	565.8	572.9	597.7
0.289	702.5	703.1	653.6	635.2	622.0	602.0	578.2	560.5		551.9	569.7	577.0	602.1
0.291	706.5	707.1	657.0	638.5	625.1	605.0	581.1	563.7		555.3	573.6	581.0	606.4
0.293	710.5	711.1	660.4	641.6	628.1	607.9	584.1	566.9		558.7	577.4	585.0	610.7
0.295	714.3	715.0	663.3	644.3	630.8	610.5	586.7	569.8		561.9	581.1	588.8	614.8
0.297	718.0	718.9	666.2	646.9	633.2	612.9	589.2	572.6		565.0	584.7	592.5	618.7

Table 7.1-7. DM-9 Pressure Distribution Summary (60°F)
Ignition: Caveny Kuo (cont)

TIME	X LOCATIONS (INCHES)											
	HEAD-END PRESSURE (489.9)	530.0	689.3	851.2	1012.1	1171.2	1332.1	1491.2	1511.0	1577.5	1697.5	1816.7	NOZZLE STAGNATION PRESSURE
0.299	721.7	722.6	669.1	649.3	635.4	615.1	591.6	575.2		567.9	588.1	595.9	622.5
0.301	725.3	726.4	671.9	651.7	637.7	617.3	593.9	577.8		570.8	591.4	599.4	626.2
0.303	728.9	730.1	674.7	654.2	639.9	619.5	596.1	580.3		573.6	594.7	602.7	629.8
0.305	732.4	733.7	677.5	656.7	642.4	621.7	598.3	582.8		576.3	597.9	606.0	633.4
0.308	735.8	737.1	680.3	659.2	644.8	624.0	600.6	585.3		579.1	601.1	609.1	636.8
0.309	739.2	740.4	683.2	662.0	647.5	626.5	603.2	588.0		582.1	604.2	612.3	640.3
0.311	742.6	743.6	686.1	664.8	650.3	629.2	605.9	590.8		585.1	607.4	615.4	643.7
0.313	745.9	746.7	688.8	667.6	653.2	632.0	608.8	593.7		588.0	610.5	618.6	647.1
0.323	761.6	765.0	706.8	684.7	672.1	653.7	630.5	616.8		610.3	632.1	641.0	671.0
0.333	776.2	779.0	721.5	699.1	686.2	666.2	643.0	629.0		623.8	648.1	657.9	689.5
0.343	789.8	791.7	735.4	714.6	702.8	683.0	659.7	645.5		640.1	663.0	671.3	704.2
0.353	802.5	803.3	750.0	730.2	718.3	698.3	675.7	660.2		654.3	678.7	688.2	722.6
0.363	813.9	813.6	763.1	745.1	734.1	713.2	689.5	673.8		668.4	693.1	701.7	737.4
0.373	824.6	823.7	776.6	759.9	748.2	726.6	703.5	687.3		681.8	706.2	714.9	751.8
0.383	834.2	833.0	787.8	771.8	760.2	738.5	715.3	698.1		692.7	716.9	725.1	762.9
0.393	843.2	842.1	798.2	783.0	771.0	748.5	725.4	707.3		701.6	725.5	733.1	771.7
0.403	851.2	850.1	807.3	792.9	780.6	757.6	734.0	714.6		708.5	731.5	738.8	777.7
0.413	858.7	857.4	814.9	800.9	788.1	764.1	739.9	719.4		712.7	735.6	742.7	782.0
0.424	865.3	863.9	821.6	807.2	793.7	768.6	743.9	722.8		715.9	738.6	745.5	785.2
0.433	871.4	870.7	826.6	811.5	797.4	771.6	746.8	725.2		718.1	740.6	747.3	787.3
0.443	876.9	876.6	831.5	816.2	801.9	775.5	750.1	728.2		721.1	743.6	750.3	790.6
0.453	881.8	882.0	836.5	821.3	807.2	780.8	755.4	733.4		726.2	748.7	755.4	796.1
0.463	886.2	886.5	840.6	825.6	811.8	785.6	760.5	738.6		731.7	754.5	761.3	802.5
0.473	890.2	890.5	844.9	829.0	815.2	789.0	764.4	742.7		736.0	758.8	765.6	807.1
0.484	893.7	893.8	847.2	832.3	818.7	792.6	768.2	746.4		739.5	762.0	768.8	810.4
0.493	896.9	896.8	850.2	835.7	822.4	796.5	772.1	750.0		743.0	765.4	772.1	813.9
0.503	899.6	899.4	852.7	838.2	824.9	798.9	774.6	752.4		745.4	768.1	774.9	816.9
0.513	902.0	901.6	854.8	839.9	826.5	800.3	776.0	753.8		747.0	769.5	776.2	818.3
0.523	904.1	903.5	856.4	841.4	827.9	801.6	777.4	755.0		748.0	770.4	777.1	819.4
0.533	906.0	905.2	858.2	843.0	829.7	803.4	779.2	756.5		749.6	772.0	778.7	821.2
0.543	907.5	906.6	859.5	844.4	831.1	804.8	780.7	758.1		751.3	773.8	780.6	823.2
0.553	908.9	907.9	860.8	845.7	832.4	806.2	782.3	759.8		753.1	775.7	782.5	825.3
0.563	910.0	909.0	862.0	846.9	833.8	807.7	783.9	761.5		754.8	777.4	784.1	827.0
0.573	911.0	909.9	863.0	848.0	835.0	808.9	785.3	762.8		756.0	778.7	785.4	828.4
0.583	911.8	910.6	863.9	848.8	835.8	809.6	786.0	763.5		756.7	779.4	786.0	829.0
0.593	912.4	911.2	864.5	849.3	836.3	810.1	786.4	763.8		757.0	779.6	786.2	829.2

Table 7.1-7. DM-9 Pressure Distribution Summary (60°F)
Steady State: SCB04 1-D Mass Addition (cont)

TIME	X LOCATIONS (INCHES)											
	HEAD-END PRESSURE (489.9)	530.0	689.3	851.2	1012.1	1171.2	1332.1	1491.2	1511.0	1577.5	1697.5	1816.7	NOZZLE STAGNATION PRESSURE
0.6	912.8	911.5	864.8	849.5	836.4	810.2	786.5	763.9	757.4	757.1	779.6	786.2	829.3
0.8	910.5	909.3	866.2	851.6	839.0	814.8	791.3	770.5	763.6	763.3	785.0	791.3	824.9
1.0	908.0	906.9	865.7	851.6	839.4	816.4	793.3	773.6	766.7	766.3	787.1	793.2	817.0
2.0	899.0	898.1	861.4	848.1	836.3	815.8	792.7	774.6	767.4	766.8	786.1	791.7	816.3
3.0	895.3	894.5	861.1	848.5	837.1	817.6	795.5	778.5	771.3	770.7	788.6	793.9	819.3
4.0	894.6	893.9	863.3	851.1	840.2	820.7	800.3	784.2	777.1	776.3	793.2	798.2	824.6
5.0	897.5	896.9	868.6	856.7	846.2	826.9	807.8	792.3	785.4	784.5	800.5	805.2	832.7
6.0	902.6	902.0	875.7	864.3	854.1	834.8	817.0	802.0	795.3	794.3	809.5	813.9	842.6
7.0	905.3	904.8	880.6	869.6	859.8	841.0	824.3	809.9	803.4	802.4	816.5	820.6	848.3
8.0	903.8	903.4	881.2	870.8	861.4	843.1	827.5	813.6	807.3	806.3	819.4	823.2	849.7
9.0	902.0	901.6	881.3	871.3	862.3	844.6	829.8	816.5	810.6	809.4	821.5	825.1	850.5
10.0	901.3	900.9	882.3	872.7	864.0	847.1	833.0	820.2	814.6	813.3	824.5	827.8	852.2
12.0	893.9	893.6	877.8	869.1	861.1	845.5	832.9	821.0	816.1	814.7	824.3	827.0	849.2
14.0	889.8	889.5	876.0	868.1	860.6	846.2	834.8	823.7	819.4	817.9	826.2	828.4	848.6
16.0	884.4	884.2	872.5	865.2	858.3	845.2	834.8	824.4	820.6	819.0	826.2	828.0	846.3
18.0	882.4	882.2	872.2	865.5	859.0	847.0	837.4	827.6	824.2	822.6	828.7	830.3	846.7
20.0	878.2	878.0	869.3	863.2	857.2	846.2	837.3	828.1	825.1	823.5	828.7	830.0	844.7
22.0	868.0	867.9	861.0	855.5	849.9	839.9	831.6	822.9	820.2	818.6	822.8	823.7	836.6
24.0	834.1	834.0	828.6	823.9	818.8	810.0	802.5	794.4	792.1	790.3	793.7	794.2	805.9
26.0	804.5	804.4	800.3	796.2	791.6	783.7	776.9	769.4	767.4	765.6	768.2	768.4	779.1
28.0	779.5	779.4	776.3	772.7	768.5	761.5	755.2	748.2	746.4	744.7	746.7	746.7	756.5
30.0	757.5	757.5	755.1	751.9	748.1	741.9	736.1	729.5	728.0	726.3	727.7	727.6	736.6
32.0	736.7	736.7	734.9	732.1	728.8	723.1	717.7	711.7	710.3	708.6	709.6	709.3	717.7
34.0	717.6	717.5	716.2	713.8	710.7	705.6	700.7	695.0	693.8	692.1	692.8	692.4	700.1
36.0	699.8	699.8	698.8	696.8	694.0	689.5	684.8	679.5	678.4	676.8	677.2	676.7	683.9
38.0	682.4	682.4	681.7	680.0	677.6	673.4	669.1	664.1	663.1	661.6	661.7	661.1	667.8
40.0	665.5	665.5	665.1	663.6	661.4	657.6	653.7	649.0	648.1	646.6	646.6	645.9	652.1
42.0	650.8	650.8	650.6	649.3	647.3	644.0	640.2	635.9	635.0	633.6	633.4	632.7	638.5
44.0	639.4	639.4	639.2	638.2	636.4	633.3	629.8	625.7	625.0	623.6	623.2	622.5	628.0
46.0	630.0	630.0	629.9	629.0	627.4	624.6	621.3	617.4	616.7	615.4	614.9	614.1	619.4
48.0	618.3	618.3	618.2	617.5	616.1	613.5	610.4	606.7	606.0	604.7	604.1	603.3	608.3
50.0	602.7	602.7	602.7	602.1	600.7	598.3	595.3	591.9	591.3	590.0	589.5	588.6	593.4
52.0	599.2	599.2	599.2	598.5	597.2	595.0	592.2	588.8	588.3	587.1	586.5	585.7	590.3
54.0	601.4	601.5	601.4	600.8	599.6	597.4	594.7	591.5	591.0	589.9	589.3	588.5	593.0
56.0	606.7	606.7	606.7	606.1	604.9	602.8	600.3	597.2	596.7	595.6	595.0	594.2	598.6
58.0	612.3	612.3	612.3	611.8	610.6	608.6	606.2	603.3	602.9	601.8	601.1	600.3	604.5
60.0	616.6	616.6	616.6	616.1	615.0	613.1	610.7	608.0	607.6	606.5	605.9	605.1	609.1
62.0	623.2	623.2	623.2	622.7	621.7	619.9	617.6	614.9	614.6	613.5	612.9	612.1	616.1
64.0	625.8	625.8	625.8	625.4	624.3	622.6	620.4	617.9	617.6	616.6	615.9	615.2	619.0
66.0	632.8	632.8	632.8	632.4	631.4	629.8	627.6	625.2	624.9	623.9	623.3	622.5	626.2
68.0	635.4	635.4	635.4	634.9	634.0	632.5	630.4	628.1	627.8	626.8	626.2	625.5	629.0
70.0	638.4	638.4	638.4	638.0	637.1	635.7	633.7	631.5	631.2	630.3	629.6	628.9	632.4
72.0	645.6	645.6	645.6	645.3	644.4	643.0	641.1	639.0	638.7	637.8	637.1	636.4	639.8
74.0	643.5	643.5	643.5	643.1	642.3	641.0	639.2	637.2	636.9	636.0	635.3	634.7	637.9
76.0	642.1	642.1	642.1	641.7	640.9	639.7	637.9	636.0	635.8	634.9	634.2	633.6	636.8
78.0	643.3	643.3	643.3	643.0	642.2	641.0	639.3	637.4	637.2	636.4	635.7	635.2	638.2
80.0	621.1	621.1	621.1	620.8	620.0	618.9	617.2	615.4	615.2	614.5	613.8	613.4	616.3
82.0	610.6	610.6	610.6	610.3	609.6	608.4	606.8	605.1	604.9	604.1	603.4	603.2	606.0
84.0	596.0	596.0	596.0	595.7	595.0	593.9	592.3	590.6	590.4	589.7	589.1	588.8	591.6

Table 7.1-7. DM-9 Pressure Distribution Summary (60°F)
Steady State: SCB04 1-D Mass Addition (cont)

TIME	HEAD-END PRESSURE (489.9)	X LOCATIONS (INCHES) 530.0	689.3	851.2	1012.1	1171.2	1332.1	1491.2	1511.0	1677.5	1697.5	1816.7	NOZZLE STAGNATION PRESSURE
86.0	577.8	577.8	577.8	577.6	576.8	575.8	574.3	572.7	572.5	571.8	571.1	571.0	573.7
88.0	556.6	556.6	556.6	556.4	555.7	554.7	553.3	551.7	551.5	550.8	550.2	550.2	552.8
90.0	544.4	544.4	544.4	544.2	543.5	542.6	541.2	539.7	539.5	538.8	538.2	538.2	540.8
92.0	535.9	535.9	535.9	535.7	535.0	534.1	532.7	531.3	531.1	530.5	529.9	529.9	532.4
94.0	525.7	525.7	525.7	525.5	524.9	524.0	522.6	521.3	521.1	520.4	520.0	520.0	522.4
96.0	508.1	508.1	508.1	507.9	507.3	506.5	505.2	503.9	503.7	503.1	502.7	502.7	505.1
98.0	496.2	496.2	496.2	496.0	495.4	494.6	493.3	492.0	491.9	491.3	490.9	490.9	493.2
100.0	482.1	482.1	482.1	481.9	481.3	480.6	479.3	478.1	477.9	477.3	477.0	477.0	479.3
100.4	479.0	479.0	479.0	478.8	478.3	477.5	476.2	475.0	474.9	474.3	474.0	474.0	476.3
100.8	476.2	476.2	476.2	476.0	475.4	474.7	473.4	472.2	472.1	471.5	471.3	471.3	473.5
101.2	473.3	473.3	473.3	473.1	472.5	471.8	470.5	469.4	469.3	468.6	468.4	468.4	470.6
101.6	470.2	470.2	470.2	470.0	469.5	468.7	467.5	466.3	466.2	465.6	465.4	465.4	467.6
102.0	467.1	467.1	467.1	466.9	466.4	465.7	464.4	463.2	463.1	462.5	462.3	462.3	464.5
102.4	464.3	464.3	464.3	464.1	463.6	462.9	461.6	460.5	460.4	459.8	459.6	459.6	461.7
102.8	461.9	461.9	461.9	461.7	461.1	460.4	459.2	458.0	458.0	457.3	457.2	457.2	459.3
103.2	459.5	459.5	459.5	459.3	458.8	458.1	456.8	455.7	455.6	455.0	454.8	454.8	457.0
103.6	456.5	456.5	456.5	456.4	455.8	455.1	453.9	452.7	452.7	452.0	451.9	451.9	454.0
104.0	452.5	452.5	452.5	452.4	451.8	451.1	449.9	448.8	448.7	448.1	448.0	448.0	450.1
104.4	447.7	447.7	447.7	447.5	447.0	446.3	445.1	444.0	443.9	443.3	443.2	443.2	445.3
104.8	442.8	442.8	442.8	442.7	442.1	441.5	440.3	439.1	439.1	438.5	438.4	438.4	440.5
105.2	438.8	438.8	438.8	438.7	438.1	437.5	436.3	435.1	435.1	434.5	434.4	434.4	436.5
105.6	436.1	436.1	436.1	435.9	435.4	434.7	433.5	432.4	432.4	431.8	431.7	431.7	433.8
106.0	434.1	434.1	434.1	434.0	433.4	432.8	431.6	430.4	430.4	429.8	429.8	429.8	431.9
106.4	431.8	431.8	431.8	431.7	431.1	430.5	429.3	428.2	428.2	427.5	427.5	427.5	429.6
106.8	428.6	428.6	428.6	428.5	427.9	427.3	426.1	425.0	425.0	424.3	424.3	424.3	426.4
107.2	425.1	425.1	425.1	425.0	424.4	423.8	422.6	421.5	421.4	420.9	420.9	420.9	422.9
107.6	422.4	422.4	422.4	422.2	421.7	421.1	419.9	418.8	418.7	418.2	418.2	418.2	420.2
108.0	420.8	420.8	420.8	420.6	420.1	419.4	418.3	417.2	417.1	416.6	416.6	416.6	418.6
108.4	419.6	419.6	419.6	419.4	418.9	418.2	417.1	416.0	415.9	415.4	415.4	415.4	417.4
108.8	417.8	417.8	417.8	417.7	417.1	416.5	415.3	414.3	414.2	413.7	413.7	413.7	415.7
109.2	415.1	415.1	415.0	414.9	414.4	413.8	412.6	411.6	411.5	411.0	411.0	411.0	413.0
109.6	411.7	411.7	411.7	411.5	411.0	410.4	409.2	408.2	408.1	407.7	407.7	407.7	409.6
110.0	408.1	408.1	408.1	407.9	407.4	406.8	405.6	404.5	404.5	404.1	404.1	404.1	406.1
110.4	403.2	403.2	403.2	403.0	402.5	401.9	400.7	399.6	399.6	399.3	399.3	399.3	401.2
110.8	394.8	394.8	394.8	394.6	394.1	393.4	392.3	391.2	391.2	391.0	391.0	391.0	392.8
111.2	382.1	382.1	382.1	382.0	381.4	380.8	379.7	378.6	378.6	378.5	378.5	378.5	380.3
111.6	366.0	366.0	366.0	365.9	365.3	364.8	363.6	362.6	362.6	362.6	362.6	362.6	364.3
112.0	346.9	346.9	346.9	346.7	346.2	345.7	344.6	343.6	343.6	343.6	343.6	343.6	345.2
112.4	325.0	325.0	325.0	324.8	324.4	323.9	322.8	321.9	321.9	321.9	321.9	321.9	323.5
112.8	301.5	301.5	301.5	301.3	300.9	300.4	299.4	298.7	298.7	298.7	298.7	298.7	300.1
113.2	278.1	278.1	278.1	278.0	277.5	277.2	276.2	275.5	275.5	275.5	275.5	275.5	276.8
113.6	255.6	255.6	255.6	255.5	255.0	254.8	253.9	253.3	253.3	253.3	253.3	253.3	254.4
114.0	233.7	233.8	233.8	233.6	233.1	233.0	232.1	231.6	231.6	231.6	231.6	231.6	232.7
114.4	212.9	212.9	212.9	212.7	212.2	212.1	211.2	210.9	210.9	210.9	210.9	210.9	211.9
114.8	194.0	194.0	194.0	193.8	193.3	193.3	192.4	192.2	192.2	192.2	192.2	192.2	193.1
115.2	178.1	178.1	178.1	178.1	178.0	177.5	177.5	176.6	176.5	176.5	176.5	176.5	177.3
115.6	165.6	165.6	165.6	165.6	165.5	165.0	165.0	164.2	164.1	164.1	164.1	164.1	164.8
116.0	155.0	155.0	155.0	155.0	154.9	154.5	154.5	153.6	153.6	153.6	153.6	153.6	154.3

Table 7.1-7. DM-9 Pressure Distribution Summary (60°F)
Steady State: SCB04 1-D Mass Addition (cont)

TIME	X LOCATIONS (INCHES)												
	HEAD-END PRESSURE (489.9)	530.0	689.3	851.2	1012.1	1171.2	1332.1	1491.2	1511.0	1577.5	1697.5	1816.7	NOZZLE STAGNATION PRESSURE
116.4	143.9	143.9	143.9	143.8	143.4	143.4	142.5	142.6	142.6	142.6	142.6	142.6	143.2
116.8	130.7	130.7	130.7	130.6	130.2	130.2	129.5	129.5	129.5	129.5	129.5	129.5	130.1
117.2	116.9	116.9	116.9	116.8	116.5	116.5	115.8	115.8	115.8	115.8	115.8	115.8	116.4
117.6	104.4	104.4	104.4	104.2	104.0	104.0	103.4	103.4	103.4	103.4	103.4	103.4	103.9
118.0	93.8	93.8	93.8	93.7	93.4	93.4	92.9	92.9	92.9	92.9	92.9	92.9	93.4
118.4	85.0	85.0	85.0	84.9	84.7	84.7	84.2	84.2	84.2	84.2	84.2	84.2	84.6
118.8	77.4	77.4	77.4	77.3	77.1	77.1	76.7	76.7	76.7	76.7	76.7	76.7	77.0
119.2	70.4	70.5	70.5	70.3	70.2	70.2	69.8	69.8	69.8	69.8	69.8	69.8	70.1
119.6	63.8	63.8	63.8	63.7	63.6	63.6	63.2	63.2	63.2	63.2	63.2	63.2	63.5
120.0	57.4	57.4	57.3	57.2	57.1	57.1	56.8	56.8	56.8	56.8	56.8	56.8	57.1

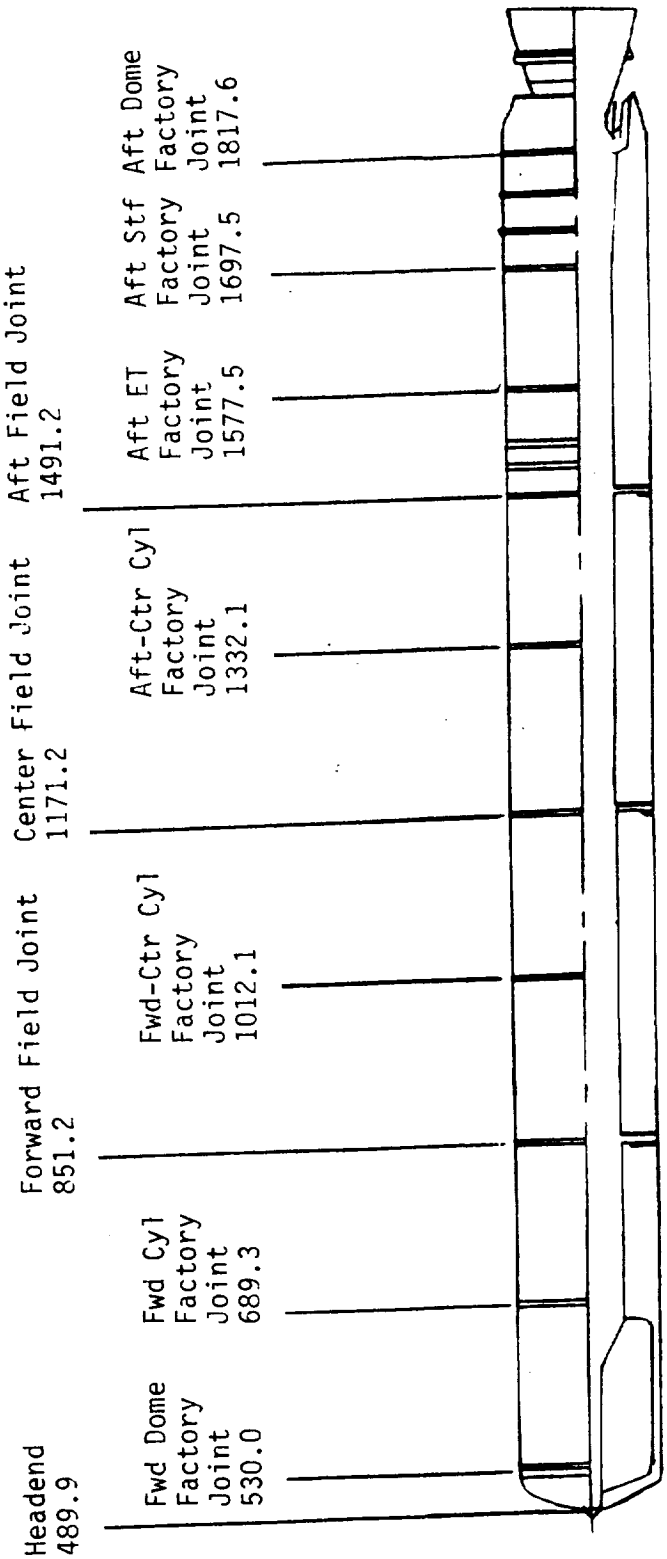

Figure 7.1-13. SRM Axial Station Location Summary (in.)

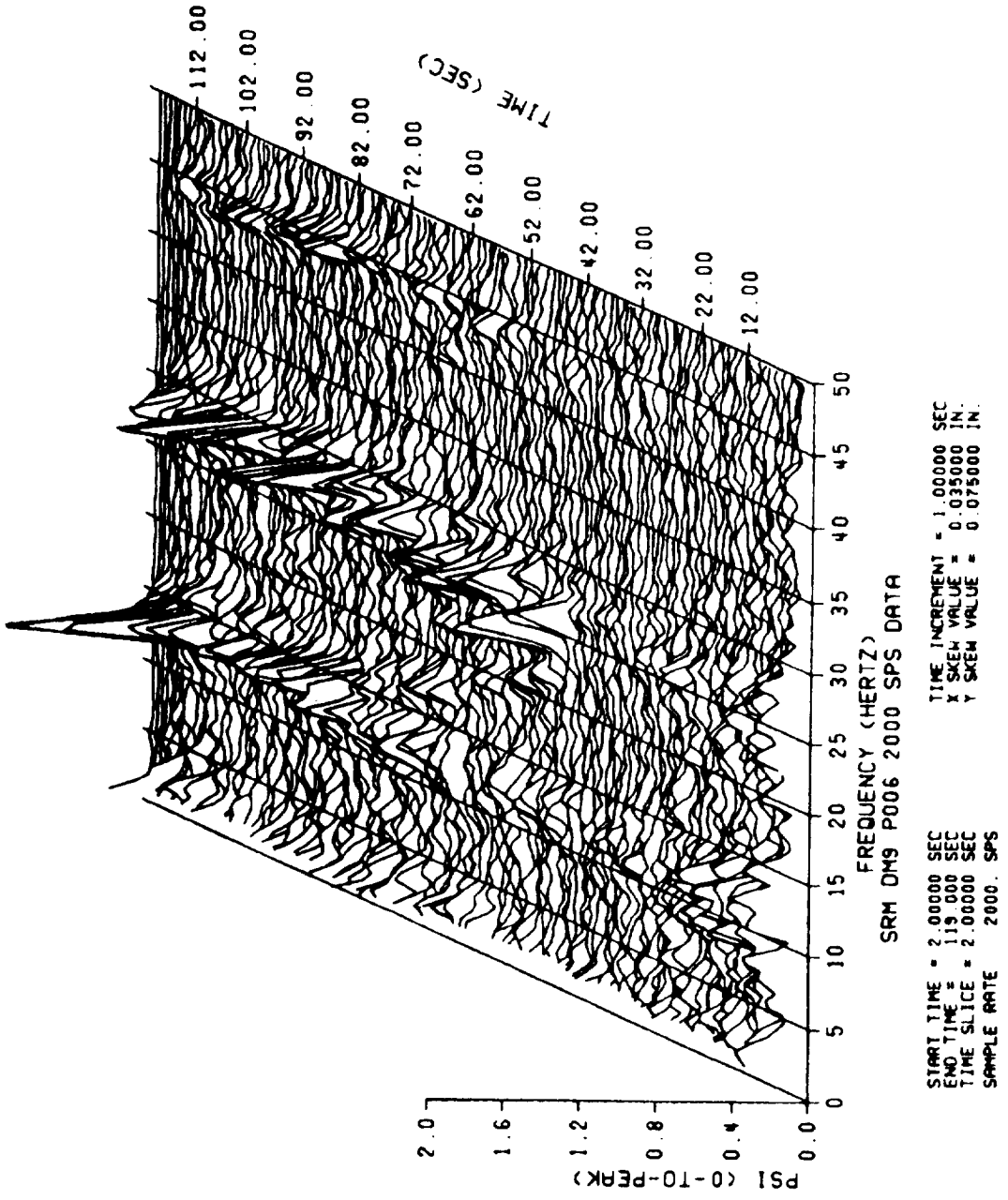

Figure 7.1-14. DM-9 Oscillatory Pressure Data: P006

Figure 7.1-15 is a waterfall plot of P006 data from the DM-8 static test, which was the last RSRM steel case HPM motor to undergo static testing. This figure is provided for comparison purposes, and the following observations regarding the two motors can be made:

a. DM-9 has slightly higher oscillation amplitudes than DM-8.

b. Overall, both motors behaved in a similar fashion.

When using waterfall plots to compare static test motor oscillation amplitudes, it is important to remember that this format uses an averaging method of analysis. This presents no difficulty for steady state signals, but has an attenuating effect on transient signals. Since most of the data obtained from a SRM are transient, any oscillation magnitudes referred to as maxima are, in fact, not true but averaged values. Nonetheless, these numbers are very useful for comparison. Table 7.1-8 shows such a comparison for the DM-9, DM-8, ETM-1A, DM-7, DM-6, and QM-4 static test motors. DM-6 and DM-7 were filament wound case (FWC) motors.

Figures 7.1-16 and 7.1-17 show oscillatory data obtained from the DM-9 and DM-8 thrust gages, respectively. A comparative examination of these data shows relatively close agreement between the two.

7.2 AERO/THERMAL

7.2.1 Introduction

This section discusses the temperature data and the possible causes of the large amounts of slag deposited in the DM-8 aft segment.

7.2.2 Objectives

The main objective of the flow/thermal/erosion analysis was to compare the flow/thermal/erosion analysis predictions with test results.

There were no test objectives from Section 2 that dealt specifically with the aero/thermal section.

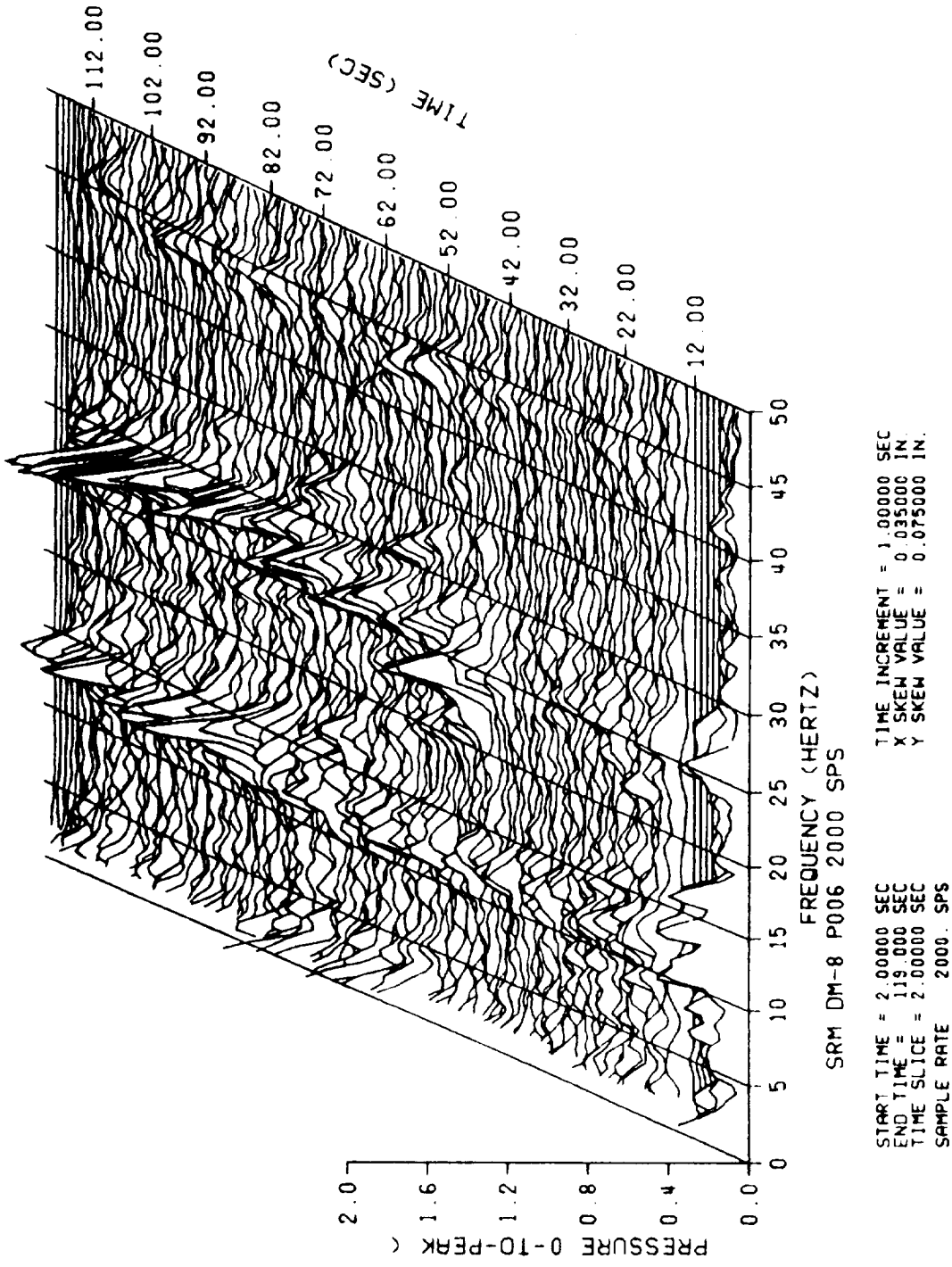

Figure 7.1-15. DM-8 Oscillatory Pressure Data: P006

Table 7.1-8. Maximum Pressure Oscillation Amplitude Comparison

Motor	Source of Measurement	Mode	Time of Measurement	Frequency (Hz)	Maximum Pressure (psia-to-peak)
DM-9	Waterfall	1-L 2-L	107 96	14.5 30.0	1.15 0.88
DM-8	Waterfall	1-L 2-L	78 97	16.0 29.5	0.83 0.85
ETM-1A	Waterfall	1-L 2-L	83 100	15.5 29.5	0.47 0.55
DM-7	Waterfall	1-L 2-L	77 93,96	15.5 29.5	1.29 0.86
DM-6	Waterfall	1-L 2-L	76 86	15.5 29.0	0.51 0.78
QM-4	Waterfall	1-L 2-L	93 83	14.0 29.0	0.21 0.35

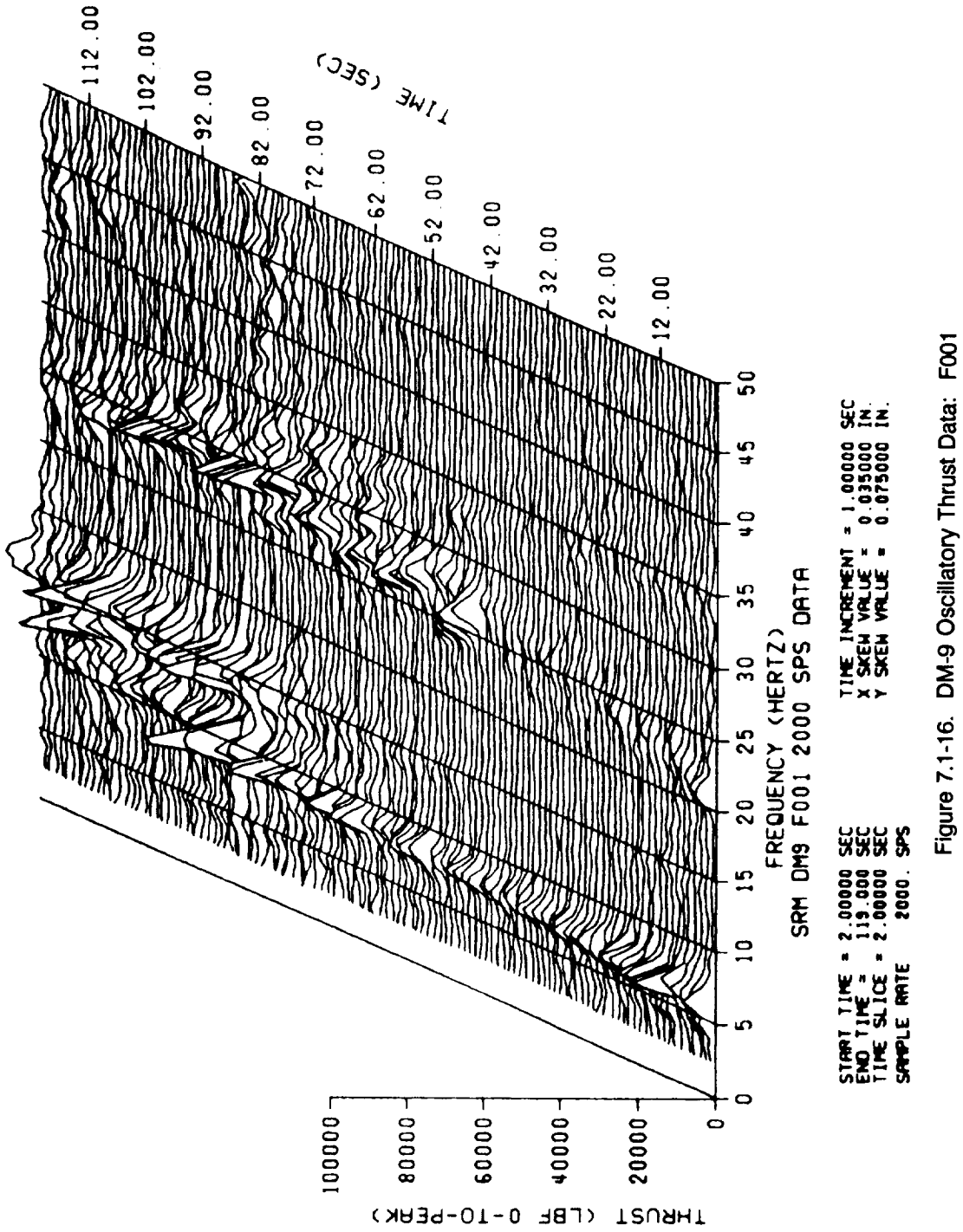

Figure 7.1-16. DM-9 Oscillatory Thrust Data: F001

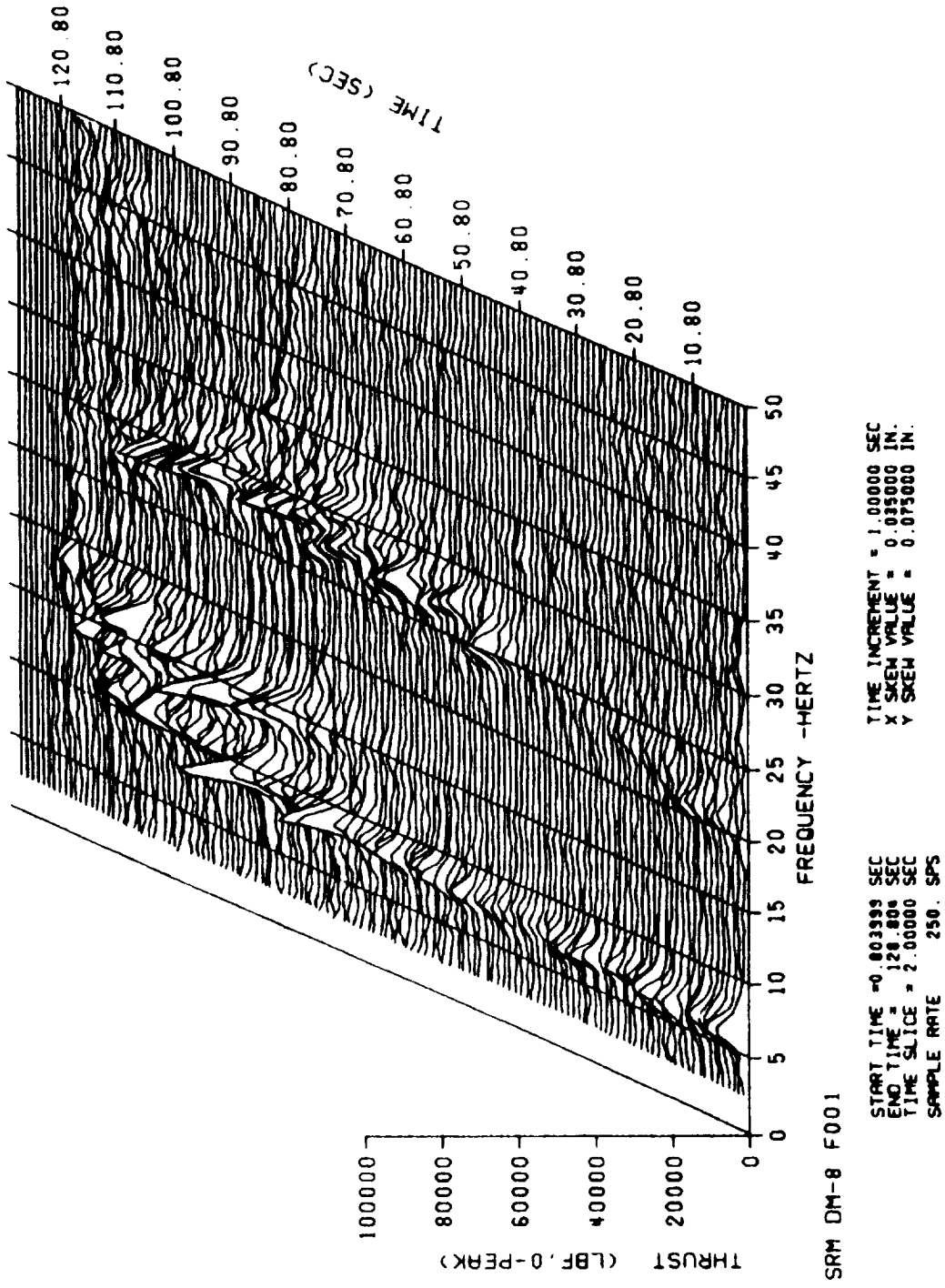

Figure 7.1-17. DM-8 Oscillatory Thrust Data: F001

7.2.3 Conclusions/Recommendations

Ambient temperature at the time of ignition was 25°F. Most component temperatures at the time of firing were between 80° and 120°F because of the three heating systems in operation:

- The field joint heaters
- The igniter heating system
- The aft skirt heating system

Temperature data collected appear to match expected results at all locations. The total slag weight was 2,270 lbm which is near the predicted DM-8 slag weight (2,381 lbm). The deluge system performed exactly as planned. The maximum case temperature was 196°F occurring at approximately T+6 minutes. To ensure against any slag-related damage to the case in a worst-case scenario, two additional water nozzles should be added to the deluge system at the instrumentation box.

7.2.4 Results/Discussion

7.2.4.1 Slag Deposits. The total slag weight in the DM-9 motor was 2,269 lbm. This amount of slag is similar to the amount collected in the DM-8 static test (2,381 lbm). Studies indicate that slag quantity is a strong function of AP particle size, and this was discussed in the DM-8 final test report (TWR-16658).

7.2.4.2 Temperature Data

Igniter

Igniter temperature readings, T875 to T878, are in the expected range. Because of the shroud, the initial temperatures were at 80°F instead of at ambient.

Nozzle Exit Cone

Eight thermocouples (T561 to T568) were mounted on the exterior of the nozzle exit cone, about 5 in. forward of the nozzle exit plane and at the carbon phenolic/glass phenolic interface. Thermocouples T561 to T568 were at the 1-, 89-, 91-, 179-, 181-,

and 269-deg positions, respectively. Thermocouples T562 and T564 apparently did not function, while thermocouple T561 performed correctly following motor firing although it oscillated during motor firing. The six functioning thermocouples all registered normal temperature rises over the 500-sec record time. Thermocouples T566 and T567 had temperature spikes of 625° and 1,000°F, respectively. This same temperature spike condition occurred on ETM-1A (Reference 1) and on DM-8 (Reference 2). It was explained by the fact that at the end of motor firing, the residual burning resulted in a low-velocity flame which was blown back by the wind and engulfed part of the nozzle.

Nose Inlet Housing

Temperature readings at the nose inlet housing (T126), nozzle throat (T130), aft exit cone/forward (T132), aft exit cone/aft (T136), fixed housing/aft (T142 to T145), and flex bearing (T801) all appear normal.

TVC System

Thermocouples T301, T302, T304, T305, T307, T308, T309, and T310 are mounted on the equipment in the base region, which is protected from the plume heat by a thermal curtain. The thermal analysis of this equipment is done by United Space Boosters, Inc. (USBI), the NASA SRB integrator. Thermocouples T301 and T302 on the gas generator bed and T305 and T309 at the gas turbine exhaust registered much higher temperatures than the other thermocouples in this area. This was expected because of their specific locations, and all other measurements in the base region seem reasonable. The reason for the T301 temperature spike before ignition is unknown.

Hydraulic temperatures (T221, T222, and T312) all appear to have the normal temperature increase.

Case (Slag)

Thermocouples at slag locations T638 through T642 and T830 through T846 registered reasonably low temperature increases due to the deluge system. Of these

thermocouples, only T834 appears bad. Temperature data collected appear to match expected results at all locations.

The deluge system performed as planned. It was activated at the specific time. Peak temperature rise occurred approximately 6 min after ignition. The maximum case temperature was 196°F occurring at the 1,547-in. 0-deg location. To ensure against any slag-related damage to the case, two additional nozzles should be added to the deluge system.

All thermocouples were applied securely to the case and insulated from the water of the deluge system, and gave accurate data throughout the cooling process. The thermocouples were carefully monitored, resulting in a very safe procedure for determining when the motor was cooled and the deluge could be safely shut off. The peak temperature was very close to that predicted from analysis done prior to designing the system for the 2,261 lb of slag measured in DM-9. When data are available for the exact insulation and slag thicknesses, a comparison of the theoretical model and actual thermocouple response data will be made.

In previous motors, the slag has run into the center aft section as far back as 66 inches. Considering this, there is adequate coverage of water over the instrumentation box. Excess erosion of the field joint inhibitor or excess slag could allow slag to flow over the instrumentation box area where there is a 48-in. gap between the nozzles. To address this possibility, it is proposed that two nozzles be added, one on each side of the instrumentation box, so that there will be a maximum nozzle spacing of 32 in. between nozzles under the three forward sections of the motor. Thus, the system would guarantee proper cooling for the worst-case scenario.

Figure 7.2-1 shows the thermocouple response data from ignition in various locations directly under the motor (0-deg location). Figure 7.2-2 shows a blownup version of Figure 7.2-1 from ignition to 20 min after ignition. The spikes in Figure 7.2-1 occur when the system shuts down momentarily for visual inspection. It can be concluded from these plots that there is proper cooling provided by the new deluge system.

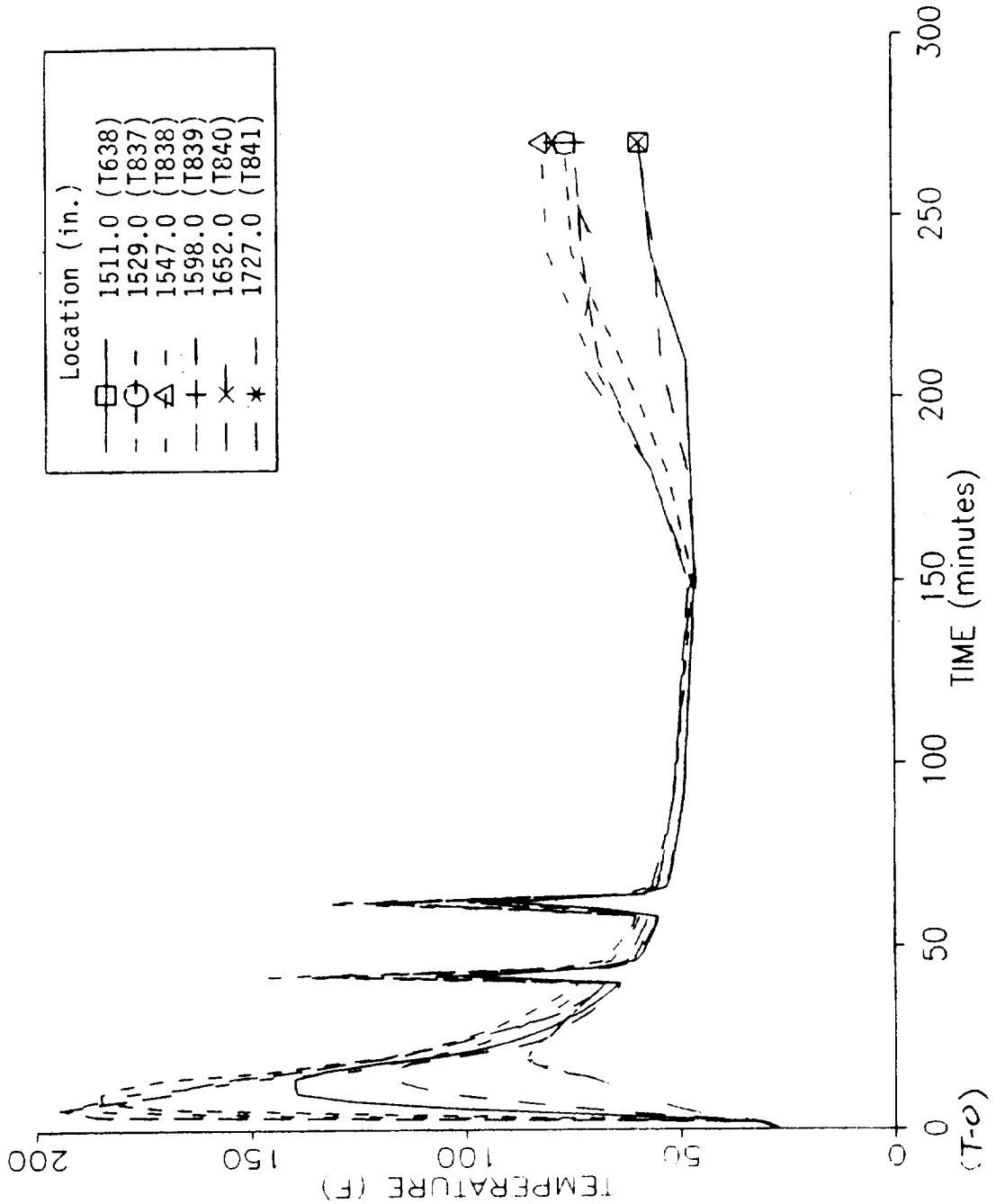

Figure 7.2-1. Temperature History Outer Steel Case

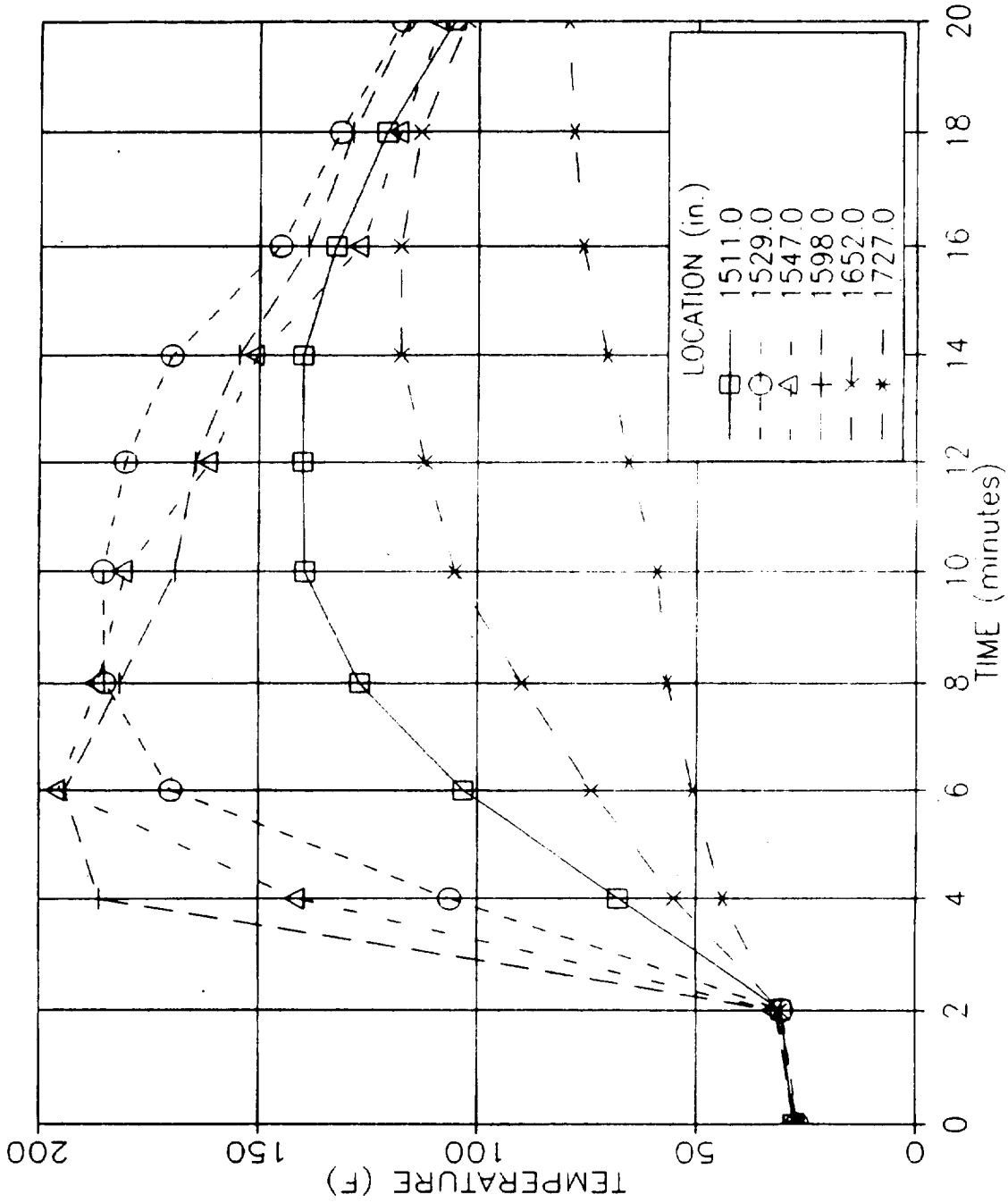

Figure 7.2-2. Temperature History Outer Steel Case Location

Joints

Joint exterior temperatures (T146 to T151) begin cooling down when the joint heater was turned off.

7.3 DYNAMICS

7.3.1 Introduction

Transducers mounted on DM-9 included accelerometers, displacement gages, force cells, pressure transducers, and strain gages. There were a total of 29 accelerometers installed at various locations on DM-9 to monitor dynamic behavior during static firing. Thirteen were installed along the case, four on the nozzle, and the remainder located at the TVC actuators. The accelerometers and displacement gages installed on DM-9 are listed in the instrumentation list in Appendix B. Only part of the data is discussed and summarized in this report.

7.3.2 Objectives

The qualification test objectives from Section 2 with regard to motor dynamic behavior are:

X Determine pressure distribution within the motor during ignition and main burn.
BK Obtain data to verify finite element models.

An additional test objective is to:

Certify the structural integrity of the case, ignition system, and nozzle from displacement and acceleration data.

7.3.3 Conclusions/Recommendations

The numerous transducers used to monitor DM-9 during static firing gathered valuable data for assessing and analyzing the dynamic behavior of the RSRM. The first bending frequency noted in the data is 1.8 Hz.

7.3.4 Results/Discussion

The nonstationary characteristics of the RSRM during static firing are evident in the time history of Channel A409 (Figure 7.3-1). The amplitude of the acceleration response shows some decay within the first 30 sec, remains stationary for the next 60 sec, and shows some nonstationary response through the end of burn. Channel A409 was installed at the center of the motor (center field joint, Station 1159.50) in the radial direction.

Simulated as a simple beam, the RSRM response at the mid-length is a good representation for bending response. The direct waterfall plot (Figure 7.3-2) yields some approximate idea of the increasing trend in modal frequency. (The modal frequency will increase with time due to the decrease of the mass of the propellant during motor burn). The first bending frequency at 1.8 Hz, obtained from analysis, cannot be seen in Figure 7.3-2.

Since the acceleration in time history behaves randomly, a good approach to observe the behavior of frequency spectrum is to employ the power spectral density (PSD). The result is shown in Figure 7.3-3. Randomness is reduced in the PSD plot (Figure 7.3-3); however, the first bending frequency still cannot be seen.

An analysis is underway to identify and verify the accuracy of the first bending mode. In the analytical approach, the response channels A403, A409, and A415 (radial direction accelerometers) were chosen to represent the bending response. The first bending frequency was identified using the first 10 sec of data after ignition. The result is approximately 1.8 Hz, which is very close to the recent modal survey result of 1.92 Hz.

The displacement measurement, D147, was also processed. The time history result is shown in Figure 7.3-4, the regular waterfall plot in Figure 7.3-5, and the PSD waterfalls in Figures 7.3-6 and 7.3-7. The 1.8 Hz first bending frequency is noted in this data.

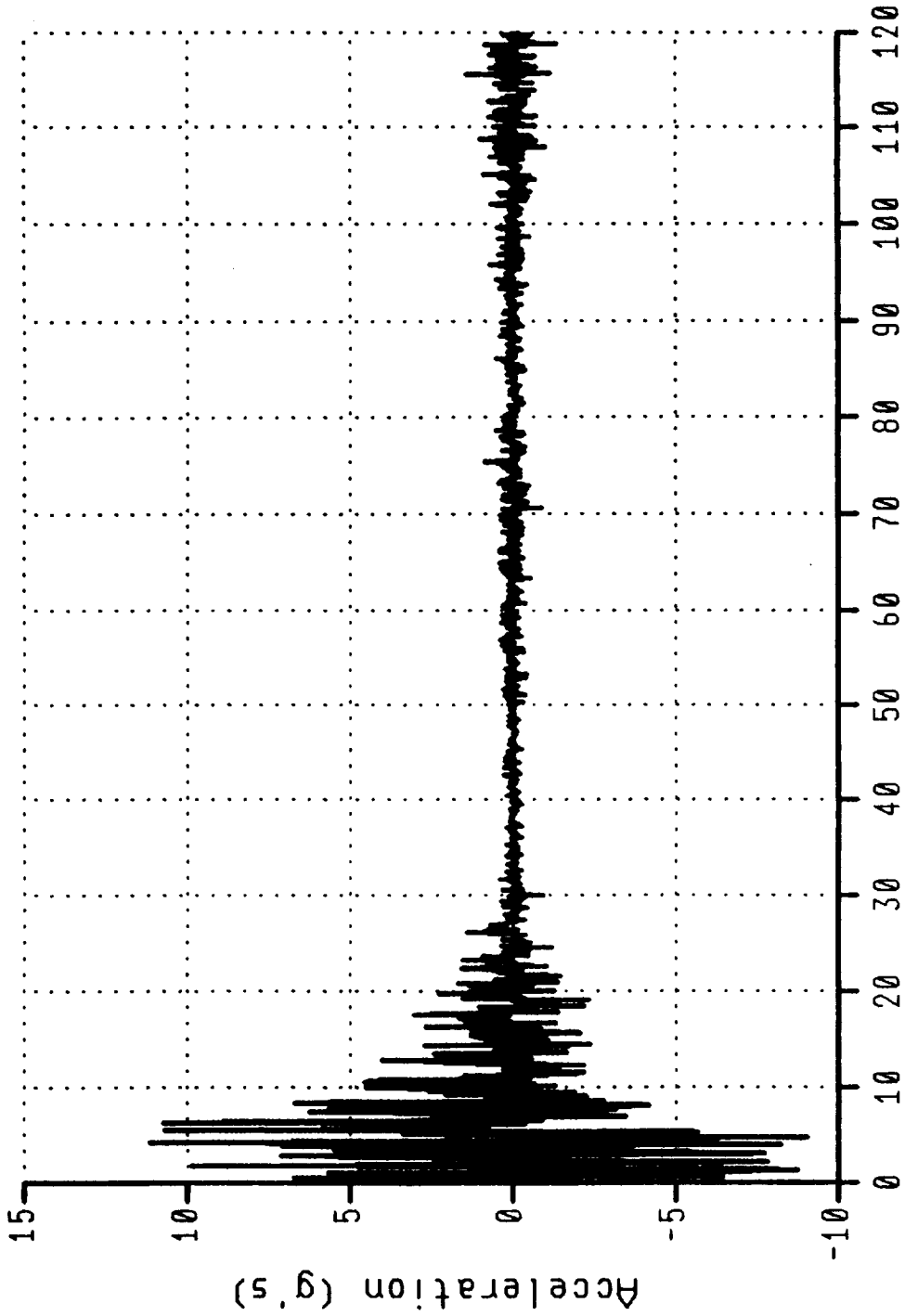

Figure 7.3-1. DM-9 Static Fire Time Response for A409

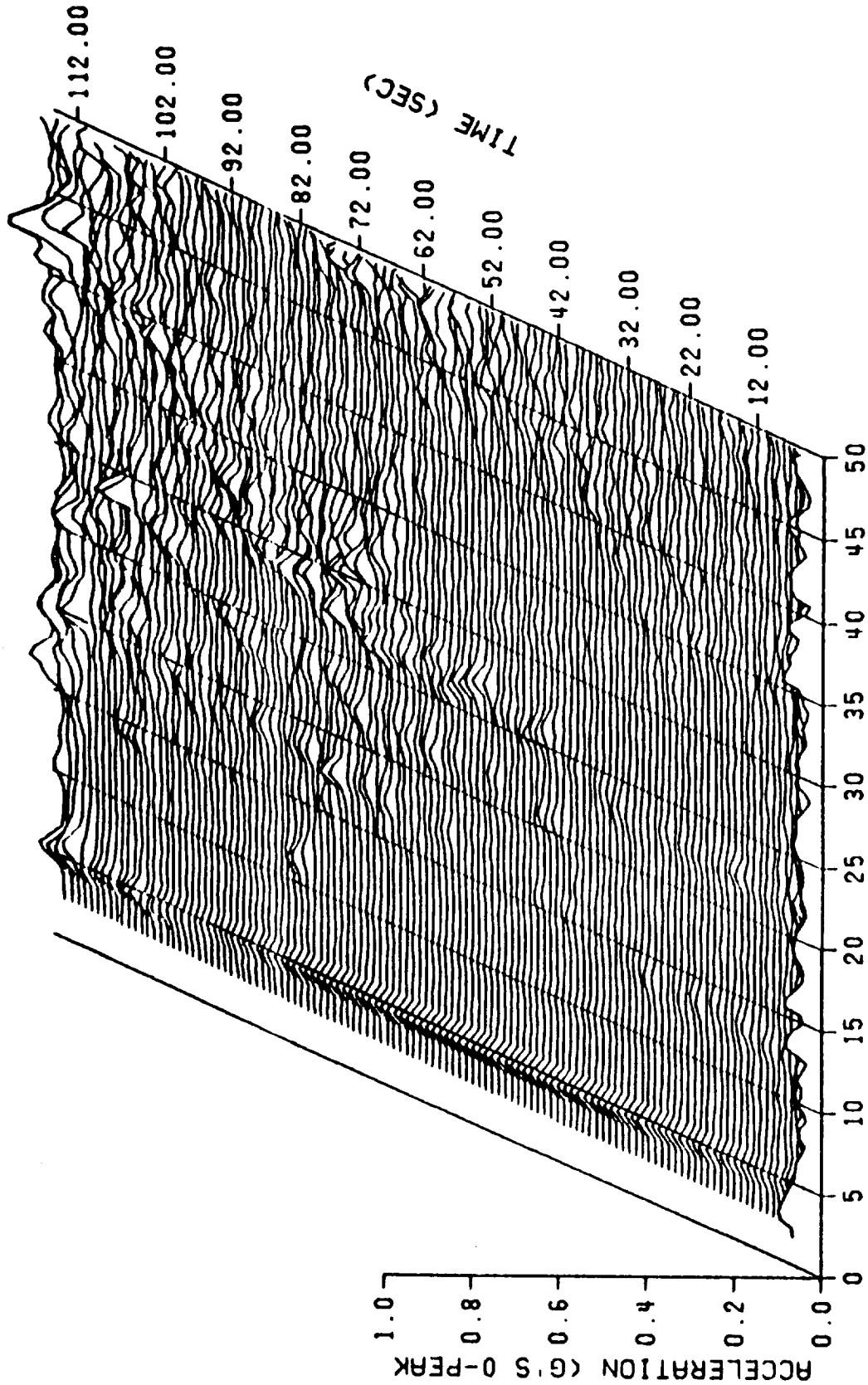

Figure 7.3-2. DM-9 Static Fire Waterfall Plot for A409

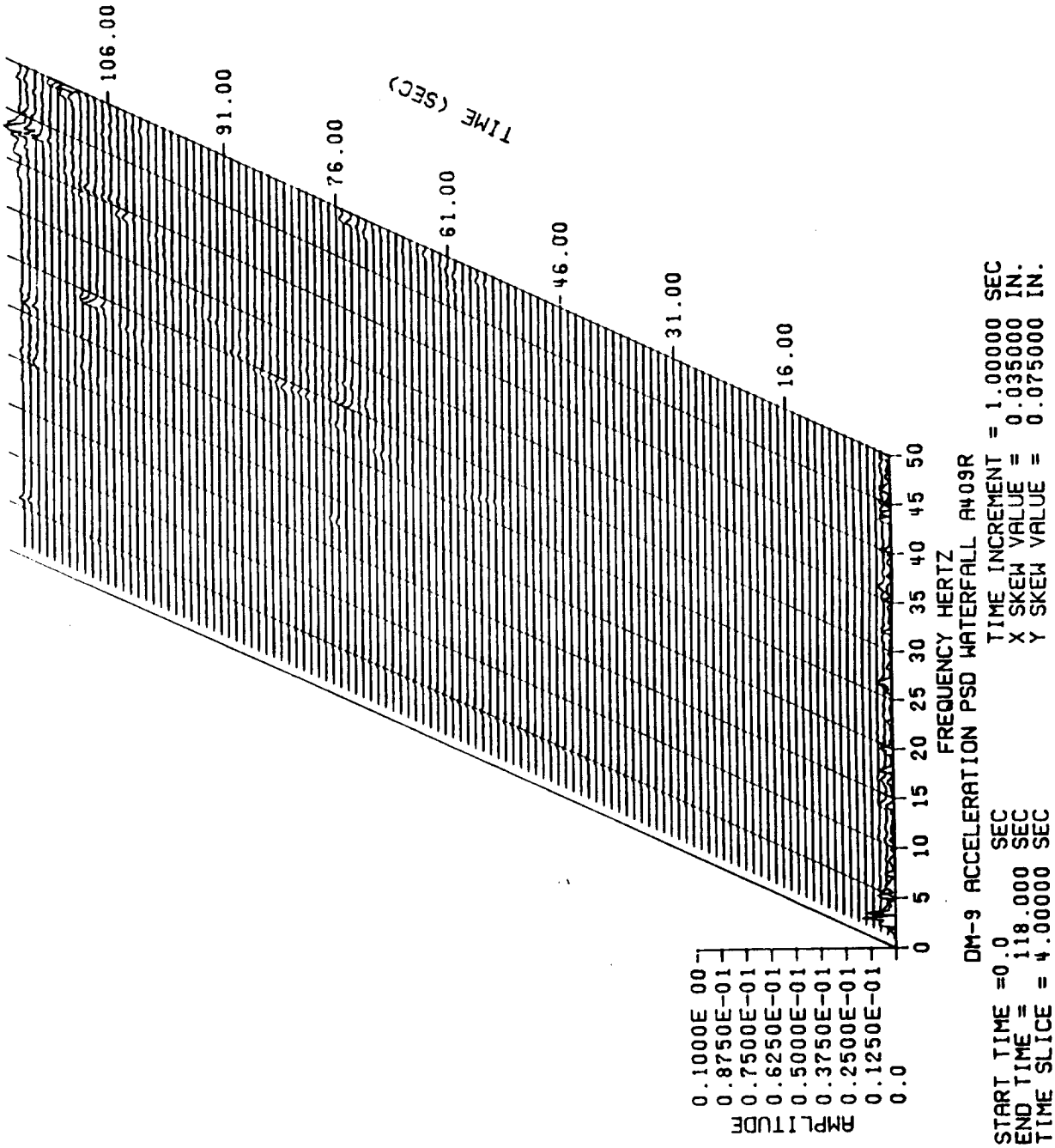

Figure 7.3-3. DM-9 Static Fire PSD Waterfall Plot for A409

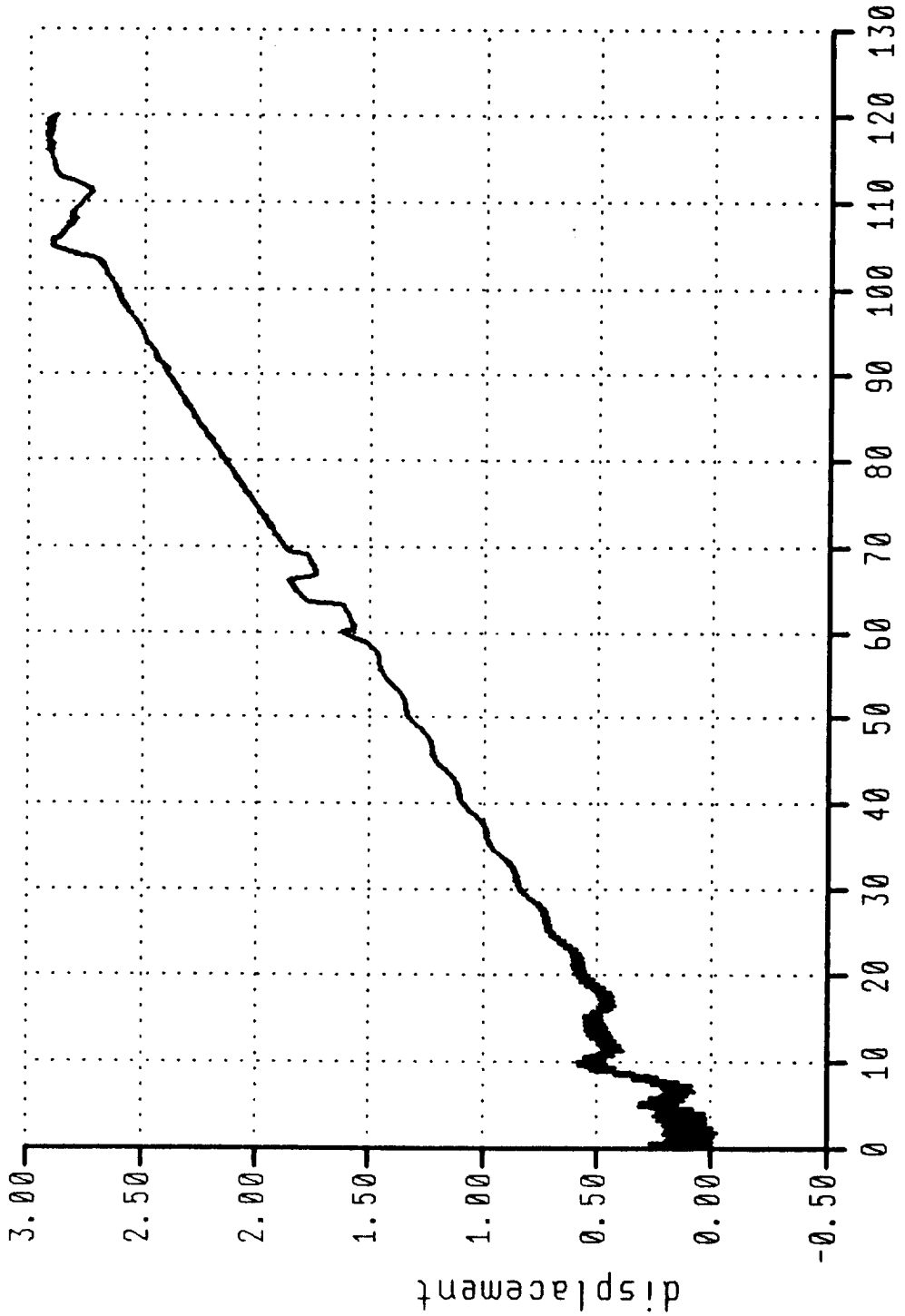

Figure 7.3-4. DM-9 Static Fire Time History Response for D147V

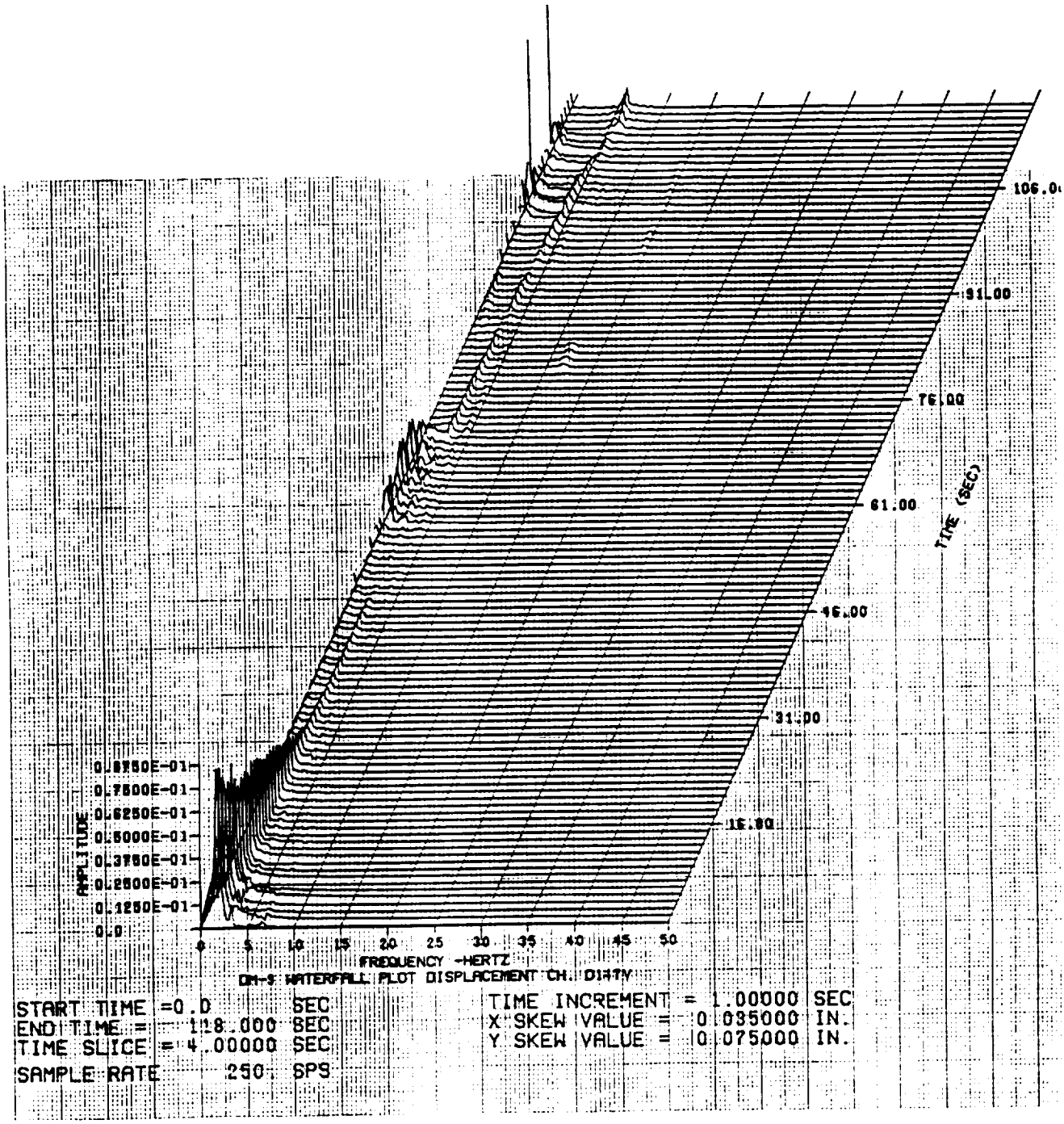

Figure 7.3-5. DM-9 Static Fire Waterfall Plot for D147V

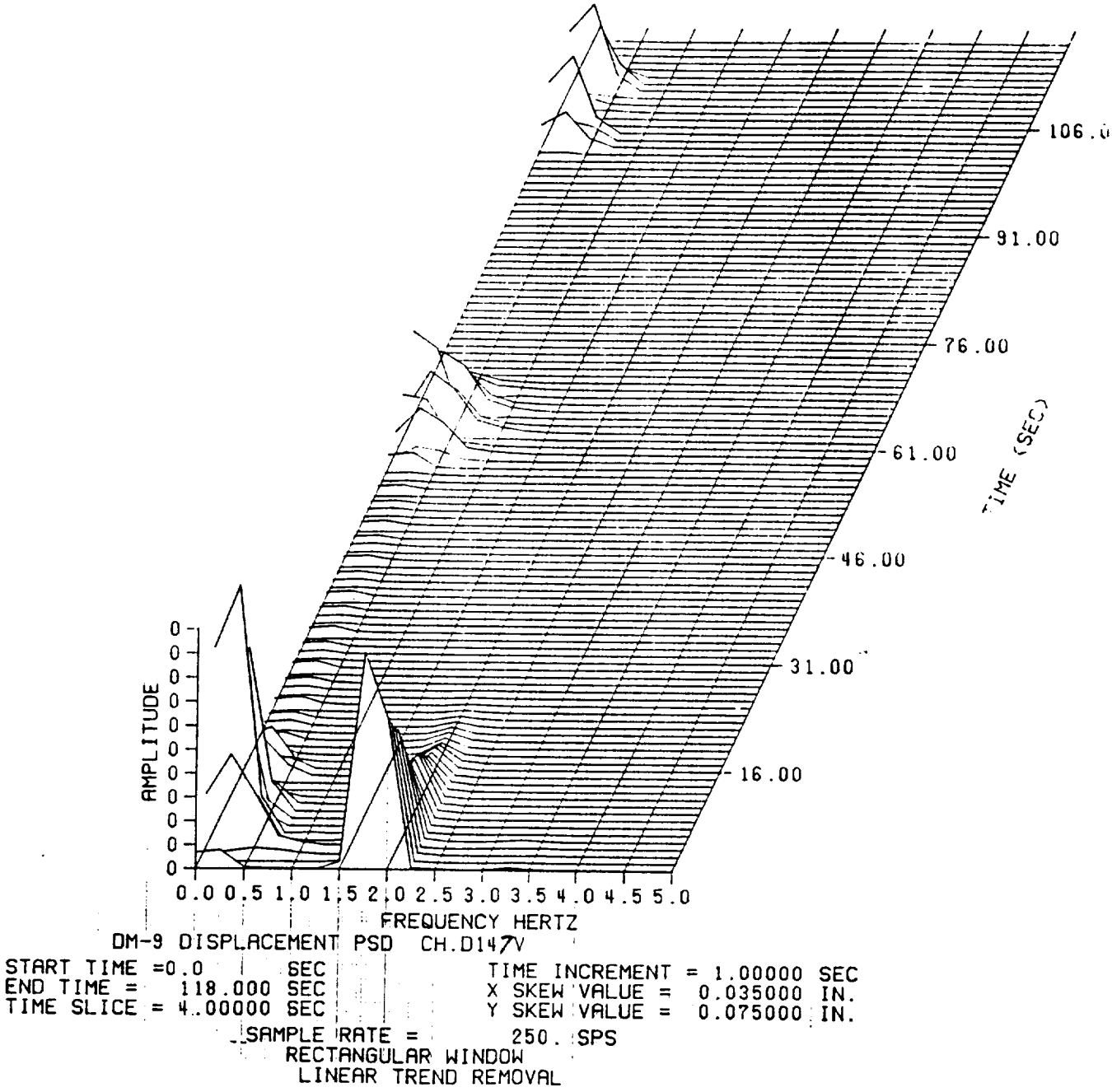

Figure 7.3-6. DM-9 Static Fire PSD Waterfall Plot for D147V (0-5 Hz)

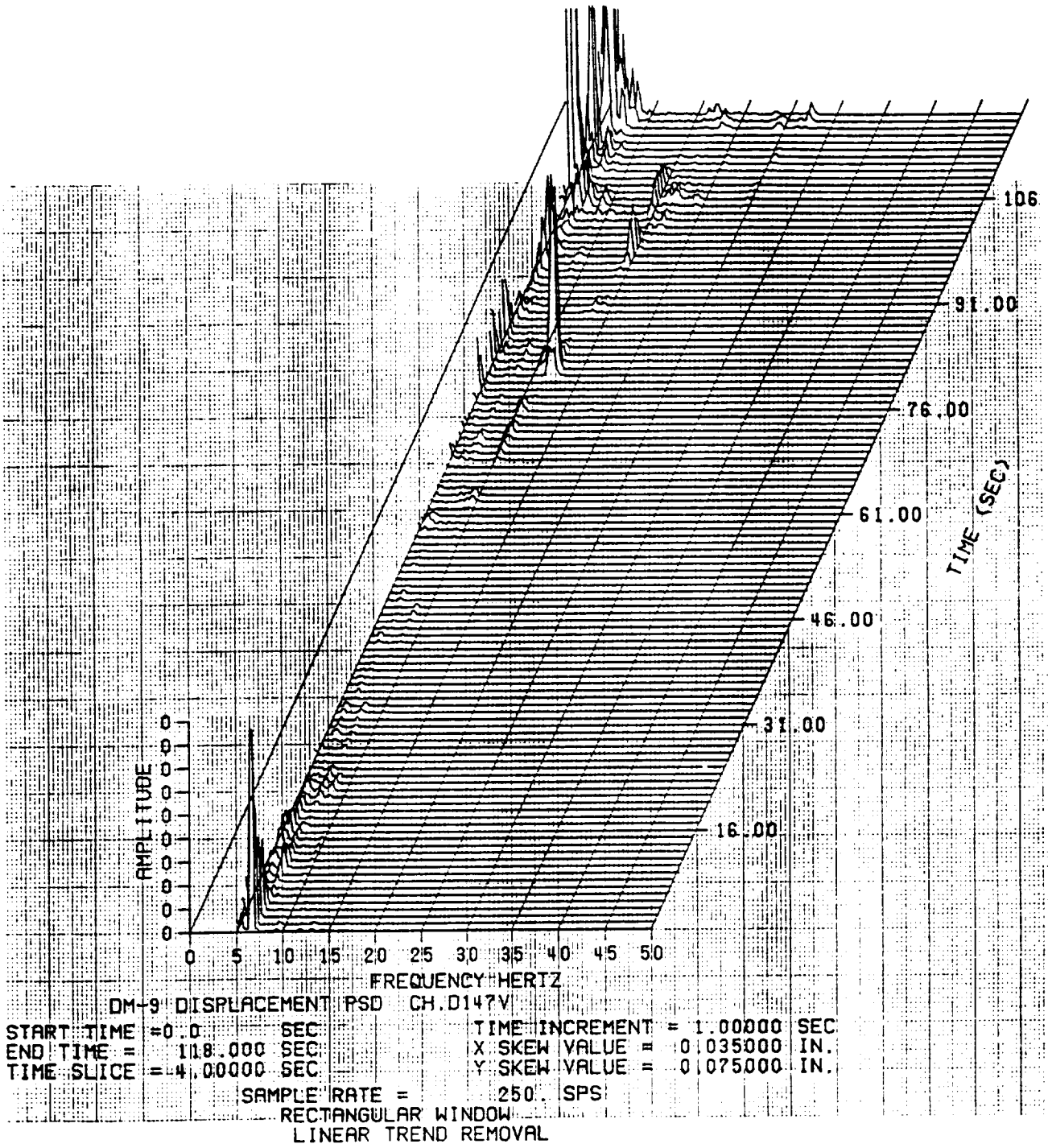

Figure 7.3-7. DM-9 Static Fire Waterfall Plot for D147V (5-50 Hz)

7.4 INSULATION

7.4.1 Introduction

DM-9 was the first full-scale, full-duration test that incorporated the actual SRM flight configurations of the redesigned case field joint and nozzle-to-case joint. The case field joint, factory joint, and nozzle-to-case joint configurations are shown in Figures 7.4-1 through 7.4-3, respectively.

In an attempt to standardize and document the evaluation of static test motors, a standard evaluation plan has been written (TWR-16472). Appropriate procedures contained in this plan were used to evaluate the internal insulation, with emphasis on the case field joints and the nozzle-to-case joint. The intent of these procedures is to ensure that all pertinent evaluation points of DM-9 are examined and documented in a consistent and complete manner.

7.4.2 Objectives

The qualification test objectives from Section 2, with regard to insulation performance were:

F Certify that the insulation ensures that system performance and structural integrity are maintained during the assembly process and operation.

G Certify that the insulation protects the primary and secondary seals from visible degradation from motor combustion gas.

H Certify the ability of the insulation to protect case joints from thermal degradation during a full-duration (ambient temperature) burn.

I Certify that the insulation does not shed fibrous or particulate matter during assembly which could prevent sealing.

J Certify that the field joint insulation withstands slag accumulation during motor operation.

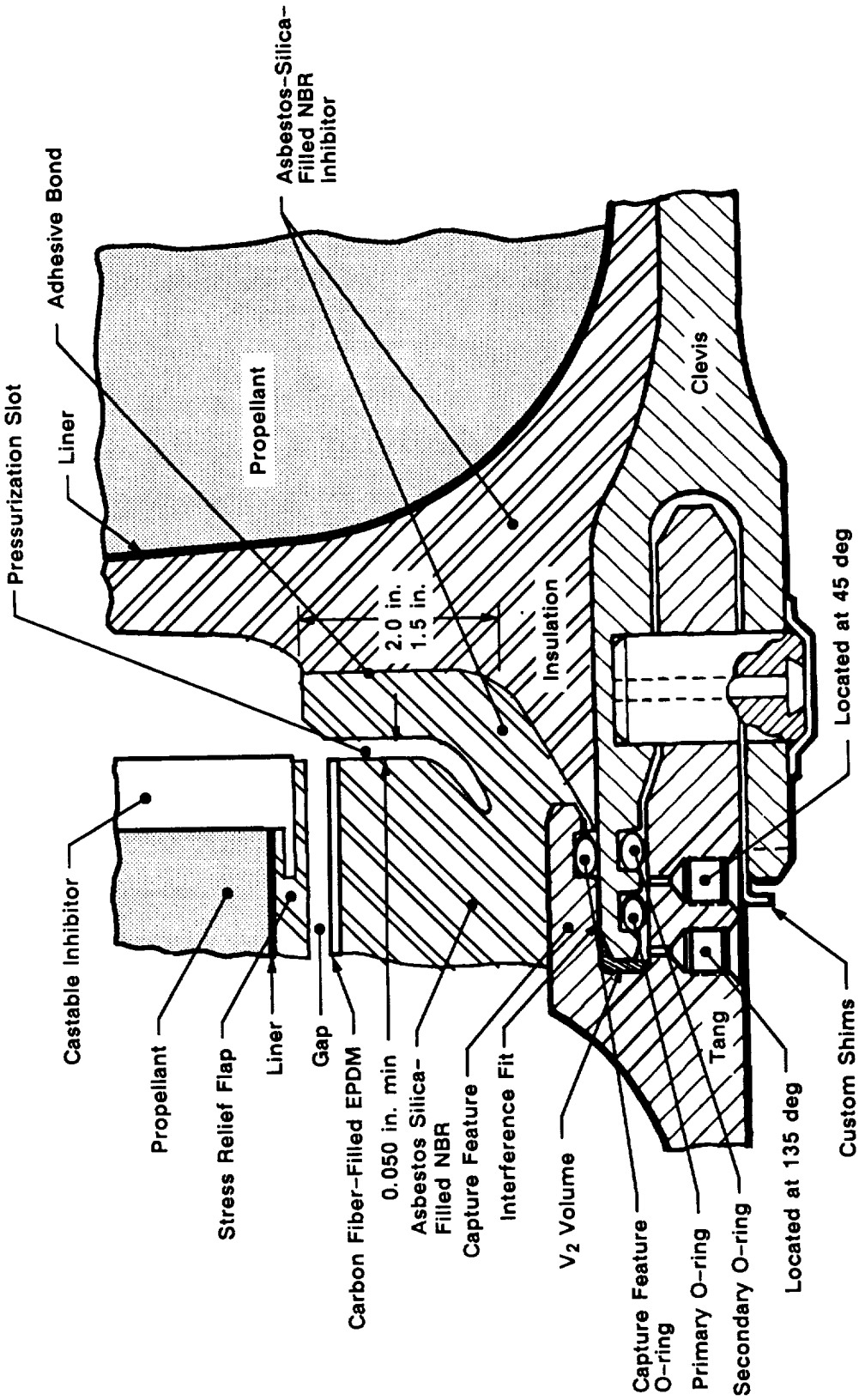

A010527a R4

Figure 7.4-1. Assembled Field Joint

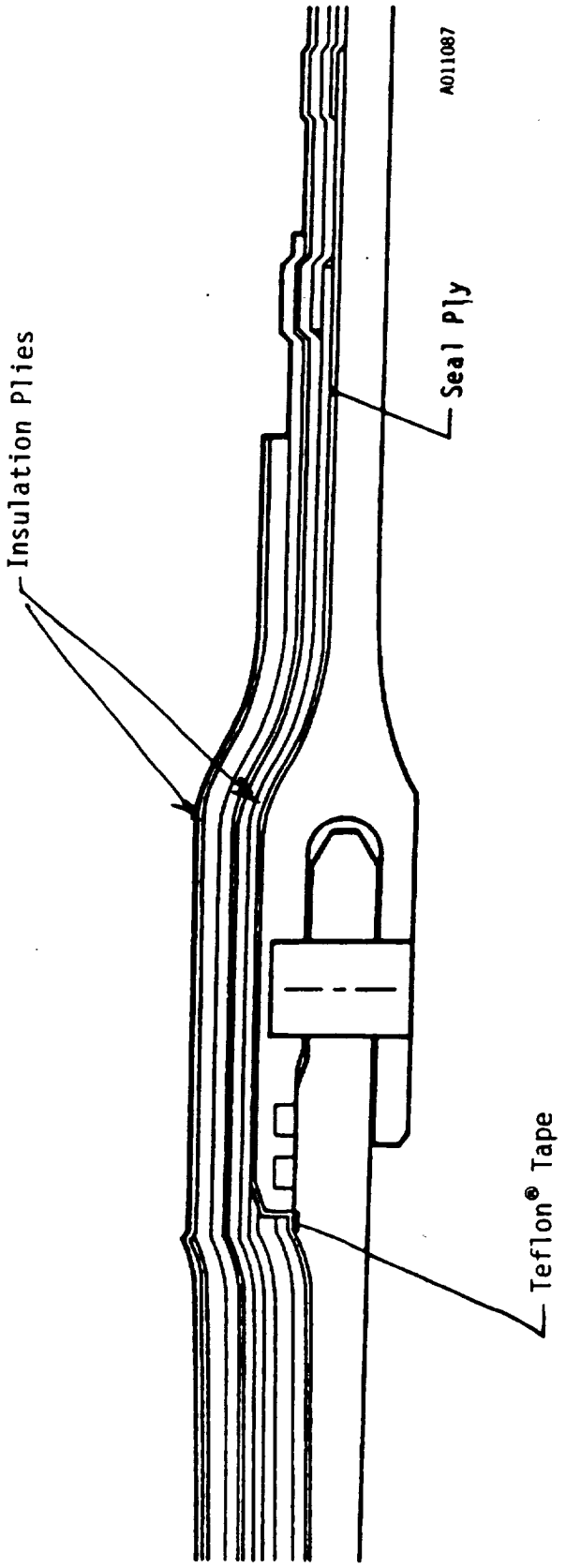

Figure 7.4-2. RSRM Case-to-Case Factory Joint Insulation Layup

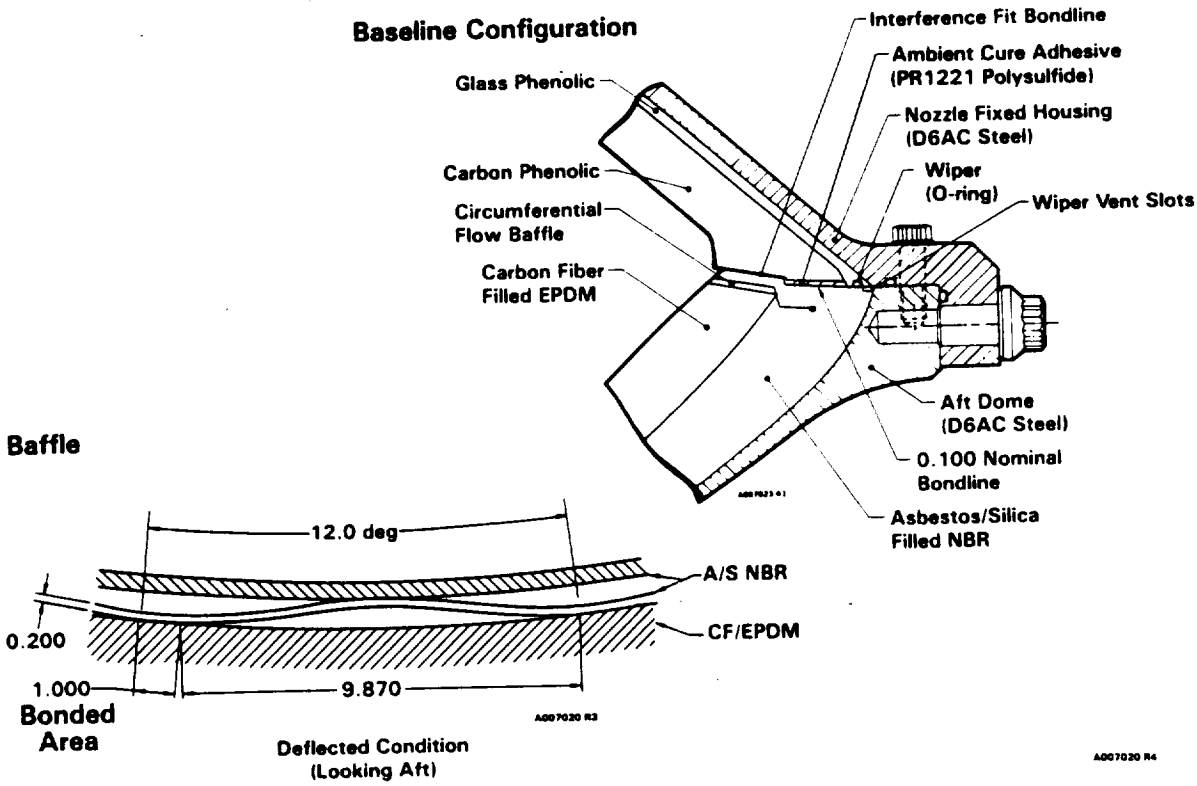

Figure 7.4-3. Nozzle-to-Case Joint

K Certify that the field joint insulation does not induce changes to the propellant grain design which could invalidate the existing ballistic performance database.

L Certify that the nozzle-to-case joint insulation withstands slag accumulation during motor operation.

M Certify that the nozzle-to-case joint insulation does not induce changes to the propellant grain design which could invalidate the existing ballistic performance database.

AK Verify that the RSRM segments are capable of horizontal assembly and disassembly.

AW Certify that the factory joint insulation can accommodate static test motor structural deflection and erosion.

AX Certify that the factory joint insulation is capable of sealing after normal manufacturing processes and during static test at ambient conditions.

AZ Certify that at least one virgin ply of insulation remains over the factory joint after the motor is fired.

BM Evaluate the performance of the nozzle-to-case and field joint adhesive.

7.4.3 Conclusions/Recommendations

Field Joints

The insulation performance in all three of the redesigned case field joints was excellent. The joint bondline for all three case field joints appeared to have contact for the full circumference as evidenced by a postfire witness line of adhesive contact. The glossy adhesive region between contact areas on the forward and center joint indicates that the V_3 volume section inboard of the radius region was compressed, but may not have been completely eliminated. The lack of glossy adhesive on the aft field joint indicates that this V_3 volume section was probably eliminated. There was no

evidence of circumferential flow or hot gas penetration (i.e., sooting or charring) into the joint beyond the nominal expected char and erosion.

Factory Joints

No problems were found after the factory joints were disassembled.

Nozzle-to-Case Joint

The nozzle-to-case joint had a gas path through the polysulfide to the wiper O-ring at 46.8 deg. There was no evidence of erosion or hot gas past the wiper O-ring. This shows that the new joint design is tolerant to this type of defect condition. One large void was noted in the adhesive bondline forward of the insulation step from 74 to 109 deg, but it did not create a through path to the wiper O-ring. There was also less erosion in the joint region that had been analytically predicted, but the erosion was similar to DM-8.

Case

There were no hot spots on the external case, unlike DM-8 and ETM-1A, which both had hot spots on the aft segment. The slag weight in the aft and aft center segments of DM-9 was 2,270 lb total, which was slightly less than that measured on DM-8 (2,381 lb). The deluge system and internal CO_2 forward and aft end quench systems operated correctly on DM-9.

Anomaly

The Insulation Component Program Team initially evaluated the observations presented in this document using Table 7.4-1 as a guide for establishing the classification of a potential anomaly.

No critical, major, or minor potential anomalies were identified by the team, but three potential anomalies which remained observations were identified. These are described in Section 7.4.4.5.

Table 7.4-1. Criteria for Classifying Potential Anomalies

Remains Observation	Anomaly		
	Minor	Major	Critical
• Requires no specific action	• Requires corrective action, but has no impact on: —Motor performance —Program schedule • Does not reduce usability of part for its intended function • Could cause damage preventing reuse of hardware in combination with other anomaly • Significant departure from the historical data base	• Could cause failure in combination with other anomaly • Could cause damage preventing reuse of hardware • Program acceptance of cause, corrective action, and risk assessment required before subsequent static test/flight	• Violates CEI spec requirements • Could cause failure and possible loss of mission/life • Mandatory resolution before subsequent static test/flight

Note: This criteria is to be applied to the specific observed potential anomaly as it relates to the observed article and as it relates to subsequent articles.

7.4.4 Results/Discussion

Insulation Design Engineering performed a postfire evaluation of the DM-9 forward, center, aft, and nozzle-to-case joints. During the postfire evaluation of the aft field joint, a preliminary inspection of the acreage internal insulation was also performed.

The discussion of this report is divided into four sections covering insulation at the field joints, nozzle-to-case joint, and internal acreage. The fourth section discusses observations that have been assessed by the Insulation Component Program Team.

7.4.4.1 Field Joint Insulation

Forward Field Joint

The tang and clevis joint insulation were in excellent condition. Both the tang and clevis joint insulation were charred with some heat-affected areas outboard of the char layer. Measurements of the tang and clevis material decomposition depths and heat-affected depths are provided in Table 7.4-2. The depth measurements on the tang side were taken from the inside diameter (ID) surface of the tang leg at the pinhole. The depth measurements on the clevis side were taken from the ID surface of the inner clevis leg.

The general appearance of the pressure-sensitive adhesive was noted. There appeared to be a distinct witness line which defined the farthest outboard point of contact between the insulation sealing surfaces which had been coated with adhesive. The adhesive outboard of the witness line appeared glossy, indicating no contact between the tang and clevis insulation sealing surface had occurred. This observation indicates that the J-seal deflected leg appeared to have made contact from the tip of the J-seal leg to approximately 0.85 in. below the material remaining, measured radially outboard from the inboard tip of the J-seal leg (Figure 7.4-4). There was minimal contact over the next 0.50 in. and good contact through the radius region.

There was no evidence of any gas flow within the joint beyond the char layer of the J-seal interface over the full circumference. No heat effect or erosion of the capture feature seal or the primary or secondary O-rings was identified.

Table 7.4-2. Field Joint Measurements - Forward (Sta 851.5)

Clevis End Measurements		Location (deg)	Measurements (in.) (1)	(2)	(3)
		0	2.58	2.52	2.14
		90	2.74	2.50	2.36
		180	2.86	2.62	2.40
		270	2.82	2.63	2.40
	Minimum	309	2.62	2.32	2.07

Tang End Measurements		Location (deg)	Measurements (in.) (1)	(2)	(3)
		0	3.32	3.20	2.80
		90	3.34	3.07	2.82
		180	3.27	3.08	2.86
		270	3.34	3.12	2.85
	Minimum	309	3.10	2.84	2.58

All measurements are taken from the ID of the tang leg (pinhole) or inner clevis leg.

Measurements:
(1) To the tip of the remaining material
(2) To the outboard edge of the char layer
(3) To the outboard edge of the heat-affected material (i.e. measurement of the virgin material remaining)*

* Location based on the tan discoloration of the adhesive

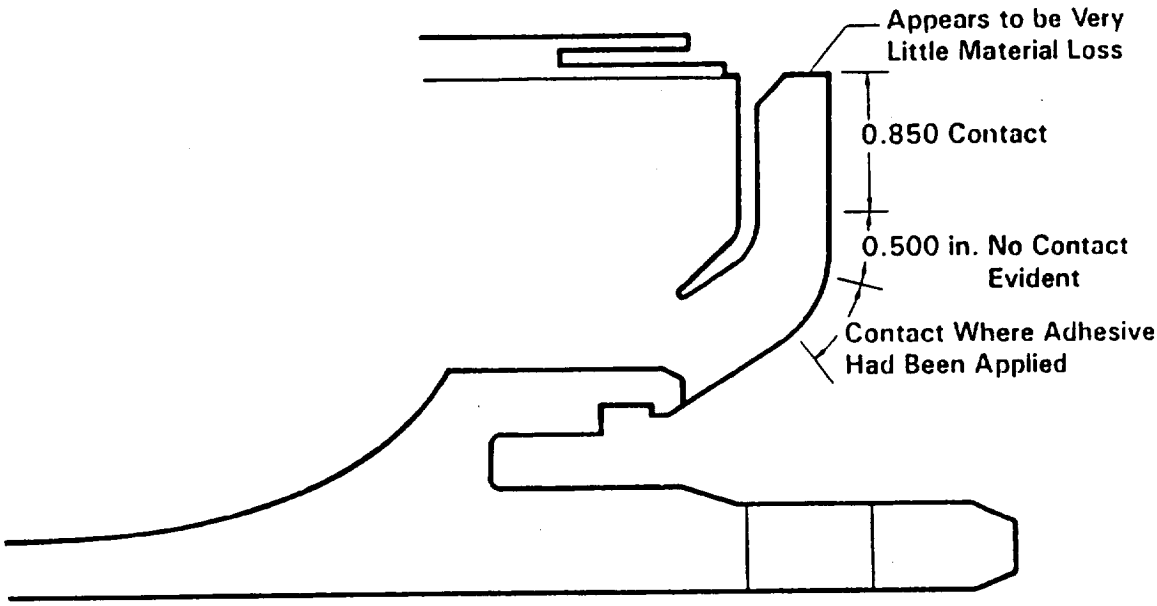

Figure 7.4-4. DM-9 Forward Field Joint Post-Test

Soot was identified in the bottom sector of the joint just beyond the radius of the J-seal leg. This soot accumulation occurred during the disassembly process, since surfaces on each side of this area were very clean.

No evidence of foreign material, ply separations, or tang-edge unbonds were identified. Fourteen clevis edge unbonds were found with the largest unbond measuring 0.29 in. deep by 1.1 in. circumferentially. The J-seal pressurization gap was partially filled (approximately 50 percent) with charred material over the full circumference. The charred material consisted of soot, charred insulation, and particulate slag.

Slag had accumulated in the J-seal pressurization gap from 307 to 310 deg, but the piece had been broken off, leaving what appeared to be an area of heat effect. It seemed that molten slag had run along the gap to this location prior to solidifying. During inspection of the fired DM-8 motor, slag was identified in this same region. Slag had also accumulated in the J-seal pressurization gap on the opposite side between 62 and 66 deg. These two areas with slag accumulation are approximately symmetrical with respect to the 0-deg location at the bottom of the motor. The slag remained intact and was approximately 1 in. in height. The insulation in these regions showed slightly more heat effect than the surrounding regions after the char was rinsed out, but it did not effect the performance of the joint. Design Engineering feels that this condition results from slag accumulation due to the height of the remaining NBR inhibitor in the forward center segment and will have no effect during an SRM flight.

Center Field Joint

The tang and clevis joint insulation were in good condition. Both were charred, with some heat-affected area outboard of the char layer. Measurements of the tang and clevis material decomposition depths and heat-affected depths are provided in Table 7.4-3. The depth measurements on the tang side were taken from the ID surface of the tang leg at the pinhole. The depth measurements on the clevis side were taken from the ID surface of the inner clevis leg.

Table 7.4-3. Field Joint Measurements - Center (Sta 1171.5)

Clevis End Measurements	Location (deg)	Measurements (in.) (1)	(2)	(3)
	0	2.77	2.57	2.22
	90	2.80	2.55	2.10
	180	2.75	2.37	1.91
	270	2.77	2.44	2.23

Tang End Measurements	Location (deg)	Measurements (in.) (1)	(2)	(3)
	0	3.38	3.10	2.62
	90	3.36	2.87	2.50
	180	3.38	3.00	2.56
	270	3.37	3.00	2.52

All measurements are taken from the ID of the tang leg (pinhole) or inner clevis leg.

Measurements: (1) To the tip of the remaining material
(2) To the outboard edge of the char layer
(3) To the outboard edge of the heat-affected material (i.e. measurement of the virgin material remaining)*

* Location based on the tan discoloration of the adhesive

The general appearance of the pressure-sensitive adhesive was noted. There appeared to be a distinct witness line which defined the farthest outboard point of contact between the insulation sealing surfaces, which had been coated with adhesive. The adhesive outboard of the witness line appeared glossy, indicating no contact between the tang and clevis insulation sealing surfaces had occurred. This observation indicates that the J-seal deflected leg appeared to have made contact from the tip of the J-seal leg to approximately 0.80 in. below the material remaining, measured radially outboard from the inboard tip of the J-seal leg (Figure 7.4-5). There was minimal contact over the next 0.70 in. and good contact through the radius region. The glossy adhesive region indicates that the V_3 volume section inboard of the radius region was compressed, but may not have been completely eliminated. Since contact was evident on both sides of this volume, the volume probably occurred at joint assembly, formed by an entrapped air pocket that received no hot gas flow during motor operation.

There was no evidence of gas flow within the joint beyond the char layer of the J-seal interface over the full circumference. No heat effect or erosion of the capture feature seal or the primary or secondary O-rings was identified.

Soot covered the bottom sector of the joint just beyond the radius of the J-seal leg. This soot accumulation occurred during the disassembly process, since surfaces on each side of this area were very clean.

No evidence of foreign material, ply separations, or tang- or clevis-edge unbonds were identified. The J-seal pressurization gap was partially filled (approximately 50 percent) with charred material over the full circumference. The charred material consisted of soot and charred insulation.

Aft Field Joint

The tang and clevis joint insulation were in good condition. The inboard surfaces of the tang and clevis joint insulation were nominally charred with some heat-affected area outboard of the char layer. Measurements of the tang and clevis material

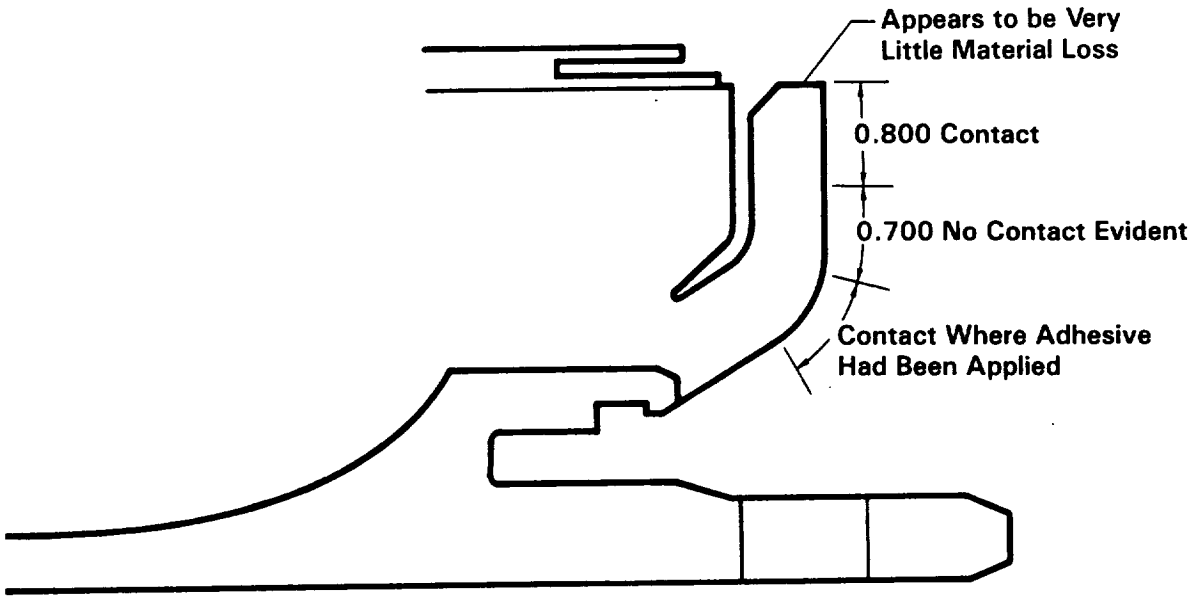

Figure 7.4-5. DM-9 Center Field Joint Post-Test

decomposition depths and heat-affected depths are provided in Table 7.4-4. The depth measurements on the tang side were taken from the ID surface of the tang leg at the pinhole. The depth measurements on the clevis side were taken from the ID surface of the inner clevis leg.

The general appearance of the pressure-sensitive adhesive was noted. There was no adhesive that appeared glossy, indicating contact between the tang and clevis insulation sealing surfaces had occurred everywhere in the adhesive-coated region. this observation indicates that the J-seal deflected leg appeared to have made contact from the tip of the J-seal leg to approximately 1.60 in. below the material remaining, measured radially outboard from the inboard tip of the J-seal leg (Figure 7.4-6). There was good contact through the radius region. The lack of a glossy adhesive region indicates that the V_3 volume section inboard of the radius region was probably eliminated.

There was no evidence of any gas flow within the joint beyond the char layer of the J-seal interface for the full circumference. No heat effect or erosion of the capture feature seal or the primary or secondary O-rings was noticed.

Soot and slag particles were identified in the bottom sector of the joint. This soot accumulation occurred during the disassembly process. This same condition was observed on DM-8. To verify that the soot and slag particle accumulation occurred during disassembly, the DM-8 tang-end insulation was cleaned with a methylchloroform-dampened Texwipe. No heat-affected material was found under the removed soot and slag; therefore, the accumulation did not occur during motor operation. The DM-9 joint condition in the bottom sector was typical.

No evidence of foreign material, ply separations, or tang-edge unbonds were identified. Nine clevis edge unbonds were found with the largest measuring 0.19 in. deep by 4.70 in. circumferentially. The J-seal pressurization gap was completely filled with charred material over the full circumference. The charred material consisted of soot, charred insulation, and particulate slag.

Table 7.4-4. Field Joint Measurements - Aft (Sta 1491.5)

Clevis End Measurements	Location (deg)	Measurements (in.) (1)	(2)	(3)
	0	2.90	2.18	1.67
	90	2.94	2.76	2.44
	180	2.84	2.52	2.38
	270	2.82	2.66	2.59

Tang End Measurements	Location (deg)	Measurements (in.) (1)	(2)	(3)
	0	3.46	2.78	1.79
	90	3.46	2.80	2.50
	180	3.00	2.78	2.38
	270	3.10	2.78	2.40

All measurements are taken from the ID of the tang leg (pinhole) or inner clevis leg.

Measurements: (1) To the tip of the remaining material
(2) To the outboard edge of the char layer
(3) To the outboard edge of the heat-affected material (i.e. measurement of the virgin material remaining)*

* Location based on the tan discoloration of the adhesive

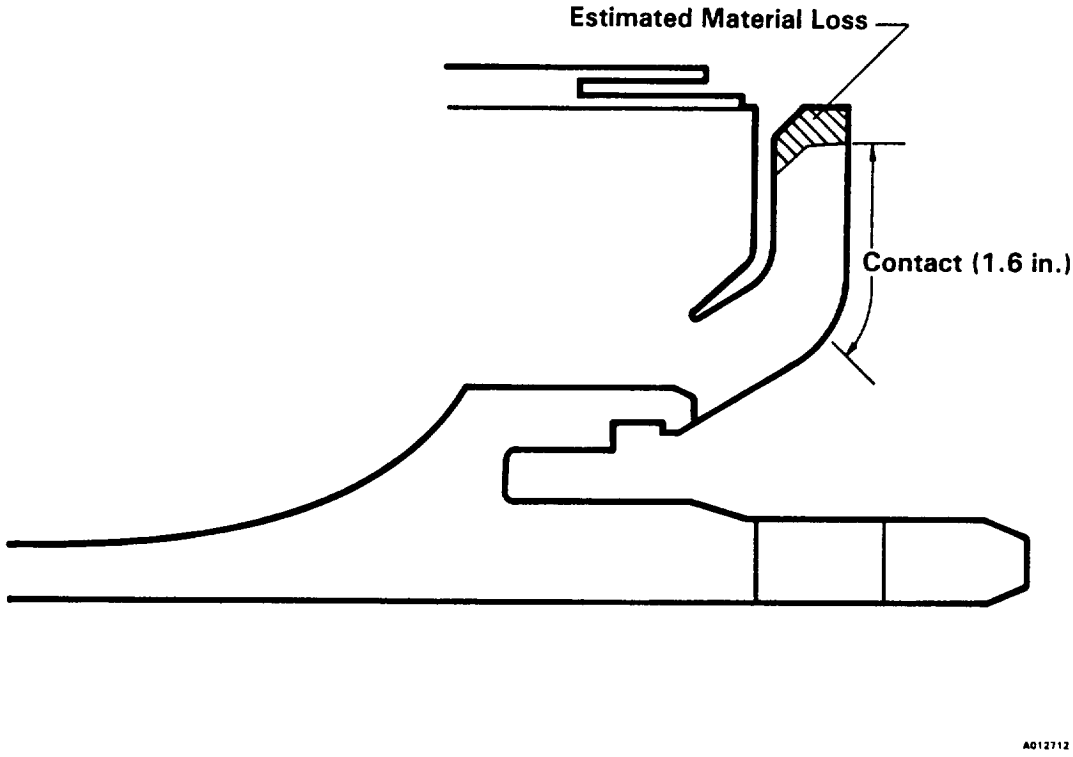

Figure 7.4-6. DM-9 Aft Field Joint Post-Test

7.4.4.2 Factory Joint. All seven factory joints were disassembled and inspected. No problems were found. There were no gas paths, sooting, abnormal heat-affected material, foreign material, or ply separations. Areas of apparent insulation-to-case separations were found intermittently on several of the joints, but they appeared to be caused by the disassembly process.

7.4.4.3 Nozzle-to-Case Joint. A fiber optic video inspection of the joint bondline was performed prior to disassembly. The joint bondline and the face of the joint stress relief flap were visible and appeared to show little erosion. Following the demate, it was evident that a layer of char existed at the original flap face, and that erosion of the flap behind this char layer had occurred (Figure 7.4-7).

The erosion in the joint region appeared to be less than had been analytically predicted, but was approximately the same as DM-8. This was less than the HPM static motor average loss for this region. The char layer on the carbon-fiber-filled/ethylene-propylene-diene monomer (CF/EPDM) had swollen to the point that the material thickness at the joint exceeded the material prefire thickness by approximately 0.5 in. (Figure 7.4-7). The joint stress relief flap and the baffle exhibited approximately 0.5 to 0.75 in. of erosion from the prefire condition, which is similar to DM-8 and close to the expected erosion.

The effects of slag on the nozzle-to-case joint insulation were minimal. Full evaluation of slag accumulation will have to be completed on a flight motor when the motor is fired in a vertical attitude.

A gas path into the polysulfide bondline region was noted at 46.8 deg. The path was filled with a black, viscous substance with the consistency of grease. This material was later identified as decomposed polysulfide, containing no grease. This indicated hot gas had flowed to the wiper O-ring, but there was no evidence of any gas past the wiper. The wiper O-ring was not damaged. The size of the path was 0.20 in. wide at the forward edge of the flap, 0.23 in. wide at the step region, and 0.20 in. wide

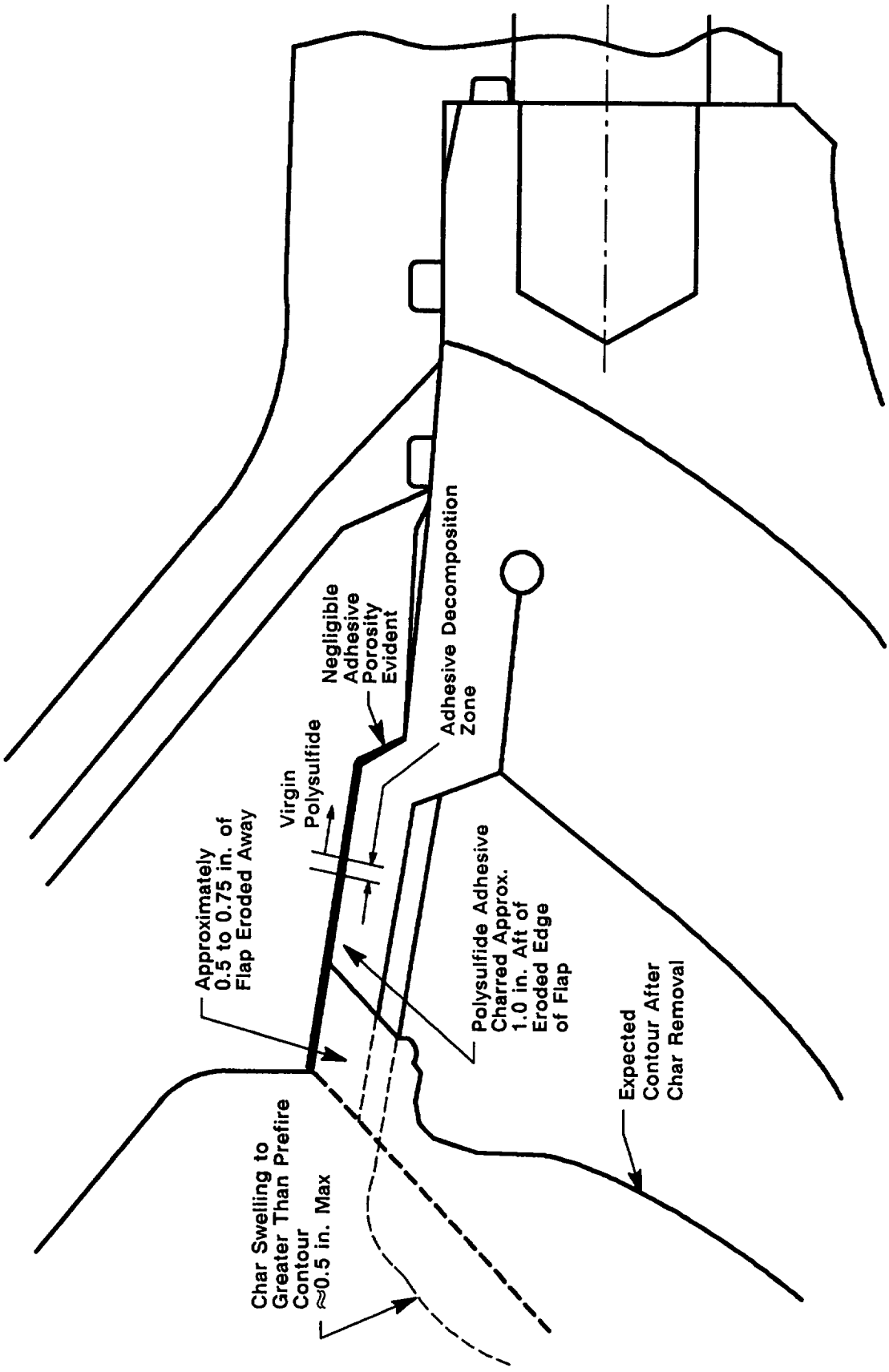

A012607a

Figure 7.4-7. Nozzle-to-Case Joint Erosion Profile

at the wiper O-ring. A sketch of the gas path is shown in Figure 7.4-8. Decomposed polysulfide was also noted just forward of the wiper O-ring from 0 to 63 deg. Intermittently around the full circumference, discoloration of the polysulfide was noted in void areas ahead of the wiper. This indicates there was hot gas penetration practically full circumference just forward of the wiper O-ring.

The DM-9 gas path was very similar to a gas path found in the nozzle-to-case joint of TPTA 1.1. One probable cause of these gas paths is short wiper vent slots. The purpose of the slots is to allow air to vent aft past the wiper O-ring during nozzle installation. If the slots are too short, air is trapped forward of the wiper O-ring, causing a void or path for gas to form in the polysulfide bondline. The slots on DM-8 were longer than DM-9 and there was no gas path in DM-8. The distance from the forward edge of the slot to the nozzle boss ranged from 2.75 to 2.79 in. on DM-9 and from 2.80 to 2.87 in. on DM-8. Another indication of inadequate venting in the joint is the fact that there was no polysulfide fill in any of the vent slots on DM-9.

One large void was noted in the polysulfide adhesive forward of the step in the phenolic. The void extended from 74 to 109 deg circumferentially and measured from 0.15 to 1.30 in. wide longitudinally. There was discoloration indicating gas flow and erosion into the void. A diagram of the void is shown in Figure 7.4-9.

The polysulfide adhesive bondline was decomposed approximately 1.0 in. farther into the joint (6.0 in. from the aft face of the nozzle boss, as shown in Figure 7.4-7) than the flap erosion. The decomposed adhesive formed a hard char layer and remained intact on the nozzle fixed housing. The adhesive in the small decomposition zone aft of the decomposed material was black and had a consistency similar to grease. Although the material was decomposed, no gas flow had occurred in the adhesive bondline region, except at the gas path located at 46.8 deg and the void located at 74 to 109 deg. The surface of the NBR flap under the decomposed adhesive was heat affected and hardened, but showed no signs of erosion.

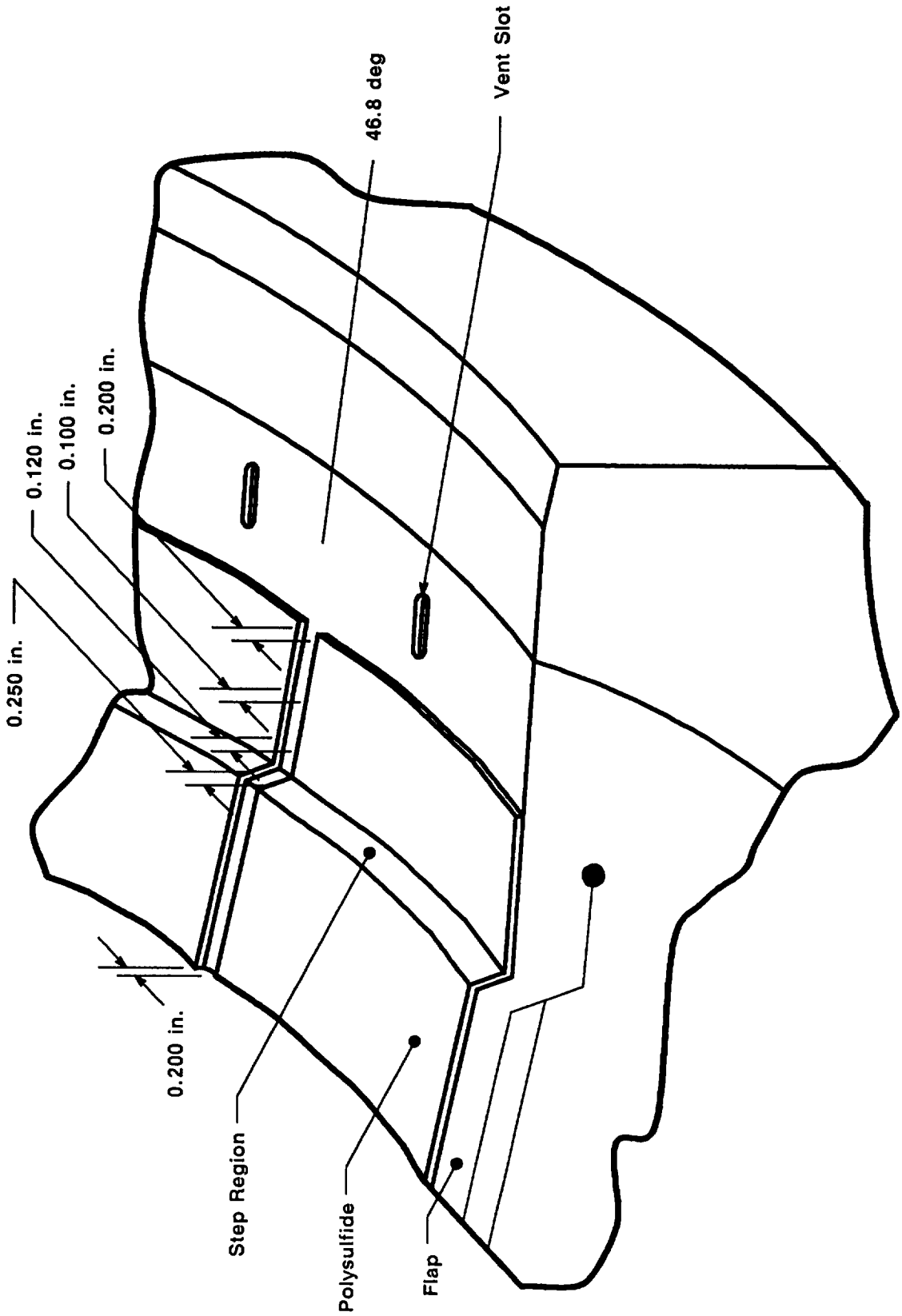

Figure 7.4-8. Nozzle-to-Case Joint Gas Path to Wiper O-ring

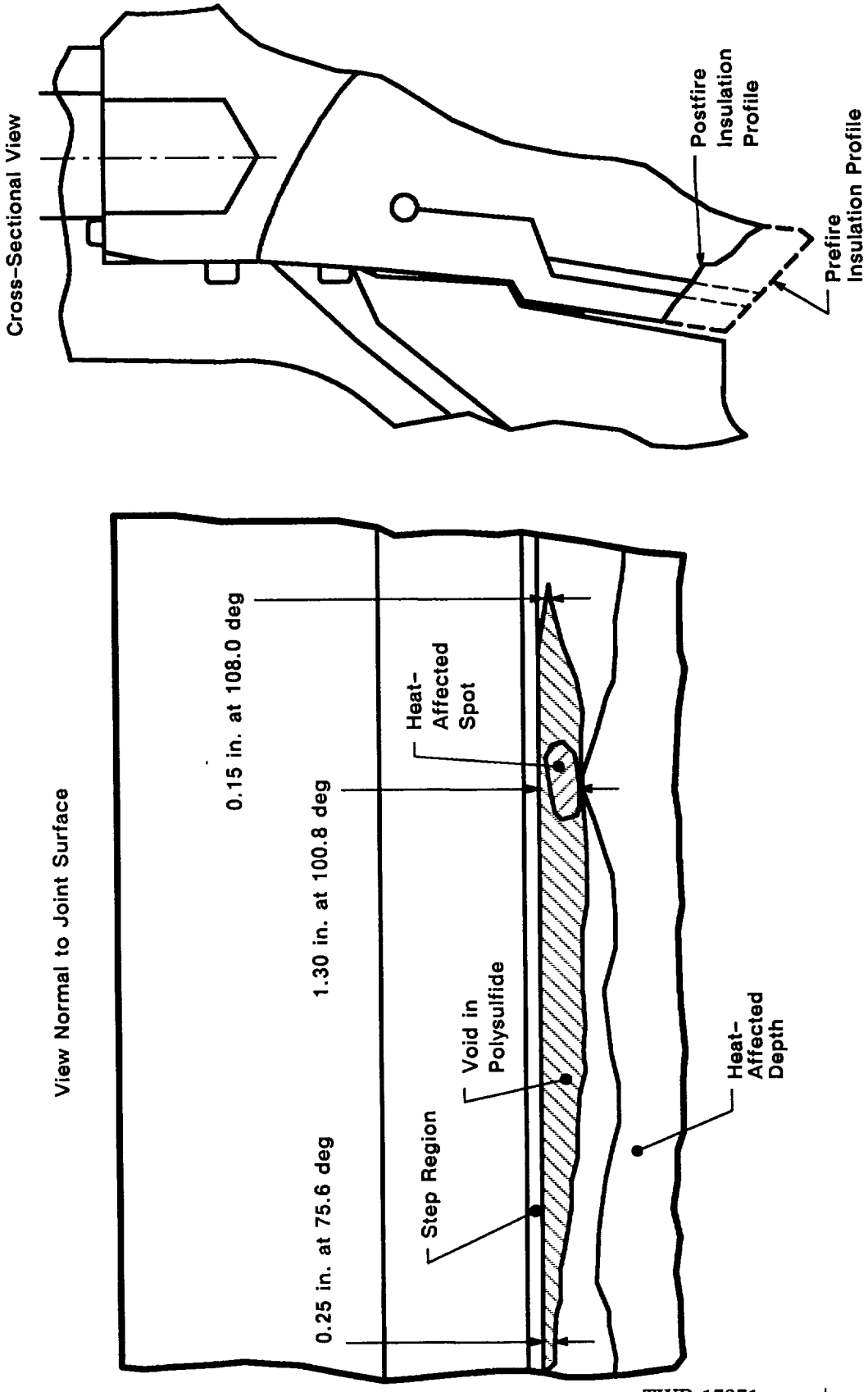

Figure 7.4-9. Nozzle-to-Case Joint Void in Polysulfide Bondline

The failure mode of the polysulfide upon disassembly showed approximately 80 percent adhesive failure at the polysulfide-to-NBR interface and approximately 20 percent cohesive failure within the polysulfide adhesive. Inadequate abrasion of the NBR prior to assembly is the most probable cause of this high adhesive failure. No porosity was noted at the insulation step region of the joint within the polysulfide, but there was porosity at the forward edge of the heat-affected area of the bondline. DM-8 exhibited much more porosity in the polysulfide at the step region.

The baffle appeared to be in excellent shape, and the Teflon tape was intact in the upper baffle. There were no ply separations noted visually in the insulation layup of the aft dome. Four edge unbonds at the nozzle boss were noted, with the deepest measuring 0.075 in. deep by 0.150 in. circumferentially. There were also no cracks noted at the wiper vent slots in the aft dome insulation.

Insulation Design Engineering is pleased with the performance of the nozzle-to-case joint. Even though there was a gas path through the bondline, no gas reached the primary O-ring and none of the joint components were damaged, including the wiper O-ring. This verifies that the new joint design is tolerant of polysulfide gas paths and voids without compromising the performance of the joint. Steps are being taken to reduce the chances of gas paths, but it is not possible to totally eliminate them.

7.4.4.4 Internal Insulation

Forward Segment

The stress relief flap remained intact full circumference. The flap was curled forward approximately perpendicular to the case wall. The edge of the flap in the upper sector showed signs of heating, and the outboard surface of the flap in the lower sector showed areas of light discoloration that resulted from slag heating. A small amount of slag was found in the lower sector of the forward segment near the field joint.

There was no castable inhibitor remaining, unlike ETM-1A and DM-8 which had castable inhibitor remaining intact in the lower sector. No abnormal erosion patterns were identified.

Forward Center Segment

The forward-facing NBR inhibitor exhibited uniform erosion for the full circumference.

The stress relief flap was eroded back to the flap bulb over most of the circumference. This erosion is typical of past static test motors. The CF/EPDM was heat affected and loose.

Aft Center Segment

The forward-facing NBR inhibitor exhibited uniform erosion for the full circumference.

Slag was observed in the lower sector of the aft end of the segment. The slag extended from the J-seal to 17 in. forward of the J-seal, with a maximum width of 26 in. and a maximum depth of 1.5 in. at the J-seal.

The stress relief flap was eroded back to the flap bulb over the full circumference. This erosion is typical of past static test motors. The CF/EPDM under the stress relief flap was eroded away, which is normal.

Aft Segment

The forward-facing NBR inhibitor exhibited uniform erosion over the full circumference.

A slag pool existed over the length of the segment. The maximum surface width of the pool was 46 in. and the maximum depth was 3 in. at the forward end of the segment. The slag pool dimensions were taken at several axial locations throughout the aft segment. These dimensions are listed in Table 7.4-5.

Table 7.4-5. Internal Slag - Aft/Aft Center Segments

Aft Segment	Estimated Depth (in.)	Width (in.)
Stiffener-to-dome joint	5	22
Stiffener-to-stiffener joint	3	39
ETA-to-stiffener	3	43
Forward end of ETA	3	46
Aft Center Segment	**Estimated Depth (in.)**	**Width (in.)**
Maximum width 0-in. axial location	1.5	26
Minimum width 17-in. axial loation	0	0

The postfire insulation decomposition profile on DM-8 and DM-9 was significantly different in the region of the aft dome near the nozzle-to-case joint when compared to HPM aft dome decomposition profiles. The most notable differences were at Stations 2 and 3 where there was less material decomposition than has previously been seen. The redesign of the nozzle-to-case joint included a change in CF/EPDM ply direction in the region under the stress relief baffle. The plies are now laid up perpendicularly rather than parallel to the dome surface. The investigation of the nozzle problems in the DM-9 test motor have raised questions as to whether nonuniform erosion was seen in the aft dome insulation in the plane of this occurrence on past static test motors.

Figure 7.4-10 is a plot showing the material decomposition depth (MDD) of DM-9 at the 291.6-deg location plotted against the median MDD at 291.6 deg from the HPM database.

Figures 7.4-11 through 7.4-21 are polar plots of the MDD at each station as measured on the DM-9 aft dome. The MDD are plotted with the HPM mean MDD (QM-4, DM-5, DM-6, and DM-7). These figures are not final, as there has not been sufficient time to completely evaluate the data. Station 1 is not plotted since changes in the joint configuration and the addition of a flap gap make the comparison misleading.

Figure 7.4-22 is a plot of the duty cycle experienced during the DM-9 test firing. The vector plane was predominately in the 90- to 270-deg plane. The motor was fired at the 0-deg down position.

The figures show that although the erosion is circumferentially nonuniform, this condition is typical of previous static test motors. No unusual erosion was seen in the MDD in the 45-, 135-, 225-deg sector (location of the boot ring problems). No MDD measurements exceeded the maximum MDD in the database.

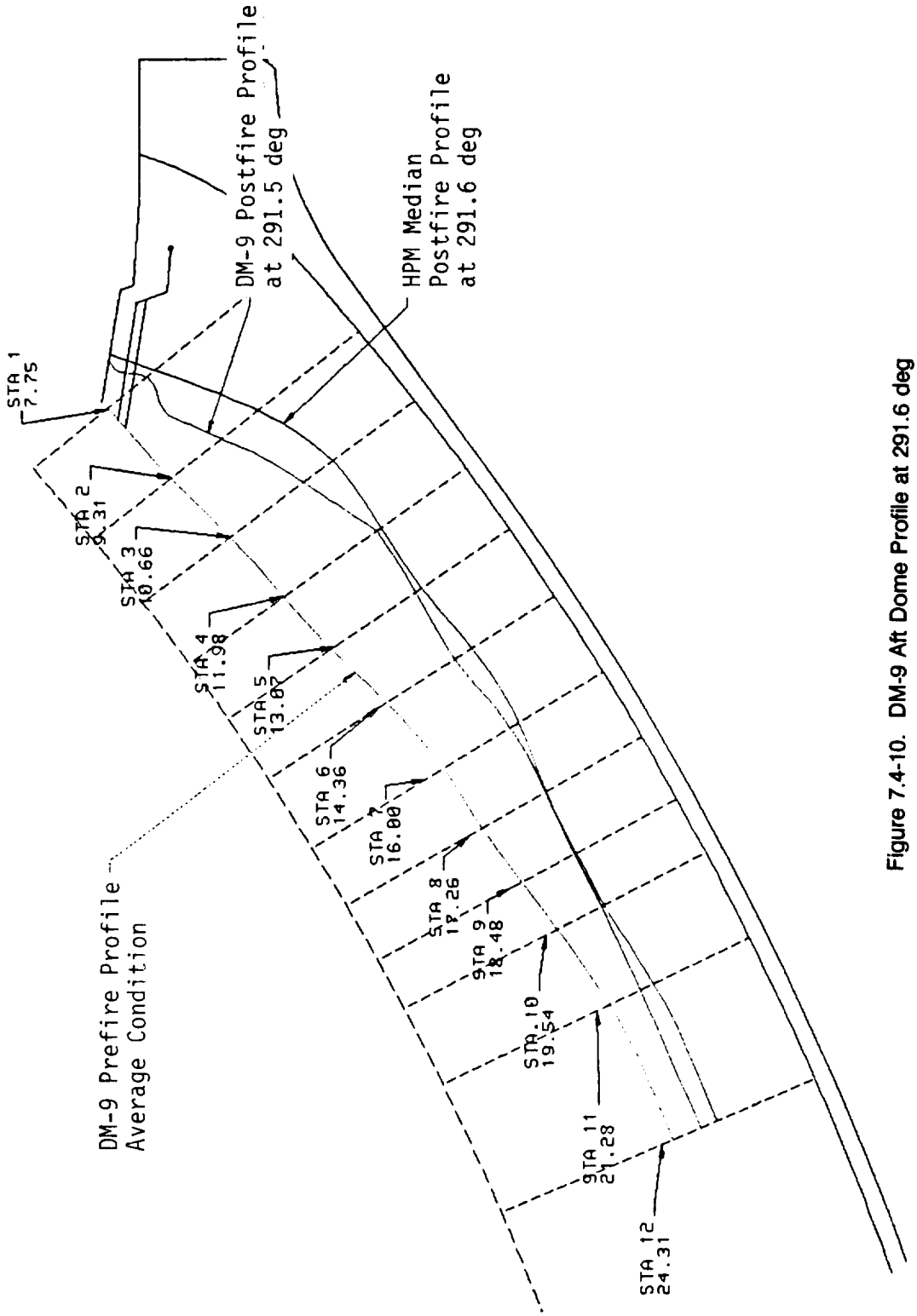

Figure 7.4-10. DM-9 Aft Dome Profile at 291.6 deg

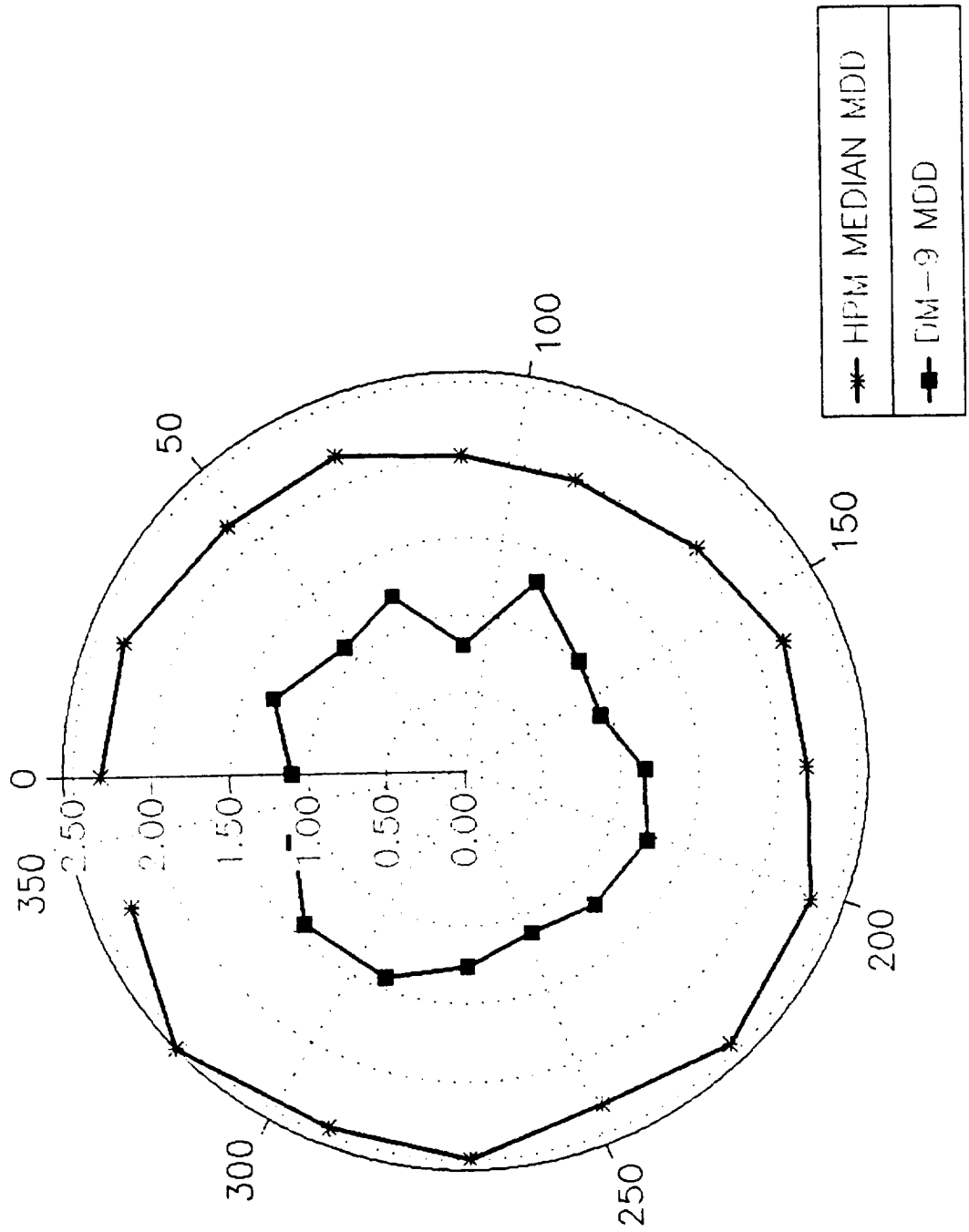

Figure 7.4-11. DM-9 Aft Dome 9.3 in. Station

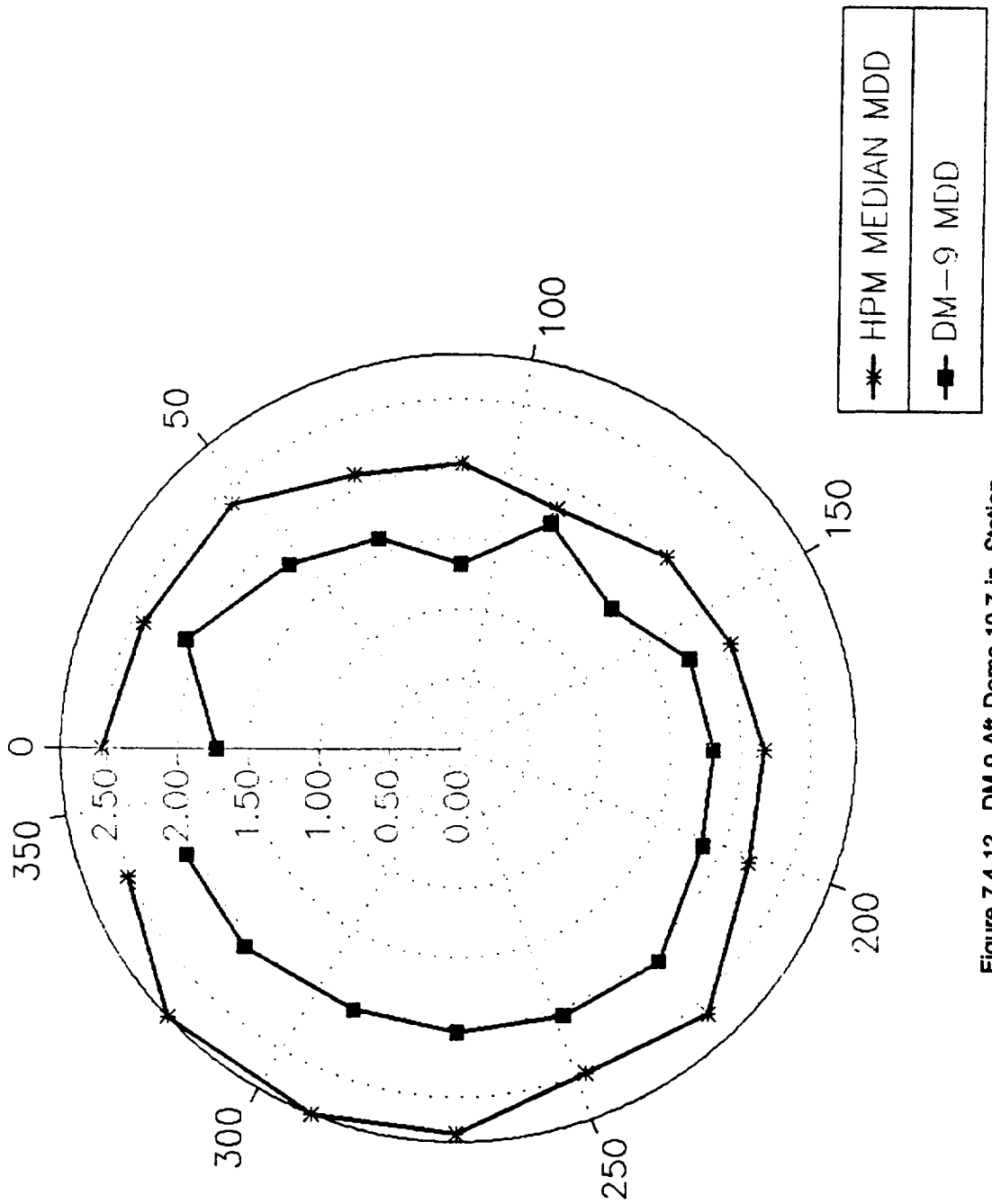

Figure 7.4-12. DM-9 Aft Dome 10.7 in. Station

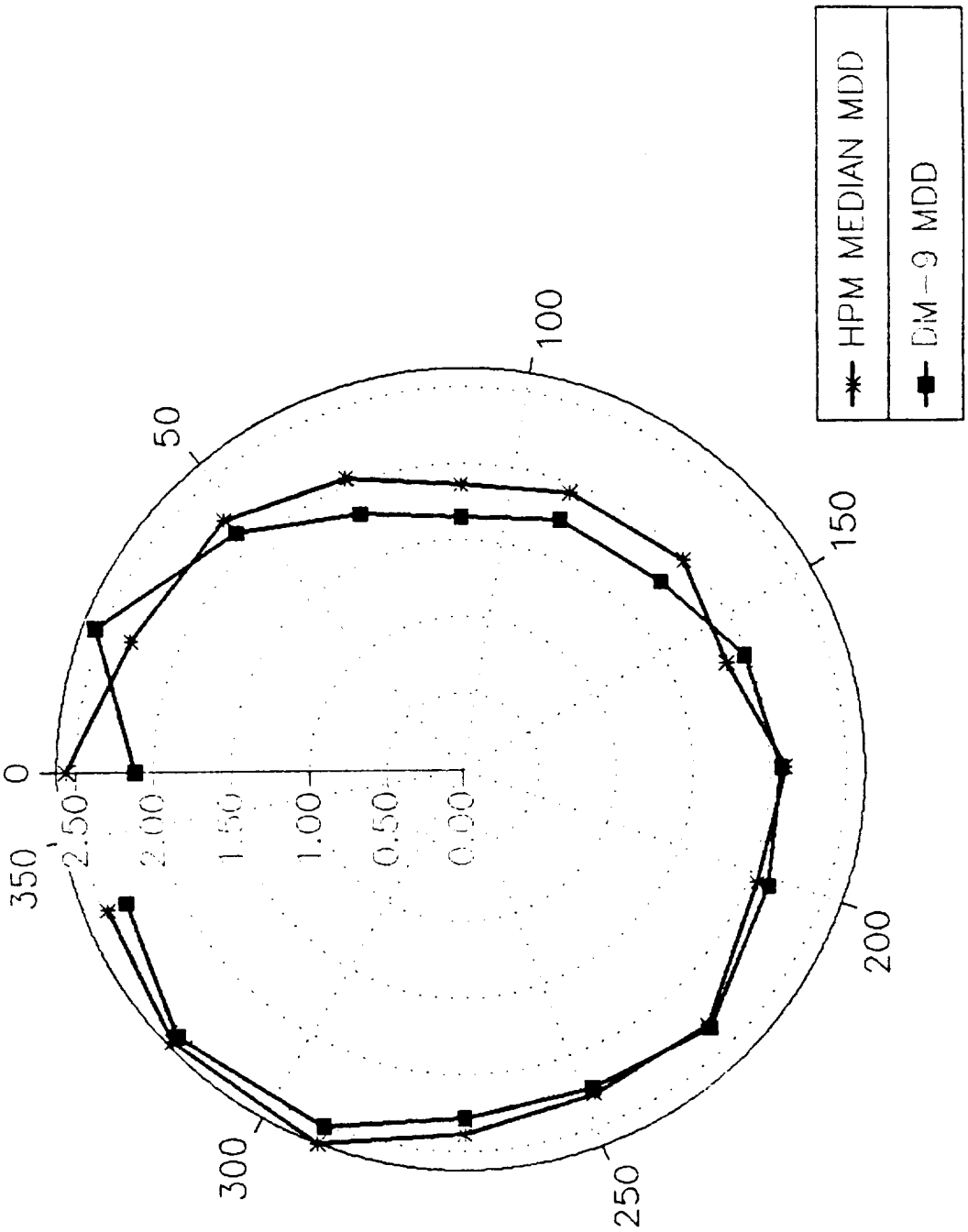

Figure 7.4-13. DM-9 Aft Dome 12.0 in. Station

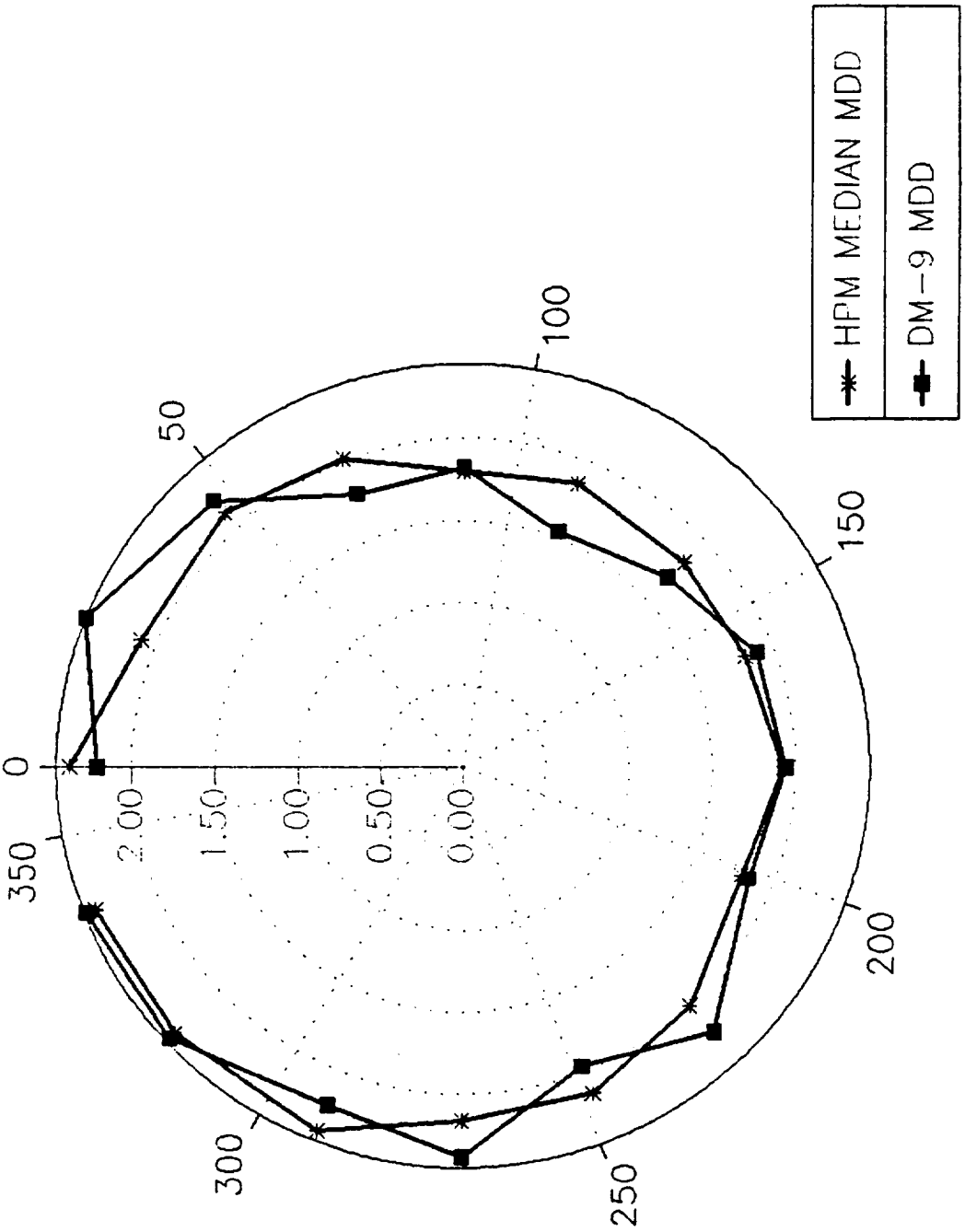

Figure 7.4-14. DM-9 Aft Dome 13.1 in. Station

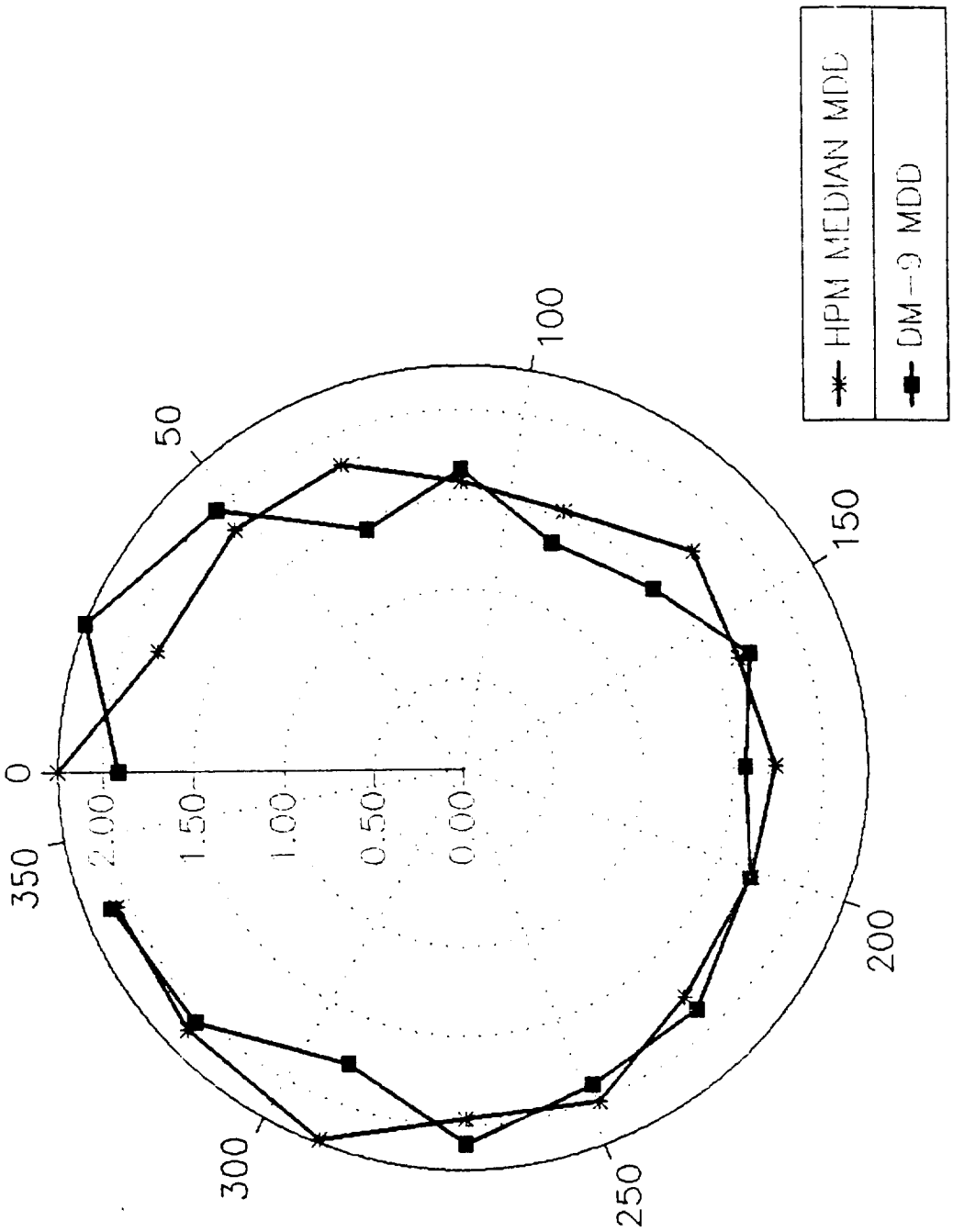

Figure 7.4-15. DM-9 Aft Dome 14.4 in. Station

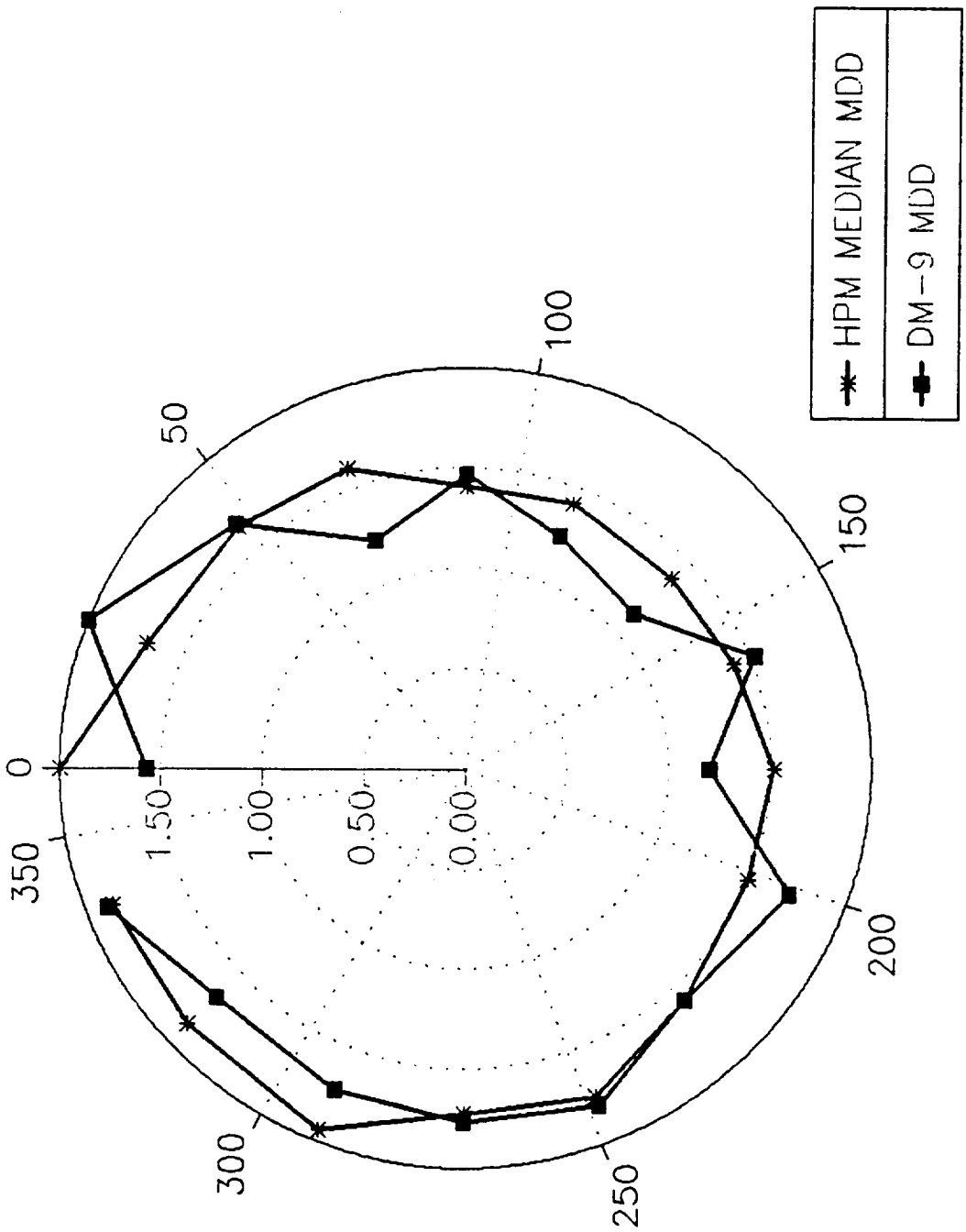

Figure 7.4-16. DM-9 Aft Dome 16.0 in. Station

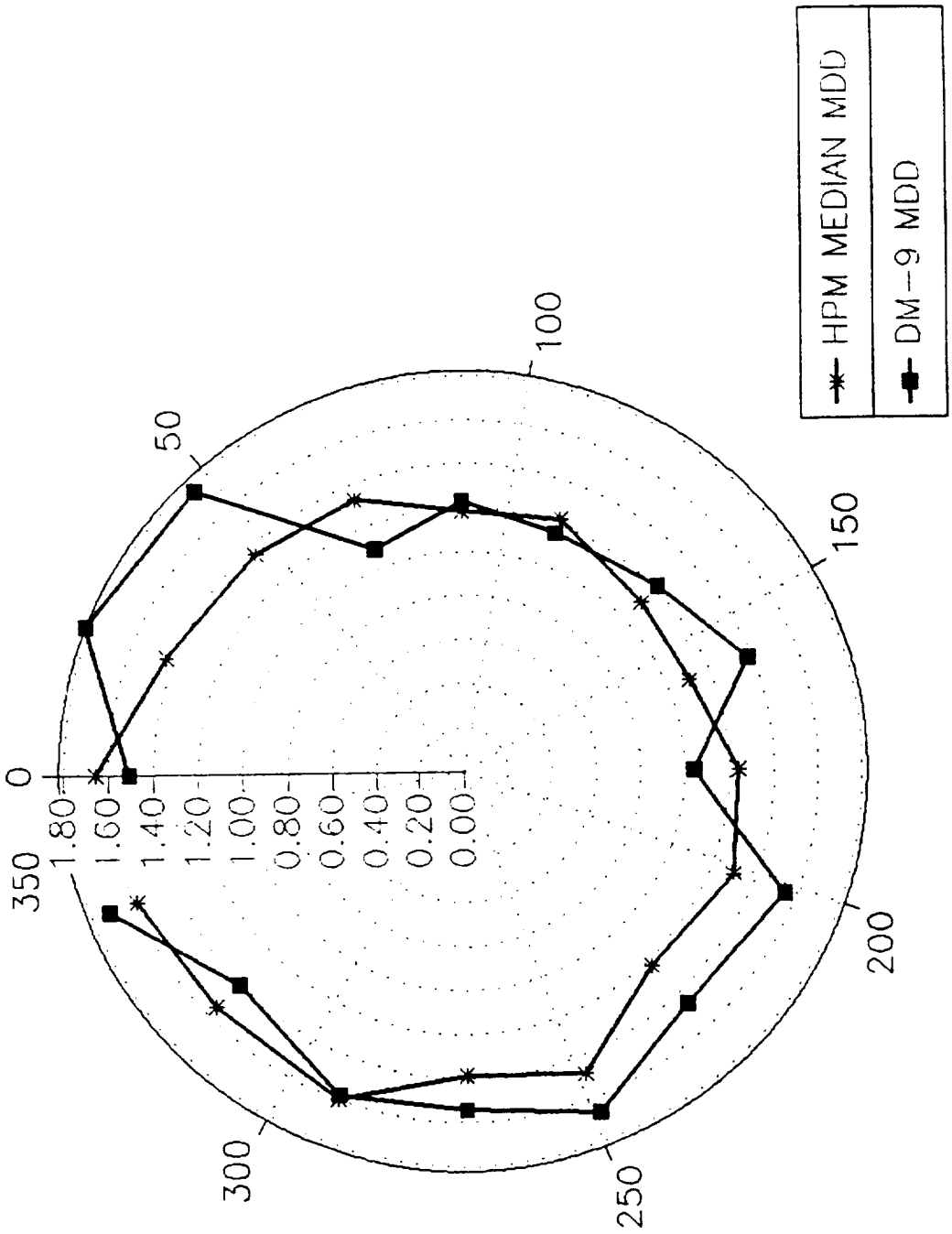

Figure 7.4-17. DM-9 Aft Dome 17.3 in. Station

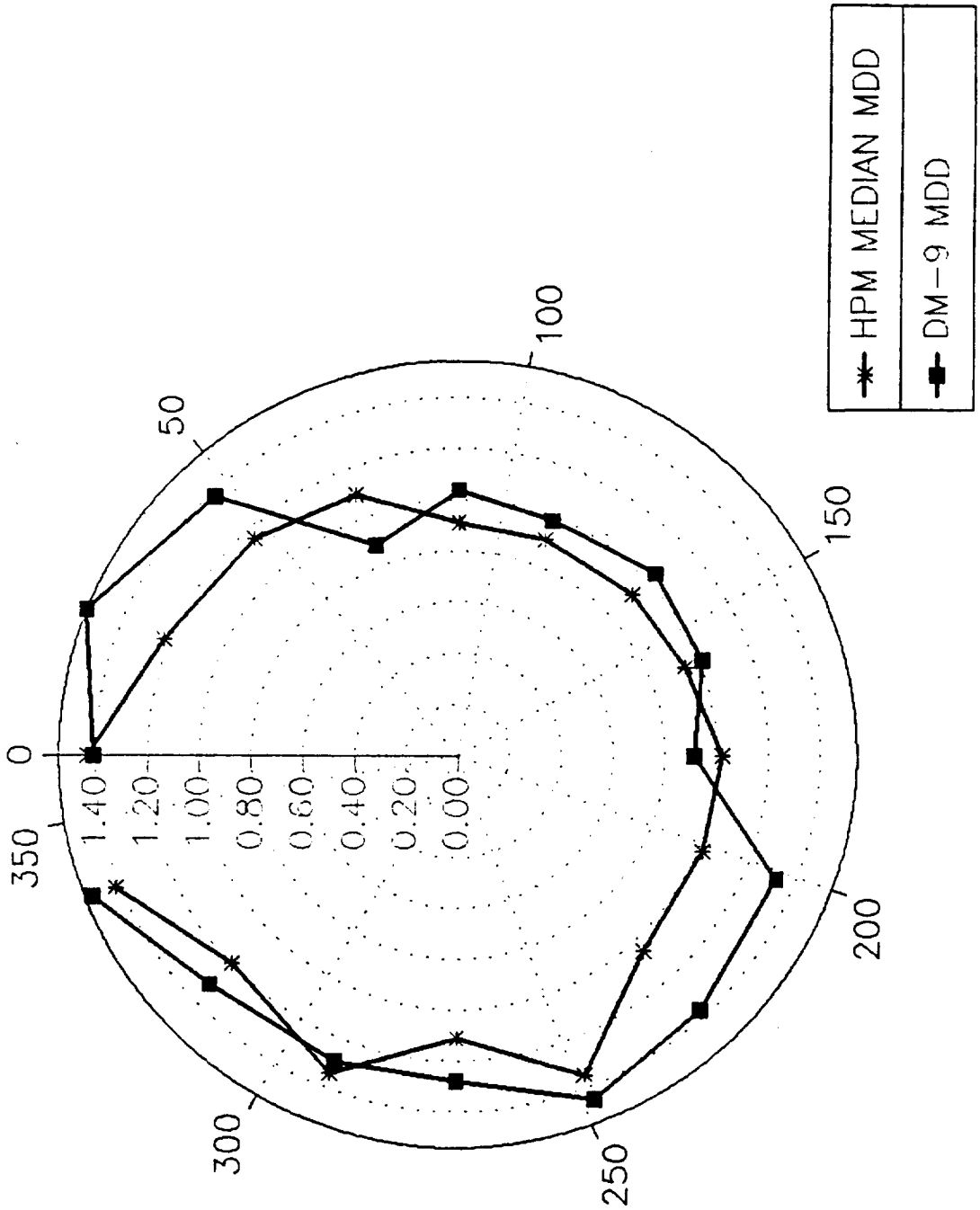

Figure 7.4-18. DM-9 Aft Dome 18.5 in. Station

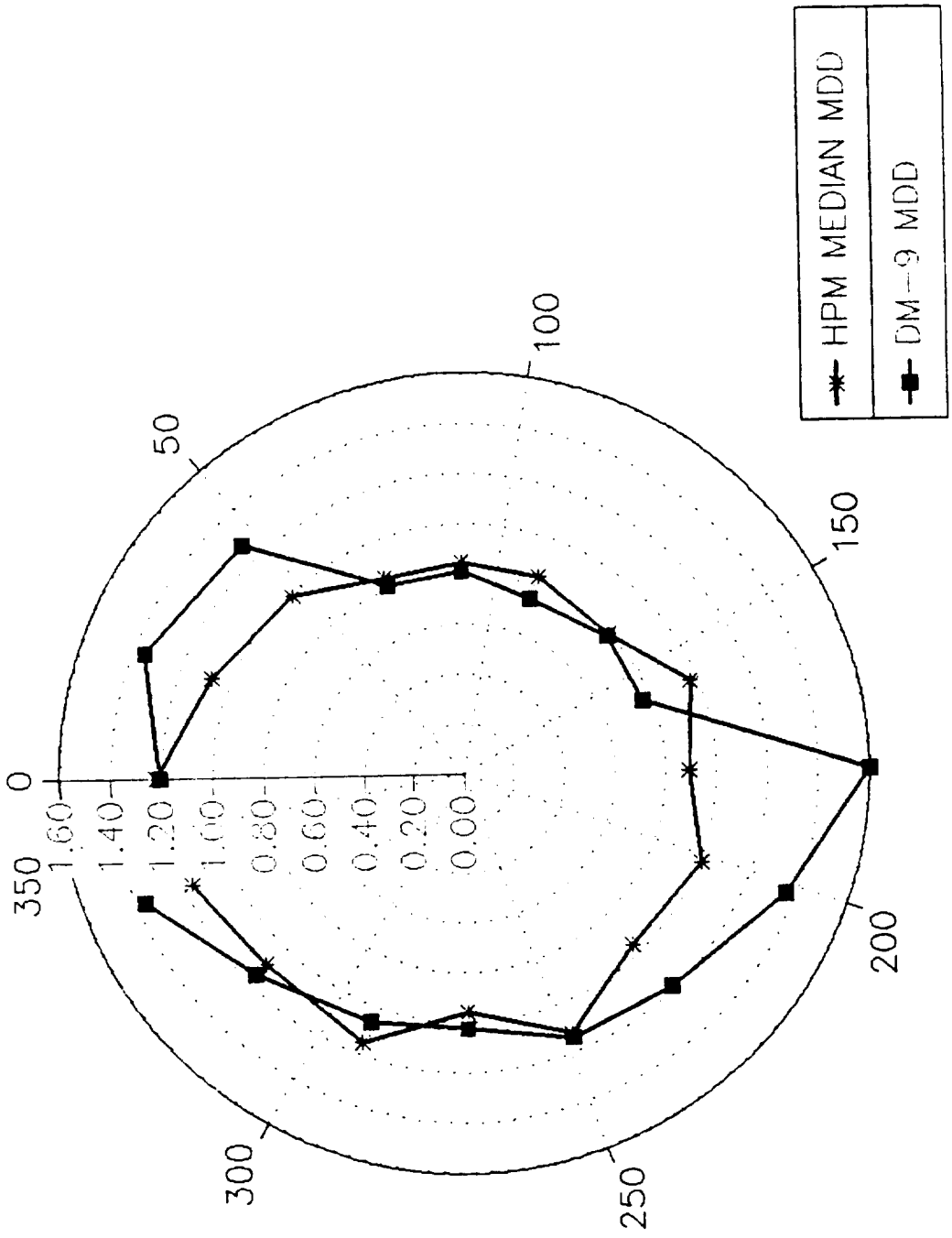

Figure 7.4-19. DM-9 Aft Dome 19.5 in. Station

C-3

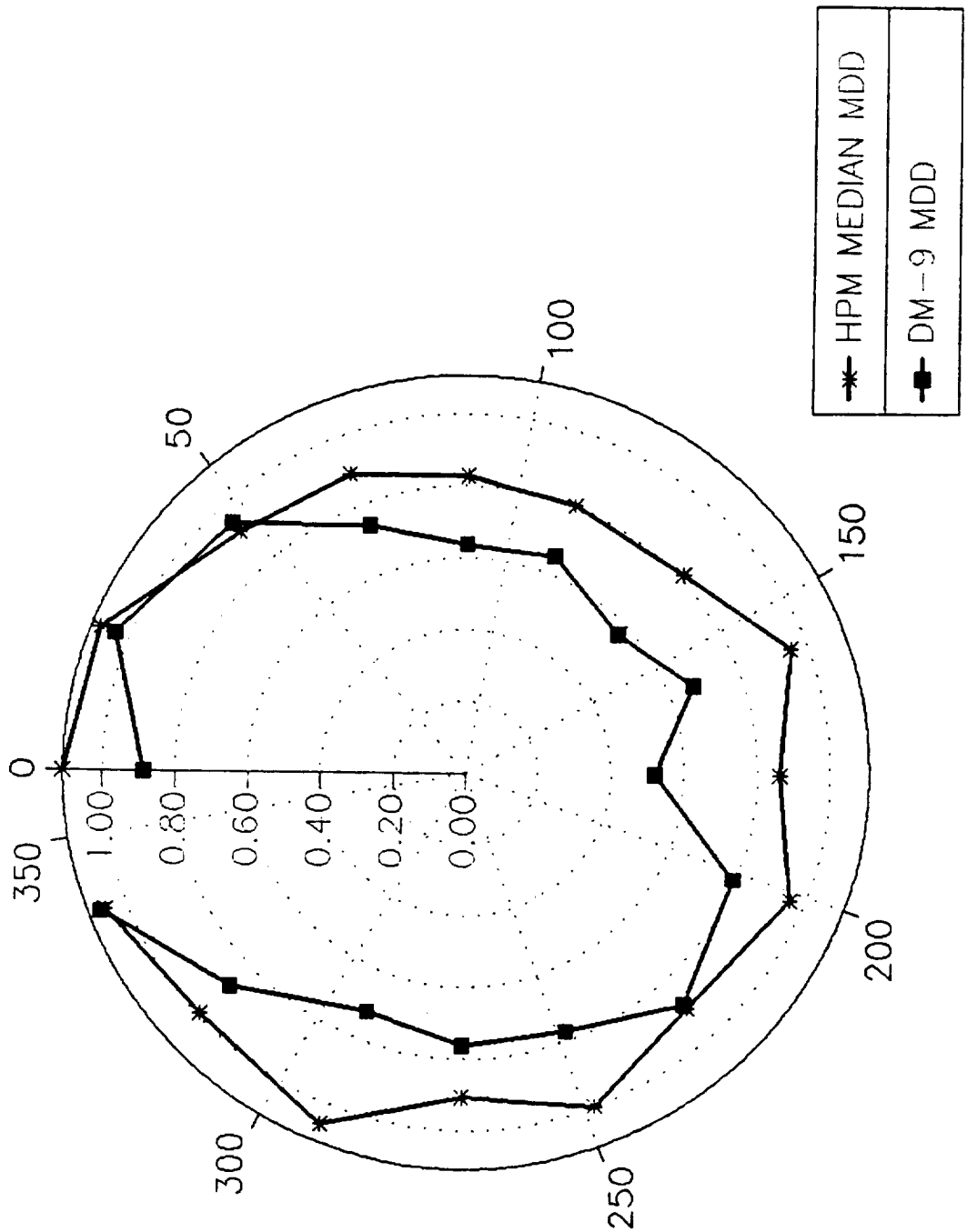

Figure 7.4-20. DM-9 Aft Dome 21.3 in. Station

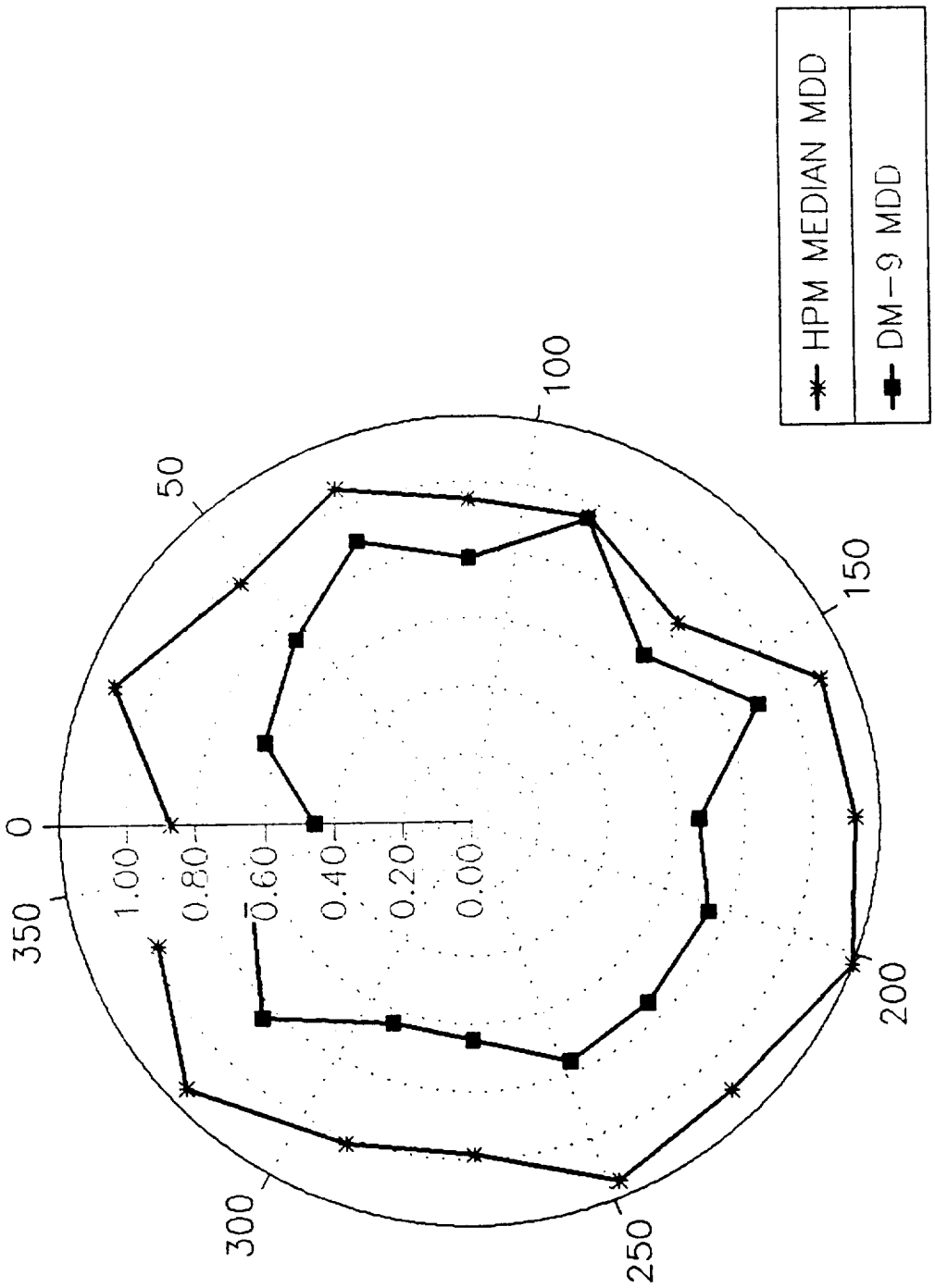

Figure 7.4-21. DM-9 Aft Dome 24.3 in. Station

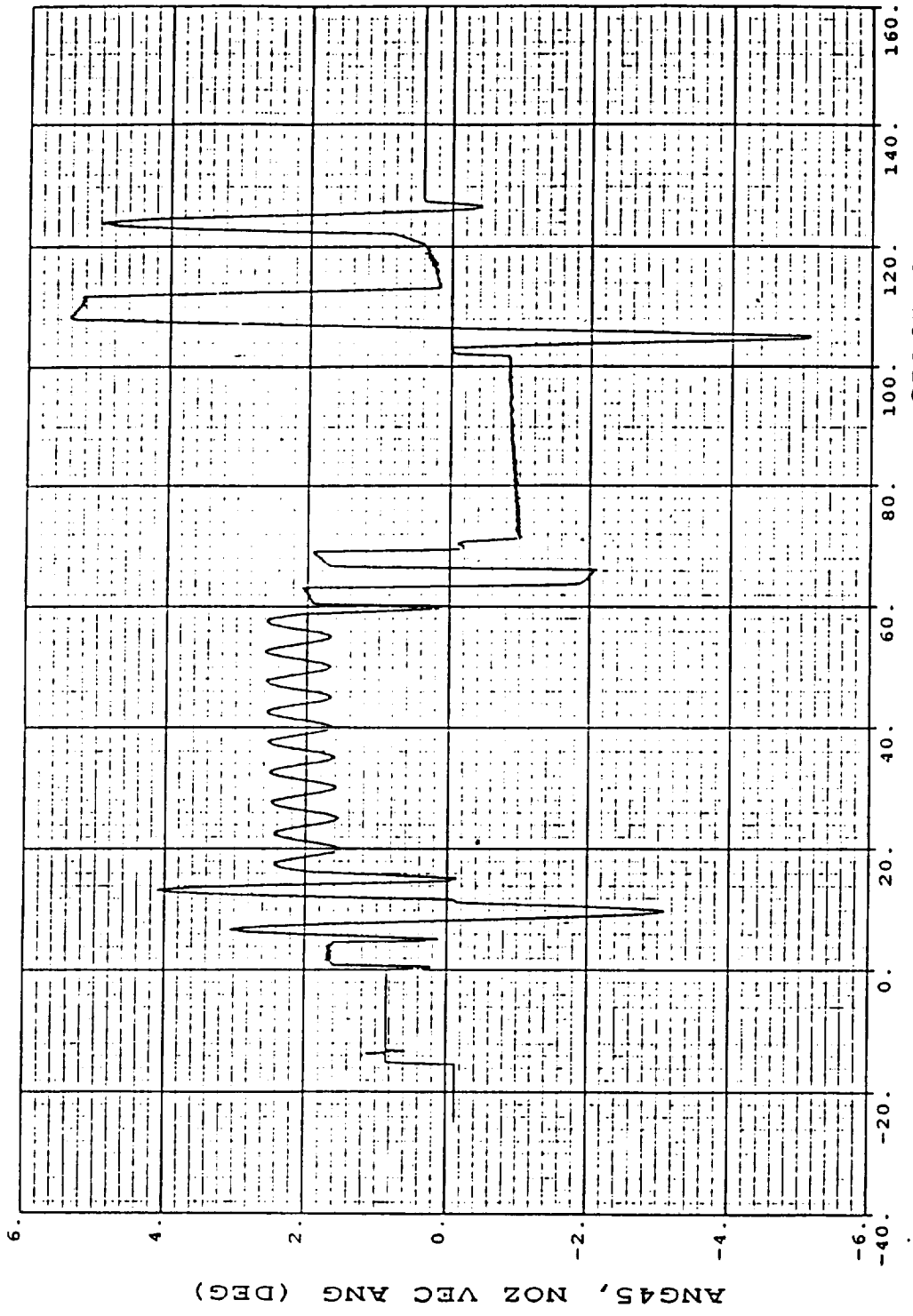

Figure 7.4-22. DM-9 Nozzle Vector Angle

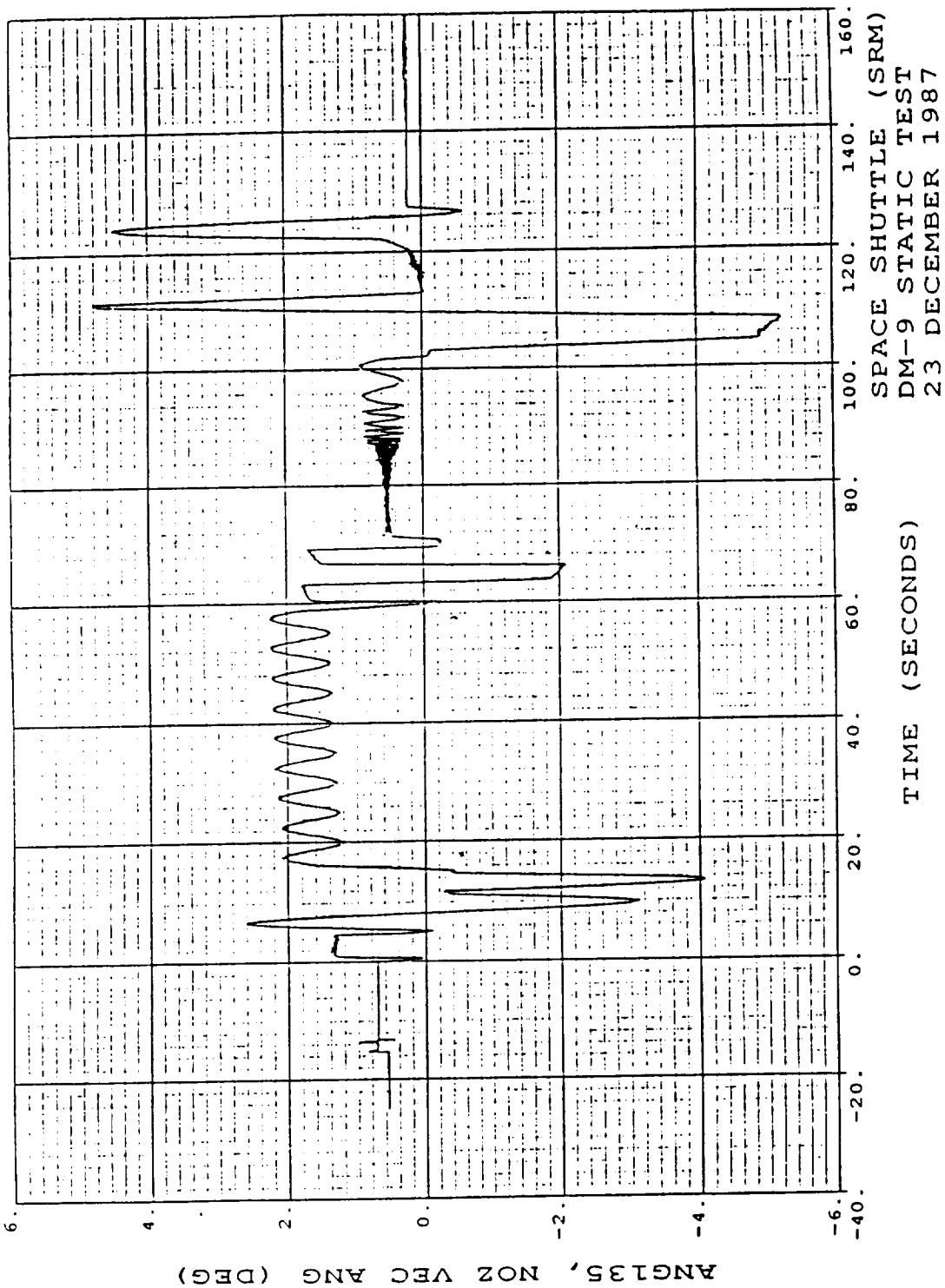

Figure 7.4-22. DM-9 Nozzle Vector Angle (cont)

ORIGINAL PAGE IS
OF POOR QUALITY

The aft dome erosion did not appear to have been affected by the nozzle vector cycle or the nozzle boot ring problems. The dome had a typical nonuniform pattern that has been seen in previous static test motors.

7.4.4.5 Insulation Component Program Team Recommendations. The Insulation Component Program Team has reviewed all observations presented in this document and has determined that the following three observations are potential anomalies. Each of the potential anomalies was further classified as a critical, major, or minor anomaly, or it remained an observation as defined in the Table 7.4-1 criteria.

Critical Anomalies: None

Major Anomalies: None

Minor Anomalies: None

Remains Observations

a. There was a gas path in the nozzle-to-case joint to the wiper O-ring, but not past wiper O-ring at 46.8 deg. No erosion or heat effects were noted on the wiper O-ring. The path was filled with a black, viscous substance which has been identified as decomposed polysulfide.
b. There was a large void in the polysulfide adhesive bondline forward of the step region, extending from 74 to 109 deg. There was evidence of gas flow into the void, resulting in decomposed polysulfide.
c. There was 85-percent adhesive failure at the polysulfide-to-aft dome interface. Inadequate abrasion of the NBR prior to assembly is the most probable cause.

7.5 NOZZLE

7.5.1 Introduction

Nozzle Assembly

The DM-9 nozzle was a partially submerged convergent/divergent movable design with an aft pivot point flexible bearing. There was no snubber assembly or aft exit cone linear shaped charge (LSC) severance system on the nozzle. The nozzle as shown in

Figure 7.5-1 consisted of the following subassemblies:

a. RSRM forward exit cone assembly

b. RSRM fixed housing

c. RSRM nose inlet assembly (PAA and primer on nose inlet housing)

d. RSRM throat inlet assembly

e. Thicker cowl with involute outer boot ring

f. Flex bearing, added O-ring groove on aft end ring (RSRM configuration)

g. RSRM aft exit cone

h. Room temperature vulcanization (RTV) backfill in Joints 1, 3, and 4

i. Redundant and verifiable seals in all five joints

j. RSRM nozzle plug

Figure 7.5-2 presents the differences between the DM-9 nozzle and the DM-8 nozzle design. The DM-9 nozzle subassembly liners and insulators were fabricated from the materials shown in Figures 7.5-3 and 7.5-4.

Flex Bearing

The 1U51060-01 S/N 000005R4 flex bearing shown in Figure 7.5-5 was static tested in the DM-9 nozzle. This flex bearing was previously used in the SRM-1A, SRM-6B, SRM-13A, and SRM-21B flight motors.

Nozzle - Composite Structures

Essential strain and temperature data were measured to verify the structural integrity of the nozzle and analytical modeling. Static motor tests, with conditions and loads close to those in actual flight, provide the only valid opportunity to obtain this data. Due to the severe environmental conditions on critical phenolic nozzle components during static firing, strain and temperature data is currently obtained only on the cool-side metal components. Verification of thermostructural analytical models and

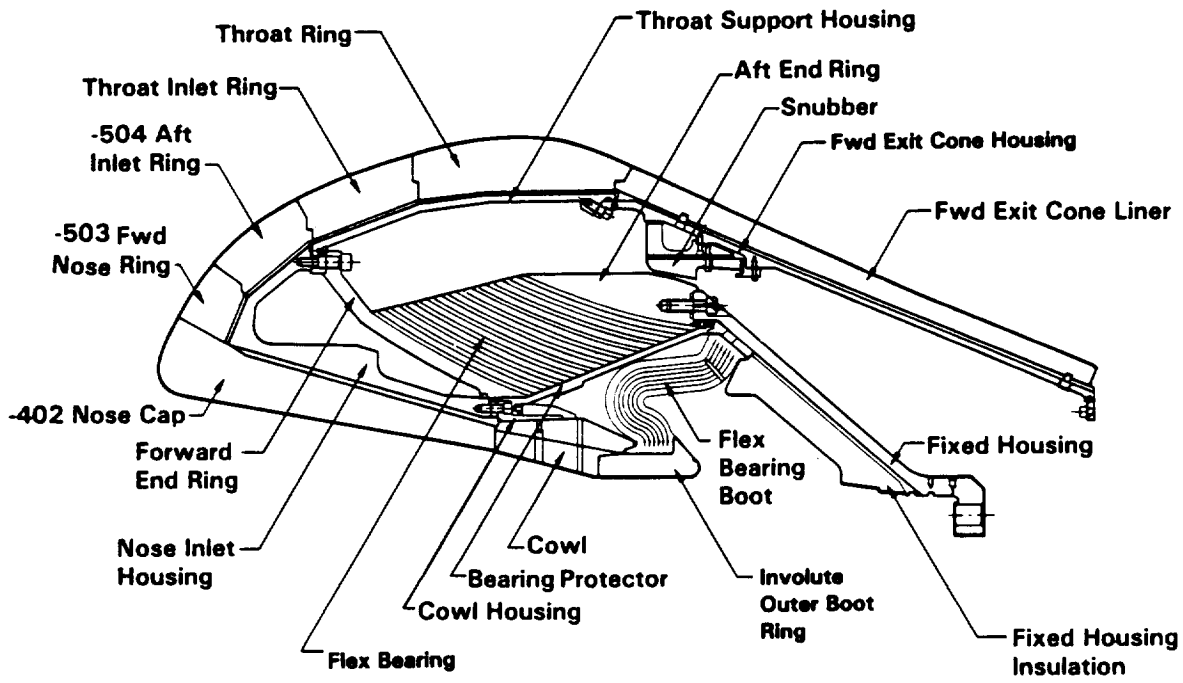

A006350 R1

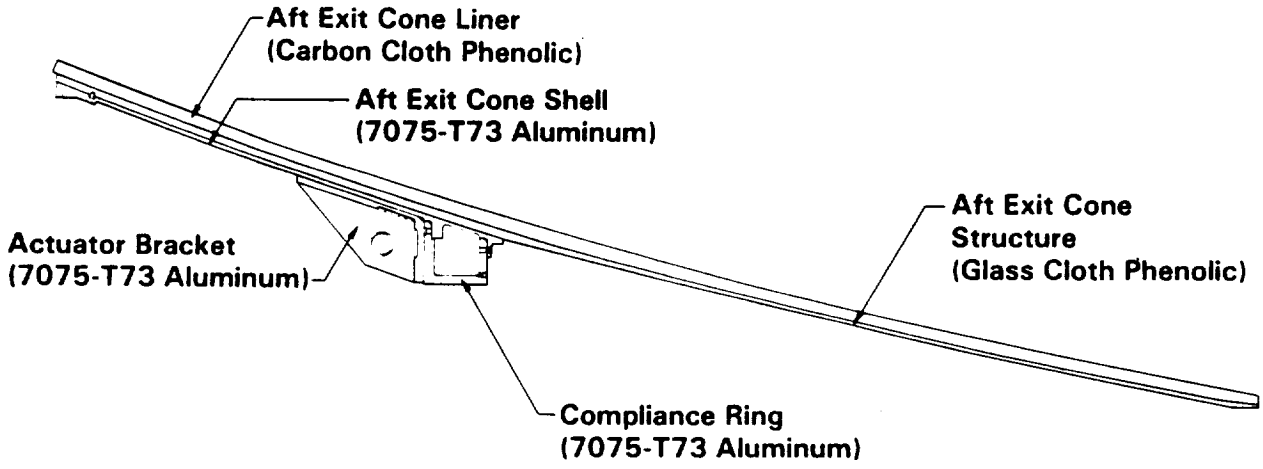

A006348 R1

Figure 7.5-1. DM-9 Nozzle Components

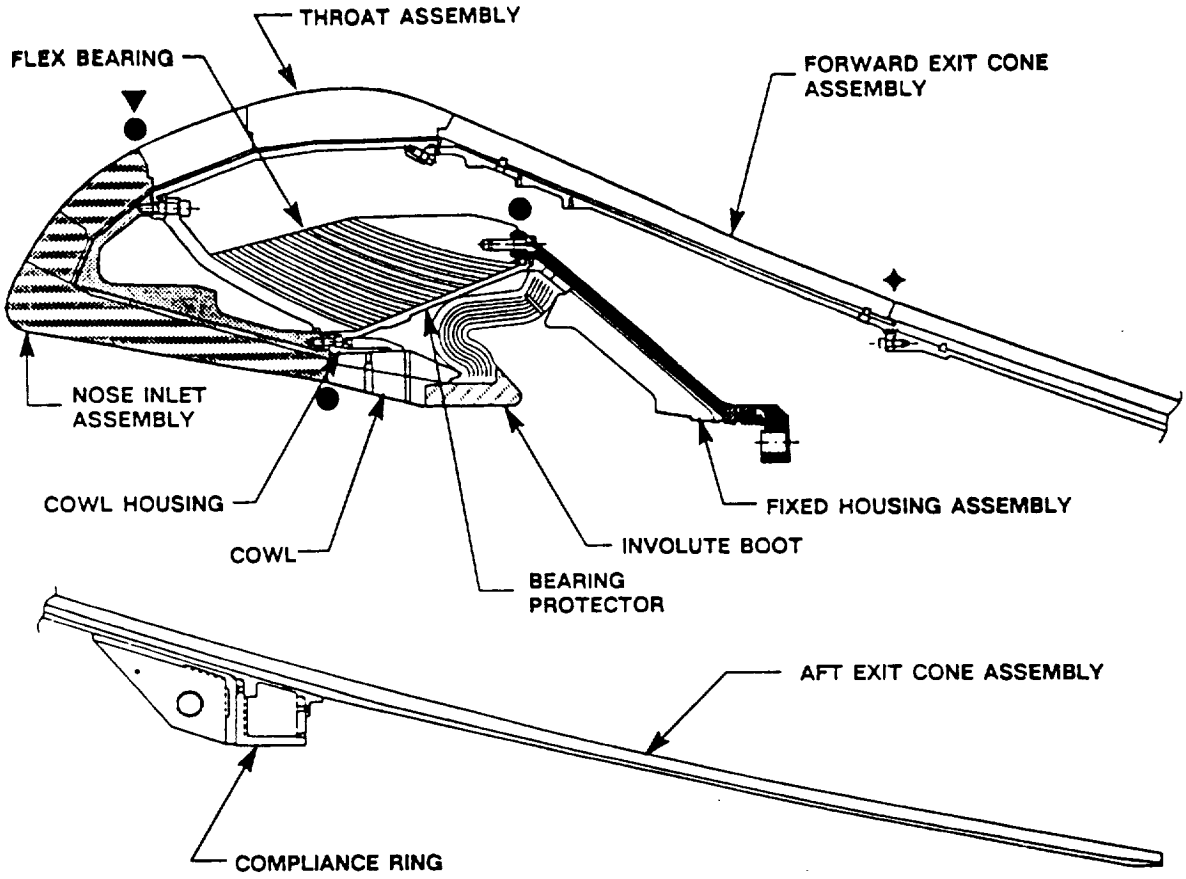

DESIGN CHANGES FROM THE DM-8 CONFIGURATION

- THICKER NOSE INLET HOUSING
- INVOLUTE OUTER BOOT RING
- THICKER FIXED HOUSING
- RETOLERANCED NOSE-INLET ASSEMBLY
- BACKFILLED RTV JOINT
- REDUNDANT SEALS WITH LEAK CHECK PORTS
- BACKFILLED POLYSULFIDE AT GCP/HOUSING INTERFACE AT FORWARD END OF AFT EXIT CONE ASSEMBLY

Vented shear pins and thicker EA 946 bondline in fwd and aft exit cone assemblies

EA 913 adhesive replaced with EA 913NA

A013990

Figure 7.5-2. DM-9 Nozzle Configuration

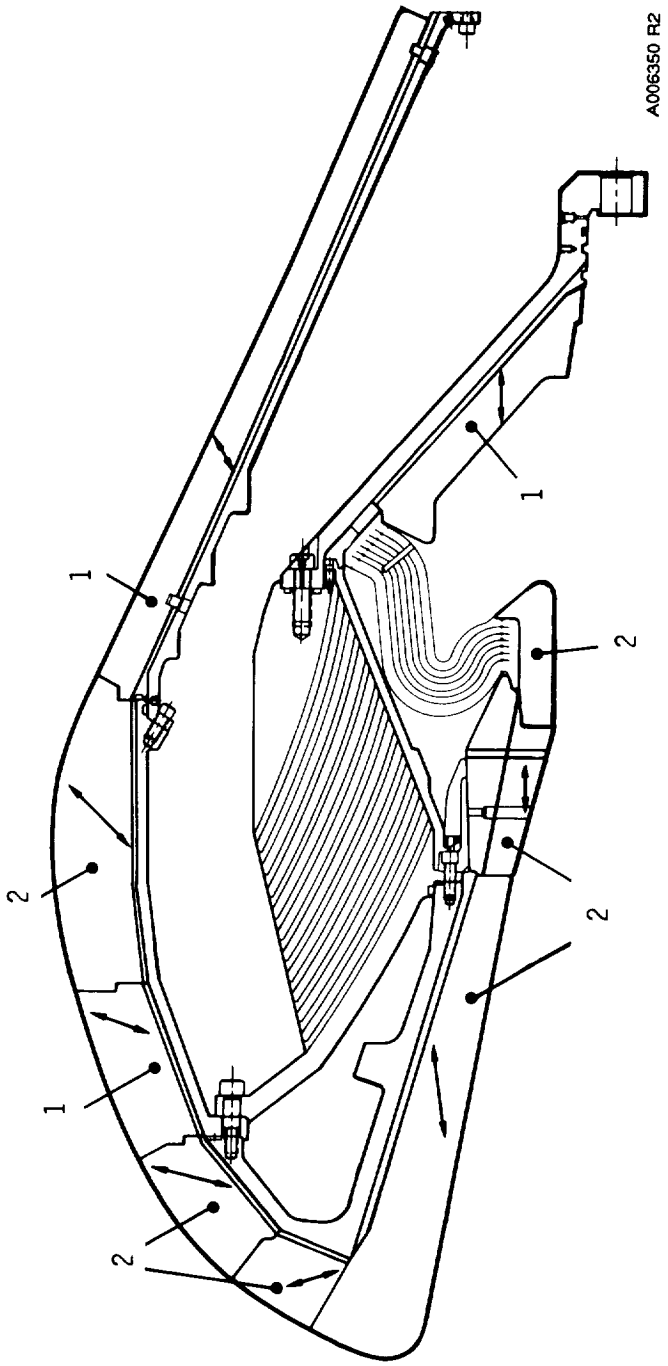

Figure 7.5-3. RSRM Forward Nozzle Assembly, DM-9 Nozzle Materials

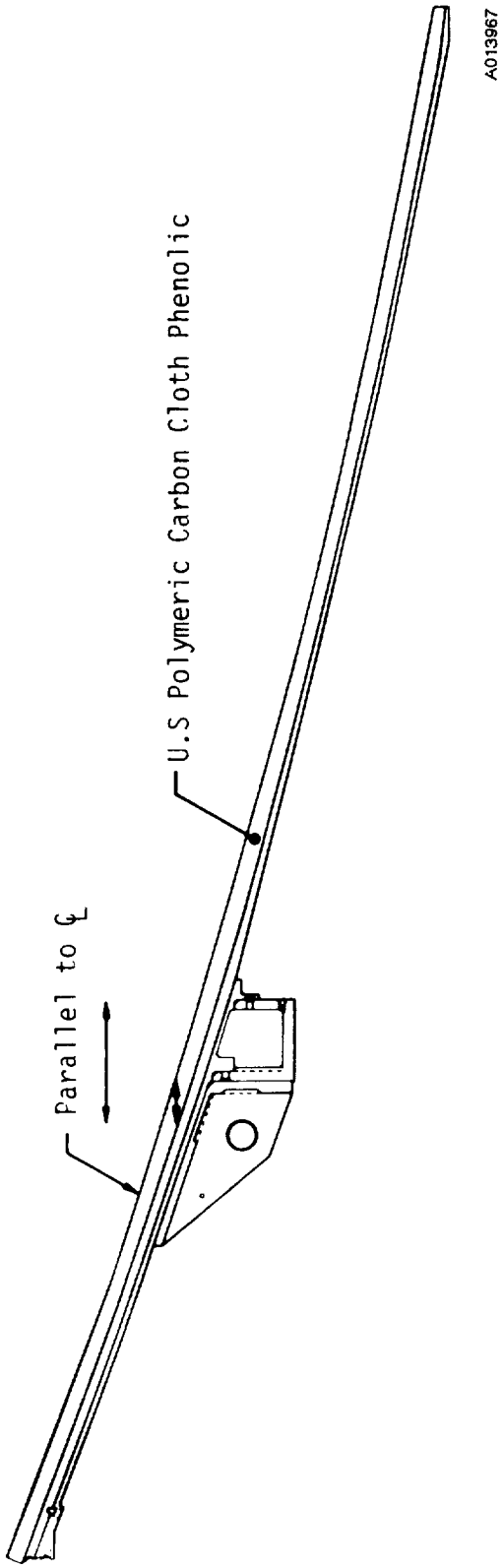

Figure 7.5-4. DM-9 Aft Exit Cone Assembly Liner and Insulator Materials

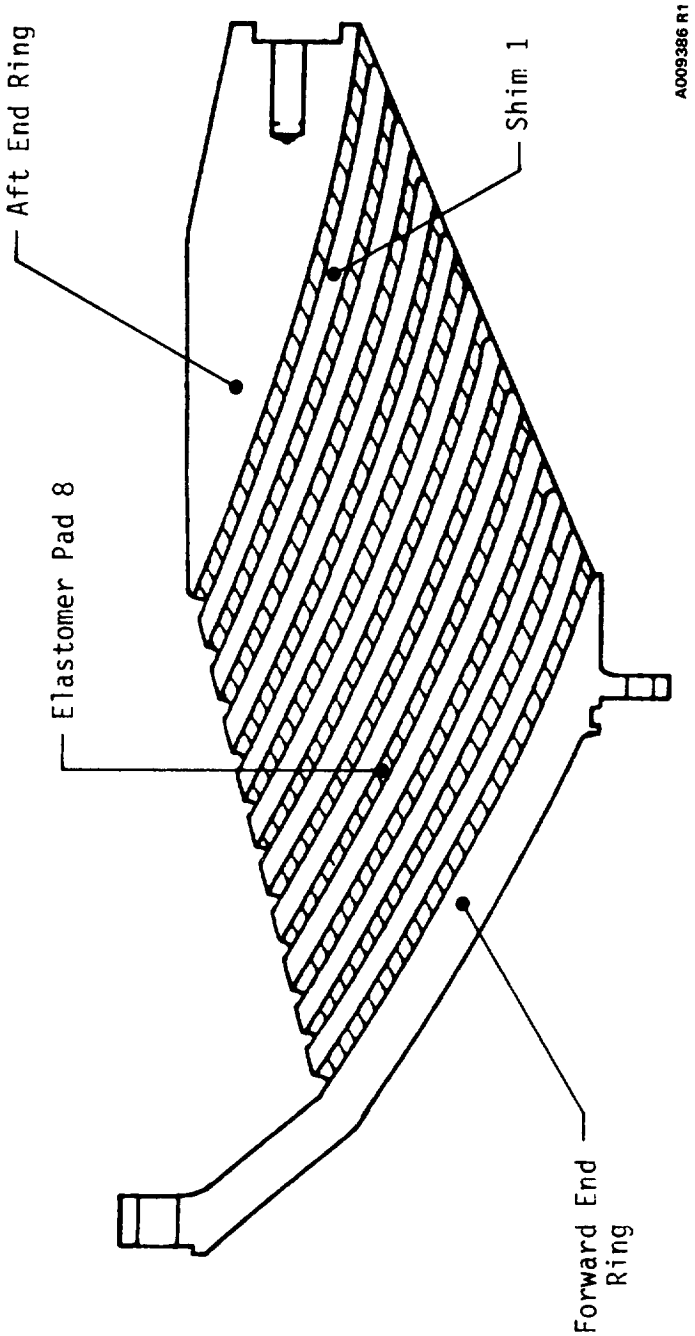

Figure 7.5-5. Space Shuttle Flexible Bearing

predicted MS is primarily dependent on this data. This instrumentation also provides valuable data for evaluation of TVC effects (which are difficult to model) on nozzle components and it provides valuable clues in the event of anomalies.

TVC System

NASA supplied the TVC subsystem, a hydraulic system which positions the nozzle in response to commands from the orbiter guidance system. NASA also supplied the kickring, aft skirt, and heat shield. These components were all flight items except for the heat shield, which lacked the extra inner layer of material used on the flight design.

The TVC subsystem consists primarily of two separate fluid power modules and two hydraulic servoactuators, which are mounted 90 deg apart in the rock and tilt planes. The major components of the fluid power modules are illustrated in Figure 7.5-6, while a typical servoactuator and its attachment to the aft skirt is depicted in Figure 7.5-7. Figure 7.5-8 shows the orientation of the TVC subsystems on the SRB system. The operation of the TVC subsystem is briefly described as follows: 1) the fuel supply module (FSM) supplies liquid hydrazine to the auxiliary power unit (APU), in which the hydrazine is decomposed and the resulting gas drives a turbine; 2) the turbine shaft power drives a hydraulic pump which provides a high-pressure fluid to the servoactuator; 3) electrical commands from the orbiter guidance system cause servovalves in the actuator to open so that the piston and connecting rod extend or retract accordingly and position the nozzle; and 4) mechanical position feedback in the actuator causes the piston and shaft to achieve and hold the commanded position. If one of the fluid power modules fails, the other continues to supply high-pressure fluid to both actuators, but with slightly degraded performance capability.

7.5.2 Objectives

The qualification test objectives from Section 2 with regard to nozzle performance were to:

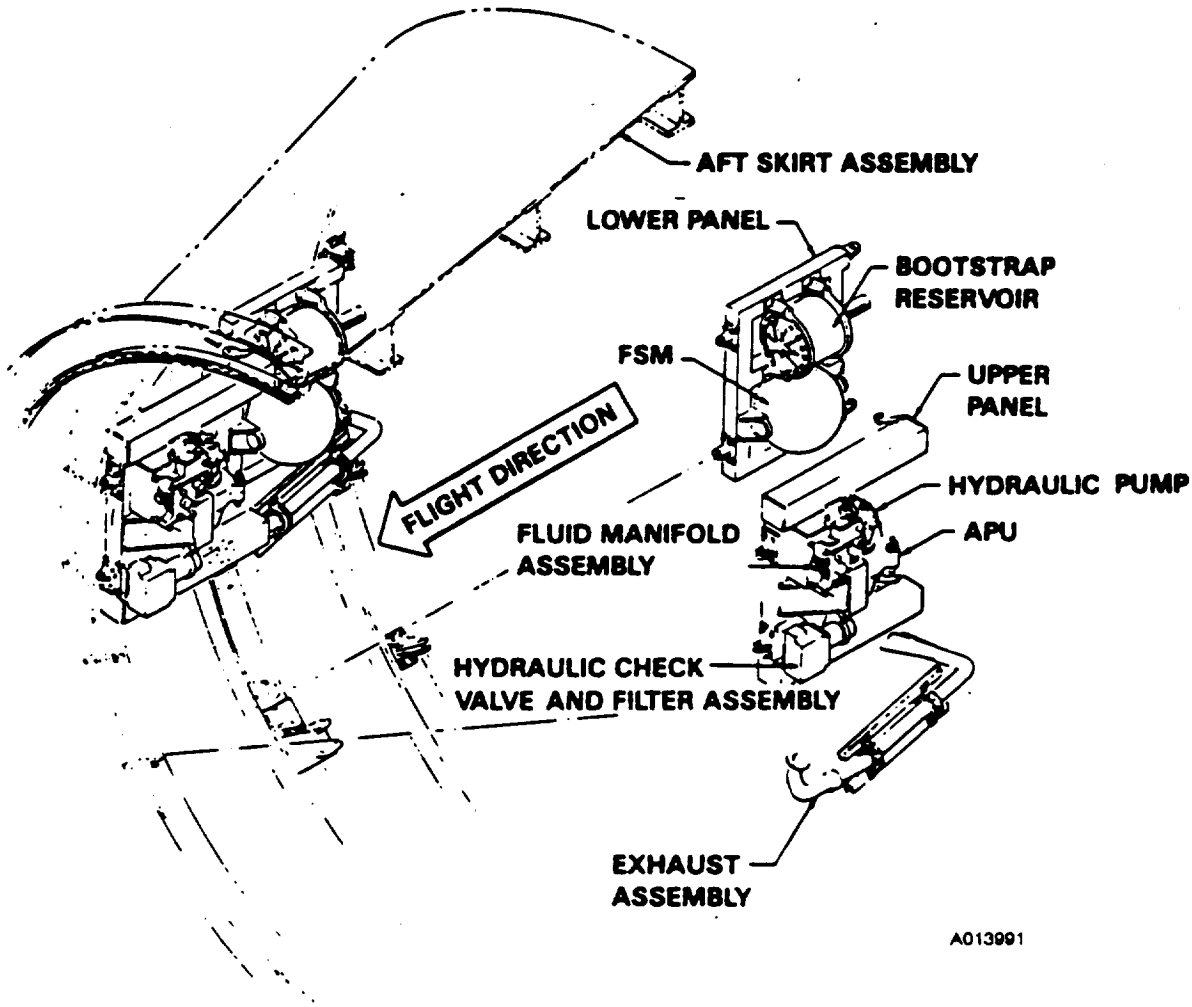

NOTE: FUEL ISOLATION VALVE, SERVICE PANELS, SERVOACTUATOR, WIRING, TUBING, AND INSTRUMENTATION NOT SHOWN

Figure 7.5-6. TVC Subsystem

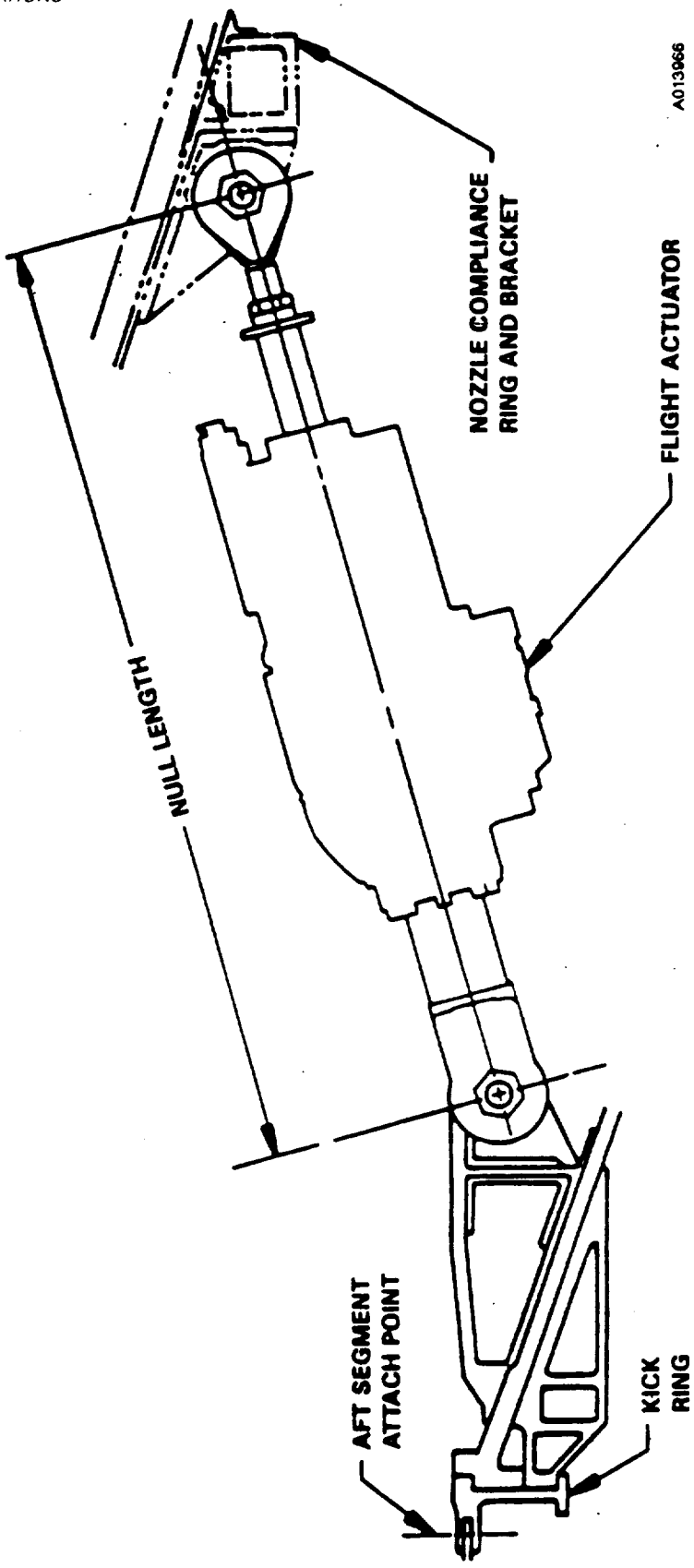

Figure 7.5-7. Thrust Vector Actuator Configuration

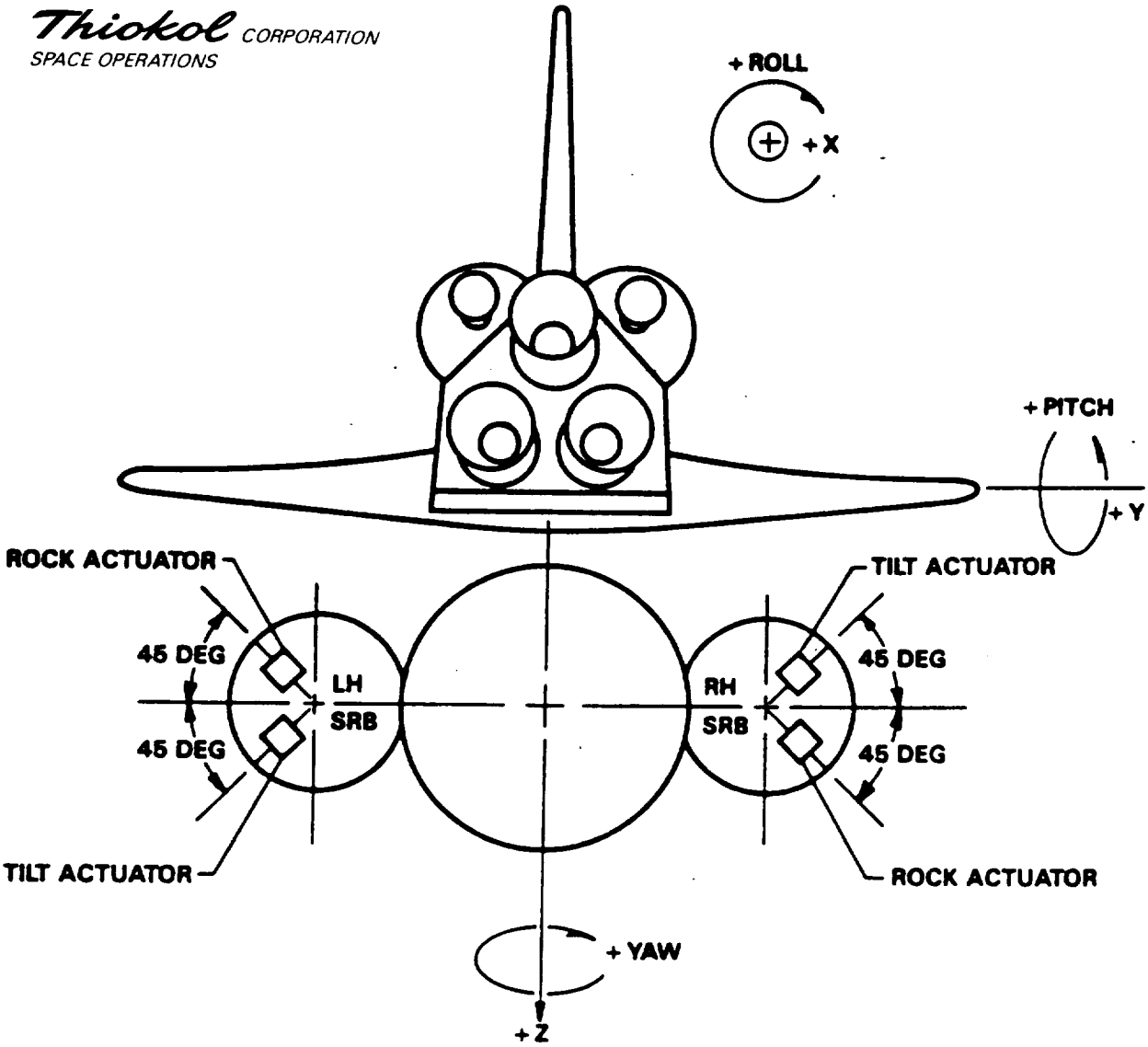

SHUTTLE VEHICLE MANEUVER	LH SOLID ROCKET BOOSTER ROCK ACTUATOR	LH SOLID ROCKET BOOSTER TILT ACTUATOR	RH SOLID ROCKET BOOSTER ROCK ACTUATOR	RH SOLID ROCKET BOOSTER TILT ACTUATOR
+ PITCH	−	+	+	−
− PITCH	+	−	−	+
+ YAW	+	+	−	−
− YAW	−	−	+	+
+ ROLL	+	−	+	−
− ROLL	−	+	−	+

+ INDICATES ACTUATOR EXTENSION
− INDICATES ACTUATOR RETRACTION

A013968

Figure 7.5-8. SRB TVC Actuator Polarity

R Certify the backfill of internal nozzle joints (flight configuration).

AE Certify that the nozzle assembly and exit cone design are compatible with the performance requirement specified in CPW1-3600A.

AM Certify that the nozzle liner design prevents the formation of pockets, wedge outs, and anomalies as defined.

AN Certify that nozzle assembly primary ablatives meet the design safety factors.

AO Certify that the nozzle performance MS are zero or greater.

AP Certify that the nozzle meets vectoring requirements.

AQ Certify that the nozzle radial offset does not exceed the limits.

AR Certify that the nozzle meets dynamic thrust vector requirements.

AS Certify that the nozzle meets null offset angle requirements.

AT Certify that the nozzle plug can be expelled without damage to other components or adversely affecting RSRM performance.

AU Certify by demonstration that the TVC actuator attach points meet the requirements of ICD 3-44003.

AV Certify that the flex bearing is capable of vectoring a total of 85 cumulative degrees during each flight duty cycle.

BA Certify that the flex bearing will remain sealed throughout TVC duty cycle during static test.

BB Certify proper flex bearing sealing capability at ambient conditions after processing in a normal manufacturing environment.

BC Certify that the flex bearing seal verification does not degrade the performance or integrity of the system.

BD Certify that there are no gas leaks between the flex bearing internal components.

BE Certify that the nozzle internal seals and the aft exit cone joint can accommodate static test motor induced-structural deflections.

Development objectives associated with the nozzle TVC system were to:

BJ Acquire engineering data for validation of joint models.

BK Obtain data to verify finite element models.

BL Determine the effects of dither/TVC performance at elevated hydraulic oil temperatures (MSFC test objective).

7.5.3 Conclusions/Recommendations

Nozzle Assembly

Compliance of the nozzle test objectives listed in Section 2 is discussed in the following paragraphs.

a. The RTV sealant backfill extended below the joint char line 360 deg circumferentially in the nose inlet/throat joint, and aft exit cone/forward exit cone joint.

The RTV backfilled throat/forward exit cone joint did not meet the criteria outlined in TWR-17198 (Postfire Engineering Evaluation Limits). RTV did not extend below the char line at the 335-deg location. The backfill extending below the joint char line 360 deg circumferentially is a design goal. This is not a certification issue and will not affect flight. The joint showed no blowby, erosion, or heat effect to the primary O-ring. This condition was also observed on the DM-8 throat/forward exit cone joint with no blowby, erosion, or heat effect to the primary O-ring.

b. The CPW1-3600 specification (paragraph 3.2.1.4.13b) in effect when DM-9 was fired stated that the nozzle flame front liners shall be designed and fabricated to prevent the formation of wedge outs greater than 0.250 inch. Specification change notice 49 (SCN 49) rewords this portion of CPW1-3600. The change reads as follows: "The nozzle flame front liners shall be designed and fabricated to prevent the formation of wedge outs during motor operation that result in negative performance MS."

Charred CCP material wedged out and popped up over the aft 2 in. of the nose cap intermittently around the part circumference. Examination showed that

the wedge outs occurred after motor operation. This condition has appeared on the majority of post-test and postflight nozzles and is not considered anomalous.

Charred CCP material also wedged out on the aft 3 in. of the cowl ring from 220 to 240 deg, and from 335 to 10 deg. These wedge outs occurred late in motor operation. Post-test char and erosion measurements, however, yielded positive performance MS in the areas of the wedge outs. This violates the current CPW1-3600 specification, but does not violate the proposed change noted above.

The involute OBR fractured and separated from the nozzle over a 150-deg arc from 220 to 10 deg. Examination showed signs of flow at the OBR/cowl axial bondline, and between the flex boot and cowl aft tip. Flow was also evident within the OBR while it remained on the nozzle. The fracturing of the OBR during motor operation is considered anomalous. As a result of the DM-9 involute OBR anomaly, future static test and flight nozzles will use the structural backup design successfully tested on DM-8.

c. Positive performance MS were obtained on the intact portion of the OBR, on the cowl ring aft end, and on all remainder parts of the nozzle with the exception of three locations on the forward exit cone and one location on the aft exit cone.

d. The nozzle plug performed nominally. The plug burst into multiple pieces at motor ignition.

e. Upon examination of the nozzle internal seals and the aft exit cone joint, it was determined that the seals and joints performed nominally and accommodated static test motor-induced structural deflections with no adverse effects.

f. The pretest seal verification did not degrade any of the nozzle internal joints or the aft exit cone joint. All joints performed nominally with no indications of primary O-ring blowby, erosion, or heat effect.

g. Evaluation of postfired hardware is documented in TWR-17269.

Flex Bearing

Overall performance of the flex bearing was acceptable. The bearing was in excellent condition and showed no indications of exposure to heating or damage. This was the fifth usage of this assembly and there were no detectable anomalies in function or performance throughout the test.

Nozzle - Composite Structures

The review of instrumentation data has verified the structural integrity of the nozzle in all locations measured. In general, predicted strains compared well with measured strains and nozzle strains were small. Excluding the fixed housing forward and aft end rings, strains are less than 1,150 in./in. in the hoop direction and 290 in./in. in the meridional direction. Hoop strains tend to follow the pressure trace. Although no strain gages could be located on or near the OBR, other nozzle gages aided in determining the time of failure.

However, the discrepancies between predictions and measurements indicate a continued need for improvement in thermostructural analytical tools. A lack of correlation between thermally-dominated strain results and predictions is particularly evident toward the end of the firing, where in most cases strains are closer to zero than predicted.

Measured strain due to TVC actuation during firing is generally less than 170 in./in. in the hoop direction and 150 in./in. in the meridional direction. However, the magnitude of these induced strains could be significant at critical joint regions, including the aft nose inlet housing joint and the fixed housing aft dome joint.

Differences in prefire and static test strains due to vectoring require further study to understand the effects of pressure, temperature, and erosion.

Assumptions used in the thermostructural analyses of the involute OBR have to be reevaluated. A more appropriate model with the boot loads will have to be studied. The boot loads test will provide valuable data that can be used in the analytical model to simulate loads due to TVC actuation.

TVC System

The TVC system performed as planned and followed the specified duty cycle well. The geometric thrust vector alignment requirements were demonstrated and adequately met in DM-9. The procedures for calculating and measuring the actuator null length to give a null vector angle at a desired motor pressure were adequately demonstrated.

7.5.4 Results/Discussion

7.5.4.1 Nozzle Assembly. Erosion of the DM-9 forward nozzle assembly and aft exit cone CCP ablative liner was smooth and uniform. The involute OBR was fractured and missing from the nozzle over a 150-deg arc. Overall external and internal views of the DM-9 nozzle are presented in Figures 7.5-9 through 7.5-16.

Nose Inlet Assembly

All regions of the DM-9 nose inlet assembly eroded smoothly, with no visible pockets or wash areas. The aft inlet ring (-504), forward nose ring (-503), and nose cap showed minimal post-test surface delaminations. The aft portion of the forward nose ring experienced more surface delaminations than the aft inlet ring. Overall views of the nose inlet assembly flow surfaces are shown in Figures 7.5-17 through 7.5-19. The nose cap showed minor washing (0.20-in. maximum depth) approximately 6 in. aft of the forward end from 280 to 310 deg (Figure 7.5-19).

The flow surface bond gap between the aft inlet ring (-504) and the forward nose ring (-503) measured 0.15 inch. The flow surface bond gap between the nose cap and forward nose ring was approximately 0.05 inch.

Charred CCP plies wedged out on the nose cap aft end intermittently around the nozzle circumference. Figures 7.5-9 through 7.5-12 and 7.5-19 show views of the wedged out areas. The poppedup and missing material occurred over the aft 2 to 2.5 in. of the nose cap and was a maximum of 0.5 in. deep radially at the cowl interface. Plies exposed after the material wedged out showed signs of heat effect,

ORIGINAL PAGE
BLACK AND WHITE PHOTOGRAPH

N1010208-1

Figure 7.5-9. DM-9 Nozzle Overall View (0 deg)

N101208-2

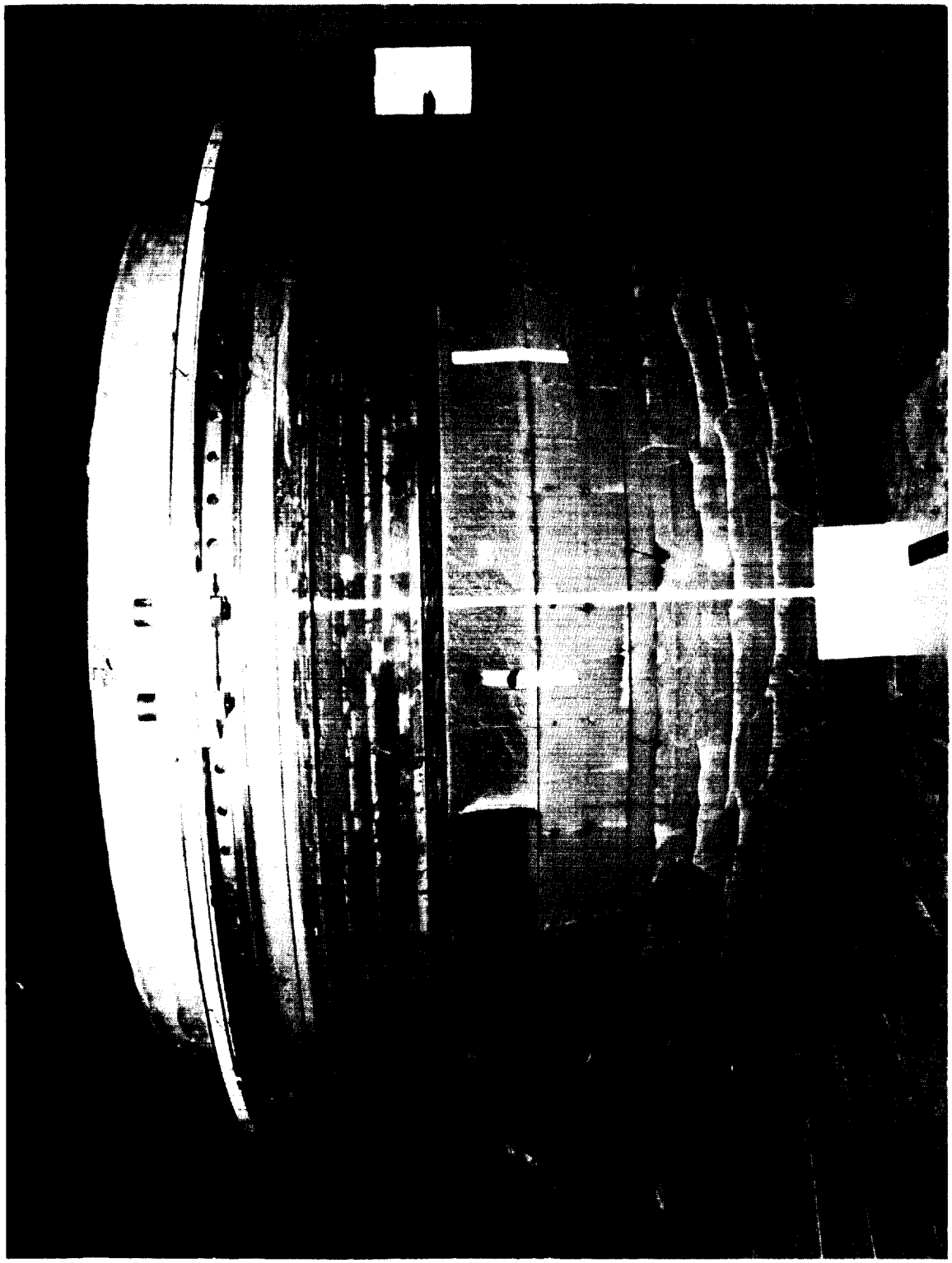

Figure 7.5-10. DM-9 Nozzle Overall View (90 deg)

N101208-3

Figure 7.5-11. DM-9 Nozzle Overall View (180 deg)

N101208-4

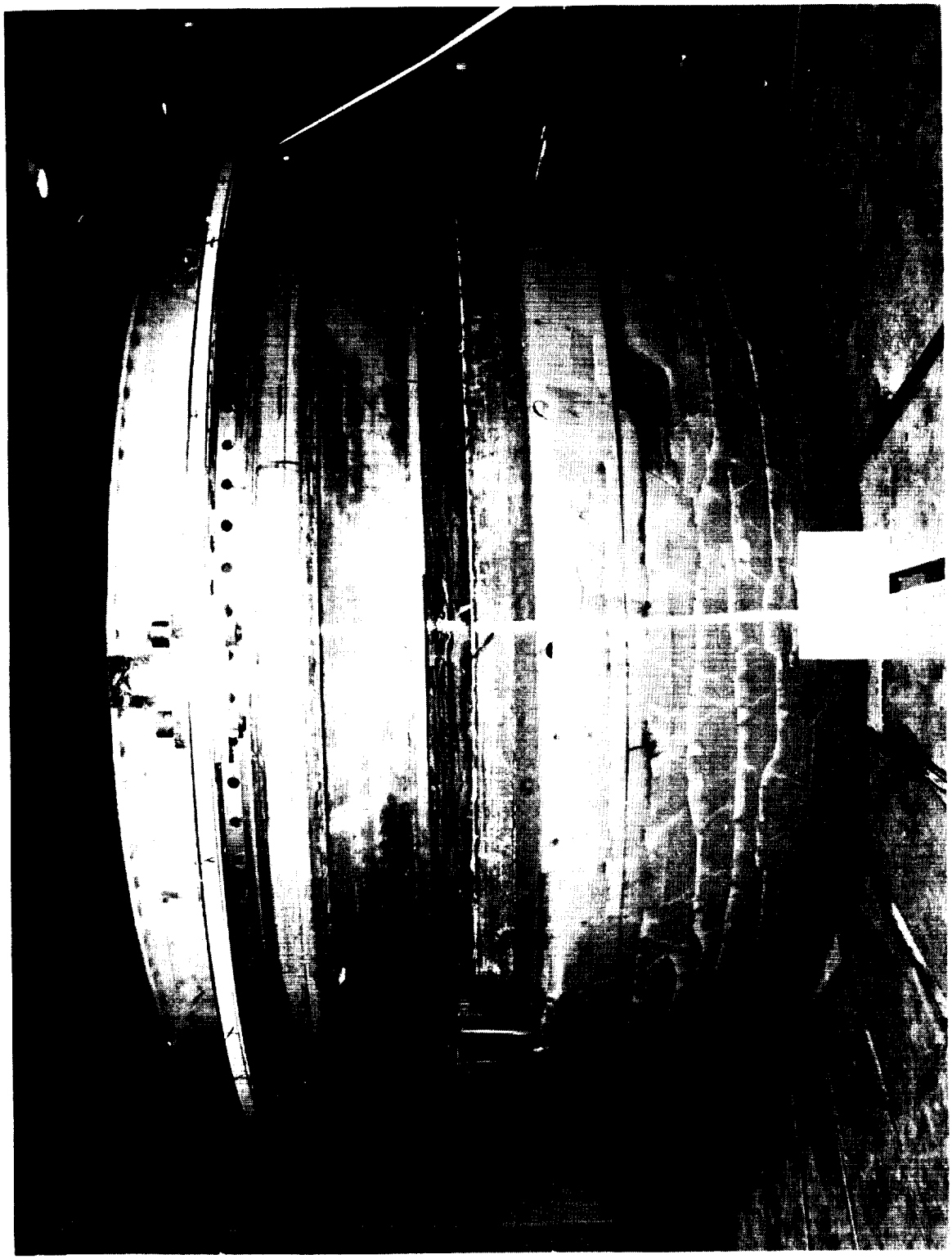

Figure 7.5-12. DM-9 Nozzle Overall View (270 deg)

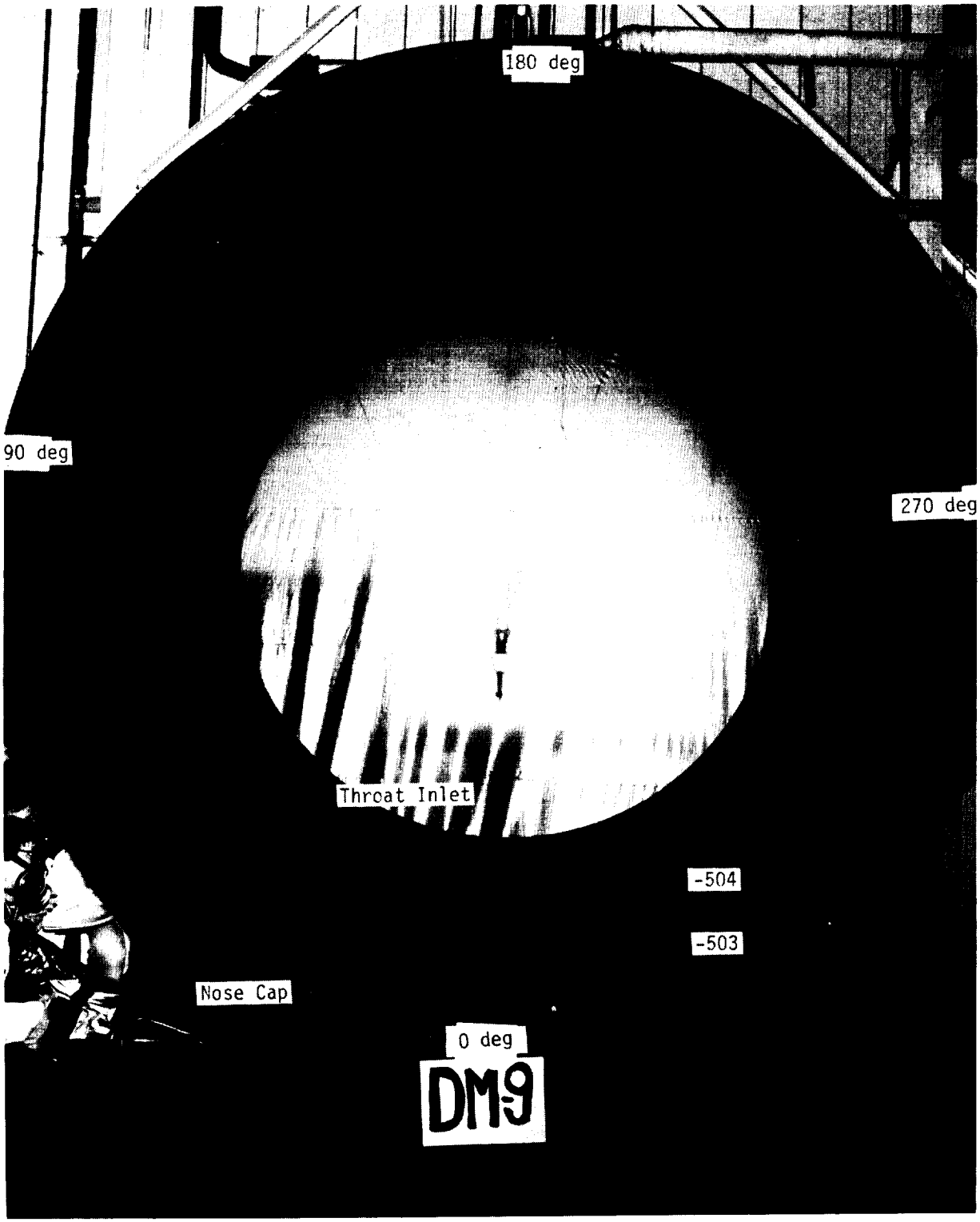

Figure 7.5-13. DM-9 Nozzle Overall Internal View

ORIGINAL PAGE
BLACK AND WHITE PHOTOGRAPH

N101197-16

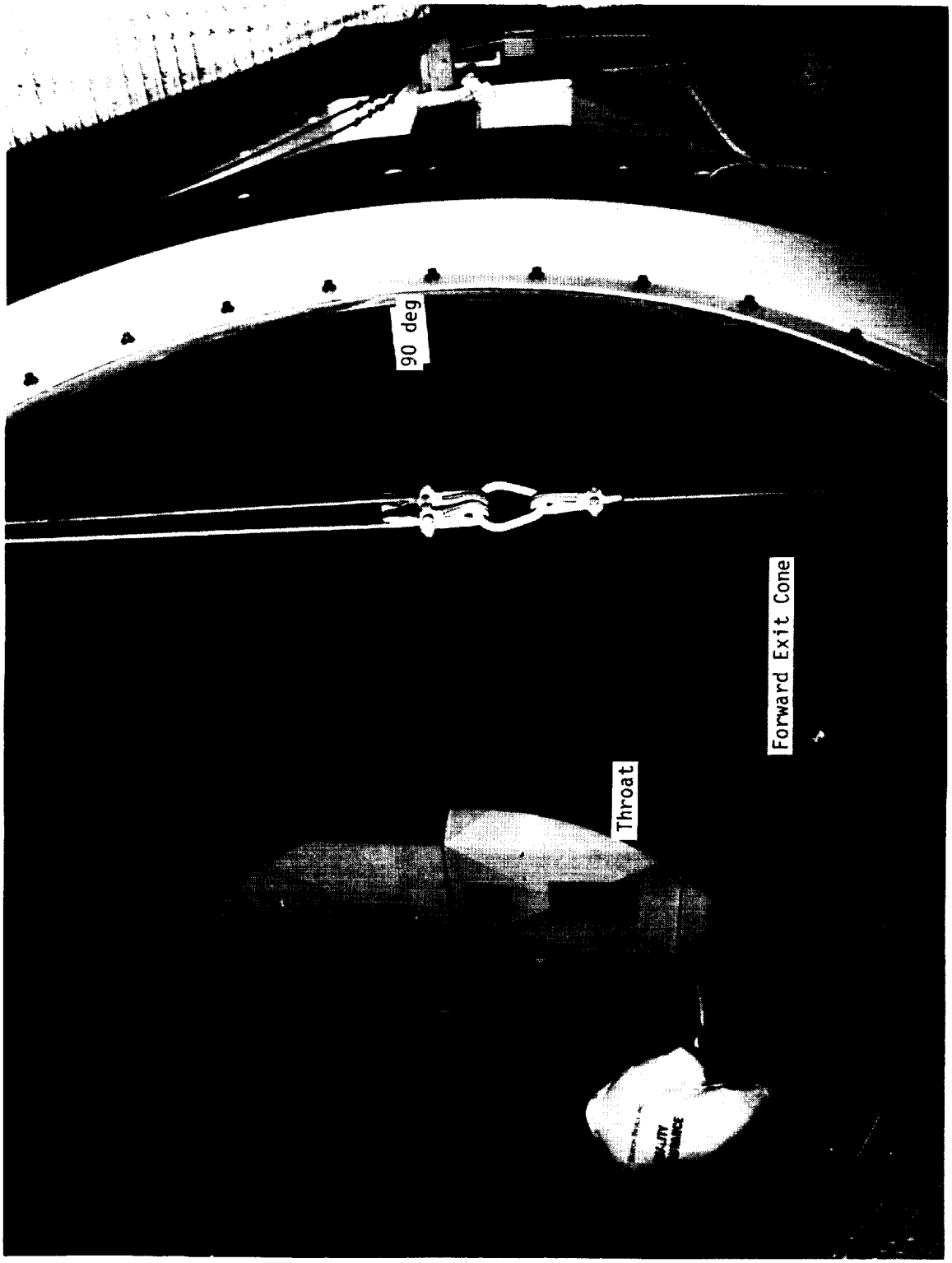

Figure 7.5-14. DM-9 Nozzle Overall Internal View

N101197-17

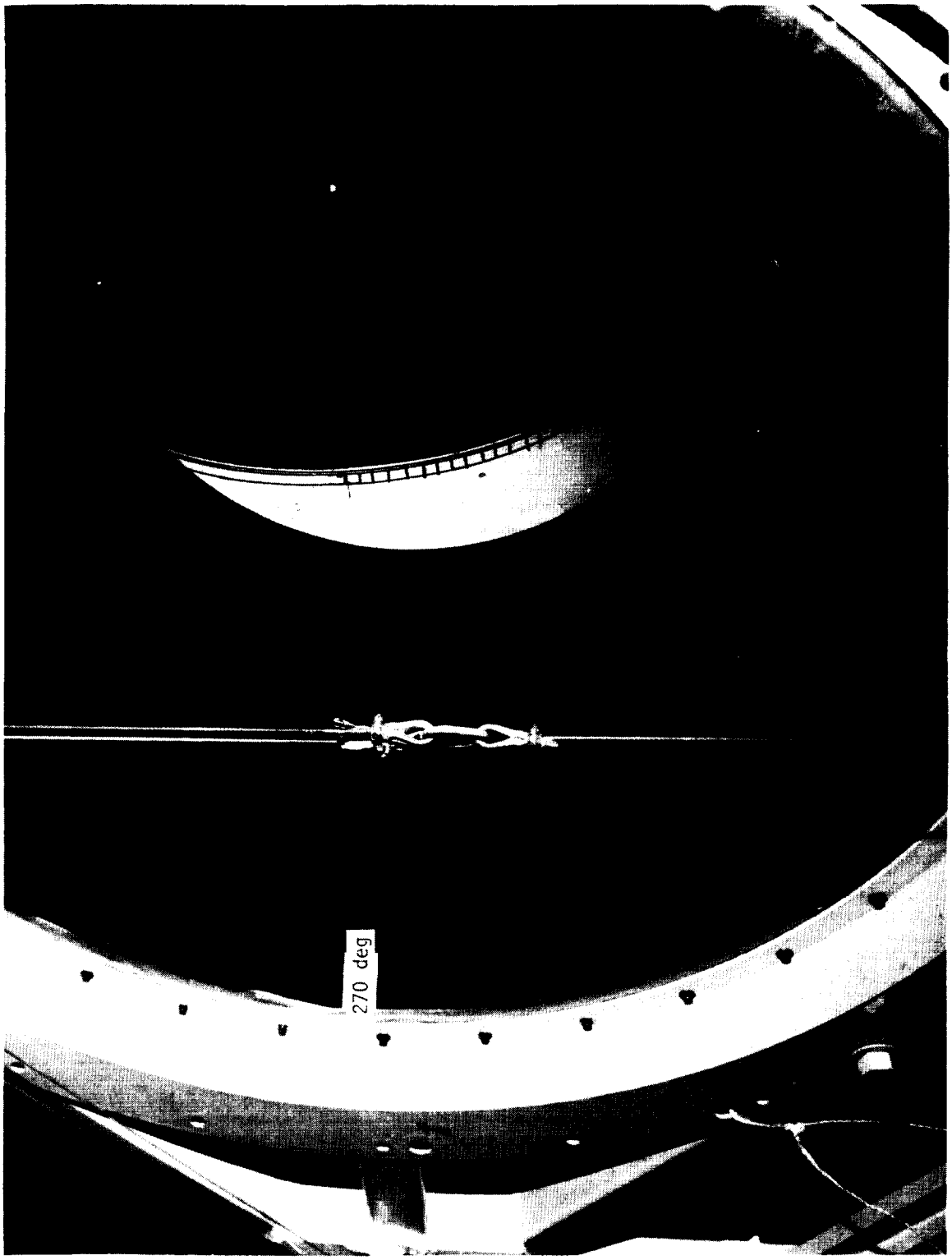

Figure 7.5-15. DM-9 Nozzle Overall Internal View

N101130-1

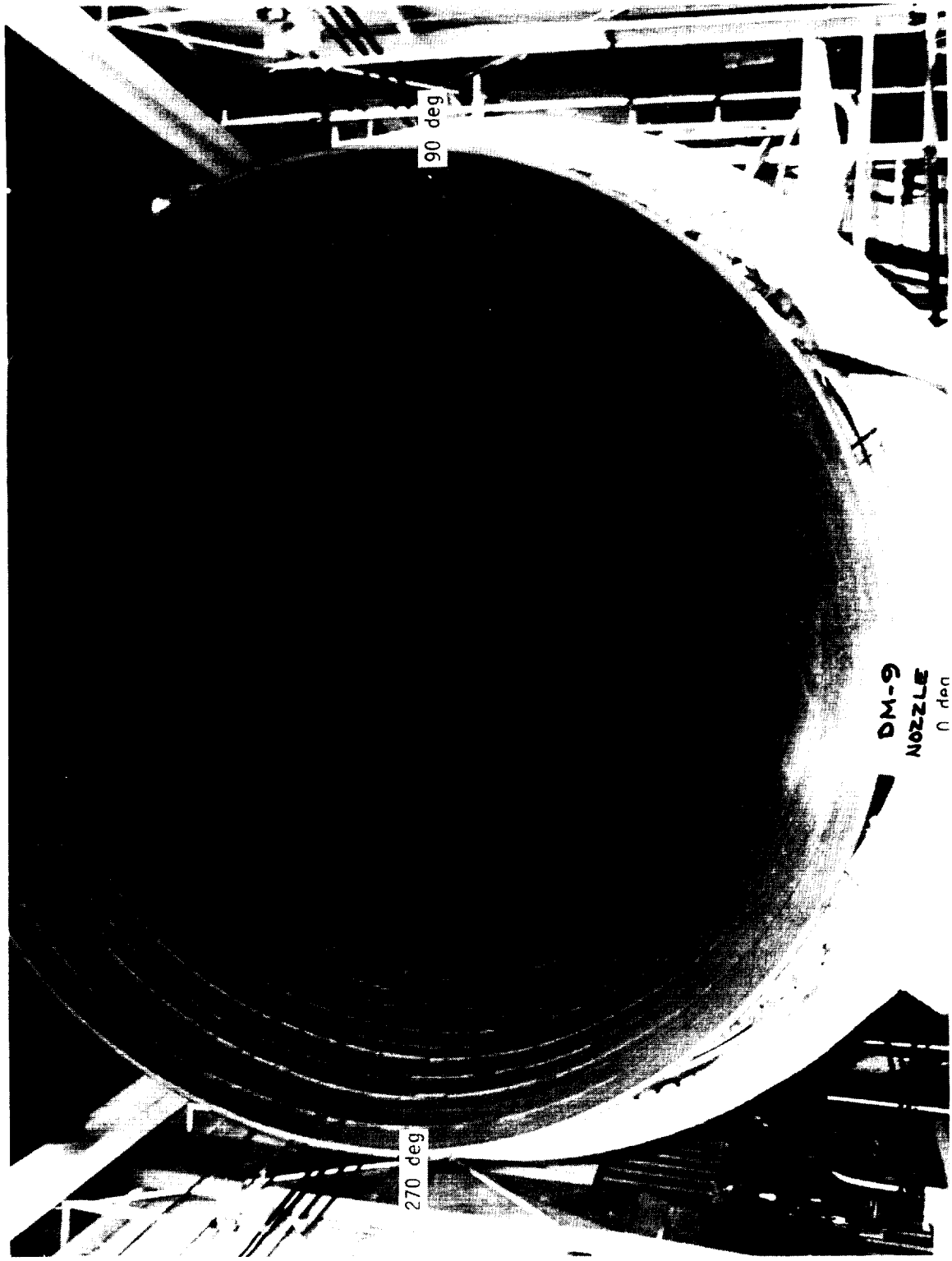

Figure 7.5-16. DM-9 Nozzle Aft Exit Cone Overall Internal View

ORIGINAL PAGE
BLACK AND WHITE PHOTOGRAPH

N101197-5

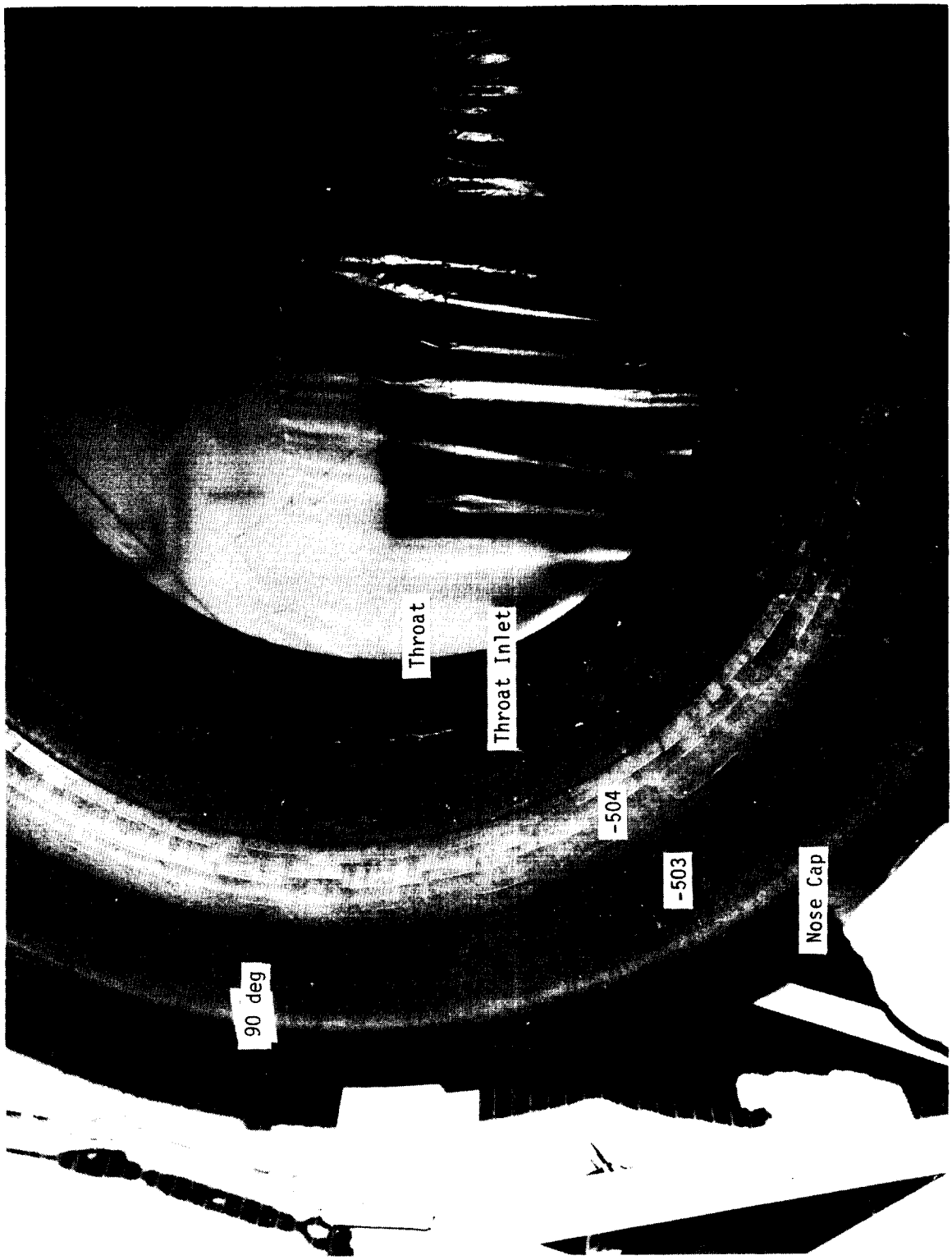

Figure 7.5-17. DM-9 Internal Flow Surface View (90 deg)

N101197-4

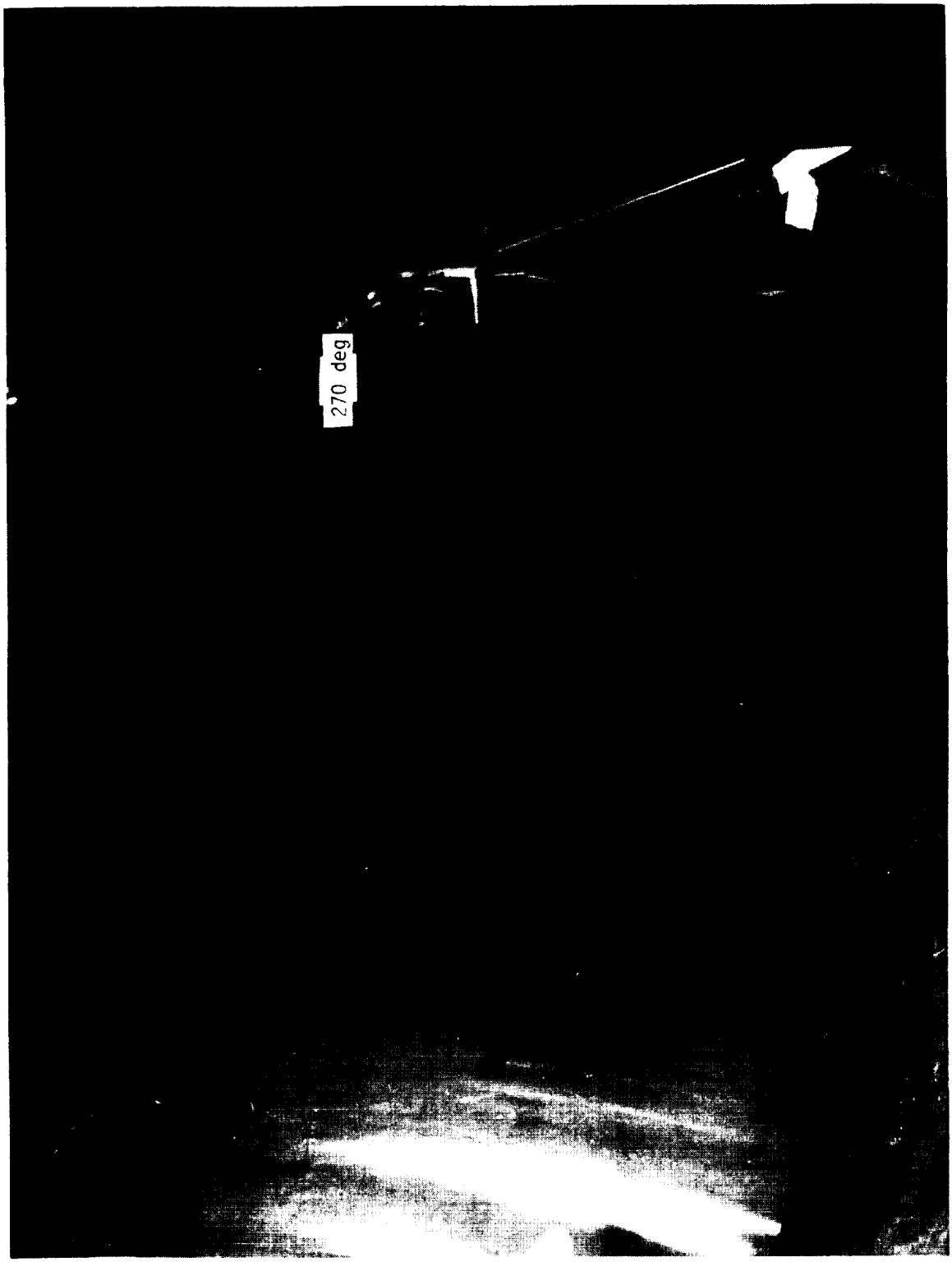

Figure 7.5-18. DM-9 Internal Flow Surface View (270 deg)

N101197-24

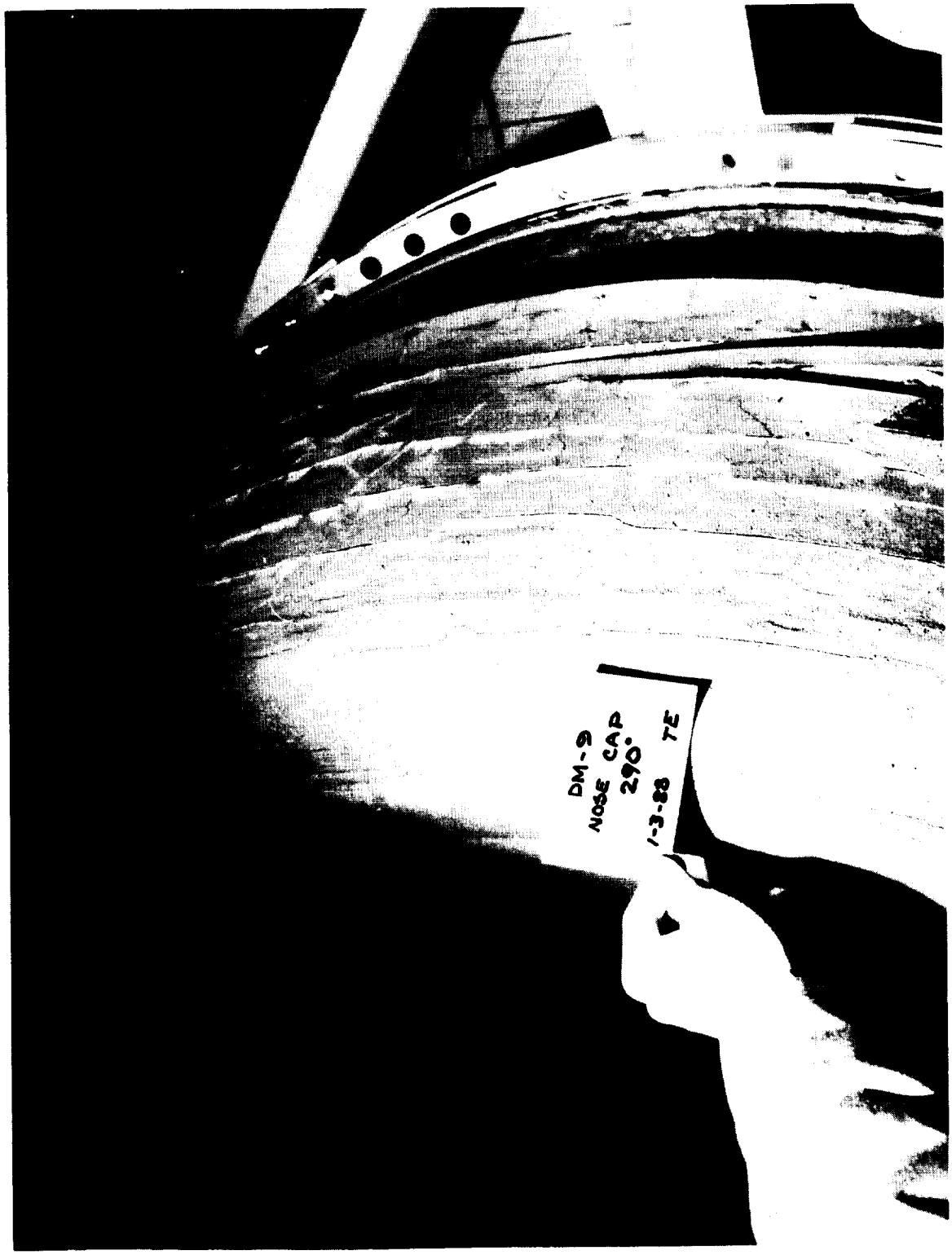

Figure 7.5-19. DM-9 Nose Cap Flow Surface (290 deg)

but no erosion. This was evidence that the CCP material wedged out after motor burn. Charred plies on the nose cap aft end have wedged out on the majority of static test and flight nozzles.

The nose cap aft end housing bondline exhibited a thin separation between the EA 946 adhesive and glass-cloth phenolic (GCP) insulator around the entire circumference. The separation was a maximum of 0.009 in. wide radially and 2.0 in. deep axially. Radial and axial gap measurements are presented in Figure 7.5-20. These separations were similar to those observed on the ETM-1A and DM-8 nose caps. No separations appeared between the EA 946 adhesive and nose inlet housing. There were also no cohesive separations observed within the adhesive at this bondline. It should be noted that the DM-9 nose inlet housing used the EA 9228 primer and PAA system.

The -504 aft inlet ring aft end housing bondline showed no adhesive or cohesive separations.

The aluminum nose inlet housing showed no damage and performed nominally. There were no signs of heat damage on the ID housing paint.

Char and erosion analysis of the aft inlet ring (-504), forward nose ring (-503), and nose cap showed positive performance MS.

Throat Inlet Assembly

Erosion of the throat and throat inlet rings was smooth and uniform. Overall views of the throat inlet assembly are shown in Figures 7.5-13 through 7.5-15, 7.5-17 and 7.5-18. The average throat postfire diameter was 55.787 in. (erosion rate of 7.88 mil/sec based on an action time of 122.2 sec). The ETM-1A post-test throat diameter was 56.083 in., and the DM-8 post-test diameter was 55.918 inches. Nozzle postflight throat diameters have ranged from 55.82 to 56.38 inches.

The throat/throat inlet ring bond gap was approximately 0.15 in. wide at the flow surface. Examination of the housing bondline showed no separations at the

Aft End Adhesive to GCP Radial Separation (in.)	Location (deg)
0.007	0
0.006	15
0.005	30
0.005	45
0.008	60
0.006	75
0.005	90
0.008	105
0.007	120
0.008	135
0.003	150
0.005	165
0.005	180
0.006	195
0.006	210
0.007	225
0.008	240
0.009	255
0.007	270
0.005	285
0.005	300
0.007	315
0.006	330
0.008	345

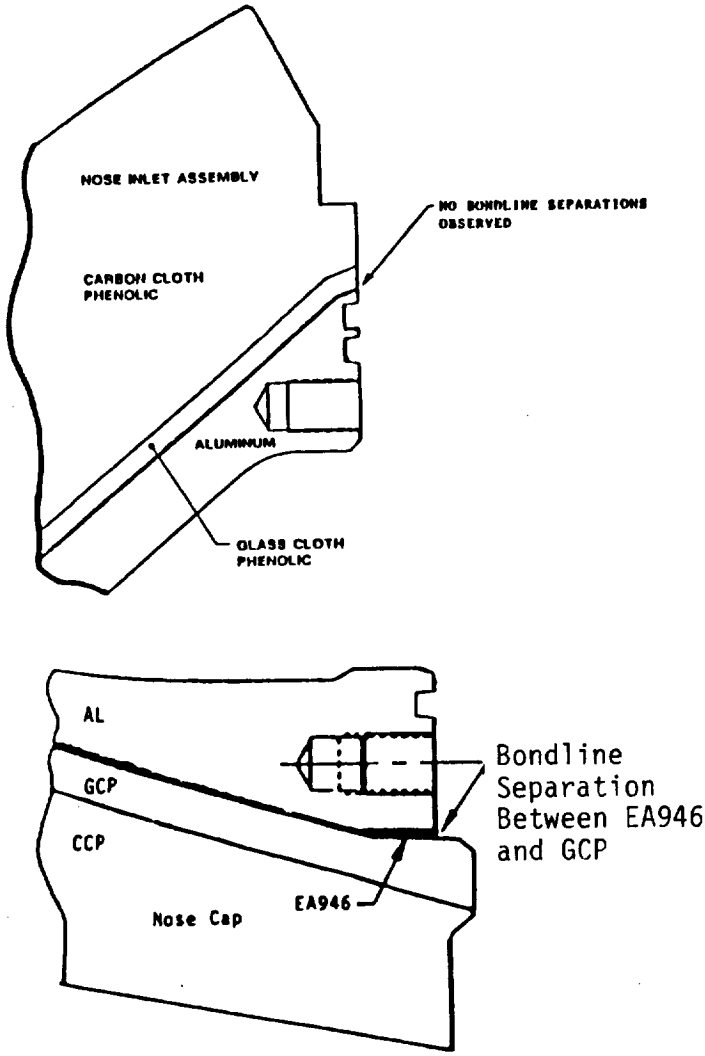

Figure 7.5-20. DM-9 Nose Inlet Assembly Bondline Separation

forward and aft ends. The ETM-1A and DM-8 throat assemblies showed adhesive and cohesive bondline separations.

The steel throat support housing showed no damage and performed nominally.

Char and erosion analysis of the throat inlet assembly insulation showed positive performance MS.

OBR

The DM-9 involute OBR separated from the nozzle over a 150-deg arc from 220 to 10 deg (Figure 7.5-21, TWR-17916). Six pieces of the OBR were found on the floor of the aft segment (Figure 7.5-22). Three pieces were observed on the slag surface during initial inspection, and three were later found buried in the slag. The six broken-off pieces made up the majority of the missing OBR. A small portion of char cap located at approximately 10 deg was not recovered. Overall photographs of the nozzle showing the missing OBR are shown in Figures 7.5-9 and 7.5-12.

The involute OBR remained intact and bonded to the nozzle from 10 to 220 deg (Figures 7.5-23 through 7.5-25). The intact portion showed cooldown cracks and delaminations that extended along the involute ply. Figure 7.5-26 presents a map of the cracks and delaminations. There were no through delaminations (OD to ID) that extended through virgin CCP material. Two through delaminations isolated in charred CCP were observed from 20 to 40 deg and 110 to 145 deg; these were aligned with ply-lift regions. Sectioning of the OBR showed delaminations extending into virgin CCP material at 40, 80, 120, and 140 deg (Figures 7.5-27 and 7.5-28). These delaminations propagated from the aft end of the OBR and showed no signs of heat effect in the virgin material during cooldown.

The aft tip of the OBR fractured off and was found lodged near the flex boot and on the aft dome floor (Figure 7.5-29). The fractured aft tip was charred material only. Examination of the fracture edges showed sharp breaks, indicating no erosion after fracture. Sectioning of the OBR showed that the char line was not affected by the fractured aft tip, which indicates that the fracture occurred after motor burn.

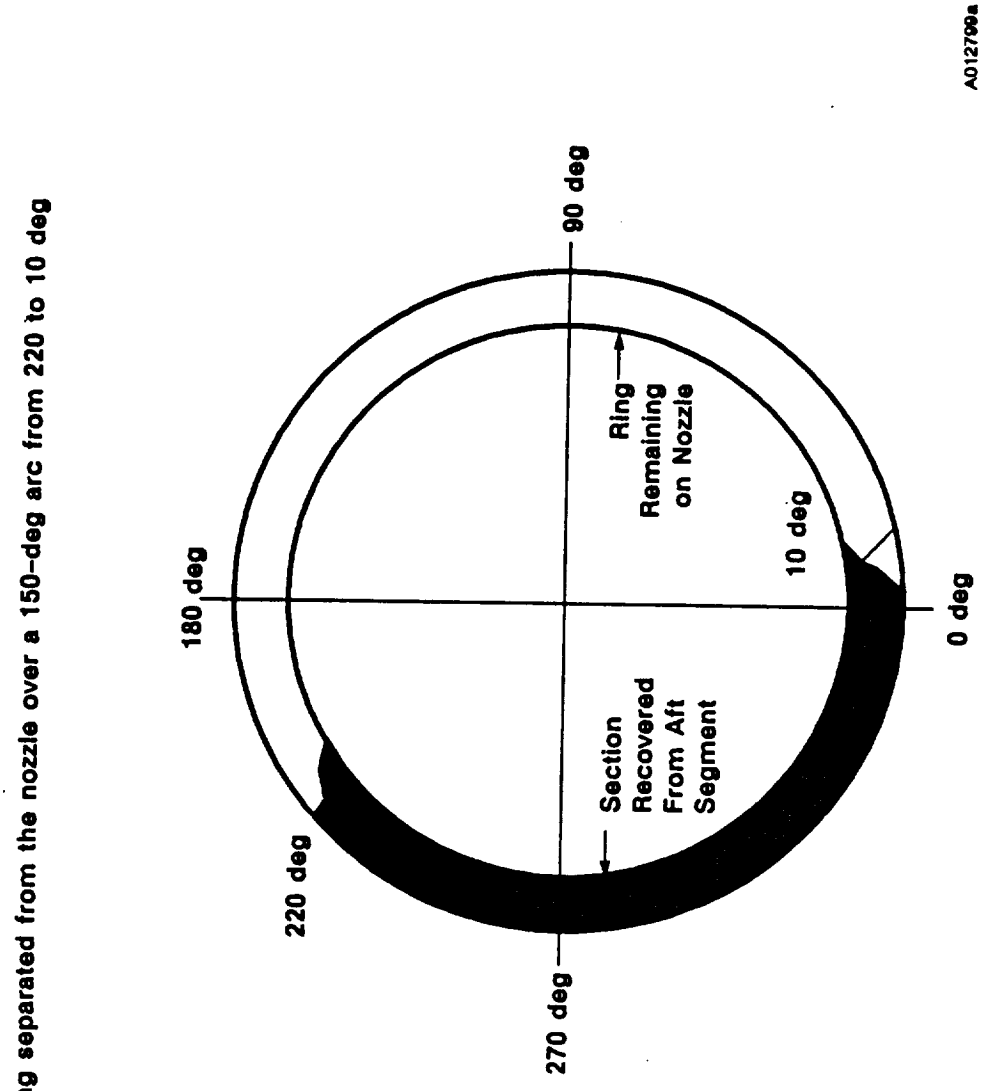

Figure 7.5-21. DM-9 OBR Post-Test Condition

A012838a

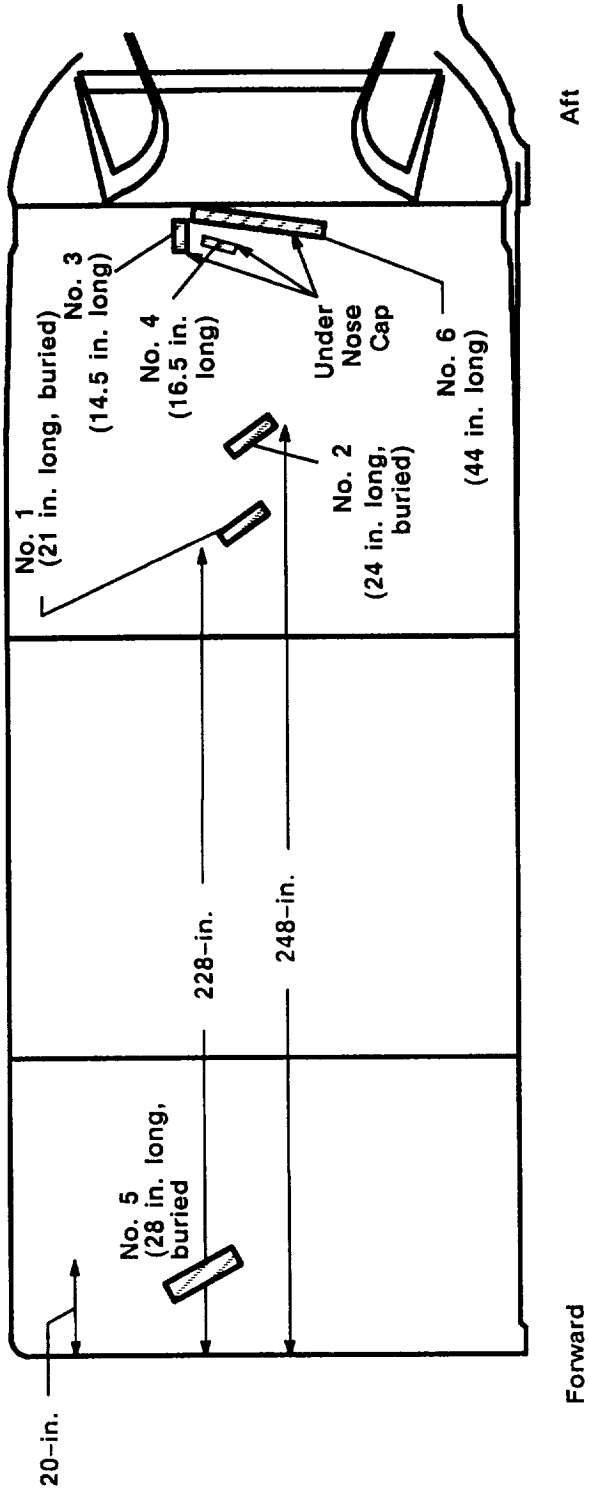

Figure 7.5-22. Locations of Six Recovered Pieces From DM-9 Aft Segment

ORIGINAL PAGE
BLACK AND WHITE PHOTOGRAPH

Figure 7.5-23. DM-9 Intact Portion of OBR (40 deg)

ORIGINAL PAGE
BLACK AND WHITE PHOTOGRAPH

N101197-20

Figure 7.5-24. DM-9 Intact Portion of OBR (150 deg)

N101197-21

Figure 7.5-25. DM-9 Intact Portion of OBR (210 deg)

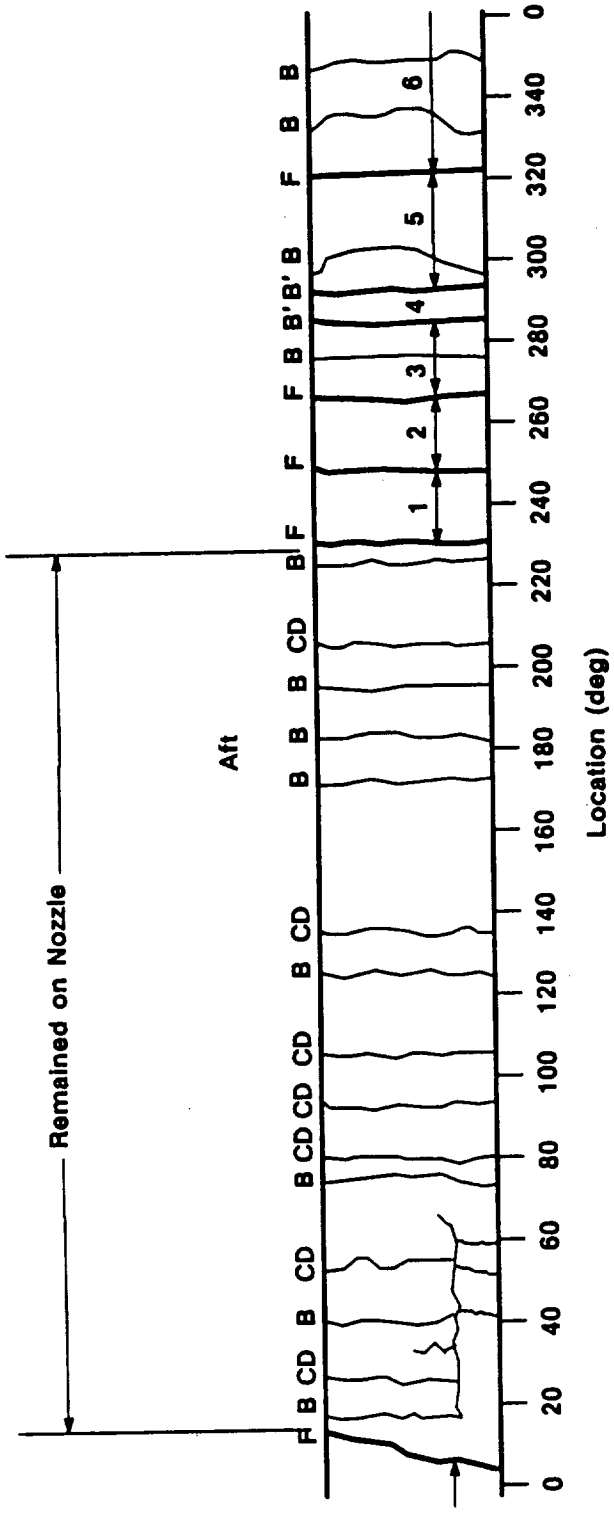

Figure 7.5-26. DM-9 OBR Map of Cracks and Delaminations

N101233-8

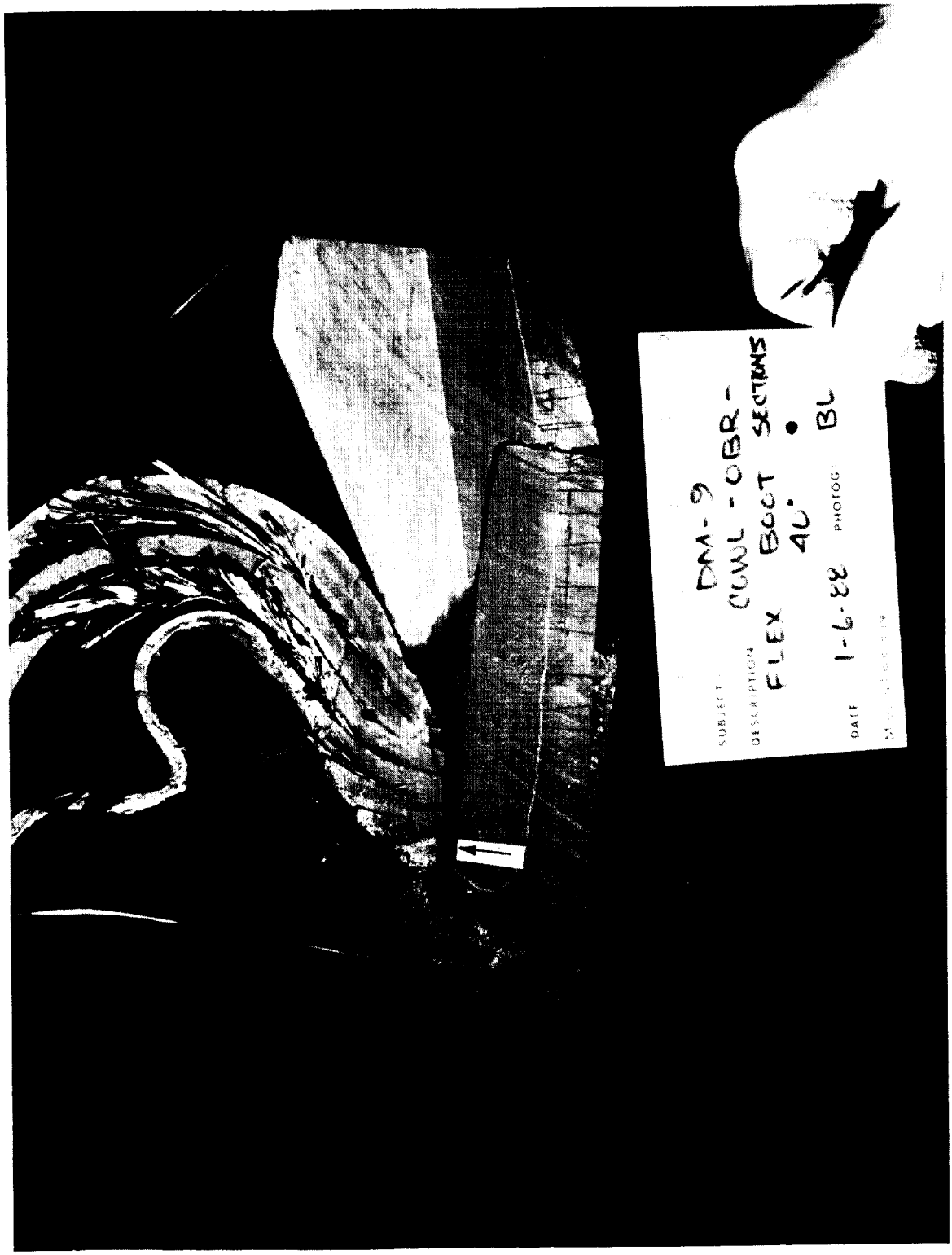

Figure 7.5-27. DM-9 Delam Extending Into Virgin CCP Material on OBR (40 deg)

ORIGINAL PAGE
BLACK AND WHITE PHOTOGRAPH

N101233-3

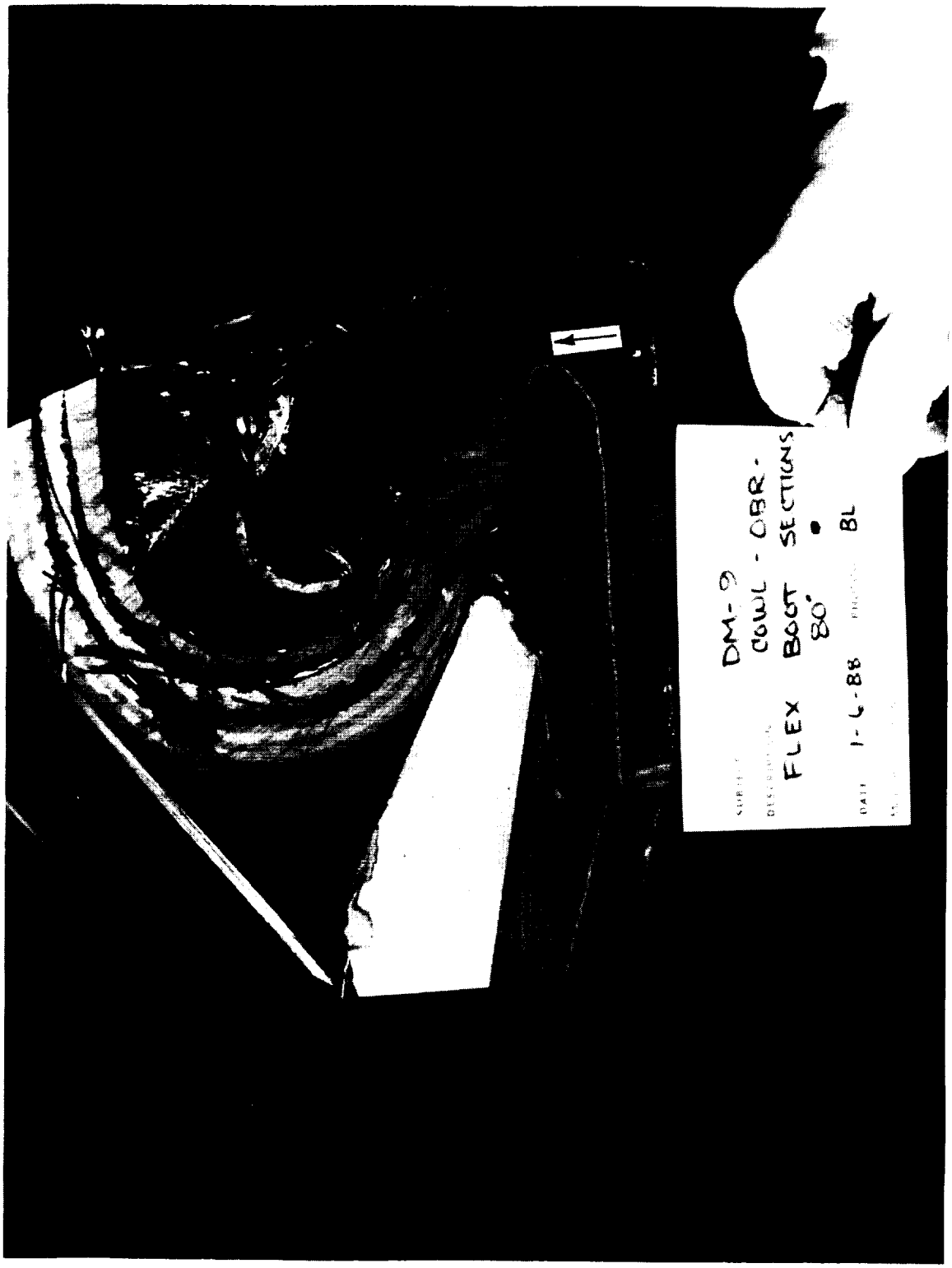

Figure 7.5-28. DM-9 Delam Extending Into Virgin CCP Material on OBR (80 deg)

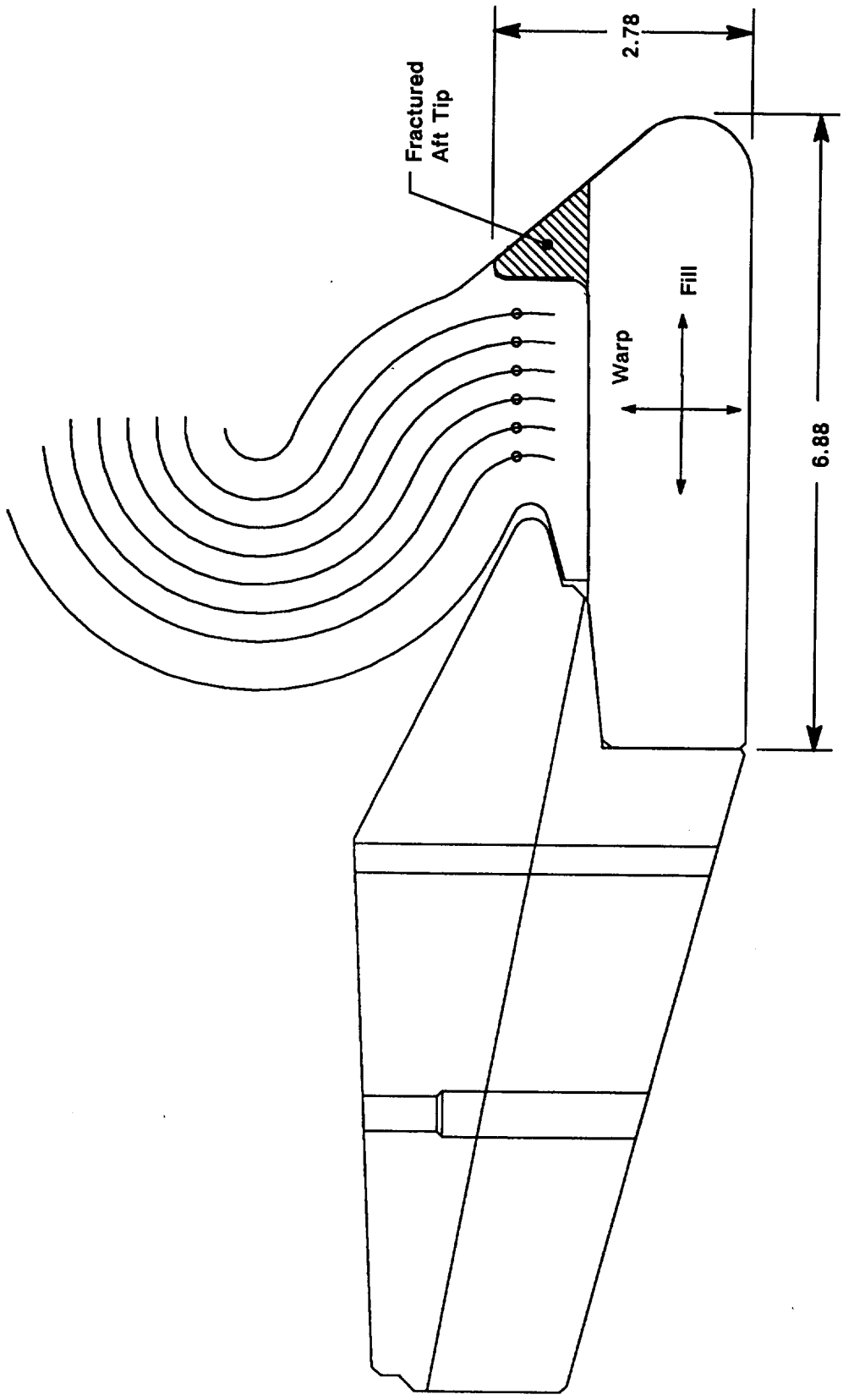

Figure 7.5-29. DM-9 OBR Fractured Aft Tip

An intact 100-deg arc of the fractured-off aft tip was found during initial inspection. This is additional evidence that the fracture occurred after motor operation, because flow would have broken the intact arc of charred material.

Table 7.5-1 presents the DM-9 involute OBR measured char and erosion data and performance MS for the portion which remained on the nozzle. The MS in this table were based on measured erosion, measured char, and minimum RSRM liner thicknesses. The measured char included heat soak from the time of motor burnout until total cooldown. All calculated MS were greater than 0.00. The worst-case margin of 0.25 occurred at the aft end of the OBR (40 deg, Station 12). Figure 7.5-30 shows the locations of the measurement stations. Table 7.5-2 presents corresponding OBR MS using measured erosion, corresponding measured char adjusted to the end of action time, and minimum RSRM liner thicknesses. The adjusted char values used in these calculations do not include motor postburn heat soak. All MS were again greater than 0.00 when using the adjusted char values.

The six pieces of the OBR found on the floor of the aft segment were reassembled and examined (Figures 7.5-31 through 39). Figure 7.5-40 is a map of the reassembled pieces. Figure 7.5-41 describes the fracture edges and overall condition of Piece No. 1. Piece No. 2 is summarized in Figure 7.5-42. Figures 7.5-43 through 7.5-46 describe Piece No. 3, and Figures 7.5-47 through 7.5-50 characterize Piece No. 4. Piece No. 5 is described in Figure 7.5-51, and Figures 7.5-52 and 7.5-53 summarize Piece No. 6.

Cowl Ring

The DM-9 cowl ring showed irregular erosion patterns intermittently around the part circumference (Figures 7.5-54 and 7.5-55). The forward portion of the cowl ring appeared to erode approximately 0.20 in. more than the aft portion of the ring in the areas of the irregular erosion. This type of erosion was observed on the DM-8 cowl ring. Previous flight and static test cowl rings have also shown minor washing patterns.

Table 7.5-1. DM-9 OBR Erosion and Char Data

Angular Location	STATIONS				
0 degrees	8	9	10	11	12
Erosion *	NA	NA	NA	NA	NA
Char **	NA	NA	NA	NA	NA
2E + 1.25C	NA	NA	NA	NA	NA
Liner Thickness ***	1.597	1.675	1.687	1.700	1.712
Safety Factor	NA	NA	NA	NA	NA
Margin of Safety	NA	NA	NA	NA	NA
20 degrees					
Erosion *	0.08	0.08	0.10	0.00	0.00
Char **	0.72	0.74	0.70	0.78	0.98
2E + 1.25C	1.06	1.09	1.08	0.98	1.23
Liner Thickness ***	1.597	1.675	1.687	1.700	1.712
Safety Factor	1.51	1.54	1.57	1.74	1.40
Margin of Safety	0.51	0.54	0.57	0.74	0.40
40 degrees					
Erosion *	0.12	0.15	0.20	0.08	0.16
Char **	0.70	0.64	0.55	0.70	0.84
2E + 1.25C	1.12	1.10	1.09	1.04	1.37
Liner Thickness ***	1.597	1.675	1.687	1.700	1.712
Safety Factor	1.43	1.52	1.55	1.64	1.25
Margin of Safety	0.43	0.52	0.55	0.64	0.25
60 degrees					
Erosion *	0.15	0.10	0.12	0.10	0.09
Char **	0.58	0.66	0.65	0.70	0.90
2E + 1.25C	1.03	1.03	1.05	1.08	1.31
Liner Thickness ***	1.597	1.675	1.687	1.700	1.712
Safety Factor	1.56	1.63	1.60	1.58	1.31
Margin of Safety	0.56	0.63	0.60	0.58	0.31
80 degrees					
Erosion *	0.02	0.00	0.04	0.05	0.04
Char **	0.73	0.74	0.75	0.76	0.85
2E + 1.25C	0.95	0.93	1.02	1.05	1.14
Liner Thickness ***	1.597	1.675	1.687	1.700	1.712
Safety Factor	1.68	1.81	1.66	1.62	1.50
Margin of Safety	0.68	0.81	0.66	0.62	0.50

* Measured Erosion
** Measured Char
*** RSRM Minimum Liner Thickness

Table 7.5-1. DM-9 OBR Erosion and Char Data (cont)

Angular Location	STATIONS				
100 degrees	8	9	10	11	12
Erosion *	0.00	0.00	0.00	0.00	0.02
Char **	0.69	0.70	0.71	0.75	0.75
2E + 1.25C	0.86	0.88	0.89	0.94	0.98
Liner Thickness ***	1.597	1.675	1.687	1.700	1.712
Safety Factor	1.85	1.91	1.90	1.81	1.75
Margin of Safety	0.85	0.91	0.90	0.81	0.75
120 degrees					
Erosion *	0.06	0.03	0.04	0.04	0.08
Char **	0.60	0.58	0.57	0.54	0.62
2E + 1.25C	0.87	0.79	0.79	0.76	0.94
Liner Thickness ***	1.597	1.675	1.687	1.700	1.712
Safety Factor	1.84	2.13	2.13	2.25	1.83
Margin of Safety	0.84	1.13	1.13	1.25	0.83
140 degrees					
Erosion *	0.00	0.00	0.00	0.00	0.00
Char **	0.79	0.76	0.70	0.69	0.75
2E + 1.25C	0.99	0.95	0.88	0.86	0.94
Liner Thickness ***	1.597	1.675	1.687	1.700	1.712
Safety Factor	1.62	1.76	1.93	1.97	1.83
Margin of Safety	0.62	0.76	0.93	0.97	0.83
160 degrees					
Erosion *	0.11	0.07	0.07	0.11	0.16
Char **	0.61	0.69	0.68	0.61	0.66
2E + 1.25C	0.98	1.00	0.99	0.98	1.15
Liner Thickness ***	1.597	1.675	1.687	1.700	1.712
Safety Factor	1.63	1.67	1.70	1.73	1.50
Margin of Safety	0.63	0.67	0.70	0.73	0.50
180 degrees					
Erosion *	0.03	0.03	0.04	0.02	0.07
Char **	0.59	0.58	0.53	0.56	0.59
2E + 1.25C	0.80	0.79	0.74	0.74	0.88
Liner Thickness ***	1.597	1.675	1.687	1.700	1.712
Safety Factor	2.00	2.13	2.27	2.30	1.95
Margin of Safety	1.00	1.13	1.27	1.30	0.95

* Measured Erosion
** Measured Char
*** RSRM Minimum Liner Thickness

A012818a-4

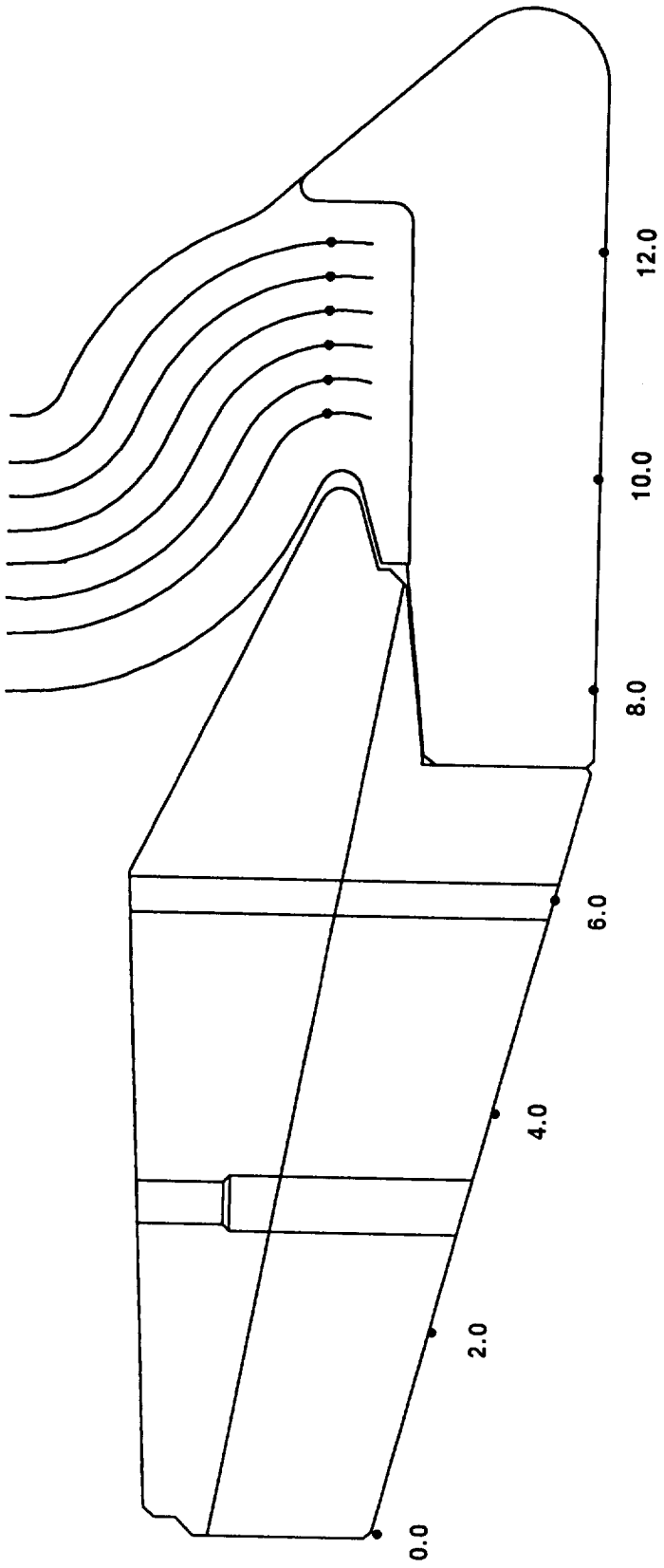

Figure 7.5-30. Cowl Ring and OBR Erosion Measurement Stations

Table 7.5-2. DM-9 OBR Erosion and Char Data

Angular Location	STATIONS				
0 degrees	8	9	10	11	12
Erosion *	NA	NA	NA	NA	NA
Char **	NA	NA	NA	NA	NA
2E + 1.25C	NA	NA	NA	NA	NA
Liner Thickness ***	1.597	1.675	1.687	1.700	1.712
Safety Factor	NA	NA	NA	NA	NA
Margin of Safety	NA	NA	NA	NA	NA
20 degrees					
Erosion *	0.08	0.08	0.10	0.00	0.00
Char **	0.61	0.63	0.60	0.66	0.83
2E + 1.25C	0.93	0.95	0.94	0.83	1.04
Liner Thickness ***	1.597	1.675	1.687	1.700	1.712
Safety Factor	1.73	1.77	1.79	2.05	1.64
Margin of Safety	0.73	0.77	0.79	1.05	0.64
40 degrees					
Erosion *	0.12	0.15	0.20	0.08	0.16
Char **	0.60	0.54	0.47	0.60	0.71
2E + 1.25C	0.98	0.98	0.98	0.90	1.21
Liner Thickness ***	1.597	1.675	1.687	1.700	1.712
Safety Factor	1.62	1.71	1.71	1.88	1.41
Margin of Safety	0.62	0.71	0.71	0.88	0.41
60 degrees					
Erosion *	0.15	0.10	0.12	0.10	0.09
Char **	0.49	0.56	0.55	0.60	0.77
2E + 1.25C	0.92	0.90	0.93	0.94	1.14
Liner Thickness ***	1.597	1.675	1.687	1.700	1.712
Safety Factor	1.74	1.86	1.81	1.80	1.51
Margin of Safety	0.74	0.86	0.81	0.80	0.51
80 degrees					
Erosion *	0.02	0.00	0.04	0.05	0.04
Char **	0.62	0.63	0.64	0.65	0.72
2E + 1.25C	0.82	0.79	0.88	0.91	0.98
Liner Thickness ***	1.597	1.675	1.687	1.700	1.712
Safety Factor	1.96	2.13	1.92	1.87	1.74
Margin of Safety	0.96	1.13	0.92	0.87	0.74

* Measured Erosion
** Measured Char times 0.85
(adjusted to end of action time)
*** RSRM Minimum Liner Thickness

Table 7.5-2. DM-9 OBR Erosion and Char Data (cont)

Angular Location	STATIONS				
100 degrees	8	9	10	11	12
Erosion *	0.00	0.00	0.00	0.00	0.02
Char **	0.59	0.60	0.60	0.64	0.64
2E + 1.25C	0.73	0.74	0.75	0.80	0.84
Liner Thickness ***	1.597	1.675	1.687	1.700	1.712
Safety Factor	2.18	2.25	2.24	2.13	2.05
Margin of Safety	1.18	1.25	1.24	1.13	1.05
120 degrees					
Erosion *	0.06	0.03	0.04	0.04	0.08
Char **	0.51	0.49	0.48	0.46	0.53
2E + 1.25C	0.76	0.68	0.69	0.65	0.82
Liner Thickness ***	1.597	1.675	1.687	1.700	1.712
Safety Factor	2.11	2.48	2.46	2.60	2.09
Margin of Safety	1.11	1.48	1.46	1.60	1.09
140 degrees					
Erosion *	0.00	0.00	0.00	0.00	0.00
Char **	0.67	0.65	0.60	0.59	0.64
2E + 1.25C	0.84	0.81	0.74	0.73	0.80
Liner Thickness ***	1.597	1.675	1.687	1.700	1.712
Safety Factor	1.90	2.07	2.27	2.32	2.15
Margin of Safety	0.90	1.07	1.27	1.32	1.15
160 degrees					
Erosion *	0.11	0.07	0.07	0.11	0.16
Char **	0.52	0.59	0.53	0.52	0.56
2E + 1.25C	0.87	0.87	0.86	0.87	1.02
Liner Thickness ***	1.597	1.675	1.687	1.700	1.712
Safety Factor	1.84	1.92	1.96	1.96	1.68
Margin of Safety	0.84	0.92	0.96	0.96	0.68
180 degrees					
Erosion *	0.03	0.03	0.04	0.02	0.07
Char **	0.50	0.49	0.45	0.48	0.50
2E + 1.25C	0.69	0.68	0.64	0.64	0.77
Liner Thickness ***	1.597	1.675	1.687	1.700	1.712
Safety Factor	2.33	2.48	2.62	2.68	2.23
Margin of Safety	1.33	1.48	1.62	1.68	1.23

* Measured Erosion
** Measured Char times 0.85
(adjusted to end of action time)
*** RSRM Minimum Liner Thickness

ORIGINAL PAGE
BLACK AND WHITE PHOTOGRAPH

N101171-3

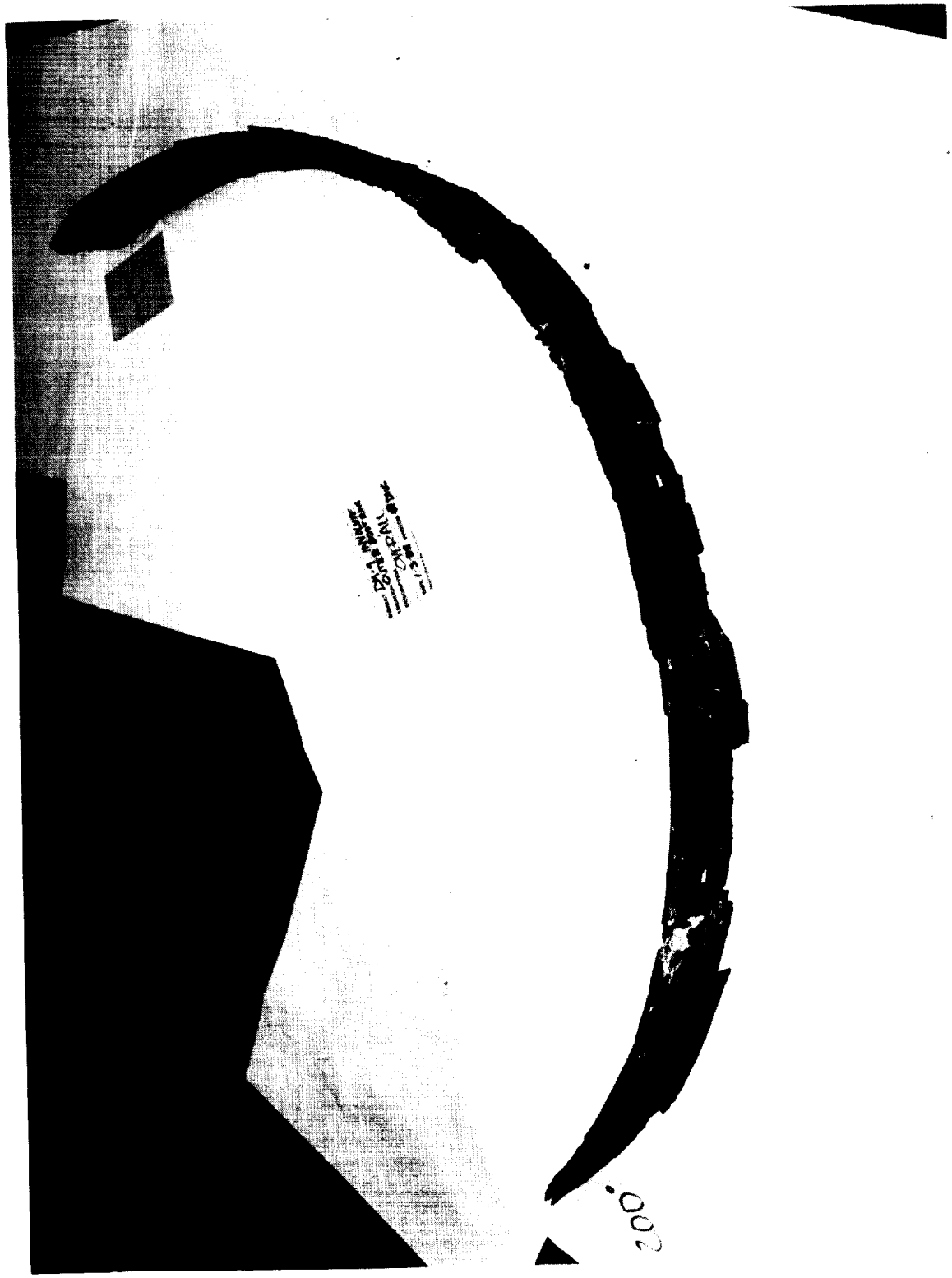

Figure 7.5-31. DM-9 Reassambled Six Pieces of Involute OBR

N101171-2

Figure 7.5-32. DM-9 Reassembled Six Pieces of Involute OBR

N101171-24

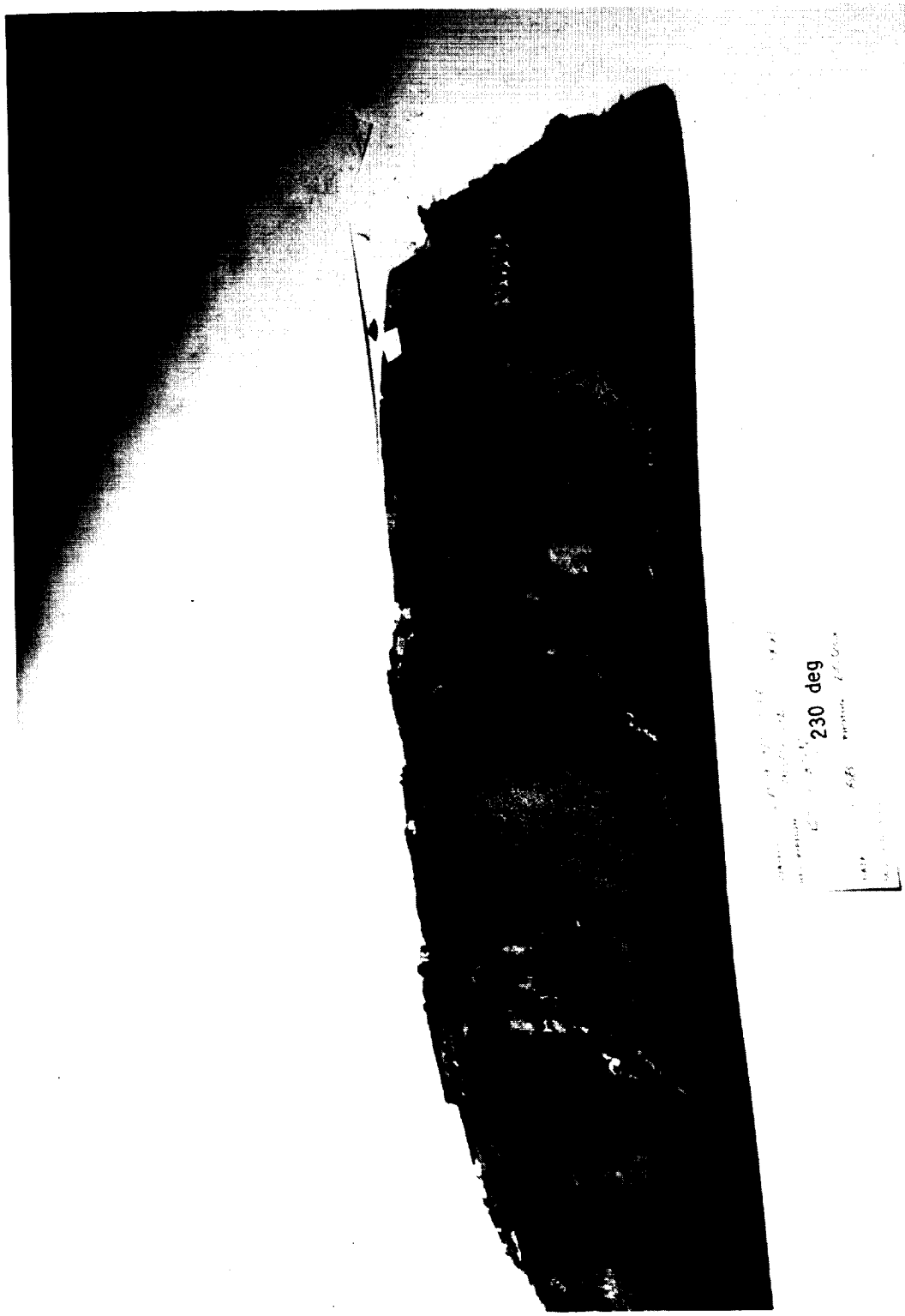

Figure 7.5-33. DM-9 OBR Piece No. 1 Recovered

N101171-25

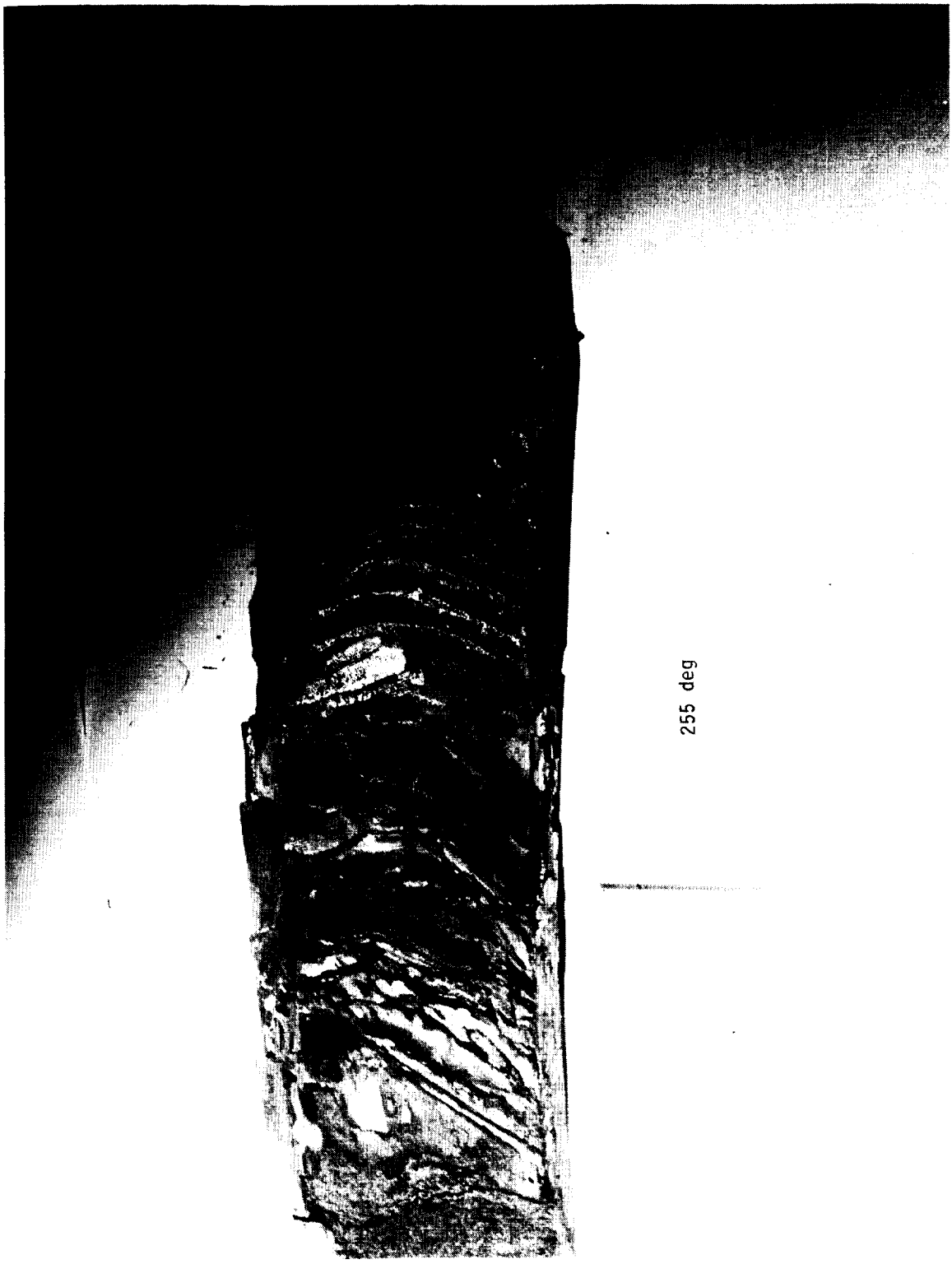

Figure 7.5-34. DM-9 OBR Piece No. 2 Recovered

ORIGINAL PAGE
BLACK AND WHITE PHOTOGRAPH

N101171-26

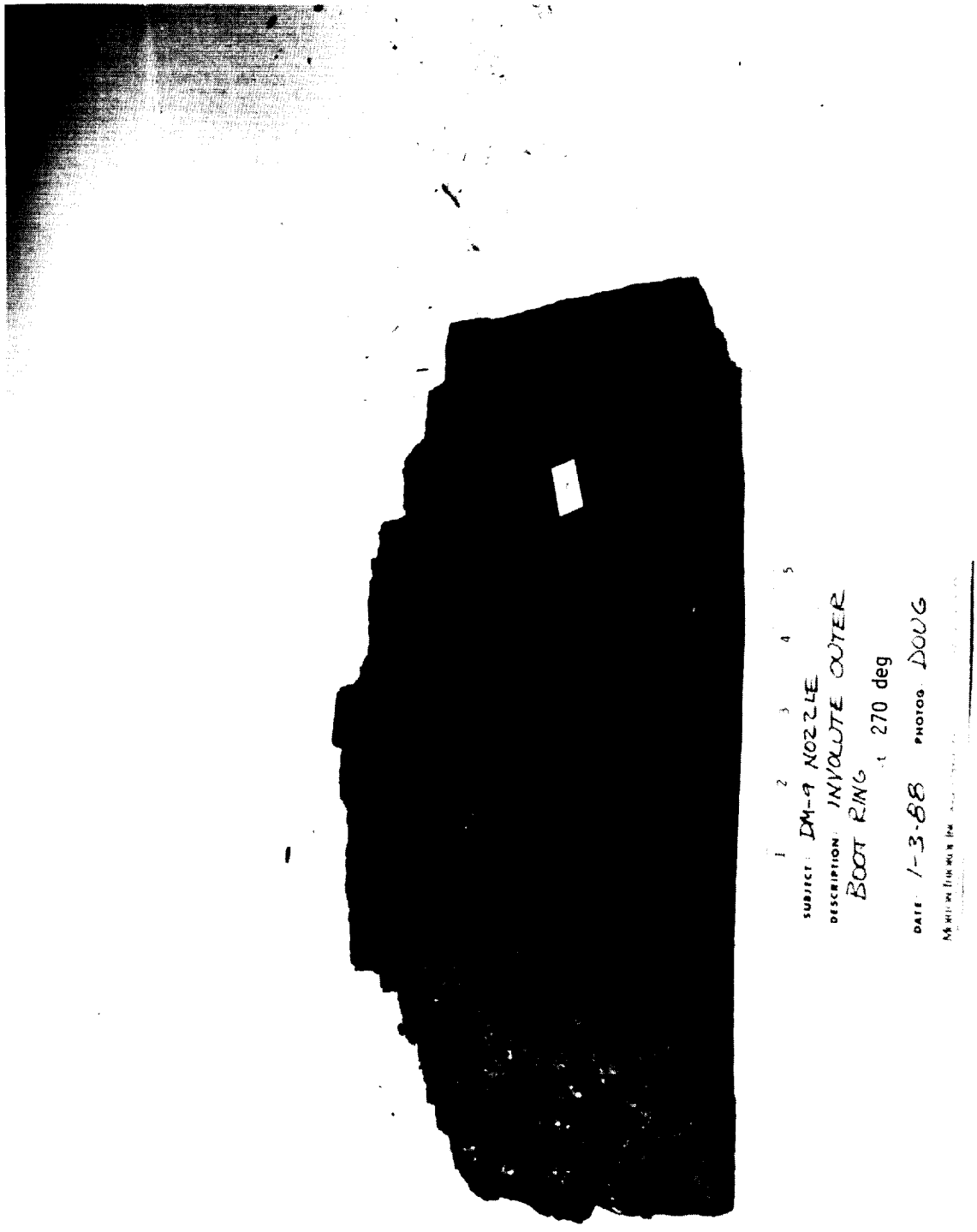

Figure 7.5-35. DM-9 OBR Piece No. 3 Recovered

N101171-22

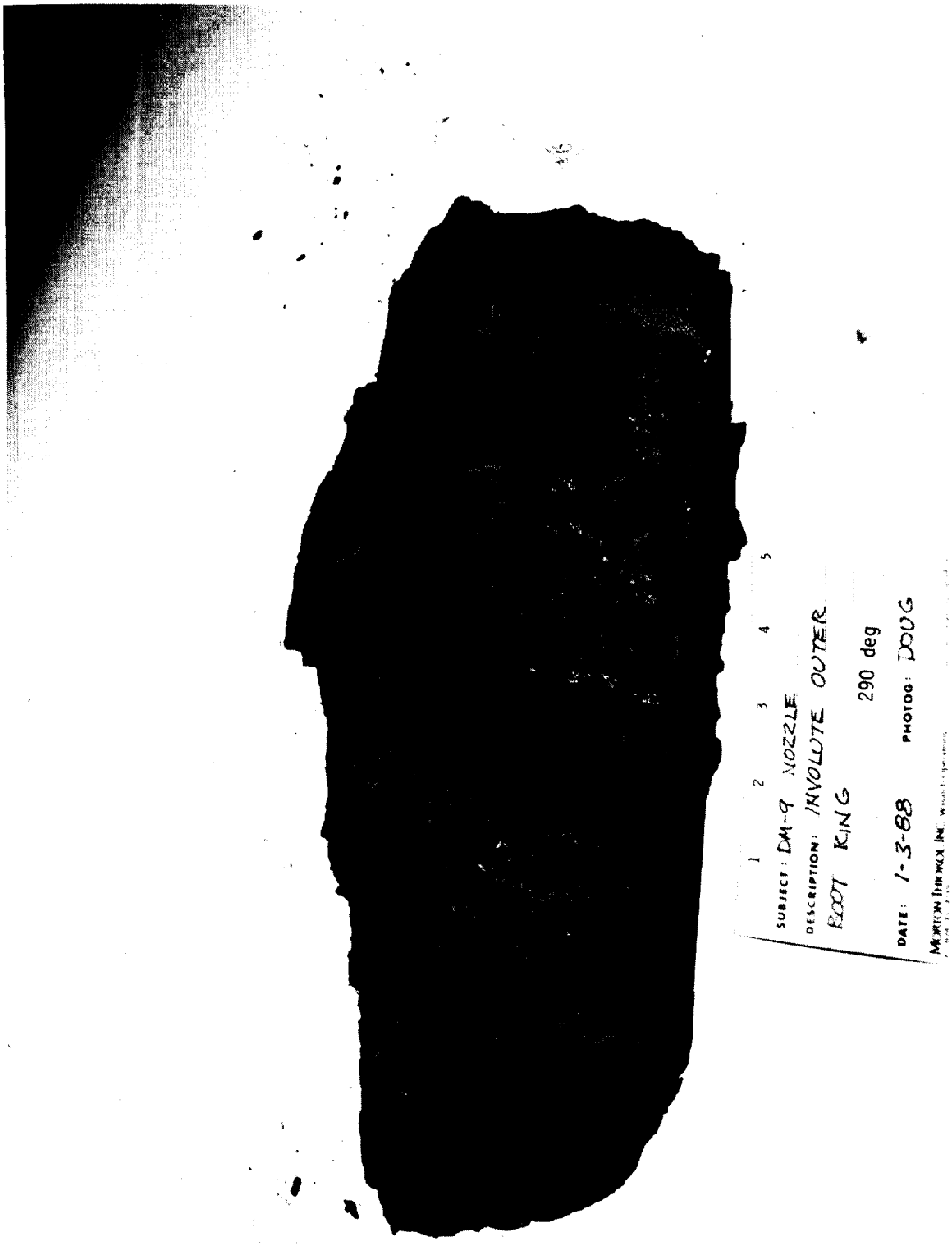

Figure 7.5-36. DM-9 OBR Piece No. 4 Recovered

N101171-20

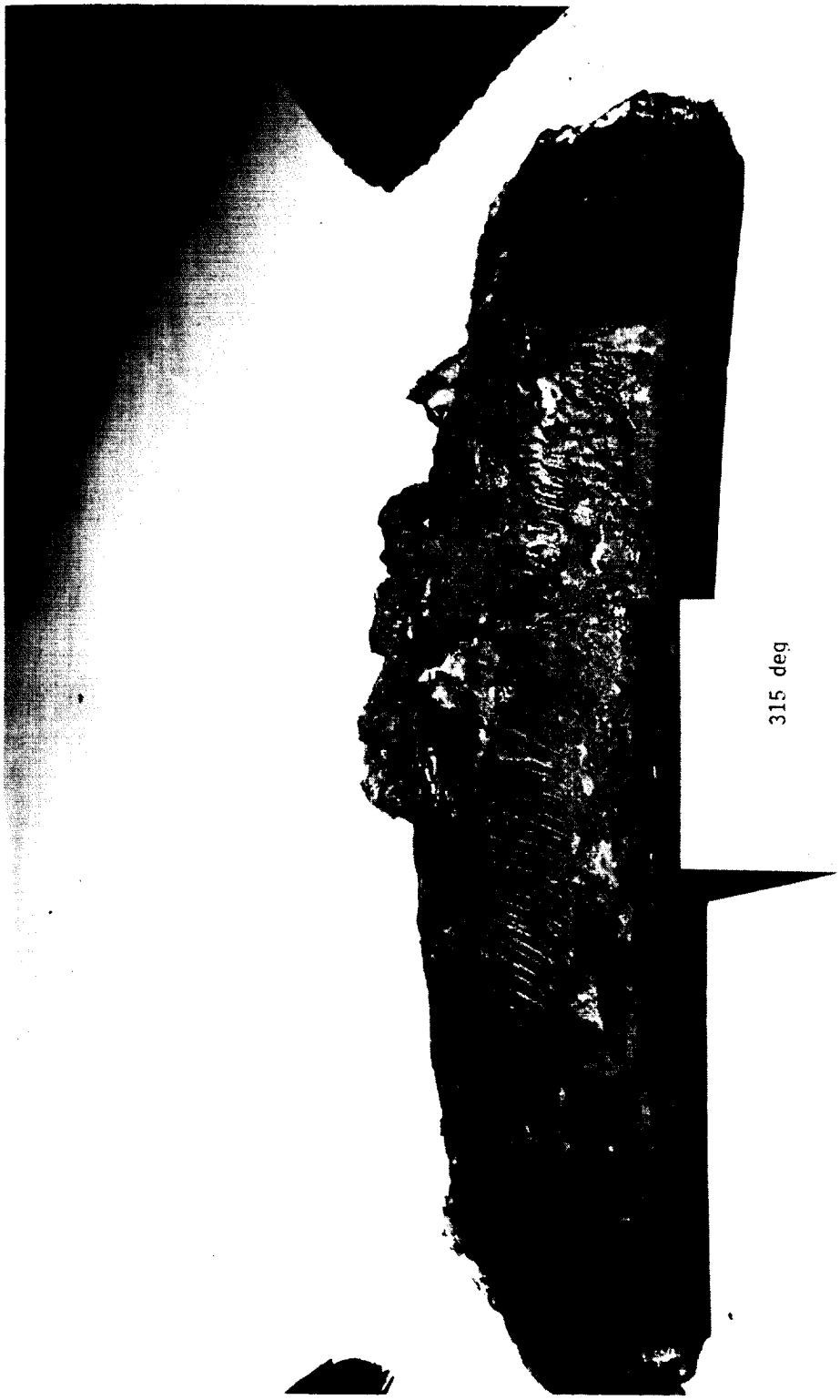

Figure 7.5-37. DM-9 OBR Piece No. 5 Recovered

N101171-19

Figure 7.5-38. DM-9 OBR Piece No. 6 Recovered

N101171-8

10 deg

Figure 7.5-39. DM-9 OBR Piece No. 6 Recovered

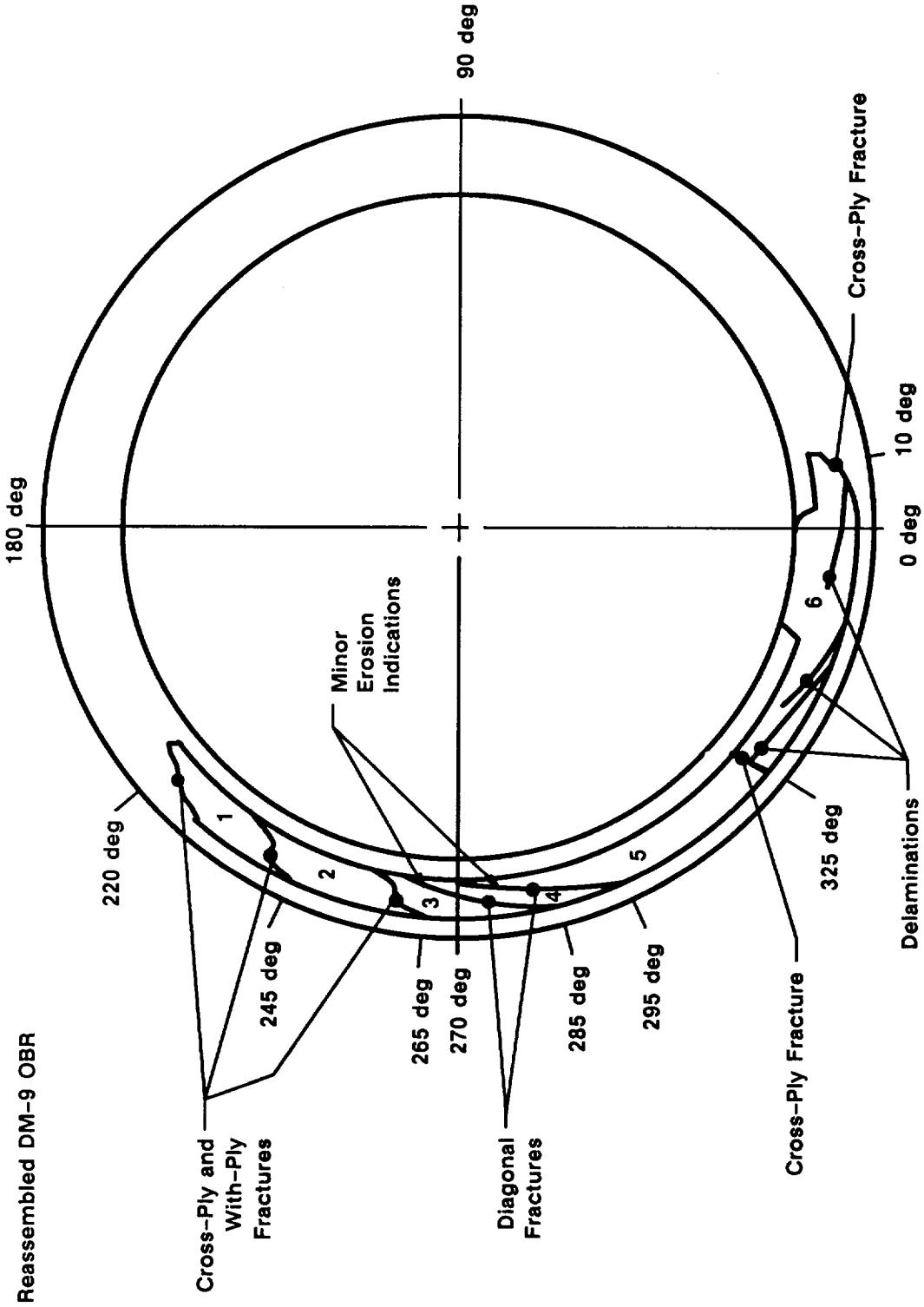

Figure 7.5-40. DM-9 Mapping of Reassembled Pieces of OBR

- Piece No. 1—220 to 245 deg— was found buried in slag approximately 8.0 ft forward of the nozzle nose cap

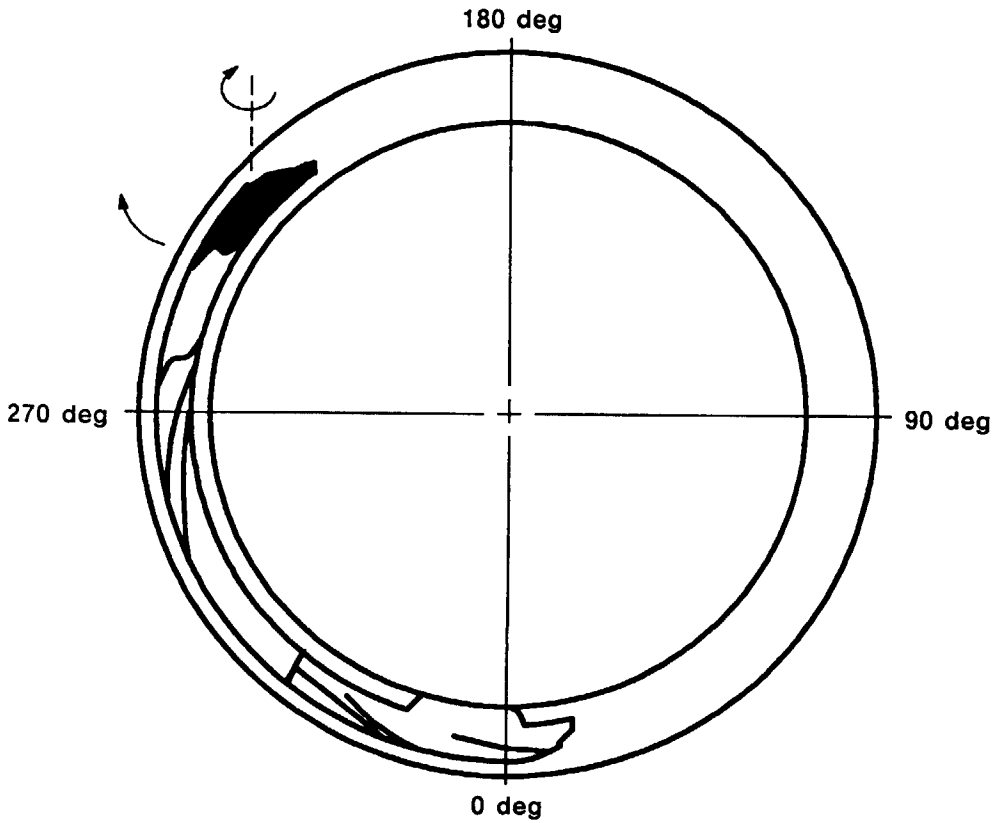

- Sectioning revealed that Piece No. 1 was completely charred through
- The 220-deg and 245-deg fractured ends of Piece No. 1 showed signs of both cross-ply and with-ply failure
- The 220-deg fractured end contained indications of bending/torsion fracture
- The 245-deg fractured end contained indications of bending fracture
- Erosion was not present on fractured or ID surfaces

Figure 7.5-41. DM-9 OBR Piece No. 1 Description

A012792a

- Piece No. 2—245 to 265 deg— was found buried in slag approximately 6.0 ft forward of the nozzle nose cap

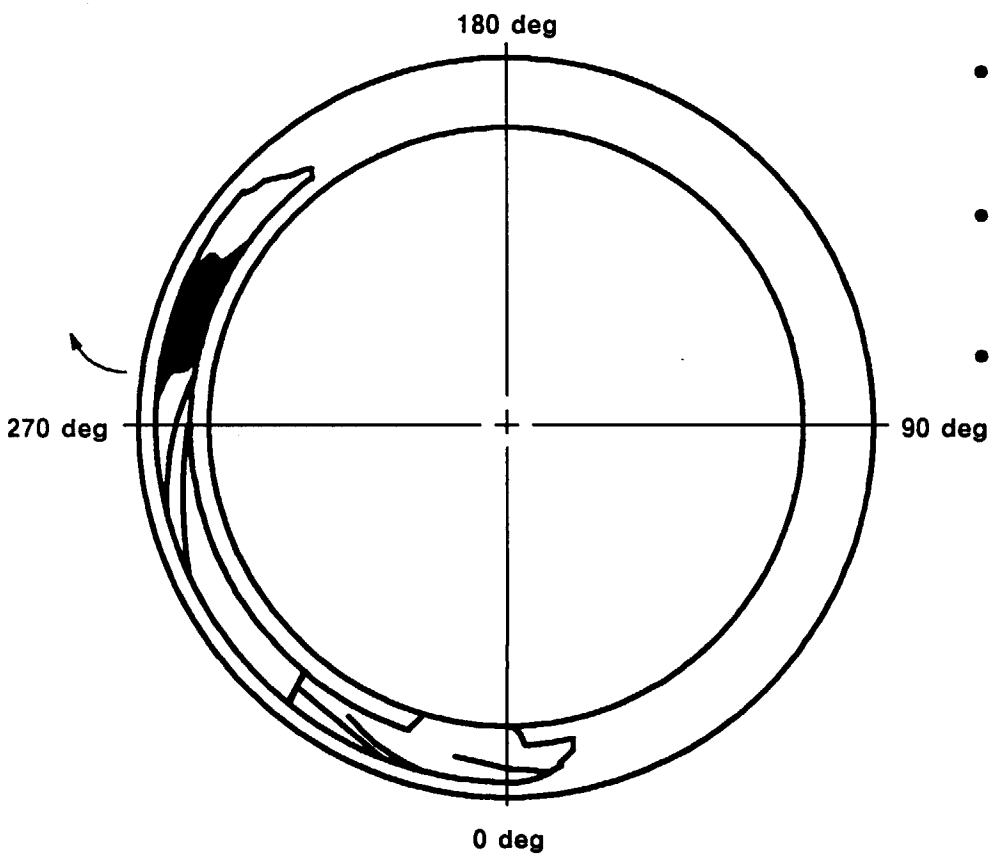

- Sectioning revealed that Piece No. 2 was completely charred through
- The 245-deg and 265-deg fractured ends of Piece No. 2 showed signs of both cross-ply and with-ply failure
- The 245-deg and 265-deg fractured ends contained indications of bending fracture
- Erosion was not present on fractured or ID surfaces

Figure 7.5-42. DM-9 OBR Piece No. 2 Description

A012793a

- Piece No. 3 —265 to 285 deg—was found lying on top of the slag under the nozzle nose cap

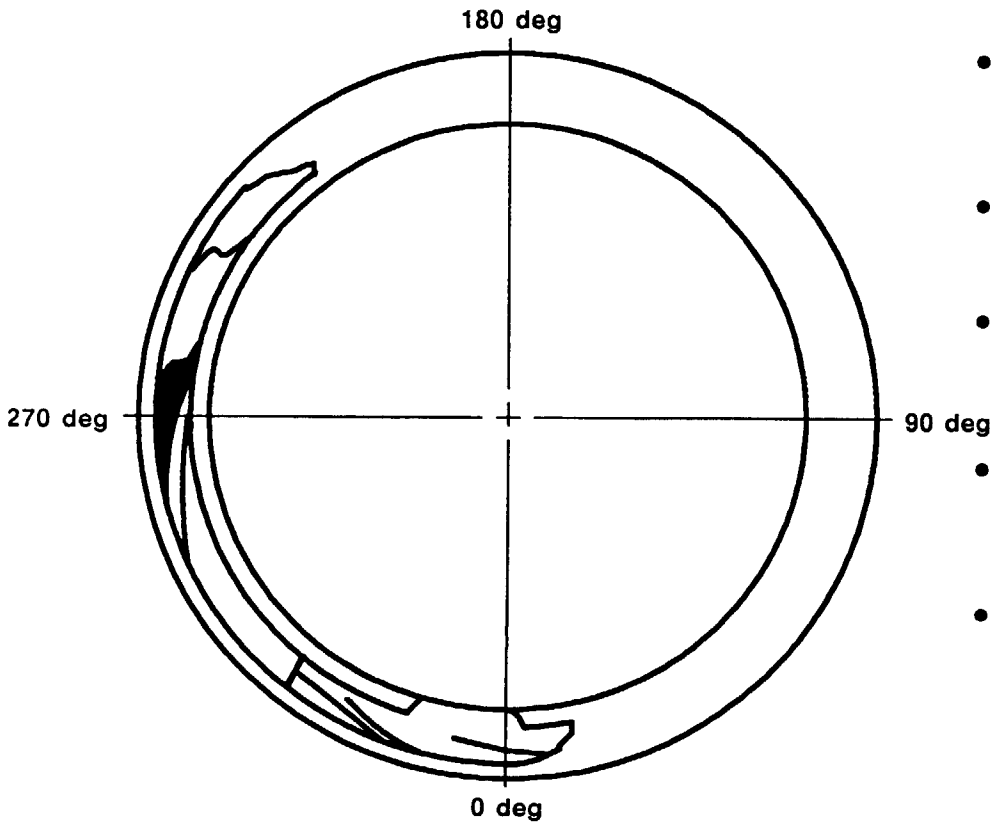

- Sectioning revealed that Piece No. 3 was completely charred through
- The 265-deg fractured end of Piece No. 3 showed signs of both cross-ply and with-ply failure
- The 265-deg fractured end contained indications of bending fracture
- The 285-deg fractured end of Piece No. 3 failed with-ply, with localized cross-ply fracture
- The 285-deg fractured end contained indications of delamination with mechanical load assist
- Erosion and flow indications were found near the ID surface along diagonal fracture (photo micrographs show rounding of the fibers - Figure 7.5-46)

Figure 7.5-43. DM-9 OBR Piece No. 3 Description

A012794a

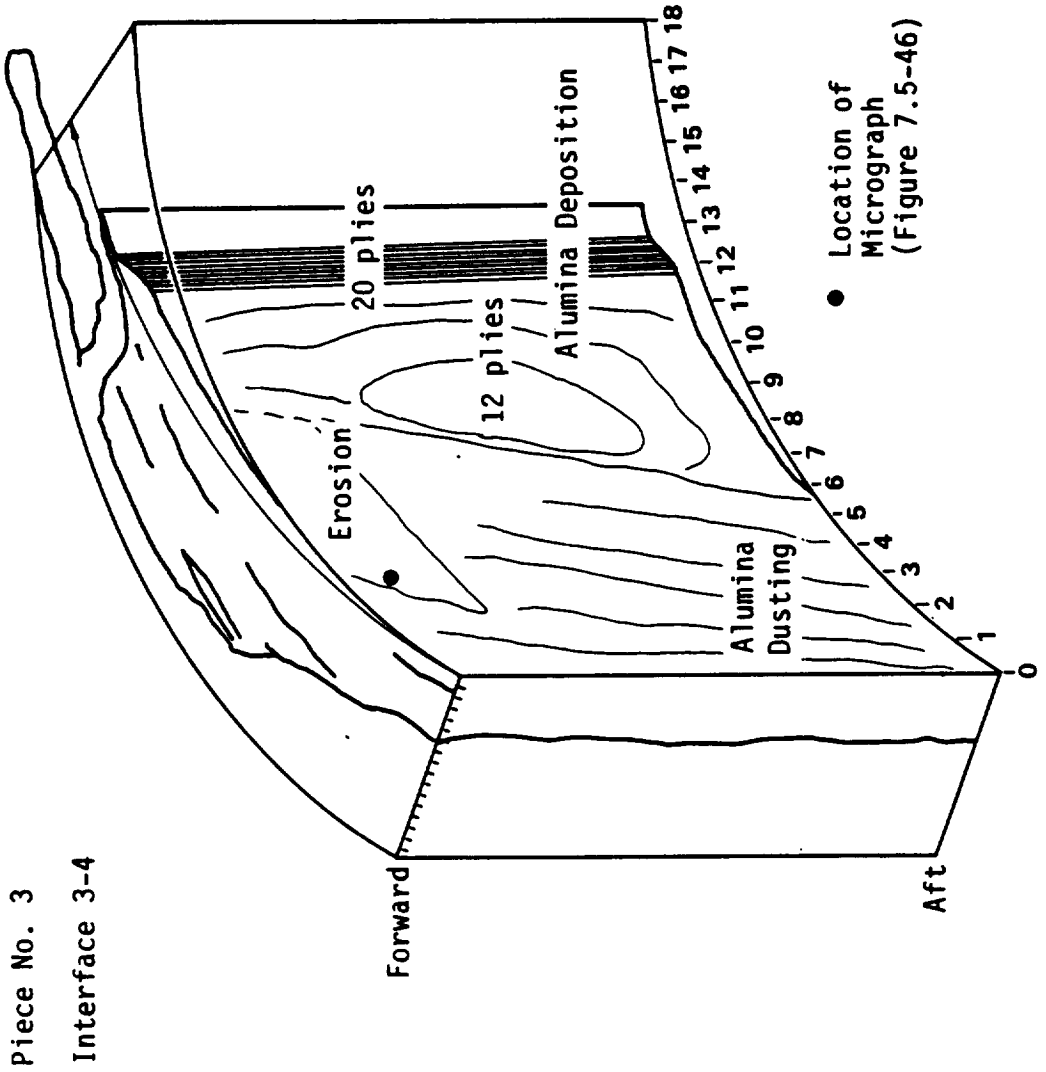

Figure 7.5-44. DM-9 OBR Ring Piece No. 3 Description

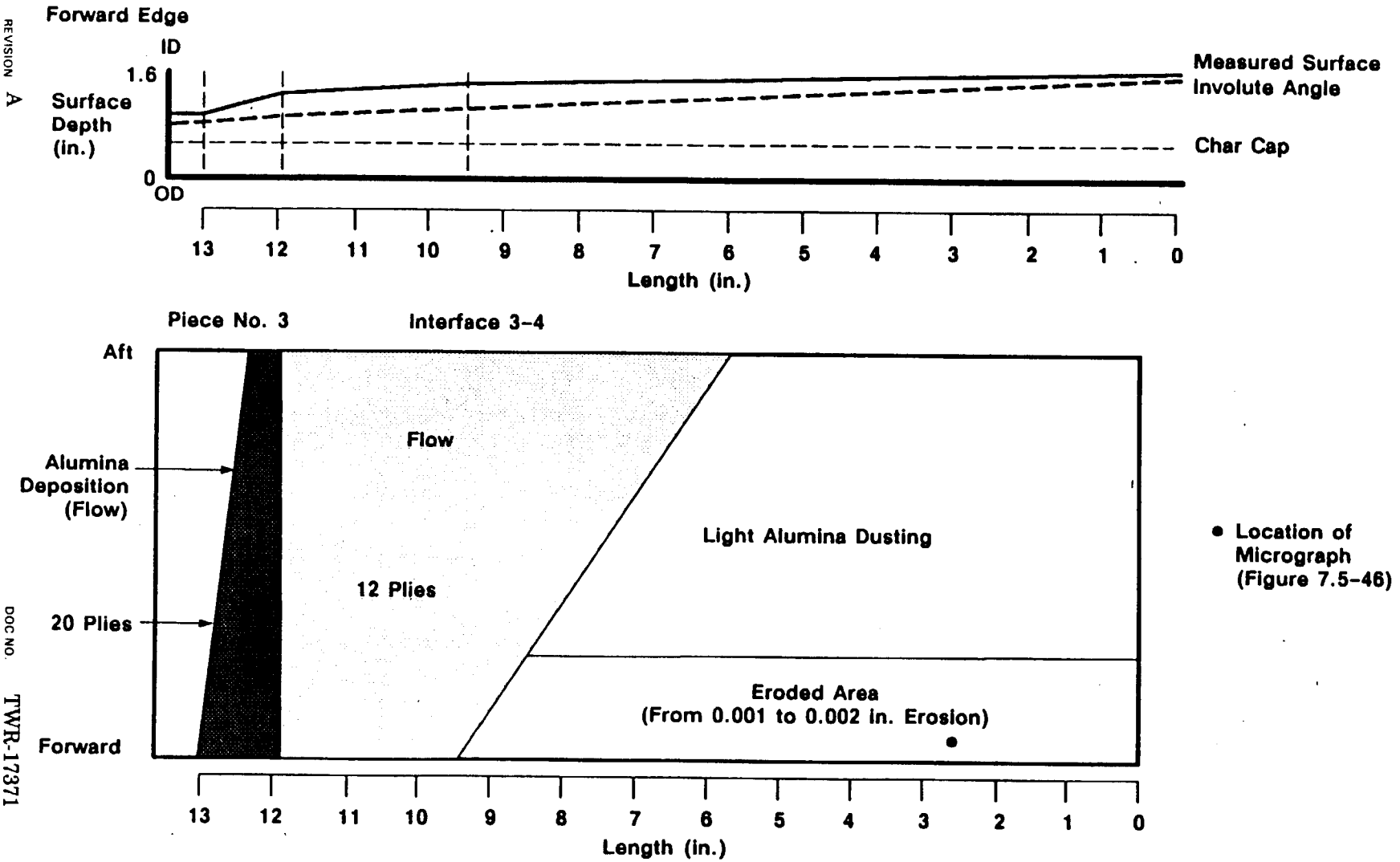

Figure 7.5-45. DM-9 OBR Ring Piece No. 3 Description

ORIGINAL PAGE
BLACK AND WHITE PHOTOGRAPH

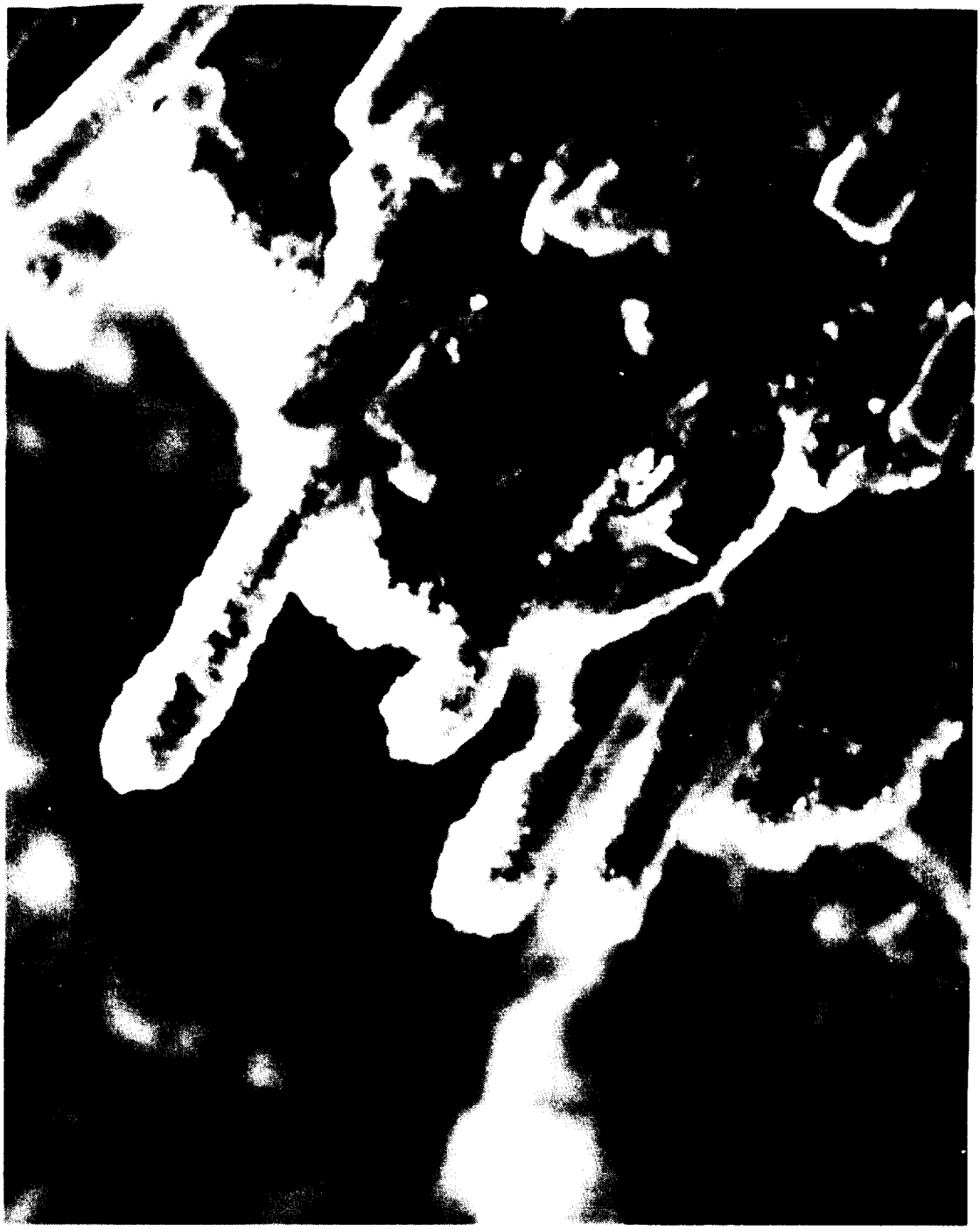

Figure 7.5-46. DM-9 OBR Piece No. 3, Micrograph Showing Alumina Dusting and Rounded Fibers

- Piece No. 4—285 to 295 deg—was found under the nozzle nose cap lying on top of the slag

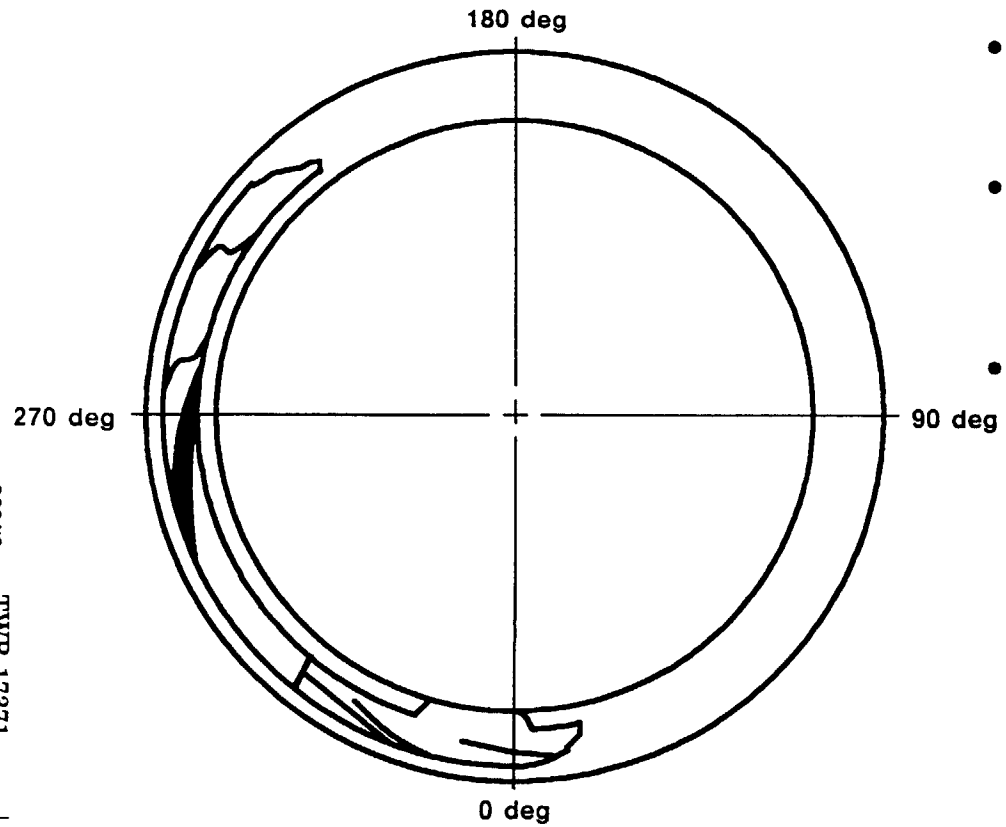

- Sectioning revealed that Piece No. 4 was completely charred through
- The 285-deg and 295-deg fractured ends of Piece No. 4 failed with-ply, with localized cross-ply fracture
- The 285-deg and 295-deg fractured ends contained indications of delamination with mechanical load assist
- Erosion and flow indications were found near the ID surface along through-delamination (photo micrographs show rounding of the fibers-Figure 7.5-50)

Figure 7.5-47. DM-9 OBR Piece No. 4 Description

A012795a

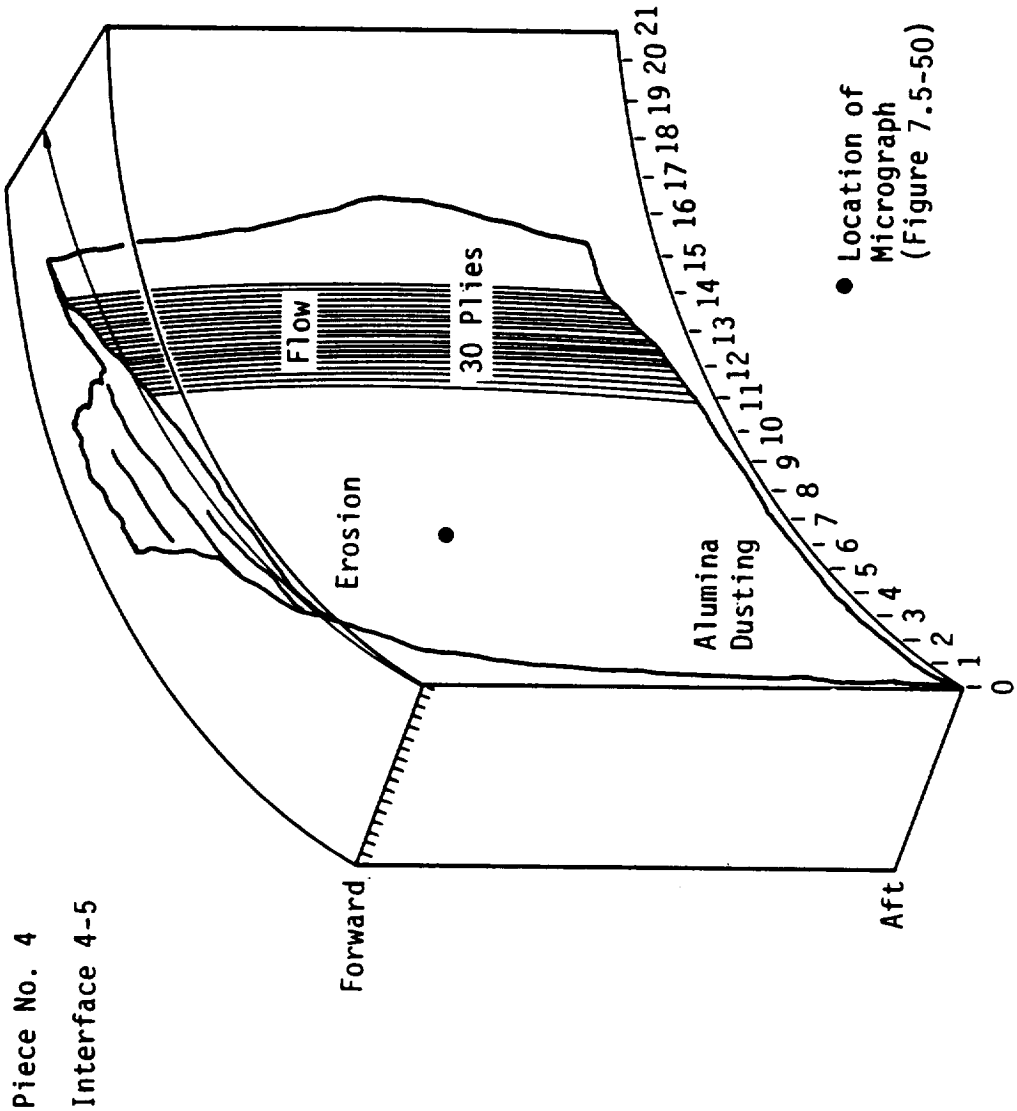

Figure 7.5-48. DM-9 OBR Ring Piece No. 4 Description

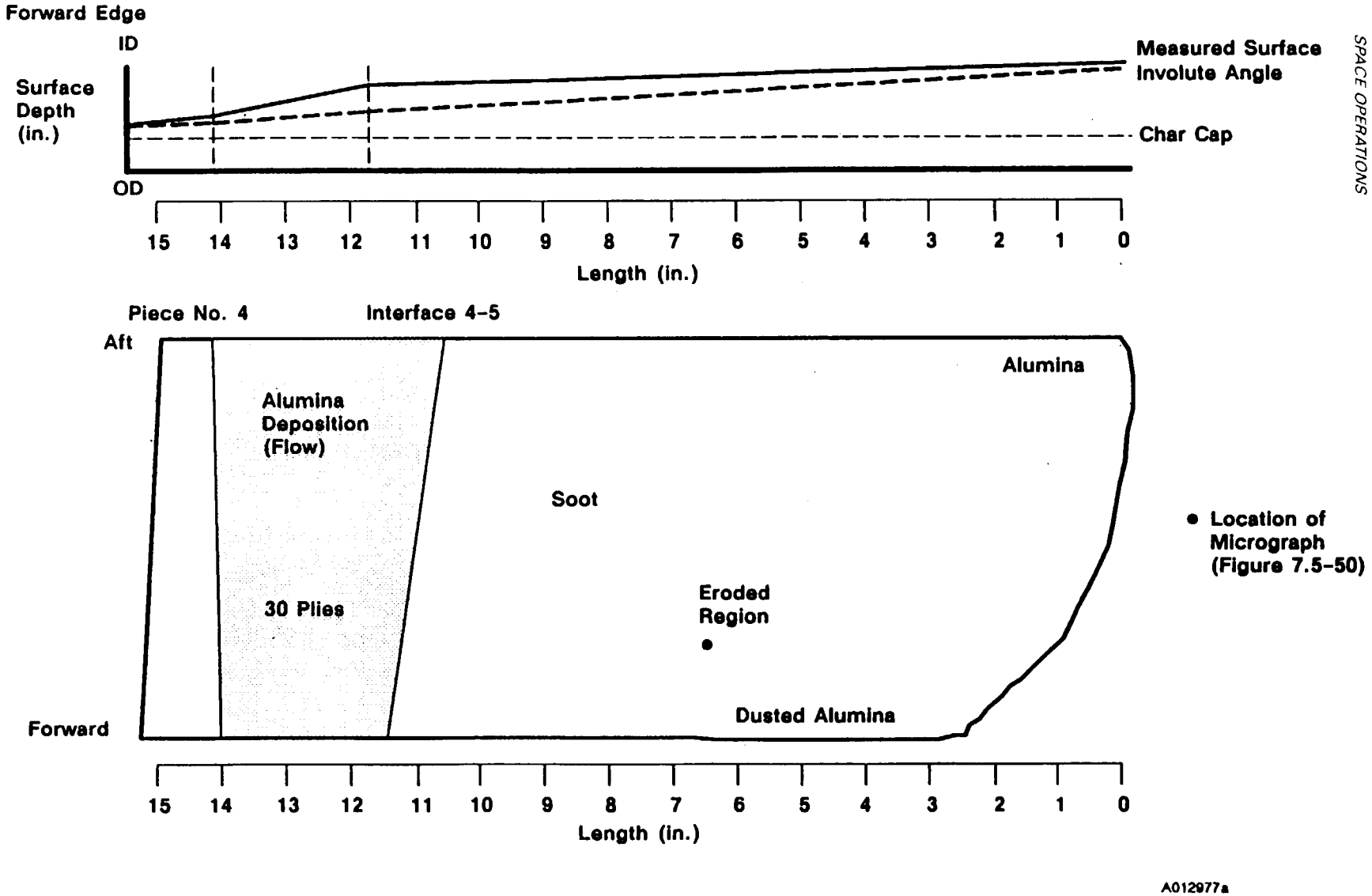

Figure 7.5-49. DM-9 OBR Ring Piece No. 4 Description

ORIGINAL PAGE
BLACK AND WHITE PHOTOGRAPH

Figure 7.5-50. DM-9 OBR Piece No. 4 Micrograph Showing Flow Indications (alumina dusting and rounded fibers)

- Piece No. 5—295 to 325 deg—was found buried in the slag 27 ft forward of the nozzle nose cap

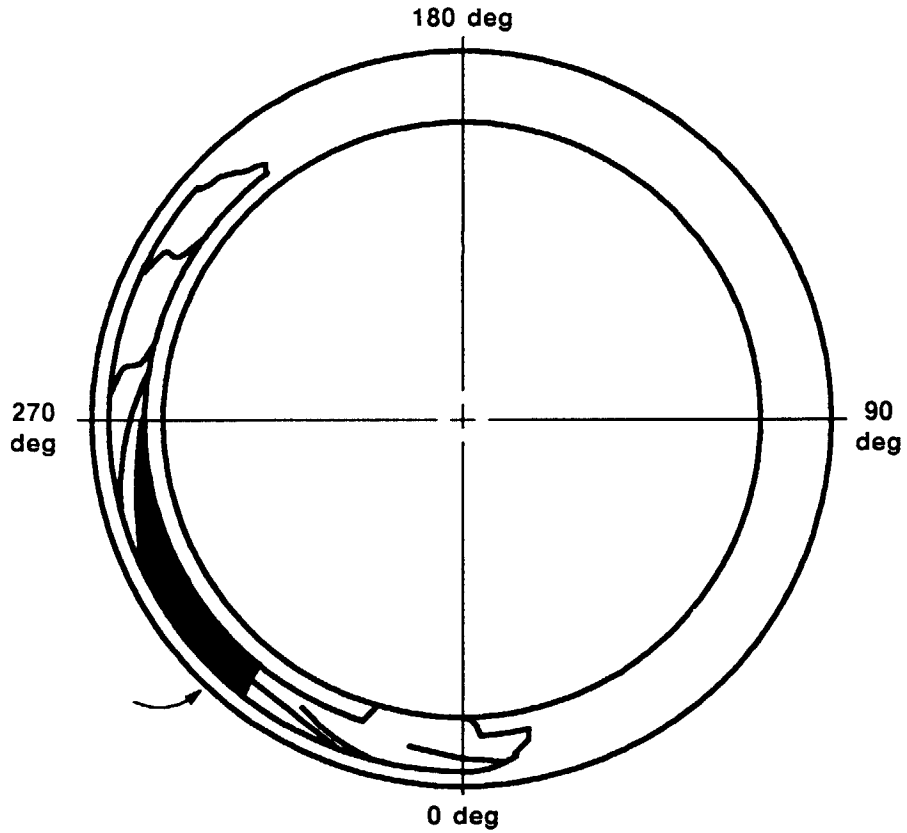

- Sectioning revealed that Piece No. 5 was completely charred through
- The 295-deg fractured end of Piece No. 5 was with-ply, with localized cross-ply fracture
- The 295-deg fractured end contained indications of delamination with mechanical load assist
- The 325-deg fractured end of Piece No. 5 showed a complete radial (cross-ply) failure
- The 325-deg fractured end contained indications consistent with hoop tension or bending fracture
- Erosion was not present on fractured or ID surface

Figure 7.5-51. DM-9 OBR Piece No. 5 Description

A012796a

- Piece No. 6—325 to 10 deg—was found under the nozzle nose cap, lying on top of the slag

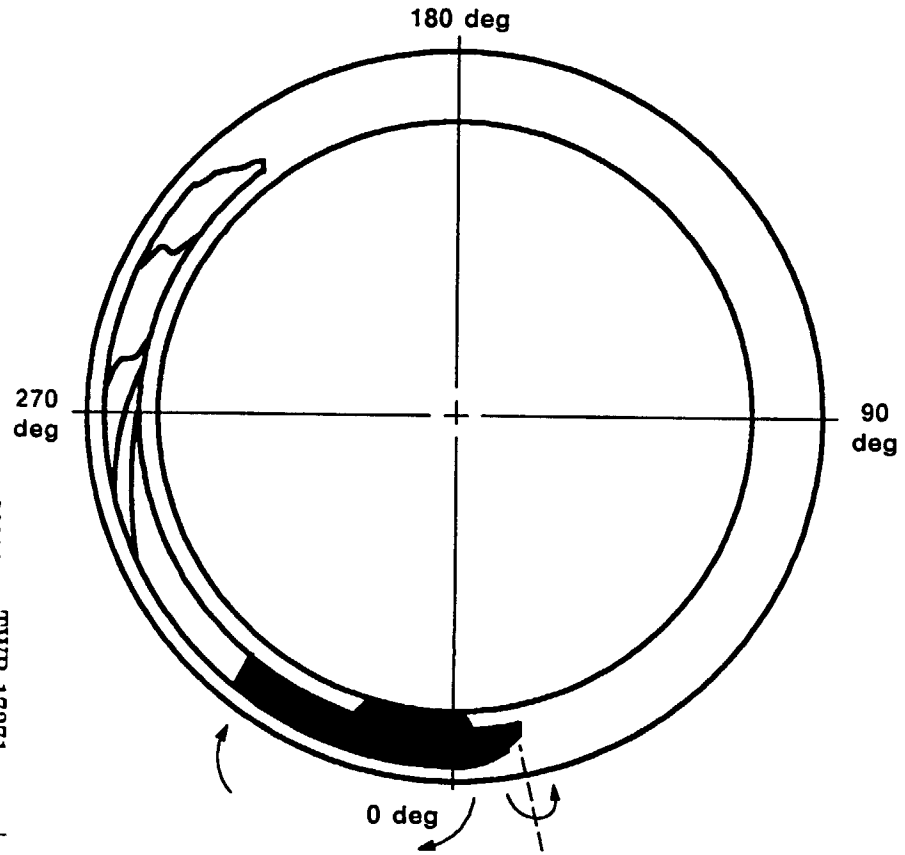

- Sectioning revealed one location (325-deg end) less heat affected (Figure 4.1.3-35d)
- The 325-deg fracture end of Piece No. 6 showed a radial (cross-ply) failure
- The 325-deg fractured end contained indications of hoop tension or bending fracture
- The 10-deg fracture end of Piece No. 6 showed signs of cross-ply and with-ply failure
- The 10-deg fractured end contained indications of bending/torsion fracture
- Erosion was not present on fractured or ID surface

Figure 7.5-52. DM-9 OBR Piece No. 6 Description

A012797a

A012817a

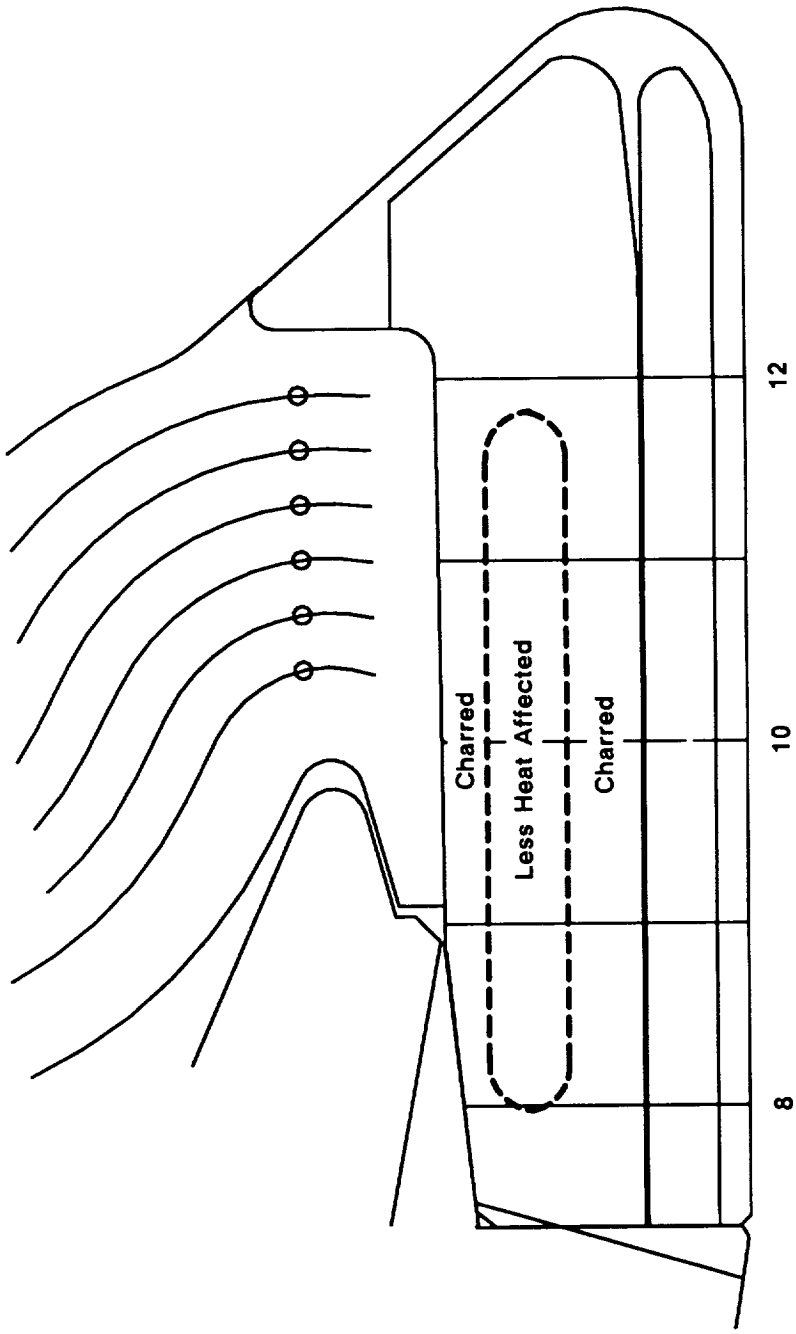

Piece No. 6 (at approximately 325 deg)

Figure 7.5-53. DM-9 OBR Piece No. 6 Description

N101197-3

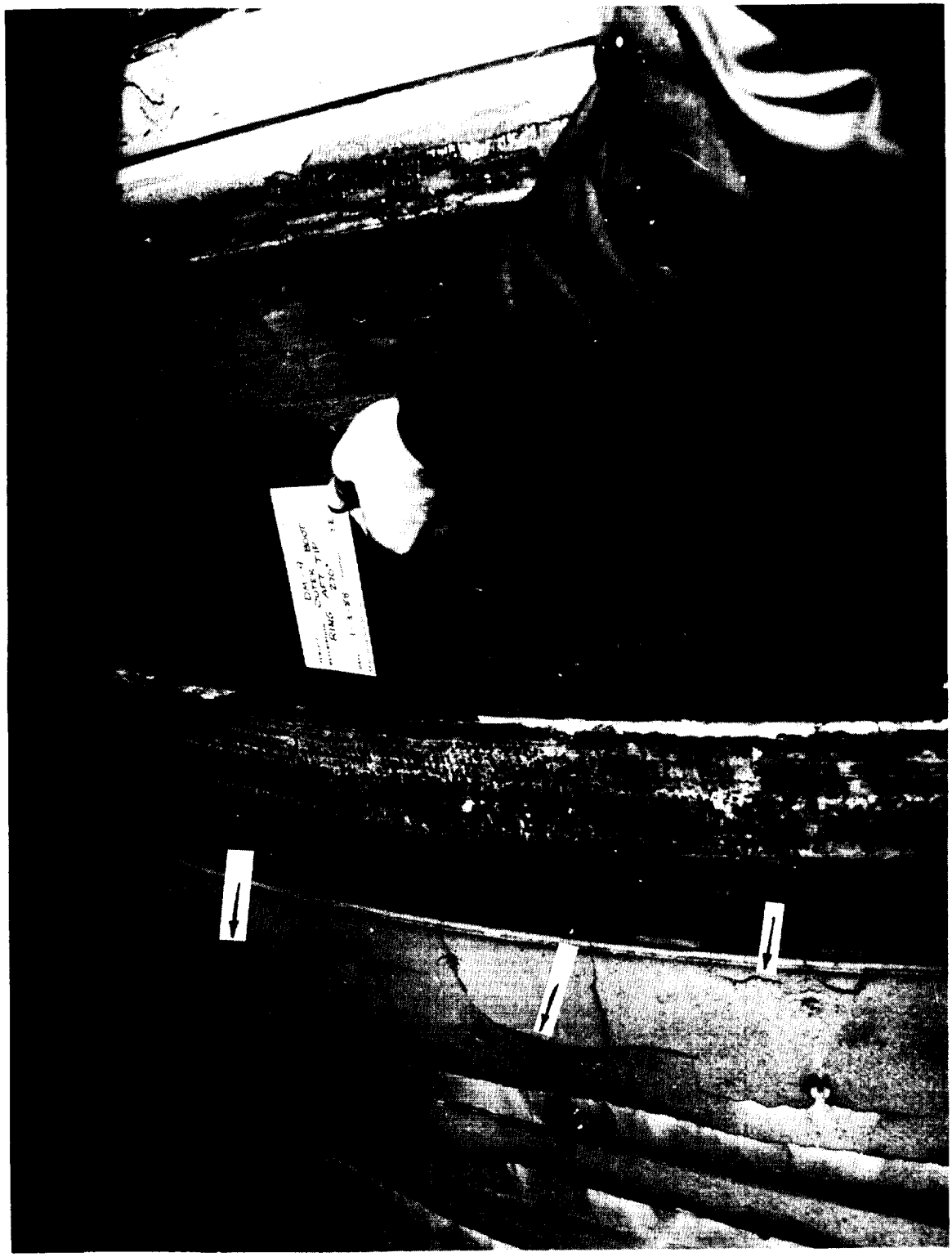

Figure 7.5-54. DM-9 Cowl Ring Irregular Erosion Patterns (270 deg)

ORIGINAL PAGE
BLACK AND WHITE PHOTOGRAPH

N101197-1

Figure 7.5-55. DM-9 Cowl Ring Irregular Erosion Patterns (300 deg)

The cowl ring showed cross-ply cracks extending axially through the port vent and shear pinholes. Axial cracks were also observed spaced between ventholes. These axial cracks have occurred on all previous nozzles and have been shown to be isolated within charred CCP material only.

Charred CCP material wedged out on the aft 3.0 in. of the cowl ring from 220 to 240 deg and from 335 to 10 deg (Figures 7.5-9, 7.5-11 and 7.5-56). Three pieces of the wedged out CCP were found downstream of the motor (Figures 7.5-57 through 7.5-60). One of the pieces showed erosion and slag on the fracture surface. Sectioning of the cowl ring revealed that the char line was only slightly affected in the areas of the wedge outs. This indicates the material wedged out late in motor operation. The char line indicates that the 220- to 240-deg wedge out occurred earlier than the 335- to 10-deg wedge out.

Visual examination showed that the majority of the DM-9 cowl vent holes were plugged with slag. When using a probe measurement method (0.125 in. wire), 2 of the 36 cowl vent holes were open. DM-8 showed three open vent holes and ETM-1A showed seven open vent holes. When using a gas flow method (100 psi air), 20 of the DM-9 vent holes allowed flowthrough. Slag coated each vent hole wall circumferentially from ID to OD. The holes were typically plugged near the ID and OD of the ring. Slag was removed from each vent hole and weighed (Figure 7.5-61). The average weight of slag per hole was 1.68 g.

The cowl aft tip remained bonded to the flex boot around most of the circumference (Figure 7.5-62). Separations occurred between 240 and 300 deg. From 240 to 260 deg, approximately 60 percent of the bondline between the cowl and flex boot showed NBR remaining on the cowl aft tip. The bondline showed a 40-percent adhesive failure between the EA 913 adhesive and cowl aft tip. The separation from 240 to 260 deg resulted from a break within the flex boot and a partial adhesion degradation between the adhesive and cowl aft tip. From 260 to 300 deg, 100 percent of the bondline between the cowl and flex boot showed NBR remaining on the cowl

- The cowl ring showed wedge-out of charred CCP material from 220 to 240 deg and from 335 to 10 deg

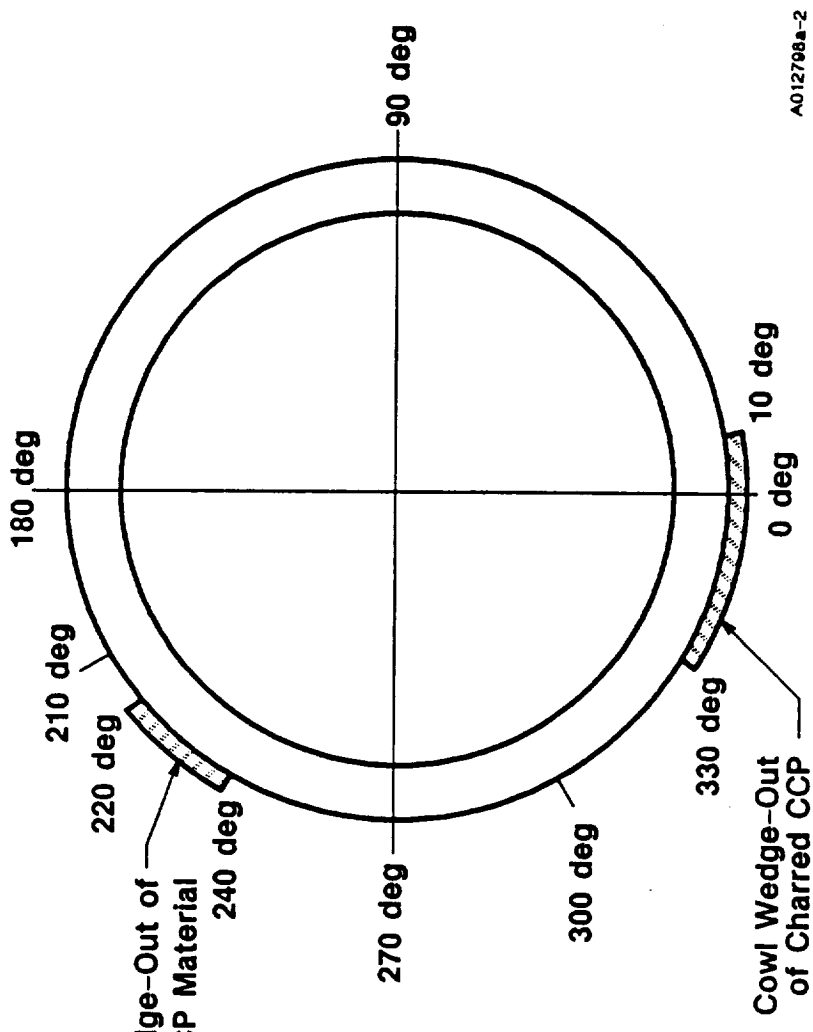

Figure 7.5-56. DM-9 Cowl Ring Wedge Out Locations

ORIGINAL PAGE
BLACK AND WHITE PHOTOGRAPH

N101171-15

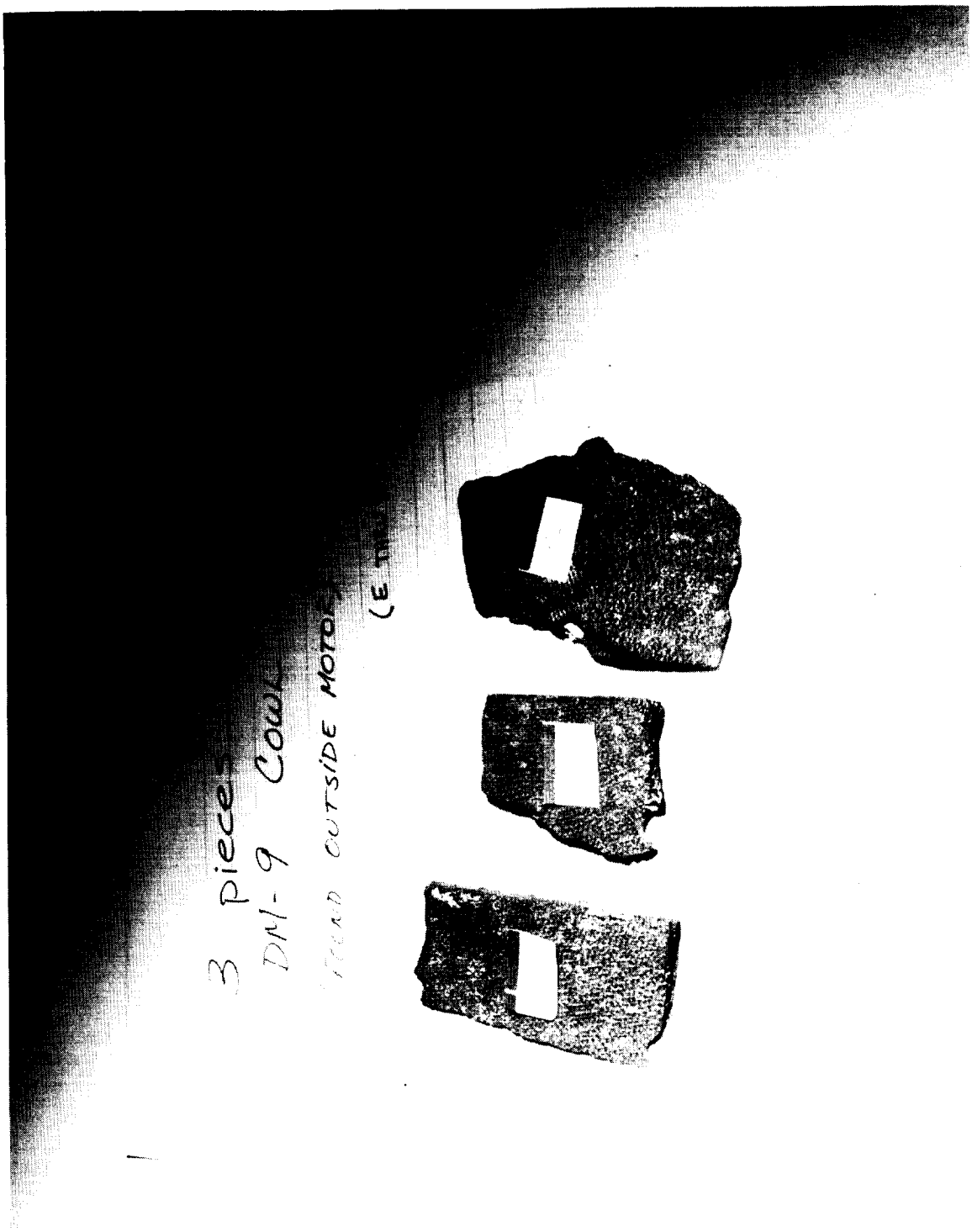

Figure 7.5-57. DM-9 Cowl Ring Pieces Found Outside of Motor

A012816a-2

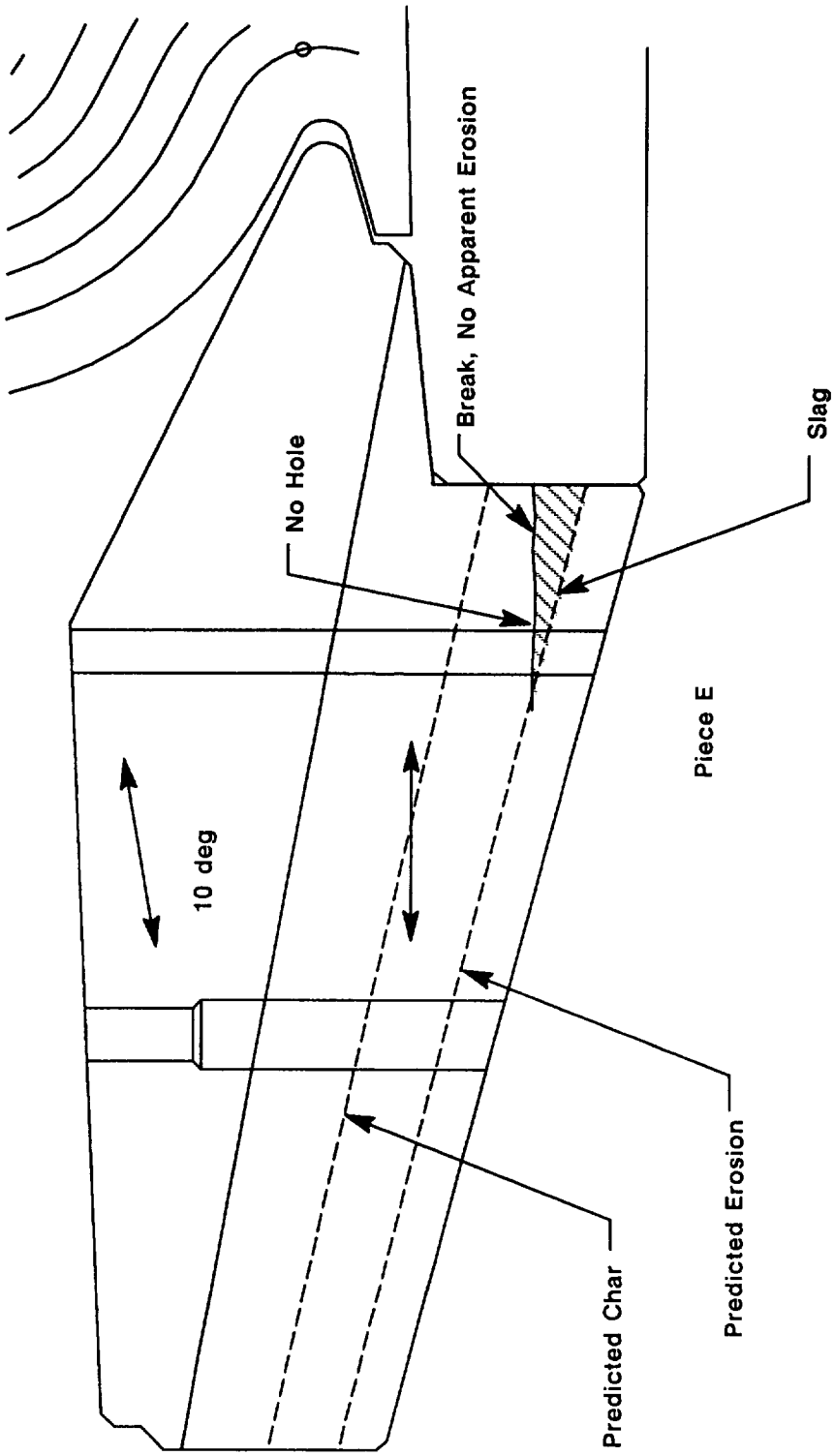

Figure 7.5-58. Cowl Piece E Found Outside of DM-9 Motor

A012813aR1

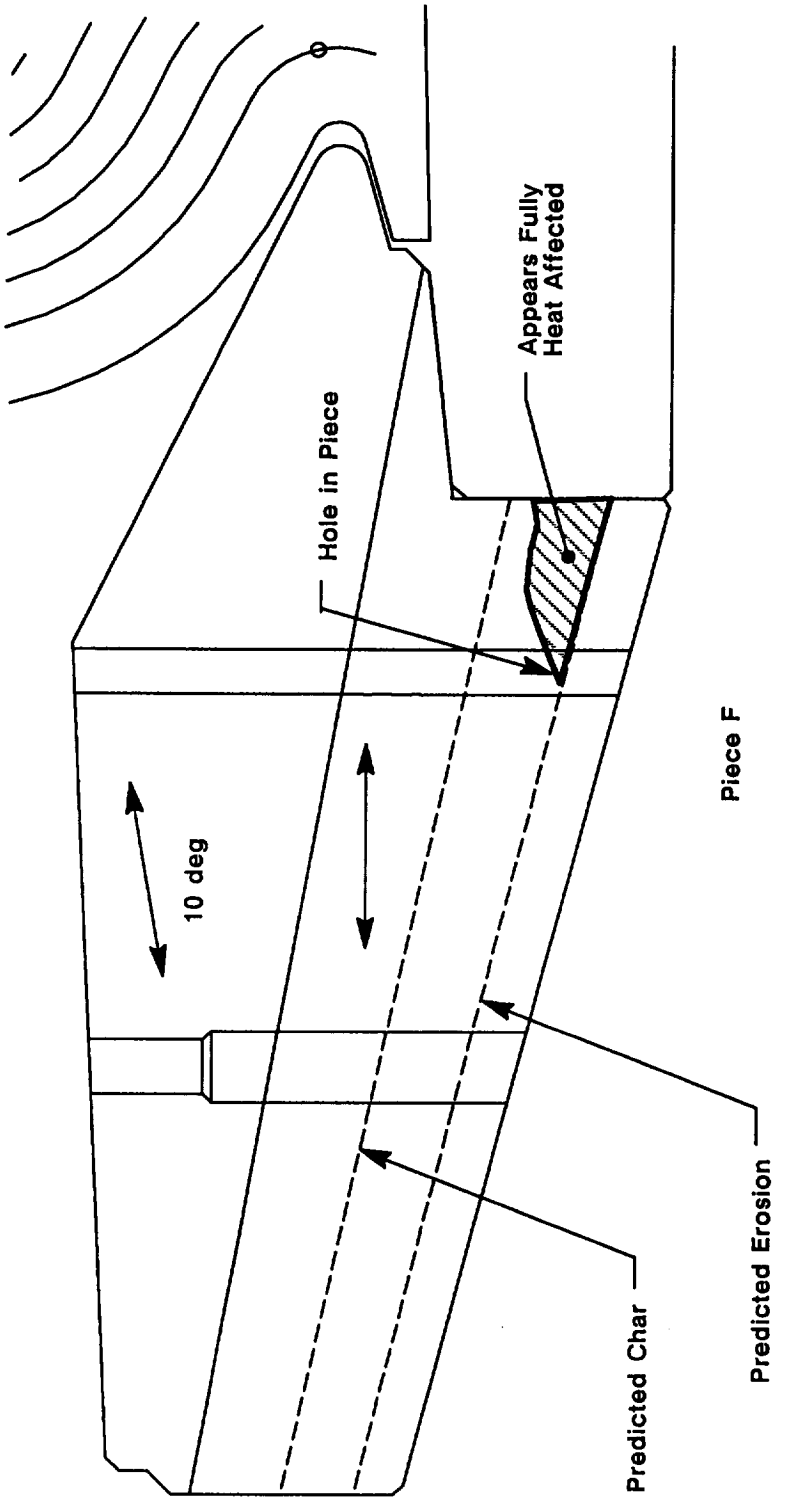

Figure 7.5-59. Cowl Piece F Found Outside of DM-9 Motor

A012813a

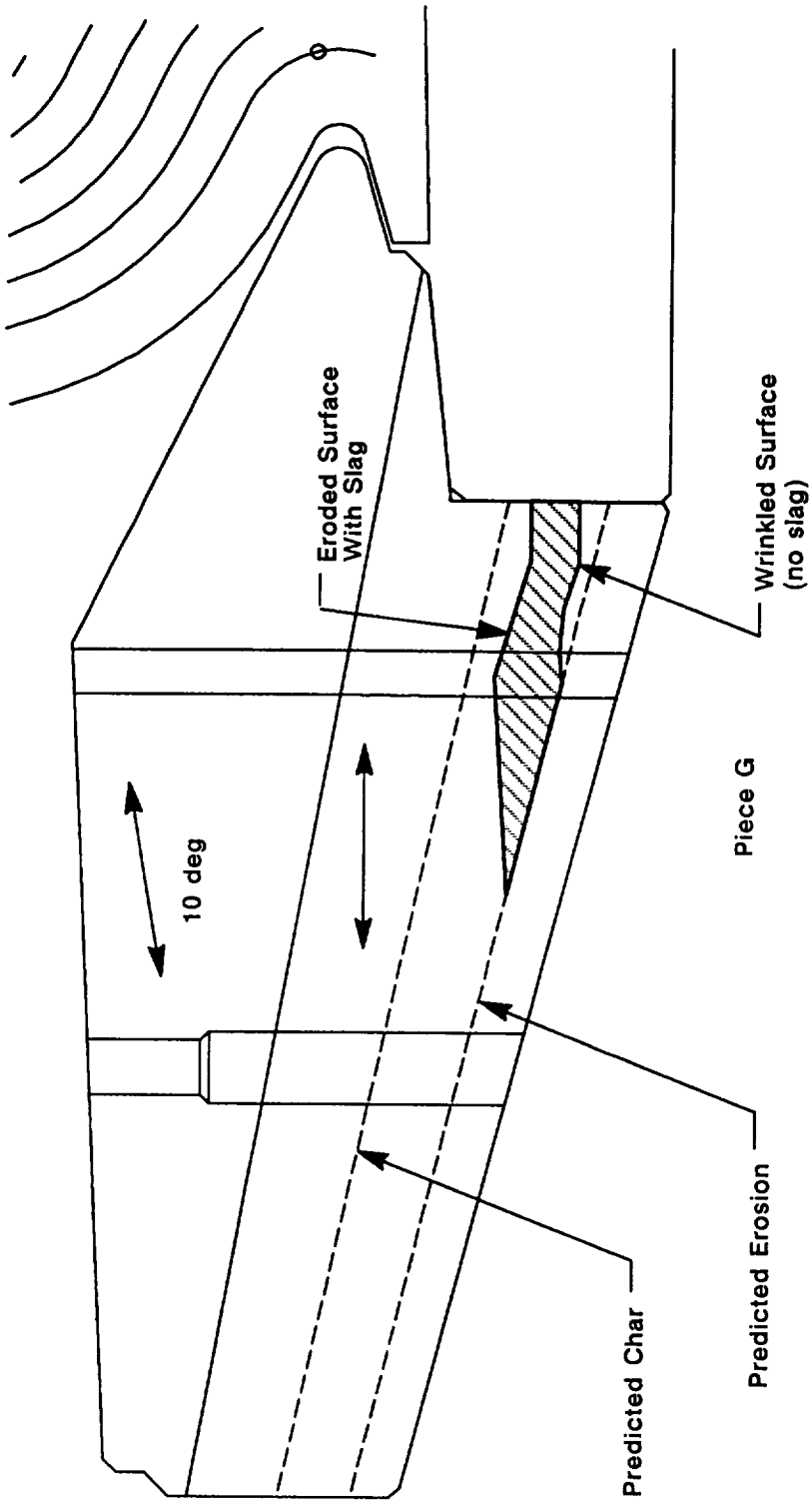

Figure 7.5-60. Cowl Piece G Found Outside of DM-9 Motor

Circumferential Location (deg)	Slag Weight (gm)	Circumferential Location (deg)	Slag Weight (gm)
0	0.66	190	0.98
10	2.23	200	2.39
20	2.88	210	0.71
30	1.45	220	1.98
40	1.10	230	2.39
50	3.02	240	2.98
60	2.83	250	2.37
70	2.21	260	2.85
80	2.33	270	NA
90	1.58	280	NA
100	0.94	290	NA
110	1.27	300	2.99
120	0.95	310	1.02
130	1.06	320	0.95
140	0.72	330	1.17
150	1.08	340	1.26
160	0.92	350	2.02
170	0.95		
180	1.07		
			1.68 Avg

Figure 7.5-61. DM-9 Slag Removed From Cowl Ventholes

A012811aR3

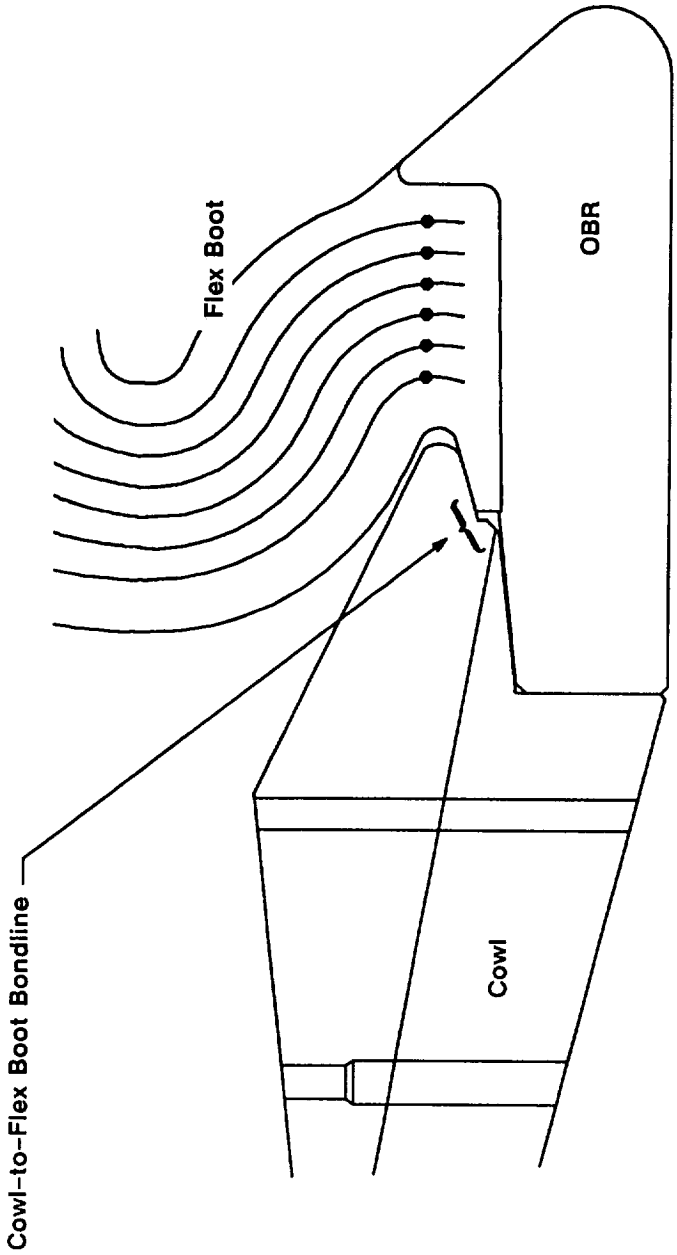

Figure 7.5-62. Cowl-to-Flex Boot Bondline Location

aft tip. The separation from 260 to 300 deg resulted from a break within the flex boot.

The axial bondline between the cowl ring and OBR (Figure 7.5-63) remained intact between 0 and 200 deg. Adhesive and cohesive failures were observed over the remainder of the bondline. From 200 to 360 deg, OBR CCP plies were observed bonded to the cowl primarily towards the forward end of the axial bondline (Figure 7.5-64). Adhesive failure between the EA 913 adhesive and cowl occurred primarily over the aft portion of the axial bondline. Figure 7.5-65 presents a map showing percent of cohesive failure along the cowl/OBR axial bondline from 200 to 360 deg. Cohesive failure was defined, as were OBR plies remaining bonded to the cowl.

An energy dispersive spectrometry (EDS) scan showed evidence of flow at the cowl-to-flex boot and cowl-to-OBR bondlines at 251, 280, and 290 deg. Figures 7.5-66 through 7.5-68 present the contents of samples taken at the indicated locations. Locations B and E showed high aluminum percentages deposited by flow. The aluminum percentages at locations A, C, and D were all significantly less than at B and E. This indicates flow did not propagate aft-to-forward along the flex boot/OBR bondline, or forward-to-aft along the cowl/OBR axial bondline.

The aft end of the aluminum cowl housing showed flattened areas approximately 4 to 5 in. wide circumferentially located at 90 and 115 deg (Figure 7.5-69). A metal gouge was also observed intermittently on the OD surface near the cowl housing aft end. The gouge was located approximately 0.05 in. forward of the housing aft end and was a maximum of 0.05 in. deep radially. Damage to the aluminum cowl housing occurred during disassembly cutting of the cowl ring.

Bondline separations at the cowl housing aft end occurred only in line with the metal damage located at 90 and 115 deg. The separations failed cohesively within the EA 913 adhesive and adhesively between the housing and adhesive. There were no bondline separations observed at the cowl housing forward end.

A012811a

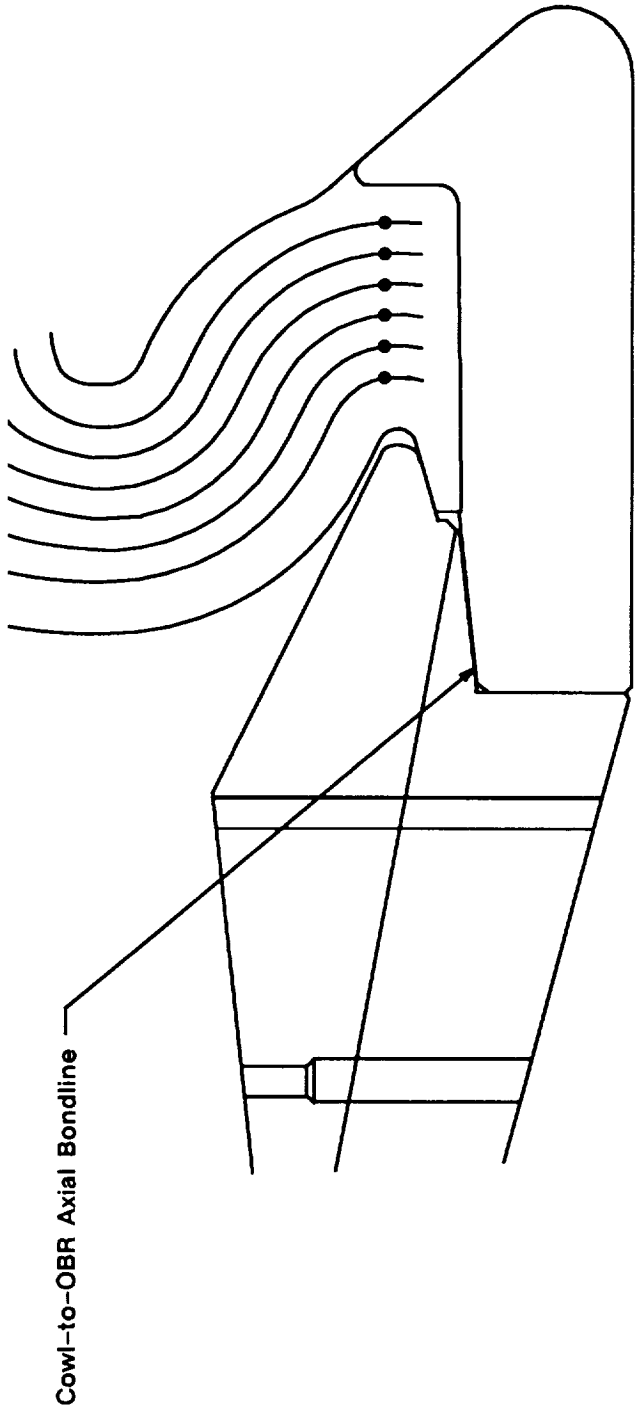

Figure 7.5-63. Cowl-to-OBR Axial Bondline Location

ORIGINAL PAGE
BLACK AND WHITE PHOTOGRAPH

N101197-14

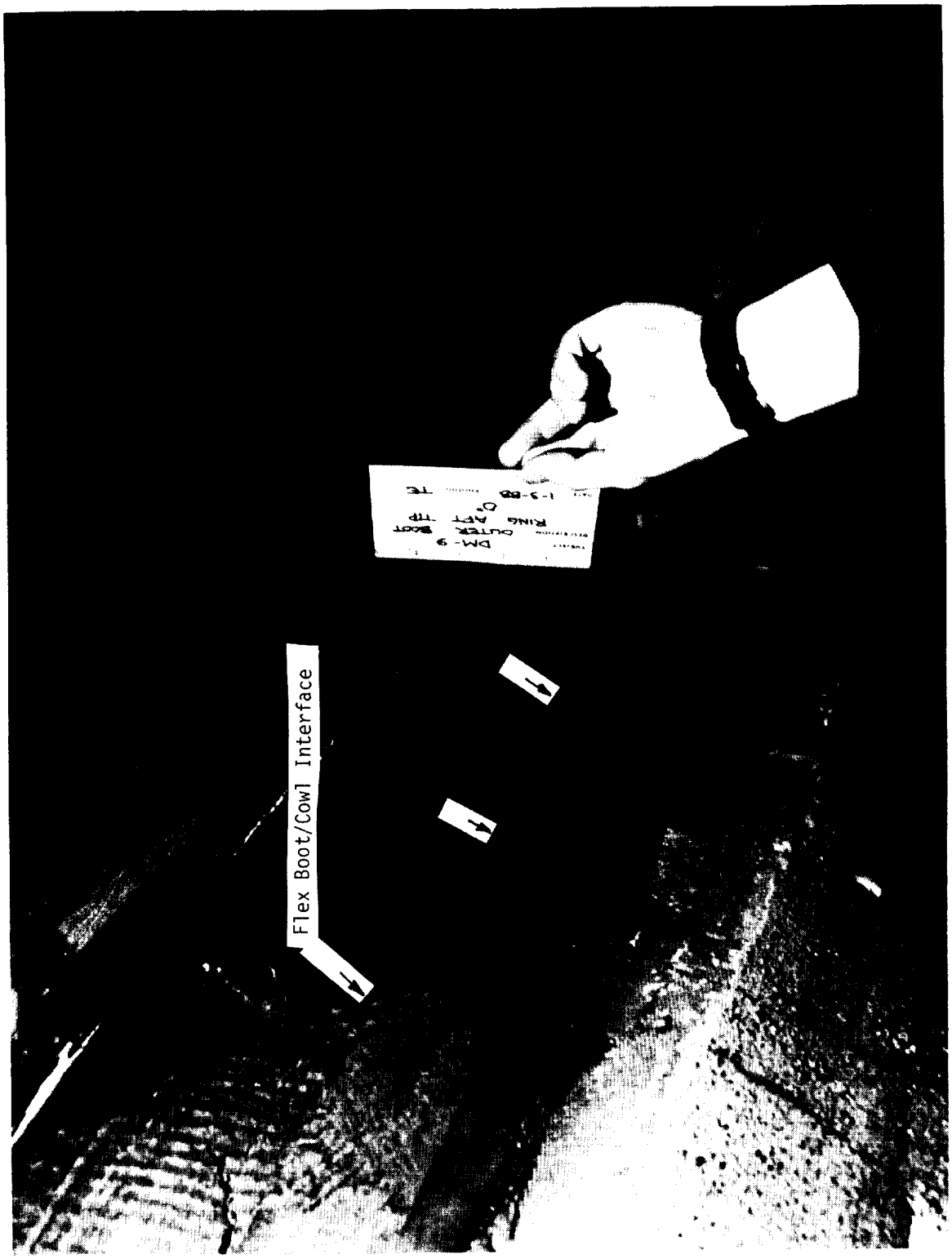

Figure 7.5-64. DM-9 Cowl/OBR Axial Bondline at 0 deg

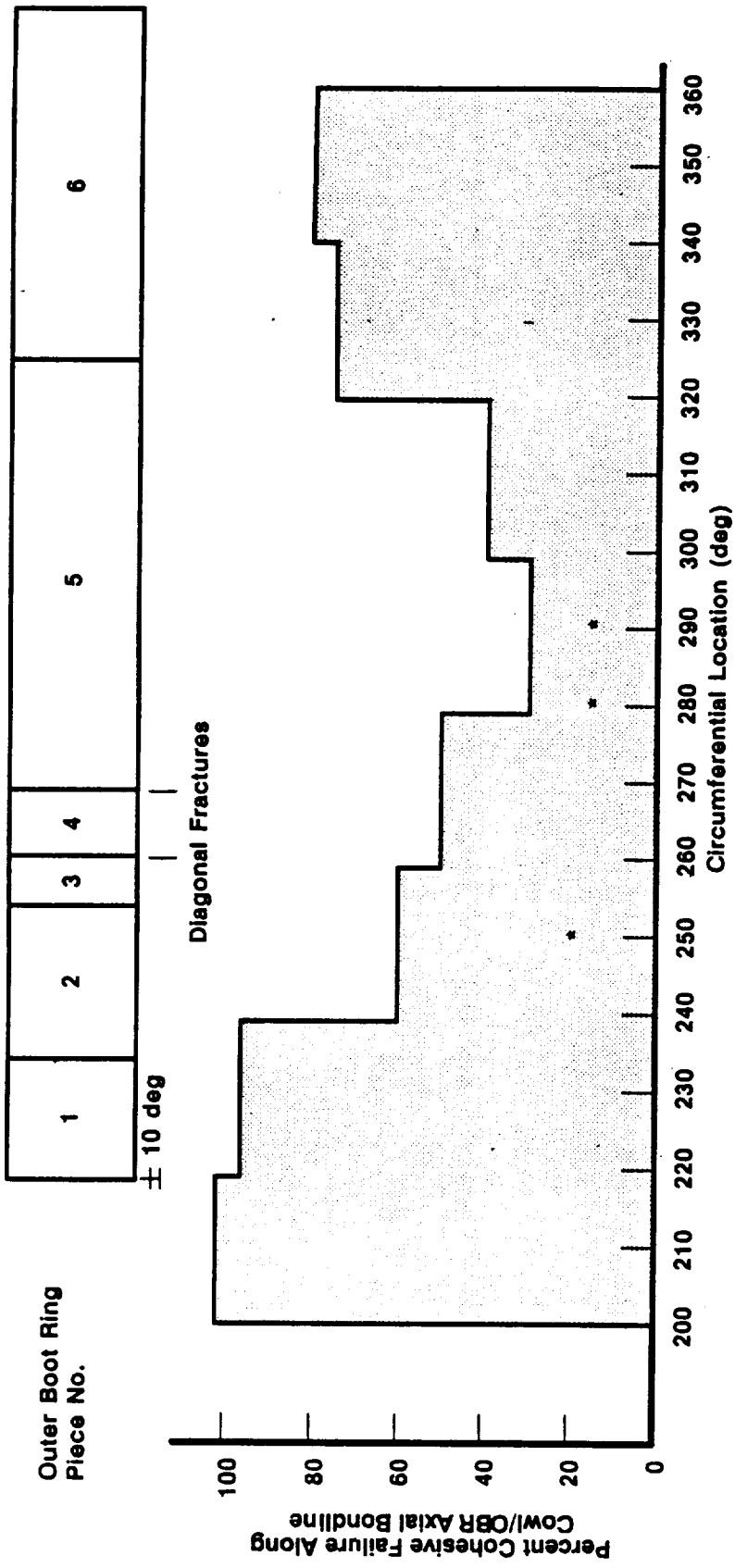

Figure 7.5-65. Percent Cohesive Failure Along Cowl/OBR Axial Bondline (200 to 360 deg)

	250-deg Specimen (wt %)				
	A	B	C	D	E
Sodium	4.90	6.33	7.91	5.09	0.66
Magnesium	3.88	6.87	18.56	22.58	4.08
Aluminum	4.45	46.68	6.18	3.38	13.15
Silicon	57.61	33.34	17.60	57.57	52.46
Sulfur	0.76	2.01	4.88	8.95	2.32
Chlorine	1.18	3.15	13.78	2.27	27.34
Calcium	27.21	1.62	1.08	0.28	--

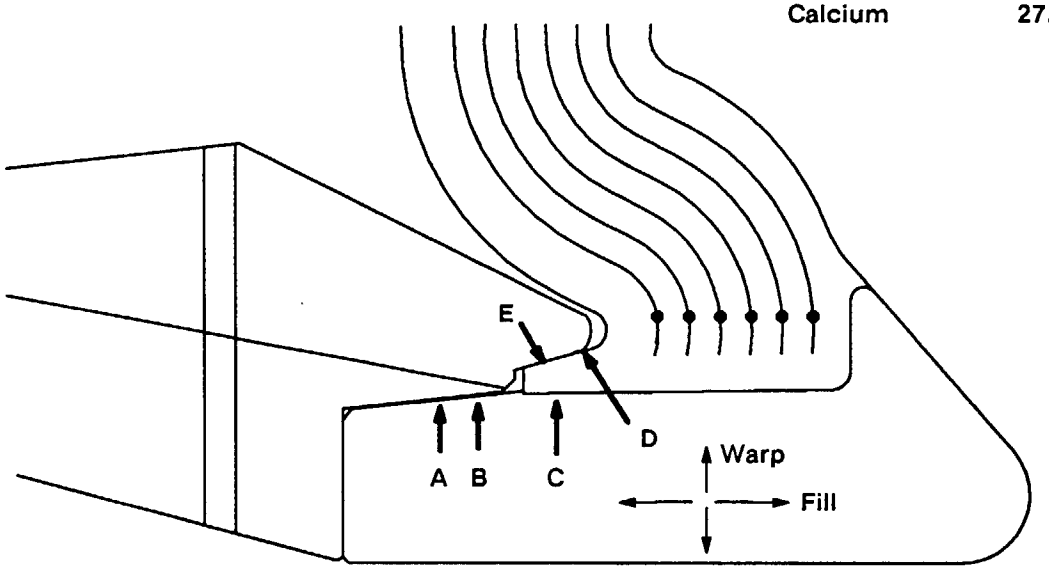

Figure 7.5-66. DM-9 EDS Results at 250 deg

A012986a

	280-deg Specimen (wt %)				
	A	B	C	D	E
Sodium	--	6.27	7.32	5.09	--
Magnesium	--	6.65	19.62	22.58	5.08
Aluminum	--	30.07	3.01	3.38	9.24
Silicon	66.63	44.84	55.43	57.47	67.55
Sulfur	4.28	4.83	7.01	2.27	15.81
Chlorine	--	3.40	6.78	8.95	2.32
Calcium	29.09	3.94	0.83	0.28	--

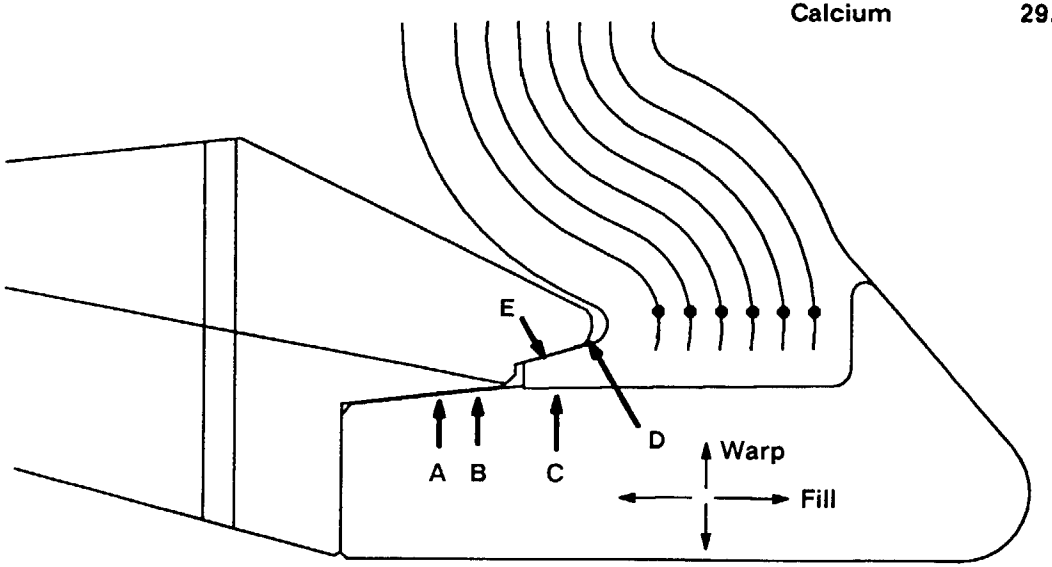

Figure 7.5-67. DM-9 EDS Results at 280 deg

A012985a

	290-deg Specimen (wt %)				
	A	B	C	D	E
Sodium	3.86	--	7.61	5.09	2.18
Magnesium	3.11	--	20.16	22.58	2.82
Aluminum	4.58	34.88	3.94	3.38	13.46
Silicon	57.05	54.26	59.12	57.47	64.11
Sulfur	1.47	1.18	6.92	8.95	1.71
Chlorine	4.64	6.57	2.02	2.27	14.32
Calcium	25.30	3.11	0.24	0.28	1.40

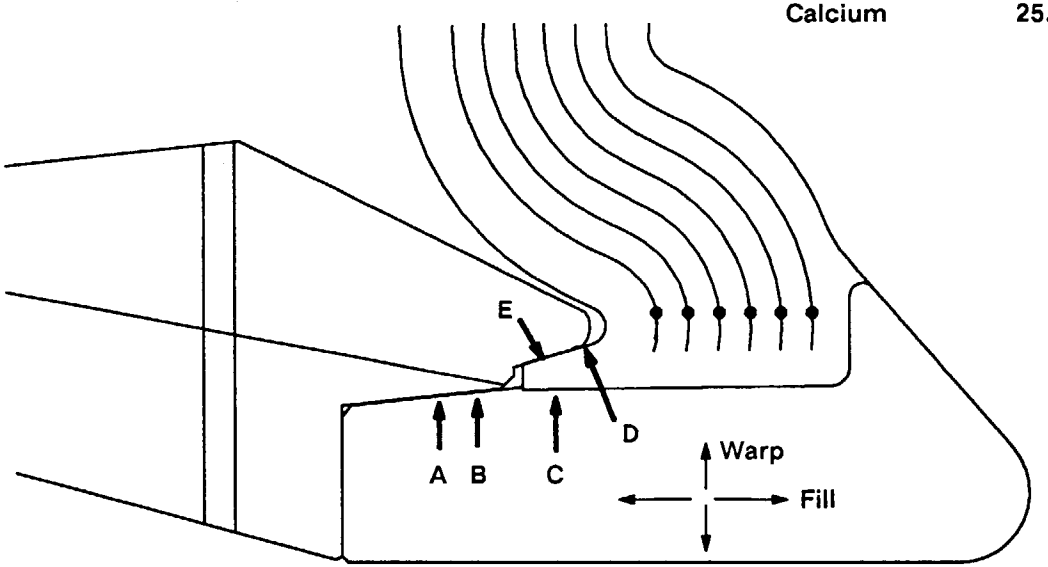

Figure 7.5-68. DM-9 EDS Results at 290 deg

A012987a-2

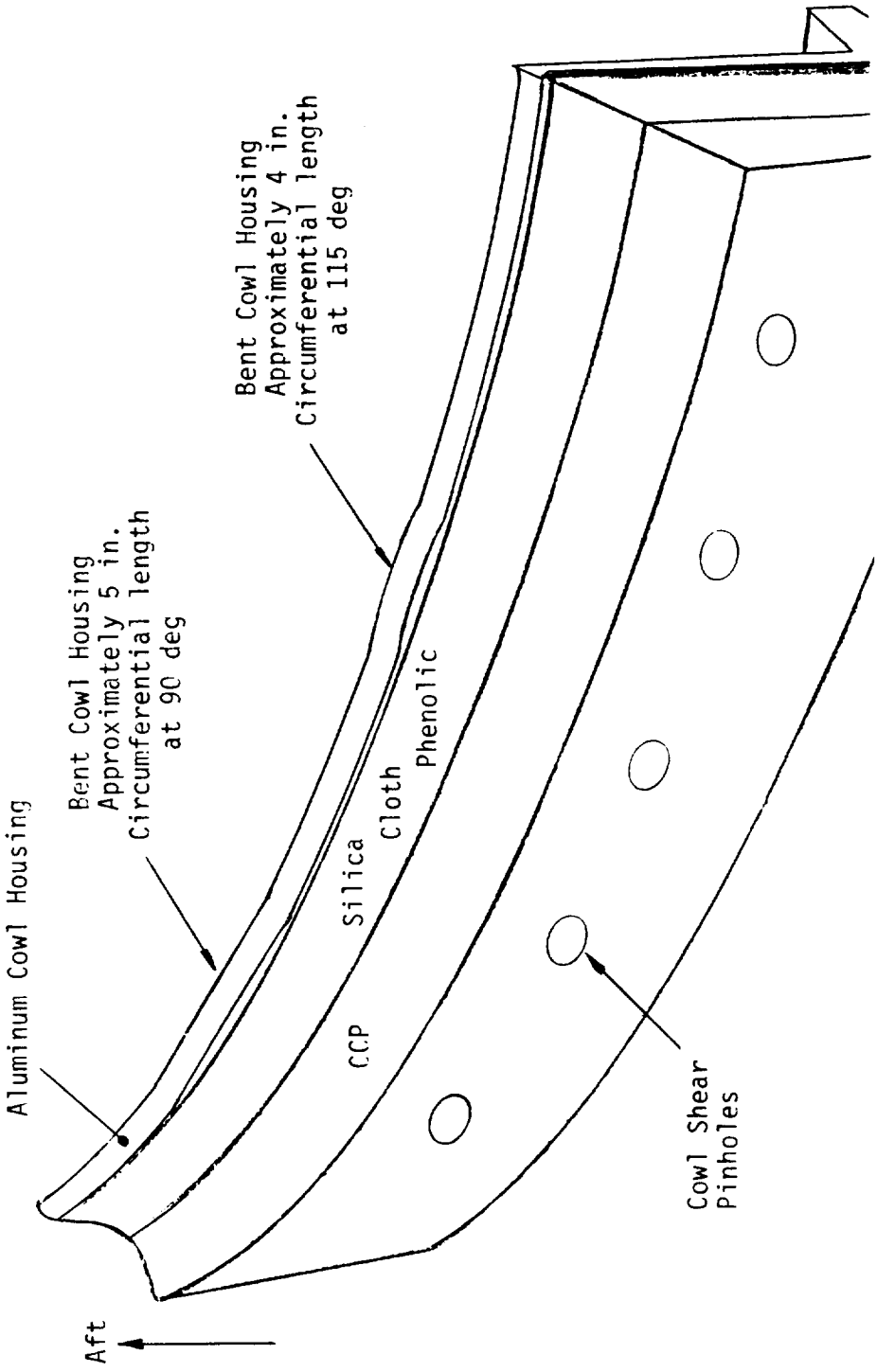

Figure 7.5-69. DM-9 Aluminum Cowl Housing Damage

Table 7.5-3 presents the DM-9 cowl ring aft end measured char and erosion data and performance MS. The MS in this table were based on measured erosion, measured char, and minimum RSRM liner thicknesses. The measured char included heat soak from the time of motor burnout until total cooldown. All locations, including wedge out areas, showed MS greater than 0.00. The worst-case margin of 0.10 occurred at a wedge out at 240 deg at Station 7. Figure 7.5-70 shows the locations of the measurement stations on the cowl. Table 7.5-4 presents corresponding cowl ring aft end MS using measured erosion, corresponding measured char adjusted to the end of action time, and minimum RSRM liner thicknesses. The adjusted char values used in these calculations do not include motor postburn heat soak. All MS were again greater than 0.00 when using the adjusted char values. Char and erosion analysis of the cowl ring forward end showed positive performance MS.

The total material-affected depth (char + erosion) for the aft portion of the cowl ring was slightly higher from 260 to 320 deg. Figures 7.5-71 and 7.5-72 show material-affected depths plotted for Stations 6 and 7 on the cowl.

Flex Boot

A minimum of three NBR plies of the DM-9 flex boot remained around the circumference following the test. Figure 7.5-73 presents the number of remaining plies per circumferential location. The cavity side of the flex boot showed no evidence of flow or erosion. It was uniformly sooted and charred and appeared typical of past flight and static test motors (Figures 7.5-74 and 7.5-75).

The vulcanized axial bondline between the flex boot and the OBR showed intermittent separations at locations where the OBR remained on the nozzle. The flex boot/OBR separations are summarized in Figure 7.5-76. Separations initiated at both the forward and aft ends of the axial bondline. There were no indications of flow running aft to forward along the bondline.

Partial tears were observed near the flex boot OD forward tip at 20 and 200 deg (Figure 7.5-77). Complete breaks through the flex boot OD forward tip appeared from

Table 7.5-3. DM-9 Cowl Erosion and Char Data

Angular Location	STATIONS		
0 degrees	5	6	7
	W	W	
Erosion *	0.58	0.70	NA
Char **	0.30	0.00	NA
2E + 1.25C	1.54	1.40	NA
Liner Thickness ***	1.811	1.889	1.967
Safety Factor	1.18	1.35	NA
Margin of Safety	0.18	0.35	NA
20 degrees			
Erosion *	0.30	0.24	0.14
Char **	0.65	0.70	0.66
2E + 1.25C	1.41	1.36	1.11
Liner Thickness ***	1.811	1.889	1.967
Safety Factor	1.28	1.39	1.78
Margin of Safety	0.28	0.39	0.78
40 degrees			
Erosion *	0.25	0.20	0.18
Char **	0.62	0.62	0.72
2E + 1.25C	1.28	1.18	1.26
Liner Thickness ***	1.811	1.889	1.967
Safety Factor	1.42	1.61	1.56
Margin of Safety	0.42	0.61	0.56
60 degrees			
Erosion *	0.22	0.22	0.24
Char **	0.62	0.66	0.66
2E + 1.25C	1.22	1.27	1.31
Liner Thickness ***	1.811	1.889	1.967
Safety Factor	1.49	1.49	1.51
Margin of Safety	0.49	0.49	0.51
80 degrees			
Erosion *	0.24	0.18	0.14
Char **	0.60	0.68	0.71
2E + 1.25C	1.23	1.21	1.17
Liner Thickness ***	1.811	1.889	1.967
Safety Factor	1.47	1.56	1.68
Margin of Safety	0.47	0.56	0.68

Angular Location	STATIONS		
100 degrees	5	6	7
Erosion *	0.25	0.19	0.18
Char **	0.59	0.62	0.69
2E + 1.25C	1.24	1.16	1.22
Liner Thickness ***	1.811	1.889	1.967
Safety Factor	1.46	1.64	1.61
Margin of Safety	0.46	0.64	0.61
120 degrees			
Erosion *	0.19	0.19	0.18
Char **	0.70	0.63	0.56
2E + 1.25C	1.26	1.17	1.06
Liner Thickness ***	1.811	1.889	1.967
Safety Factor	1.44	1.62	1.86
Margin of Safety	0.44	0.62	0.86
140 degrees			
Erosion *	0.25	0.19	0.19
Char **	0.63	0.54	0.68
2E + 1.25C	1.29	1.06	1.23
Liner Thickness ***	1.811	1.889	1.967
Safety Factor	1.41	1.79	1.60
Margin of Safety	0.41	0.79	0.60
160 degrees			
Erosion *	0.30	0.33	0.30
Char **	0.62	0.51	0.56
2E + 1.25C	1.38	1.30	1.30
Liner Thickness ***	1.811	1.889	1.967
Safety Factor	1.32	1.46	1.51
Margin of Safety	0.32	0.46	0.51
180 degrees			
Erosion *	NA	0.19	0.11
Char **	NA	0.58	0.63
2E + 1.25C	NA	1.11	1.01
Liner Thickness ***	1.811	1.889	1.967
Safety Factor	NA	1.71	1.95
Margin of Safety	NA	0.71	0.95

* Measured Erosion
** Measured Char
*** RSRM Minimum Liner Thickness
W wedge out location

Table 7.5-3. DM-9 Cowl Erosion and Char Data (cont)

Angular Location	STATIONS		
200 degrees	5	6	7
Erosion *	NA	0.60 W	0.80 W
Char **	NA	0.32	0.13
2E + 1.25C	NA	1.60	1.76
Liner Thickness ***	1.811	1.889	1.967
Safety Factor	NA	1.18	1.12
Margin of Safety	NA	0.18	0.12
240 degrees			
Erosion *	NA	0.61 W	0.84 W
Char **	NA	0.23	0.09
2E + 1.25C	NA	1.51	1.79
Liner Thickness ***	1.811	1.889	1.967
Safety Factor	NA	1.25	1.10
Margin of Safety	NA	0.25	0.10
260 degrees			
Erosion *	NA	0.19	0.20
Char **	NA	0.85	0.80
2E + 1.25C	NA	1.44	1.40
Liner Thickness ***	1.811	1.889	1.967
Safety Factor	NA	1.31	1.41
Margin of Safety	NA	0.31	0.41
280 degrees			
Erosion *	NA	0.38	0.34
Char **	NA	0.54	0.60
2E + 1.25C	NA	1.44	1.43
Liner Thickness ***	1.811	1.889	1.967
Safety Factor	NA	1.32	1.38
Margin of Safety	NA	0.32	0.38
300 degrees			
Erosion *	NA	0.30	0.24
Char **	NA	0.62	0.67
2E + 1.25C	NA	1.38	1.32
Liner Thickness ***	1.811	1.889	1.967
Safety Factor	NA	1.37	1.49
Margin of Safety	NA	0.37	0.49

Angular Location	STATIONS		
320 degrees	5	6	7
Erosion *	NA	0.20	0.22
Char **	NA	0.86	0.80
2E + 1.25C	NA	1.48	1.44
Liner Thickness ***	1.811	1.889	1.967
Safety Factor	NA	1.28	1.37
Margin of Safety	NA	0.28	0.37
340 degrees			
Erosion *	NA	0.59 W	0.84 W
Char **	NA	0.27	0.00
2E + 1.25C	NA	1.52	1.68
Liner Thickness ***	1.811	1.889	1.967
Safety Factor	NA	1.24	1.17
Margin of Safety	NA	0.24	0.17

* Measured Erosion
** Measured Char
*** RSRM Minimum Liner Thickness
w wedge out location

A012818a-4

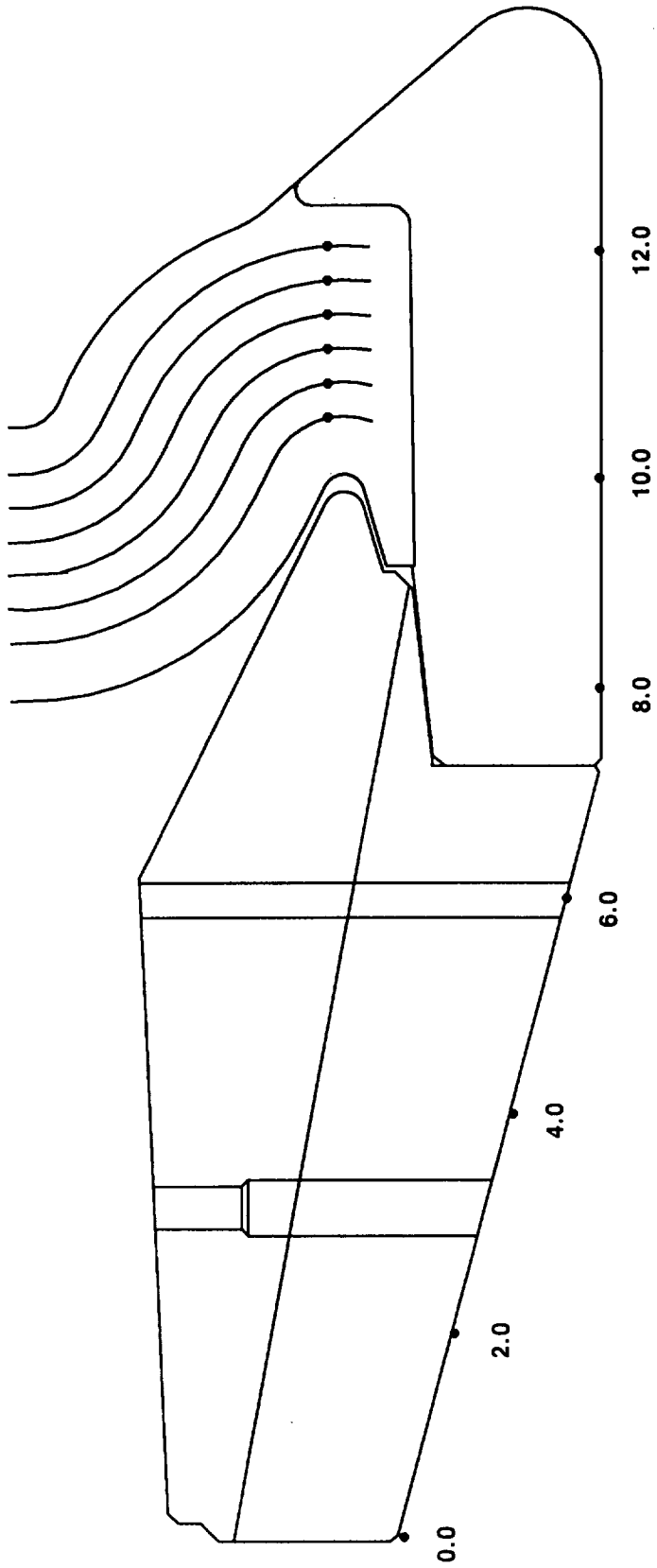

Figure 7.5-70. Cowl Ring and OBR Erosion Measurement Stations

Table 7.5-4. DM-9 Cowl Erosion and Char Data

Angular Location	STATIONS		
0 degrees	5	6	7
	W	W	
Erosion *	0.58	0.70	NA
Char **	0.26	0.00	NA
2E + 1.25C	1.48	1.40	NA
Liner Thickness ***	1.811	1.889	1.967
Safety Factor	1.22	1.35	NA
Margin of Safety	0.22	0.35	NA
20 degrees			
Erosion *	0.30	0.24	0.14
Char **	0.55	0.60	0.56
2E + 1.25C	1.29	1.22	0.98
Liner Thickness ***	1.811	1.889	1.967
Safety Factor	1.40	1.54	2.00
Margin of Safety	0.40	0.54	1.00
40 degrees			
Erosion *	0.25	0.20	0.18
Char **	0.53	0.53	0.61
2E + 1.25C	1.16	1.06	1.13
Liner Thickness ***	1.811	1.889	1.967
Safety Factor	1.56	1.78	1.75
Margin of Safety	0.56	0.78	0.75
60 degrees			
Erosion *	0.22	0.22	0.24
Char **	0.53	0.56	0.56
2E + 1.25C	1.10	1.14	1.18
Liner Thickness ***	1.811	1.889	1.967
Safety Factor	1.65	1.66	1.67
Margin of Safety	0.65	0.66	0.67
80 degrees			
Erosion *	0.24	0.18	0.14
Char **	0.51	0.58	0.60
2E + 1.25C	1.12	1.08	1.03
Liner Thickness ***	1.811	1.889	1.967
Safety Factor	1.62	1.75	1.90
Margin of Safety	0.62	0.75	0.90

Angular Location	STATIONS		
100 degrees	5	6	7
Erosion *	0.25	0.19	0.18
Char **	0.50	0.53	0.59
2E + 1.25C	1.13	1.04	1.09
Liner Thickness ***	1.811	1.889	1.967
Safety Factor	1.61	1.82	1.80
Margin of Safety	0.61	0.82	0.80
120 degrees			
Erosion *	0.19	0.19	0.18
Char **	0.60	0.54	0.48
2E + 1.25C	1.12	1.05	0.96
Liner Thickness ***	1.811	1.889	1.967
Safety Factor	1.61	1.80	2.06
Margin of Safety	0.61	0.80	1.06
140 degrees			
Erosion *	0.25	0.19	0.19
Char **	0.54	0.46	0.58
2E + 1.25C	1.17	0.95	1.10
Liner Thickness ***	1.811	1.889	1.967
Safety Factor	1.55	1.98	1.78
Margin of Safety	0.55	0.98	0.78
160 degrees			
Erosion *	0.30	0.33	0.30
Char **	0.53	0.43	0.48
2E + 1.25C	1.26	1.20	1.20
Liner Thickness ***	1.811	1.889	1.967
Safety Factor	1.44	1.57	1.65
Margin of Safety	0.44	0.57	0.65
180 degrees			
Erosion *	NA	0.19	0.11
Char **	NA	0.49	0.54
2E + 1.25C	NA	1.00	0.89
Liner Thickness ***	1.811	1.889	1.967
Safety Factor	NA	1.90	2.21
Margin of Safety	NA	0.90	1.21

* Measured Erosion
** Measured Char times 0.85
(adjusted to end of action time)
*** RSRM Minimum Liner Thickness
w wedge out location

Table 7.5-4. DM-9 Cowl Erosion and Char Data (cont)

Angular Location	STATIONS		
200 degrees	5	6	7
Erosion *	NA	0.60 W	0.80 W
Char **	NA	0.27	0.11
2E + 1.25C	NA	1.54	1.74
Liner Thickness ***	1.811	1.889	1.967
Safety Factor	NA	1.23	1.13
Margin of Safety	NA	0.23	0.13
240 degrees			
Erosion *	NA	0.61 W	0.84 W
Char **	NA	0.20	0.08
2E + 1.25C	NA	1.46	1.78
Liner Thickness ***	1.811	1.889	1.967
Safety Factor	NA	1.29	1.11
Margin of Safety	NA	0.29	0.11
260 degrees			
Erosion *	NA	0.19	0.20
Char **	NA	0.72	0.68
2E + 1.25C	NA	1.28	1.25
Liner Thickness ***	1.811	1.889	1.967
Safety Factor	NA	1.47	1.57
Margin of Safety	NA	0.47	0.57
280 degrees			
Erosion *	NA	0.38	0.34
Char **	NA	0.46	0.51
2E + 1.25C	NA	1.33	1.32
Liner Thickness ***	1.811	1.889	1.967
Safety Factor	NA	1.42	1.49
Margin of Safety	NA	0.42	0.49
300 degrees			
Erosion *	NA	0.30	0.24
Char **	NA	0.53	0.57
2E + 1.25C	NA	1.26	1.19
Liner Thickness ***	1.811	1.889	1.967
Safety Factor	NA	1.50	1.65
Margin of Safety	NA	0.50	0.65

Angular Location	STATIONS		
320 degrees	5	6	7
Erosion *	NA	0.22	0.20
Char **	NA	0.73	0.68
2E + 1.25C	NA	1.35	1.25
Liner Thickness ***	1.811	1.889	1.967
Safety Factor	NA	1.40	1.57
Margin of Safety	NA	0.40	0.57
340 degrees			
Erosion *	NA	0.59 W	0.84 W
Char **	NA	0.23	0.00
2E + 1.25C	NA	1.47	1.68
Liner Thickness ***	1.811	1.889	1.967
Safety Factor	NA	1.29	1.17
Margin of Safety	NA	0.29	0.17

* Measured Erosion
** Measured Char times 0.85
(adjusted to end of action time)
*** RSRM Minimum Liner Thickness
w wedge out location

910335-15.24

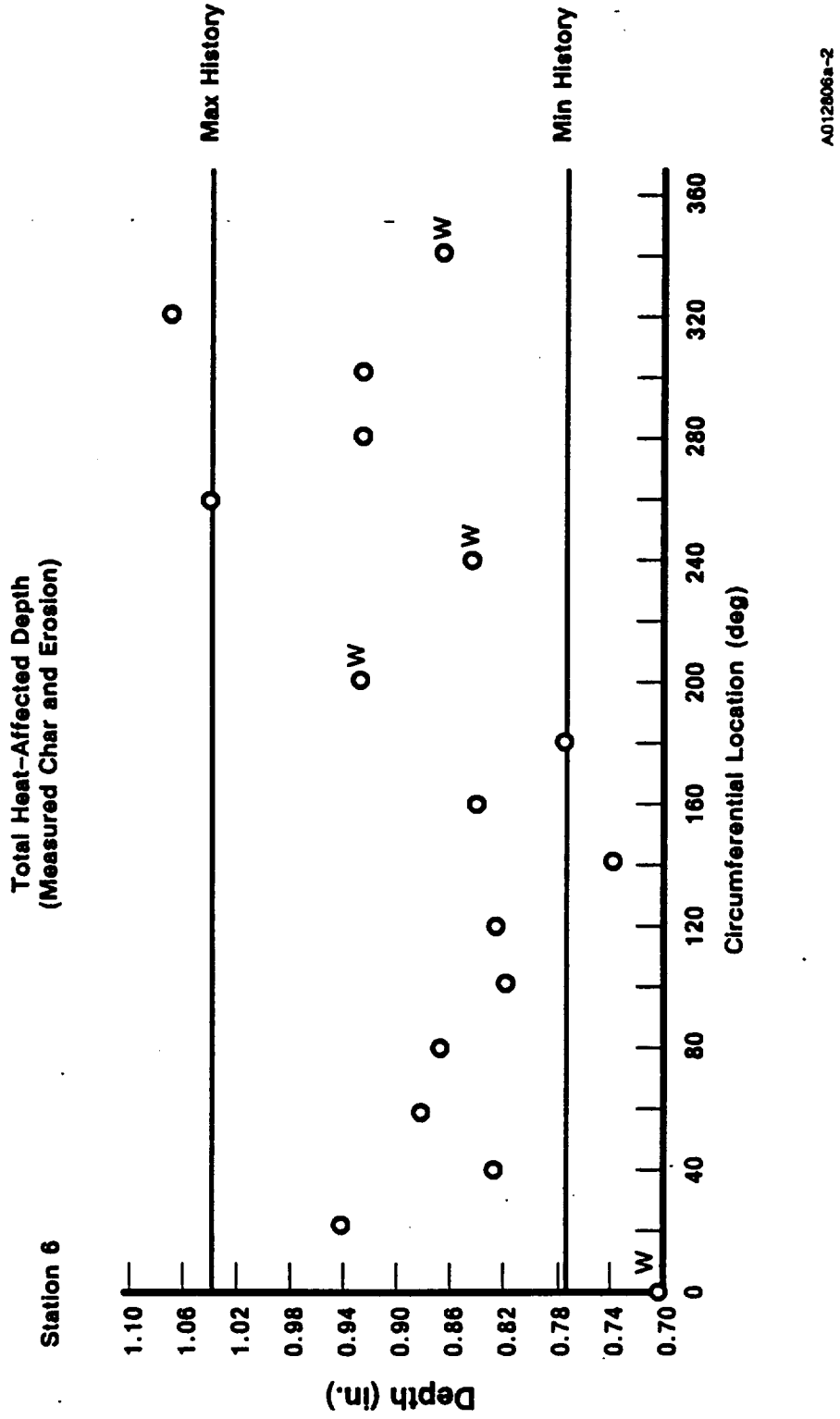

Figure 7.5-71. DM-9 Total Material Affected Depths for Cowl Aft End (Station 6)

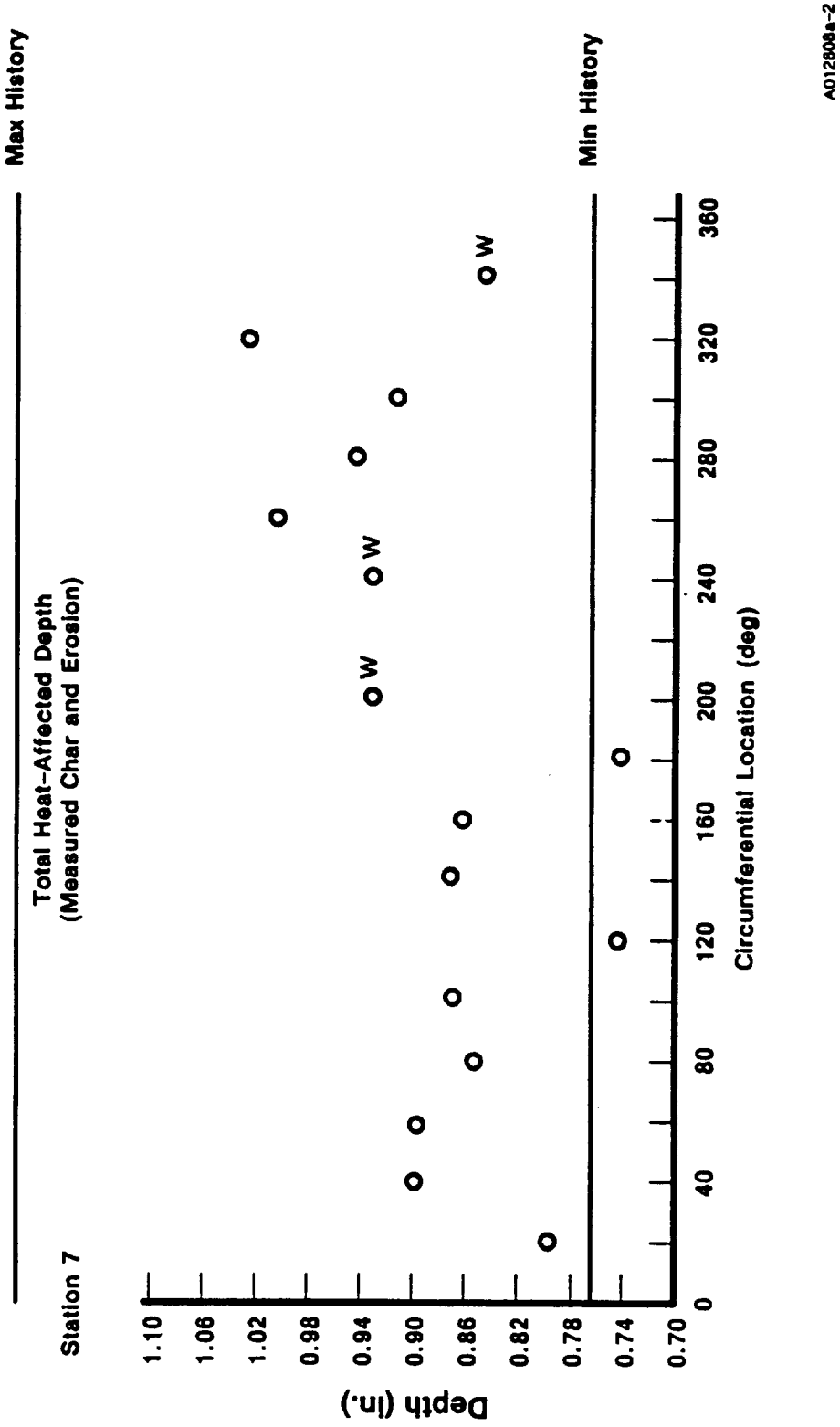

Figure 7.5-72. DM-9 Total Material Affected Depths for Cowl Aft End (Station 7)

Location (deg)	DM-8 Intact Flex Boot NBR Plies	DM-9 Intact Flex Boot NBR Plies
0	3.5	3.5
20	3.5	3.3
40	3.0	3.3
60	3.0	3.3
80	3.0	3.3
100	3.3	3.3
120	NA	3.3
140	NA	3.3
160	NA	3.0
180	4.0	3.0
200	4.0	3.0
220	3.0	3.0
240	3.0	3.0
260	3.0	3.0
280	3.0	3.0
300	3.0	3.0
320	3.0	3.0
340	3.0	3.3

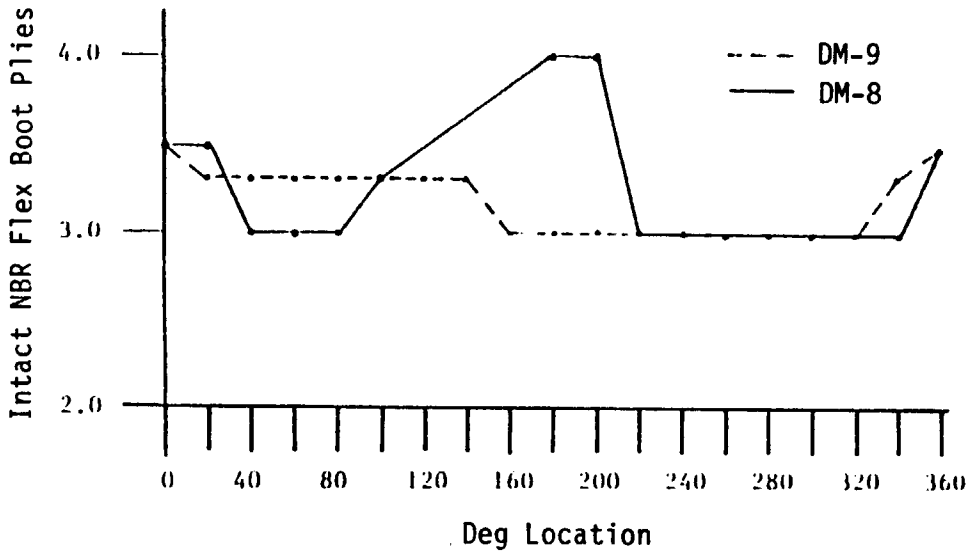

Figure 7.5-73. DM-9 and DM-8 Flex Boot Remaining NBR Plies

ORIGINAL PAGE
BLACK AND WHITE PHOTOGRAPH

N101223-4

Figure 7.5-74. DM-9 Flex Boot Cavity Side (90 deg)

N101223-10

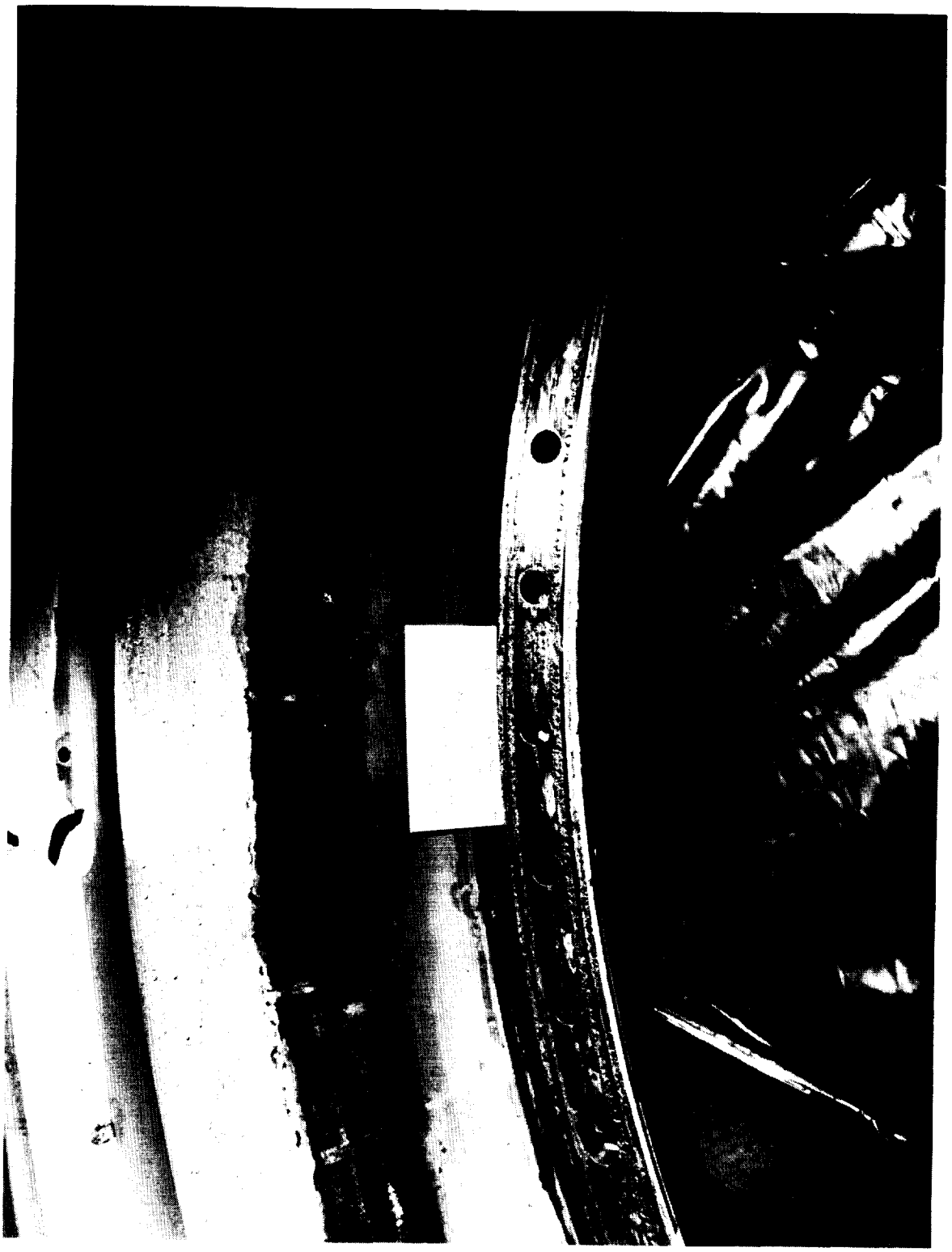

Figure 7.5-75. DM-9 Flex Boot Cavity Side (270 deg)

- OBR-to-flex boot bondline description
  - 20 deg—Separated on aft 0.75 in.
  - 40 deg—Separated on aft 0.25 in.
  - 60 deg—Separated on aft 0.50 in.
  - 80 deg—Separated on aft 0.25 in.
  - 100 to 160 deg—Completely intact
  - 180 deg—Separated on forward 0.50 in.
  - 200 to 360 deg—Completely separated
- There were no indications of flow running aft to forward along axial length of flex boot at OBR interface

Figure 7.5-76. DM-9 Flex Boot/OBR Bondline Separation Summary

A012810a-2

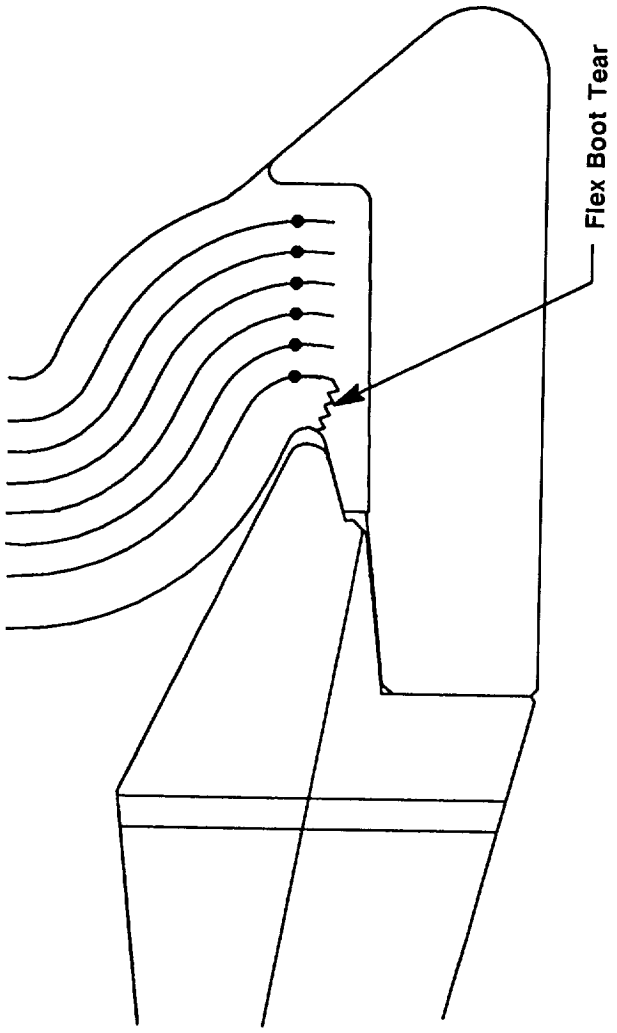

Figure 7.5-77. DM-9 Flex Boot Tears Located at 20 and 200 deg

240 to 300 deg (Figure 7.5-78). The flex boot OD forward tip remained bonded to the cowl ring where the complete breaks occurred.

Bearing Protector

The DM-9 bearing protector performed nominally with light soot and char appearing on the OD surface (Figures 7.5-79 and 7.5-80). Sooting and charring appeared to be slightly higher from 270 to 295 deg than on the remainder of the circumference. This condition, however, is no greater than previously observed. Maximum erosion of approximately 0.15 in. and heavier soot were observed in line with the cowl ring vent holes at the thickened portion of the bearing protector. There was no evidence of heat effect on the ID surface. Remaining material thicknesses are presented in Table 7.5-5.

Fixed Housing Insulation

The fixed housing insulation erosion was smooth and uniform. Photographs of the fixed housing insulation are shown in Figures 7.5-9 through 7.5-12 and 7.5-81. Wide post-test delaminations and heavy slag deposits were observed at the aft end of the CCP insulation. The fixed housing insulation flow surface showed no impact marks. Housing bondlines at the inner boot ring forward end and at the fixed housing insulation aft end were intact.

The steel fixed housing experienced no damage and performed nominally. Char and erosion analysis of the fixed housing insulation showed positive performance MS.

Forward Exit Cone Assembly

The DM-9 forward exit cone liner erosion was nominal showing no major washing or pocketing. Overall views of the forward exit cone are presented in Figures 7.5-14 and 7.5-15.

Visual inspection of the forward exit cone showed minor irregularly-shaped erosion patterns located around the circumference of the cone. The erosion patterns were a maximum of 0.10 in. deep radially. A review of prior post-test and postflight

A012754a-2

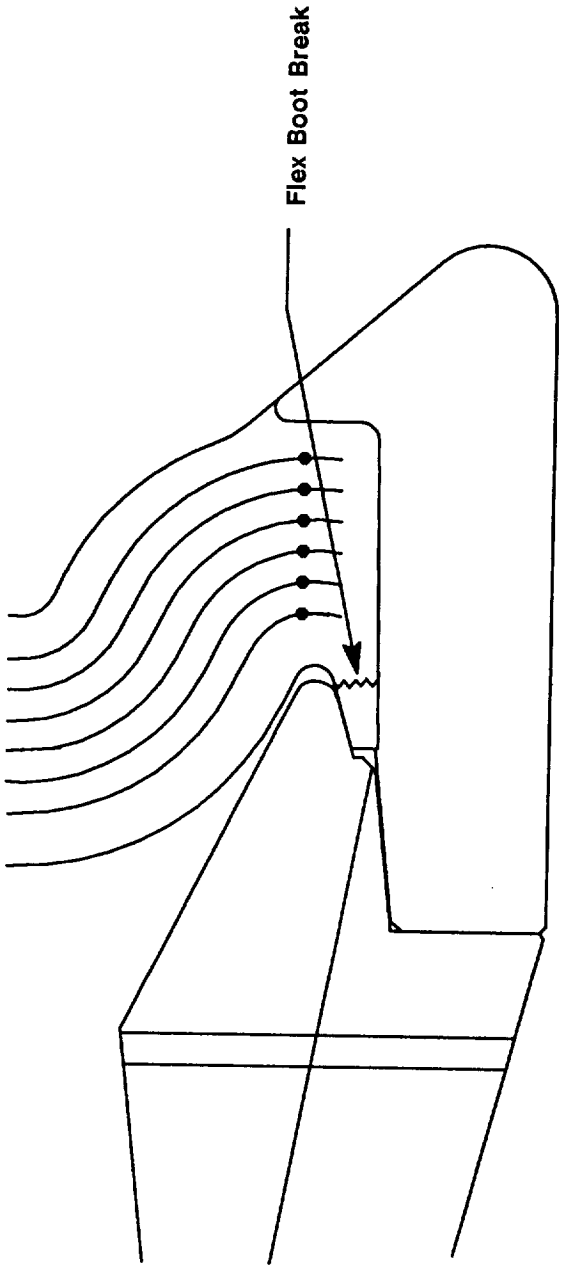

Figure 7.5-78. DM-9 Flex Boot Breaks Located From 240 to 300 deg

ORIGINAL PAGE
BLACK AND WHITE PHOTOGRAPH

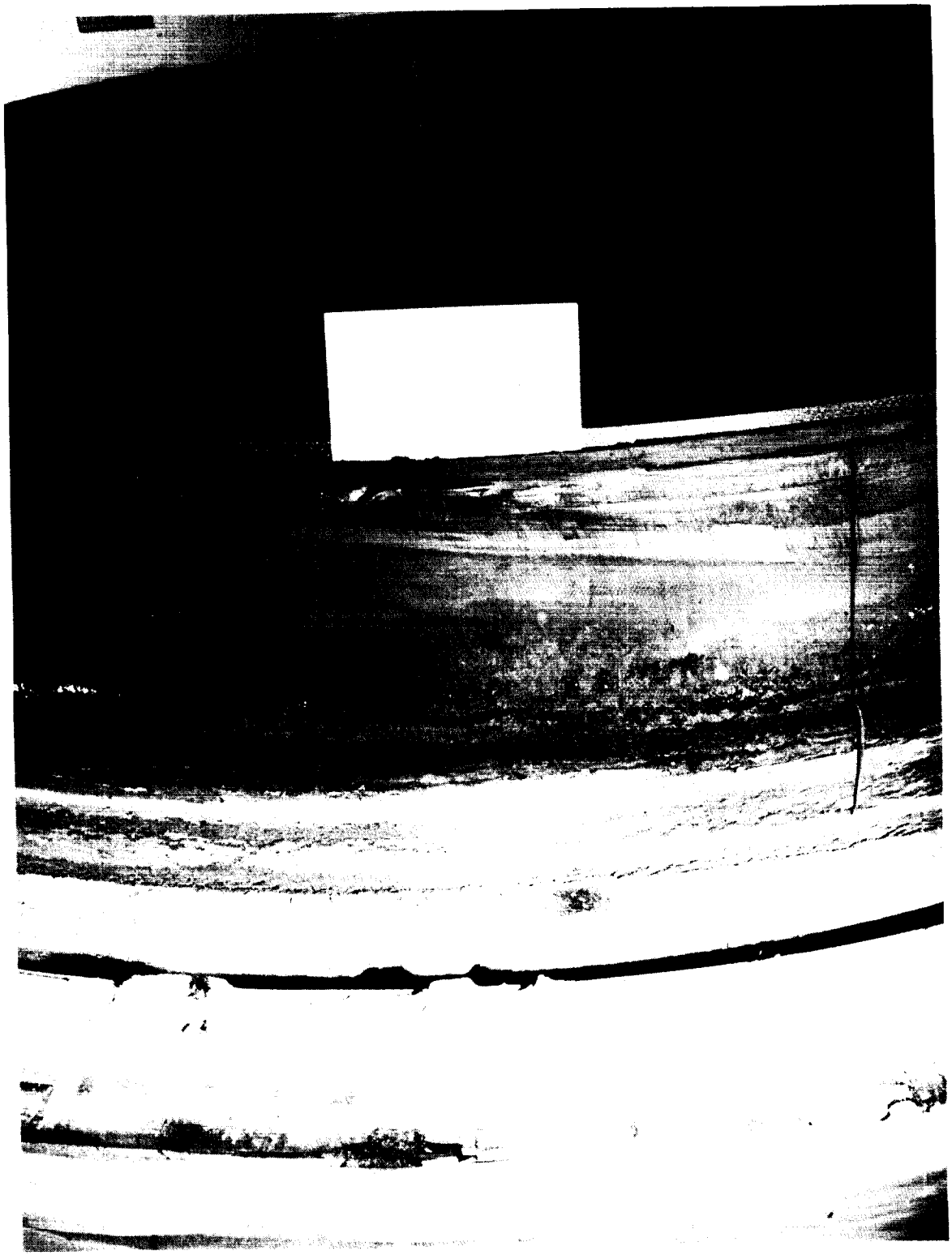

N101224-4

Figure 7.5-79. DM-9 Bearing Protector (90 deg)

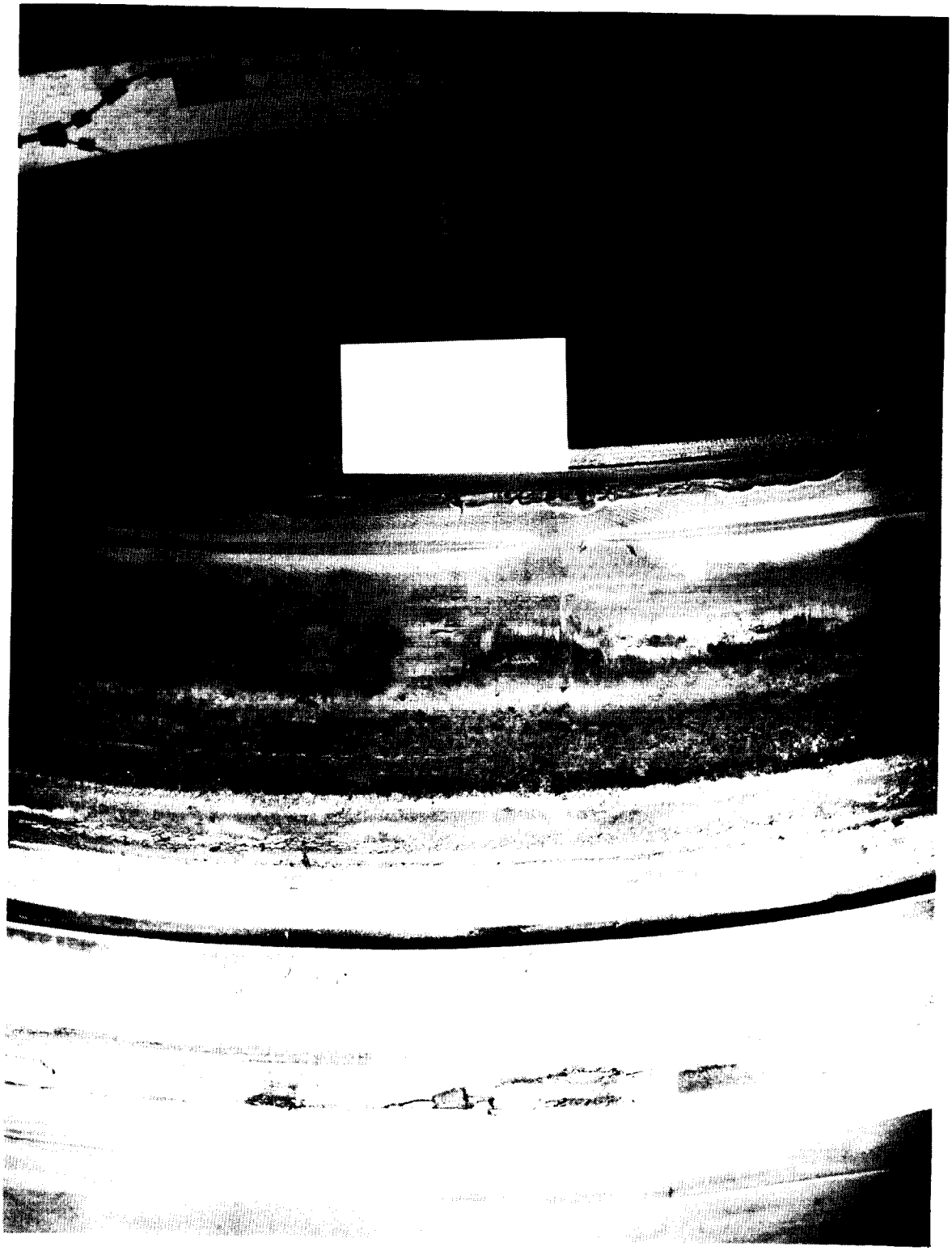

N101224-10

Figure 7.5-80. DM-9 Bearing Protector (270 deg)

Table 7.5-5. DM-9 Bearing Protector Thickness* of Remaining Material

Loc Circumferential Location (deg)	Measurement Location (see sketch) A	B	C	D	E
0	0.481	0.470	0.698	0.423	0.454
10	0.470	0.471	0.705	0.444	0.465
20	0.472	0.472	0.705	0.444	0.465
30	0.472	0.472	0.704	0.440	0.465
40	0.472	0.480	0.708	0.453	0.474
50	0.475	0.476	0.697	0.458	0.472
60	0.472	0.476	0.700	0.468	0.473
70	0.462	0.465	0.694	0.448	0.475
80	0.475	0.472	0.697	0.456	0.468
90	0.484	0.477	3.700	Q.462	0.476
100	0.484	0.477	0.700	0.451	0.476
110	0.491	0.474	0.695	0.453	0.472
120	0.476	0.462	0.688	0.430	0.464
130	0.455	0.452	0.677	0.430	0.470
140	0.452	0.448	0.675	0.429	0.470
150	0.460	0.442	0.655	0.415	0.470
160	0.453	0.438	0.647	0.406	0.465
170	0.456	0.441	0.646	0.406	0.461
180	0.461	0.461	0.650	0.404	0.462
190	0.470	0.450	0.651	0.383	0.465
200	0.473	0.469	0.652	0.402	0.460
210	0.477	0.470	0.608	0.352 (1)	0.474
220	0.482	0.464	0.666	0.375	0.480
230	0.465	0.472	0.647	0.390	0.477
240	0.460	0.458	0.672	0.434	0.458
250	0.455	0.455	0.634	0.407	0.468
260	0.458	0.443	0.652	0.404	0.461
270	0.464	0.465	0.661	0.424	0.472
280	0.484	0.469	0.667	0.425	0.472
290	0.489	0.490	0.685	0.417	0.472
300	0.468	0.465	0.678	0.422	0.456
310	0.475	0.467	0.667	0.401	0.454
320	0.462	0.454	0.677	0.433	0.446
330	0.468	0.460	0.665	0.402	0.445
340	0.481	0.472	0.688	0.422	0.435
350	0.478	0.468	0.694	0.429	0.432

* Measurements in inches

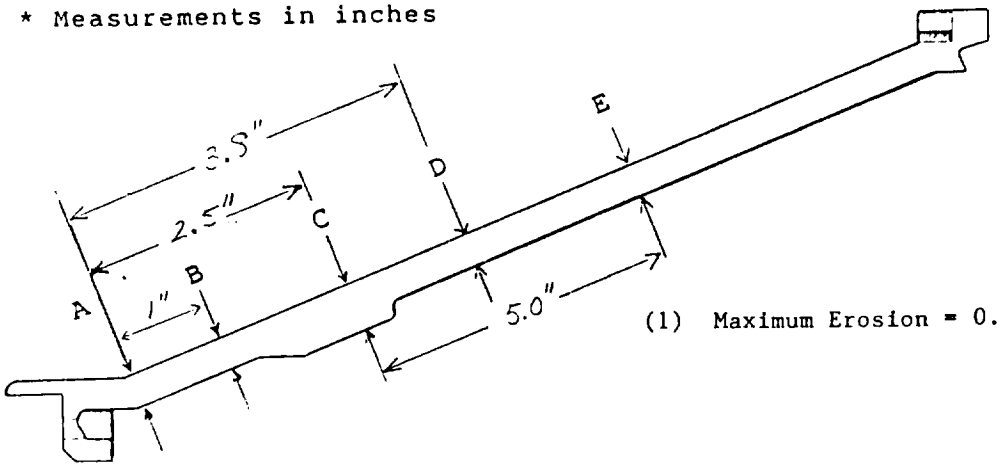

(1) Maximum Erosion = 0.148

ORIGINAL PAGE
BLACK AND WHITE PHOTOGRAPH

N101197-9

Figure 7.5-81. DM-9 Fixed Housing Insulation (60 deg)

forward exit cones, from both SRM and other programs (Peacekeeper), showed that this type of erosion pattern frequently occurred in CCP forward exit cones.

The forward exit cone insulation was separated from the forward and aft ends of the steel housing intermittently around the part circumference. Inspection showed that the separations were adhesive failures between the EA 946 adhesive and the housing, and between the adhesive and GCP overwrap. There was no indication of cohesive failure or heat effect in or adjacent to the separations. The maximum radial gap measurement was 0.050 inch.

The forward and aft interfaces of the forward exit cone assembly showed no CCP/GCP separations. There were also no separations observed within the CCP liner or within the GCP liner.

The forward exit cone steel housing experienced no damage. There was no snubber assembly fired on the DM-9 nozzle.

Char and erosion analysis of the forward exit cone insulation showed positive performance MS except at station locations 20 (90 and 270 deg) and 24 (270 deg).

Aft Exit Cone Assembly

The DM-9 aft exit cone liner eroded smoothly with no major washing, pocketing, or surface ply lifting observed (Figure 7.5-16). Higher off-gassing and a few cross-ply cracks appeared in an area axially in line with the compliance ring at 90 deg. The area was approximately 2 ft wide circumferentially by 3 ft long axially. There was no anomalous erosion in the area, and the cross-ply cracks were isolated in charred material only.

Figures 7.5-82 through 7.5-83 show views of the polysulfide backfill at the forward aluminum shell bondline. No adhesive failure was evident between the polysulfide and housing or between the polysulfide and GCP overwrap. The surface bubbles/voids within the polysulfide were present in the pretest. There was no evidence of flow within or adjacent to the shell bondline.

Figure 7.5-82. DM-9 Aft Exit Cone Polysulfide Backfill (93 deg)

ORIGINAL PAGE
BLACK AND WHITE PHOTOGRAPH

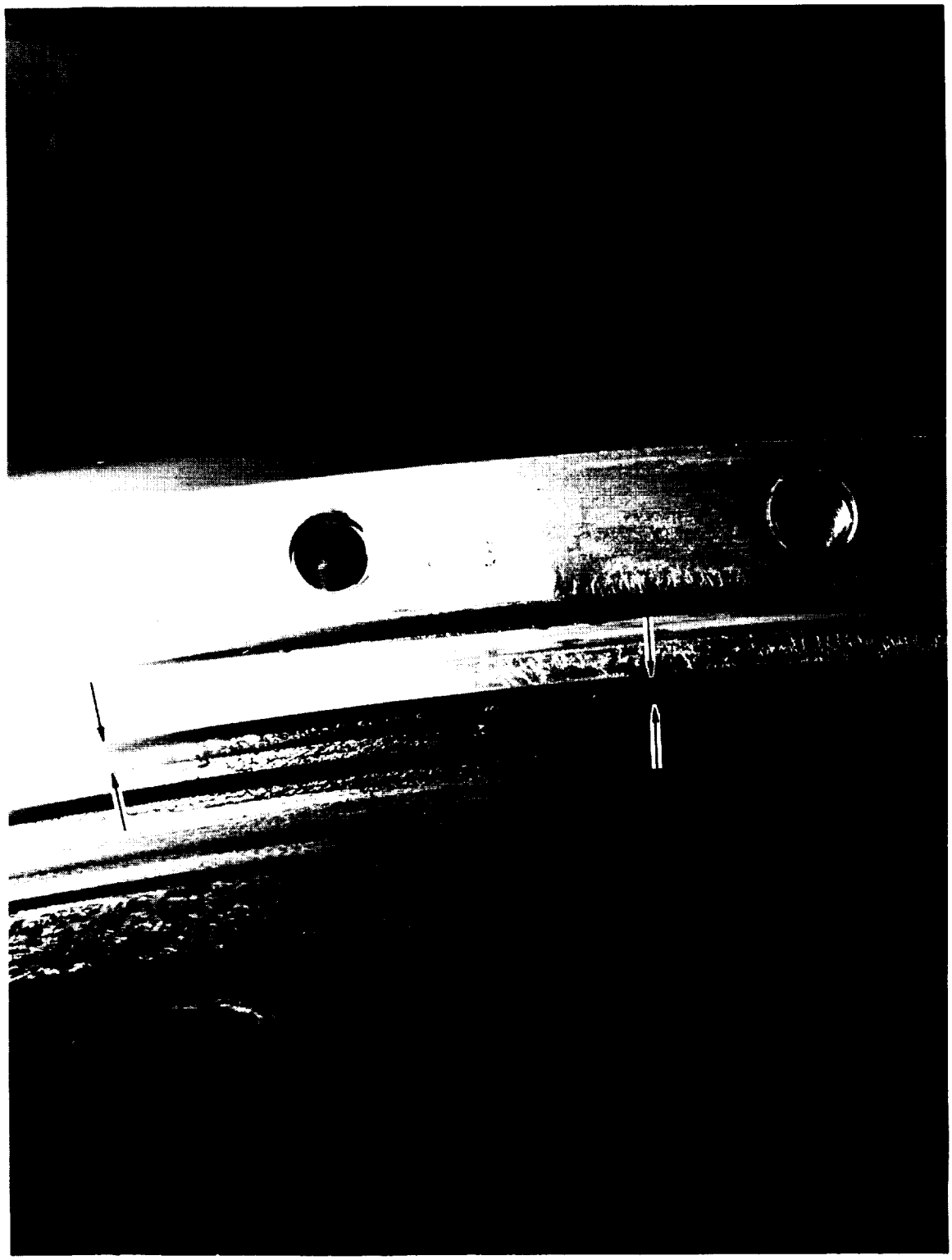

N101206-7

Figure 7.5-83. DM-9 Aft Exit Cone Polysulfide Backfill (265 deg)

The forward field joint interface of the aft exit cone assembly showed CCP/GCP separations appearing intermittently around the cone circumference. The extreme aft end of the aft exit cone showed no CCP/GCP separations. There were no separations isolated within the CCP liner or the GCP insulator.

The cork insulation covering the GCP overwrap performed nominally. Heat effect was far less than observed on the ETM-1A and DM-8 nozzles. Charring and blistering of the cork was due to exhaust plume radiation reflection off the test bay floor.

No damage occurred on the aluminum aft exit cone shell, compliance ring, or actuator brackets. Minor paint scratches were observed on both actuator brackets.

Char and erosion analysis of the aft exit cone assembly insulation showed positive performance MS except at station location 95.77 (90 deg).

Nozzle Plug

The DM-9 nozzle plug burst into multiple pieces at motor ignition. The largest chunk located following the test was approximately 6 by 7 by 11 in. in size and weighed 0.95 lb.

Nose Inlet/Throat Joint

A cross-sectioned view of the DM-9 nose inlet/throat assembly joint is shown in Figure 7.5-84. Photographs of the post-test joint are presented in Figures 7.5-85 through 7.5-87.

The backfilled RTV sealant extended below the joint char line 360 deg circumferentially. The sealant did not completely fill the radial ID portion of the bondline at 3, 10, 90, 125, 307, 315, 325, 330, and 342 deg. The RTV sealant extended past the axial portion of the bondline from 0 to 2, 15 to 20, 25 to 50, 55 to 88, 112 to 118, 175 to 185, 190 to 195, 200 to 208, 215 to 290, 300 to 305, and 338 to 340 deg. RTV reached the high-pressure side of the primary O-ring intermittently around the

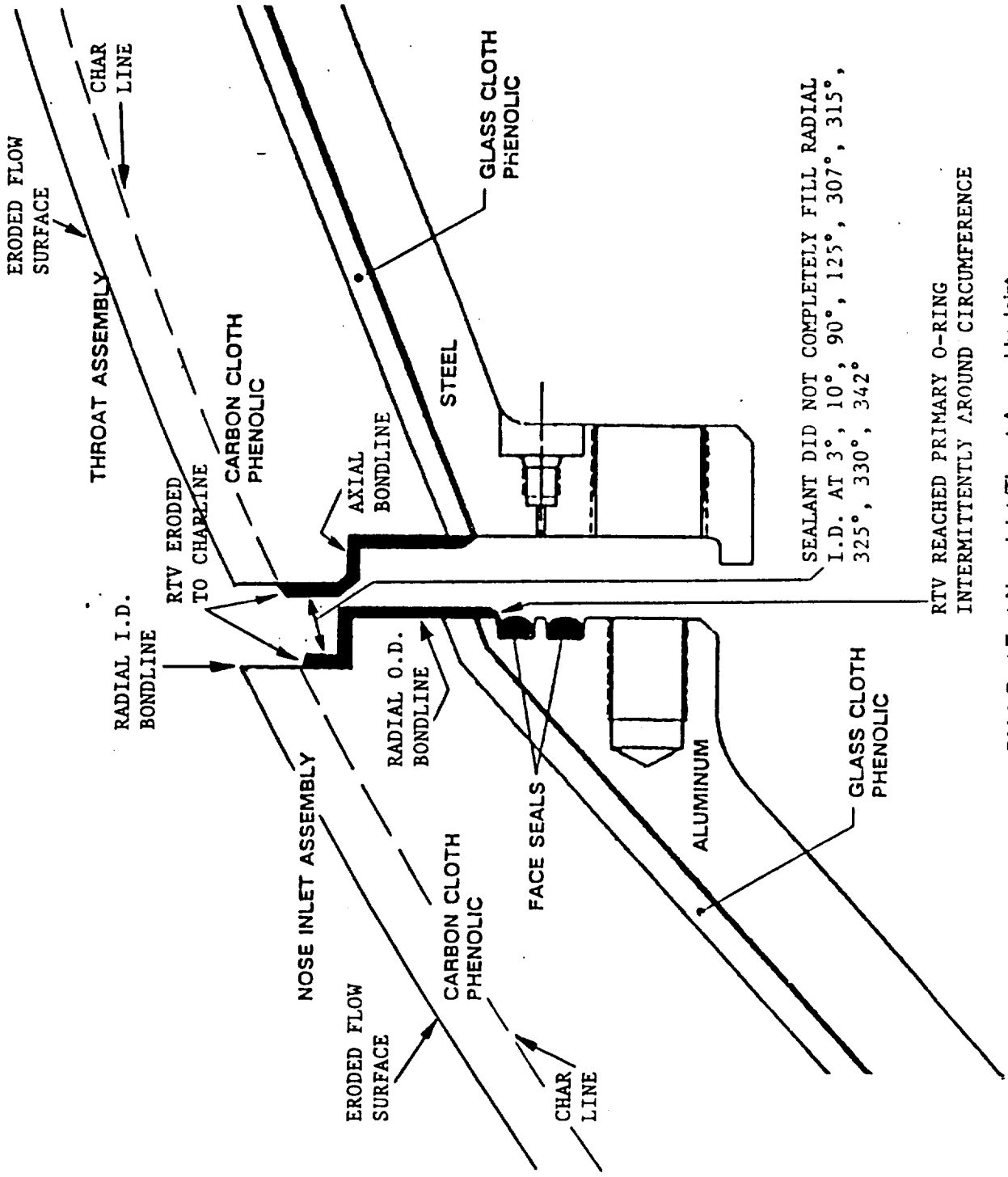

Figure 7.5-84. DM-9 Post-Test Nose Inlet/Throat Assembly Joint

ORIGINAL PAGE
BLACK AND WHITE PHOTOGRAPH

N101584-1

Figure 7.5-85. Nose Inlet/Throat Joint (0-30 deg)

ORIGINAL PAGE
BLACK AND WHITE PHOTOGRAPH

N101584-4

Figure 7.5-86. Nose Inlet/Throat Joint at 90 deg Showing Blowpath Location

N101561-9

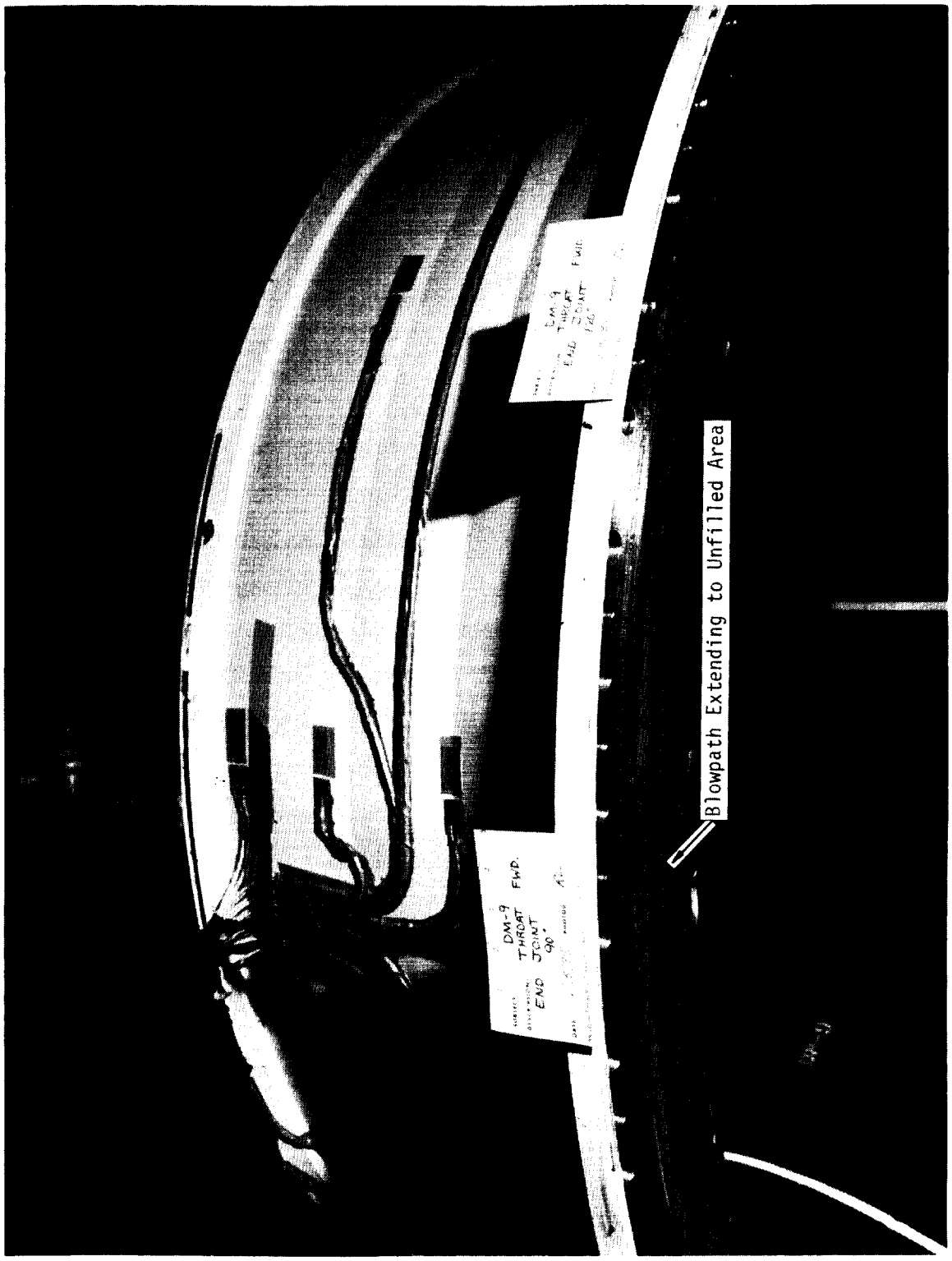

Figure 7.5-87. Nose Inlet/Throat Joint at 90 deg Showing Blowpath Location

circumference, but there was no RTV past the O-ring. The RTV eroded to the char line as expected.

A blowpath approximately 0.16 in. wide circumferentially extended from the flow surface, through the RTV sealant, to the unfilled void area located at 90 deg (Figure 7.5-86). The primary O-ring saw pressure, but showed no signs of blowby, erosion, or heat effect.

Nose Cap/Bearing/Cowl Joint

A cross-sectioned view of the nose cap/bearing/cowl joint is presented in Figure 7.5-88. Photographs of the post-test joint are presented in Figures 7.5-89 through 7.5-92.

The sealant was eroded to the char line as expected. EA 913NA adhesive was found to be mixed with the RTV. The adhesive was typically between two layers of RTV. Soot was observed between the RTV and adhesive, and also on the metal surfaces of the nose inlet housing and bearing forward end ring up to the bolt holes. The accumulation of soot was heaviest from 15 to 39, 186 to 204, and 280 to 286 deg. Soot also reached the high-pressure side of the primary O-ring from 0 to 7, 12 to 23, 37 to 39, 90 to 92, 105 to 108, 180 to 195, 200 to 210, 240. 290 to 295, 320, 335, and 345 deg. The primary O-ring was exposed to pressure, but showed no signs of erosion or heat effect. In addition, soot was observed between the cowl housing and bearing forward end ring, between the bearing protector and bearing forward end ring (cross section, Figure 7.5-88), and between the cowl housing forward flange ID surface and bearing protector.

Throat/Forward Exit Cone Joint

A cross-sectioned view of the DM-9 throat inlet/forward exit cone joint is shown in Figure 7.5-93. Photographs of the post-test joint are presented in Figures 7.5-94 through 7.5-97.

The backfilled RTV sealant extended below the joint char line circumferentially except at 333 deg. The sealant also reached the radial OD portion of the bondline

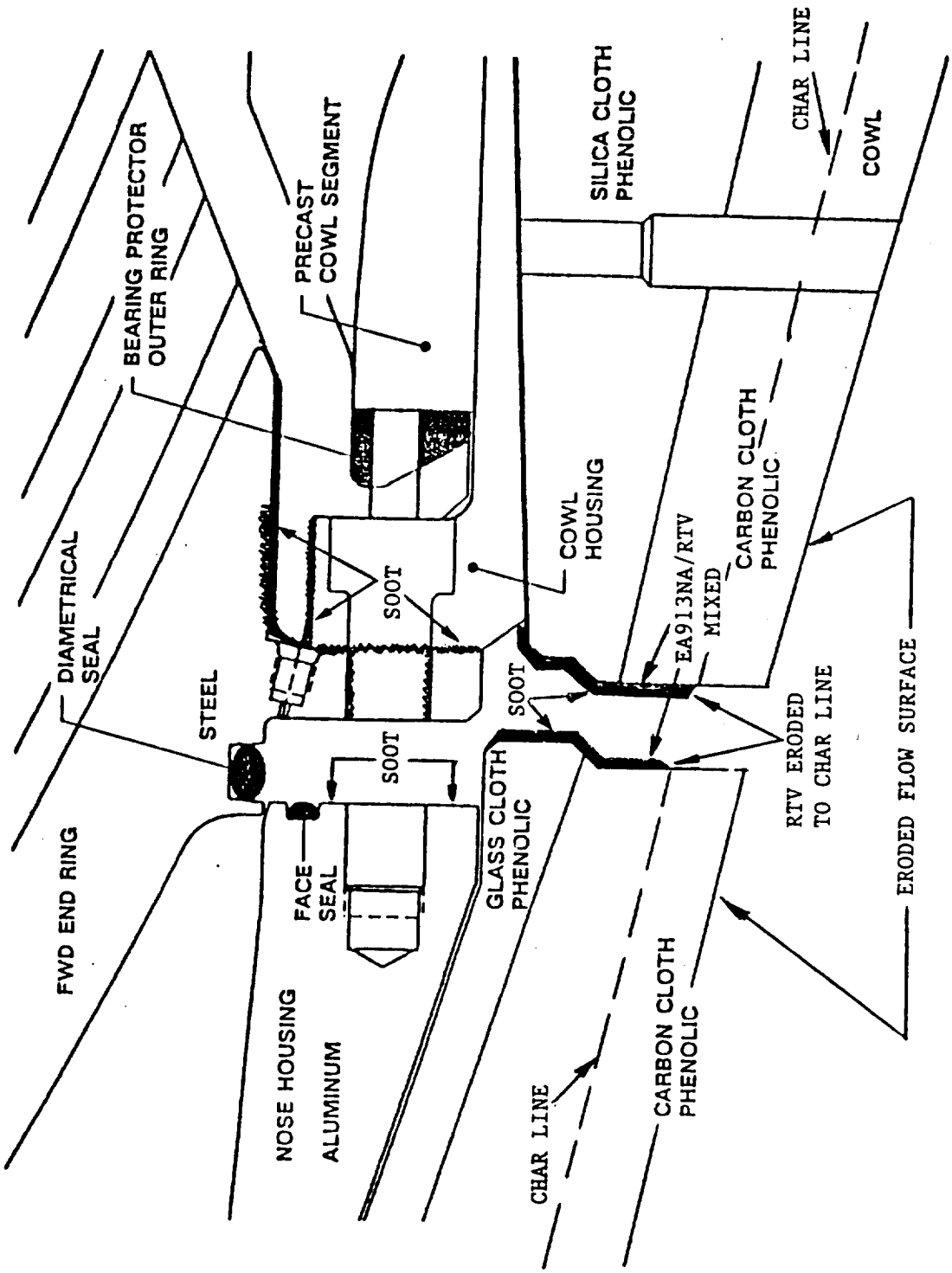

Figure 7.5-88. DM-9 Post-Test Nose Cap/Bearing/Cowl Ring Joint

ORIGINAL PAGE
BLACK AND WHITE PHOTOGRAPH

N101473-8

Figure 7.5-89. Nose Cap Aft End at 0 deg Prior to Removal of Flex Bearing

N101473-27

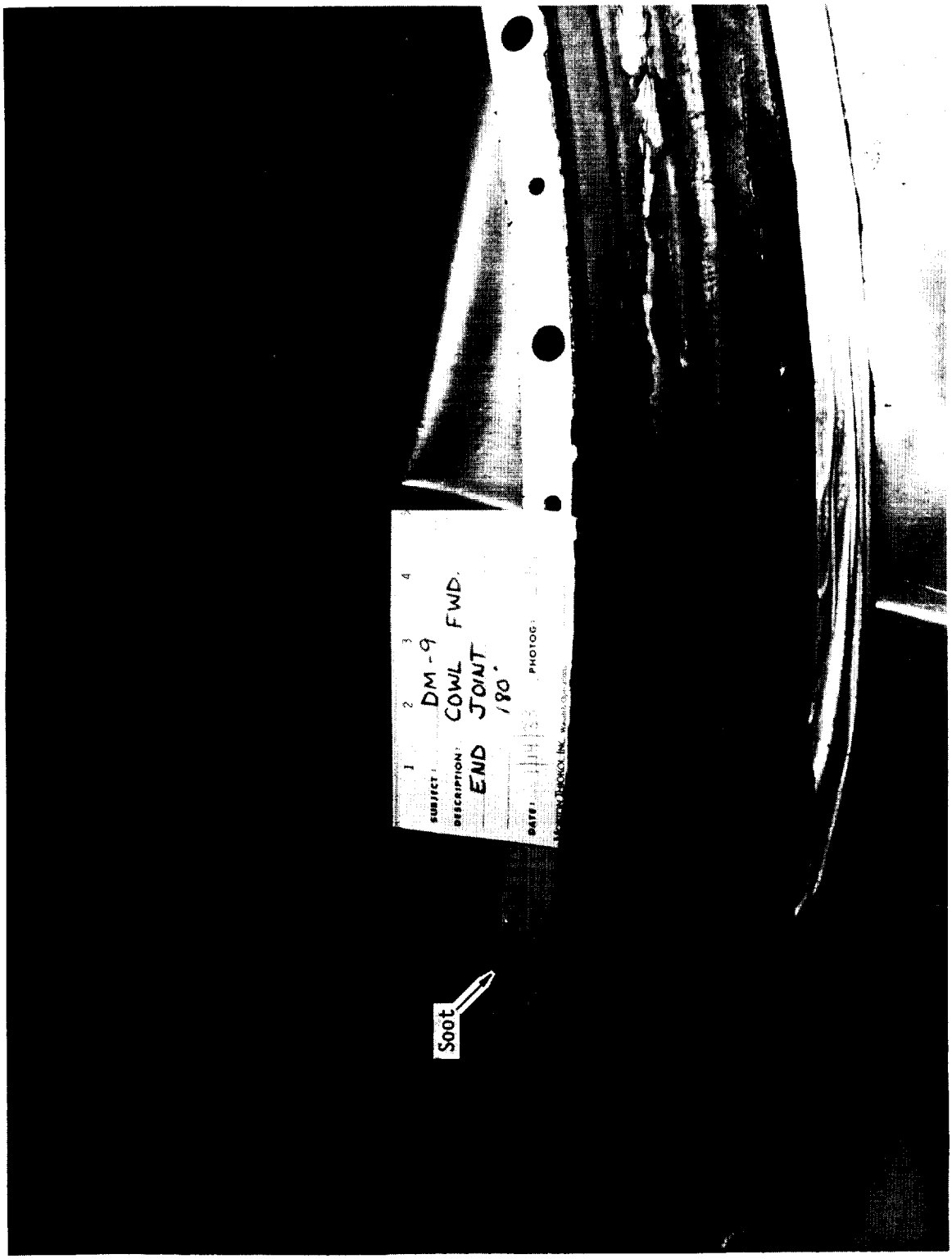

Figure 7.5-90. Cowl Forward End Joint at 180 deg

N101562-1

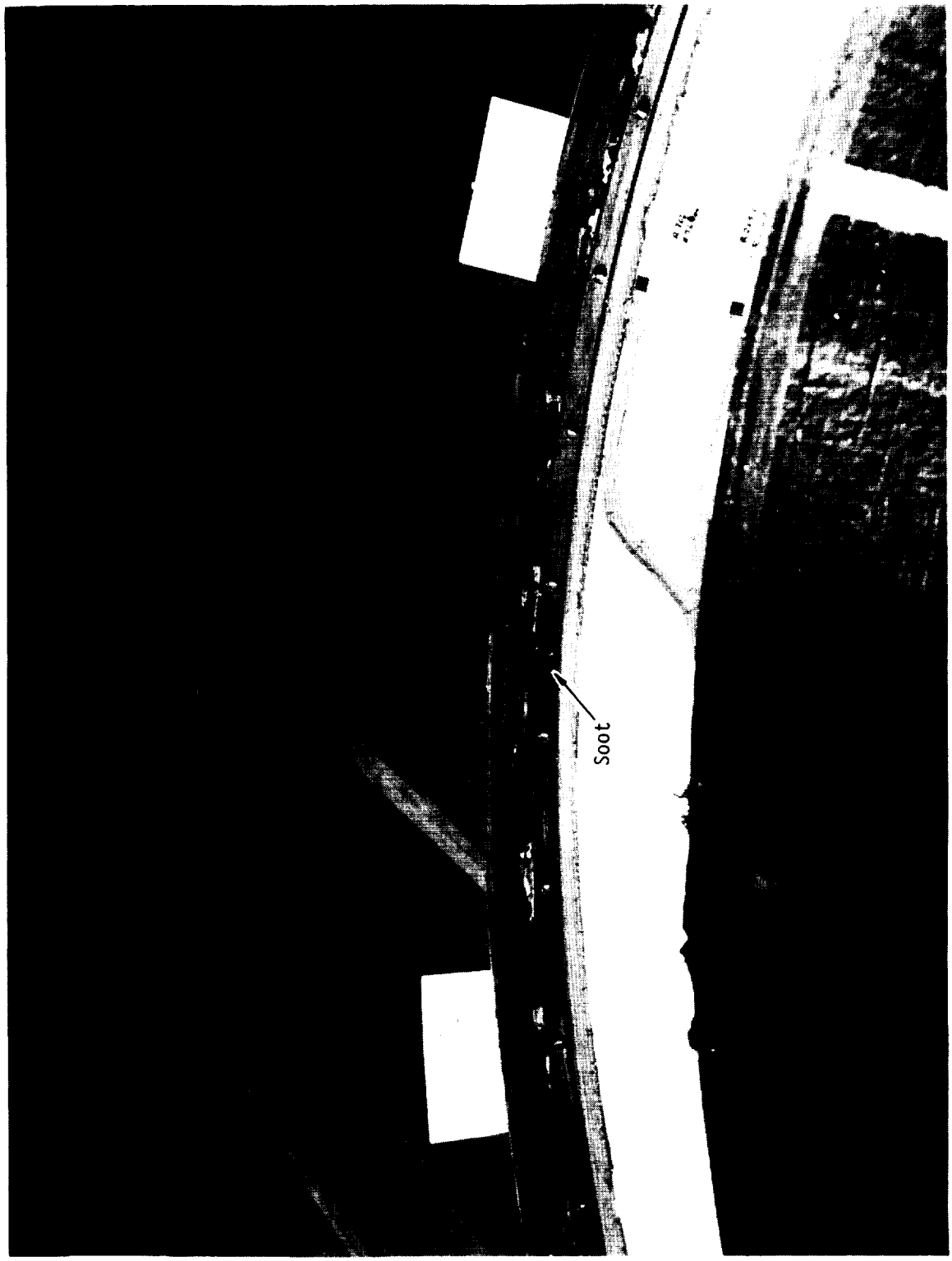

Figure 7.5-91. Nose Cap Aft End at 0-30 deg

N101562-3

Figure 7.5-92. Nose Cap Aft End at 60 to 90 deg Showing Soot

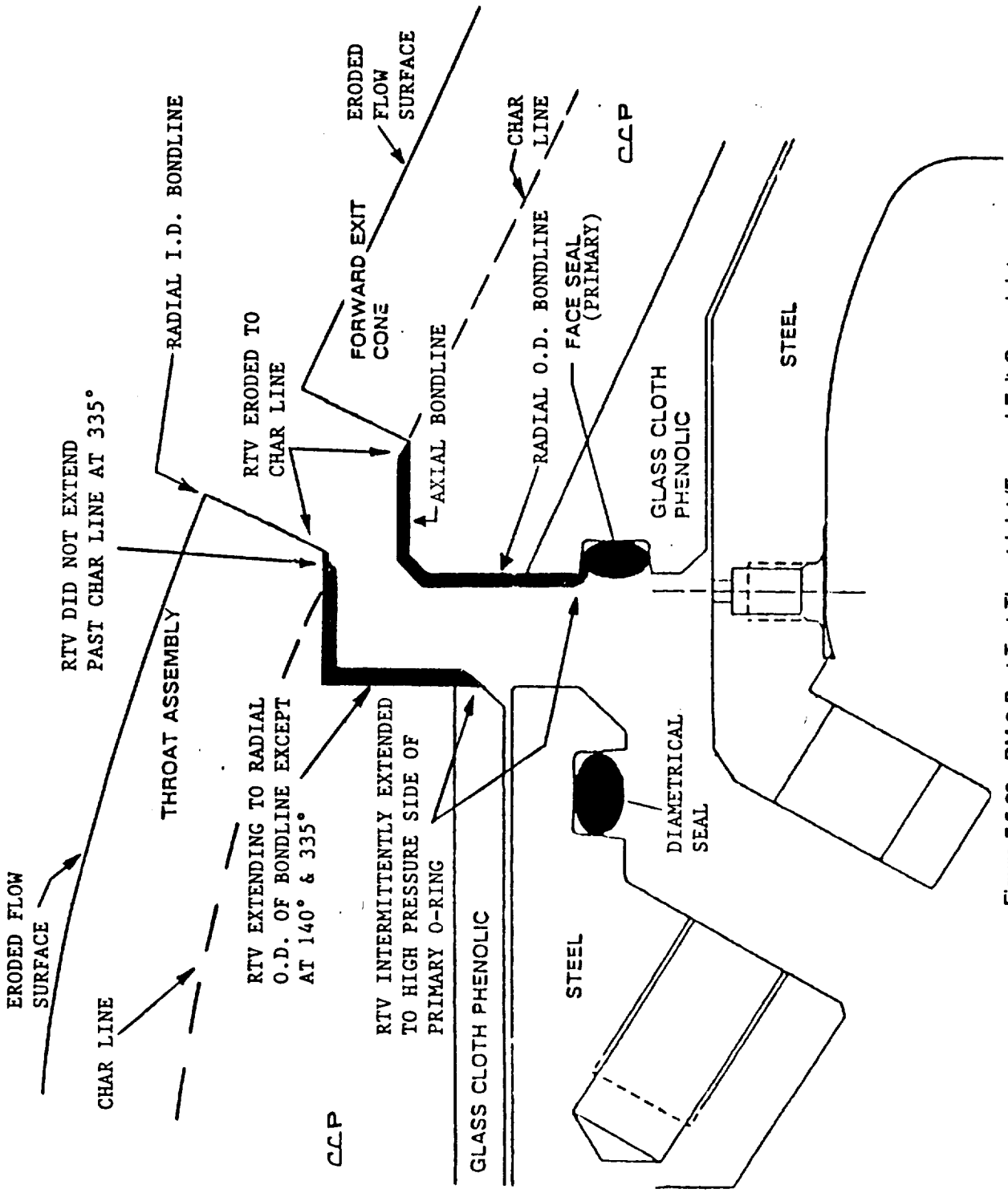

Figure 7.5-93. DM-9 Post-Test Throat Inlet/Forward Exit Cone Joint

N101256-10

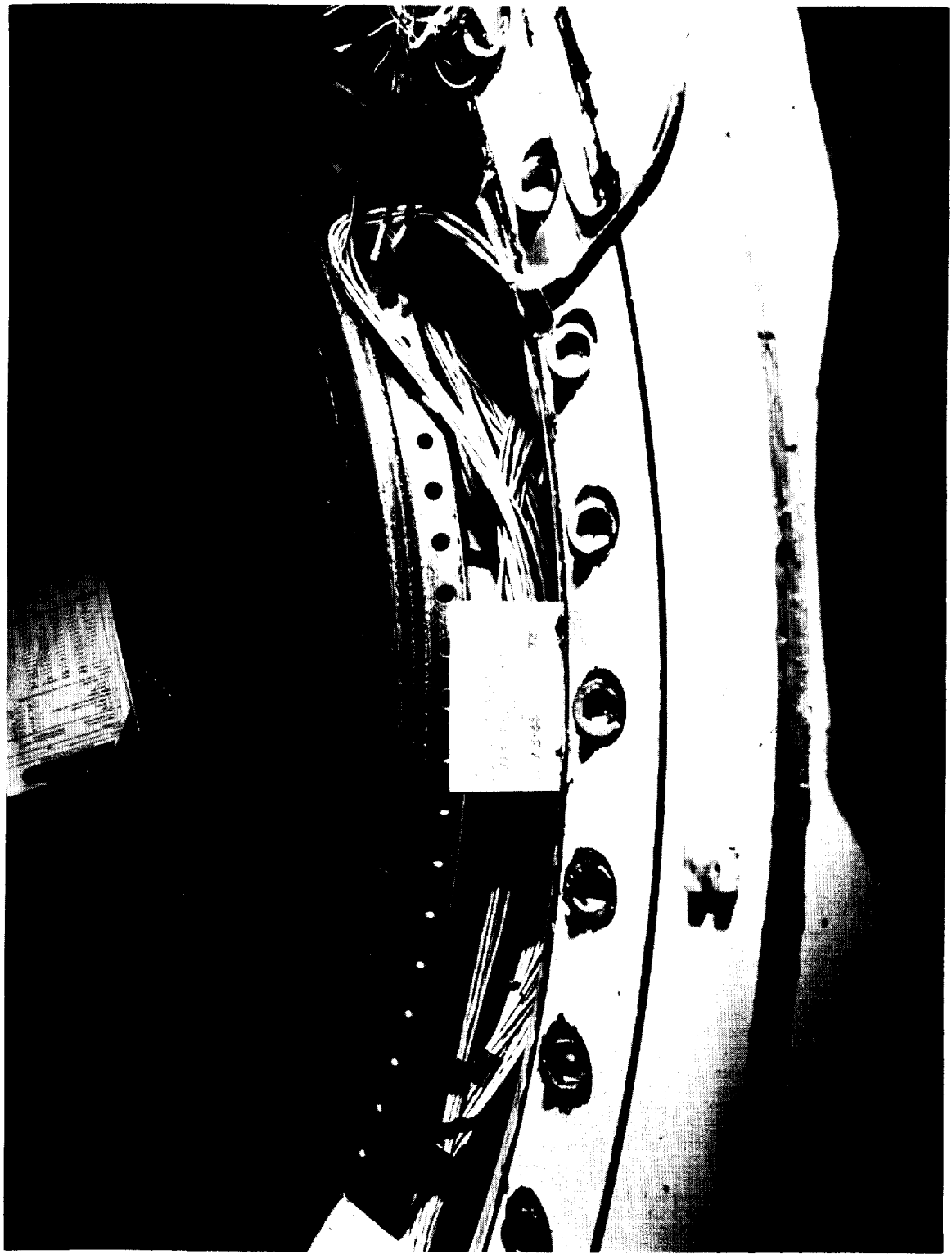

Figure 7.5-94. Throat Aft End Joint at 60 deg

N101257-11

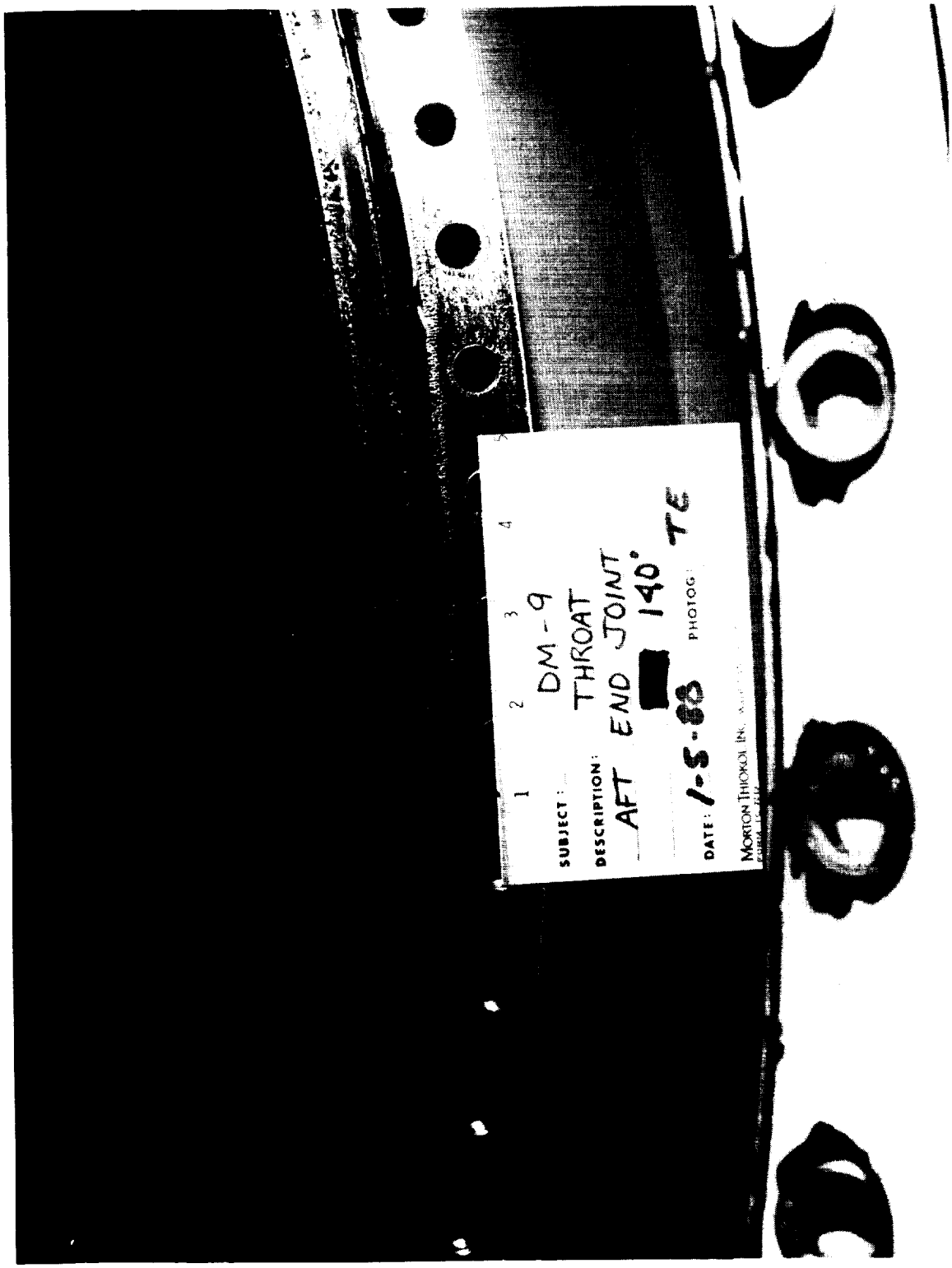

Figure 7.5-95. Throat Aft End Joint at 140 deg Showing Blowpath and Unfilled Area

N101258-1

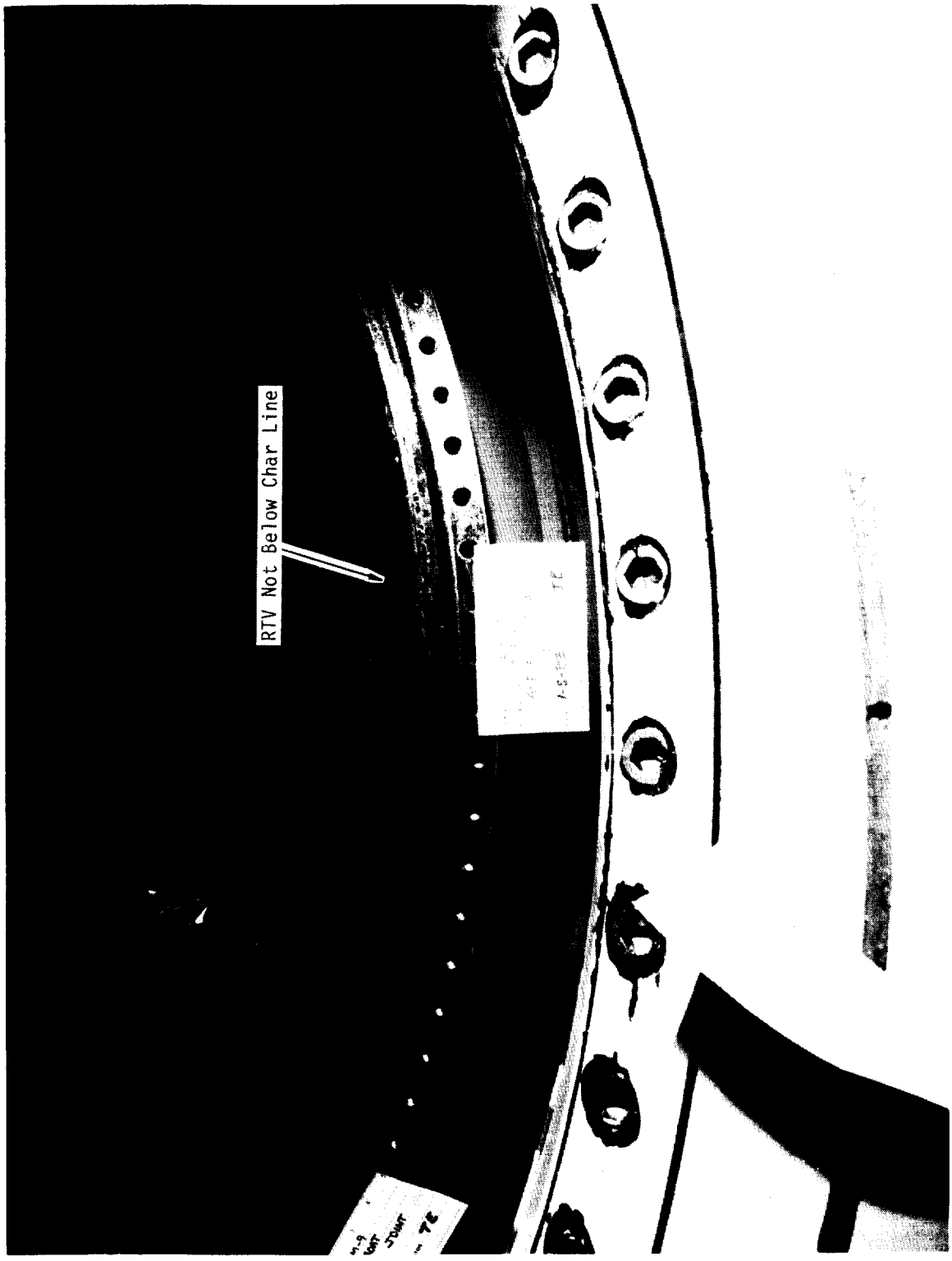

Figure 7.5-96. Throat Aft End Joint at 330 deg

N101257-1

Figure 7.5-97. Forward Exit Cone/Forward End Joint at 330 deg

circumferentially except at 140 and 335 deg. RTV extended to the high-pressure side of the primary O-ring intermittently around the joint circumference.

A blowpath approximately 0.40 in. wide circumferentially extended from the flow surface, through the RTV sealant, to an unfilled void area located at 140 deg (Figure 7.5-95). The primary O-ring at this location saw pressure, but showed no signs of blowby, erosion, or heat effect.

The backfilled RTV sealant did not extend below the char line at the 333-deg location (Figures 7.5-96 and 7.5-97). This violates the postfire engineering evaluation limit established in TWR-17198, Vol. 5. The primary O-ring at this location also saw pressure, but showed no signs of blowby, erosion, or heat effect.

Grease was observed on the post-test joint phenolic interfaces. RTV backfill depths may have been limited due to the presence of excessive grease during assembly procedure.

Fixed Housing/Bearing Aft End Ring Joint

A cross-sectioned view of the DM-9 fixed housing/bearing aft end ring joint is shown in Figure 7.5-98. Photographs of the post-test joint are presented in Figures 7.5-99 and 7.5-100.

RTV sealant completely filled the bondline between the bearing protector and inner boot ring. No voids were observed in the RTV. Approximately 95 percent of the axial gap between the bearing protector and steel fixed housing was filled with sealant. RTV reached the high-pressure side of the primary O-ring from 40 to 112, 150 to 170, 220 to 250, 260 to 270, 275 to 318, and 350 to 355 deg. Sealant did not extrude past the O-ring. There was no assembly, disassembly, or heat effect damage observed on the primary O-ring, and the joint was free of soot. Inspection of the secondary O-ring revealed 12 diagonal abrasion marks between 218 and 227 deg. The marks were a maximum length of 0.05 in. and were approximately 0.001 to 0.002 in. deep.

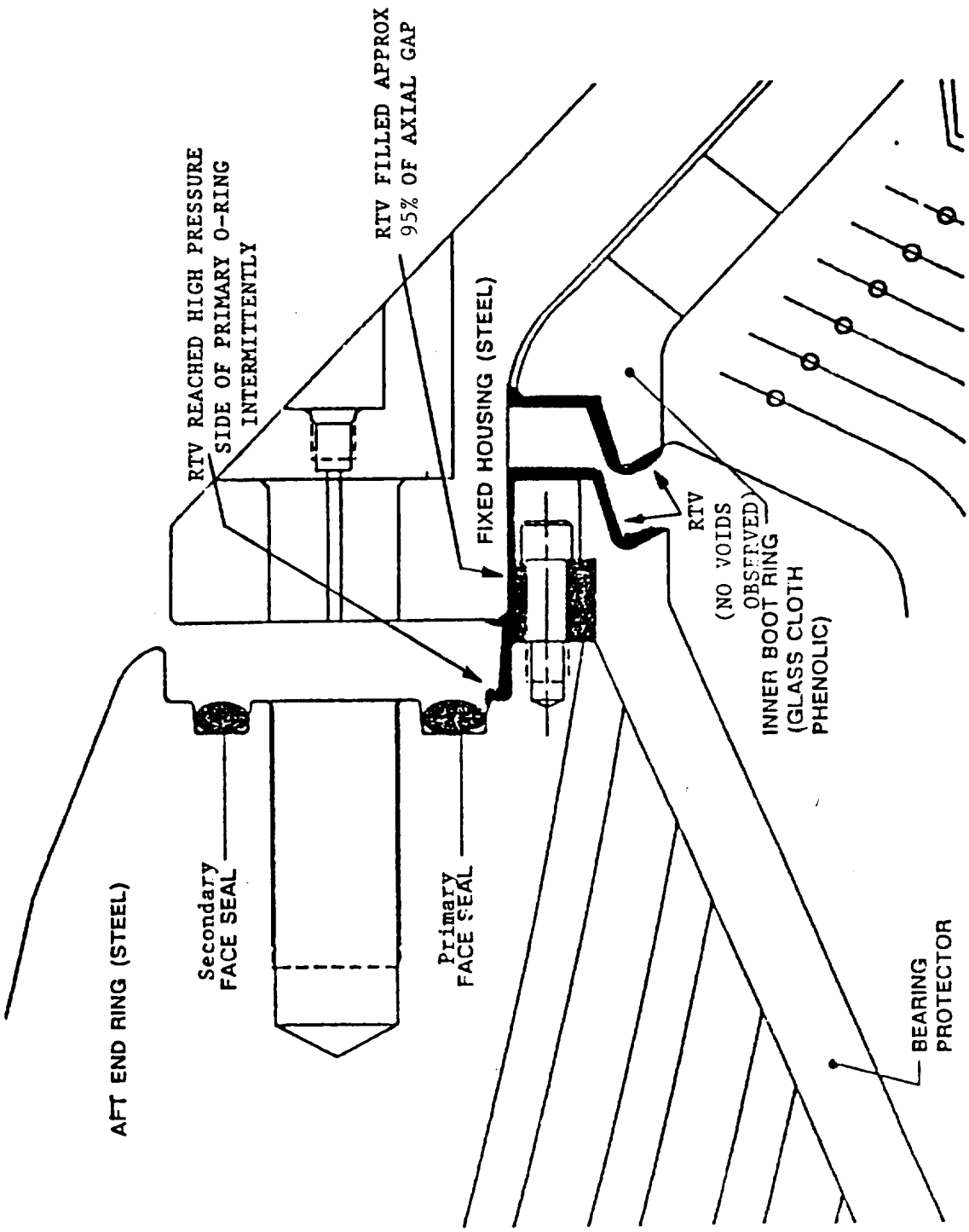

Figure 7.5-98. DM-9 Post-Test Fixed Housing/Bearing Aft End Ring Joint

ORIGINAL PAGE
BLACK AND WHITE PHOTOGRAPH

N101225-1

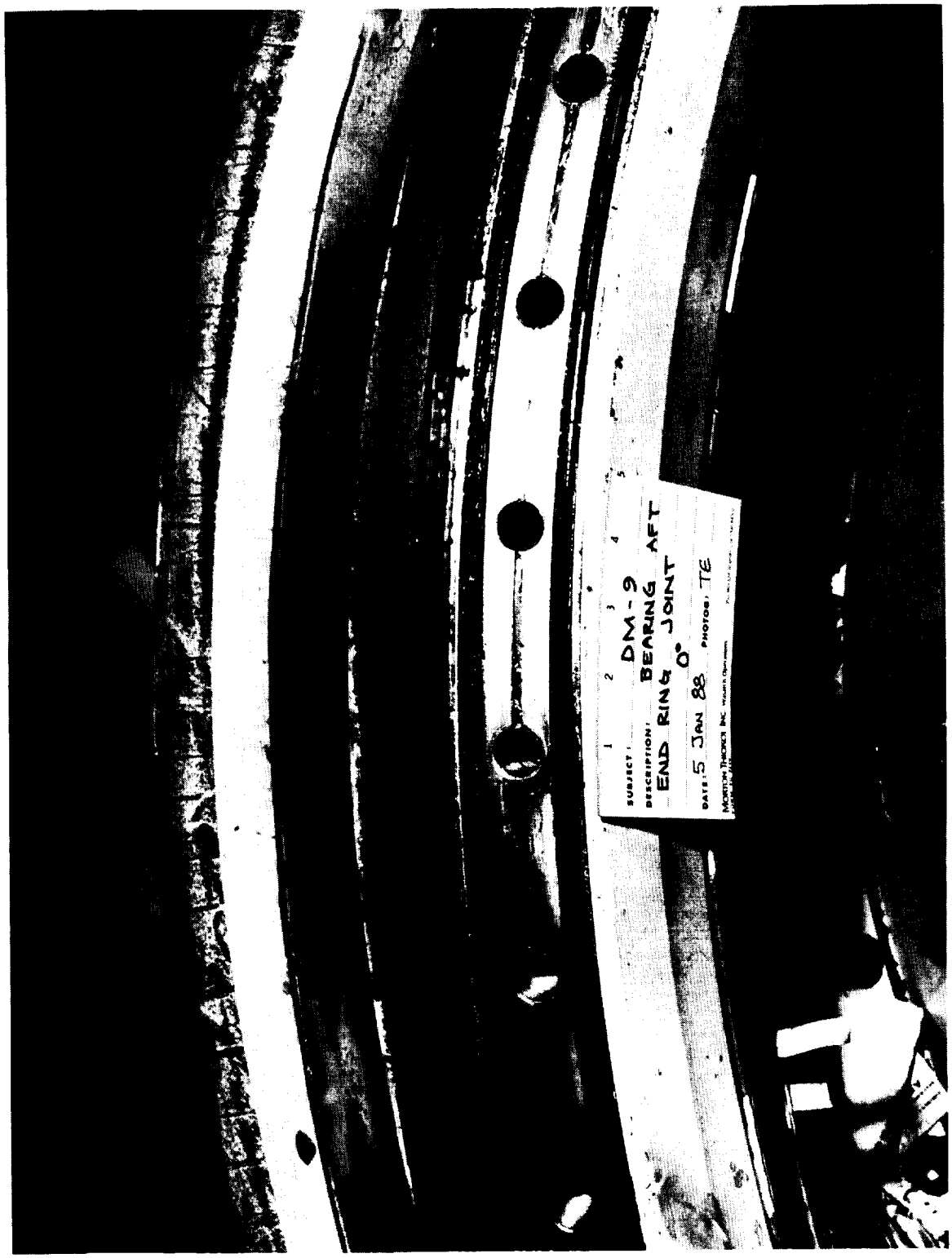

Figure 7.5-99. Bearing Aft End Ring Joint at 0 deg

N101222-1

Figure 7.5-100. Fixed Housing Foward End at 0 deg

Aft Exit Cone/Forward Exit Cone Joint

Figure 7.5-101 shows a cross-sectioned view of the DM-9 aft exit cone/forward exit cone field joint. Photographs of the post-test joint are presented in Figures 7.5-102 through 7.5-105.

The backfilled RTV sealant extended below the joint char line 360 deg circumferentially. RTV filled the radial ID portion of the joint bondline completely, and reached the high pressure side of the primary O-ring circumferentially except from 0 to 70 deg, and at 330 deg.

A blowpath approximately 0.30 in. wide circumferentially extended from the flow surface, through the RTV sealant, to an unfilled void area located at 330 deg (Figure 7.5-104). The primary O-ring at this location saw pressure, but showed no signs of blowby, erosion, or heat effect. The GCP on the high-pressure side of the O-ring groove was sooted in line with the blowpath, but was not eroded or charred.

7.5.4.2 Flex Bearing. Overall flex bearing performance during static test was acceptable. Near the end of burn time, a tensile deflection of 0.48 in. was observed. This phenomenon has occurred on previous tests and is most likely due to pressurized gas trapped in the cavity between the bearing and the boot. The magnitude of tensile deflection seen is less than the bearing experiences during unbond inspection in the refurbishment cycle.

Axial Deflection

Axial deflection of the nozzle with respect to the aft chamber dome was calculated using data from the 12 linear transducers used to measure nozzle position. The nozzle stagnation pressure is shown in Figure 7.5-106. A plot of axial nozzle deflection as a function of nozzle stagnation pressure is presented in Figure 7.5-107. The lower curve reflects ignition pressures and is considered invalid because of the rapid pressure rise experienced during this time. The upper curve defines nozzle axial deflection during the period between maximum chamber pressure and motor tailoff.

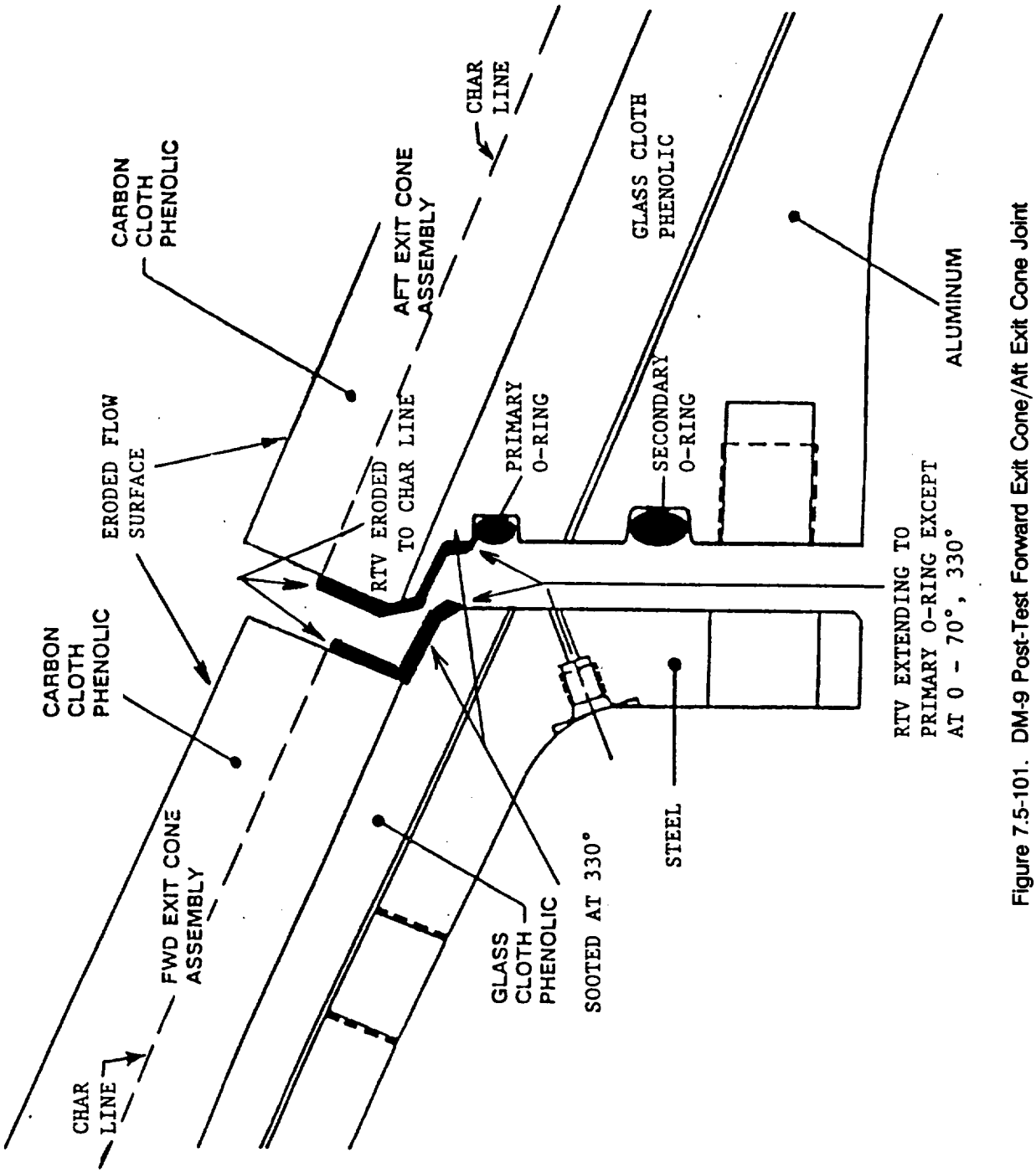

Figure 7.5-101. DM-9 Post-Test Forward Exit Cone/Aft Exit Cone Joint

N101206-33

Figure 7.5-102. Forward Exit Cone Aft End at 60 deg

ORIGINAL PAGE
BLACK AND WHITE PHOTOGRAPH

N101208-32

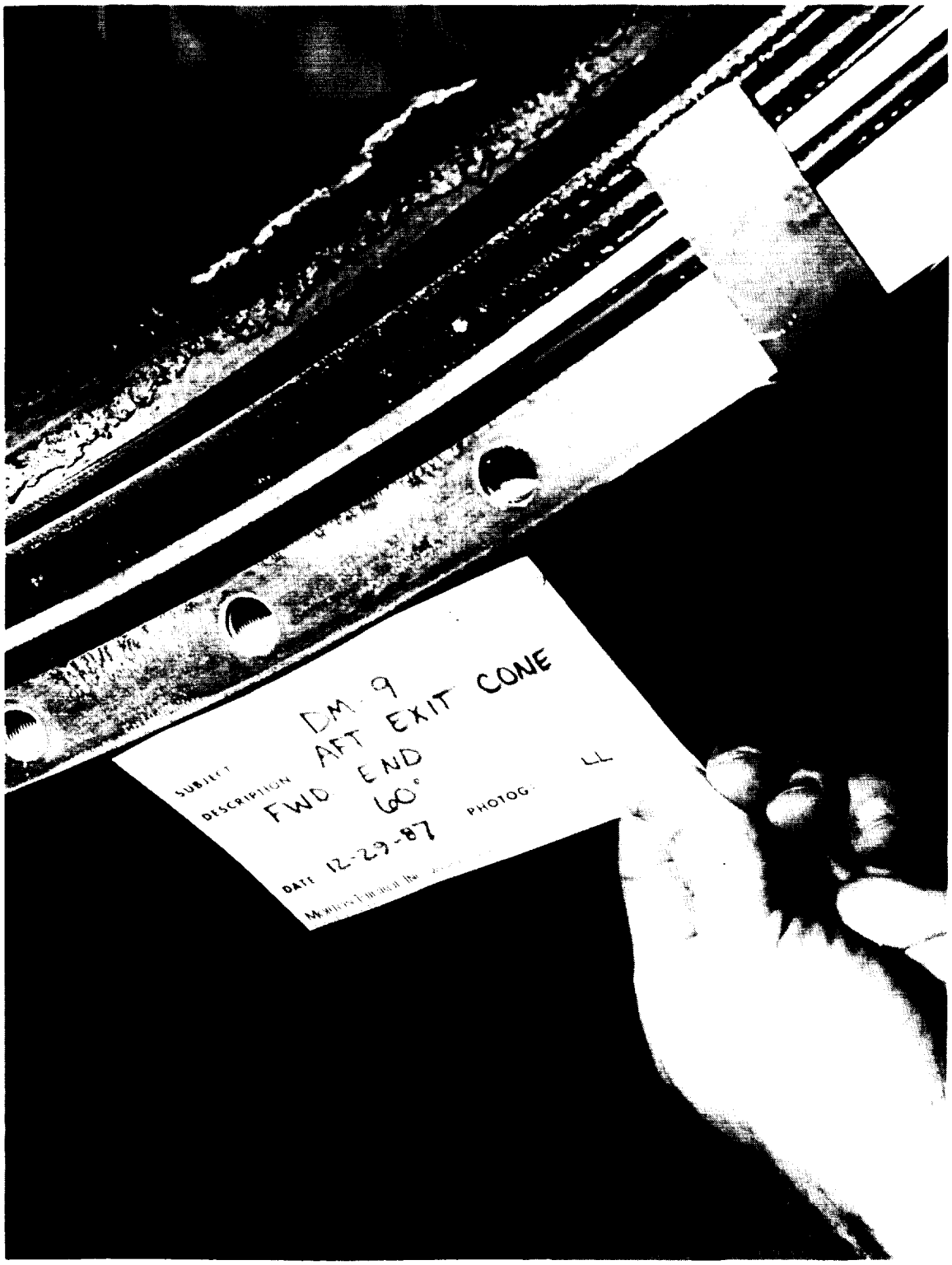

Figure 7.5-103. Aft Exit Cone Forward End at 60 deg

ORIGINAL PAGE
BLACK AND WHITE PHOTOGRAPH

N101206-36

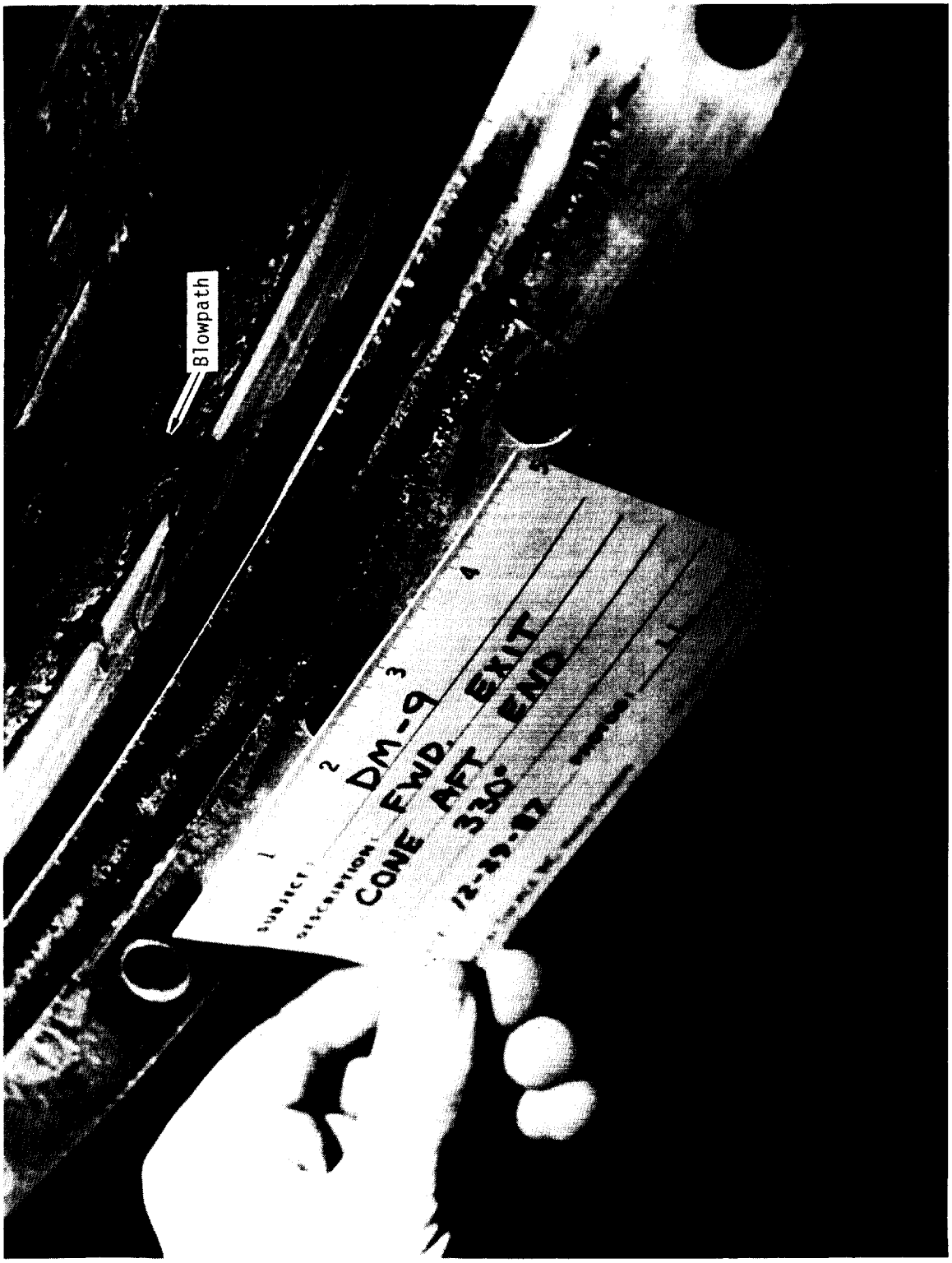

Figure 7.5-104. Forward Exit Cone Aft End at 330 deg Showing Blowpath

N101206-26

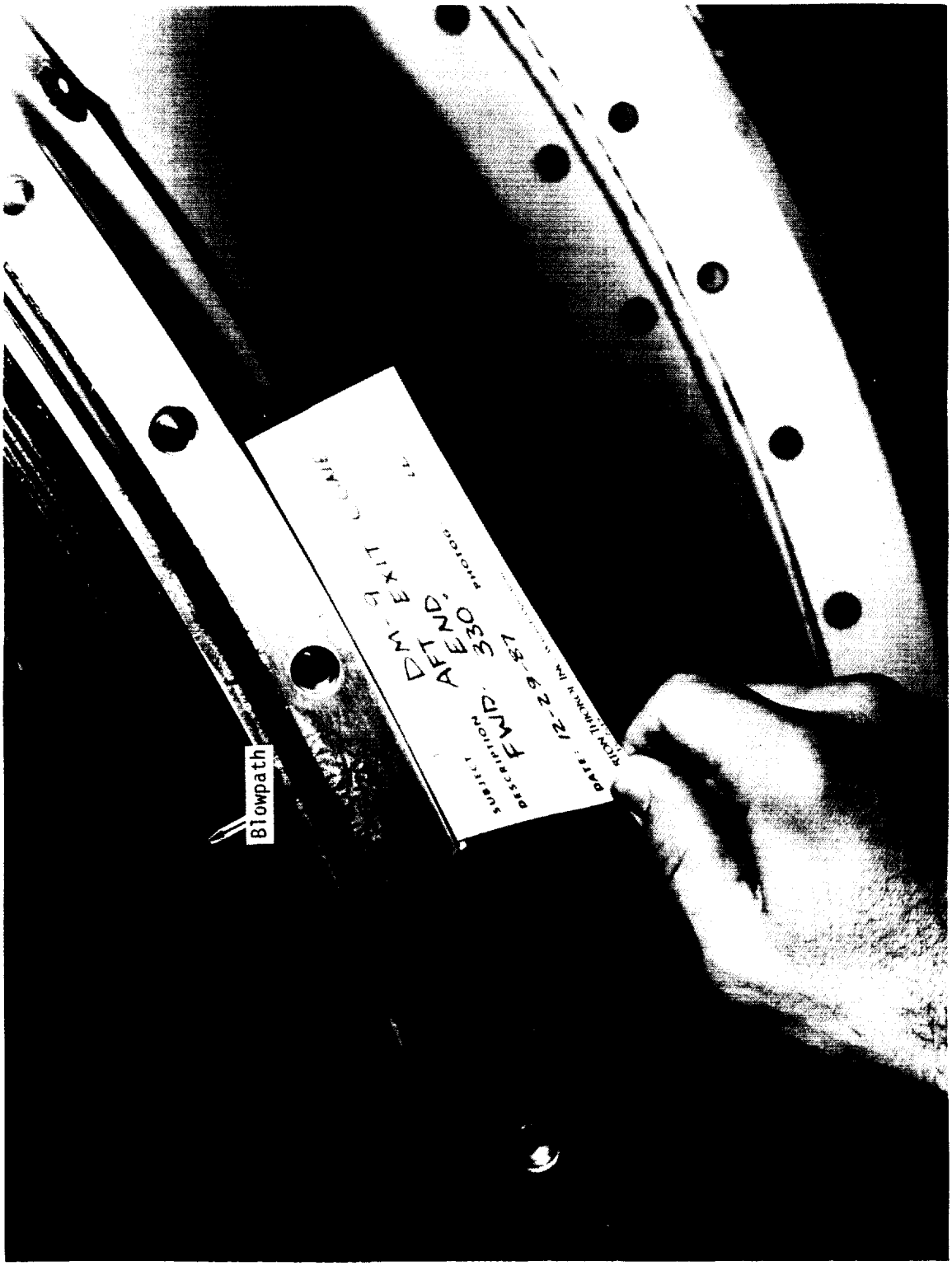

Figure 7.5-105. Aft Exit Cone Forward End at 330 deg Showing Blowpath

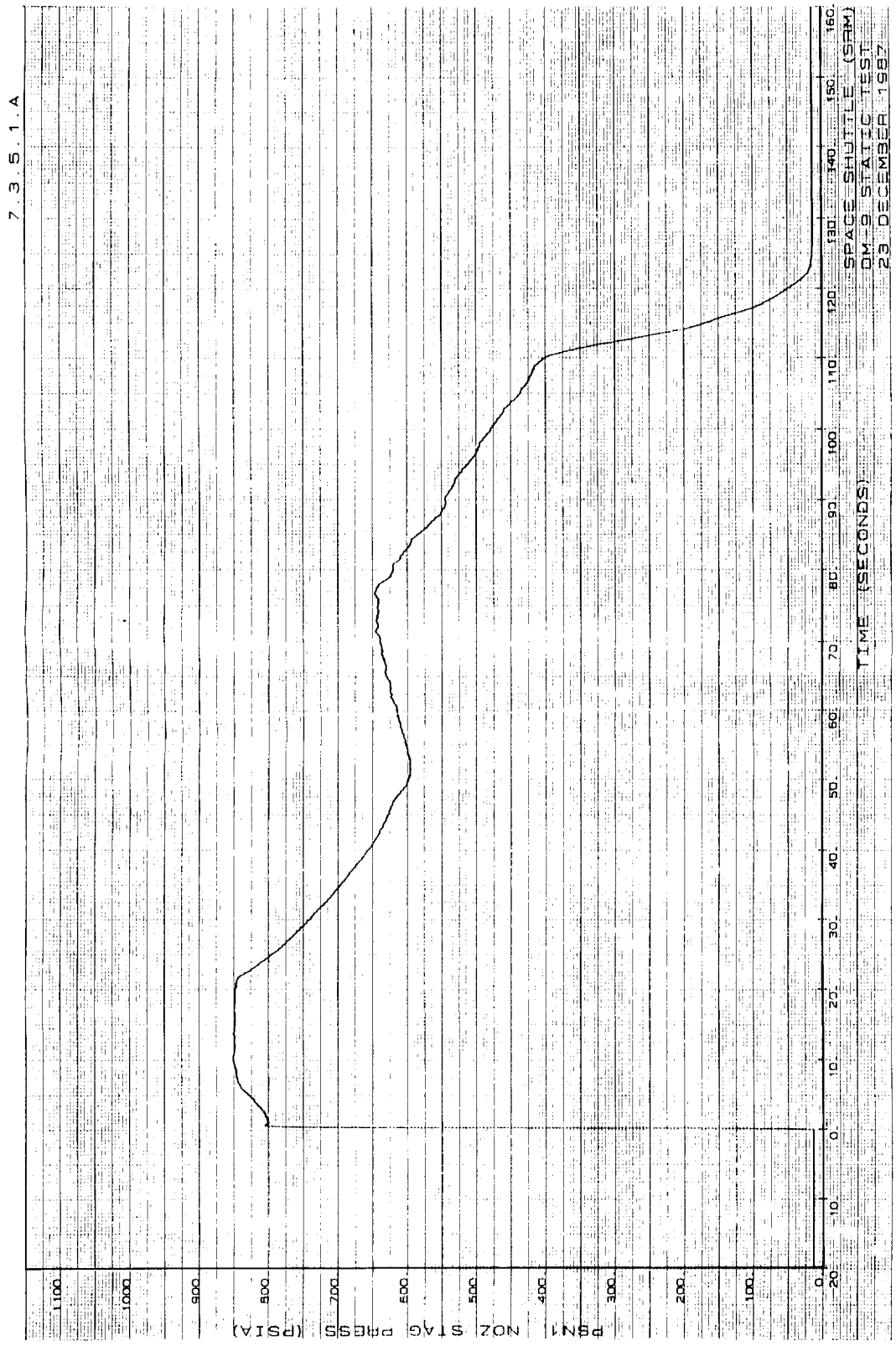

Figure 7.5-106. DM-9 Nozzle Stagnation Pressure

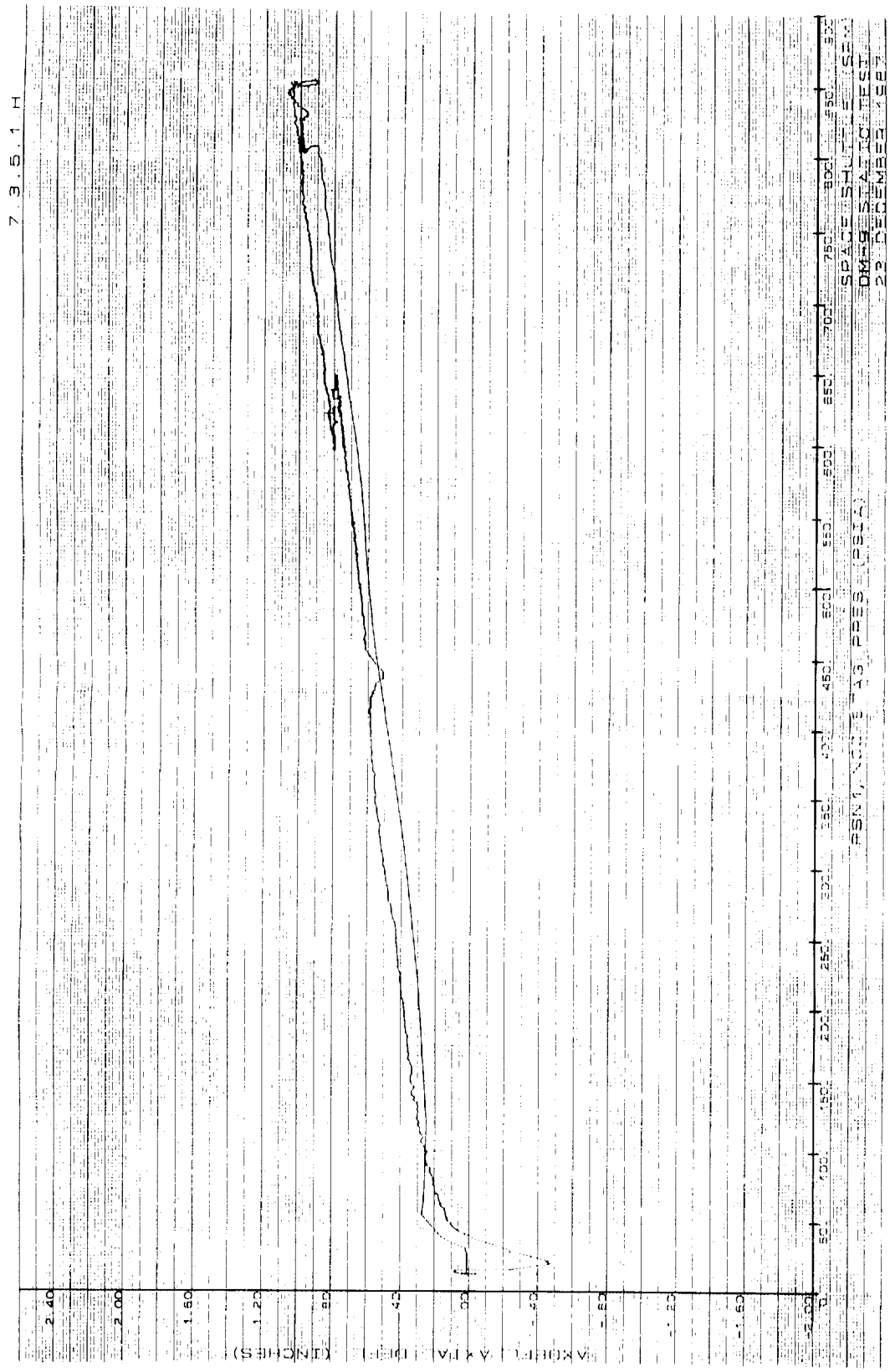

Figure 7.5-107. DM-9 Axial Deflection Versus Nozzle Stagnation Pressure

Axial deflection measured in bench test, using a thrust relief piston at 620 psig, was 0.67 inch. Measured static test nozzle axial deflection at the same pressure was 0.83 inch.

Axial deflection as a function of time is shown in Figure 7.5-108. Figure 7.5-108 shows that at the end of burn time, when the nozzle stagnation pressure was approximately ambient, there was a maximum axial deflection of 0.48 in. (forward direction). The most probable cause of the tensile deflection was pressurized gas in the cavity between the flex bearing and boot due to plugged vent holes in the cowl. It was determined that a pressure of approximately 109 psi would cause the deflection seen. Similar occurrences were experienced on previous static tests including QM-2 (-0.66 in.), QM-3 (-0.60 in.), QM-4 (-0.91 in.), DM-6 (-1.08 in.), DM-7 (-0.75 in.), DM-8 (-0.93 in.), and ETM-1A (-0.60 in.).

Pivot Point Analysis

Static test pivot point locations, which were calculated using extensometer data (obtained when the nozzle vector angle was greater than 4 deg), were input to a computer program which calculated a mean and one standard deviation for pivot point location. The equations used will only converge for vector angles equal to or greater than 4 deg. Results of the analysis are presented in Table 7.5-6. Group 1 data were calculated for time periods when motor pressure was below 50 psig and the actuators extended. Group 2 data are for chamber pressures greater than 50 psi with the actuators extended. Group 4 data are for chamber pressures greater than 50 psig with the actuators extended. Group 2 data are for chamber pressures greater than 50 psi with the actuators extended. Group 4 data are for chamber pressures greater than 50 psig with the actuators retracted.

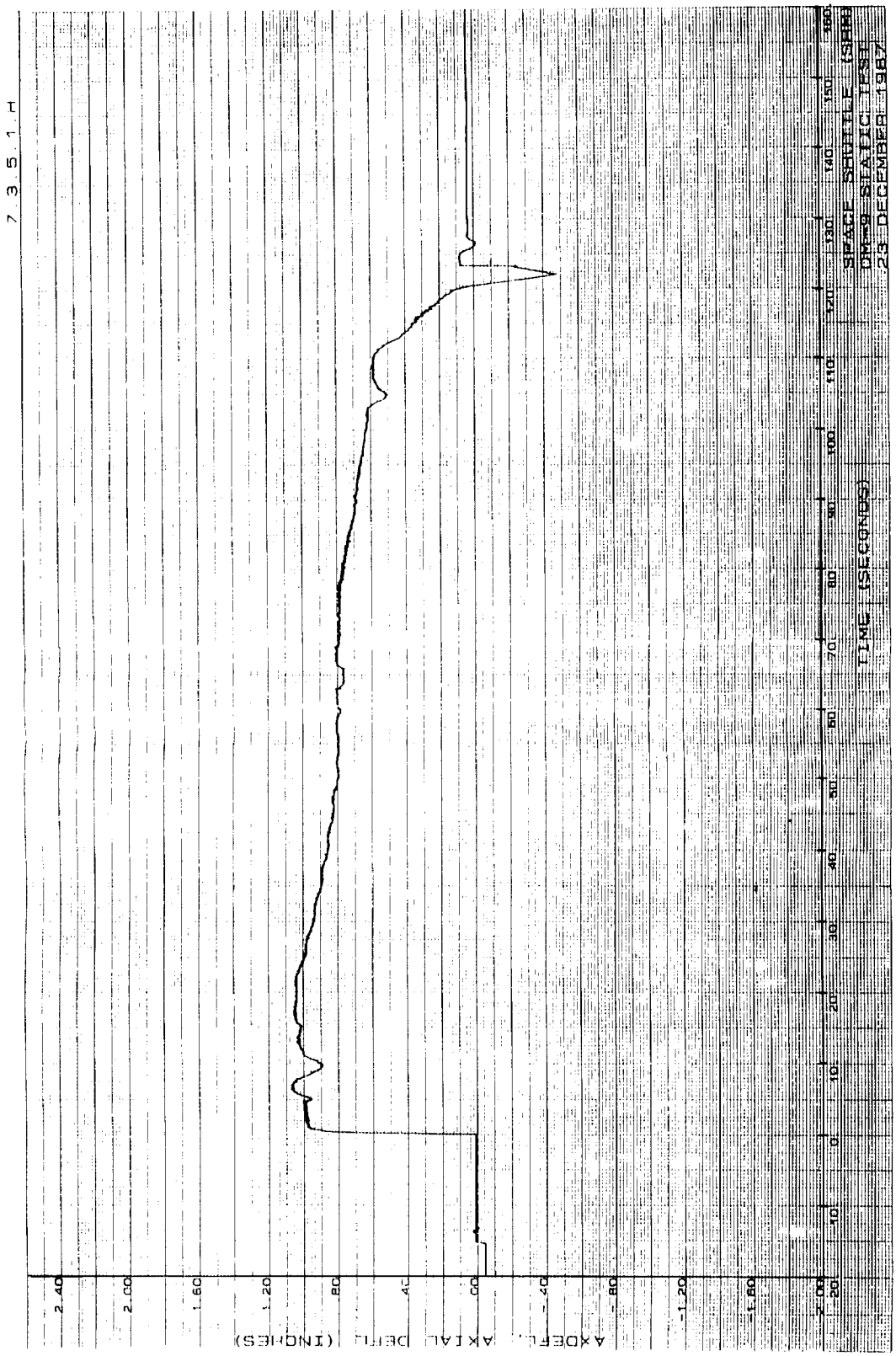

Figure 7.5-108. DM-9 Axial Deflection

Table 7.5-6. DM-9 Pivot Point Variation From Theoretical

Pressure (psi)	Group	Axial (in)	Standard Deviation	Radial (in)	Standard Deviation
<50	1 Single and Dual Extend	1.380	0.871	-0.868	0.091
≥50	2 Single and Dual Extend	3.448	1.229	0.740	0.207
≥50	4 Single and Dual Retract	6.538	1.620	0.656	0.228

The mean pivot point data from Table 7.5-6 are plotted in Figure 7.5-109 for low pressure and Figure 7.5-110 for high pressure. Also plotted are the pivot point data from the flex bearing bench test. The DM-9 static test mean pivot points for both high and low pressure fall outside the acceptance envelope. However, the validity of these points is questionable because of the high magnitude compared with those from the flex bearing bench test which were well within the acceptance limit.

Step Events

Part of the DM-9 duty cycle included step events to evaluate slew rate and angular acceleration capabilities of the nozzle. Tables 7.5-7 and 7.5-8 tabulate these values for the six step events during DM-9 dry run and static fire. The maximum slew rates and angular accelerations for each event all exceed the specified minimum levels of 5 deg/sec and 2 rad/sec^2, respectively.

7.5.4.3 Nozzle - Composite Structures. Figures 7.5-111 and 7.5-112 display the strain gage and thermocouple locations for the DM-9 nozzle. A total of 46 strain gages and 12 thermocouples were installed on the nozzle fixed housing region. The strain gages were made up of 17 biaxial (hoop and meridian) gages, 12 uniaxial gages, and 1 girth (hoop) gage. Instrumentation used on the DM-9 nozzle is listed in Table 7.5-9.

Figures 7.5-113 through Figure 7.5-115 display the actuator adjustment, dry run duty cycle (with hydrazine), and the static test duty cycle, respectively.

Static Test Predictions Versus Measurements

A two-dimensional (2-D) axisymmetric TASS Finite Element model was used as the analytical tool to predict strain results during the static test at 1, 4, 8, 22, 40, 80, and 123 sec. Figure 7.5-116 through 7.5-154 compare measured strain with predicted results for all locations. Each plot displays results of one strain component (hoop or meridian) with predictions at all locations. These strain plots were filtered. Raw data plots are found in Appendix C. Since a 2-D axisymmetric finite element model was used for the analysis, loads due to TVC actuation were not considered and predictions do not account for these loads.

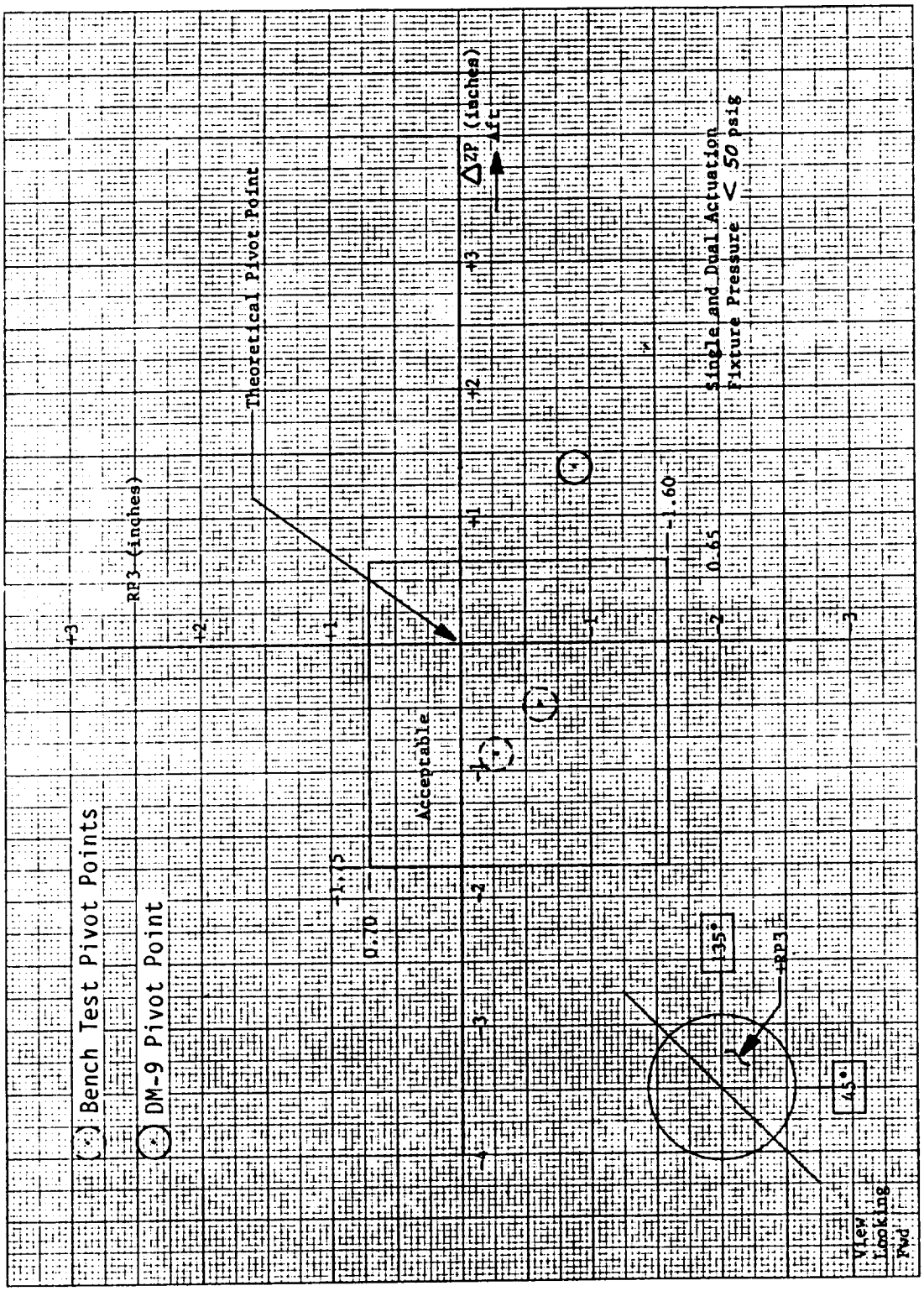

Figure 7.5-109. Low-Pressure Pivot Point Envelope

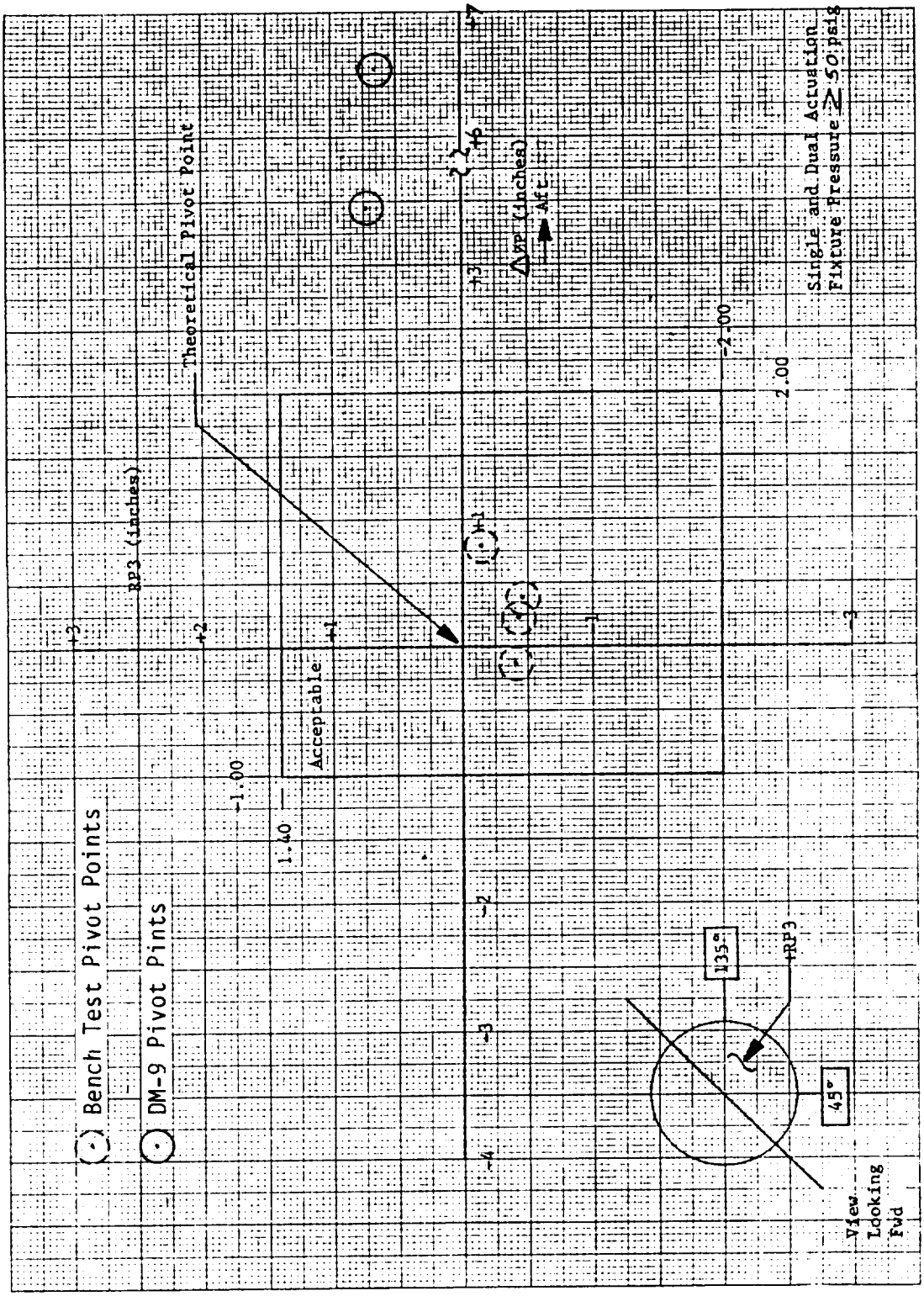

Figure 7.5-110. High-Pressure Pivot Point Envelope

Table 7.5-7. Nozzle Slew Rates for Step Events - DM-9

Event*	Dry Run/ Static	Time (Sec)	Vector Angle (Deg)	Maximum Slew Rate (Deg/Sec)	Average of Maximum Slew Rates (Deg/Sec)
10	Dry Run	0.664	1.094		
				}--> 13.00	
		0.684	1.354		}--> 12.28
				}--> 11.55	
		0.704	1.585		
10	Static	0.640	0.320		
				}--> 9.50	
		0.672	0.624		}--> 9.48
				}--> 9.47	
		0.704	0.927		
12	Dry Run	4.664	2.137		
				}--> 12.80	
		4.684	1.881		}--> 13.10
				}--> 13.40	
		4.704	1.613		
12	Static	4.640	2.059		
				}--> 12.19	
		4.672	1.669		}--> 11.05
				}--> 9.91	
		4.704	1.352		
22	Dry Run	60.164	1.062		
				}--> 14.10	
		60.184	1.344		}--> 13.20
				}--> 12.30	
		60.204	1.590		
22	Static	60.224	0.801		
				}--> 12.22	
		60.256	1.192		}--> 10.84
				}--> 9.47	
		60.288	1.495		
24	Dry Run	63.164	2.933		
				}--> 15.85	
		63.184	2.616		}--> 14.30
				}--> 12.75	
		63.204	2.361		
24	Static	63.168	2.369		
				}--> 12.84	
		63.200	1.958		}--> 11.86
				}--> 10.88	
		63.232	1.610		

Table 7.5-7. Nozzle Slew Rates for Step Events - DM-9 (cont)

Event*	Dry Run/ Static	Time (Sec)	Vector Angle (Deg)	Maximum Slew Rate (Deg/Sec)	Average of Maximum Slew Rates (Deg/Sec)
26	Dry Run	66.184	-0.902		
				}--> 14.40	
		66.204	-0.614		}--> 13.27
				}--> 12.15	
		66.224	-0.371		
26	Static	66.144	-2.900		
				}--> 13.75	
		66.176	-2.460		}--> 11.78
				}--> 9.81	
		66.208	-2.146		
28	Dry Run	69.164	2.754		
				}--> 15.80	
		69.184	2.438		}--> 14.60
				}--> 13.40	
		69.204	2.170		
28	Static	69.152	2.439		
				}--> 14.59	
		69.184	1.972		}--> 12.25
				}--> 9.91	
		69.216	1.655		

* Event	Description
10	Step to +2 Degrees yaw
12	Step to null
22	Step to +3 Degrees yaw
24	Step to -3 Degrees yaw
26	Step to +3 Degrees yaw
28	Step to null

Table 7.5-8. Nozzle Angular Acceleration for Step Events - DM-9

Event*	Dry Run/ Static	Time (Sec)	Vector Angle (Deg)	Slew Rate (Deg/Sec)	Maximum Angular Acceleration (Rad/Sec^2)
26	Dry Run	66.144	-1.269	}--> 7.10	
		66.164	-1.127	}-->	3.62
				}--> 11.25	
		66.184	-0.902		
26	Static	66.112	-2.959	}--> 1.84	
		66.144	-2.900	}-->	6.49
				}--> 13.75	
		66.176	-2.460		
28	Dry Run	69.144	2.948	}--> 9.70	
		69.164	2.754	}-->	5.32
				}--> 15.80	
		69.184	2.438		
28	Static	69.120	2.562	}--> 3.84	
		69.152	2.439	}-->	5.86
				}--> 14.59	
		69.184	1.972		

* Event	Description
10	Step to +2 Degrees yaw
12	Step to null
22	Step to +3 Degrees yaw
24	Step to -3 Degrees yaw
26	Step to +3 Degrees yaw
28	Step to null

Table 7.5-8. Nozzle Angular Acceleration for Step Events - DM-9 (cont)

Event*	Dry Run/ Static	Time (Sec)	Vector Angle (Deg)	Slew Rate (Deg/Sec)	Maximum Angular Acceleration (Rad/Sec^2)
10	Dry Run	0.644	0.948	)--> 7.30	
		0.664	1.094	)--> 13.00	)--> 4.97
		0.684	1.354		
10	Static	0.608	0.295	)--> 0.78	
		0.640	0.320	)--> 9.50	)--> 4.76
		0.672	0.624		
12	Dry Run	4.624	2.336	)--> 1.35	
		4.644	2.309	)--> 8.60	)--> 6.33
		4.664	2.137		
12	Static	4.608	2.079	)--> 0.63	
		4.640	2.059	)--> 12.19	)--> 6.31
		4.672	1.669		
22	Dry Run	60.144	0.906	)--> 7.80	
		60.164	1.062	)--> 14.10	)--> 5.50
		60.184	1.344		
22	Static	60.192	0.544	)--> 8.03	
		60.224	0.801	)--> 12.22	)--> 2.28
		60.256	1.192		
24	Dry Run	63.124	3.169	)--> 1.95	
		63.144	3.130	)--> 9.85	)--> 6.89
		63.164	2.933		
24	Static	63.104	2.713	)--> 0.22	
		63.136	2.706	)--> 10.53	)--> 5.62
		63.168	2.369		

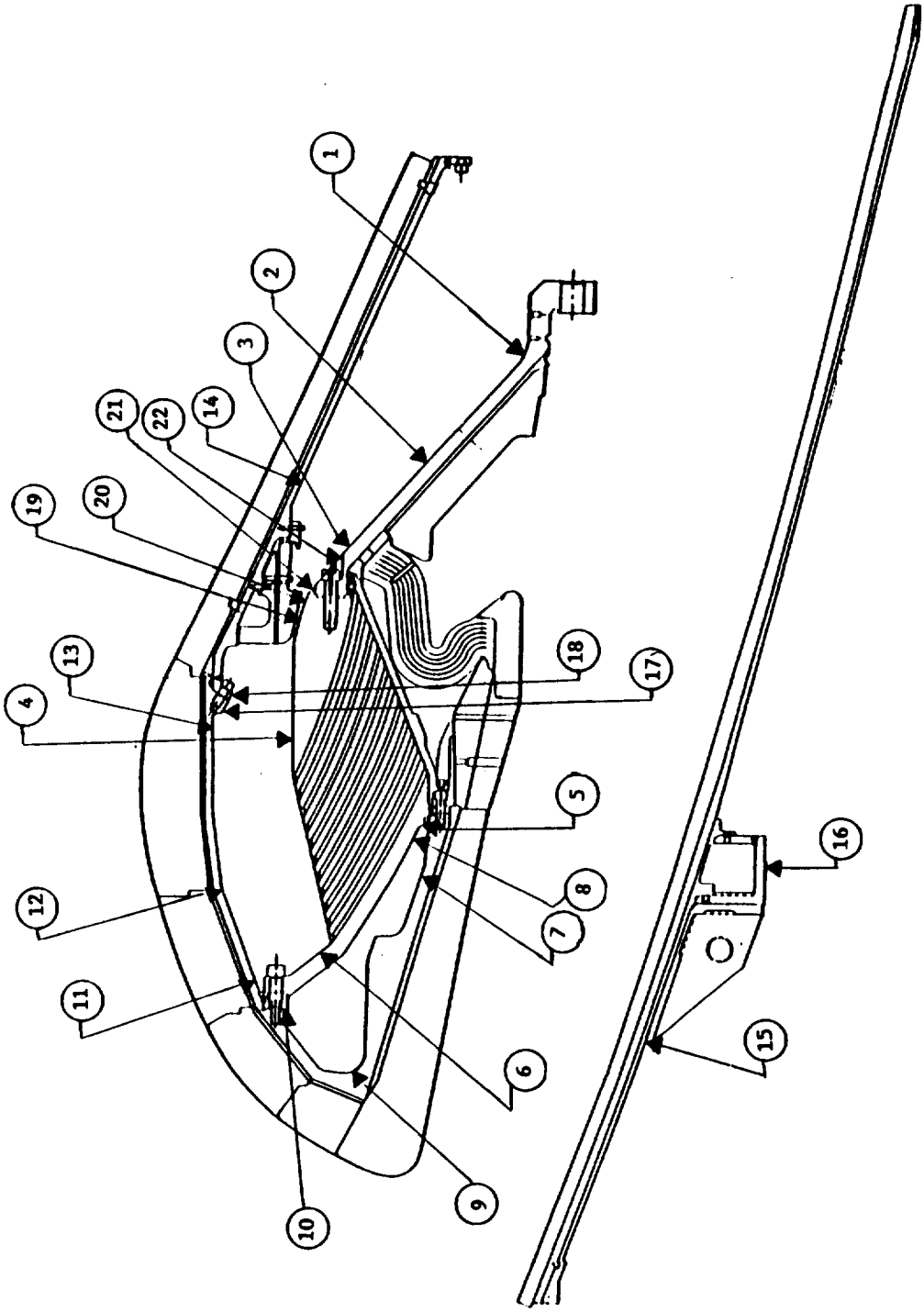

Figure 7.5-111. DM-9 Strain Gage Locations

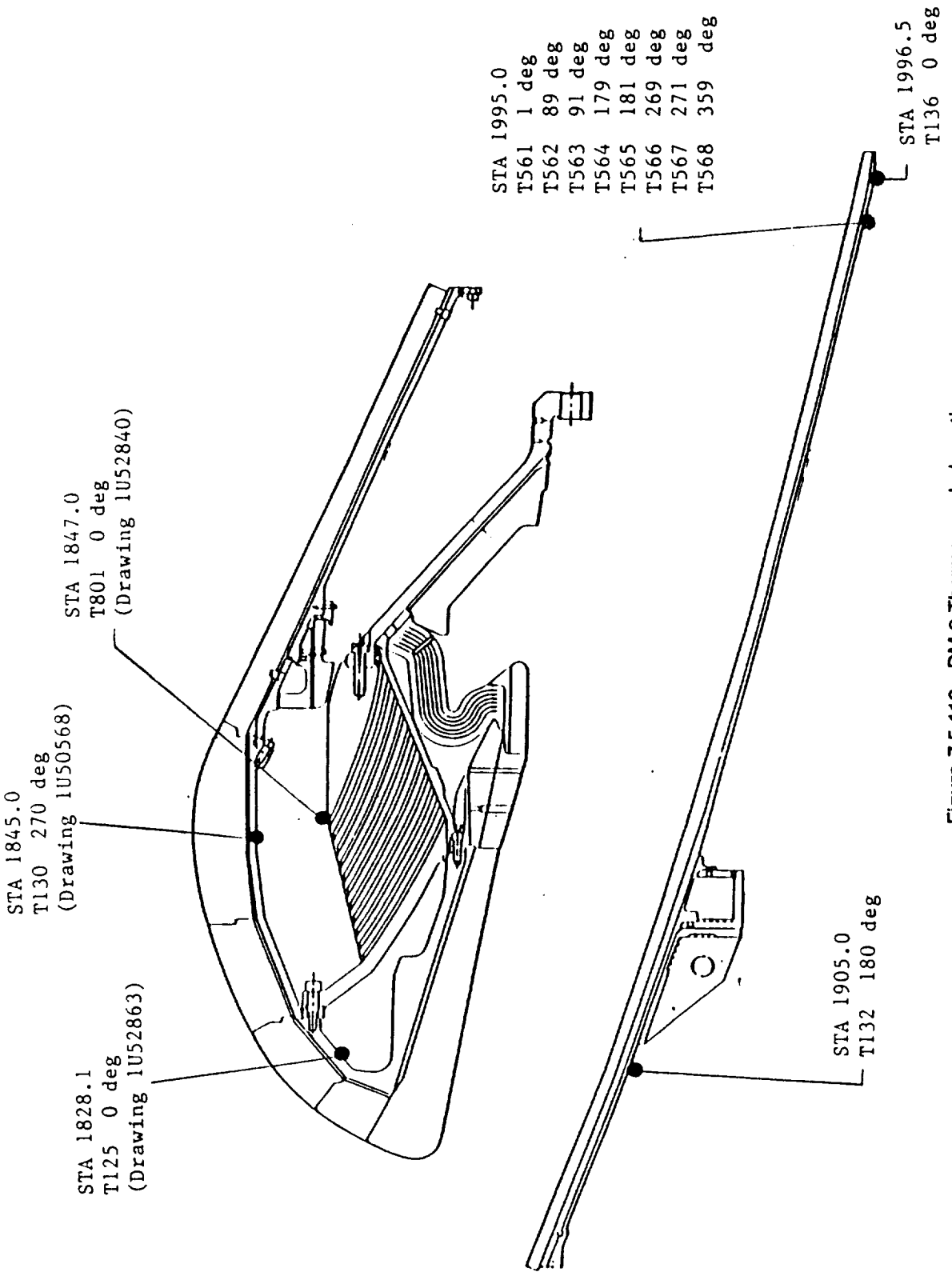

Figure 7.5-112. DM-9 Thermocouple Locations

Table 7.5-9. Nozzle Instrumentation

LOCATION # (Instrumentation Drawing #)	Gage Number	Gage Azimuth (Degrees)	Axial Station (Inches)	Gage Direction	Type of Gage
1 - FIXED HOUSING AFT END (1U75864)	R519	0	---	Meridional	Biaxial
	R520	0		Hoop	Biaxial
	R521	90		Meridional	Biaxial
	R522	90		Hoop	Biaxial
	R523	180		Meridional	Biaxial
	R524	180		Hoop	Biaxial
	R525	270		Meridional	Biaxial
	R526	270		Hoop	Biaxial
2 - FIXED HOUSING MID SECTION (1U75864)	R527	0	---	Meridional	Biaxial
	R528	0		Hoop	Biaxial
	R529	90		Meridional	Biaxial
	R530	90		Hoop	Biaxial
	R531	180		Meridional	Biaxial
	R532	180		Hoop	Biaxial
	R533	270		Meridional	Biaxial
	R534	270		Hoop	Biaxial
3 - FIXED HOUSING FWD SECTION (1U152861)	R535	0	1861.0	Meridional	Biaxial
	R536	0		Hoop	Biaxial
	R537	90		Meridional	Biaxial
	R538	90		Hoop	Biaxial
	S885	-	---	-	Girth
4 - AFT END RING FWD END (1U52480)	R284	90	1849.0	Meridional	Biaxial
	R283	90		Hoop	Biaxial
5 - Nose Inlet HSG AFT END (1U52863)	R766	90	1842.5	Meridional	Biaxial
	R765	90		Hoop	Biaxial
6 - FWD END RING FWD REGION (1U52840)	S439	90	1834.8	Meridional	Biaxial
	S437	90		Hoop	Biaxial
7 - NOSE INLET HSG AFT END (1U52863)	S268	90	1839.0	Meridional	Biaxial
	S267	90		Hoop	Biaxial
8 - FWD END RING AFT END	S276	90	1842.1	Meridional	Biaxial
(1U52480)	S275	90		Hoop	Biaxial
9 - NOSE INLET HSG FWD END (1U52863)	R260	90	1827.6	Meridional	Biaxial
	R259	90		Hoop	Biaxial
10 - NIH / THROAT JOINT REGION (1U52863)	S430	90	1829.2	Meridional	Biaxial
	S425	90		Hoop	Biaxial
11 - THROAT HSG FWD END (1U50568)	S454	90	1834.0	Meridional	Biaxial
	S452	90		Hoop	Biaxial
12 - THROAT HSG MID SECTION (1U50568)	R412	90	1839.0	Meridional	Biaxial
	R414	90		Hoop	Biaxial
13 - THROAT HSG AFT END (1U50568)	R404	90	1849.0	Meridional	Biaxial
	R403	90		Hoop	Biaxial
14 - FWD EXIT CONE (1U52839)	S484	90	1865.0	Meridional	Biaxial
	S482	90		Hoop	Biaxial
15 - AFT EXIT CONE (1U76123)	S778	90	1908.5	Meridional	Biaxial
	S777	90		Hoop	Biaxial
16 - COMPLIANCE RING (1U76123)	S259	90	1923.0	Meridional	Biaxial
	S258	90		Hoop	Biaxial
17 - THROAT HSG/ FWD EXIT CONE JOINT REGION (1U50568)	S369	90	1850.45	Hoop	Long Wire Hoop (24")
	S375	270		Hoop	Long Wire Hoop (24")
18 - THROAT HSG/ AFT END RING JOINT REGION (1U52839)	S370	90	1850.95	Hoop	Long Wire Hoop (24")
	S376	270		Hoop	Long Wire Hoop (24")
19 - AFT END RING AFT END (1U52840)	S371	90	1856.45	Hoop	Long Wire Hoop (24")
	S377	270		Hoop	Long Wire Hoop (24")
20 - AFT END RING AFT END (1U52862)	S373	90	1857.45	Hoop	Long Wire Hoop (24")
	S379	270		Hoop	Long Wire Hoop (24")
21 - FIXED HSG/ AFT END RING JOINT REGION (1U52862)	S373	90	1857.90	Hoop	Long Wire Hoop (24")
	S379	270		Hoop	Long Wire Hoop (24")
22 - FIXED HSG/ AFT END RING JOINT REGION (1U52862)	S374	90	1860.15	Hoop	Long Wire Hoop (24")
	S380	270		Hoop	Long Wire Hoop (24")

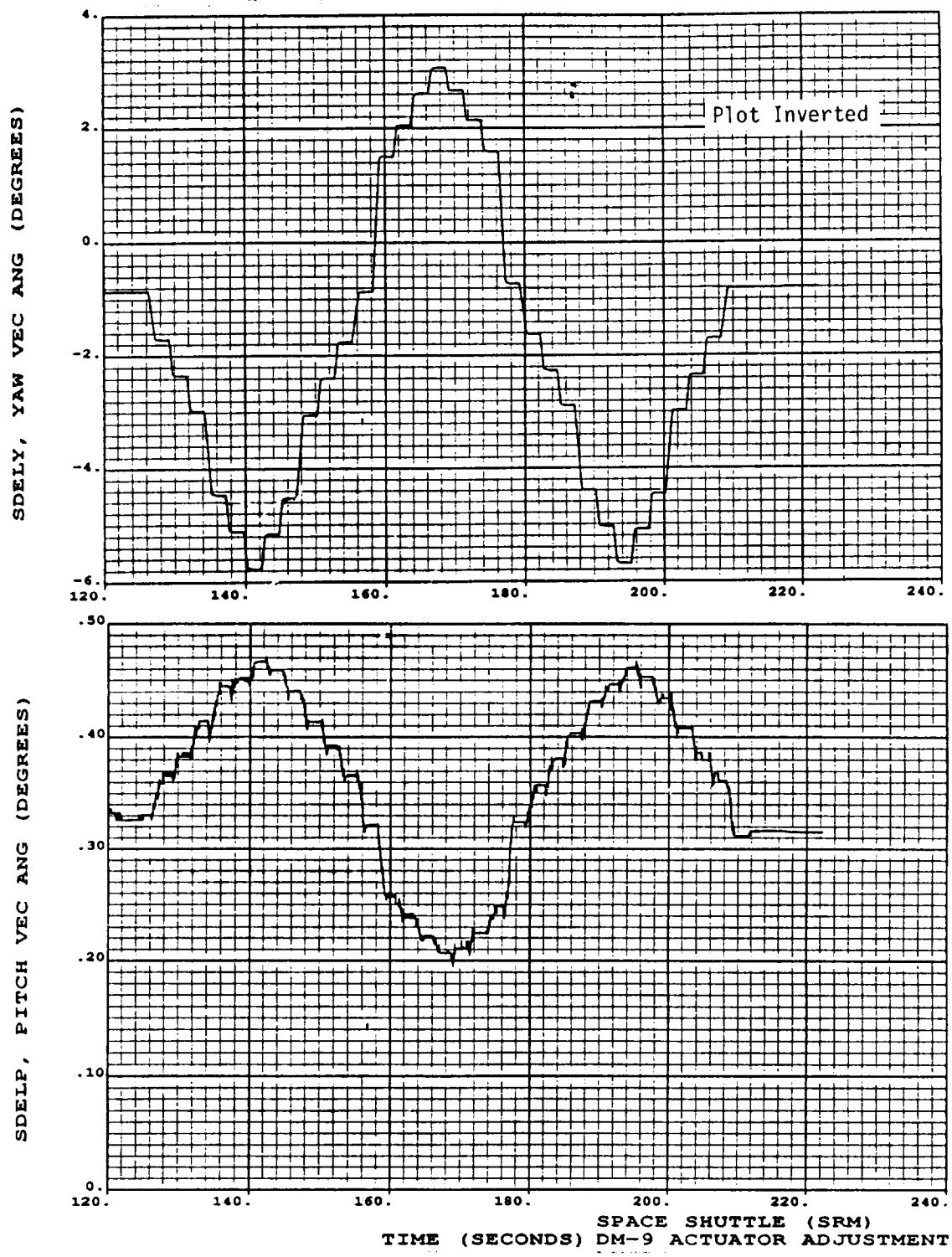

Figure 7.5-113. DM-9 Actuator Adjustment Nozzle Vector Angle

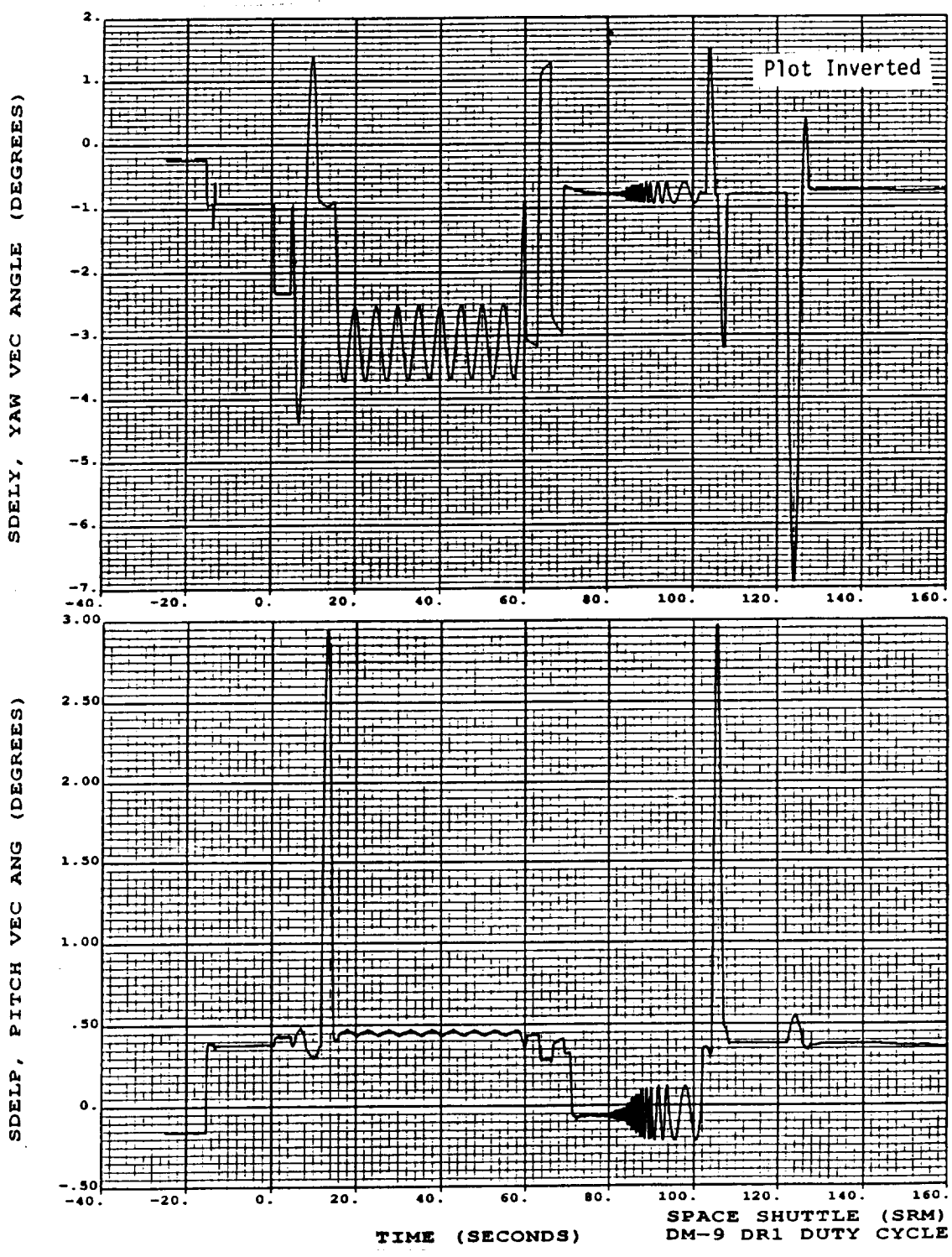

Figure 7.5-114. DM-9 Dry Run With Hydrazine

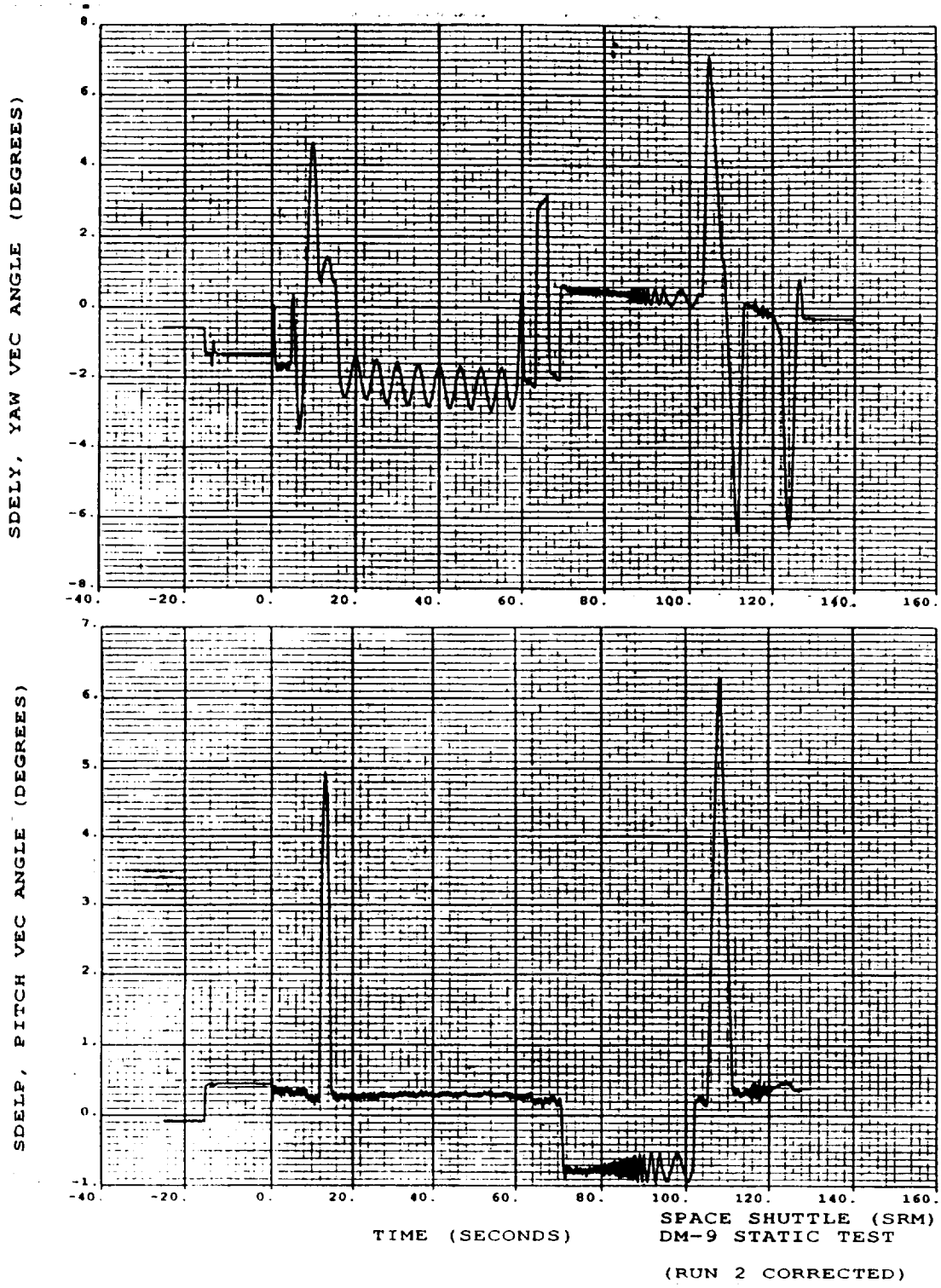

Figure 7.5-115. DM-9 Static Test Duty Cycle Nozzle Versus Vector Angle

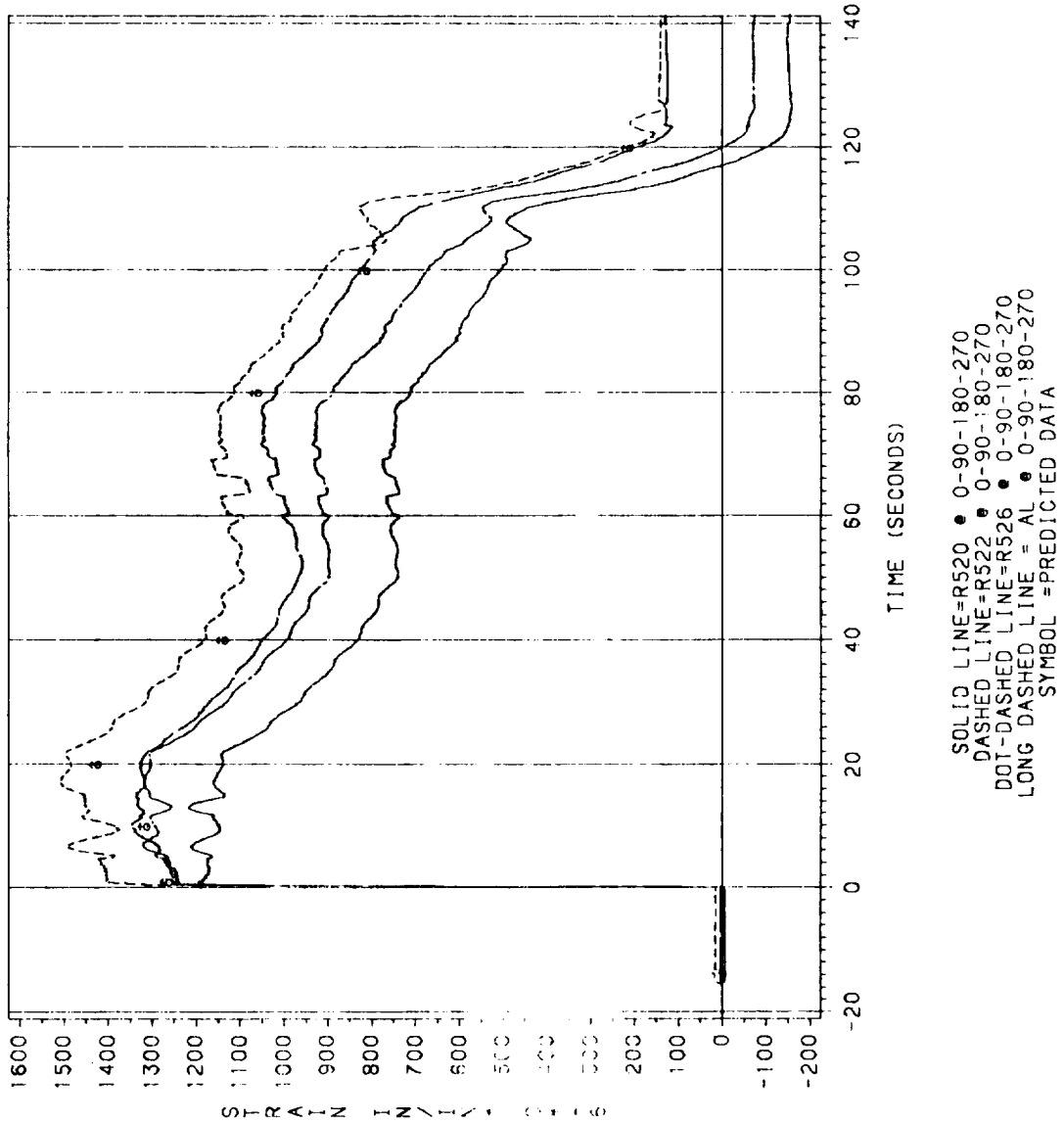

Figure 7.5-116. DM-9 Fixed Housing (hoop strain), Location 1

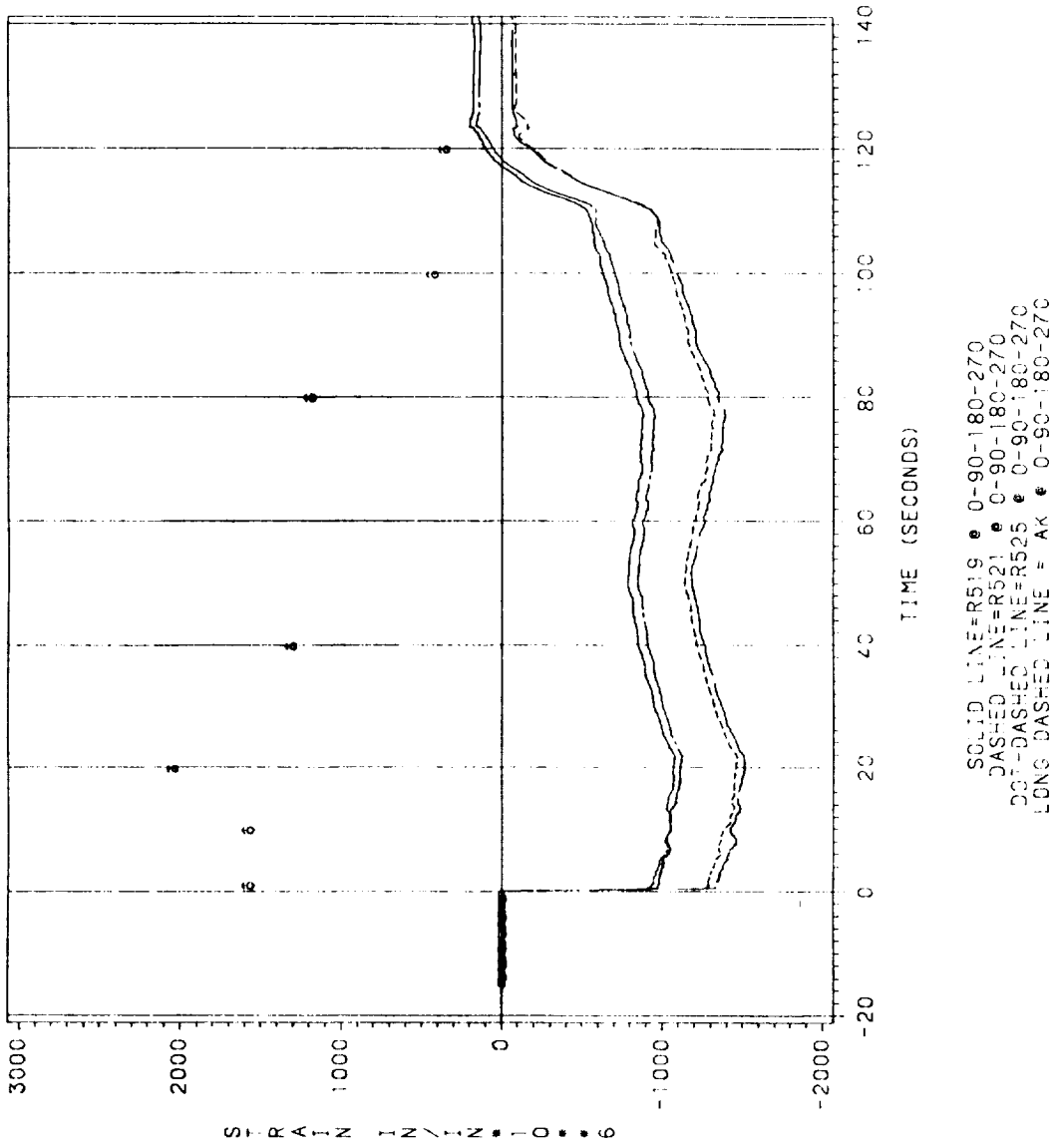

Figure 7.5-117. DM-9 Fixed Housing (meridional strain), Location 1

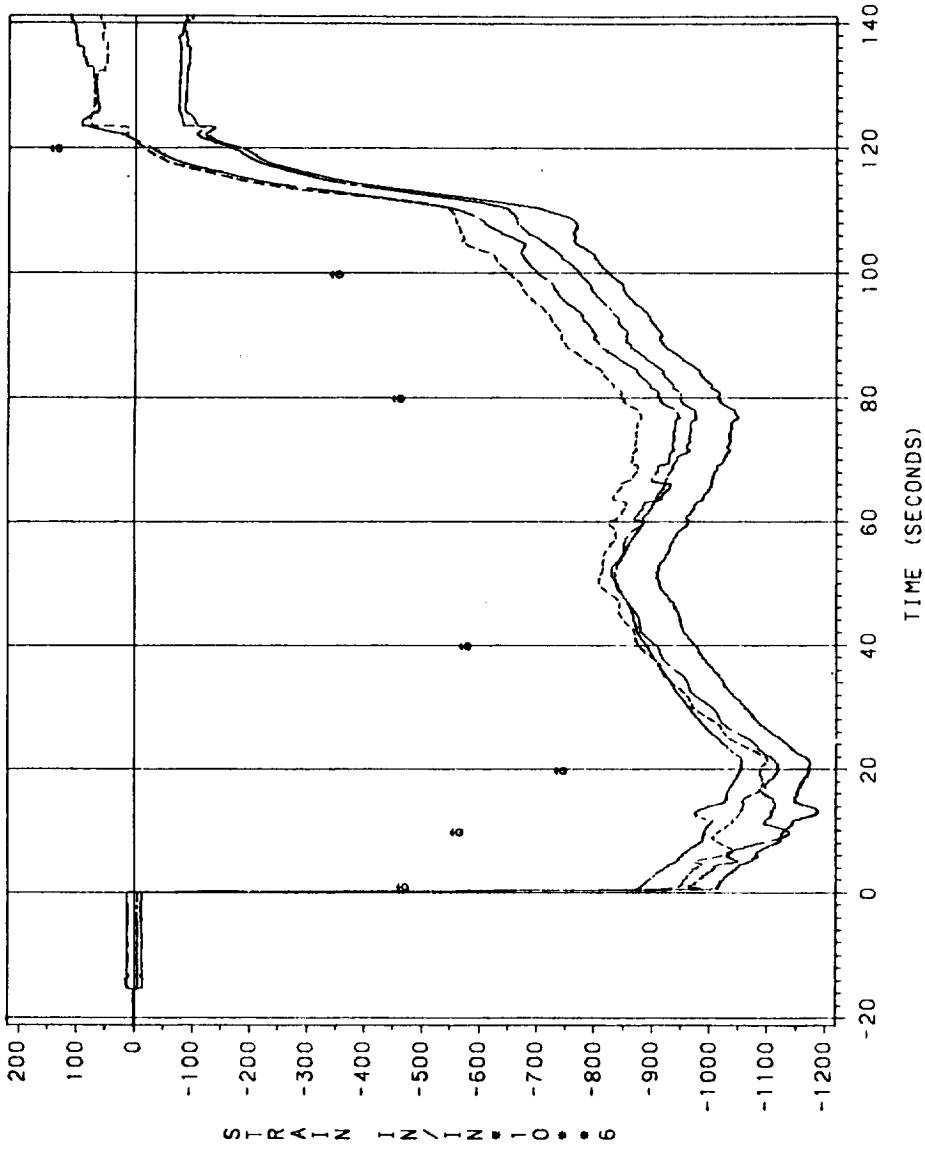

Figure 7.5-118. DM-9 Fixed Housing (hoop strain), Location 2

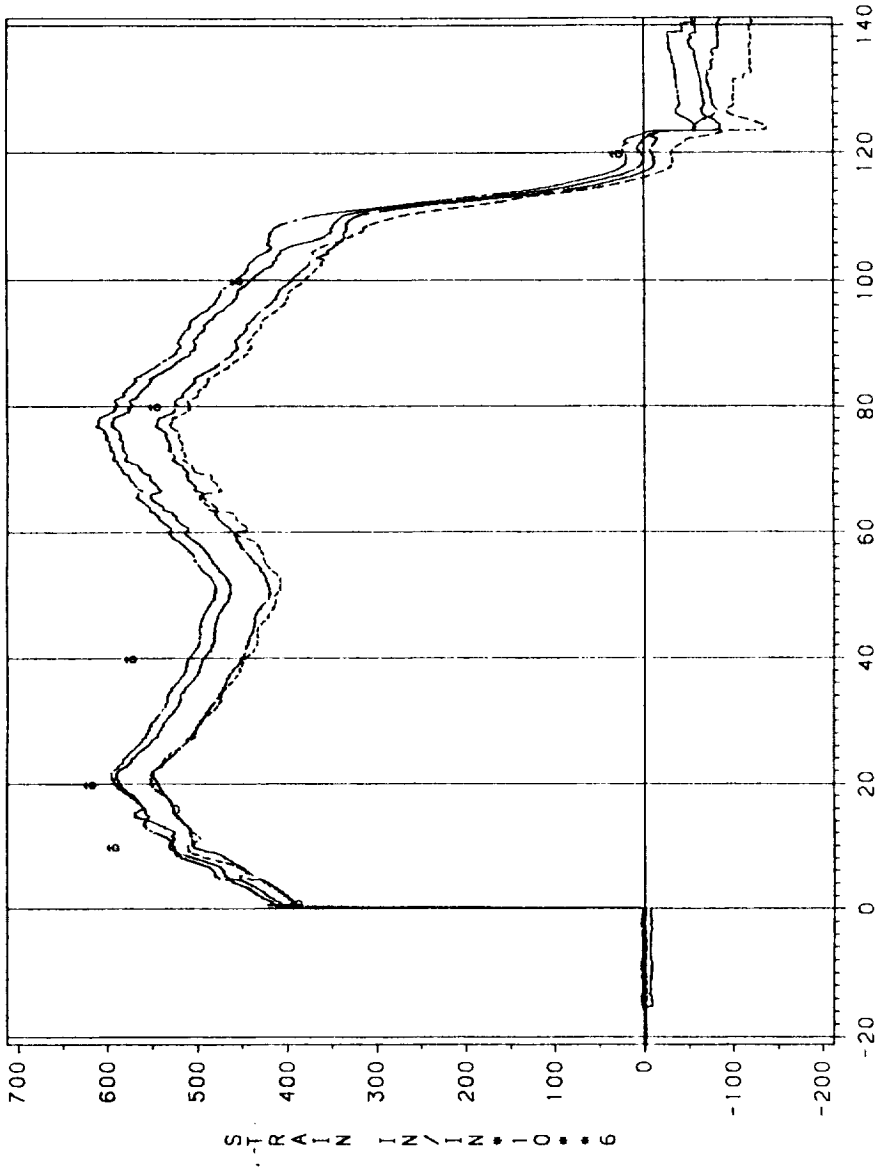

Figure 7.5-119. DM-9 Fixed Housing (meridional strain), Location 2

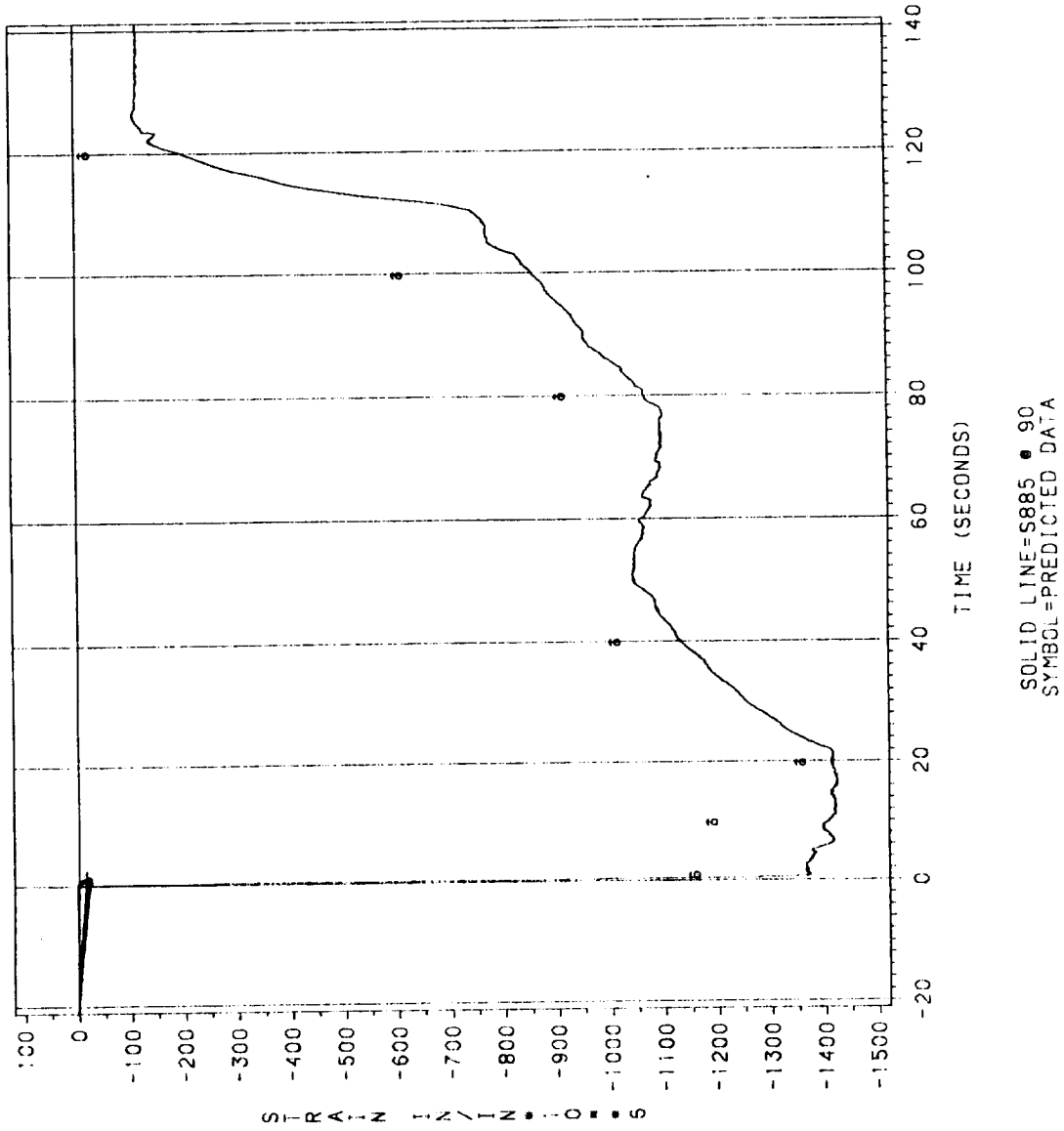

Figure 7.5-120. DM-9 Fixed Housing (hoop strain), Location 3

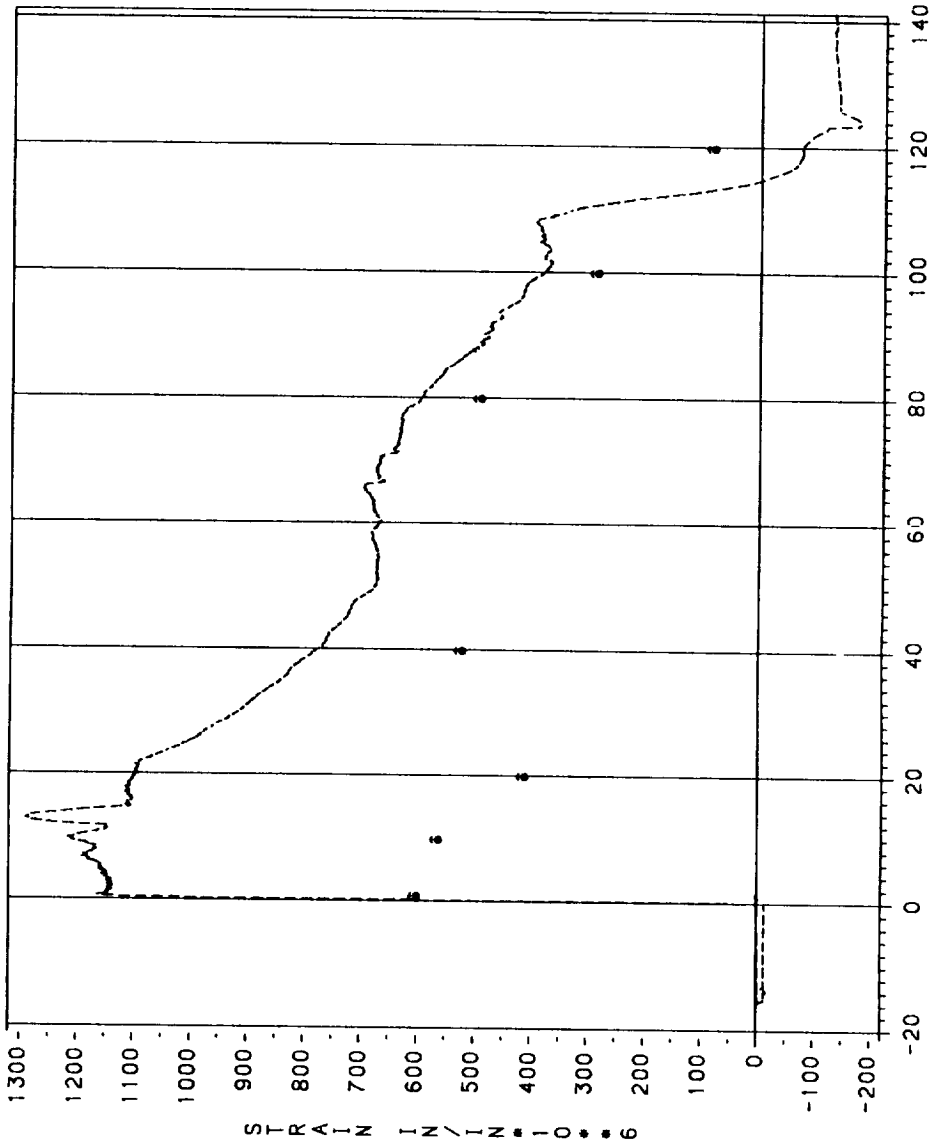

Figure 7.5-121. DM-9 Fixed Housing (meridional strain), Location 3

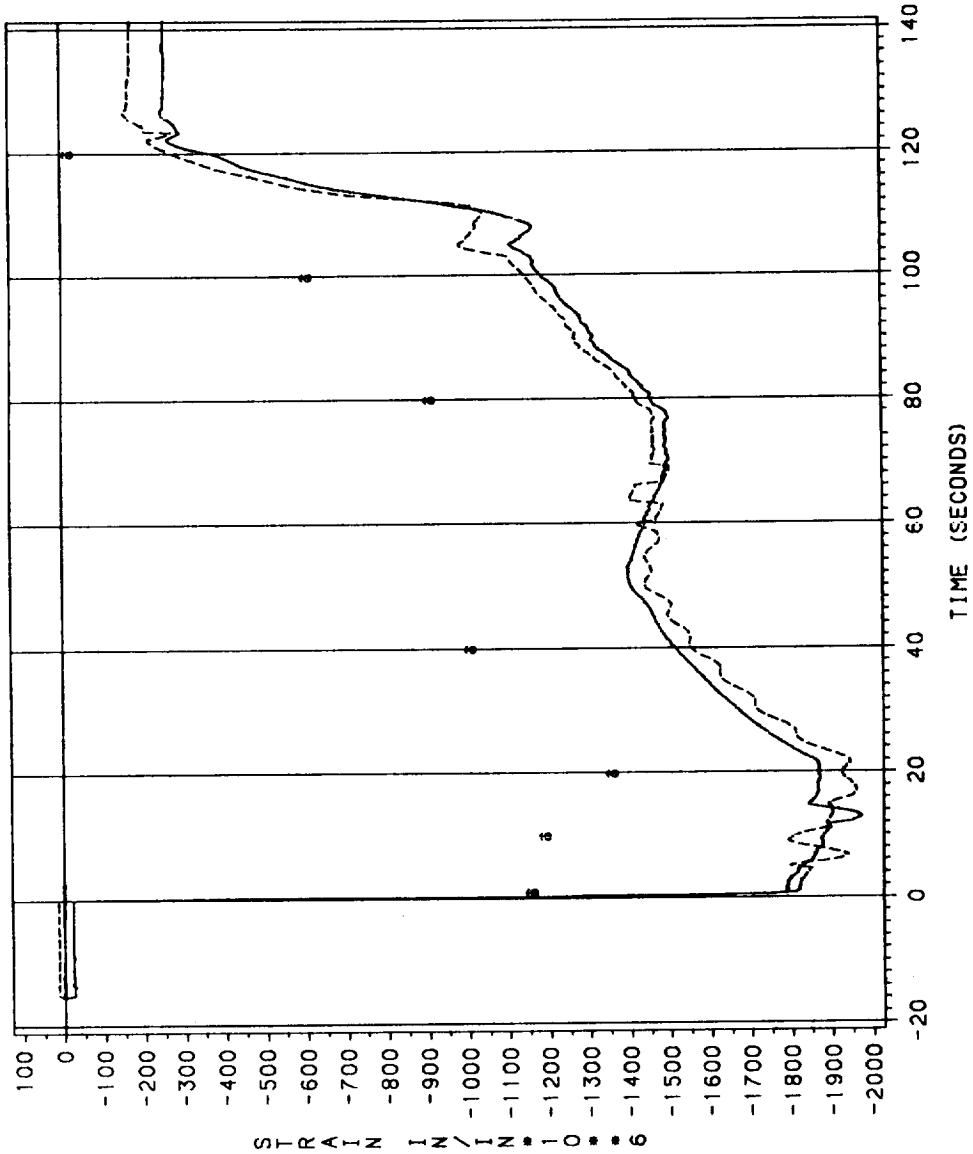

Figure 7.5-122. DM-9 Fixed Housing (girth gage), Location 3

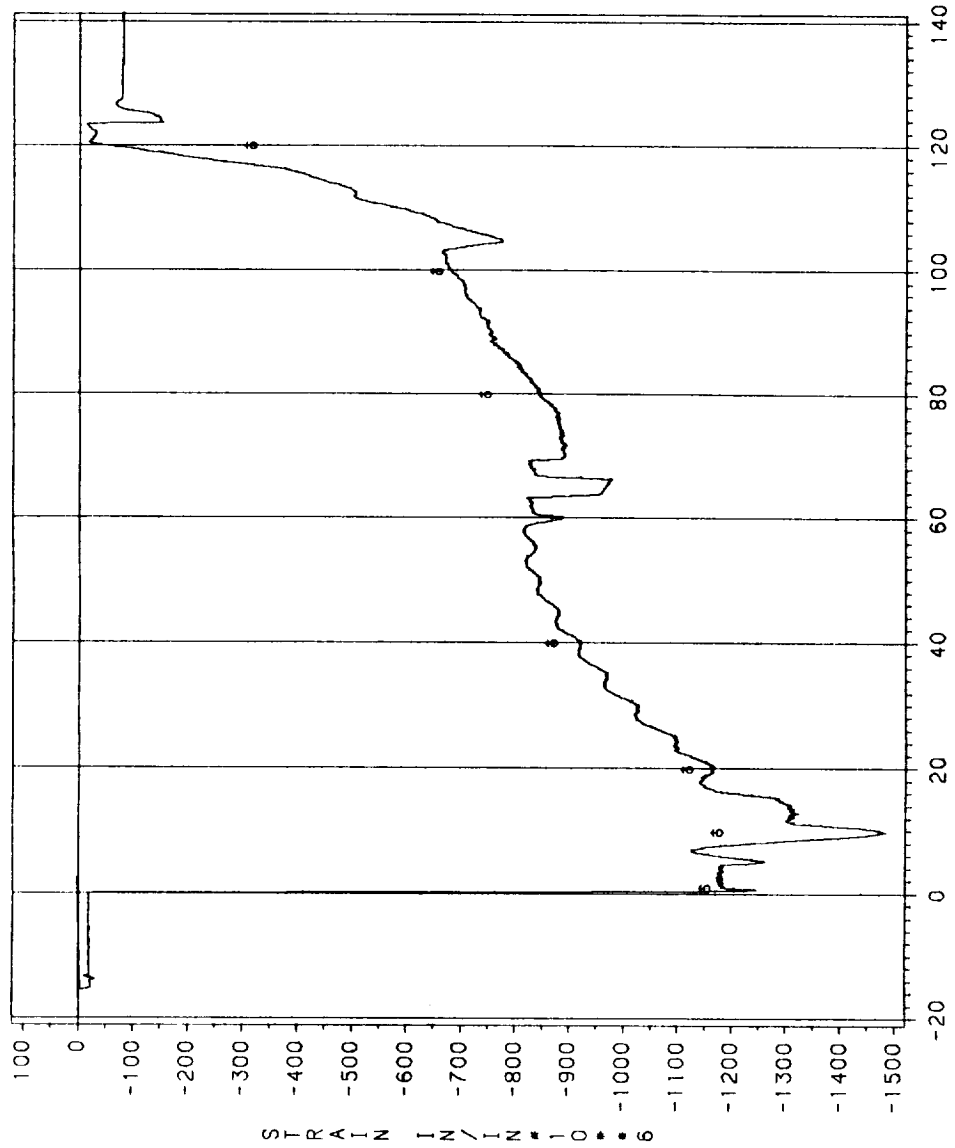

Figure 7.5-123. DM-9 Aft End Ring (hoop strain), Location 4

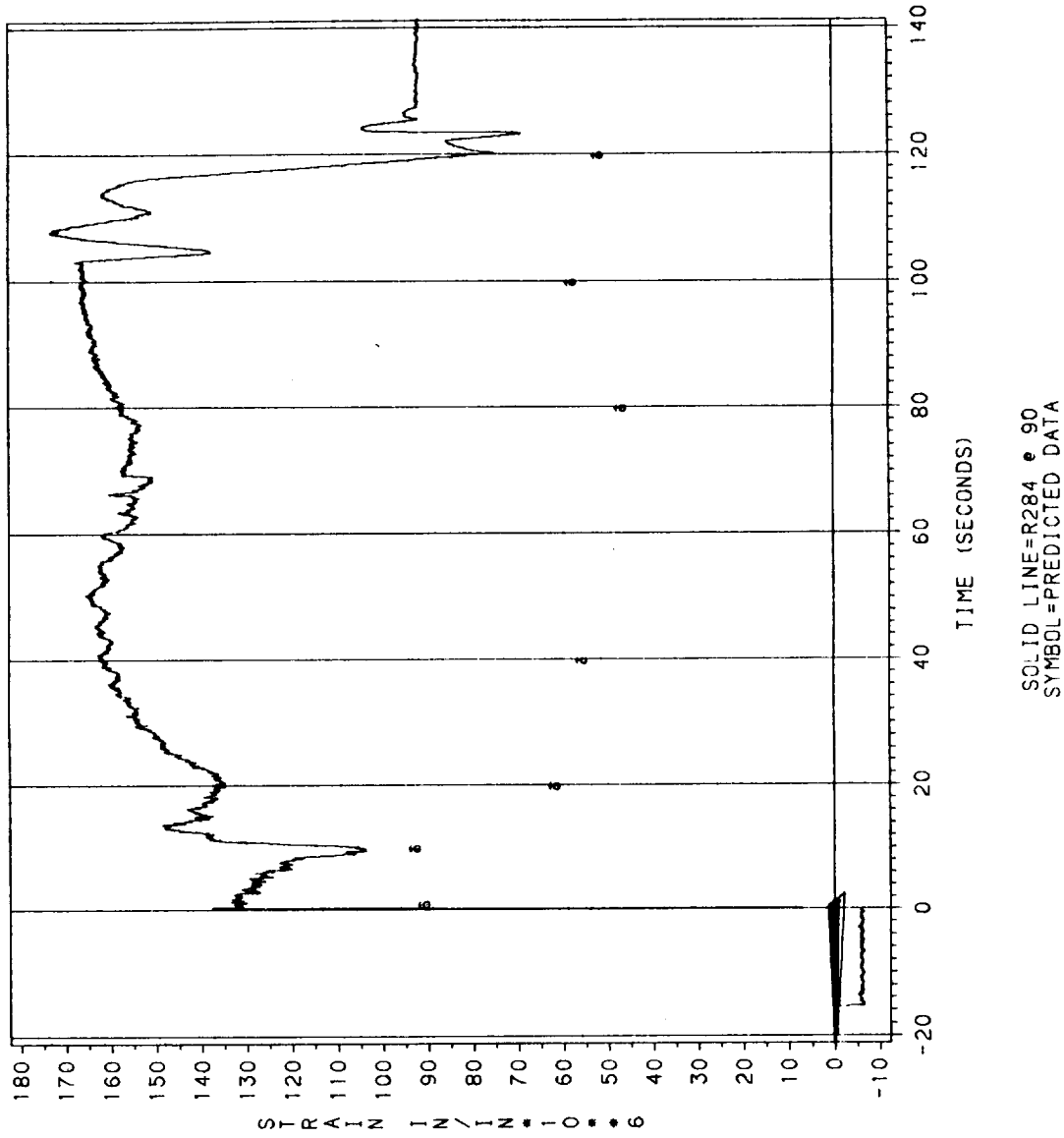

Figure 7.5-124. DM-9 Aft End Ring (meridional strain), Location 4

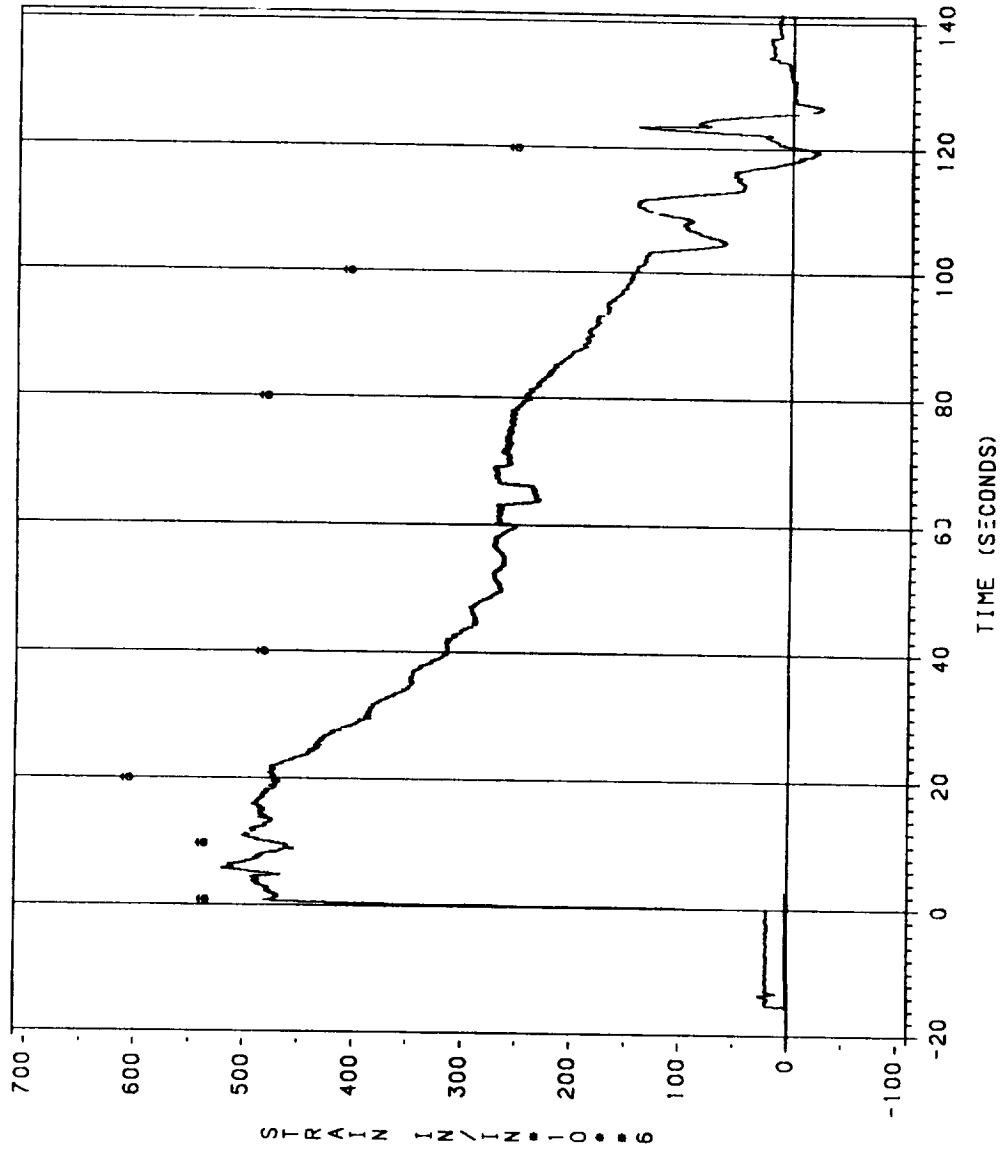

Figure 7.5-125. DM-9 Nose Inlet Housing (hoop strain), Location 5

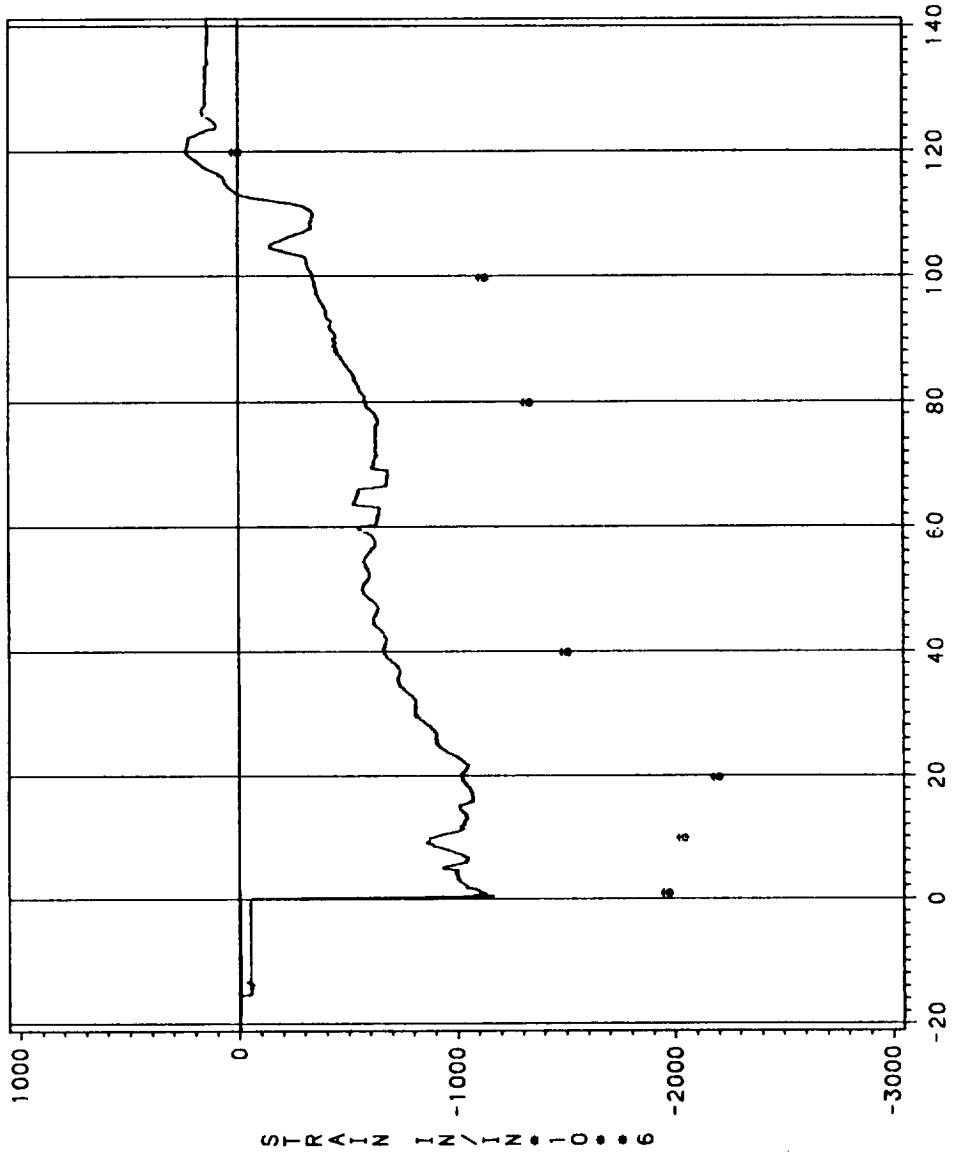

Figure 7.5-126. DM-9 Nose Inlet Housing (meridional strain), Location 5

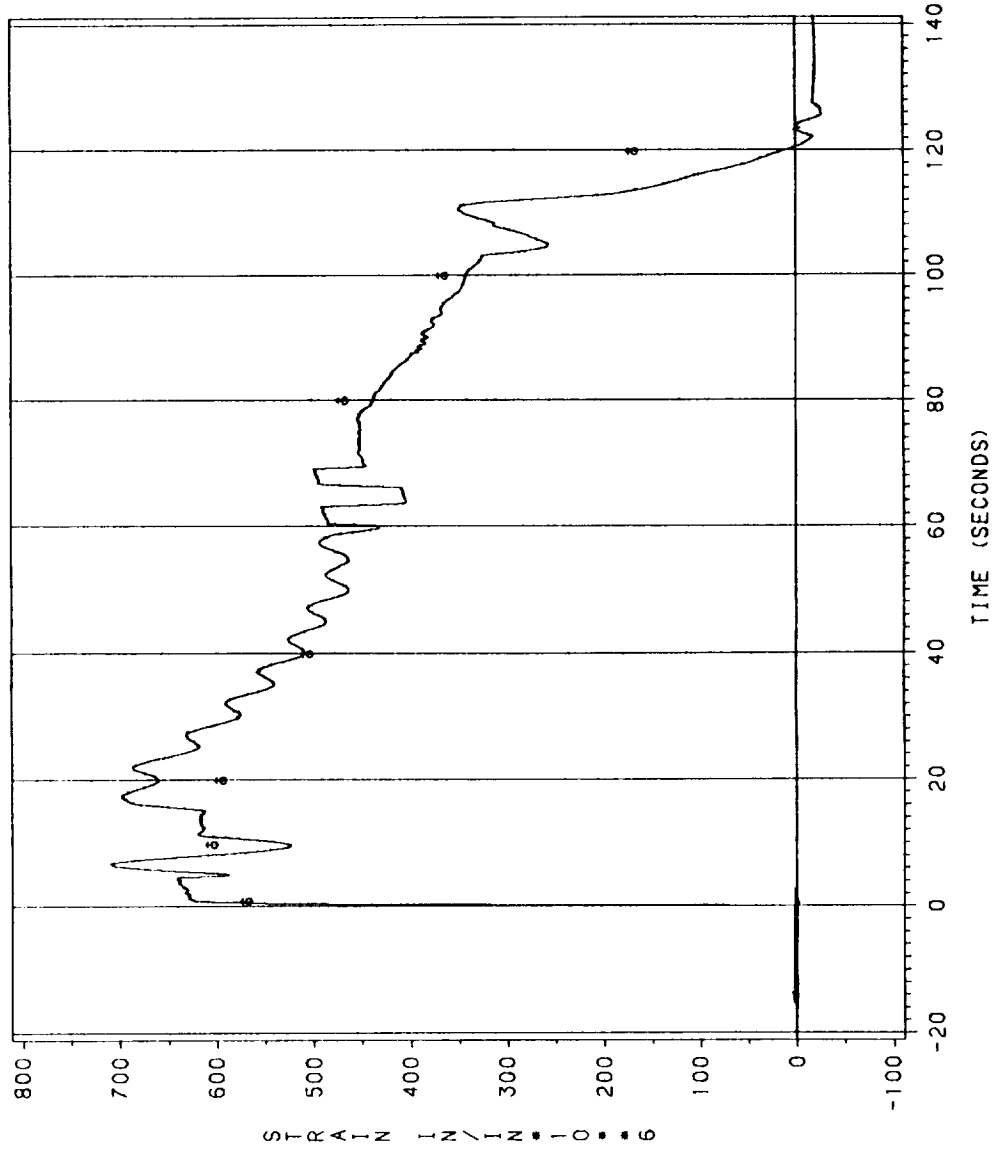

Figure 7.5-127. DM-9 Forward End Ring (hoop strain), Location 6

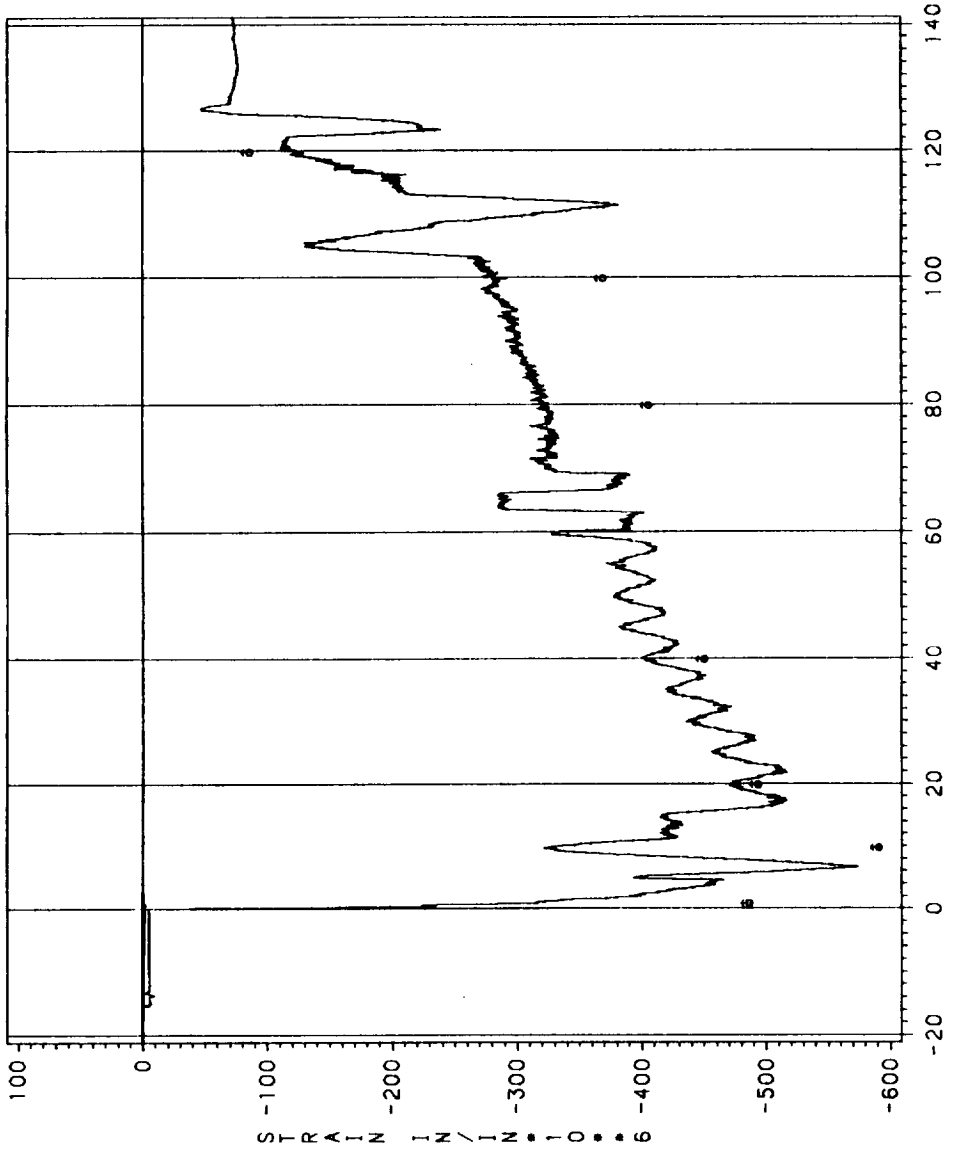

Figure 7.5-128. DM-9 Forward End Ring (meridional strain), Location 6

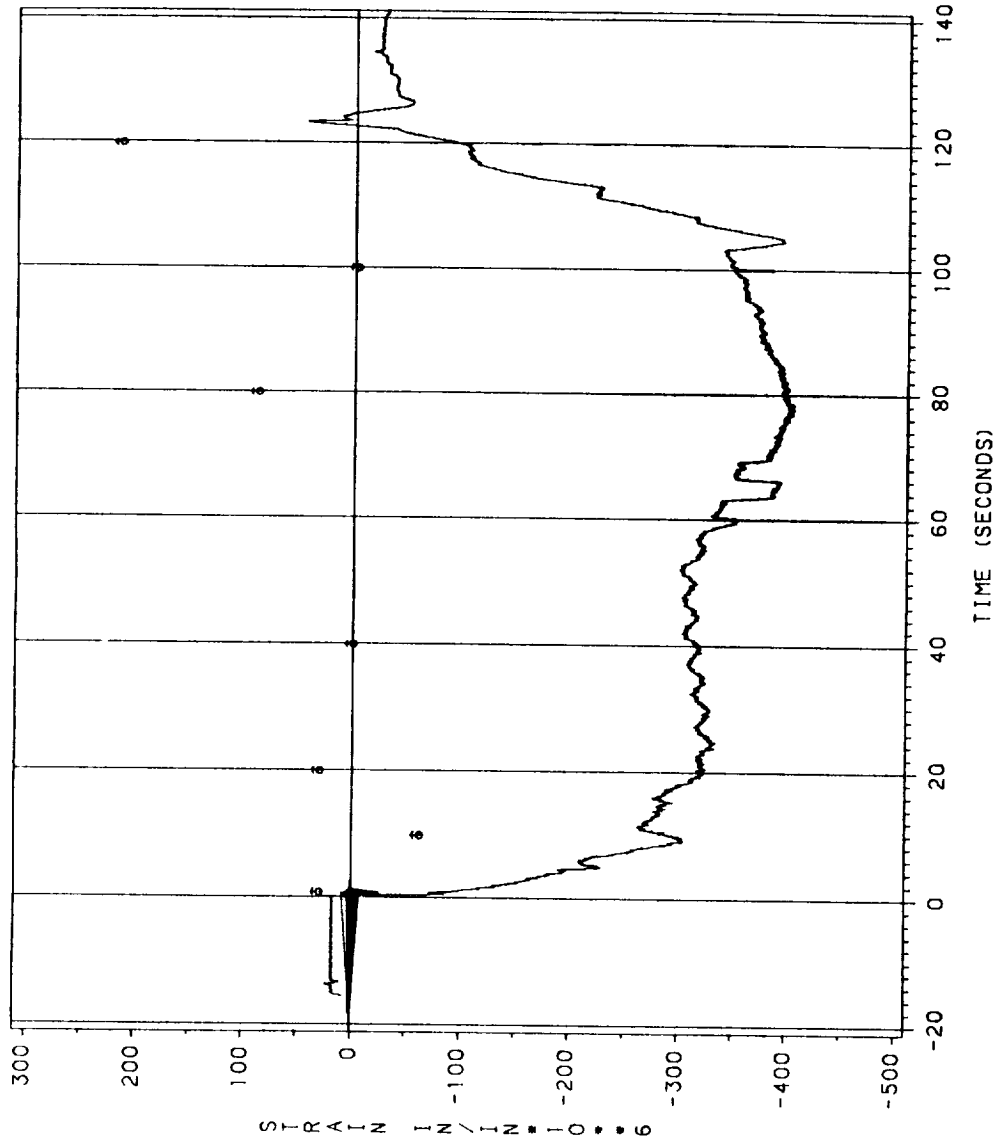

Figure 7.5-129. DM-9 Nose Inlet Housing (hoop strain), Location 7

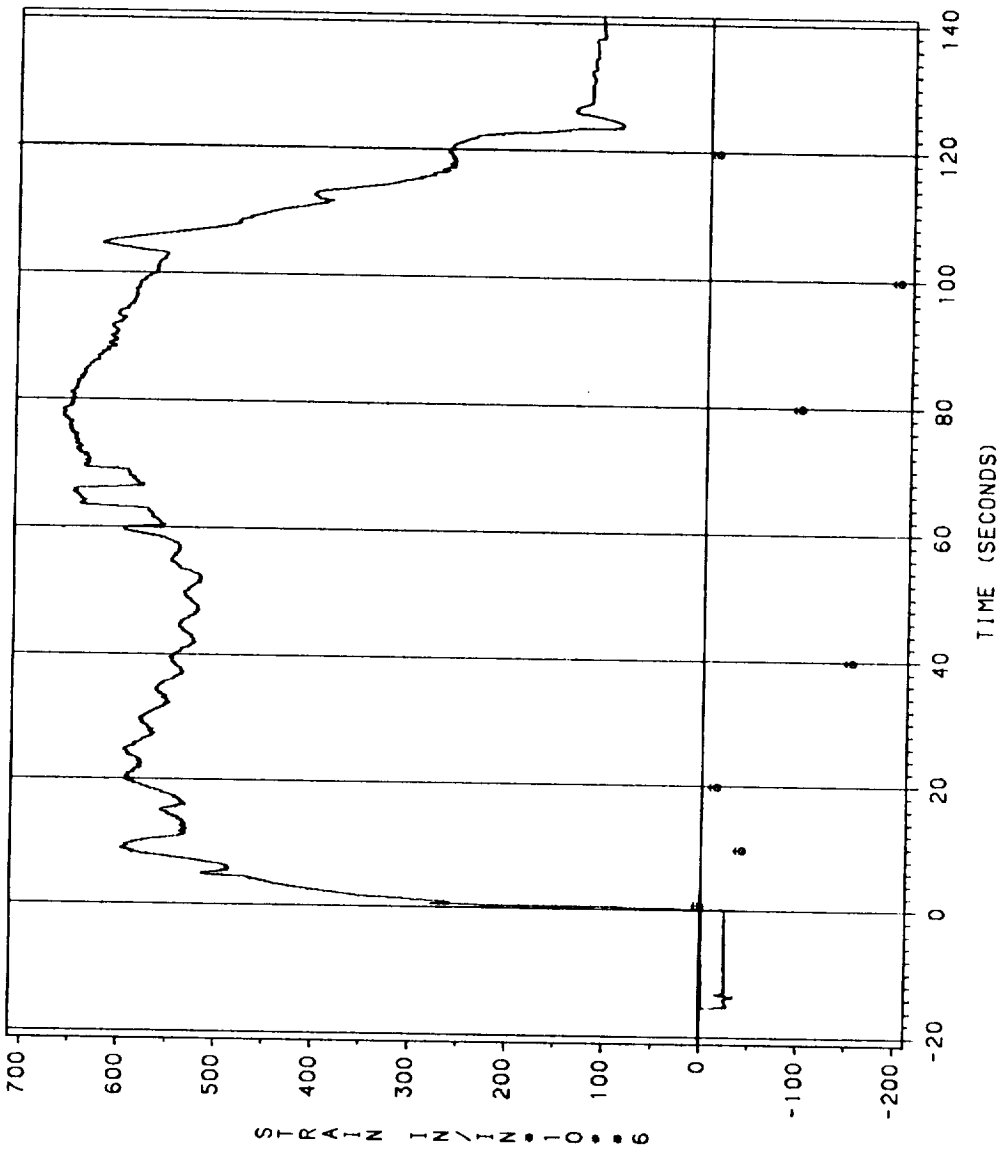

Figure 7.5-130. DM-9 Nose Inlet Housing (meridional strain), Location 7

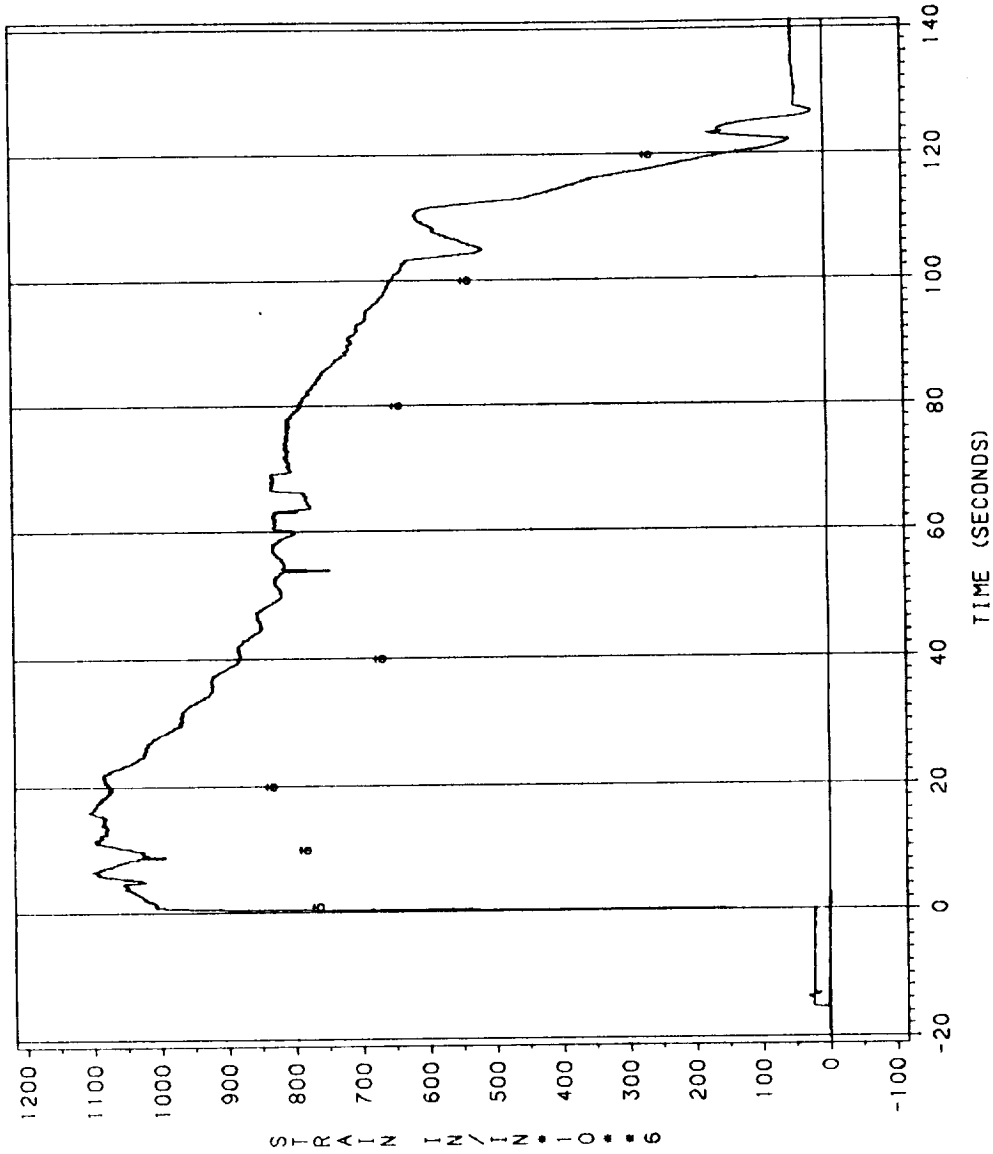

Figure 7.5-131. DM-9 Forward End Ring (hoop strain), Location 8

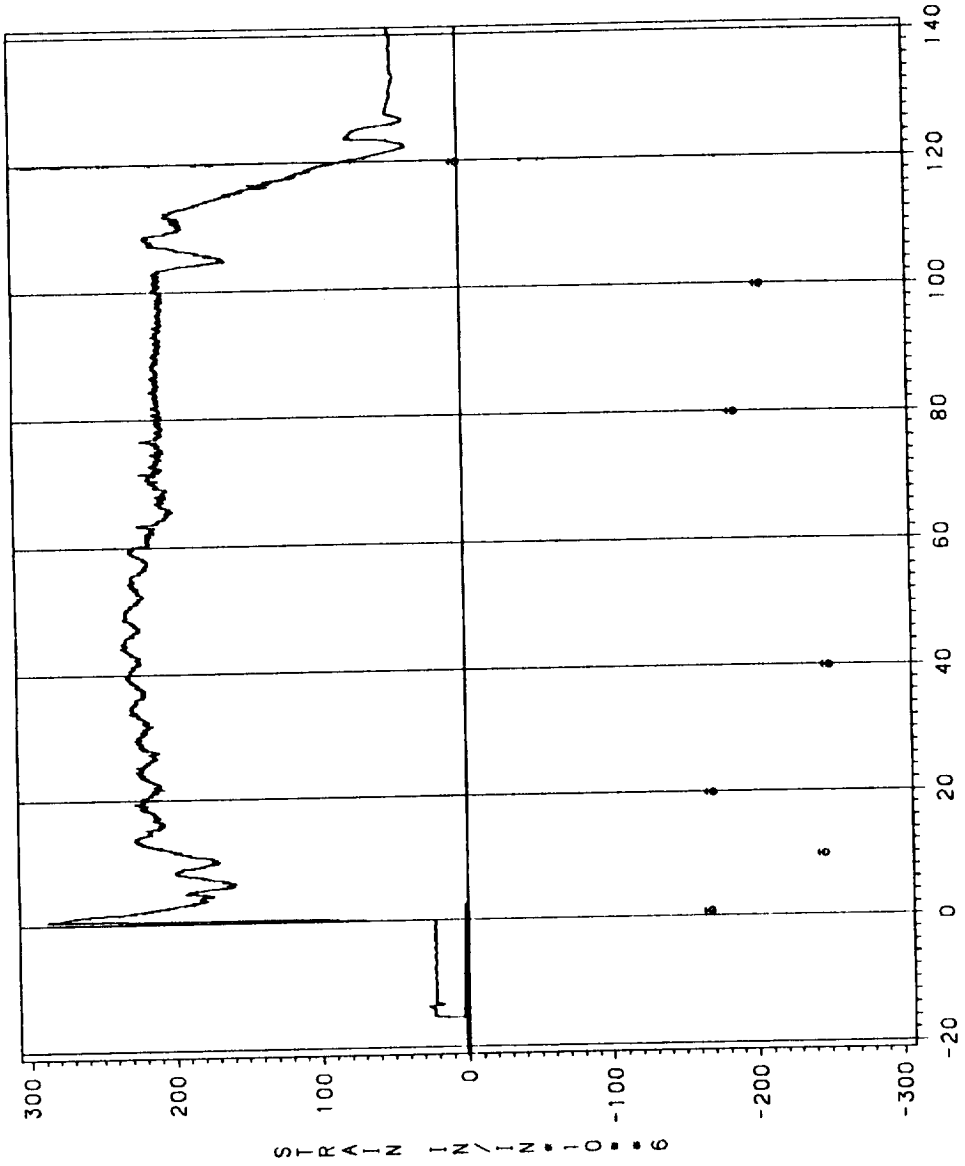

Figure 7.5-132. DM-9 Forward End Ring (meridional strain), Location 8

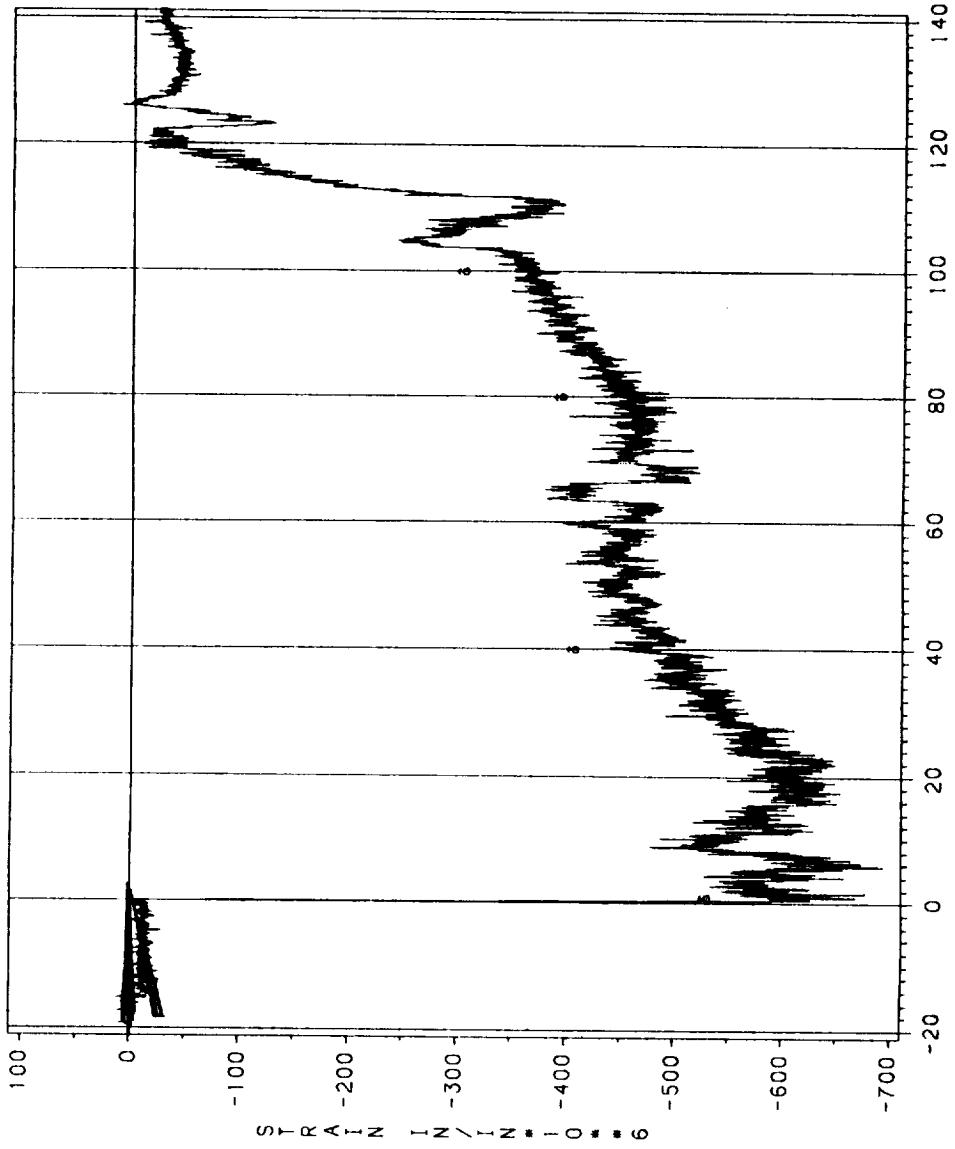

Figure 7.5-133. DM-9 Nose Inlet Housing (hoop strain), Location 9

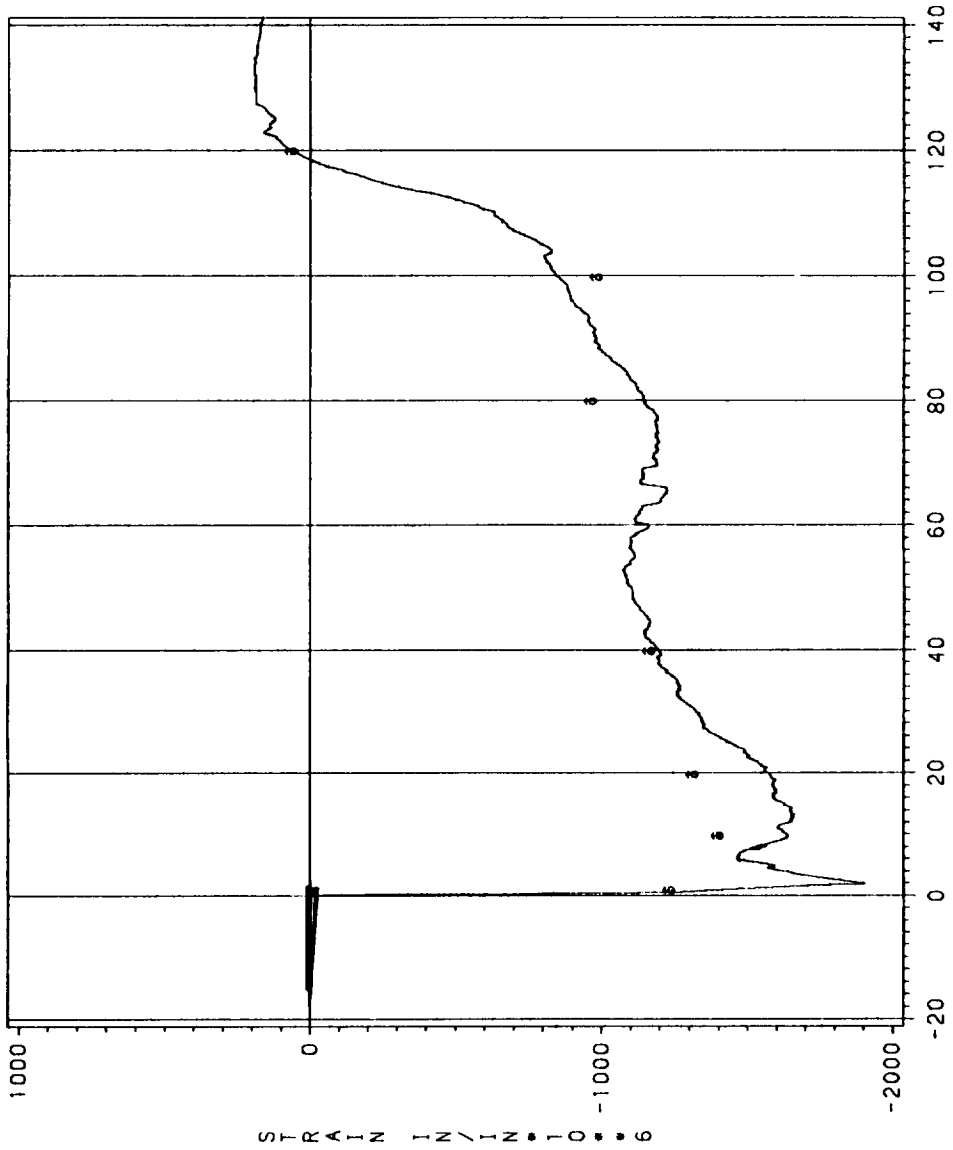

Figure 7.5-134. DM-9 Nose Inlet Housing (meridional strain), Location 9

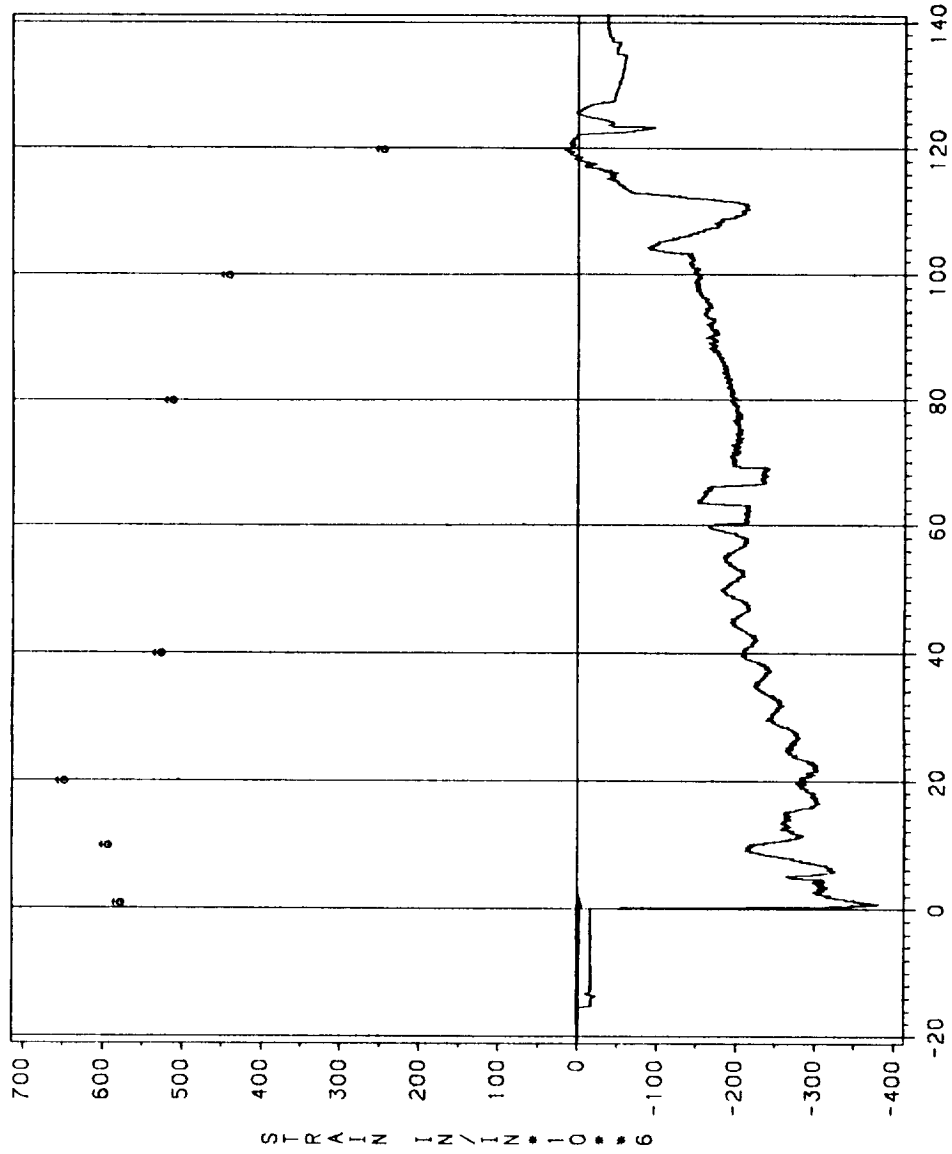

Figure 7.5-135. DM-9 Nose Inlet Housing (hoop strain), Location 10

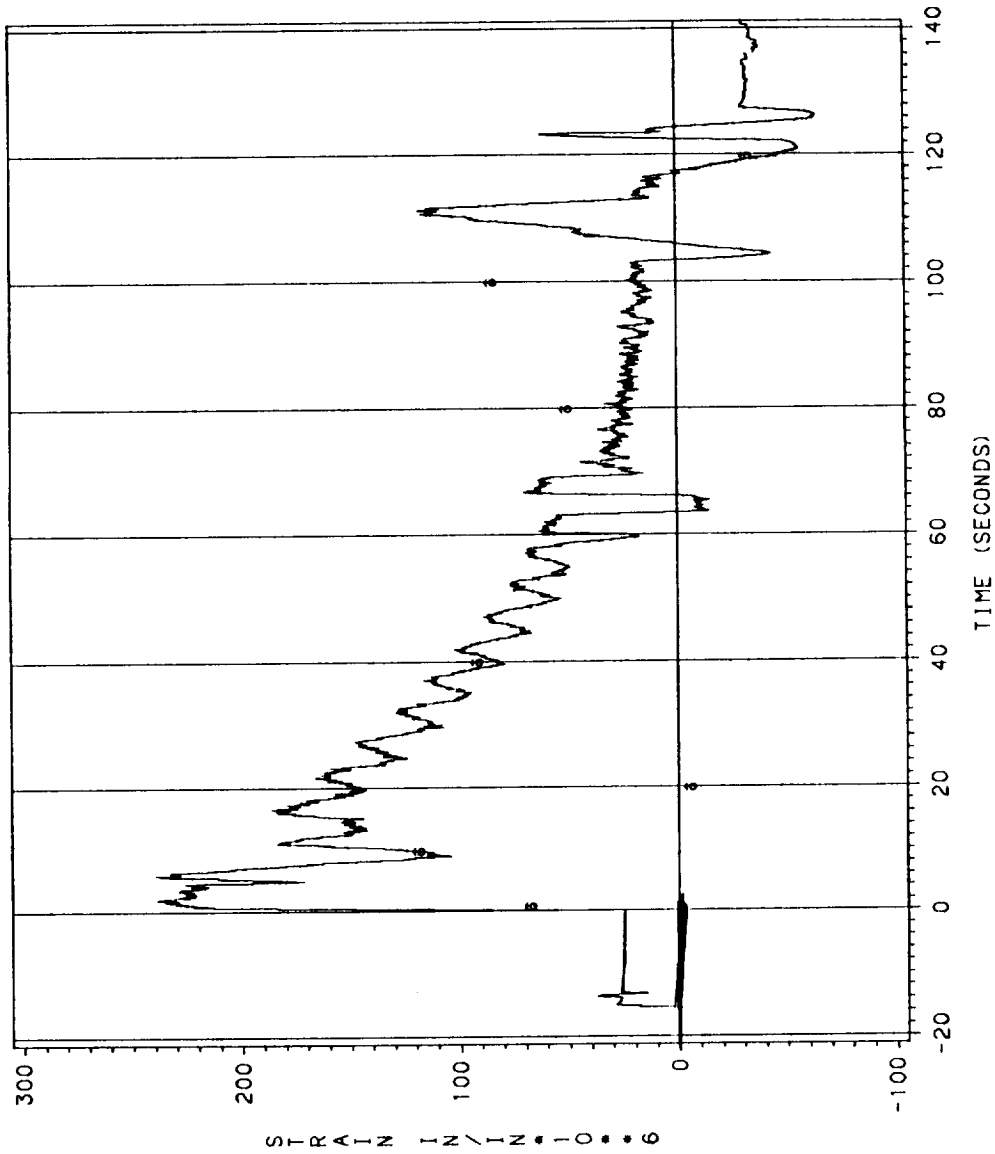

Figure 7.5-136. DM-9 Nose Inlet Housing (meridional strain), Location 10

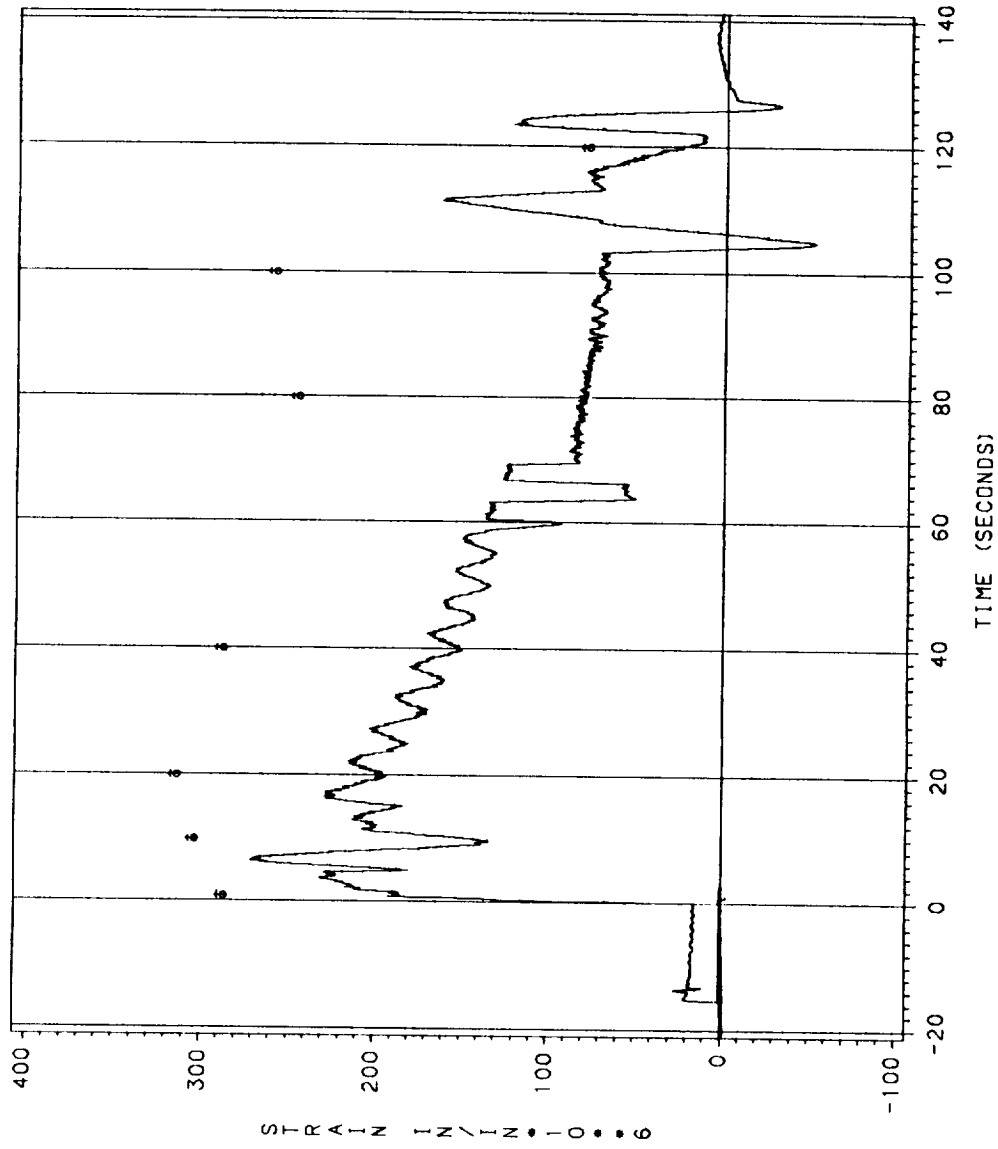

Figure 7.5-137. DM-9 Throat Housing (hoop strain), Location 11

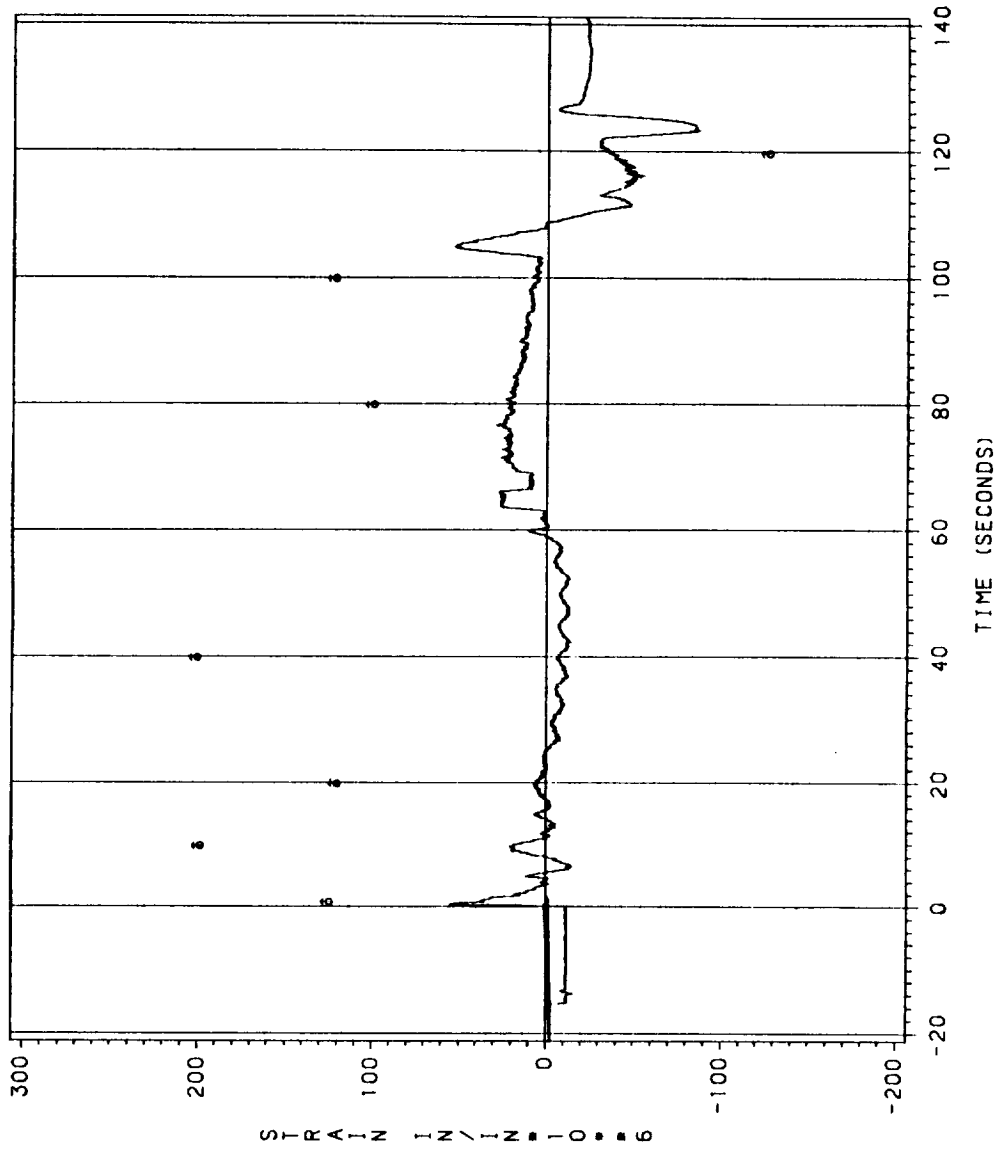

Figure 7.5-138. DM-9 Throat Housing (meridional strain), Location 11

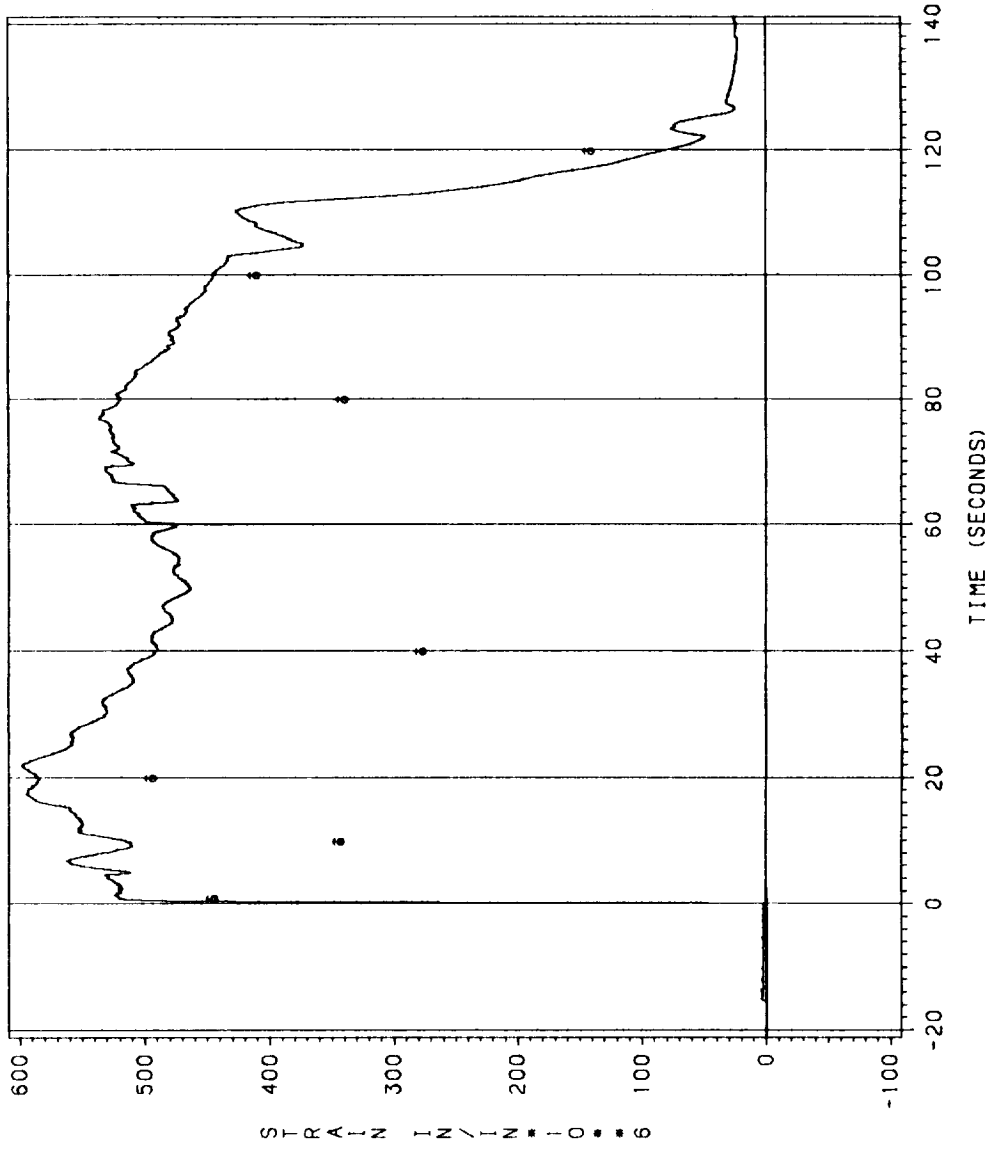

Figure 7.5-139. DM-9 Throat Housing (hoop strain), Location 12

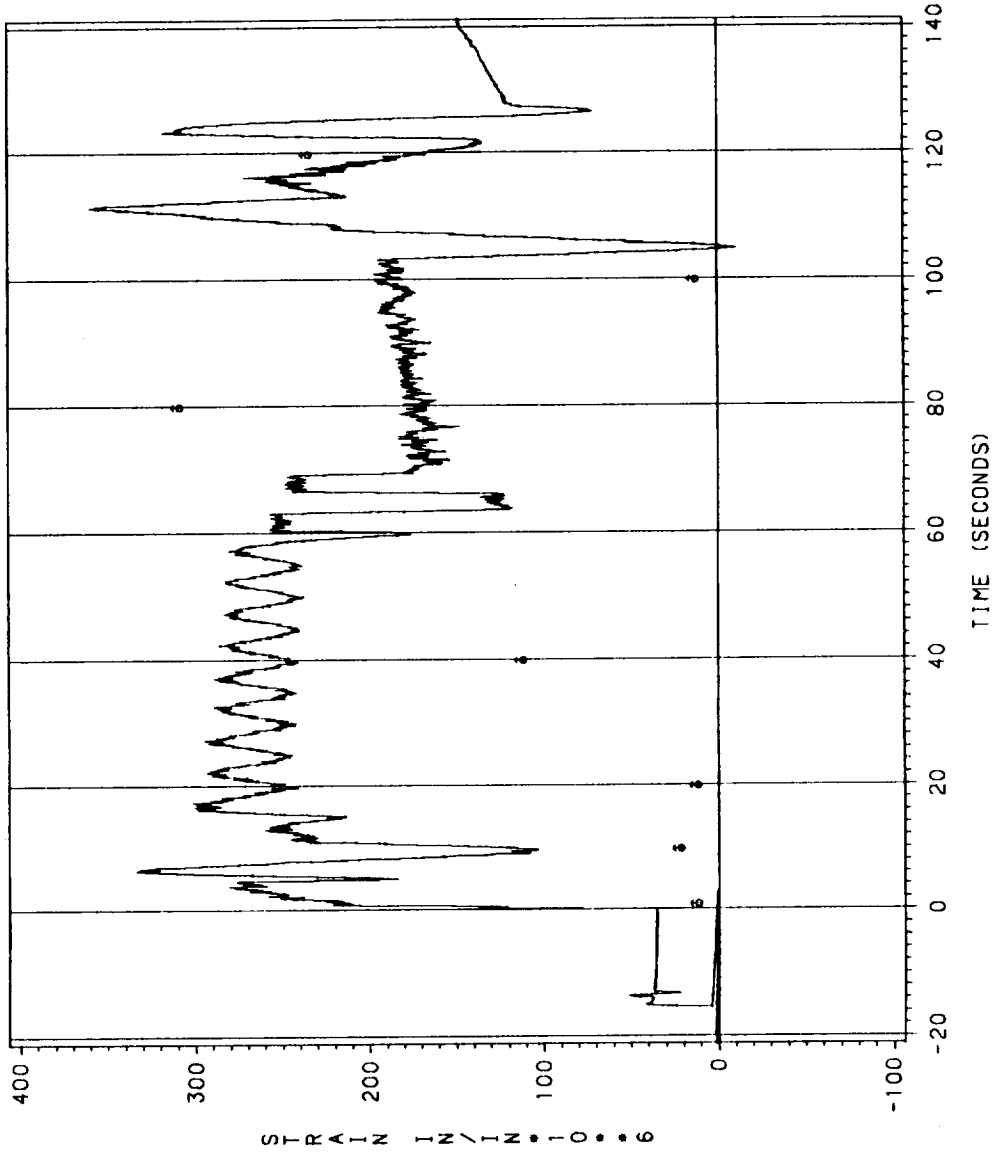

Figure 7.5-140. DM-9 Throat Housing (meridional strain), Location 12

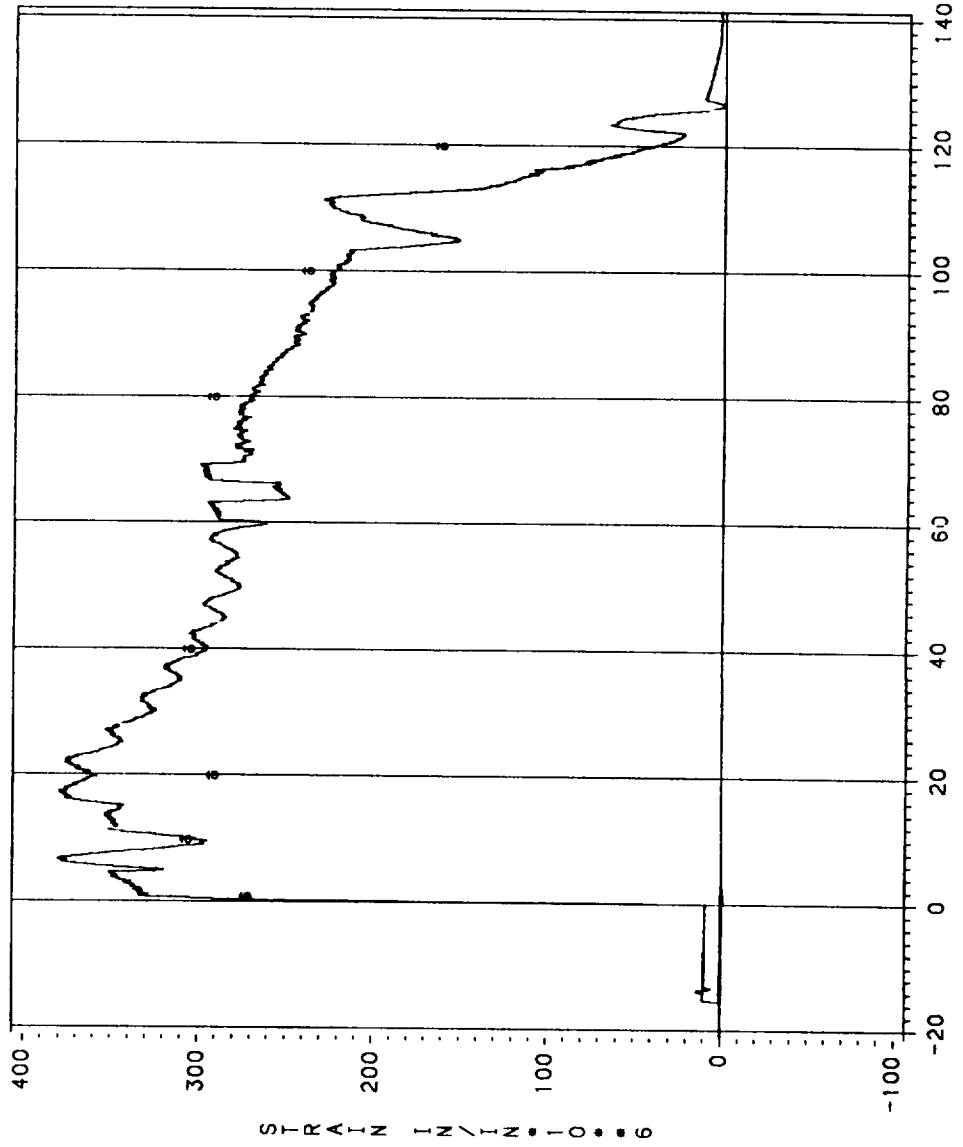

Figure 7.5-141. DM-9 Throat Housing (hoop strain), Location 13

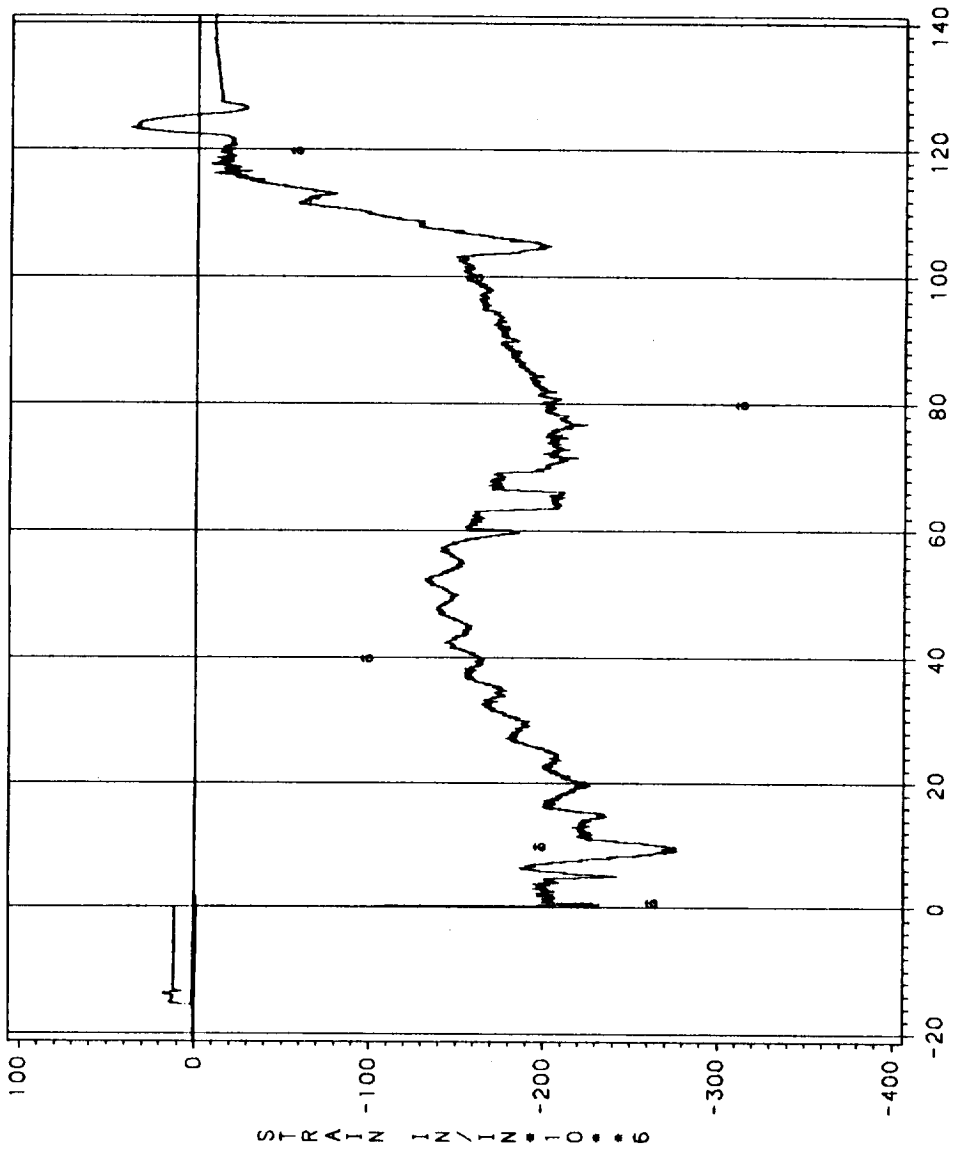

Figure 7.5-142. DM-9 Throat Housing (meridional strain), Location 13

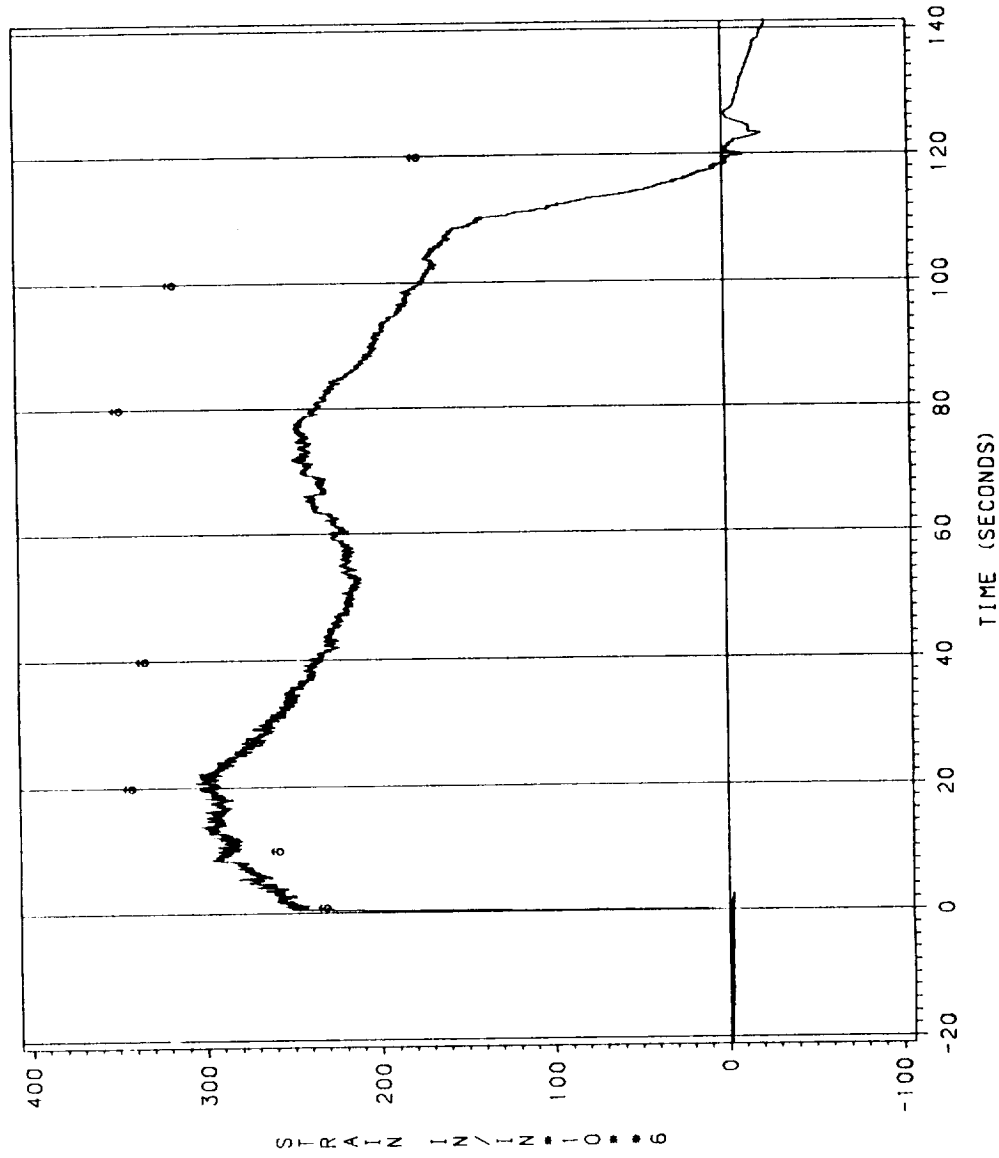

Figure 7.5-143. DM-9 Forward Exit Cone (hoop strain), Location 14

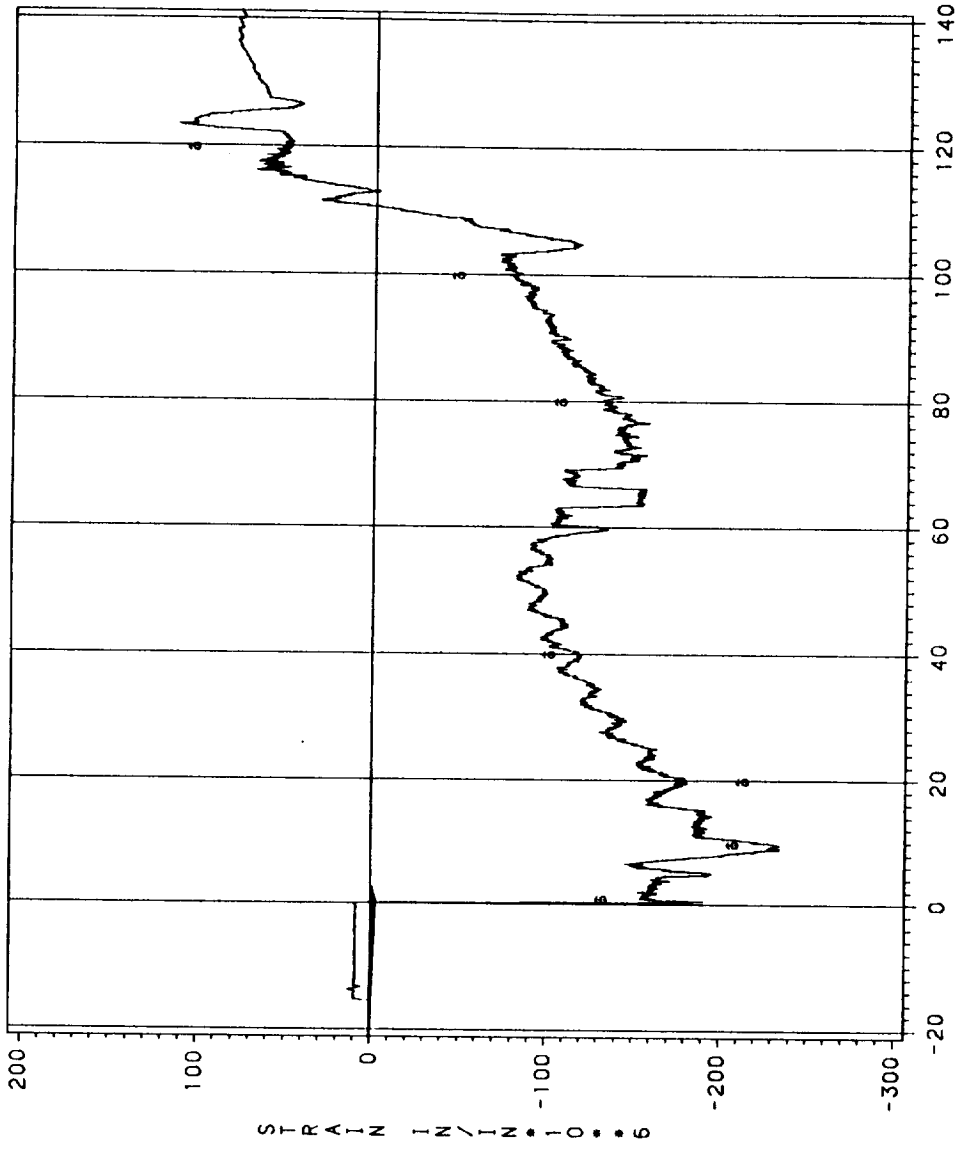

Figure 7.5-144. DM-9 Forward Exit Cone (meridional strain), Location 14

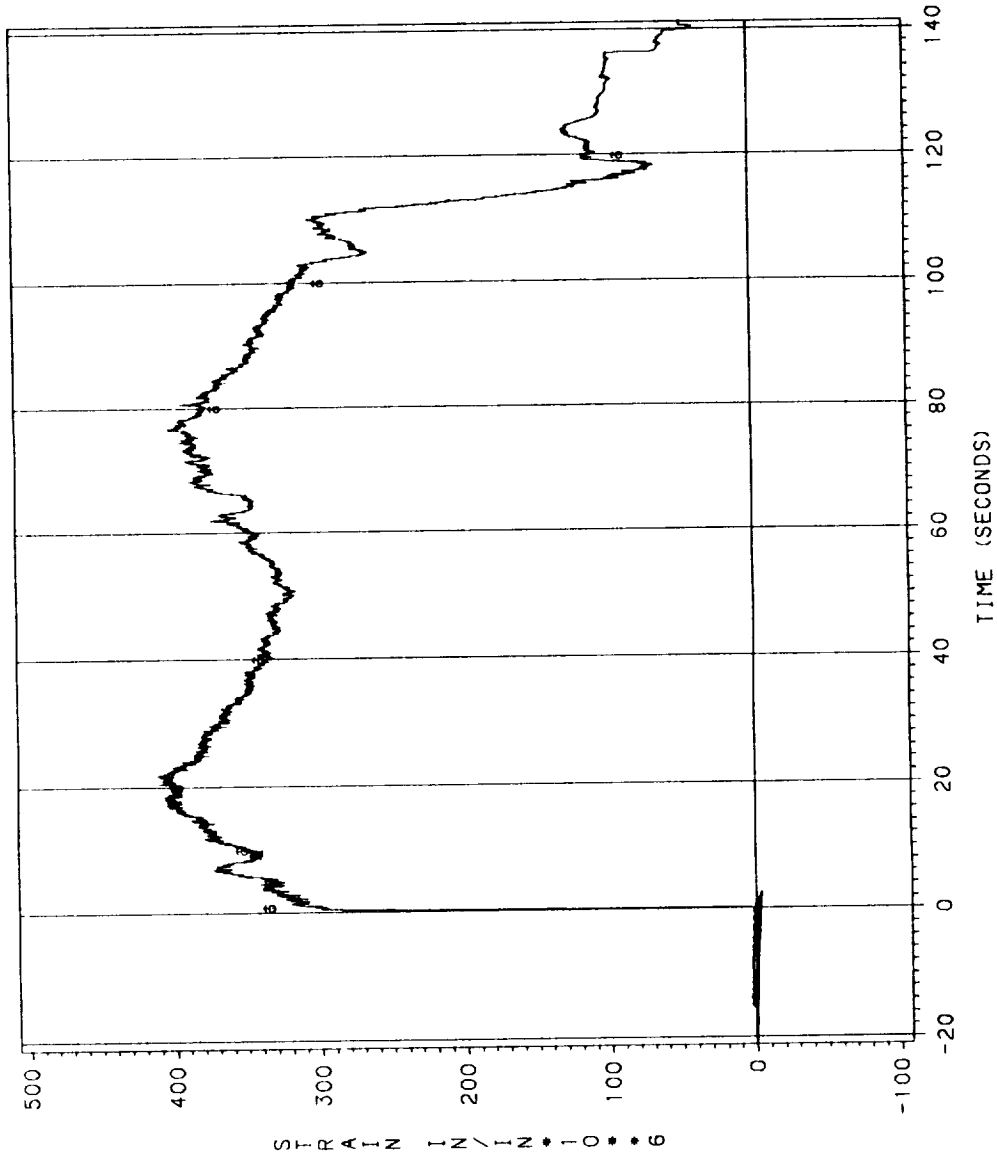

Figure 7.5-145. DM-9 Aft Exit Cone (hoop strain), Location 15

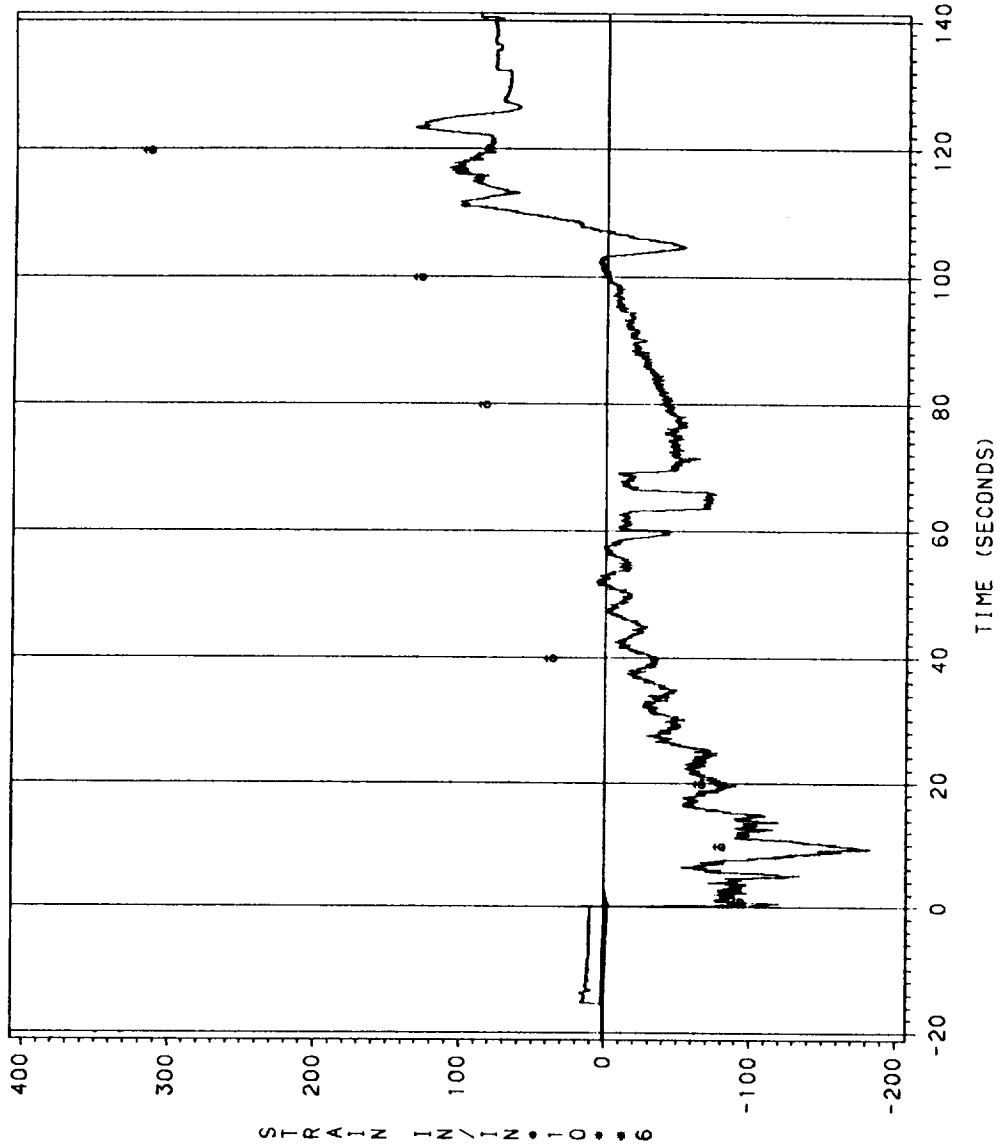

Figure 7.5-146. DM-9 Aft Exit Cone (meridional strain), Location 15

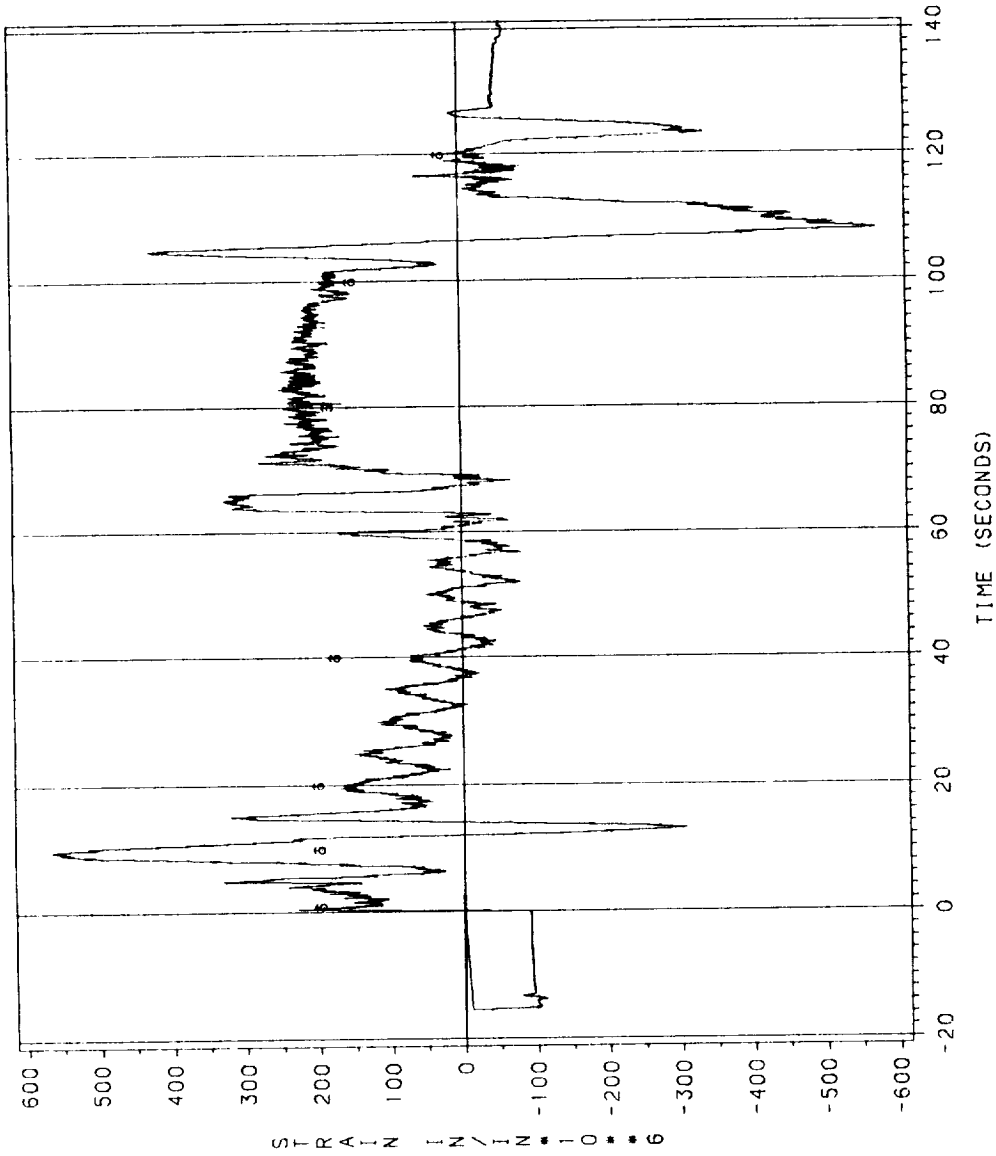

Figure 7.5-147. DM-9 Compliance Ring (hoop strain), Location 16

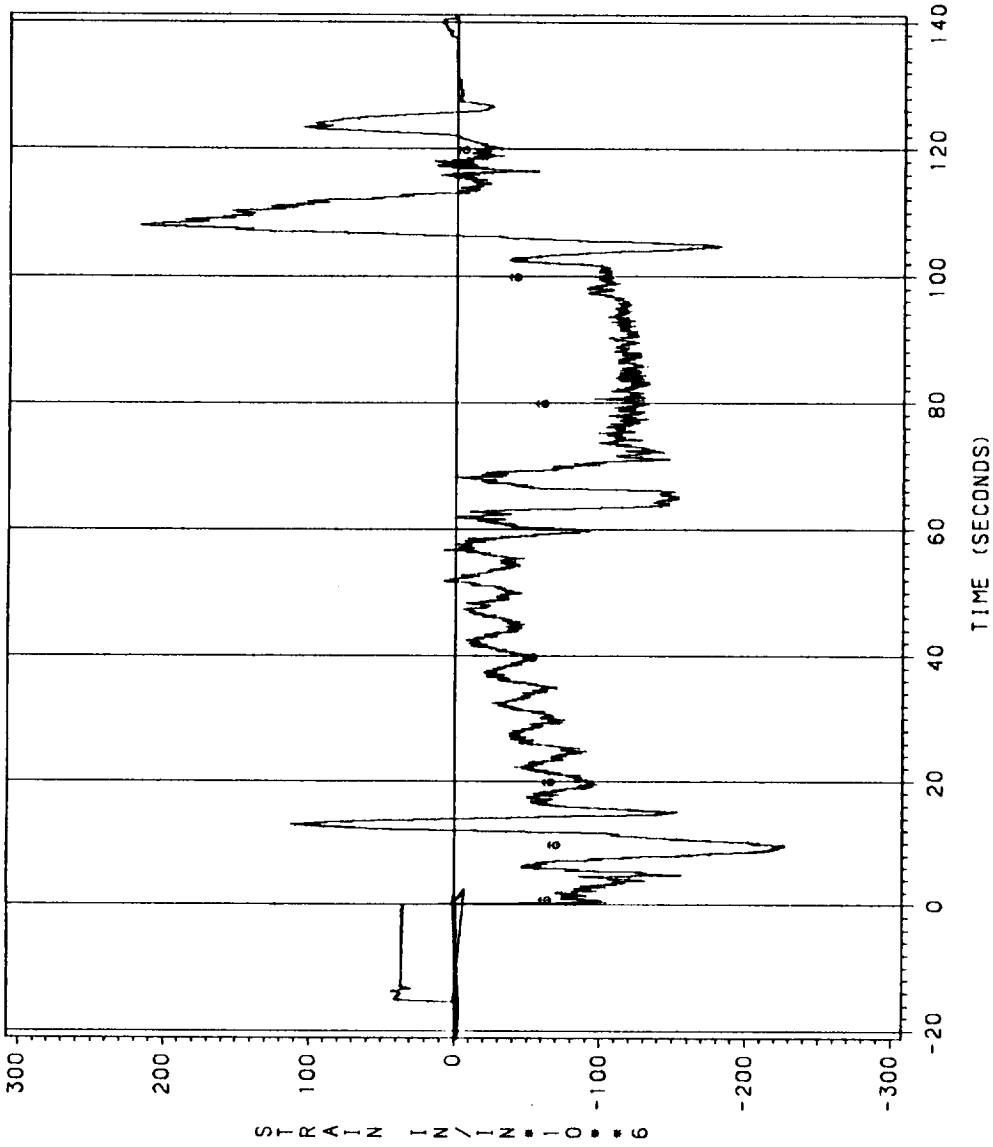

Figure 7.5-148. DM-9 Compliance Ring (meridional strain), Location 16

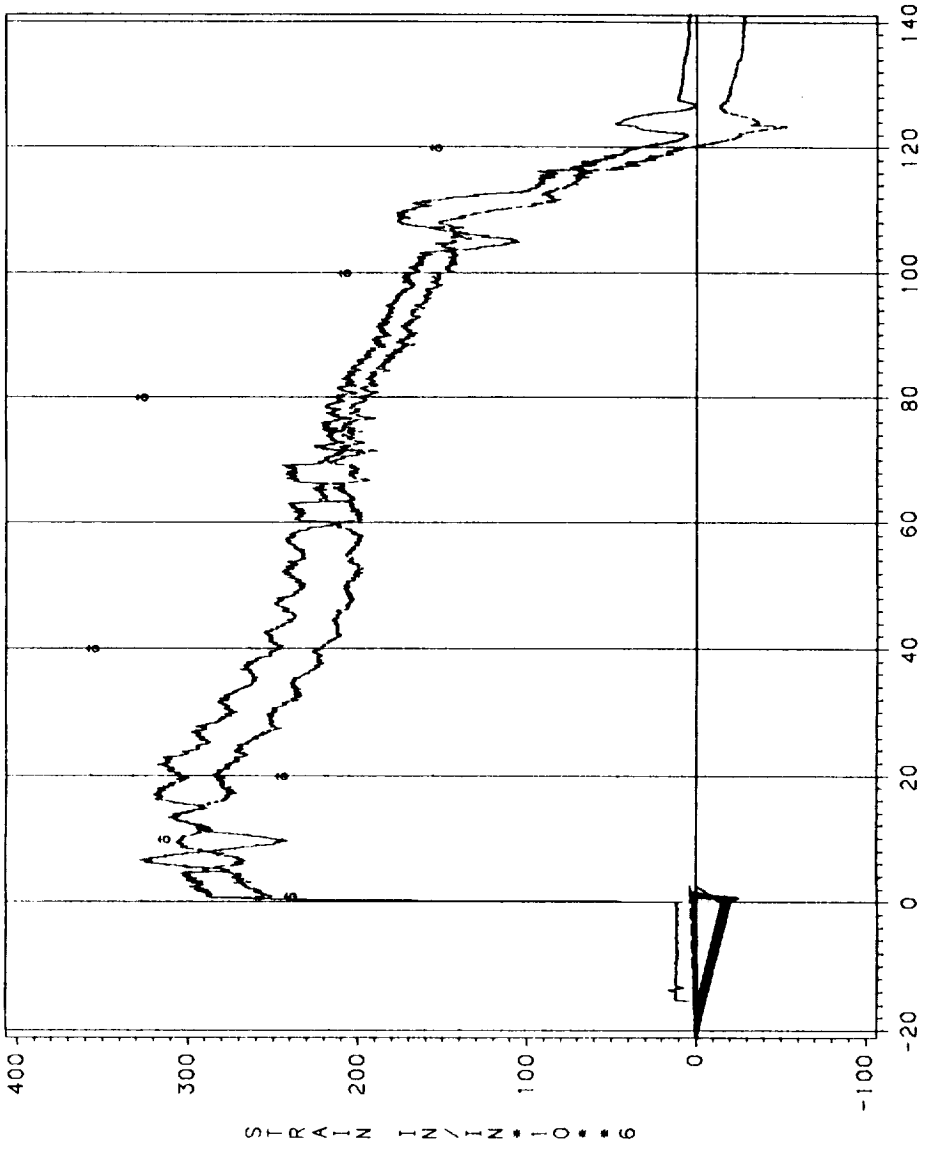

Figure 7.5-149. DM-9 Throat Housing (hoop strain), Location 17

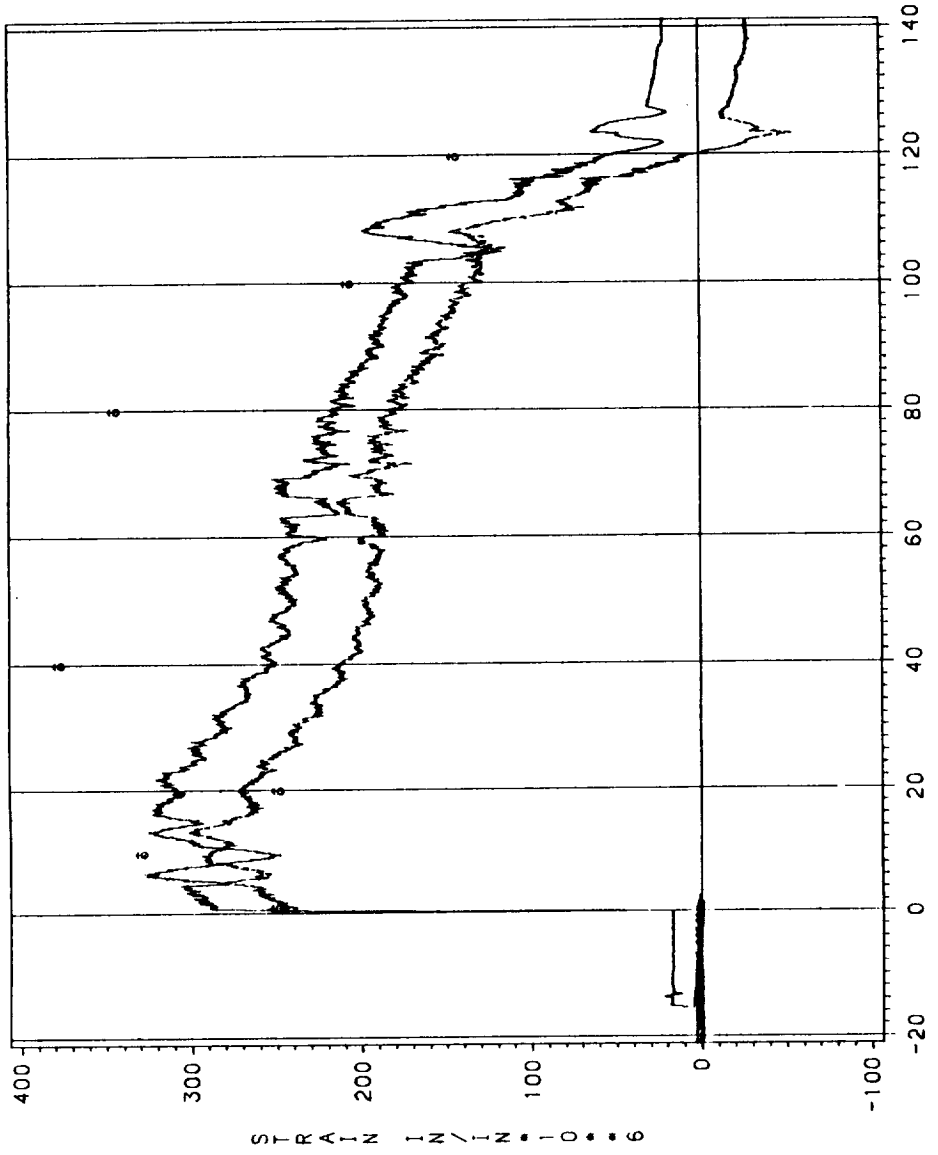

Figure 7.5-150. DM-9 Throat Housing (hoop strain), Location 18

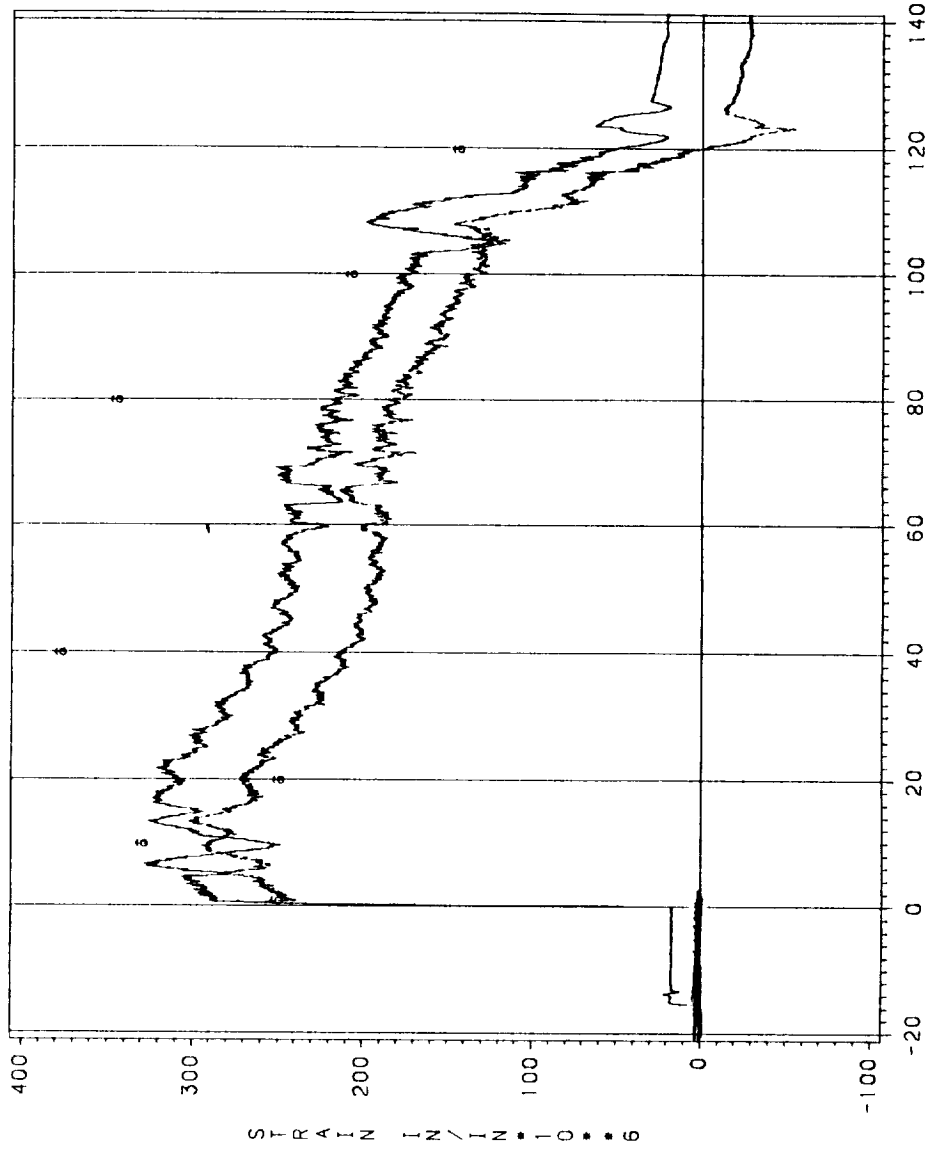

Figure 7.5-151. DM-9 Throat Housing (hoop strain), Location 18

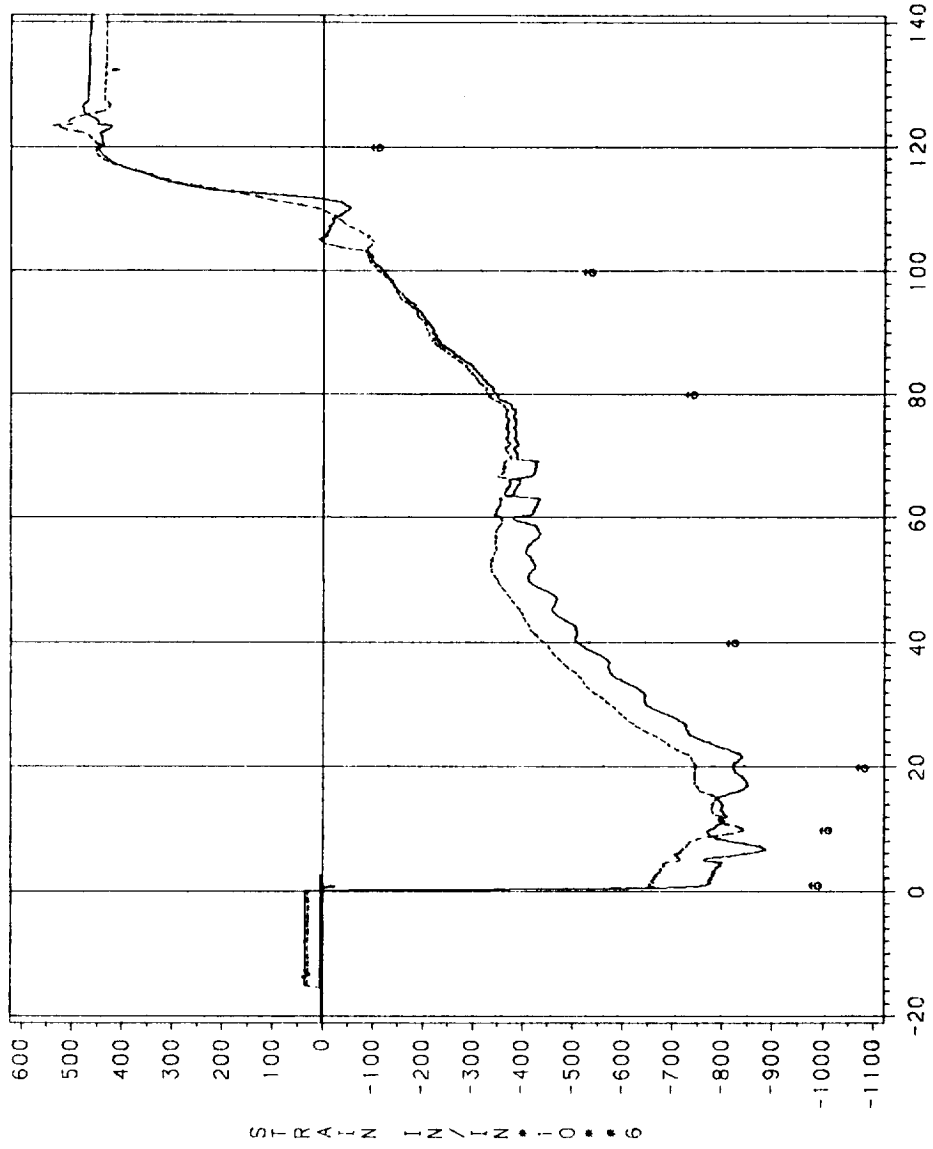

Figure 7.5-152. DM-9 Aft End Ring (hoop strain), Location 19

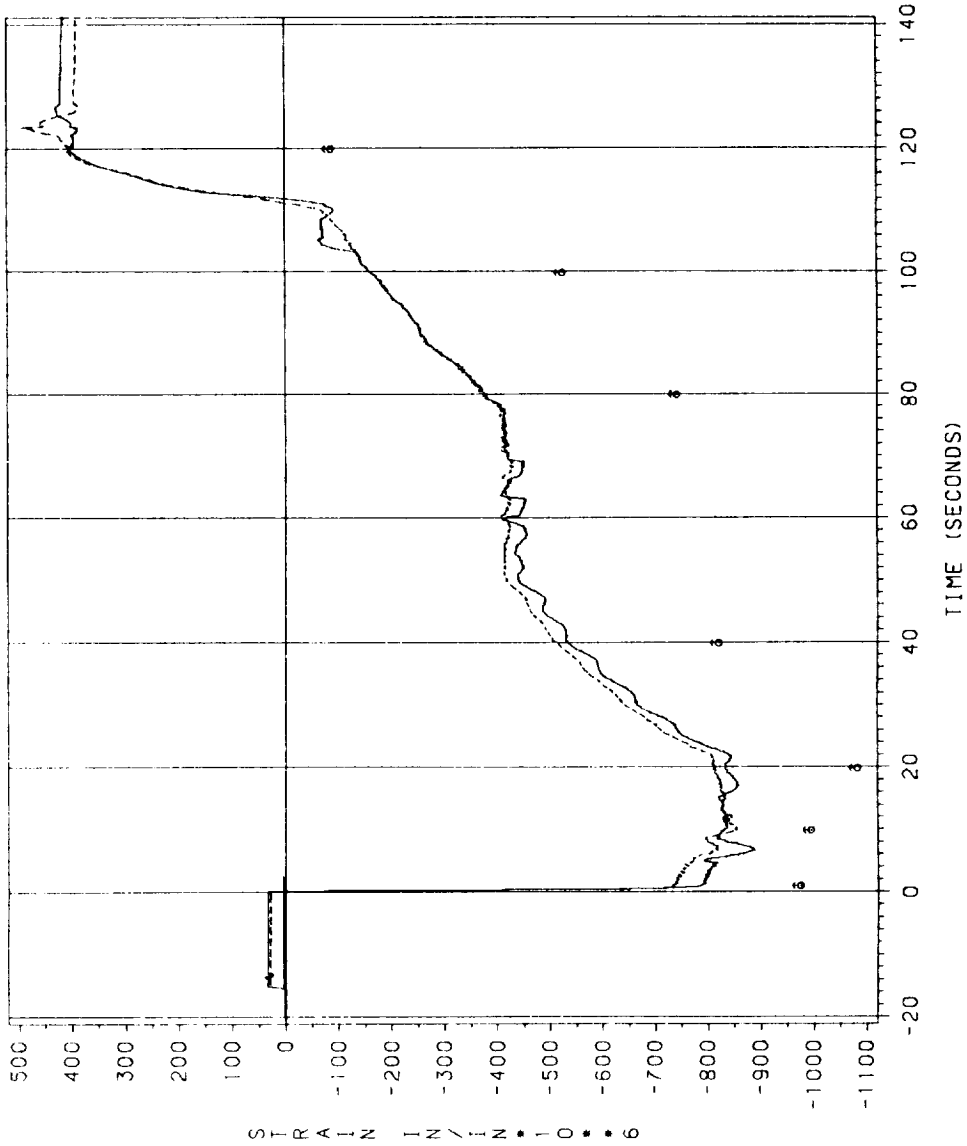

Figure 7.5-153. DM-9 Aft End Ring (hoop strain), Location 20

ORIGINAL PAGE IS
OF POOR QUALITY

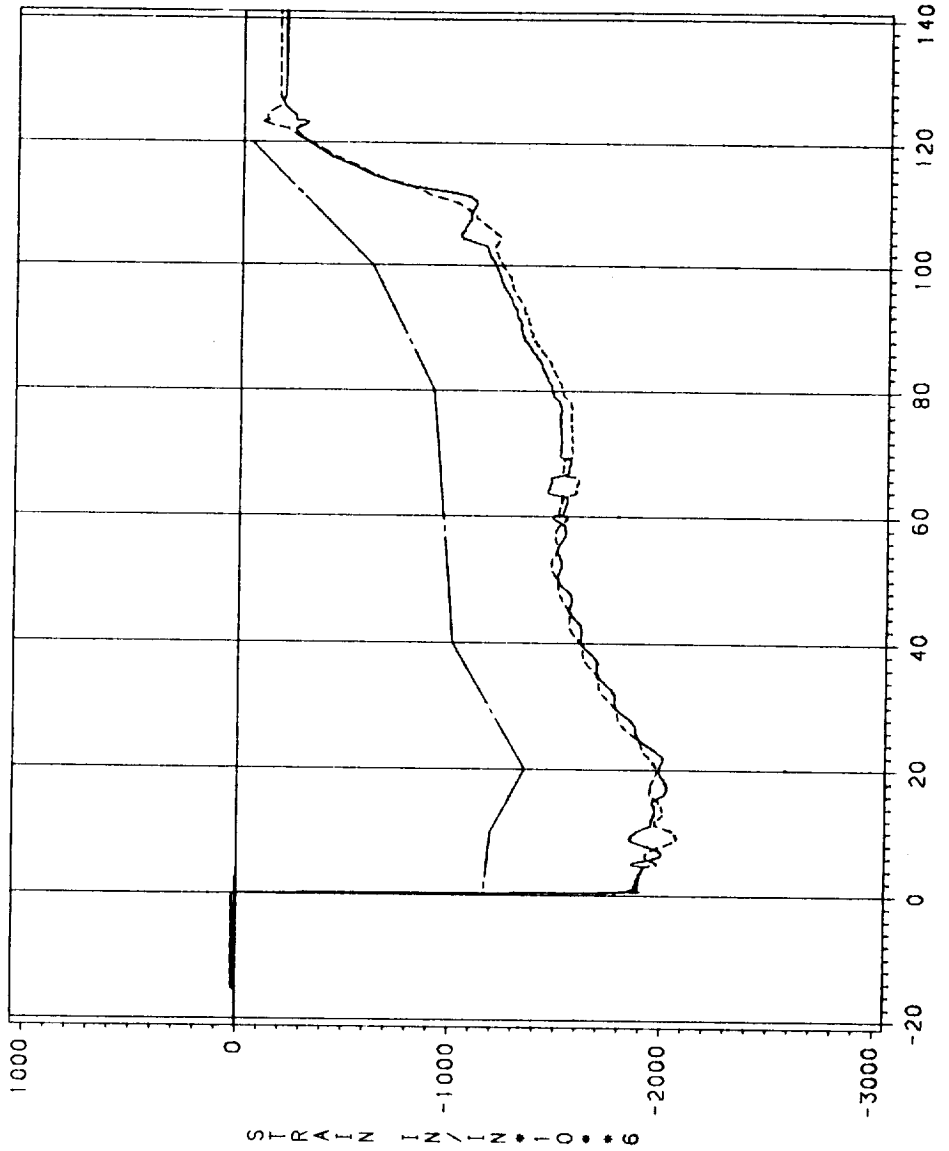

Figure 7.5-154. DM-9 Aft End Ring (hoop strain), Location 22

In general, predicted strains correlated with test data, and nozzle strains were small. Predicted hoop strains at locations 7 (aft end of the nose inlet housing) and 10 (throat joint region of the nose inlet housing), and meridional strains at locations 7 and 8 (the joint region at the nose inlet housing/forward end ring joint) need to be studied further. These gages are in regions of high-strain gradients where measurements are highly dependent on the accuracy of the gage placement. Predicted meridional strains at location 4 (forward end of the aft end ring) do not correlate with test results. However, the strains at this location are very low (less than 175 in./in.). No valid data was obtained at location 22 during the static firing due to faulty gages.

OBR Failure - Related Strain Data

On postfire inspection of the nozzle, it was found that the involute OBR had fractured and separated from the nozzle over a 150-deg arc from 220 to 10 deg. It was eroded and delaminations were noticed in several locations. The cause and time of failure was studied and conclusions were drawn.

To determine the time at which the involute OBR failed, meridional strain gage data on the fixed housing was compared with test data at the same locations on the DM-8 motor. Figures 7.5-155 to 7.5-158 show the meridional strains of DM-8 and DM-9 motors at locations 2 and 3 for various azimuth angles. There are speculations that the ring was initially damaged during the +7 deg yaw vector event at about 112 sec. At about 123.5 sec, during the 6.3-deg TVC event, discontinuities in the strain data on the DM-9 motor indicated that the OBR apparently failed at this time. These discontinuities are evident in most DM-9 nozzle strain plots at the 123.5-sec timeframe. It was also noted that the vent holes in the cowl were partially plugged allowing a pressure of about 100 psi to build up in the flex boot cavity at tailoff. This pressure load combined with the vector event at about 123.5 sec could have caused the final damage to the OBR.

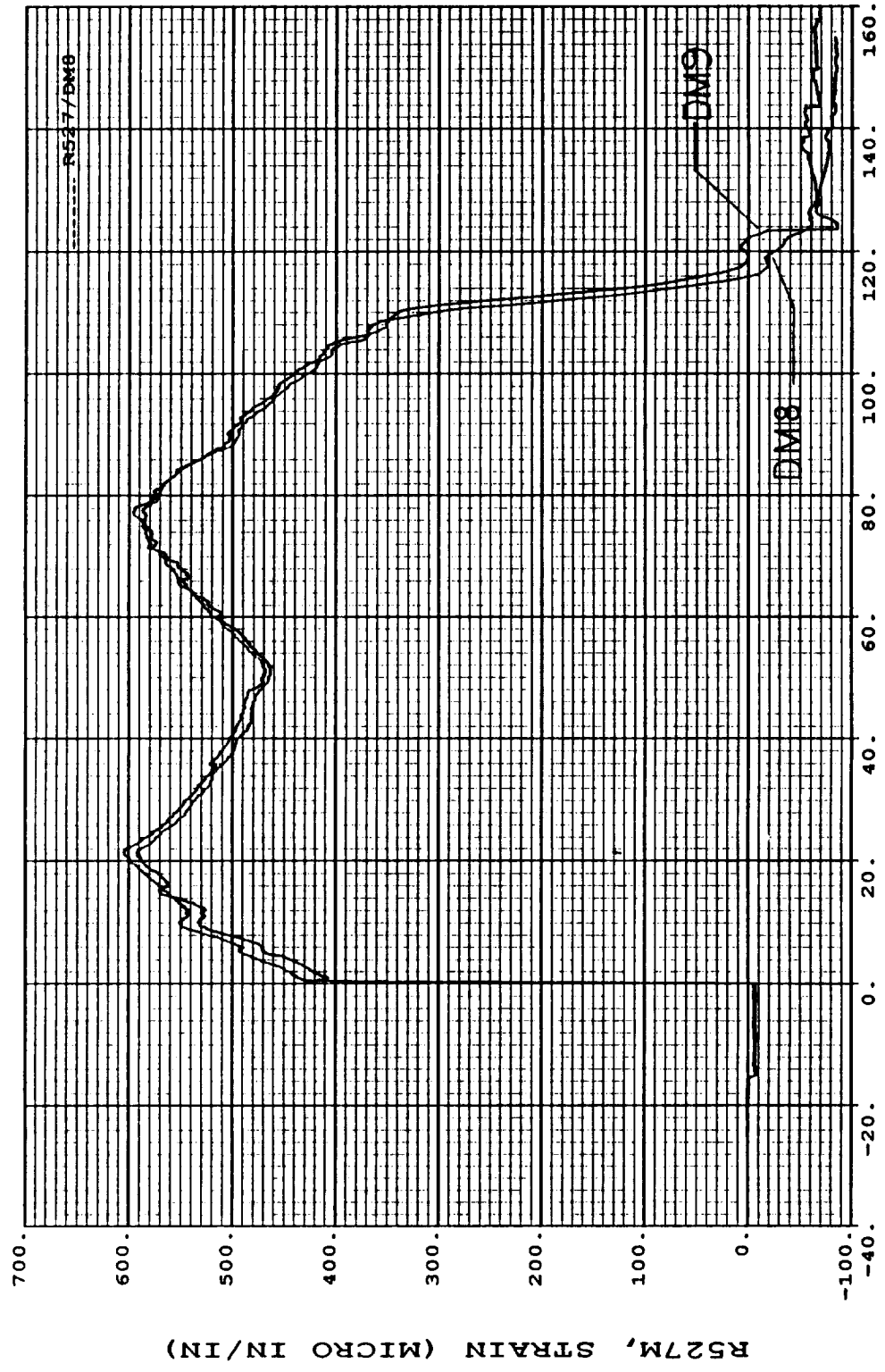

Figure 7.5-155. DM-9 and DM-8 Fixed Housing (meridional strains), 0 deg at Location 2

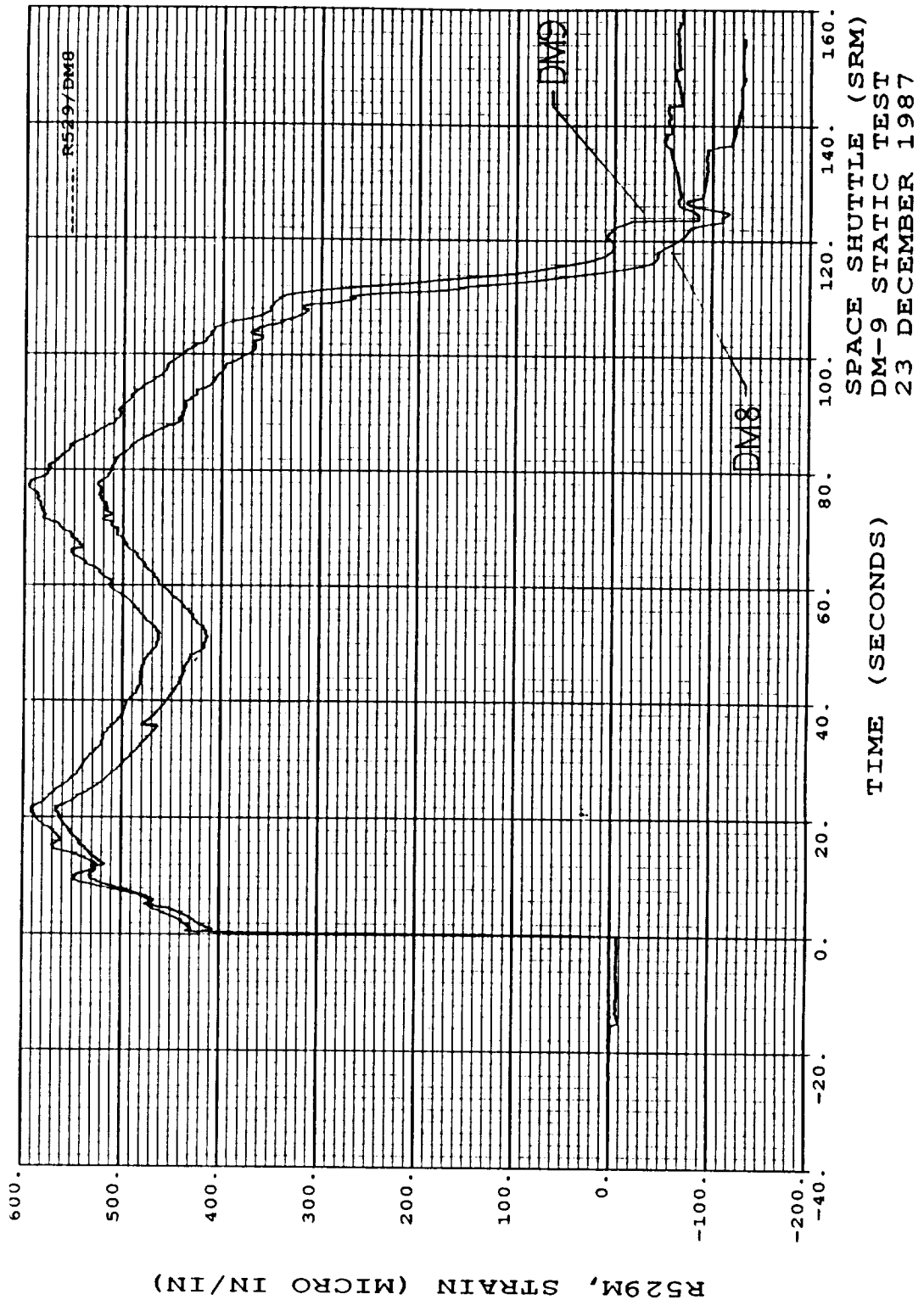

Figure 7.5-156. DM-9 and DM-8 Fixed Housing (meridional strains), 90 deg at Location 2

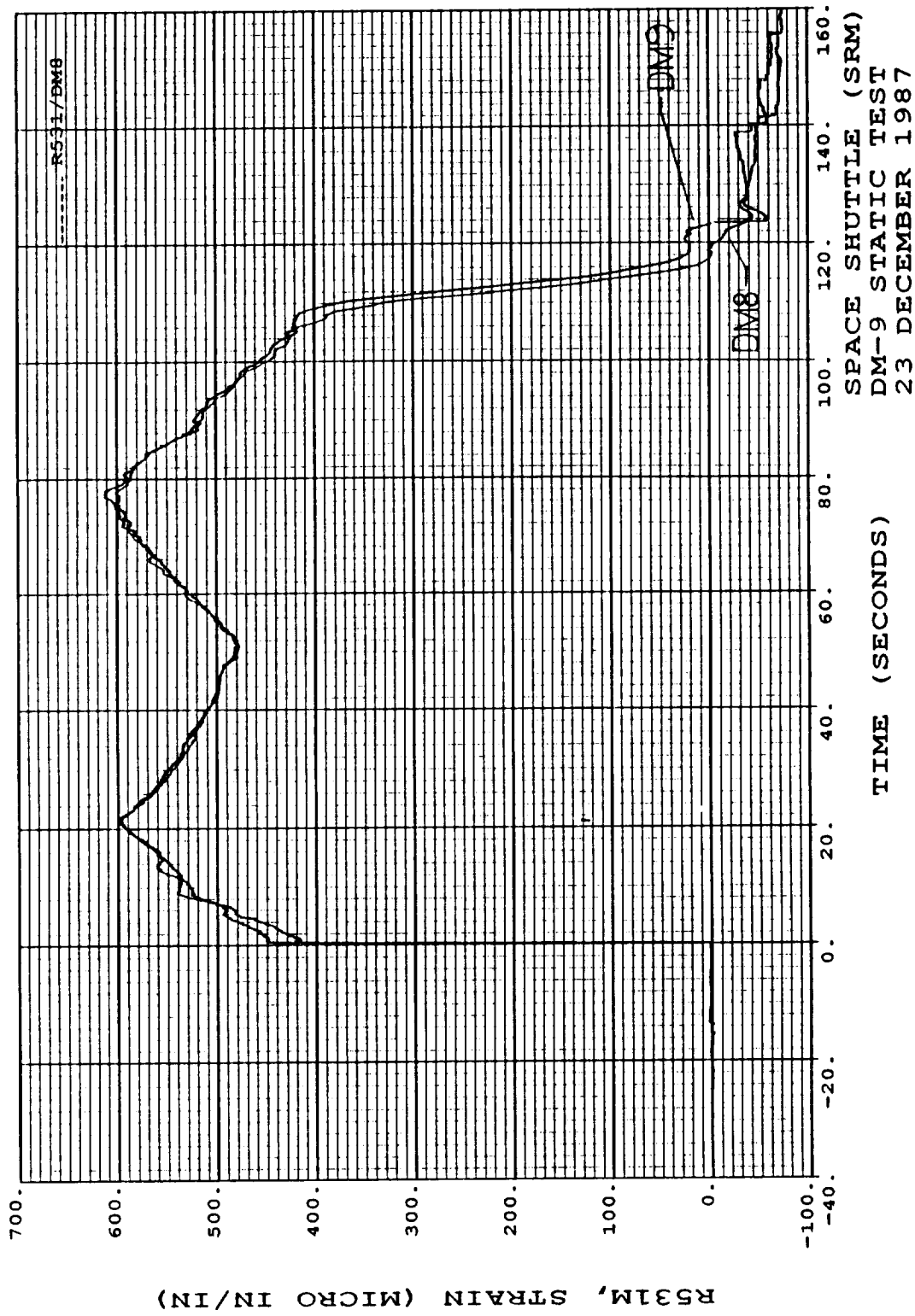

Figure 7.5-157. DM-9 and DM-8 Fixed Housing (meridional strains), 180 deg at Location 2

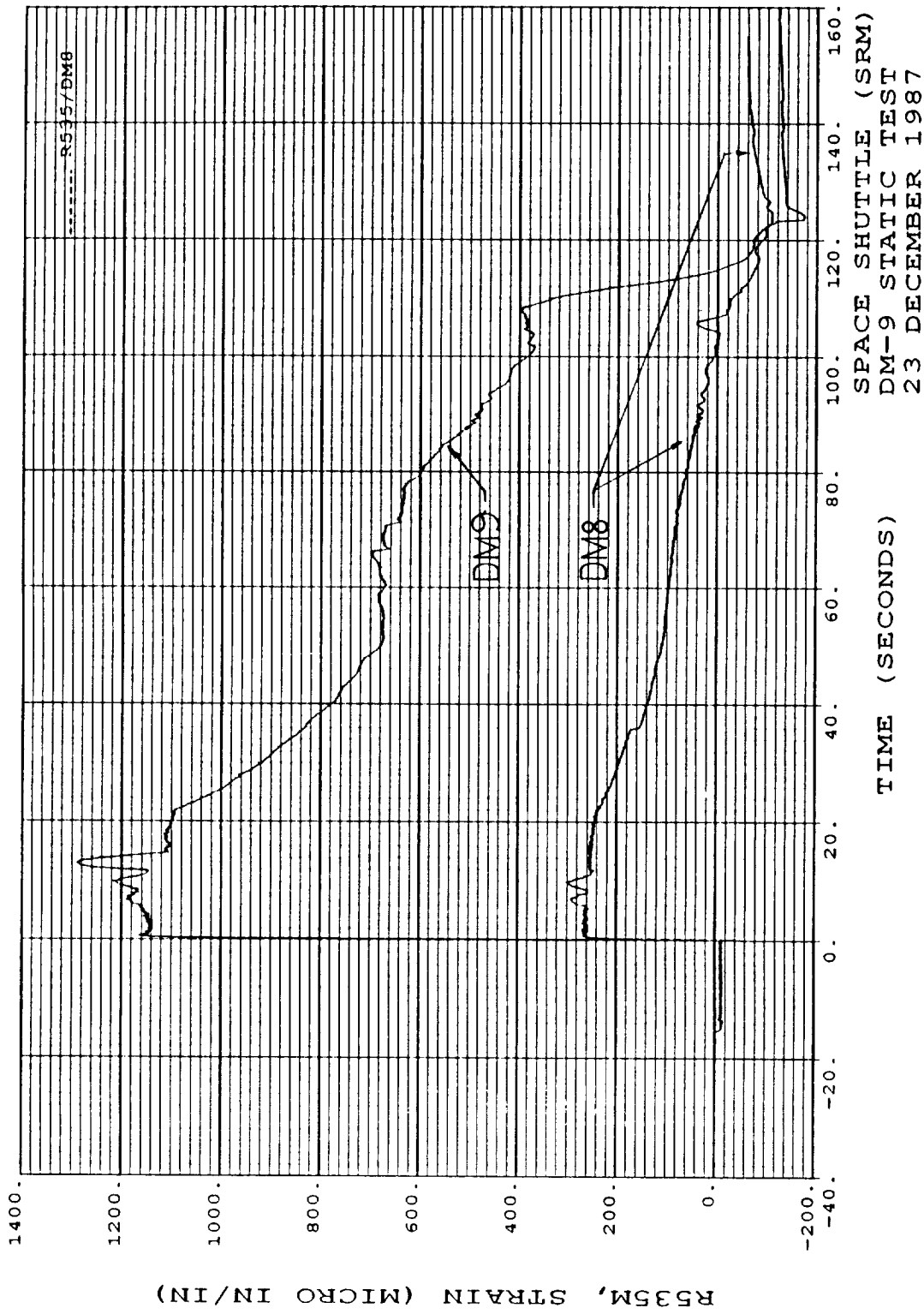

Figure 7.5-158. DM-9 and DM-8 Fixed Housing (meridional strains), 0 deg at Location 3

DM-9, DM-8, and ETM-1A Strain Comparisons

DM-9 strain gage data was also compared with DM-9, DM-8, and ETM-1A nozzle strains at common locations. In general, there was good correlation in the data measured on these motors. Locations 3 and 16 through 22 were used exclusively in DM-9 and hence could not be compared with any existing data. ETM-1A data was available only for locations 6, 11, 13, and 14. X-Y plots showing the comparisons are shown in Figures 7.5-159 to 7.5-186. At locations 2, 9, 13, 14, and 15 there was good correlation in both the hoop and meridional strains for DM-8 and DM-9 motors. Hoop strains for these motors at locations 1, 4, 7, 10, 11, and meridional strains at location 8 compared well. Hoop strains at location 8 were low compared to those measured on the DM-8 motor; this was predicted due to the thickened nose inlet housing in this region. Hoop strains at location 5 were significantly higher than data measured on the DM-8 motor. Meridional strains at location 4, 5, and 11 were significantly lower than strains measured on the DM-8 motor. Meridional strains at location 11 were also significantly lower than those measured on the ETM-1A motor. Location 1 at 0 deg azimuth and location 12 are suspect, as they have opposite signs to measurements taken at these locations at other azimuth locations on both DM-8 and DM-9 motors.

TVC Effects

In an effort to quantify effects of actuator loads on nozzle component strains during nozzle vectoring, nozzle strains are investigated for both static test and prefire duty cycles. Tables 7.5-10 and 7.5-11 compare the hoop and meridional strains measured at all locations during the actuator adjustment, dry run duty cycle, and static test duty cycle.

a. Static Test Duty Cycle. The static test duty cycle is shown in Figure 7.5-115. Vectoring at 4.0, and -4.4 deg yaw, -7.1, and 7.5 pitch, and 6.3 deg yaw occur at about 6.6, 9.8, 103.0, 104.9, and 123.5 sec, respectively, during the firing. The last vector event at 123.5 sec occurs when pressure has dropped off to near ambient. The effects of vectoring on strain during these timeframes is apparent in the strain plots. Maximum strain due to pressure, and maximum strains due

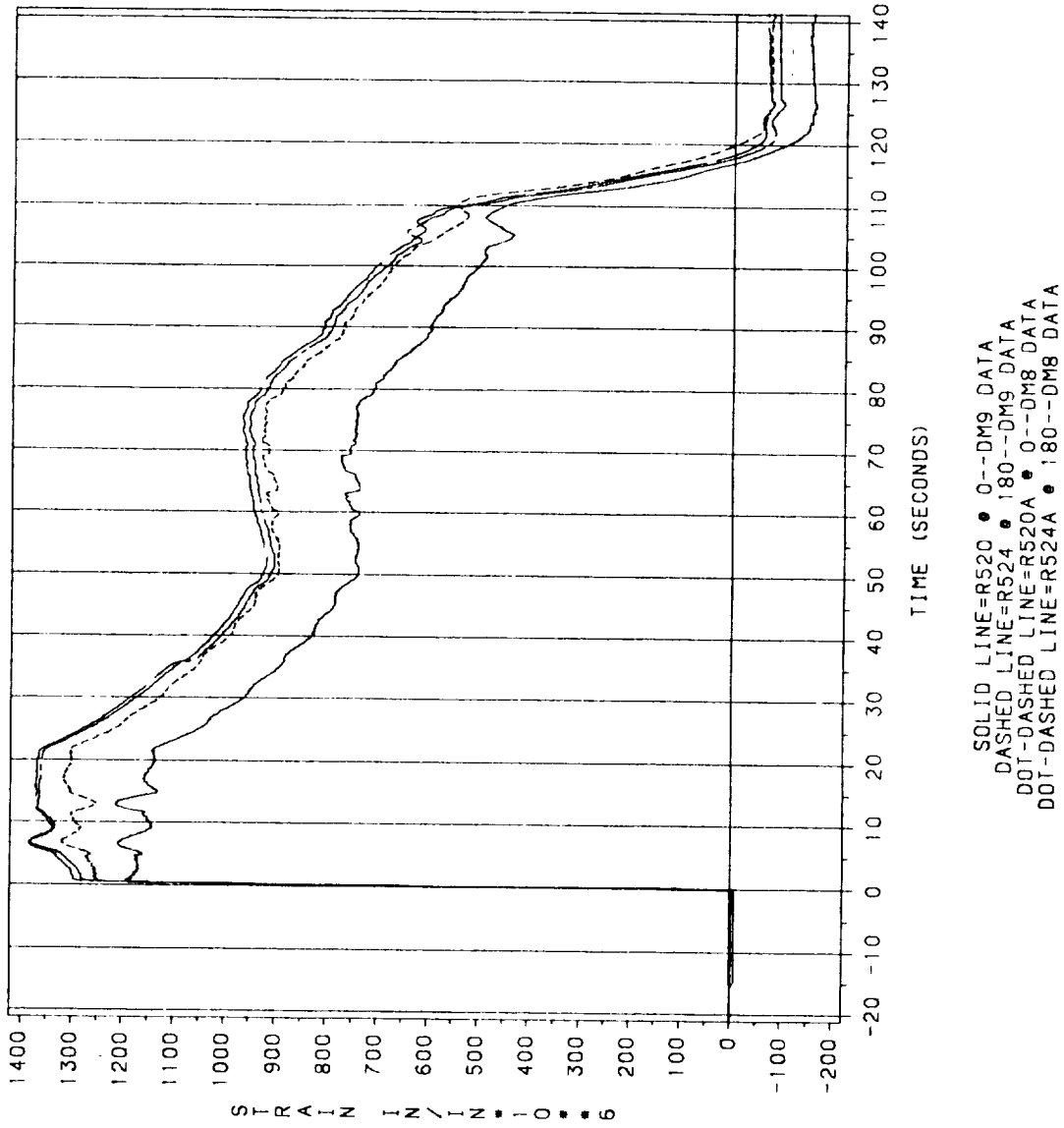

Figure 7.5-159. DM-9 and DM-8 Fixed Housing (hoop strains), 0 and 180 deg at Location 1

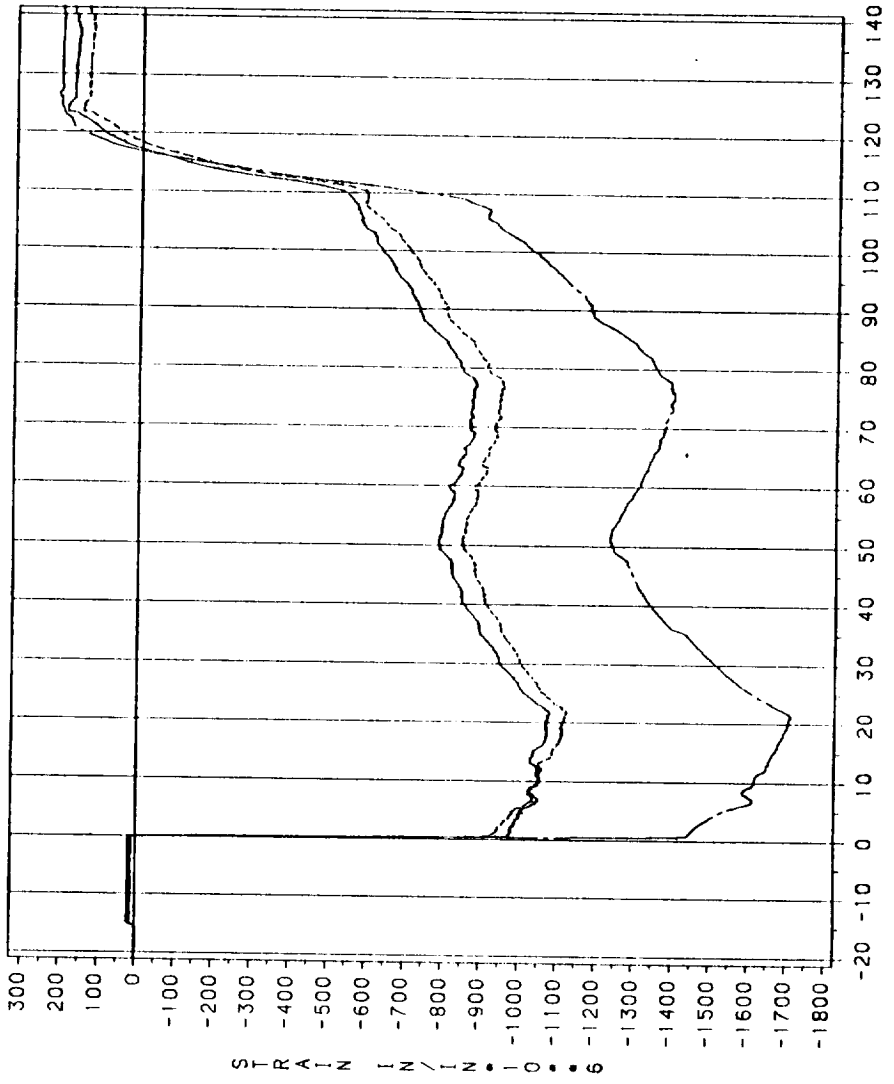

Figure 7.5-160. DM-9 and DM-8 Fixed Housing (meridional strains), 0 and 180 deg at Location 1

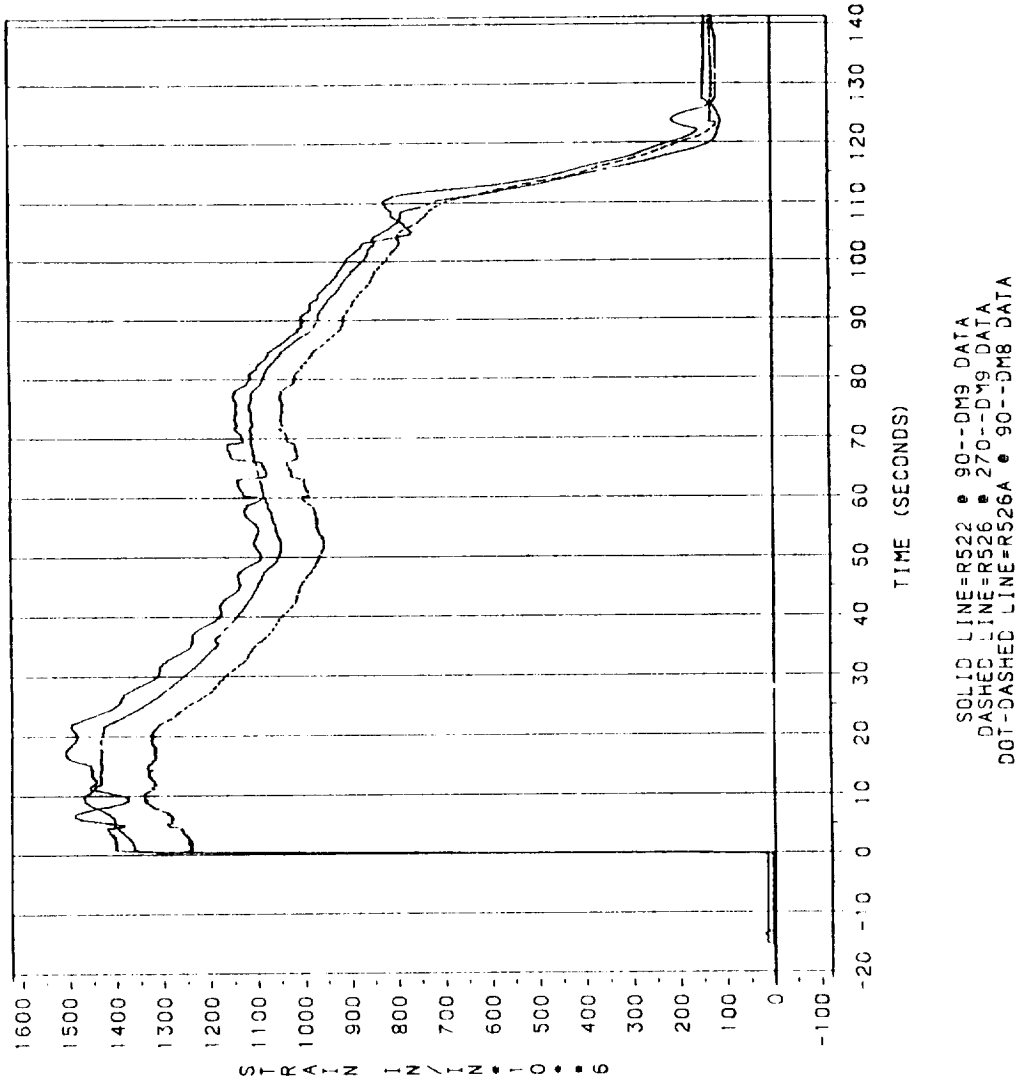

Figure 7.5-161. DM-9 and DM-8 Fixed Housing (hoop strains), 90 and 270 deg at Location 1

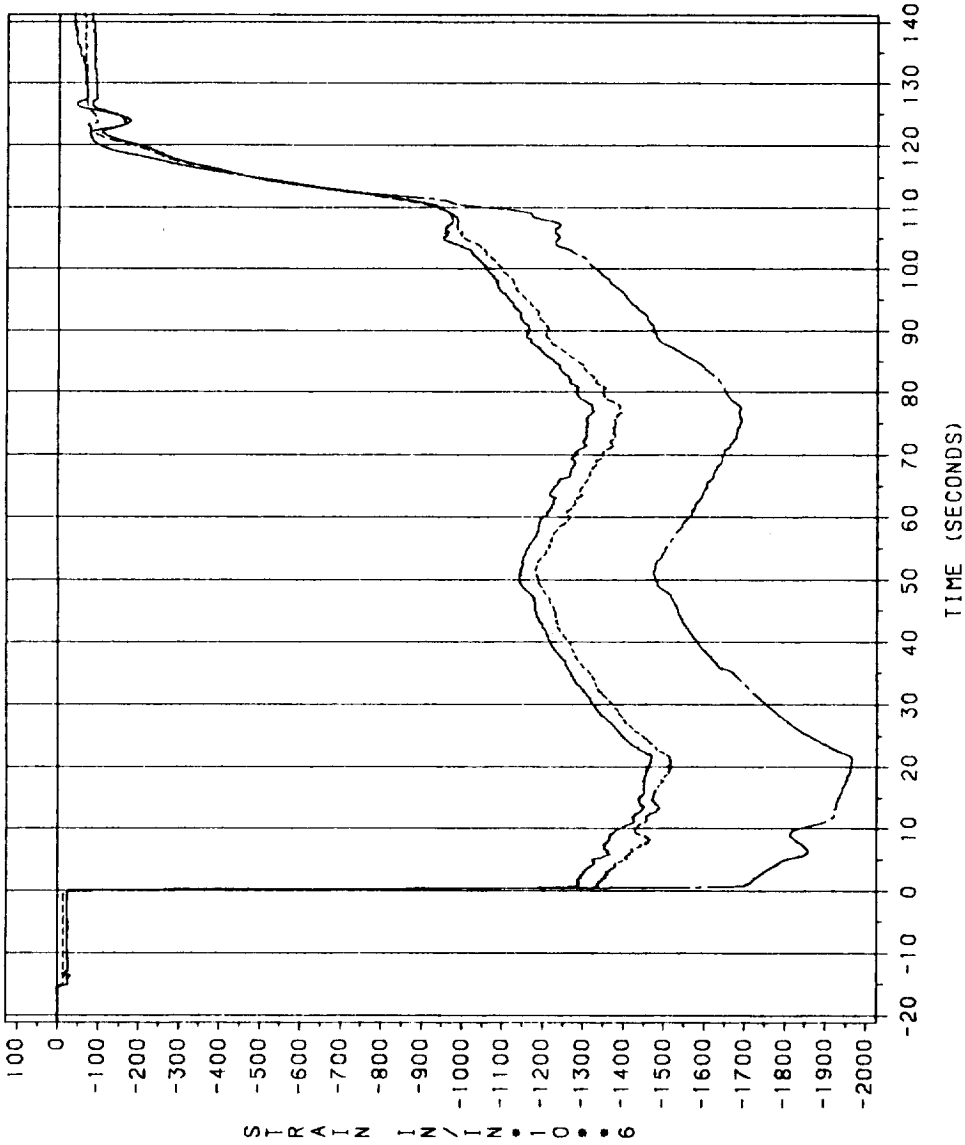

Figure 7.5-162. DM-9 and DM-8 Fixed Housing (meridional strains), 90 and 270 deg at Location 1

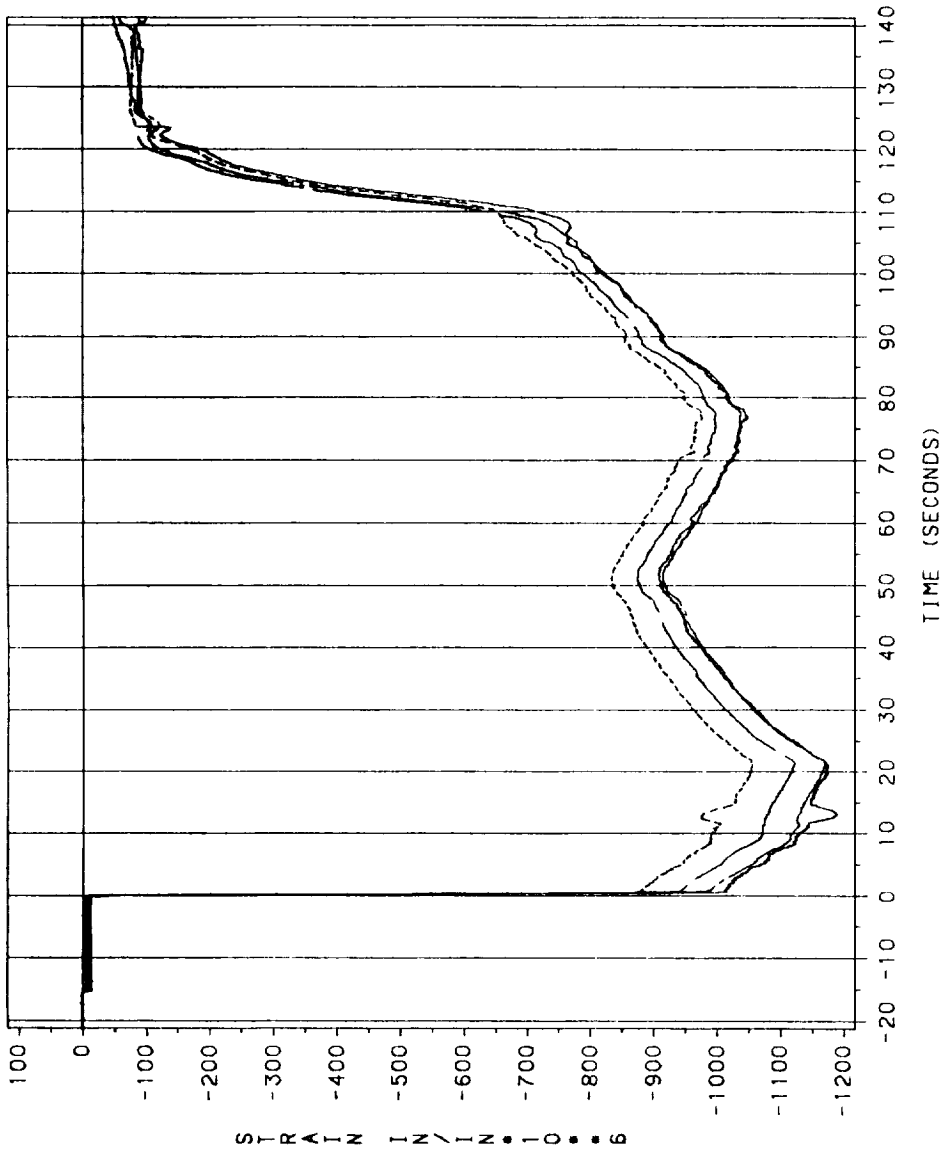

Figure 7.5-163. DM-9 and DM-8 Fixed Housing (hoop strains), 0 and 180 deg at Location 2

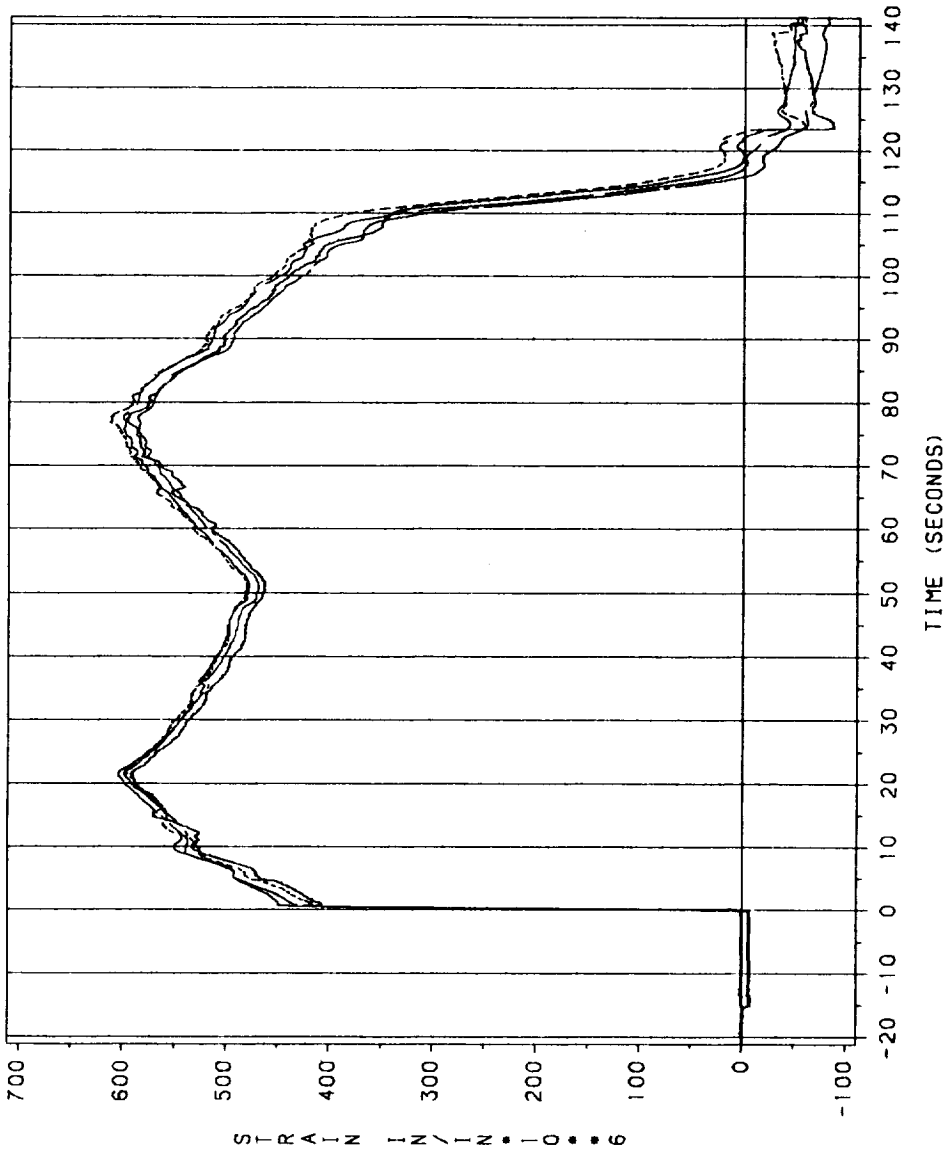

Figure 7.5-164. DM-9 and DM-8 Fixed Housing (meridional strains), 0 and 180 deg at Location 2

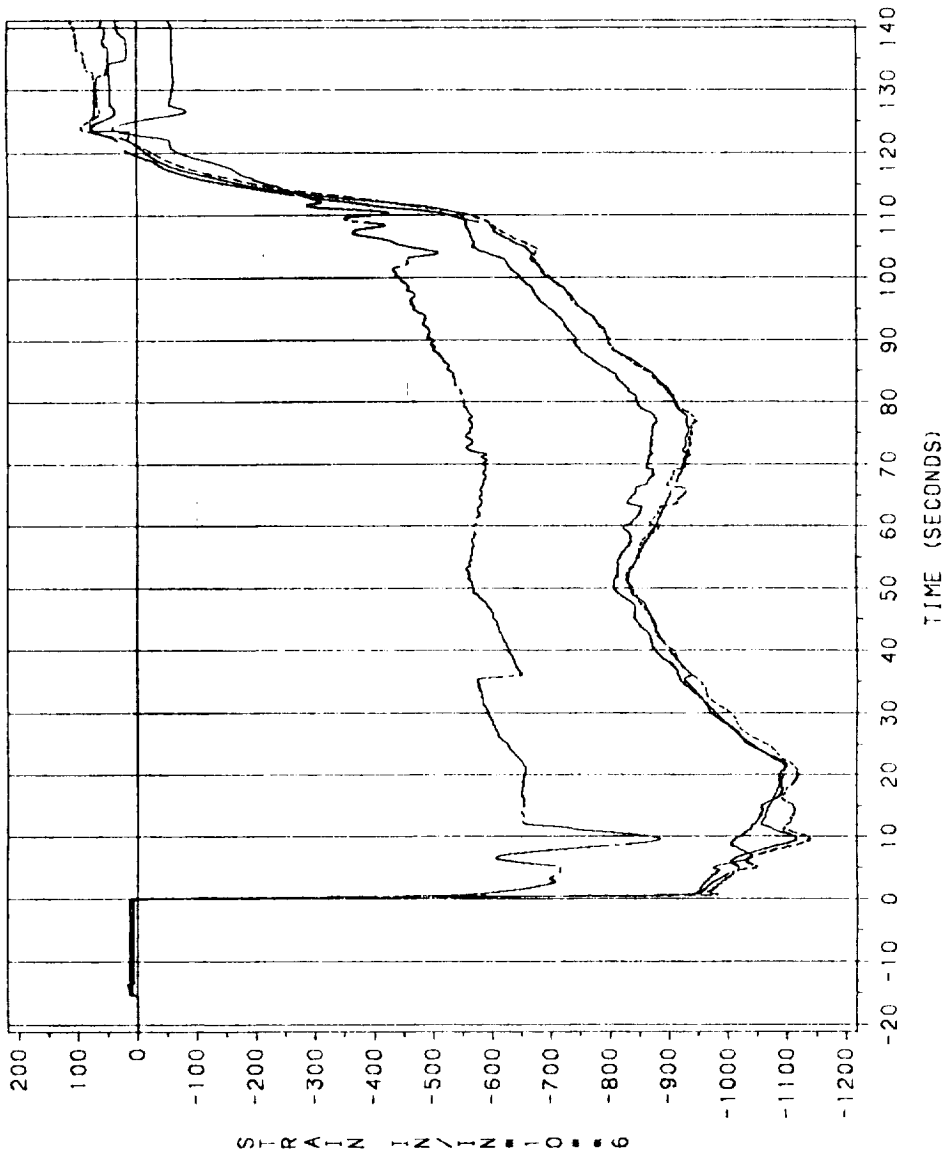

Figure 7.5-165. DM-9 and DM-8 Fixed Housing (hoop strains), 90 and 270 deg at Location 2

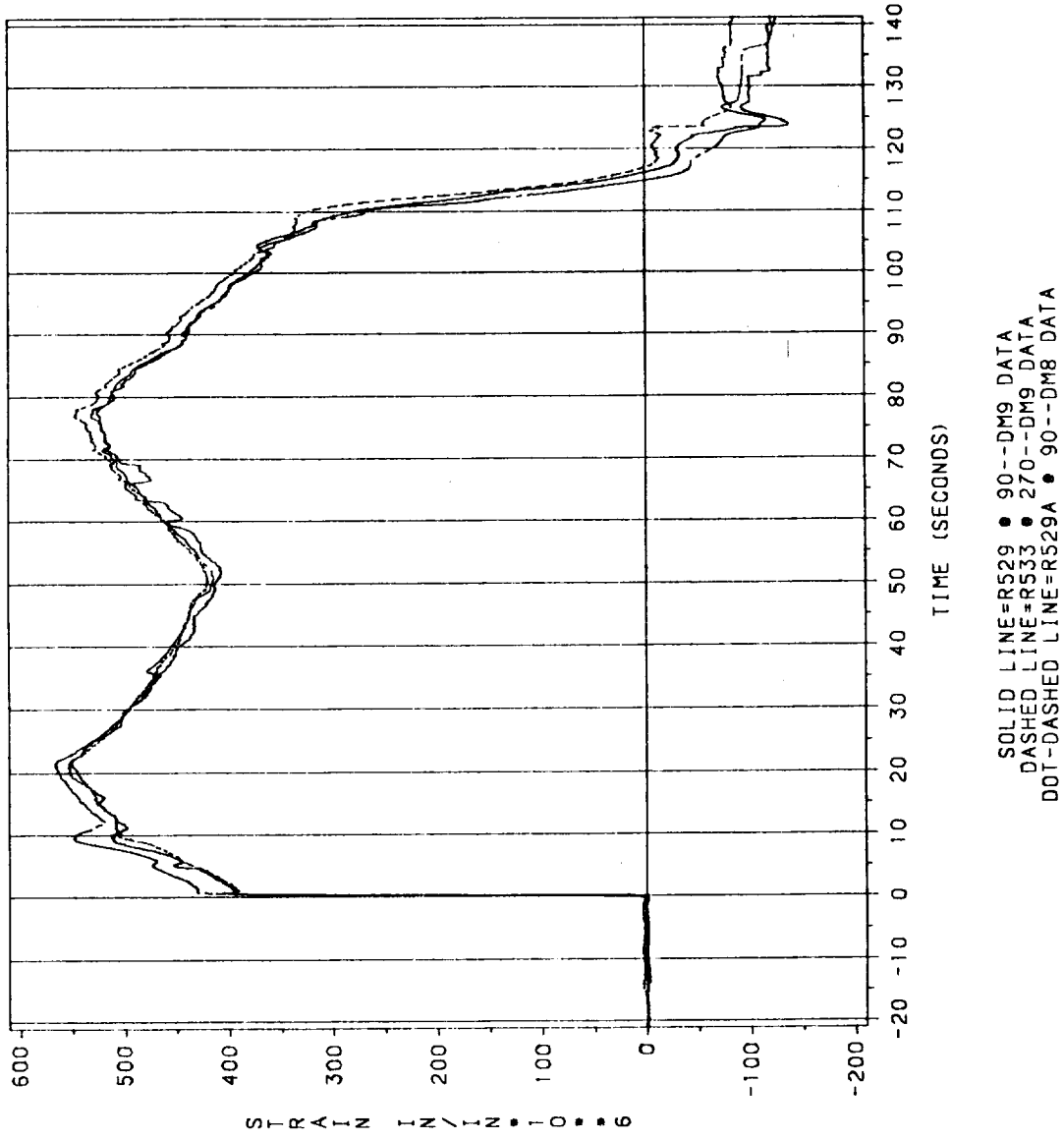

Figure 7.5-166. DM-9 and DM-8 Fixed Housing (meridional strains), 90 and 270 deg at Location 2

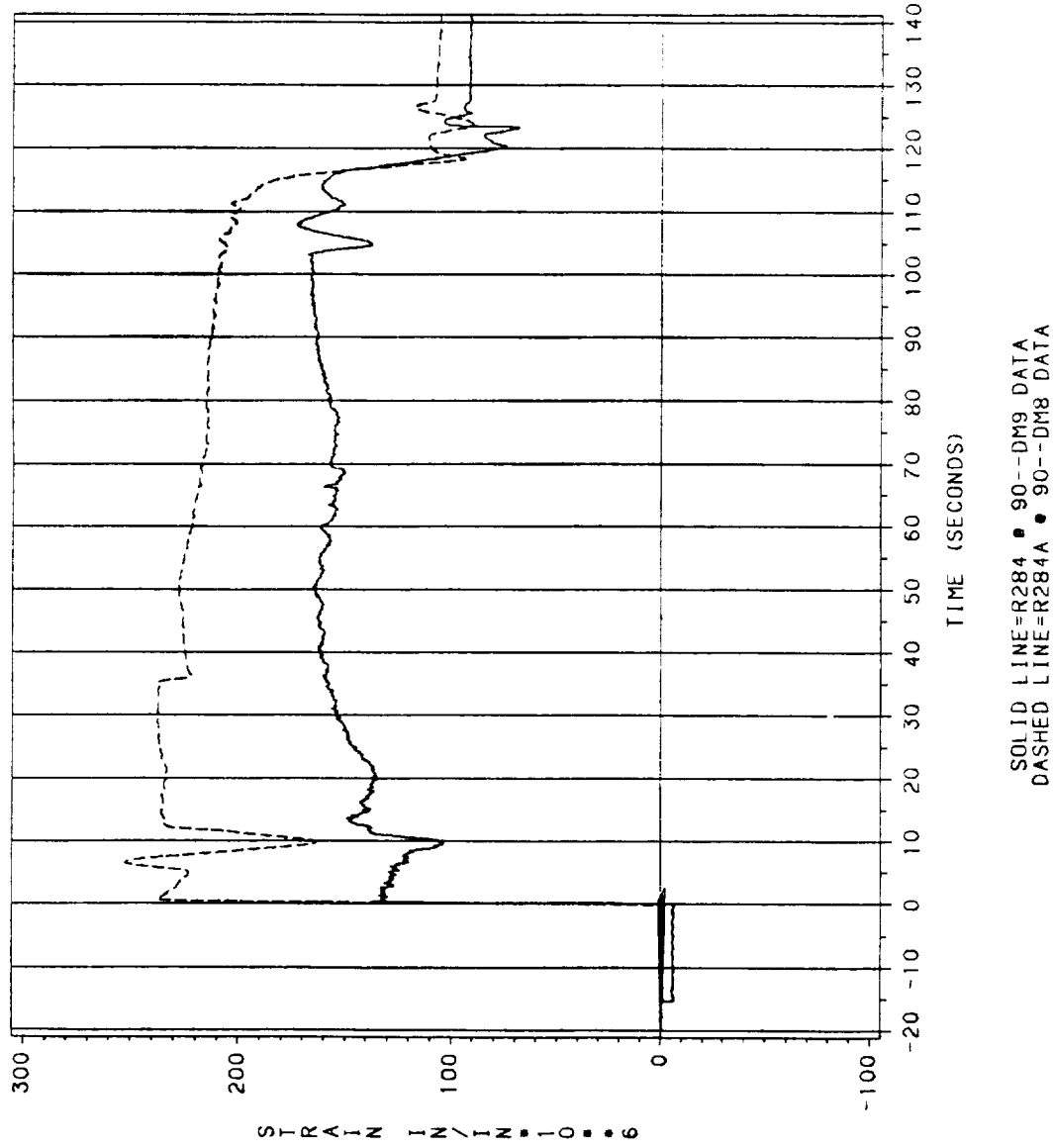

Figure 7.5-167. DM-9 and DM-8 Fixed Housing (meridional strains), 90 deg at Location 4

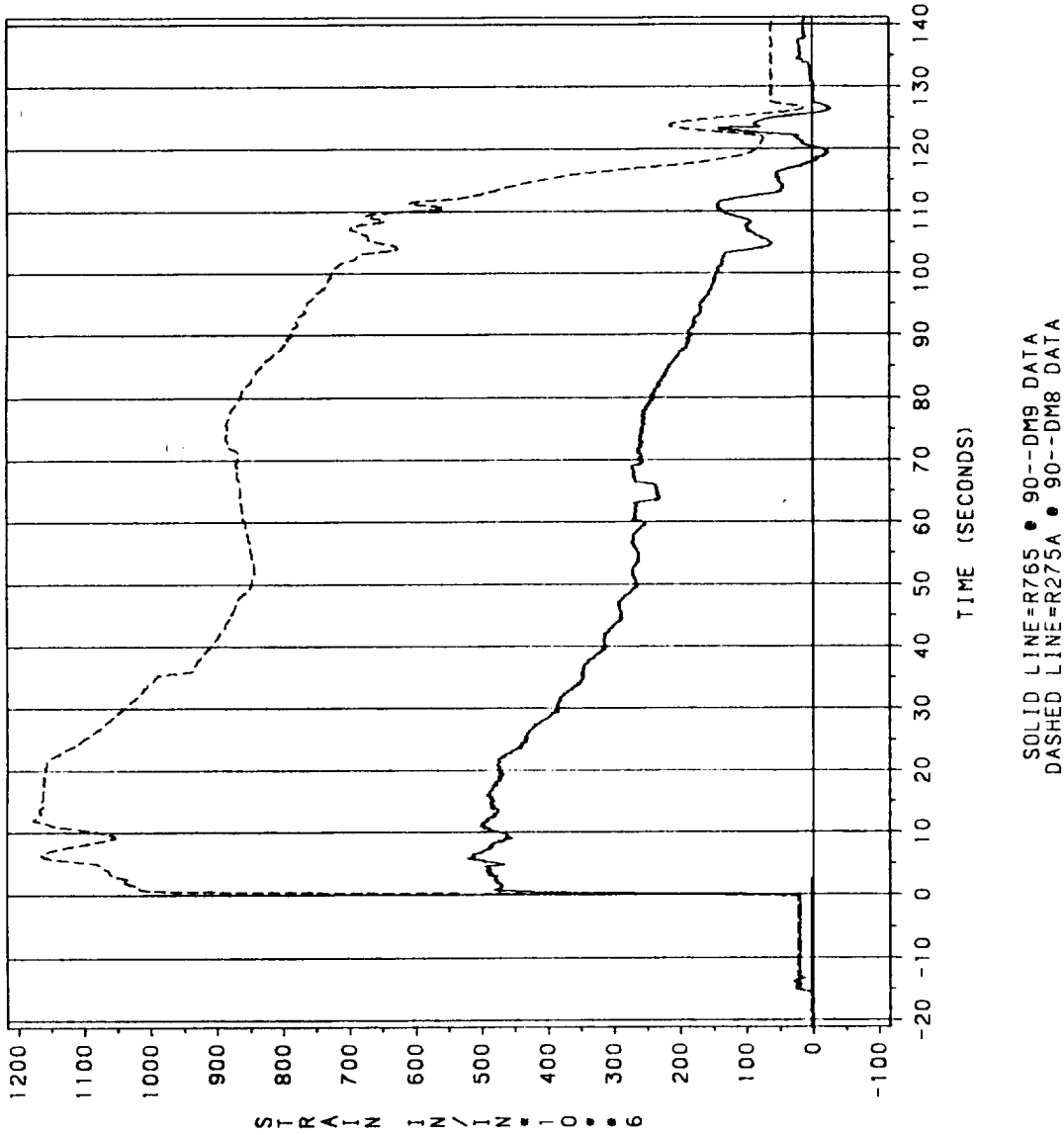

Figure 7.5-168. DM-9 and DM-8 Nose Inlet Housing (hoop strains), 90 deg at Location 5

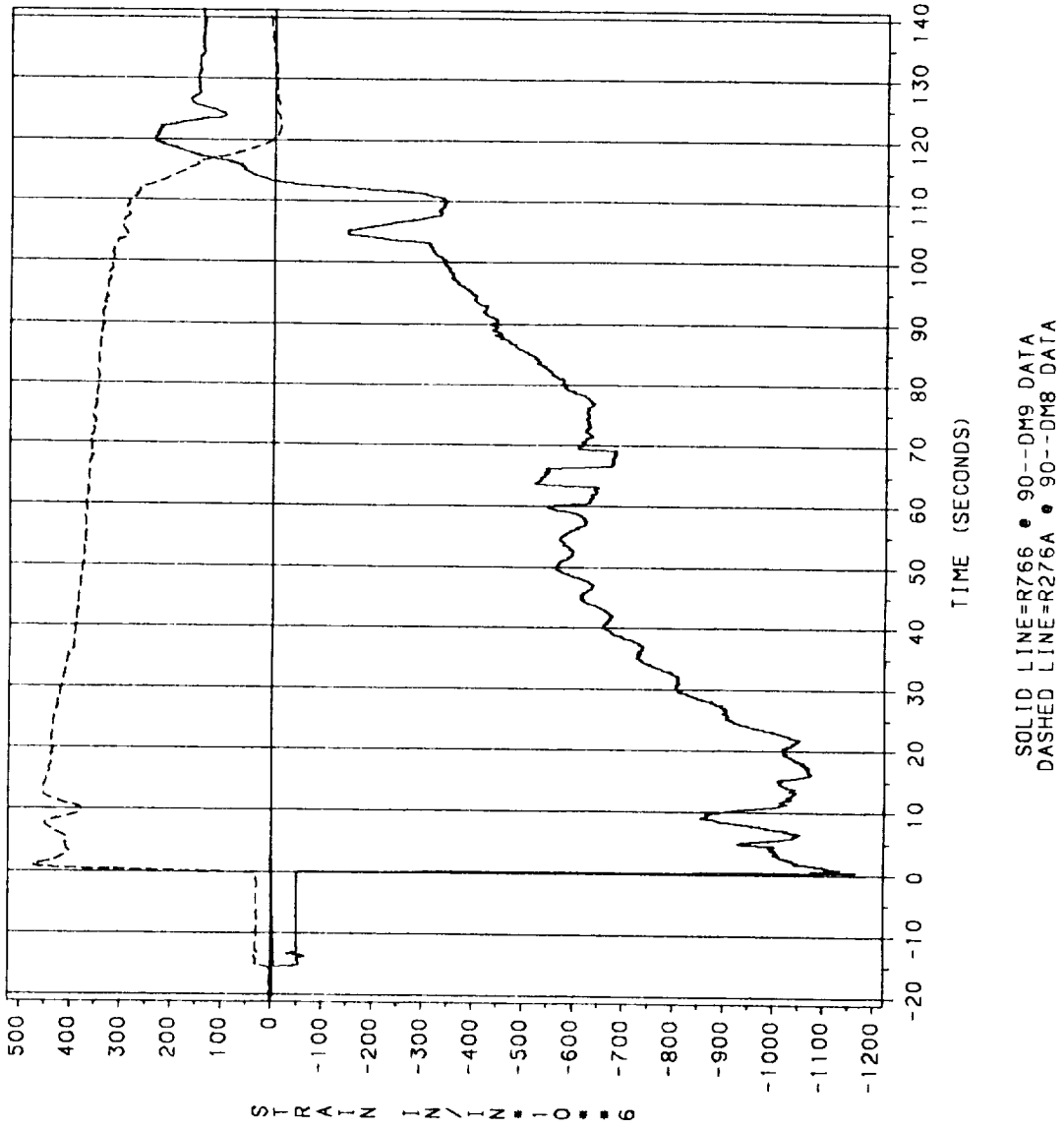

Figure 7.5-169. DM-9 and DM-8 Nose Inlet Housing (meridional strains), 90 deg at Location 5

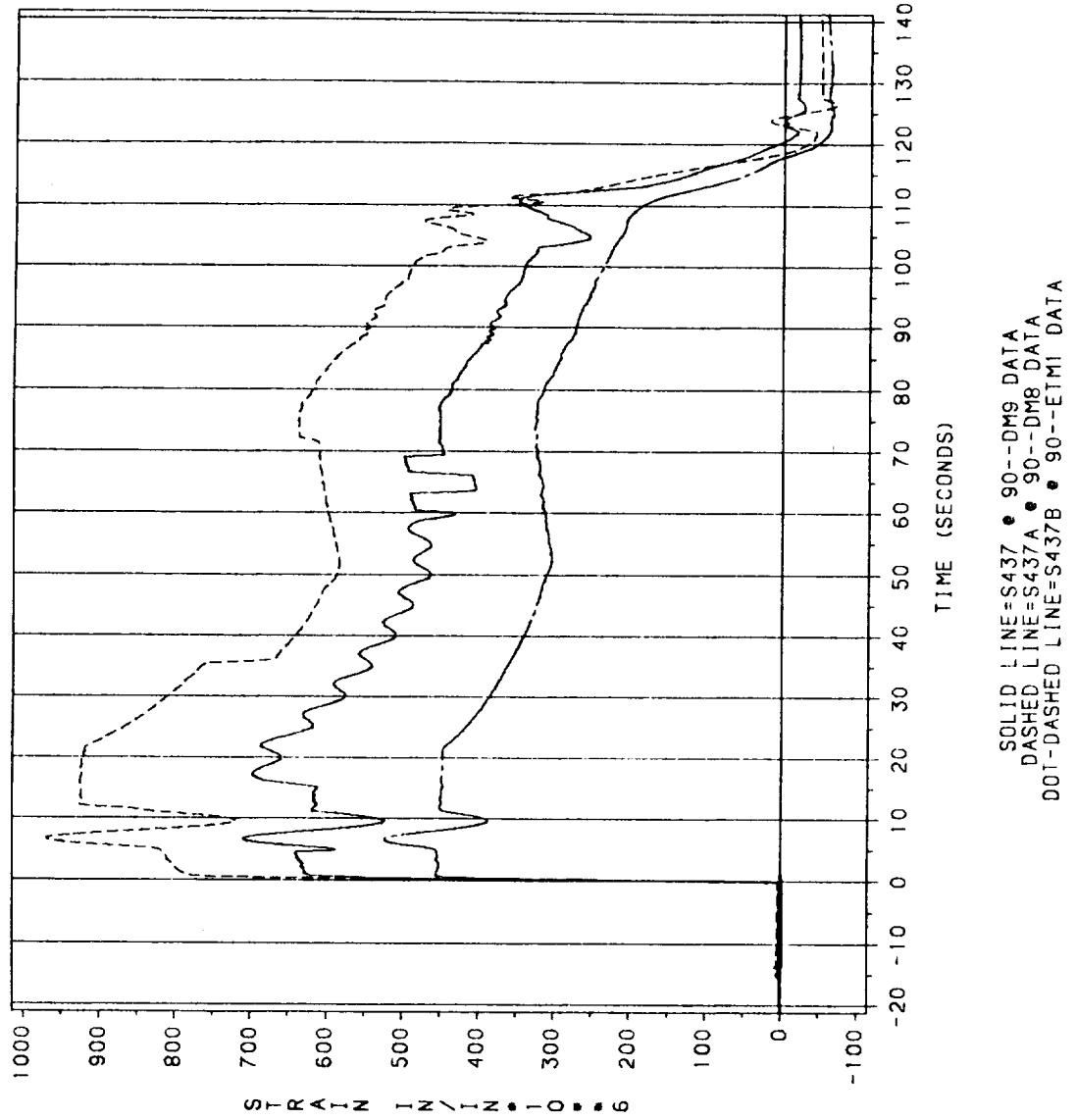

Figure 7.5-170. DM-9, DM-8, and ETM-1A Forward End Ring (hoop strains), 90 deg at Location 6

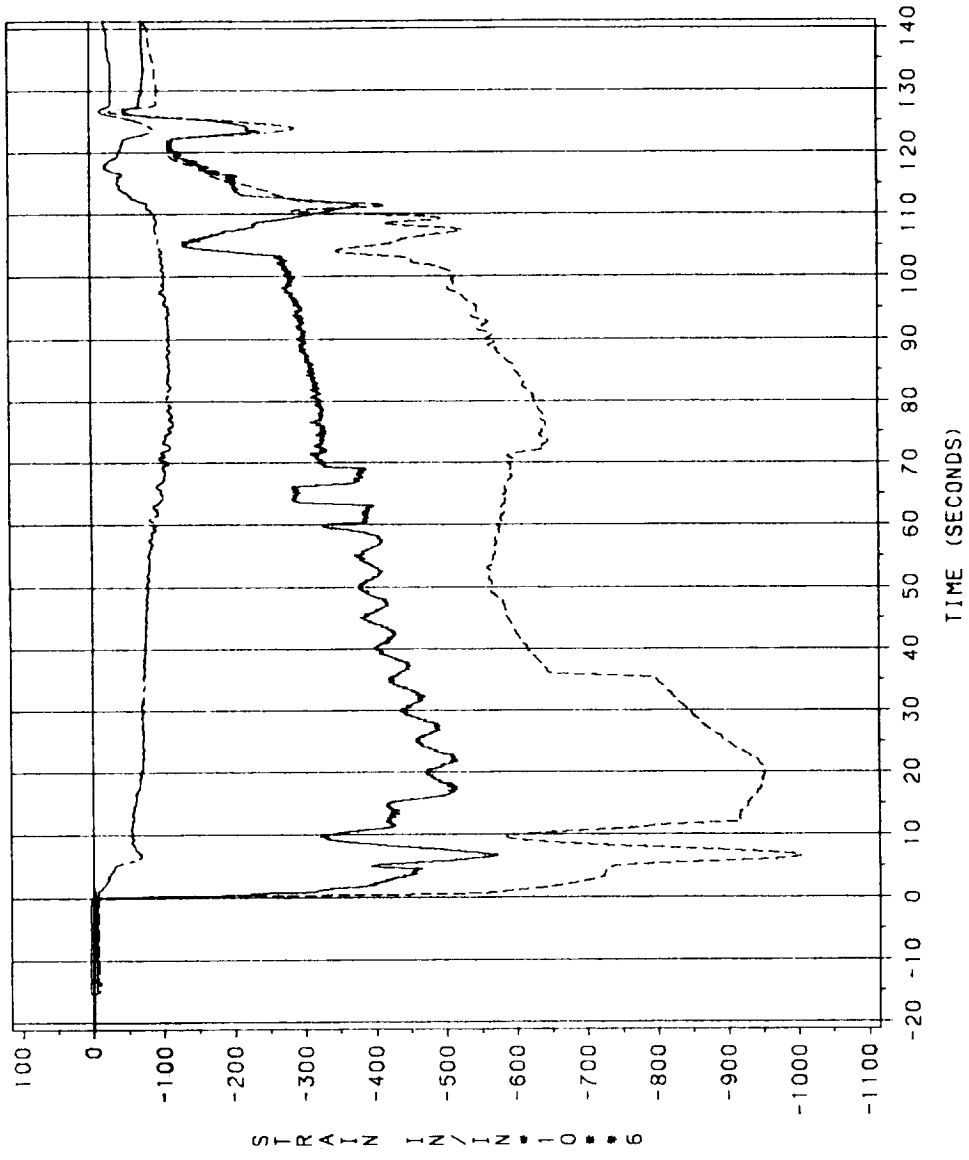

Figure 7.5-171. DM-9, DM-8, and ETM-1A Forward End Ring (meridional strains), 90 deg at Location 6

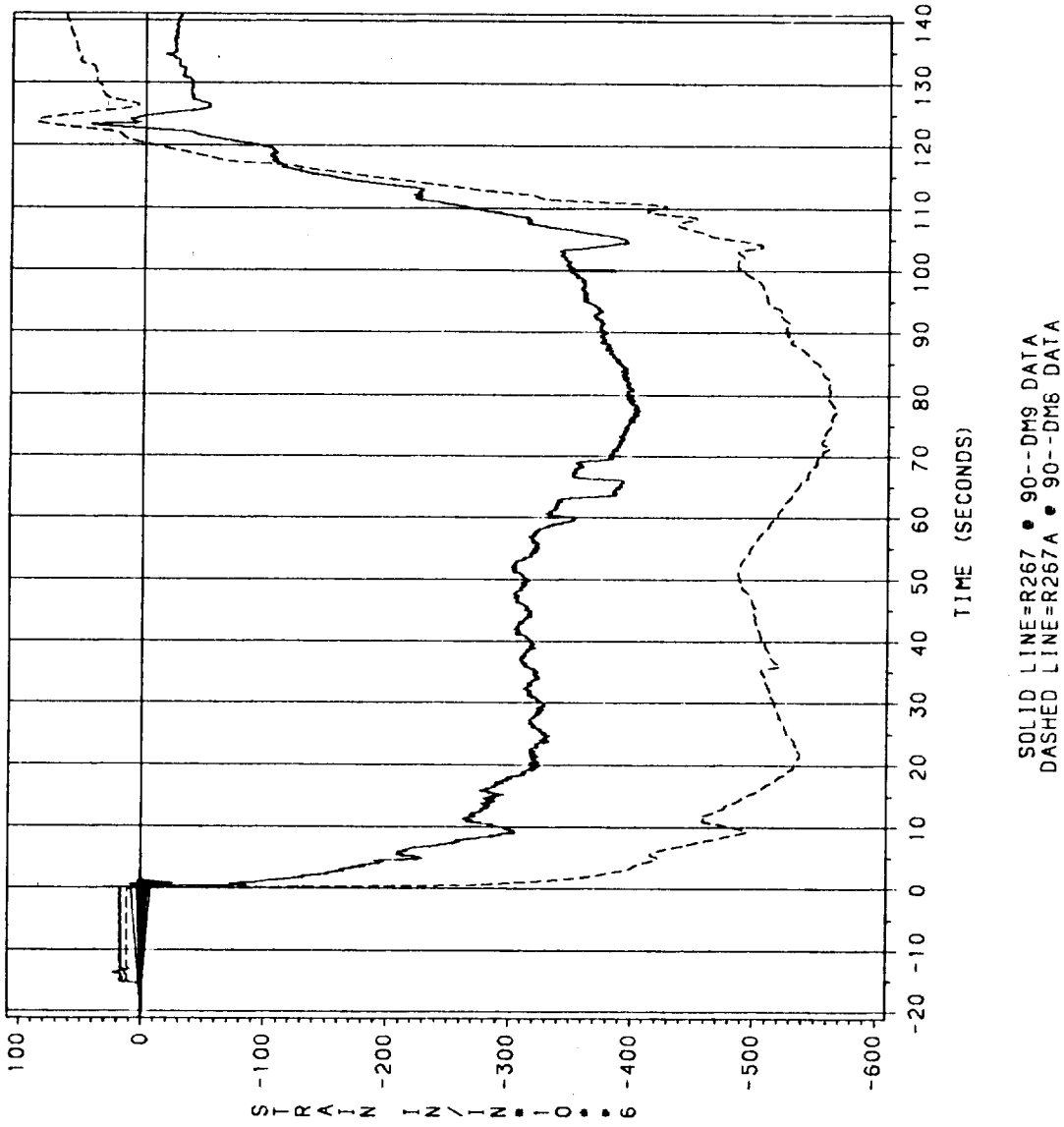

Figure 7.5-172. DM-9 and DM-8 Nose Inlet Housing (hoop strains), 90 deg at Location 7

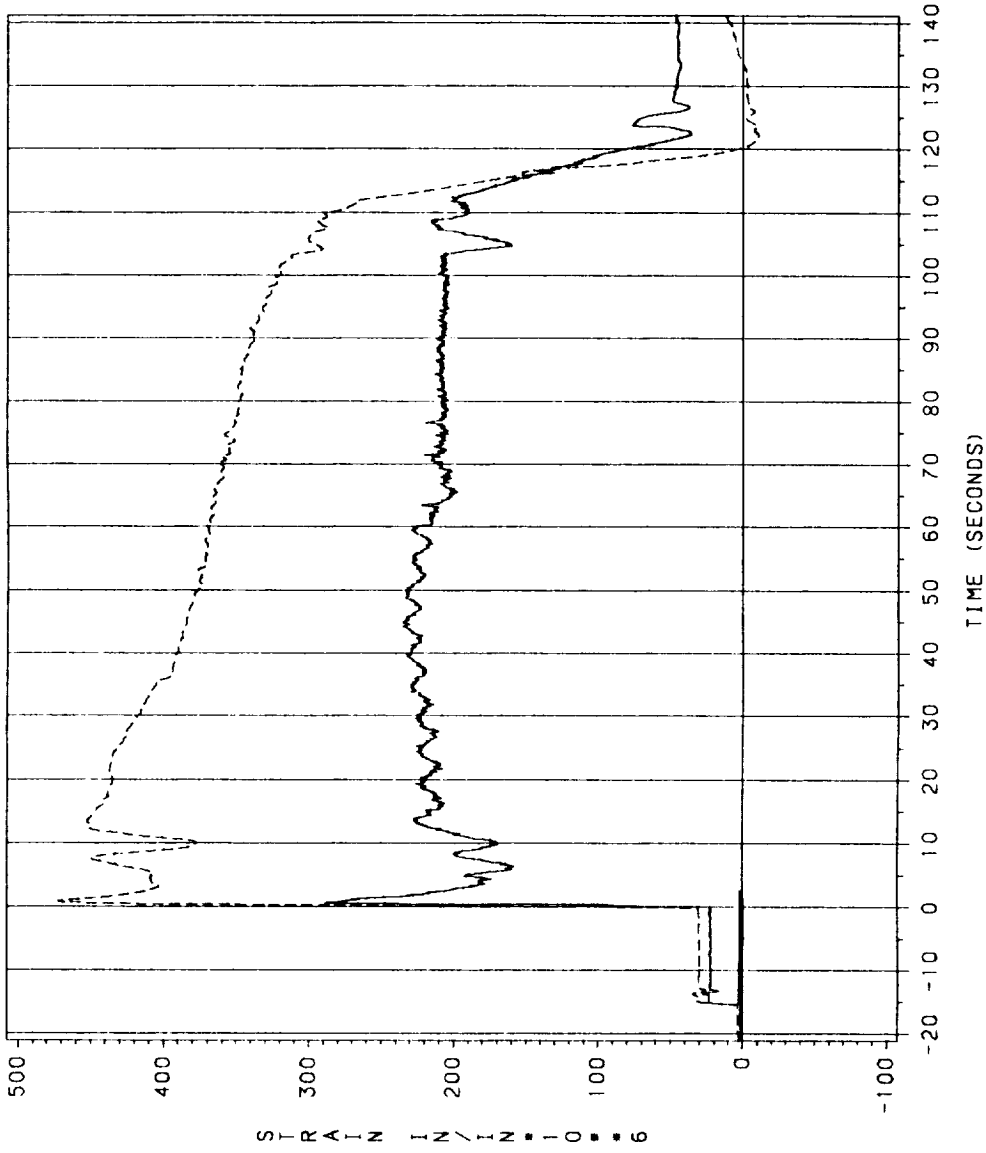

Figure 7.5-173. DM-9 and DM-8 Forward End Ring (meridional strains), 90 deg at Location 8

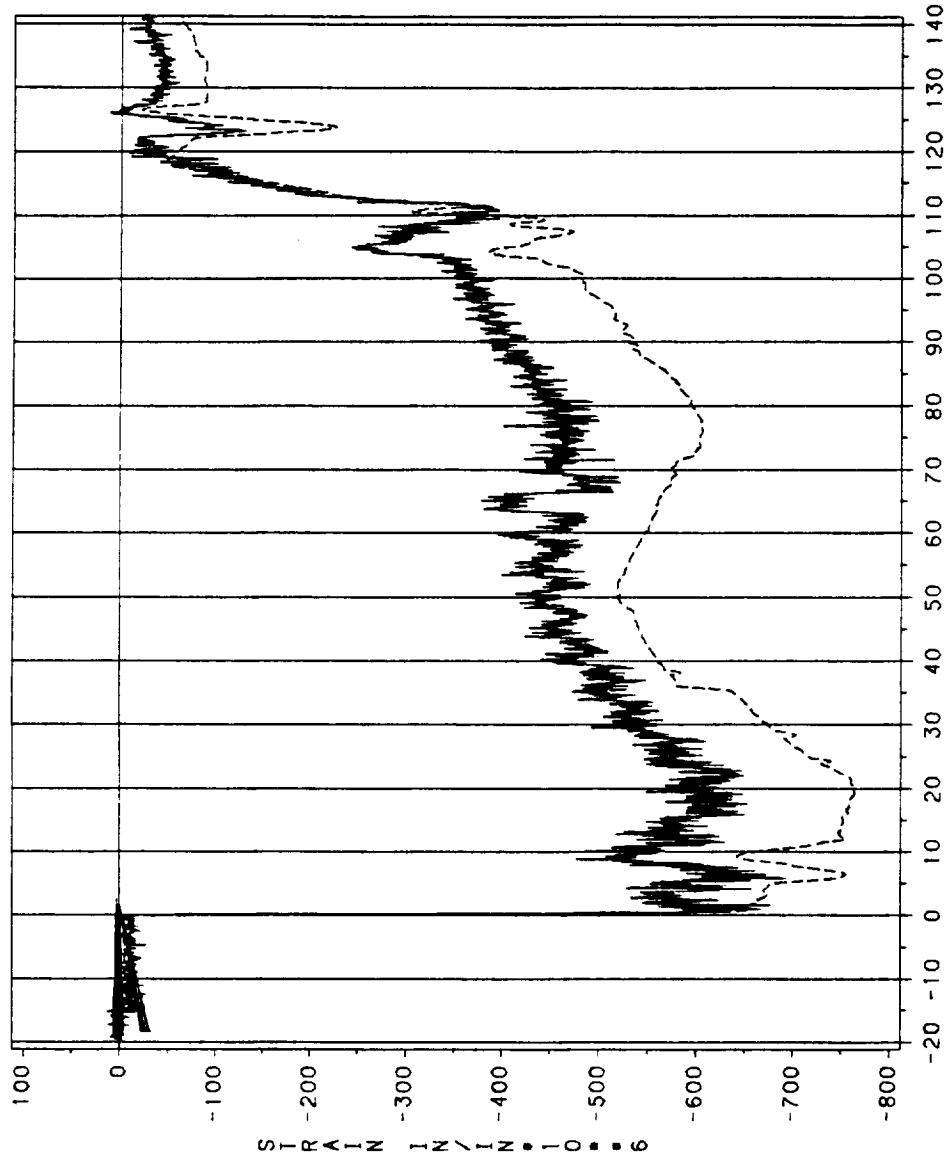

Figure 7.5-174. DM-9 and DM-8 Nose Inlet Housing (hoop strains), 90 deg at Location 9

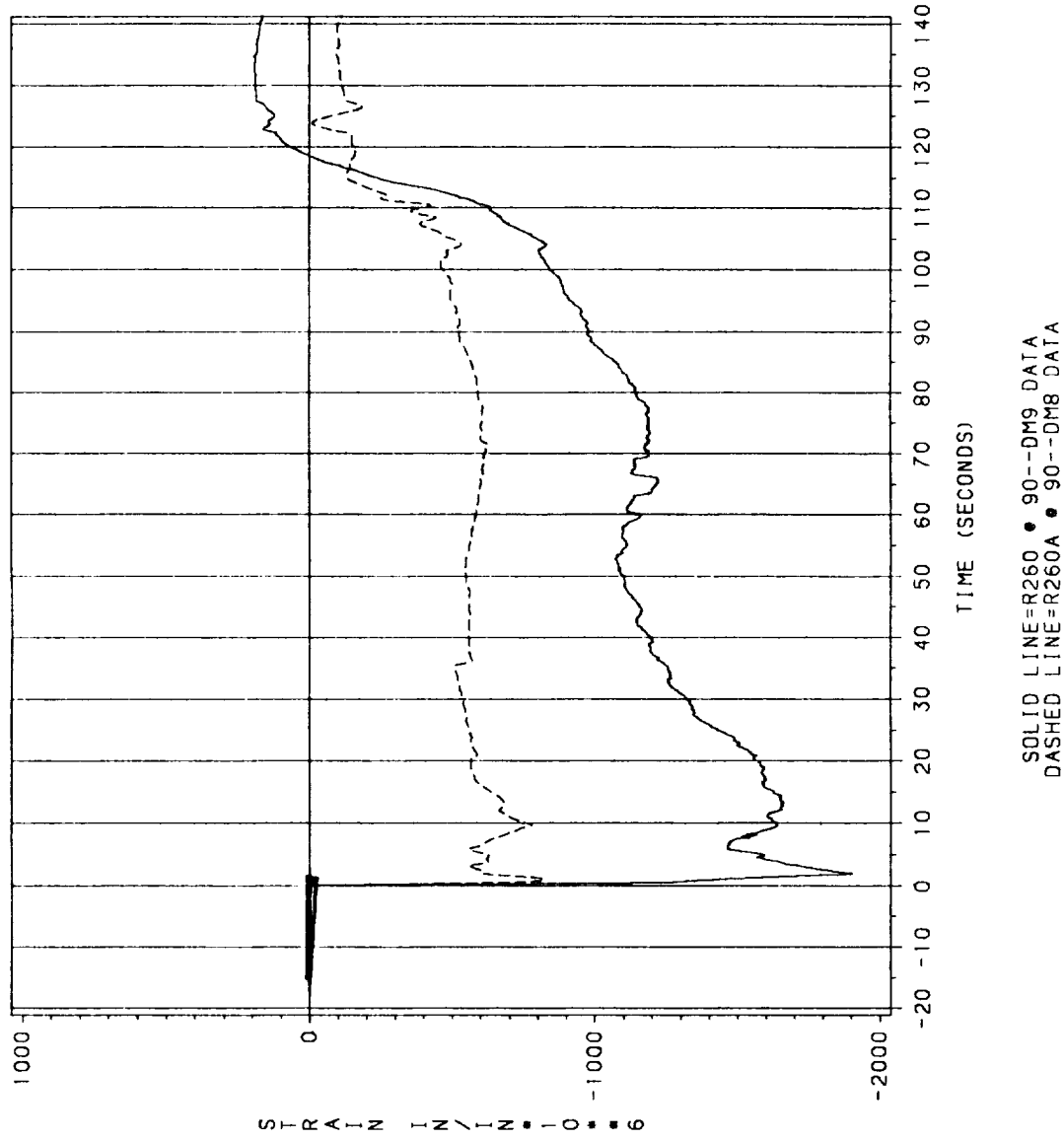

Figure 7.5-175. DM-9 and DM-8 Nose Inlet Housing (meridional strains), 90 deg at Location 9

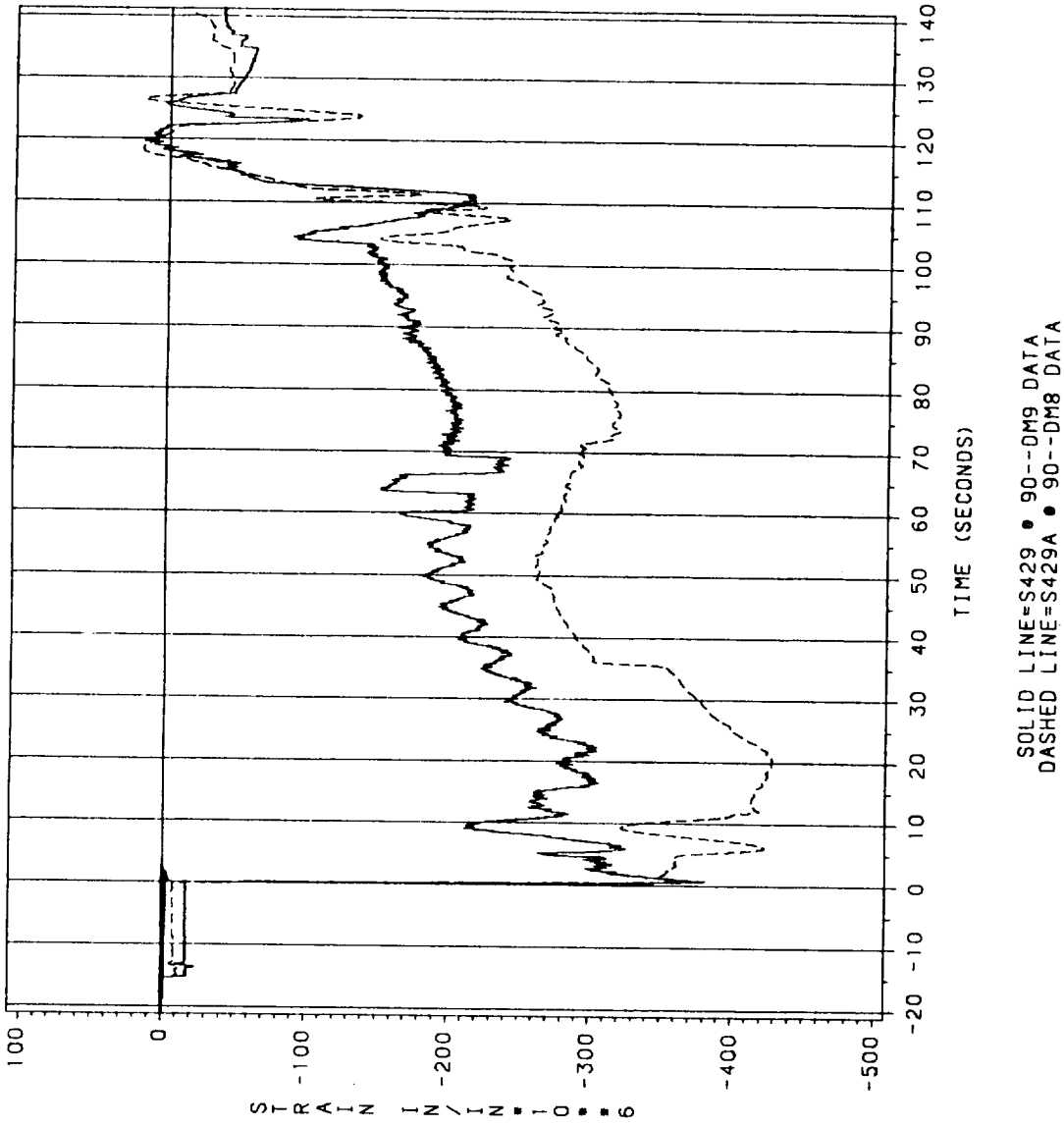

Figure 7.5-176. DM-9 and DM-8 Nose Inlet Housing (hoop strains), 90 deg at Location 10

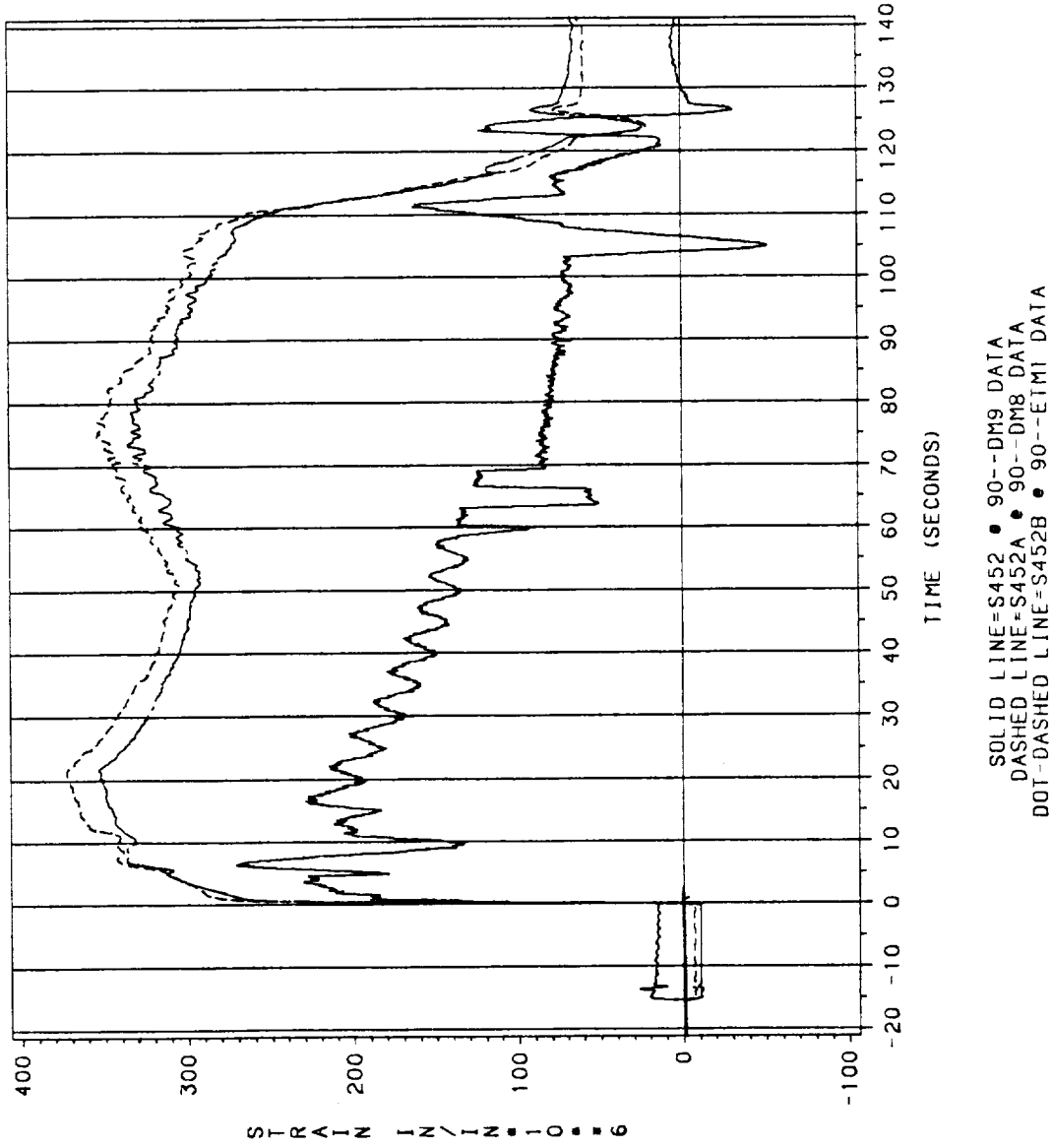

Figure 7.5-177. DM-9, DM-8, and ETM-1A Throat Housing (hoop strains), 90 deg at Location 1

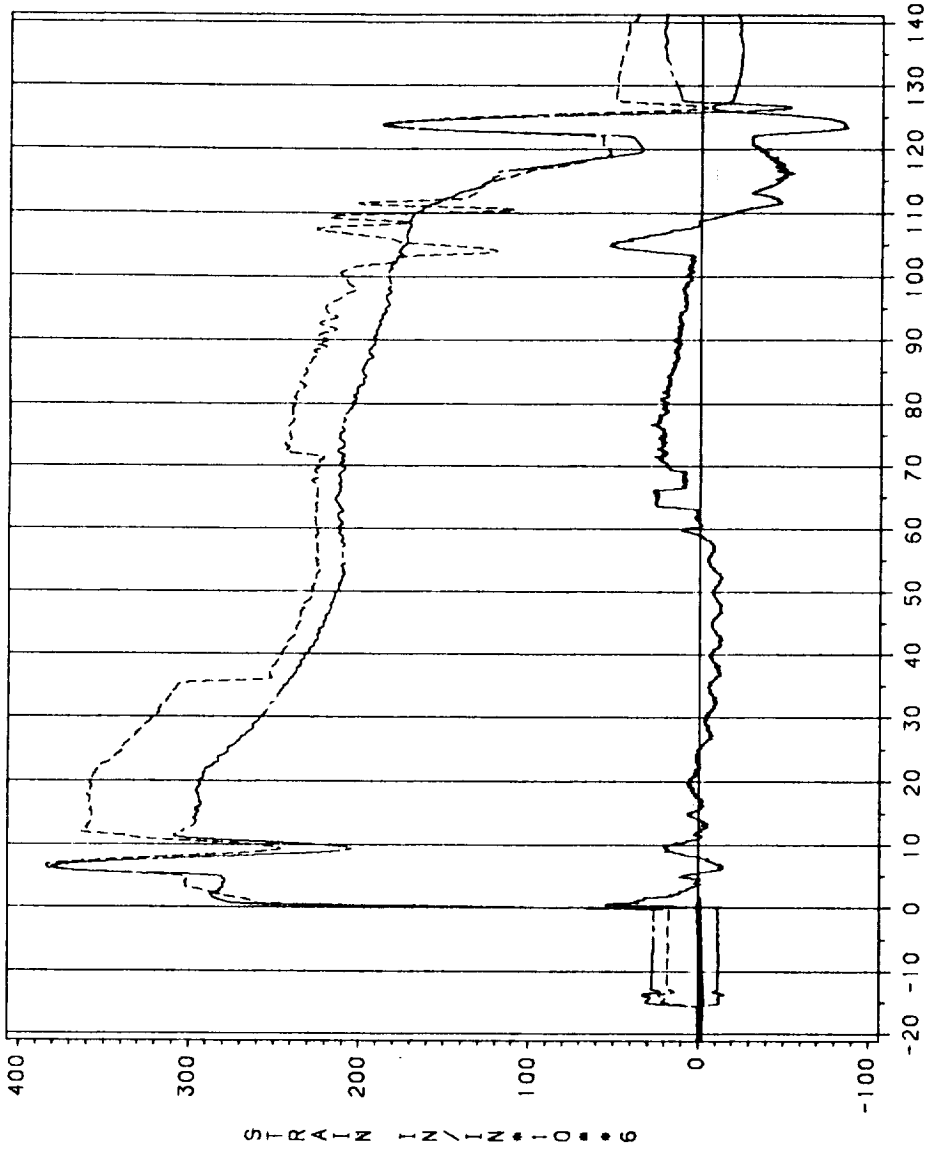

Figure 7.5-178. DM-9, DM-8, and ETM-1A Throat Housing (meridional strains), 90 deg at Location 11

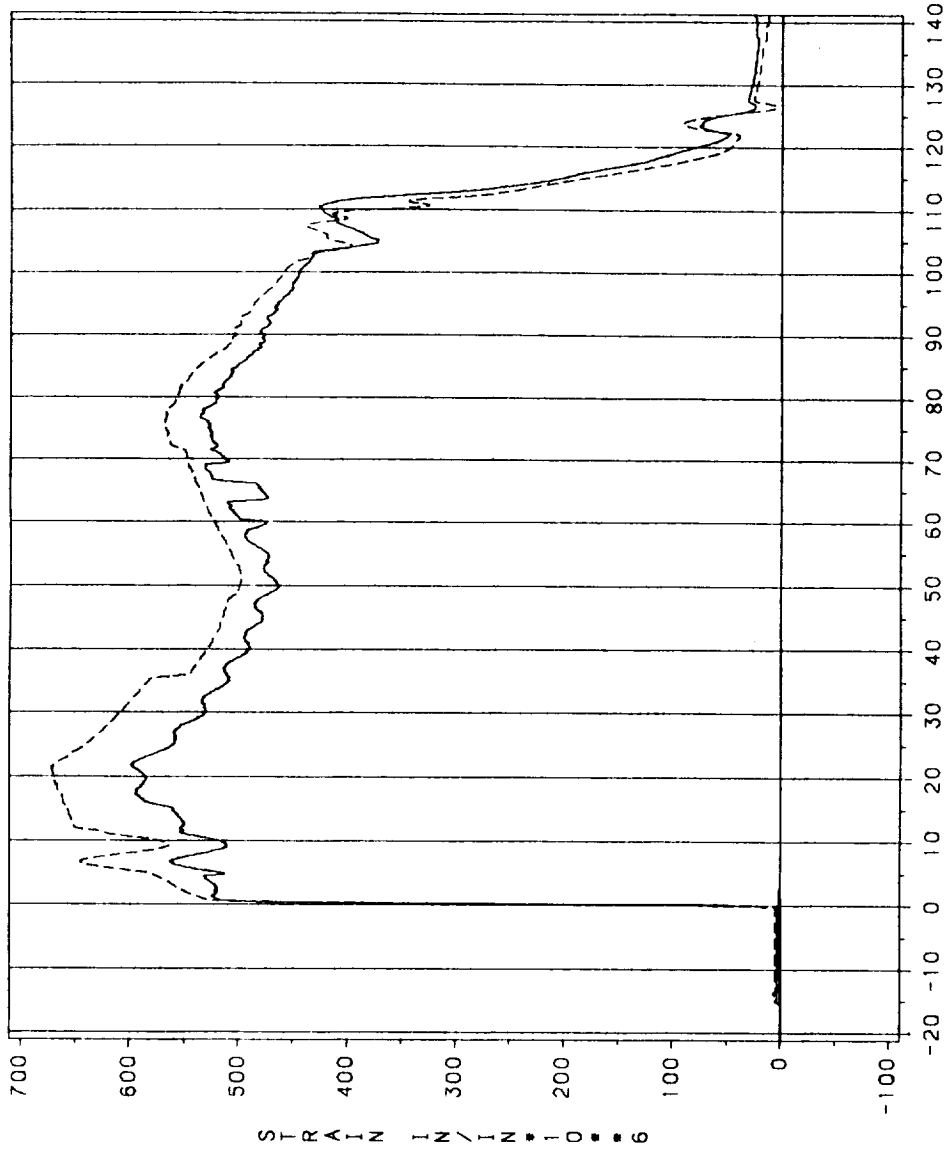

Figure 7.5-179. DM-9 and DM-8 Throat Housing (hoop strains), 90 deg at Location 12

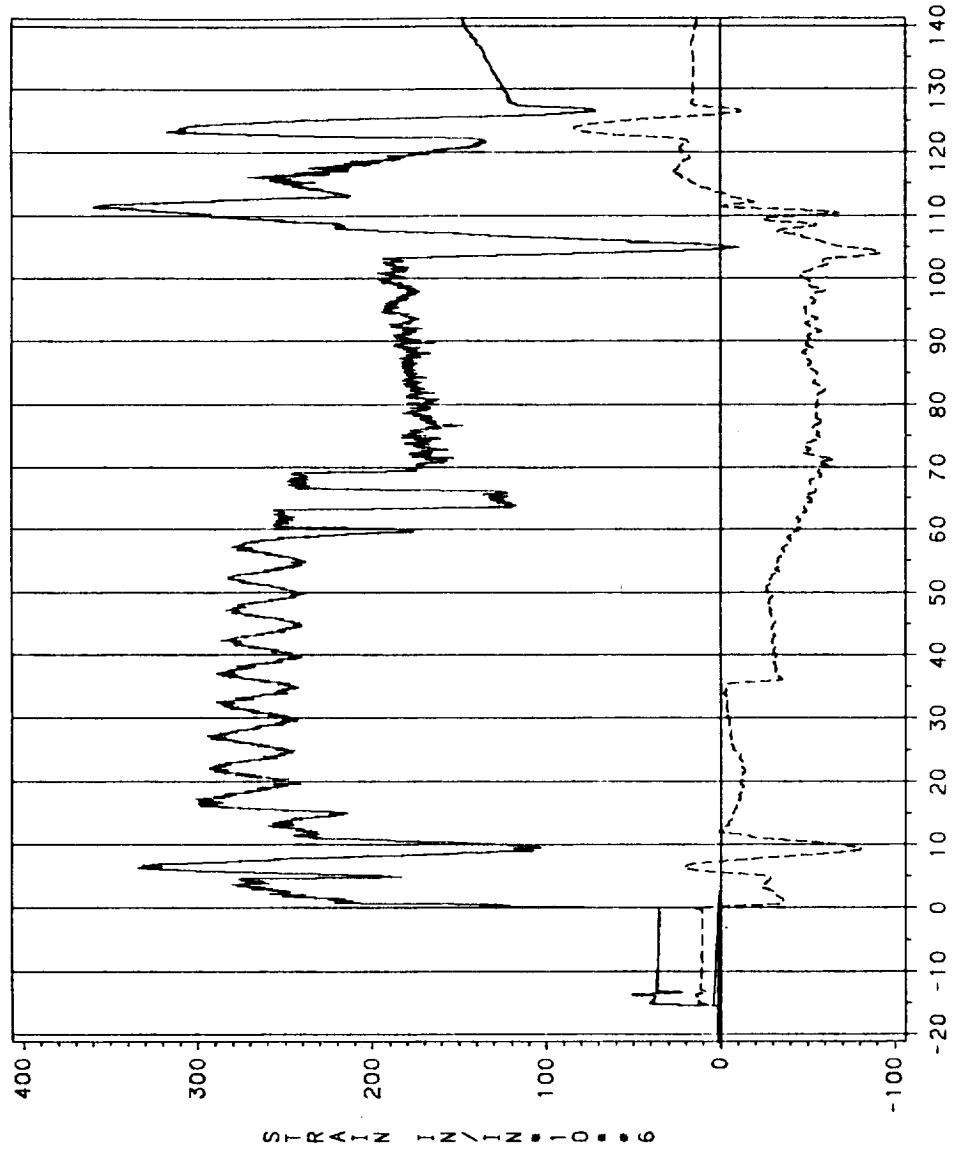

Figure 7.5-180. DM-9 and DM-8 Throat Housing (meridional strains), 90 deg at Location 12

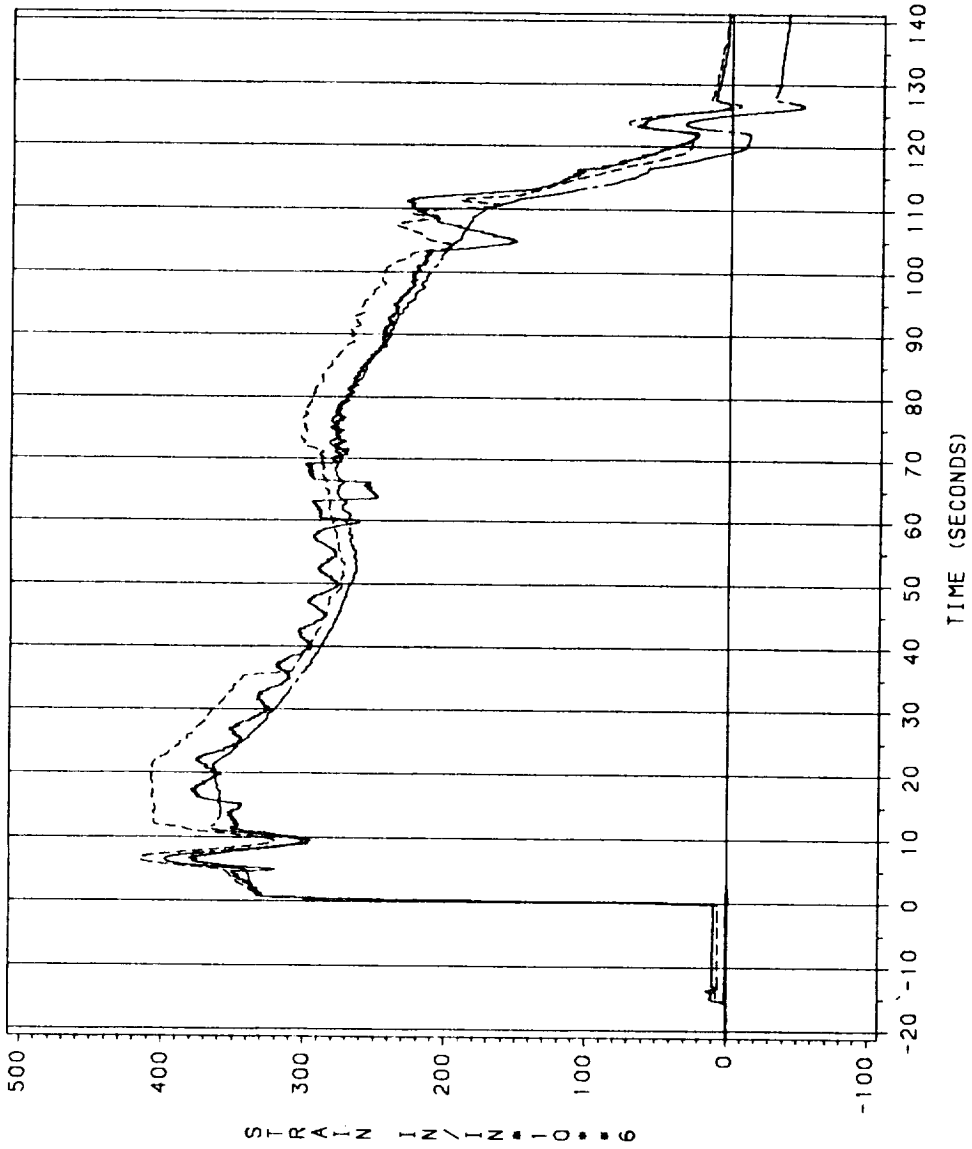

Figure 7.5-181. DM-9, DM-8, and ETM-1A Throat Housing (hoop strains), 90 deg at Location 13

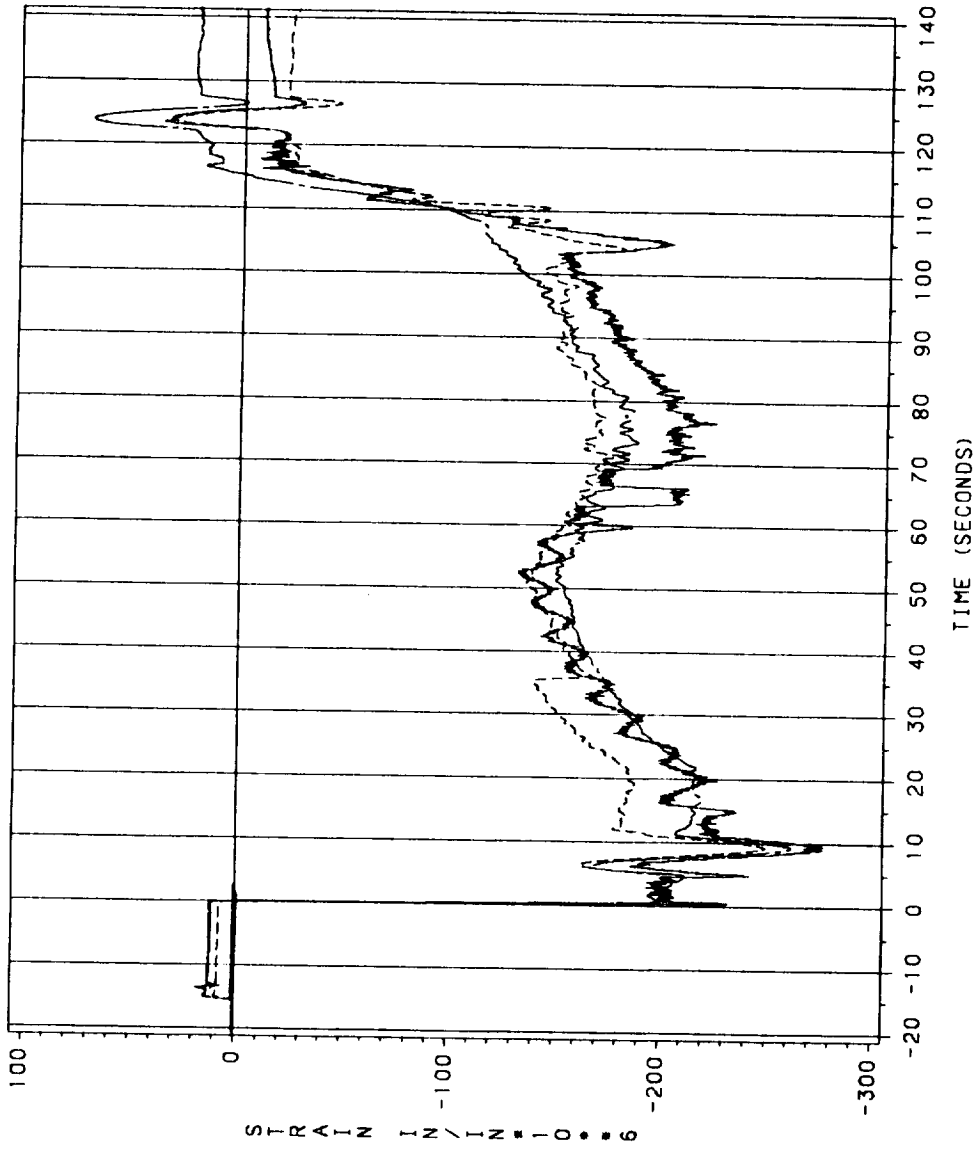

Figure 7.5-182. DM-9, DM-8, and ETM-1A Throat Housing (meridional strains), 90 deg at Location 13

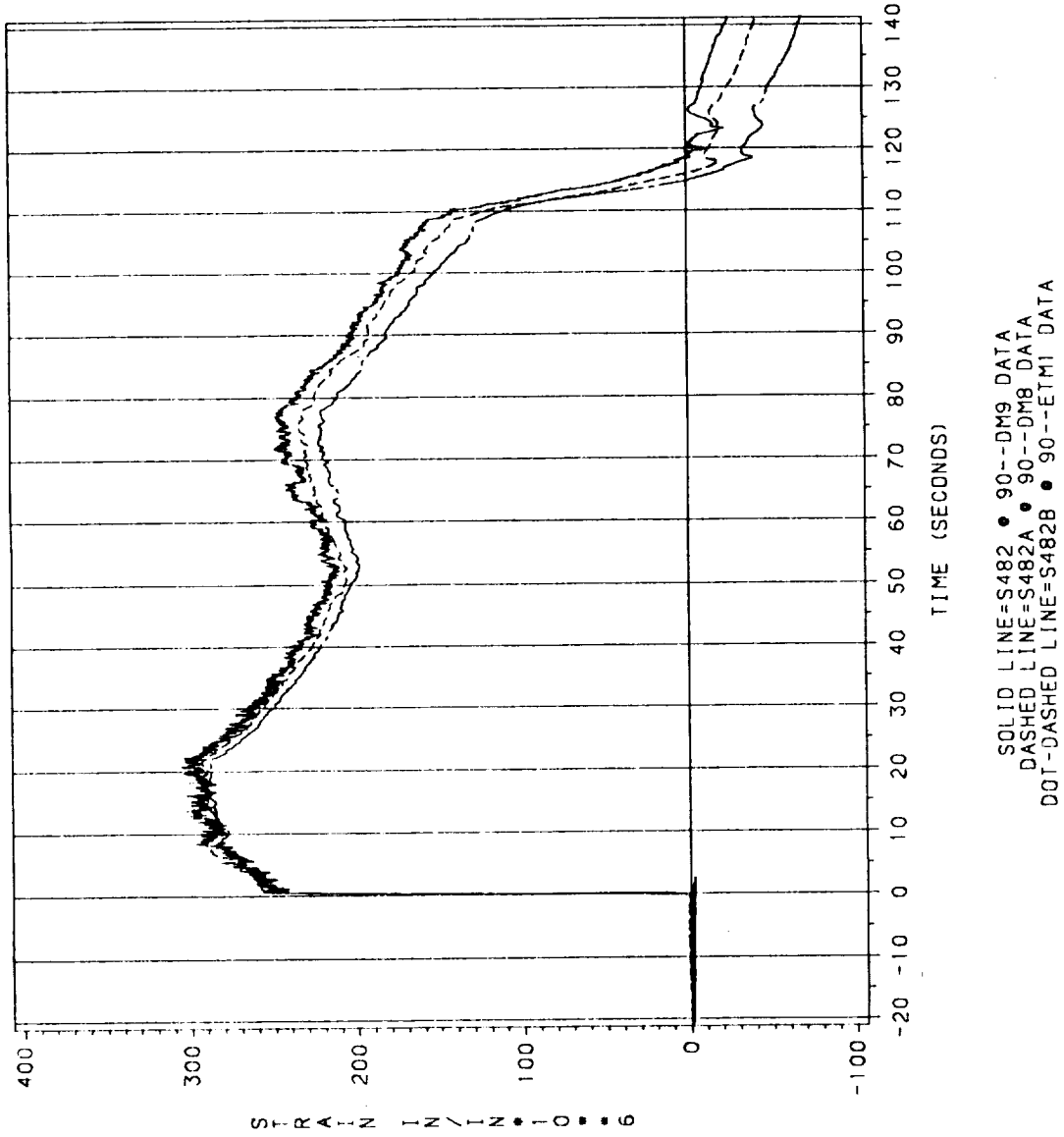

Figure 7.5-183. DM-9, DM-8, and ETM-1A Forward Exit Cone (hoop strains), 90 deg at Location 14

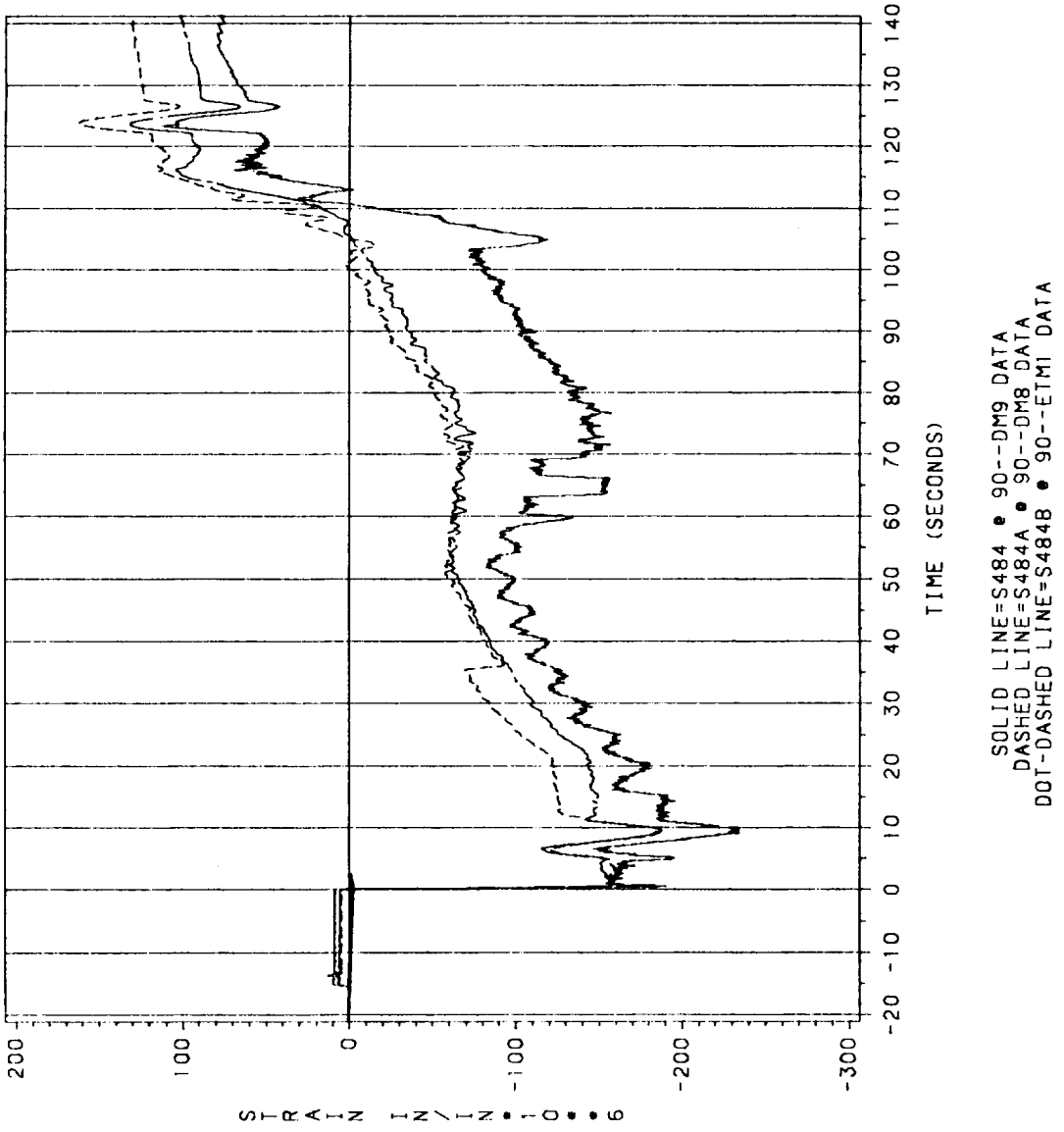

Figure 7.5-184. DM-9, DM-8, and ETM-1A Forward Exit Cone (meridional strains), 90 deg at Location 14

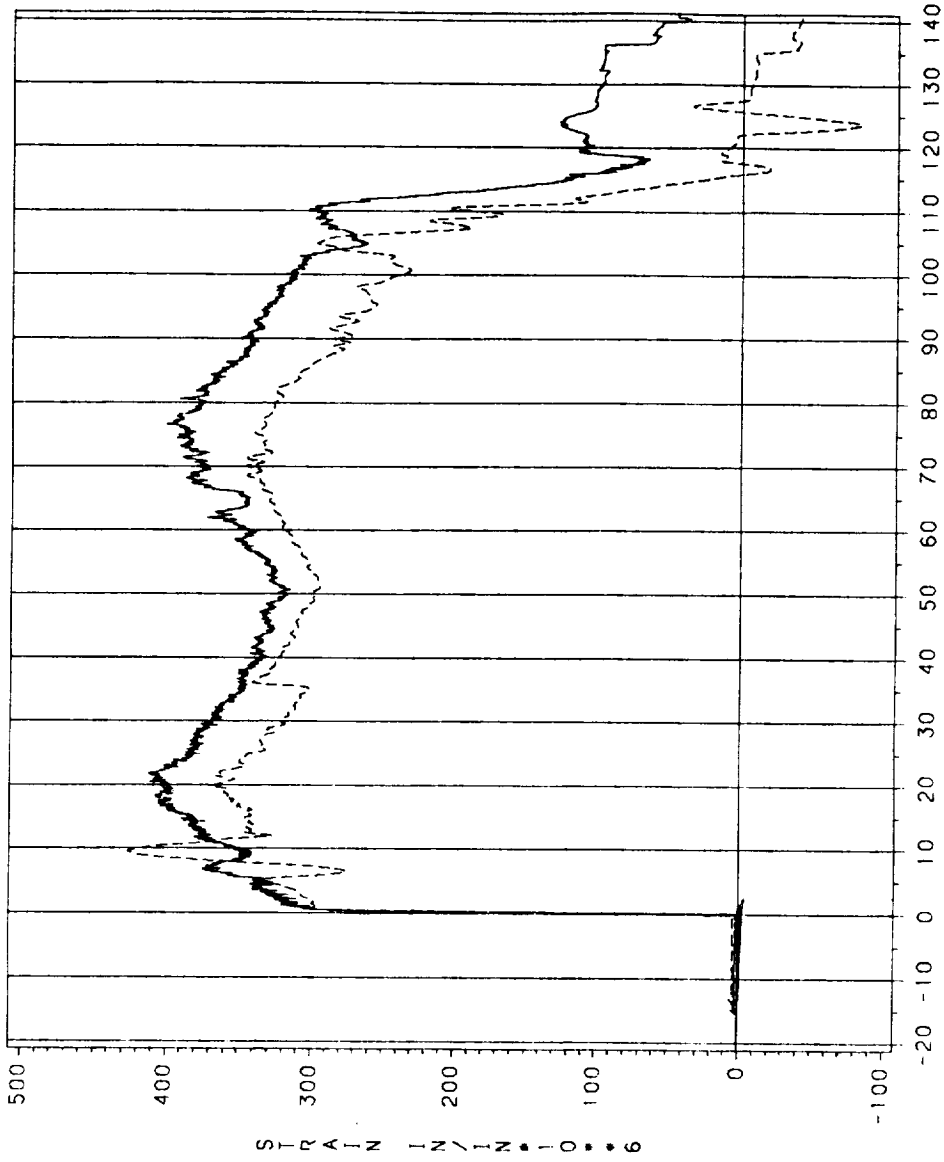

Figure 7.5-185. DM-9 and DM-8 Aft Exit Cone (hoop strains), 90 deg at Location 15

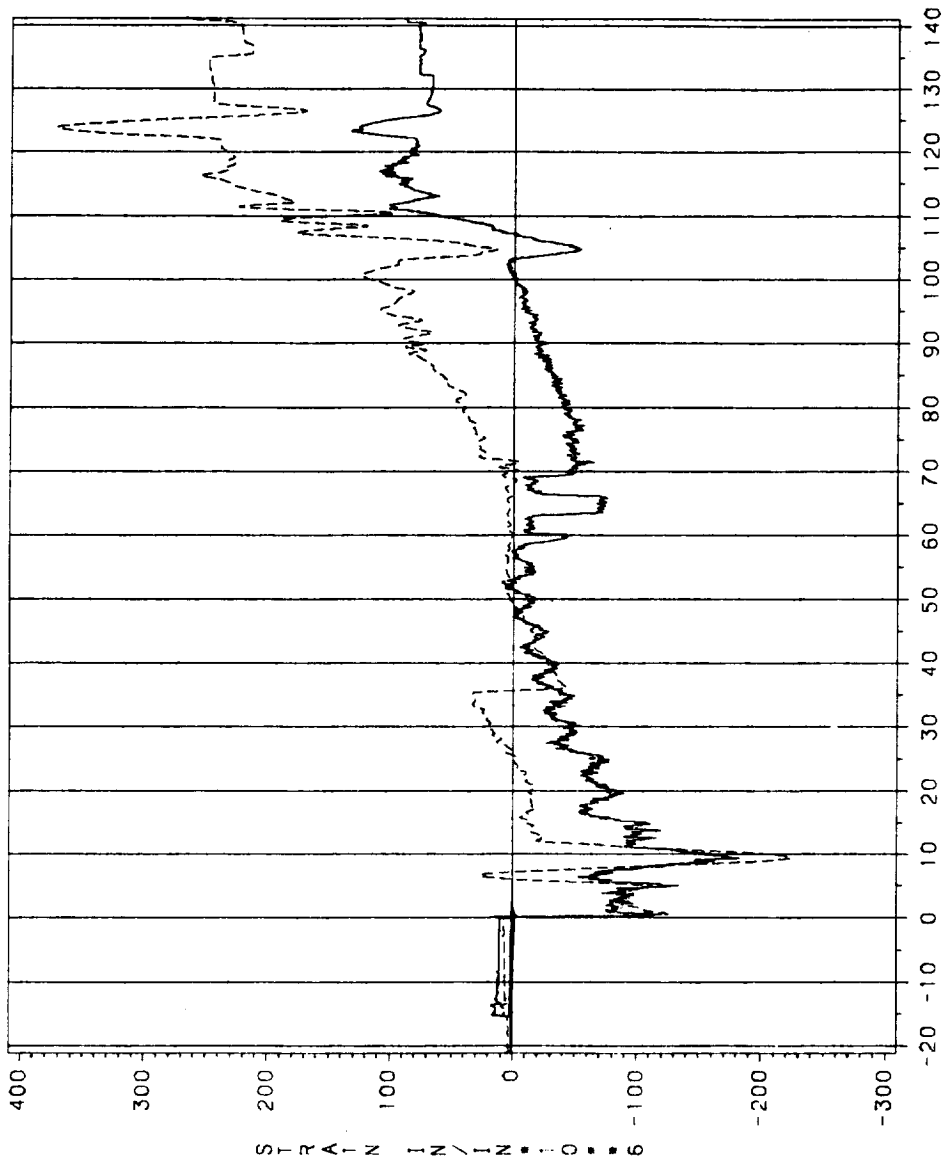

Figure 7.5-186. DM-9 and DM-8 Aft Exit Cone (meridional strains), 90 deg at Location 15

Table 7.5-10. DM-9 Static Test Nozzle Hoop Strains Due to Vectoring (gage azimuth 90 deg, μin./in.)

CONDITION	NON PRESSURIZED (ACTUATOR ADJUSTMENT)			NON PRESSURIZED (DRY RUN)			PRESSURIZED (STATIC FIRING)		
VECTOR ANGLE (DEG)	5.8	-3.2	5.7	4.4	-1.4	6.9	4.0	-4.4	6.3
VECTOR DIRECTION	90	270	90	270	90	270	270	90	270
TIME (SEC)	140.5	168.0	194.0	6.5	10.0	124.0	6.6	9.8	124.0
LOCATION #				HOOP STRAINS					
1 - FIXED HOUSING AFT END	76	-35	75	64	-30	94	70	-70	65
2 - FIXED HOUSING MID SECTION	37	-13	37	36	-14	43	-35	25	20*
3 - FIXED HOUSING FWD SECTION	20*	-5*	18*	23	-6	25	-75	75	-75
4 - AFT END RING FWD END	-110	45	-115	-95	40	-130	170	-190	-65
5 - NOSE INLET HSG AFT END	95	-65	90	79	-40	119	55	-45	150
6 - FWD END RING FWD REGION	35	-20	30	29	8	50	120	-100	100
7 - NOSE INLET HSG AFT END	80	-48	76	66	-30	96	50	-70	100
8 - FWD END RING AFT END	110	-65	110	90	-50	137	80	-40	130
9 - NOSE INLET HSG FWD END	-68	45	-68	*	*	*	-100*	90*	-100
10 - NIH / THROAT JOINT REGION	-50	45	-45	-64	11	-84	-70	70	-95
11 - THROAT HSG FWD END	105	-60	105	85	-50	128	90	-70	130
12 - THROAT HSG MID SECTION	12	-10	12	18	-3	25	35	-35	35
13 - THROAT HSG AFT END	48	-28	46	41	-20	59	60	-55	60
14 - FWD EXIT CONE	-8	4	-8	-8	3	-14	-10	10	-20
15 - AFT EXIT CONE	13	-8	13	15*	-6*	15*	20	-20	20
16 - COMPLIANCE RING (Gage Azimuth 45°)	-400	150	390	-250	40	-330	-270	300	300
17 - THROAT HSG/ FWD EXIT CONE	50	-26	48	44	-14	61	45	-45	40
JOINT REGION	(-12)	(12)	(-12)	(5*)	(10*)	(-15*)	(-20)	(15)	(-40)
18 - THROAT HSG/ AFT END RING	50	-22	50	50	-20	64	40	-45	40
JOINT REGION	(-12)	(10)	(-10)	(-9*)	(16*)	(-13*)	(20)	(20)	(-40)
19 - AFT END RING	66	18*	66	66	-24	66	-80	20	-20
AFT END	(96)	(-26)	(92)	(86)	(-20)	(118)	(20)	(-60)	(80)
20 - AFT END RING	62	14*	62	62	-20	66	-55	20	-20
AFT END	(88)	(-16)	(86)	(74)	(-24)	(102)	(-20)	(20)	(80)
22 - FIXED HSG/ AFT END RING	20*	20*	20*	18*	-13	18	-75	95	-70
JOINT REGION	(78)	(-30)	(-74)	(62)	(-26)	(96)	(70)	(-100)	(100)

Notes :

* Data not clear.

Strains in parenthesis are for gages at the 270 degree azimuth.

Table 7.5-11. DM-9 Static Test Nozzle Meridional Strains Due to Vectoring (gage azimuth 90 deg, μin./in.)

CONDITION	NON PRESSURIZED (ACTUATOR ADJUSTMENT)			NON PRESSURIZED (DRY RUN)			PRESSURIZED (STATIC FIRING)		
VECTOR ANGLE (DEG)	5.8	-3.2	5.7	4.4	-1.4	6.9	4.0	-4.4	6.3
VECTOR DIRECTION	90	270	90	270	90	270	270	90	270
TIME (SEC)	140.5	168.0	194.0	6.5	10.0	124.0	6.6	9.8	124.0**
LOCATION #	MERIDIONAL STRAINS								
1 - FIXED HOUSING AFT END	-105	30	-100	-96	26	-128	-10	10	-60
2 - FIXED HOUSING MID SECTION	-29	19	29	-20	8	-38	10	-10	-45
3 - FIXED HOUSING FWD SECTION	110	-35	105	96	-32	136	150	-140	140
4 - AFT END RING FWD END	25	10*	25	15	-10	33	0	-20	-20
5 - NOSE INLET HSG AFT END	-160	100	-155	-150	80	-200	-120	110	-90
6 - FWD END RING FWD REGION	-102	46	-100	-68	30	-120	-170	100	-120
7 - NOSE INLET HSG AFT END	-100	60	-100	-88	47	-125	-45	60	-60
8 - FWD END RING AFT END	27	-15	30	33	-20	34	-25	25	40
9 - NOSE INLET HSG FWD END	16	-30	12	28	-7	36	110	-50	40
10 - NIH / THROAT JOINT REGION	95	-85	90	110	-30	155	65	-60	100
11 - THROAT HSG FWD END	-53	27	-53	-42	19	-67	-15	20	-60
12 - THROAT HSG MID SECTION	175	-100	170	150	-70	215	125	-120	200
13 - THROAT HSG AFT END	64	-38	63	55	-26	80	45	-45	55
14 - FWD EXIT CONE	44	-24	44	42	-15	60	45	-40	60
15 - AFT EXIT CONE	120	30	110	42	-21	52	60	-70	50
16 - COMPLIANCE RING (Gage Azimuth 45°)	155	-45	150	92	-12	140	90	-100	100

Notes :

** Discontinuity in curve clouds data at this time scale.

* Data not clear.

to the 4.0 or- 4.4 deg vectoring event are compared in Table 7.5-12 in the hoop direction and in Table 7.5-13 in the meridional direction for all gage locations. Note that although vector-related strains are significant in comparison to some pressure-related strains, they are generally low (less than 400 in./in.). These measurements are significant in that they will aid in calibrating 3-D analyses which predict the contribution of TVC loads to strains in joint areas. (Strains due to vectoring were obtained by subtracting out the strains due to pressure at that time interval.)

b. Dry Run Duty Cycles. The dry run duty cycle is shown in Figure 7.5-114. Data were obtained during the dry run duty cycle to compare the effects of vectoring with and without the pressures and heat present during static firing. The hoop and meridional strains from this event are tabulated together with the strains due to actuator adjustment and the static test duty cycle in Tables 7.5-10 and 7.5-11, respectively.

c. Actuator Adjustment. Actuator adjustment was performed prior to the dry run duty cycle. The cycle used for this event is shown in Figure 7.5-113. It is performed to adjust the gain and bias to control the actuator during the duty cycles. Values of the strain gages in the nozzle section were obtained and are noted in Tables 7.5-10 and 7.5-11.

7.5.4.4 TVC System. In order to measure the vector angles and dynamic alignment performance of the system, 12 extensometers were mounted on the fixed housing around the perimeter of the nozzle as shown in Figure 7.5-187. As the nozzle was vectored, the delta-length data from the extensometers were recorded and later fed into a computer program which solved for the Euler angles and Cartesian coordinates of the nozzle centerline.

The actuator lengths were adjusted to provide a null angle at a motor chamber pressure of 620 psi. This was the predicted average pressure at the time the actuator adjustment took place. The method used to calculate actuator null length was the

Table 7.5-12. DM-9 Pressure-Related Versus Vectoring-Related Hoop Strains (μin./in.)

LOCATION #	Max Strain Due To Pressure (Sp) (Average)	Max Strain Due To Vectoring (Sv) 4.0 or -4.4	Sv/Sp*100 (%)
		HOOP STRAINS	
1 - FIXED HOUSING AFT END	1355	70	5
2 - FIXED HOUSING MID SECTION	-1130	-35	3
3 - FIXED HOUSING FWD SECTION	-1915	75	-4
4 - AFT END RING FWD END	-810	-190	23
5 - NOSE INLET HSG AFT END	500	55	11
6 - FWD END RING FWD REGION	700	120	17
7 - NOSE INLET HSG AFT END	-400	-70	18
8 - FWD END RING AFT END	1080	80	7
9 - NOSE INLET HSG FWD END	-625	-100	2
10 - NIH / THROAT JOINT REGION	-350	70	-20
11 - THROAT HSG FWD END	228	90	39
12 - THROAT HSG MID SECTION	600	35	6
13 - THROAT HSG AFT END	380	60	16
14 - FWD EXIT CONE	300	10	3
15 - AFT EXIT CONE	410	20	5
16 - COMPLIANCE RING	160	300	-188
17 - THROAT HSG/ FWD EXIT CONE JOINT REGION	304	45	15
18 - THROAT HSG/ AFT END RING JOINT REGION	314	-45	-14
19 - AFT END RING AFT END	-815	-80	10
20 - AFT END RING AFT END	-850	-55	6
22 - FIXED HSG/ AFT END RING JOINT REGION	-2020	-100	5

Table 7.5-13. DM-9 Pressure-Related Versus Vectoring-Related Meridional Strains (μin./in.)

LOCATION #	Max Strain Due To Pressure (Sp) (Average)	Max Strain Due To Vectoring (Sv) 4.0 or -4.4	Sv/Sp*100 (%)
		MERIDIONAL STRAINS	
1 - FIXED HOUSING AFT END	-1325	-10	1
2 - FIXED HOUSING MID SECTION	570	10	2
3 - FIXED HOUSING FWD SECTION	1155	150	13
4 - AFT END RING FWD END	165	-20	-12
5 - NOSE INLET HSG AFT END	-1070	-120	11
6 - FWD END RING FWD REGION	-503	-170	34
7 - NOSE INLET HSG AFT END	595	60	10
8 - FWD END RING AFT END	236	25	11
9 - NOSE INLET HSG FWD END	-1650	110	-7
10 - NIH / THROAT JOINT REGION	180	65	36
11 - THROAT HSG FWD END	26	20	75
12 - THROAT HSG MID SECTION	300	125	42
13 - THROAT HSG AFT END	-238	45	-19
14 - FWD EXIT CONE	-190	45	-24
15 - AFT EXIT CONE	-110	-70	64
16 - COMPLIANCE RING	-96	-100	101

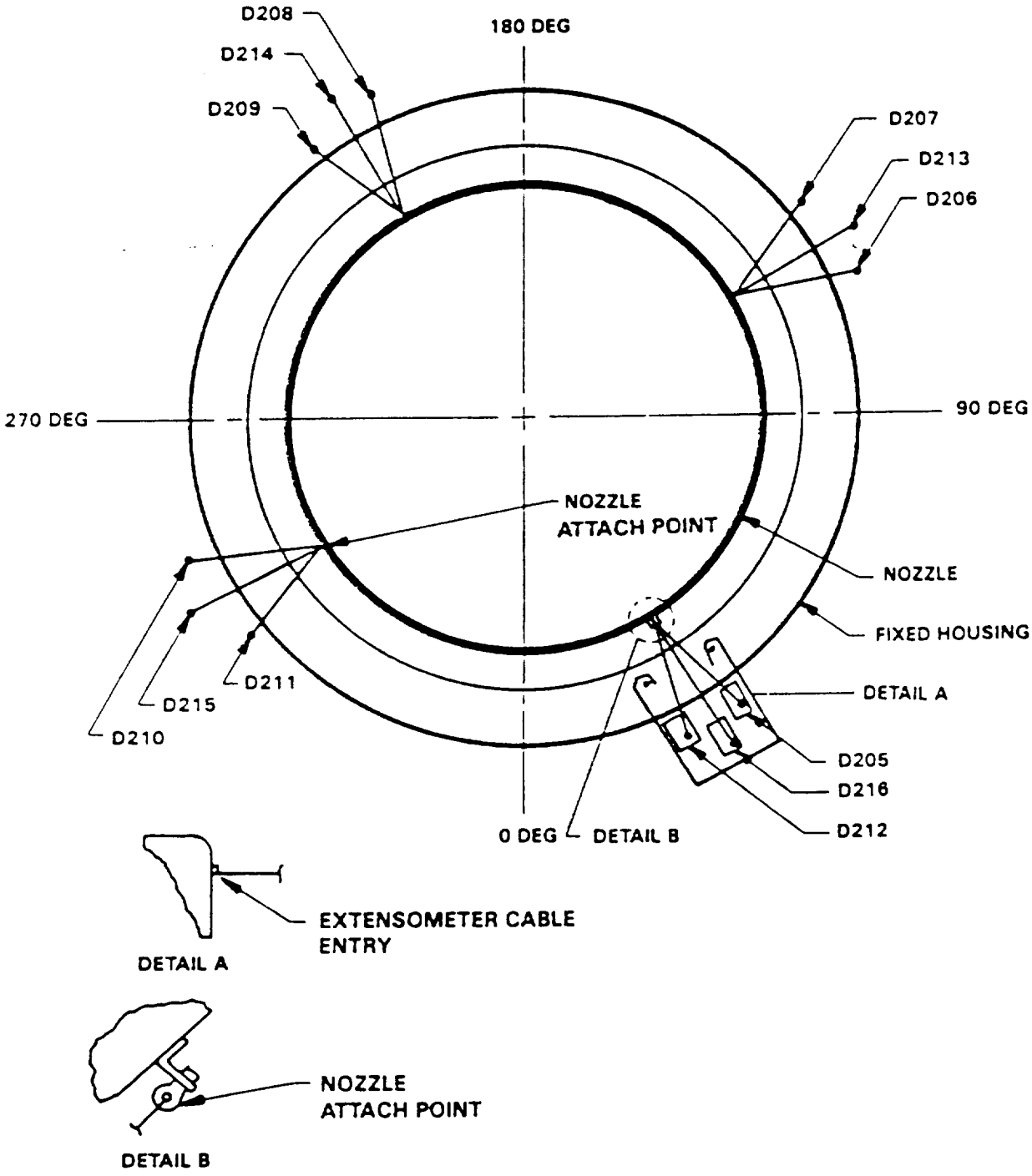

Figure 7.5-187. Location of Extensometers

same as used for the previous static tests. Nominal component dimensions were used except for the following measured values:

a. Two dimensions from the skirt assembly were measured: the axial distance from the kickring pin centerline to the center of the actuator attach point and the radial distance form the kickring inside face to the center from the actuator attach point. These dimensions were measured at both the rock (45 deg) and tilt (135 deg) actuator attach points and each actuator length calculated separately.

b. The actual axial length of the nozzle flex bearing and axial compression at an equivalent chamber pressure of 620 psia were measured in bench test for use in calculating actuator null length. The final calculated lengths were 53.056 in. for the rock actuator and 53.047 in. for the tilt actuator.

In addition to the static test itself, certain pretests were conducted to meet the test objectives. These included the nozzle alignment test and the actuator adjustment test.

Nozzle Alignment Test

The primary purpose of this test was to demonstrate that the alignment of the nozzle centerline parallel to the motor centerline was within the CEI specification. Other purposes included calibration of the extensometers for angle measurement and verification of the actuator null lengths.

The nozzle centerline was optically aligned parallel to the motor centerline using a jig transit, paragon level, and special crosshair alignment fixtures at the throat plane and exit plane. The measurements were as shown in Figures 7.5-188 and 7.5-189. The vector sum of the radial offsets at the throat plane was 0.026 inch. This was well within the requirement of 0.25 inch. The angle between the centerline was calculated to be 0.5 deg requirement.

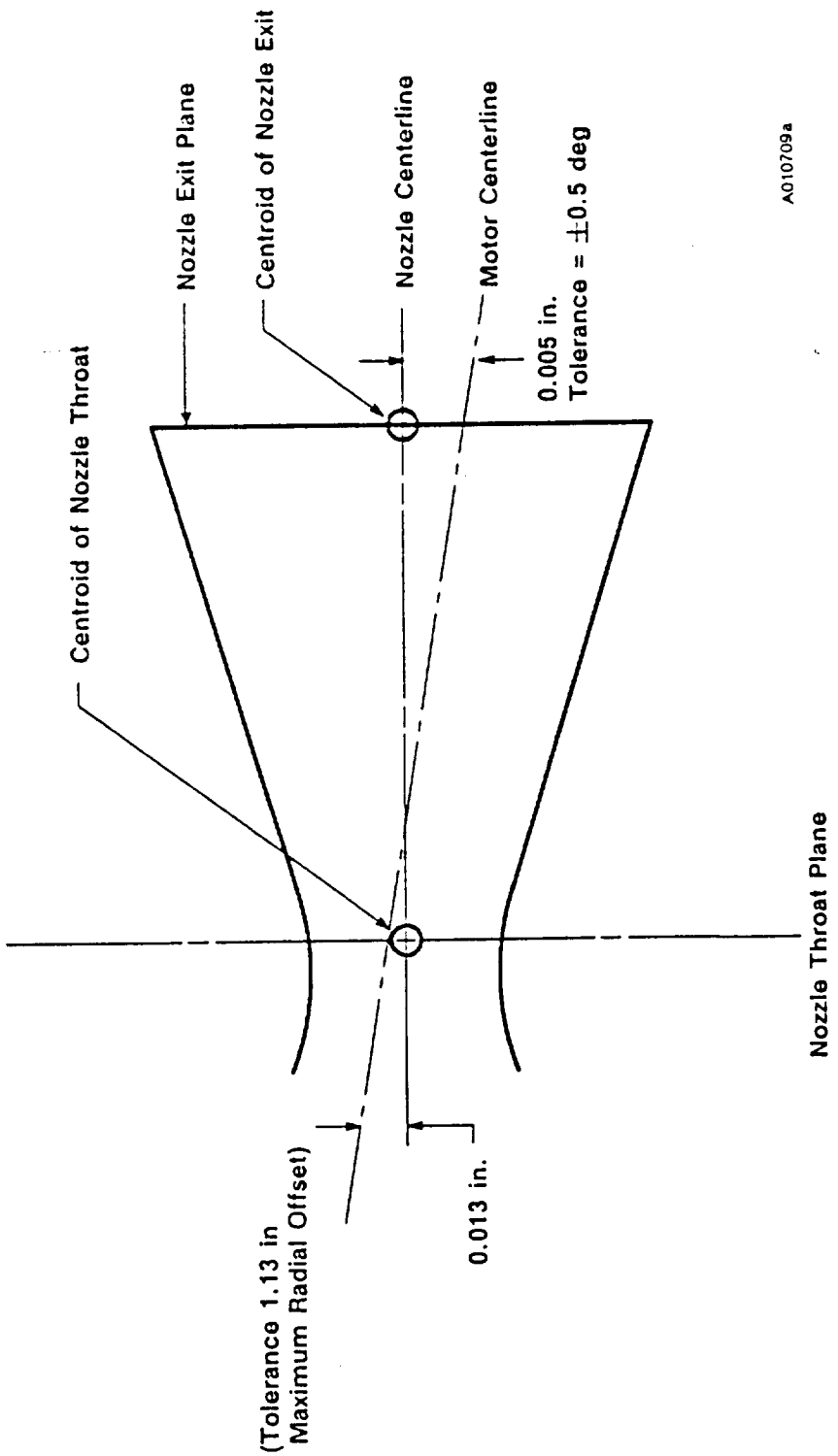

Figure 7.5-188. Side View of Nozzle and Motor Centerlines During Alignment Test

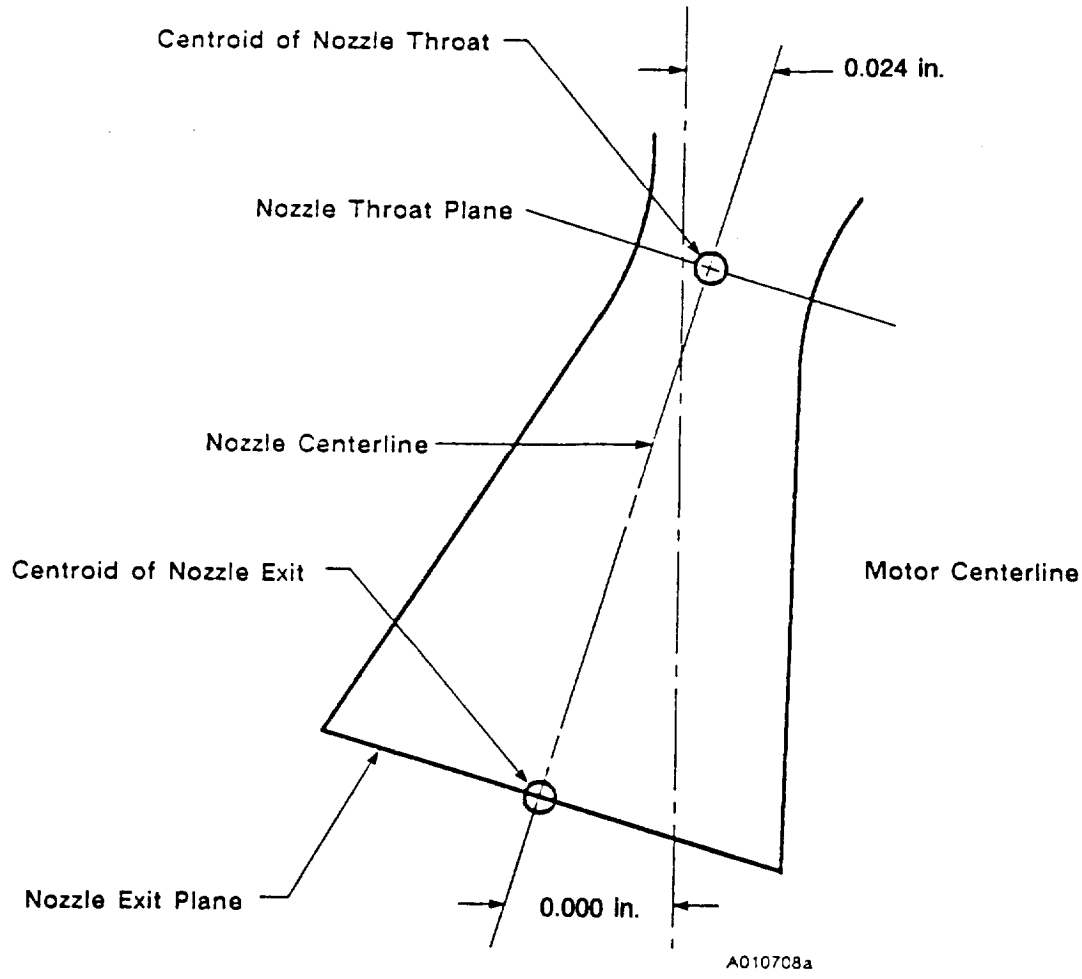

Figure 7.5-189. Top View of Nozzle and Motor Centerlines During Alignment Test

Actuator Adjustment Check-out Test

This test was conducted to determine adjustments to the actuator gains and null biases so that the actuators would provide zero position at zero command. With both actuators attached to the nozzle and each receiving identical commands, a stairstep duty cycle was conducted with the nozzle moving to a maximum vector angle of 5.4 deg, then returning in steps to null (Figure 7.5-190). The nozzle was then moved in increments to -3.3 deg, returned to null, and the initial stairstep duty cycle to 5.4 deg was repeated. Figures 7.5-191 and 7.5-192 show actuator position versus command for both planes.

A gain of 1.031 was applied to the rock actuator commands with a bias of -0.114 V. A gain of 1.031 was applied to the tilt actuator commands with a bias of -0.030 V.

The data for the static test show that prior to motor ignition, with the bias voltage applied and with null commands, the rock actuator position was 0.050 in. and the tilt actuator position was 0.100 inch. These values were well within the hysteresis of the actuators, which ranged from about 0.15 to 0.40 in. during the adjustment test (Figures 7.5-191 and 7.5-192).

Static Test

Figure 7.5-193 shows the programmed DM-9 static test duty cycle. Table 7.5-14 presents the commanded duty cycle events before pressurized motor operation (-25 to 0 sec), during pressurized motor operation (0 to 122 sec), and after pressurized motor operation (122 to 150 sec).

The duty cycle was programmed to provide 272.24 total deg-sec. The cumalitive nozzle vector angle deg-sec programmed were as follows:

a. 174.19 deg-sec in the (+) yaw plane.

b. 35.39 deg-sec in the (-) yaw plane.

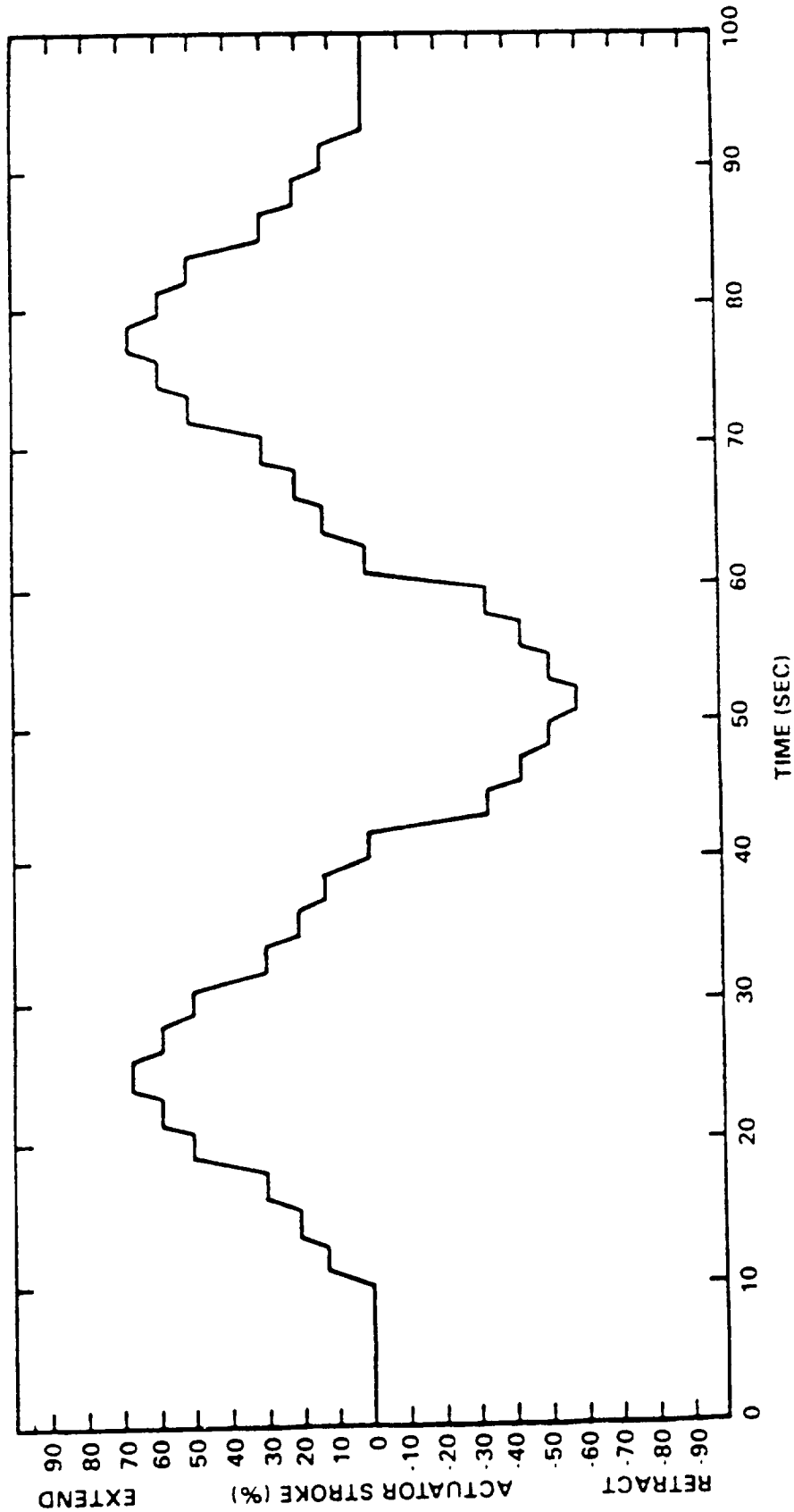

Figure 7.5-190. Actuator Adjustment Checkout Test

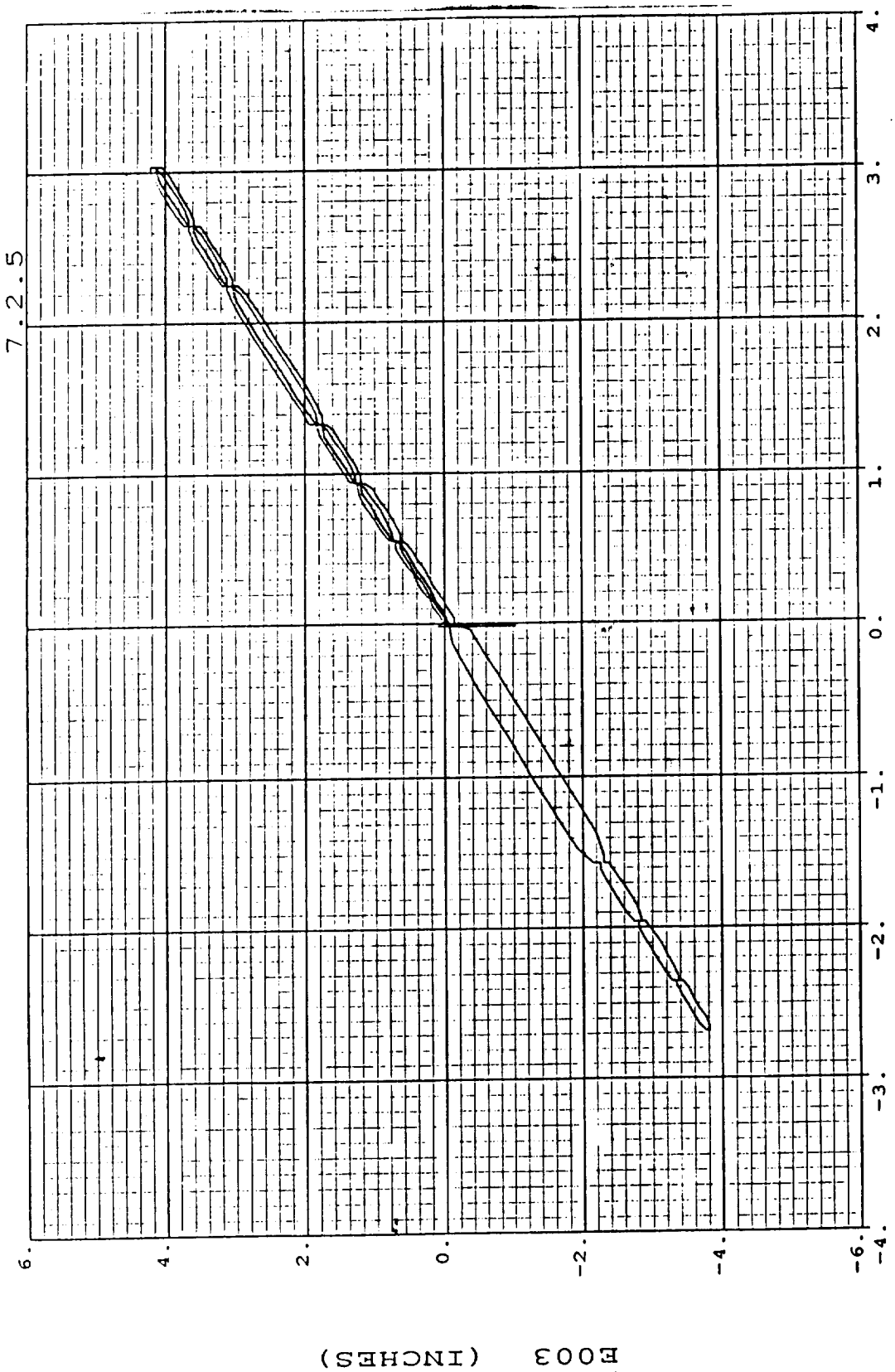

Figure 7.5-191. DM-9 Actuator Adjustment Checkout Test

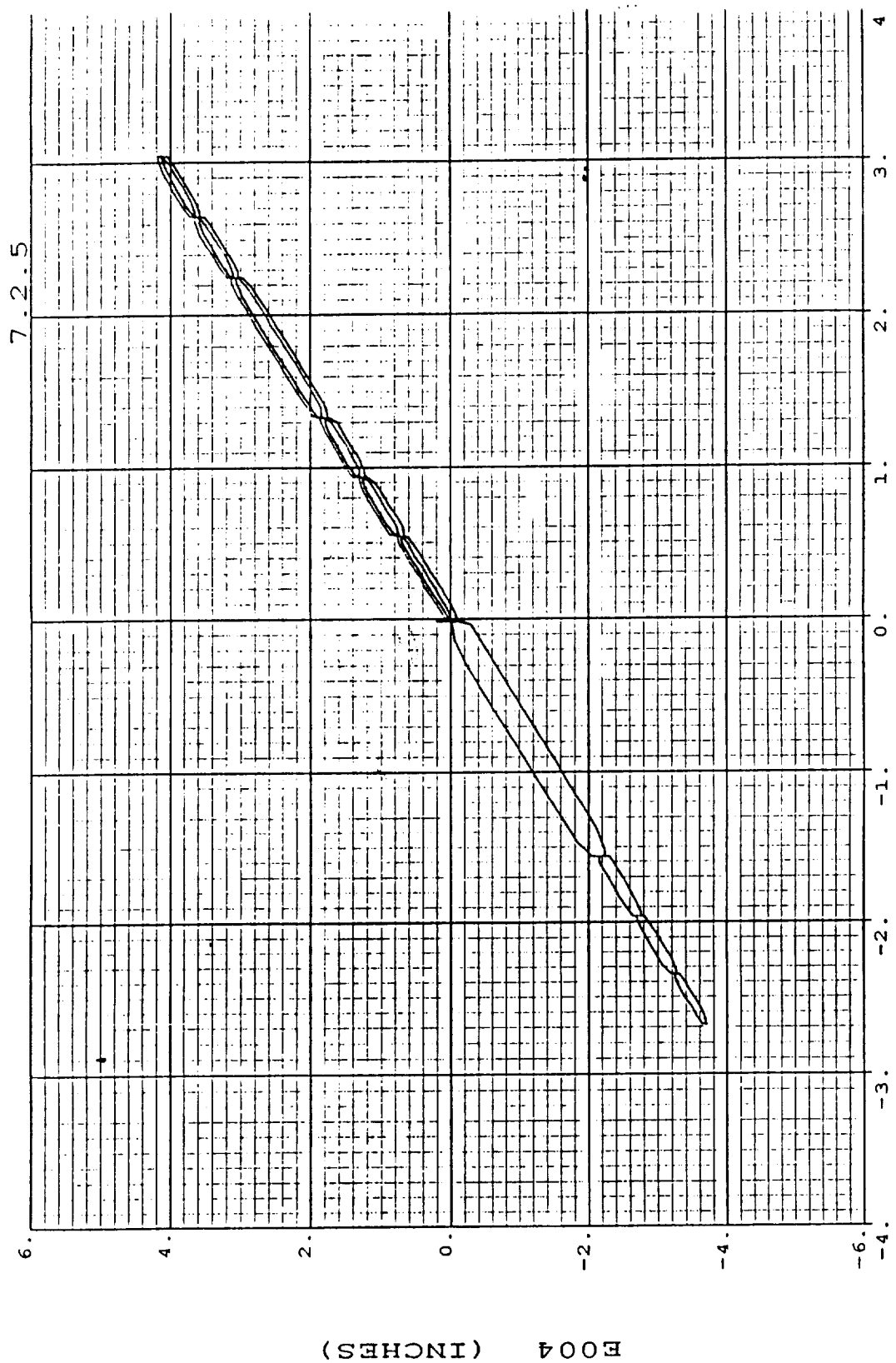

Figure 7.5-192. DM-9 Actuator Adjustment Checkout Test

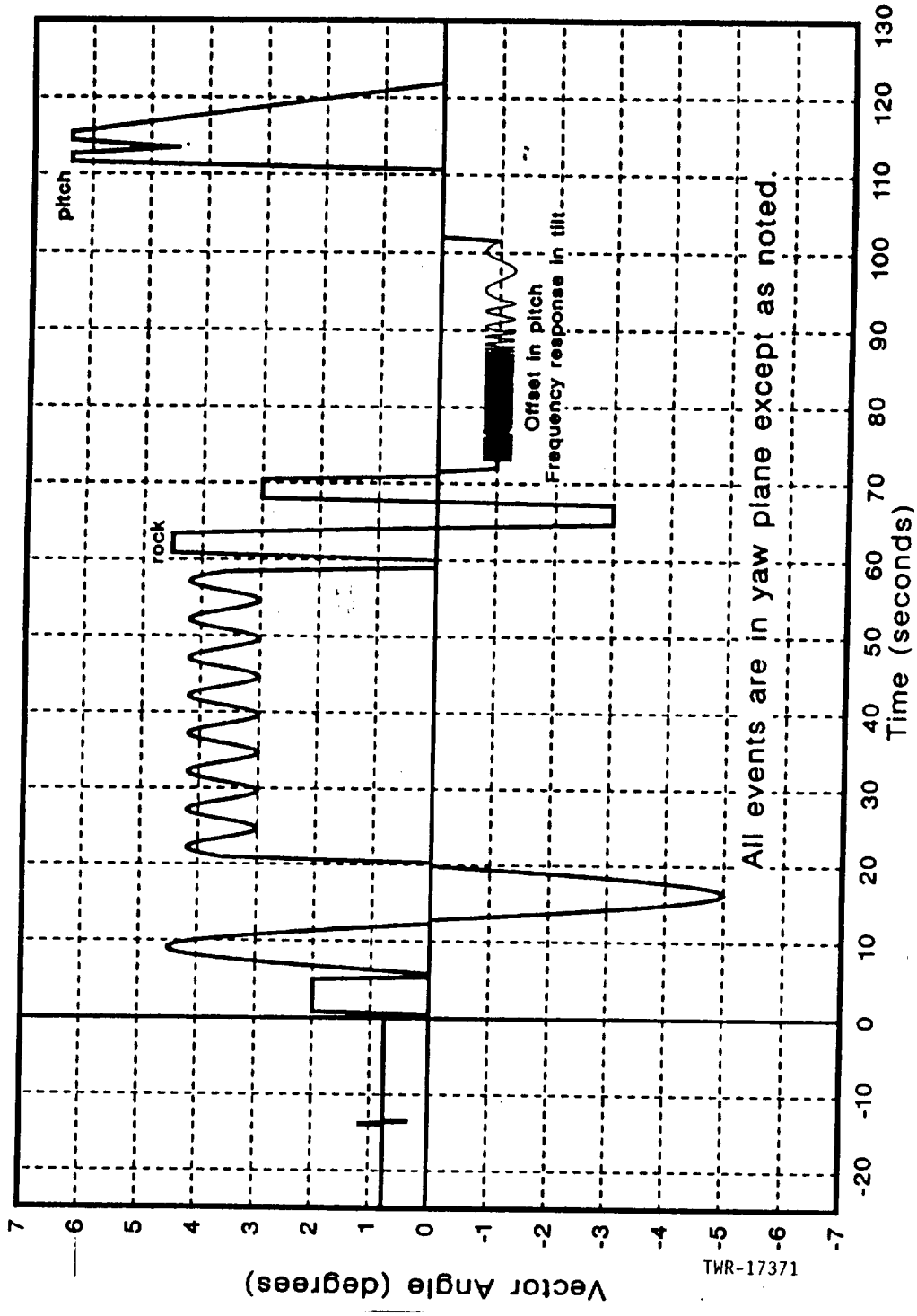

Figure 7.5-193. T-24 (QM-6) Duty Cycle

Table 7.5-14. Static Test Duty Cycle

Event	Time From	Time To	Function	Rock Act. Command % Stroke	Tilt Act. Command % Stroke	Frequency Hz	Max. Slew Rate Deg/Sec	No. of Cycles	Description
1	-25.000	-14.000	Hold	0.0	0.0	—	—	—	Hold at 0.75° Yaw
2	-14.000	-13.950	Ramp	0.0 to 5.8	0.0 to 5.8	—	8.0	—	Ramp to 1.15° Yaw
3	-13.950	-13.800	Hold	5.8	5.8	—	—	—	Hold at 1.15° Yaw
4	-13.800	-13.750	Ramp	5.8 to 0.0	5.8 to 0.0	—	-8.0	—	Ramp to 0.75° Yaw
5	-13.750	-13.600	Hold	0.0	0.0	—	—	—	Hold at 0.75° Yaw
6	-13.600	-13.550	Ramp	0.0 to -5.8	0.0 to -5.8	—	-8.0	—	Ramp to 0.35° Yaw
7	-13.550	-13.400	Hold	-5.8	-5.8	—	—	—	Hold at 0.35° Yaw
8	-13.400	-13.350	Ramp	-5.8 to 0.0	-5.8 to 0.0	—	+8.0	—	Ramp to 0.75° Yaw
9	-13.350	+0.500	Hold	0.0	0.0	—	—	—	Hold at 0.75°/Null
10	0.500	———	Step	0.0 to 29.6	0.0 to 29.6	—	—	—	Step to 2° Yaw
11	0.500	4.500	Hold	29.6	29.6	—	—	—	Hold at 2° Yaw
12	4.500	———	Step	29.6 to 0.0	29.6 to 0.0	—	—	—	Step to Null
13	4.500	5.000	Hold	0.0	0.0	—	—	—	Hold at Null
14	5.000	11.000	Sine	0.0 ± 58.1	0.0 ± 58.1	0.167	4.2	1.0	±4° Sine Yaw
15	11.000	11.500	Hold	0.0	0.0	—	—	—	Hold at Null
16	11.500	14.500	½ Sine	72.4	-72.4	0.167	5.2	0.5	+5° Sine Pitch
17	14.500	15.000	Hold	0.0	0.0	—	—	—	Hold at Null

Table 7.5-14. Static Test Duty Cycle (cont)

Event	Time From	Time To	Function	Rock Act. Command % Stroke	Tilt Act. Command % Stroke	Frequency Hz	Max. Slew Rate Deg/Sec	No. of Cycles	Description
18	15.000	16.000	Ramp	0.0 to 39.5	0.0 to 39.5	—	2.8	—	Ramp to 2.8° Yaw
19	16.000	58.500	Sine	39.5 ± 8.5	39.5 ± 8.5	0.2	0.8	8.5	+2.8°±0.6° Sine Yaw
20	58.500	59.500	Ramp	39.5 to 0.0	39.5 to 0.0	—	-2.8	—	Ramp to Null
21	59.500	61.000	Hold	0.0	0.0	—	—	—	Hold at Null
22	61.000	———	Step	0.0 to 41.3	0.0 to 41.3	—	—	—	Step to 3° Yaw
23	61.000	64.000	Hold	41.3	41.3	—	—	—	Hold at 3° Yaw
24	64.000	———	Step	41.3 to -41.3	41.3 to -41.3	—	—	—	Step to -3° Yaw
25	64.000	67.000	Hold	-41.3	-41.3	—	—	—	Hold at -3° Yaw
26	67.000	———	Step	-41.3 to 41.3	-41.3 to 41.3	—	—	—	Step to 3° Yaw
27	67.000	70.000	Hold	41.3	41.3	—	—	—	Hold at 3° Yaw
28	70.000	———	Step	41.3 to 0.0	41.3 to 0.0	—	—	—	Step to Null
29	70.000	71.500	Hold	0.0	0.0	—	—	—	Hold at Null
30	71.500	72.000	Ramp	0.0 to -15.0	0.0 to 14.0	—	2.0	—	Ramp to -1° Pitch
31	72.000	73.000	Hold	-15.0	14.0	—	—	—	Hold at -1° Pitch
32	73.000	74.000	Sine	-15.0	14.0 ± 6.0	20	31.4	20	±0.25° w/ 1° offset
33	74.000	75.000	Sine	-15.0	14.0 ± 6.0	19	29.8	19	±0.25° w/ 1° offset
34	75.000	76.000	Sine	-15.0	14.0 ± 6.0	18	28.3	18	±0.25° w/ 1° offset

Table 7.5-14. Static Test Duty Cycle (cont)

Event	Time From	Time To	Function	Rock Act. Command % Stroke	Tilt Act. Command % Stroke	Frequency Hz	Max. Slew Rate Deg/Sec	No. of Cycles	Description
35	76.000	77.000	Sine	-15.0	14.0 ± 6.0	17	26.7	17	±0.25° w/ 1° offset
36	77.000	78.000	Sine	-15.0	14.0 ± 6.0	16	25.1	16	±0.25° w/ 1° offset
37	78.000	79.000	Sine	-15.0	14.0 ± 6.0	15	23.6	15	±0.25° w/ 1° offset
38	79.000	80.000	Sine	-15.0	14.0 ± 6.0	14	22.0	14	±0.25° w/ 1° offset
39	80.000	81.000	Sine	-15.0	14.0 ± 6.0	13	20.4	13	±0.25° w/ 1° offset
40	81.000	82.000	Sine	-15.0	14.0 ± 6.0	12	18.8	12	±0.25° w/ 1° offset
41	82.000	83.000	Sine	-15.0	14.0 ± 6.0	11	17.3	11	±0.25° w/ 1° offset
42	83.000	84.000	Sine	-15.0	14.0 ± 6.0	10	15.7	10	±0.25° w/ 1° offset
43	84.000	85.000	Sine	-15.0	14.0 ± 6.0	8	12.6	8	±0.25° w/ 1° offset
44	85.000	86.000	Sine	-15.0	14.0 ± 6.0	6	9.4	6	±0.25° w/ 1° offset
45	86.000	87.000	Sine	-15.0	14.0 ± 6.0	4	6.3	4	±0.25° w/ 1° offset
46	87.000	88.000	Sine	-15.0	14.0 ± 6.0	2	3.1	2	±0.25° w/ 1° offset
47	88.000	90.000	Sine	-15.0	14.0 ± 6.0	1	1.6	2	±0.25° w/ 1° offset
48	90.000	94.000	Sine	-15.0	14.0 ± 6.0	0.5	0.8	2	±0.25° w/ 1° offset
49	94.000	101.500	Sine	-15.0	14.0 ± 6.0	0.2	0.3	1.5	±0.25° w/ 1° offset
50	101.500	102.000	Ramp	-15.0 to 0.0	14.0 to 0.0	—	—	—	Ramp to Null
51	102.000	103.000	Hold	0.0	0.0	—	—	—	Hold at Null

Table 7.5-14. Static Test Duty Cycle (cont)

Event	Time From	Time To	Function	Rock Act. Command % Stroke	Tilt Act. Command % Stroke	Frequency Hz	Max. Slew Rate Deg/Sec	No. of Cycles	Description
52	103.000	104.400	Ramp	0.0 to -95.3	0.0 to -95.3	—	-5.0	—	Ramp to -7° Yaw
53	104.400	104.900	Hold	-95.3	-95.3	—	—	—	Hold at -7° Yaw
54	104.900	107.700	Ramp	-95.3 to 95.3	—	—	5.0	—	Ramp to 7° Pitch
55	107.700	108.200	Hold	95.3	-95.3	—	—	—	Hold at 7° Pitch
56	108.200	111.000	Ramp	—	-95.3 to 95.3	—	5.0	—	Ramp to 7° Yaw
57	111.000	111.500	Hold	95.3	95.3	—	—	—	Hold at 7° Yaw
58	111.500	112.900	Ramp	95.3 to 0.0	95.3 to 0.0	—	-5.0	—	Ramp to Null
59	112.900	122.000	Hold	0.0	0.0	—	—	—	Hold at Null
60	122.000	125.570	½ Sine	84.6	84.6	0.14	5.8	0.5	6.6° Sine Yaw
61	125.570	127.230	½ Sine	-16.9	-16.9	0.30	-3.4	0.5	-1.8° Sine Yaw
62	127.230	130.000	Hold	0.0	0.0	—	—	—	Hold at Null

NOTES: (1) 100% actuator stroke = 6.4 ± 0.1 inches.
(2) Minimize discontinuities during events 32 through 50.
(3) Positive command is actuator extend.
(4) TVC system ignition is at T-20 seconds.
(5) SRM ignition is at T-0 seconds.
(6) TVC system shutdown is at T+130 seconds.
(7) Close the hydraulic pump bypass valves at T-15 seconds.
(8) Maximum slew rate and vector angle values are approximate.

c. 32.65 deg-sec in the (-) pitch plane.

d. 30.00 deg-sec in (-) pitch plane.

Actual measurements were:

a. 288.0 deg-sec with 190.0 in the (+) yaw plane.

b. 42.8 deg-sec in the (-) yaw plane.

c. 83.3 deg-sec in the (+) pitch plane.

d. 25.0 deg-sec in the (-) pitch plane.

Plots of pitch angle (SDELP), yaw angle (SDELY), and plane angles for the two actuators (ANG45 and ANG135) are in Figures 7.5-194 through 7.5-197.

The yaw thrust vector angle could not be determined due to a problem with test stand side force load train. The data was acceptable up to approximately 40 sec after which it drifted down to the 20 klb level.

The data are nonrecoverable, therefore, the yaw thrust vector angle and yaw radial offset could not be calculated.

Comparison With CEI Specifications

The CEI specification requirements which pertain to the DM-9 test objectives for the TVC subsystem are listed as follows (Reference COW1-3600, Rev. A):

a. Geometric Nozzle Alignment. With the nozzle and motor centerlines within 0.5 deg of each other, the radial offset shall not exceed the limits in Figure 7.5-198.

b. Dynamic Thrust Vector. The dynamic thrust vector during motor firing (without side load) from T+4 to T+108 sec and at times when the slew rate is zero shall not exceed the limits in Figure 7.5-199 as stated below:

   1. Misalignment of the dynamic thrust vector with respect to the nozzle centerline, between null and 8 deg, shall not deviate more than 1 deg.

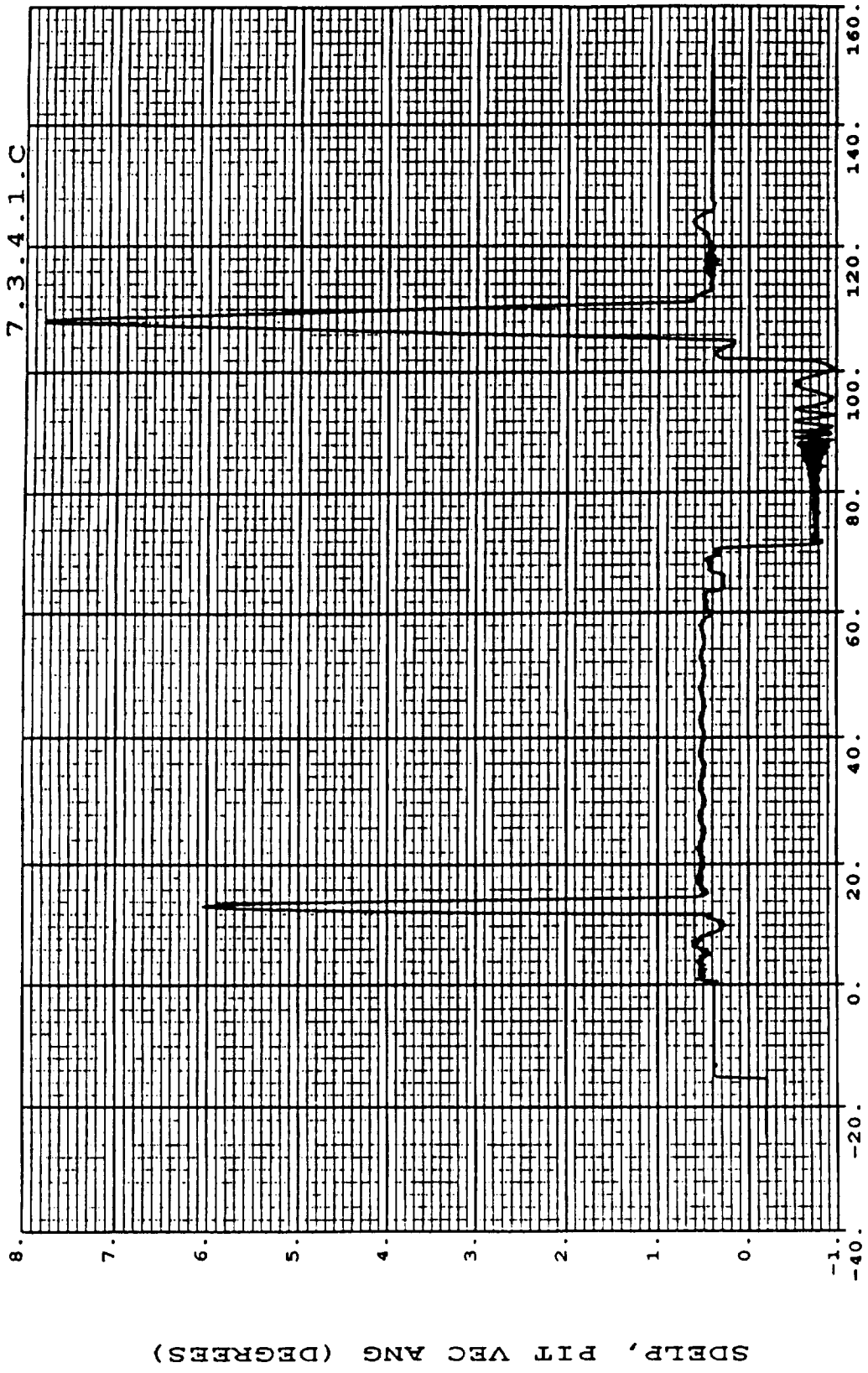

Figure 7.5-194. Pitch Angle (SDLEP)

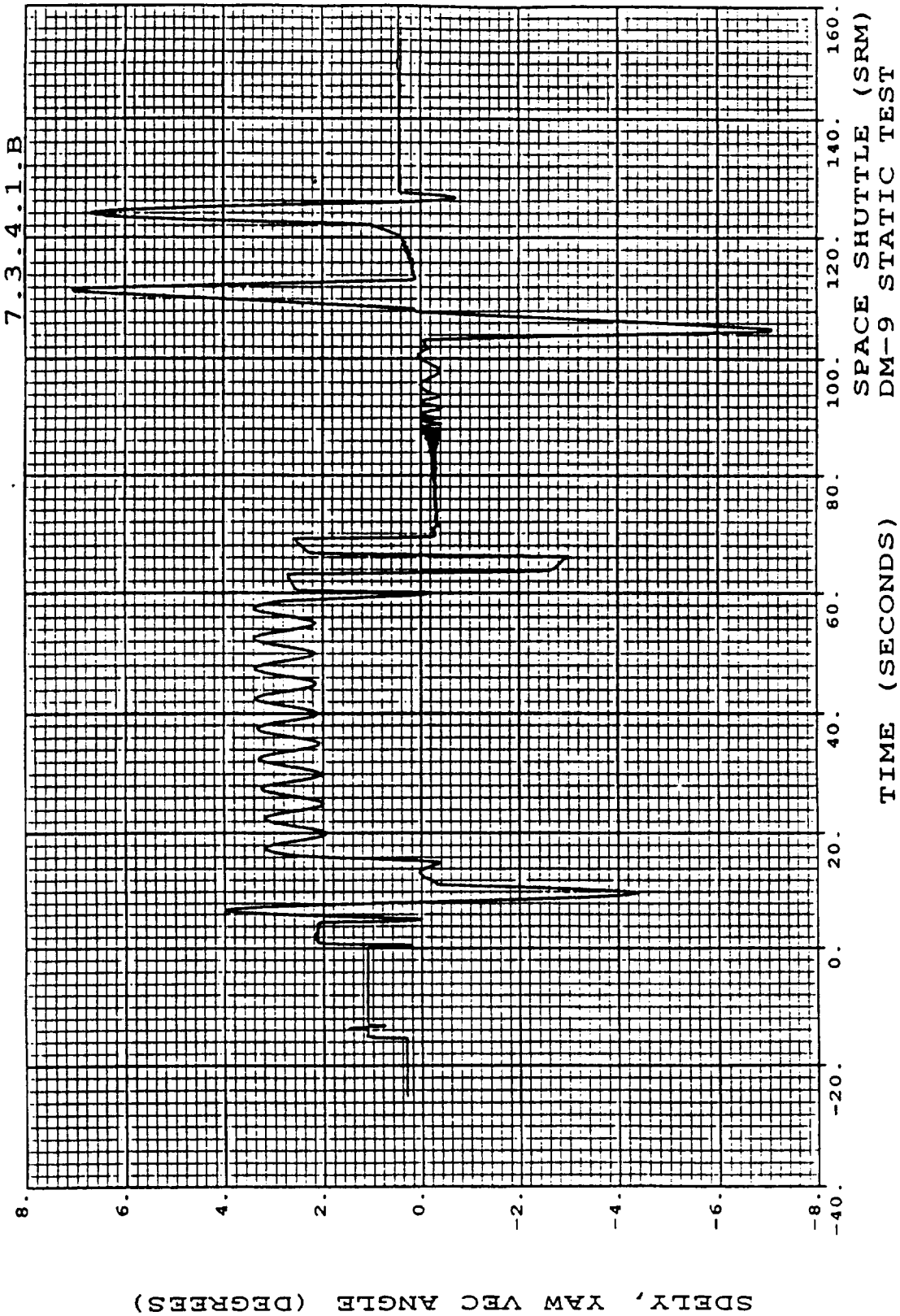

Figure 7.5-195. Yaw Angle (SDELY)

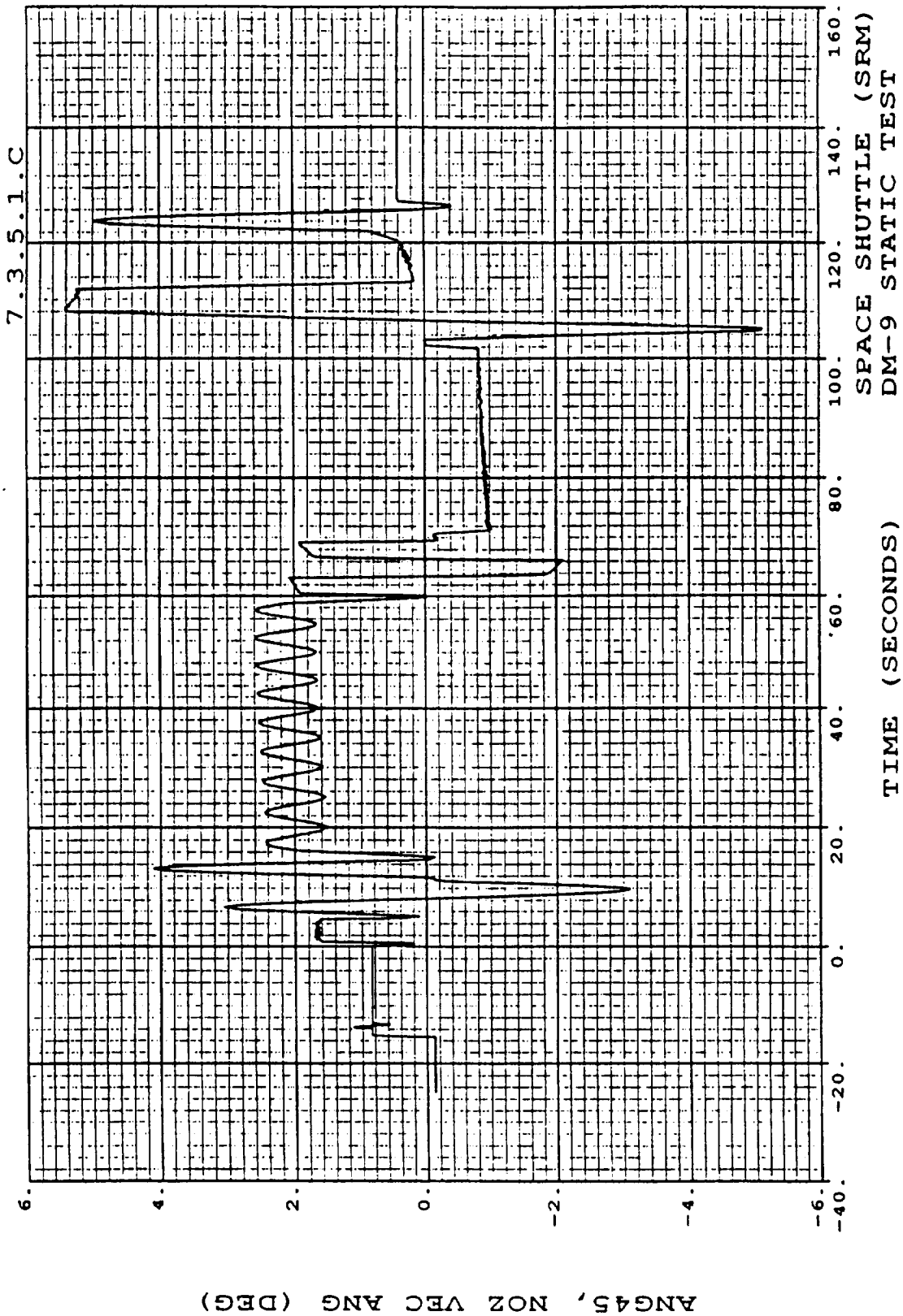

Figure 7.5-196. Plane Angle (ANG45)

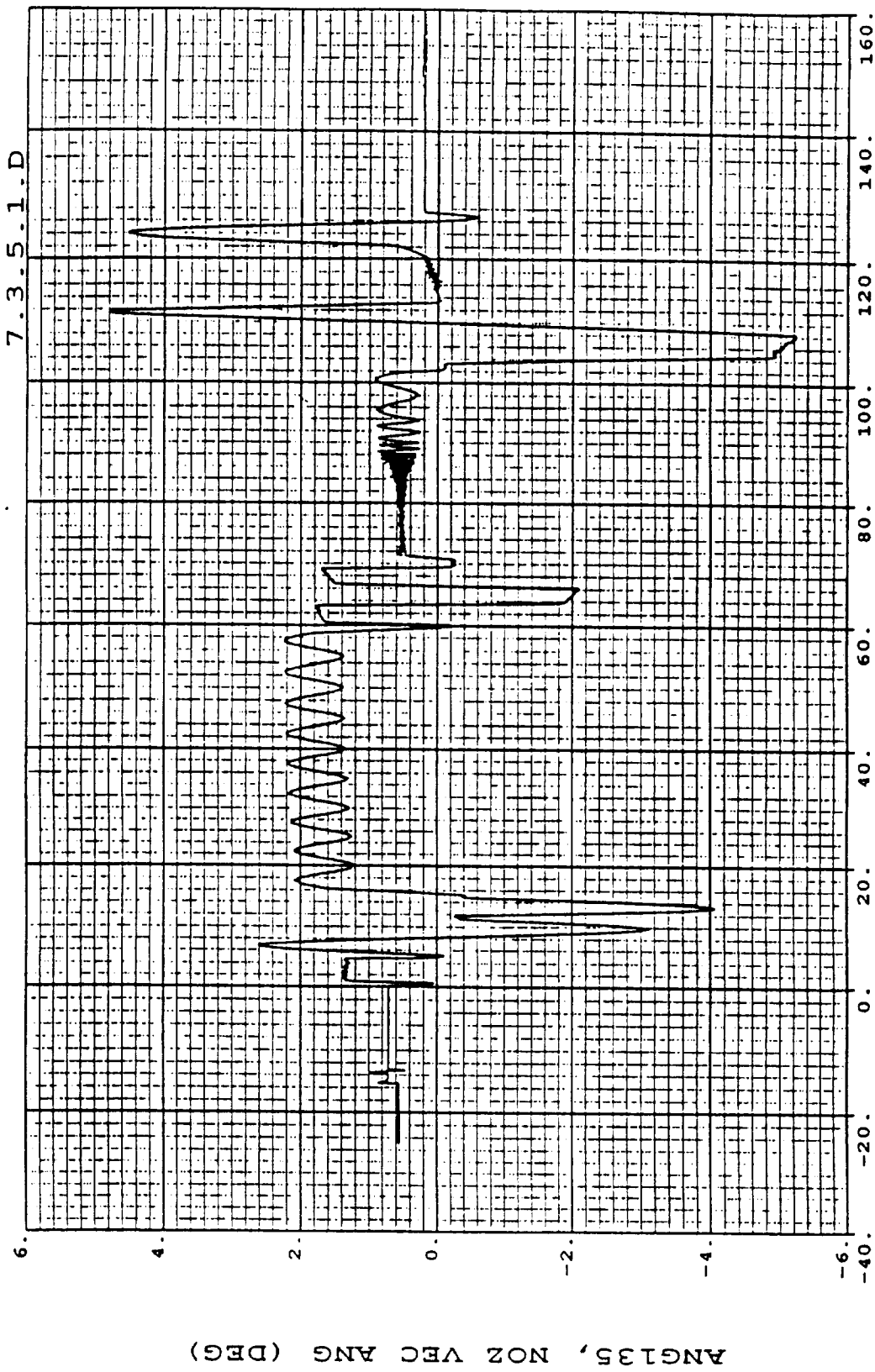

Figure 7.5-197. Plane Angle (ANG135)

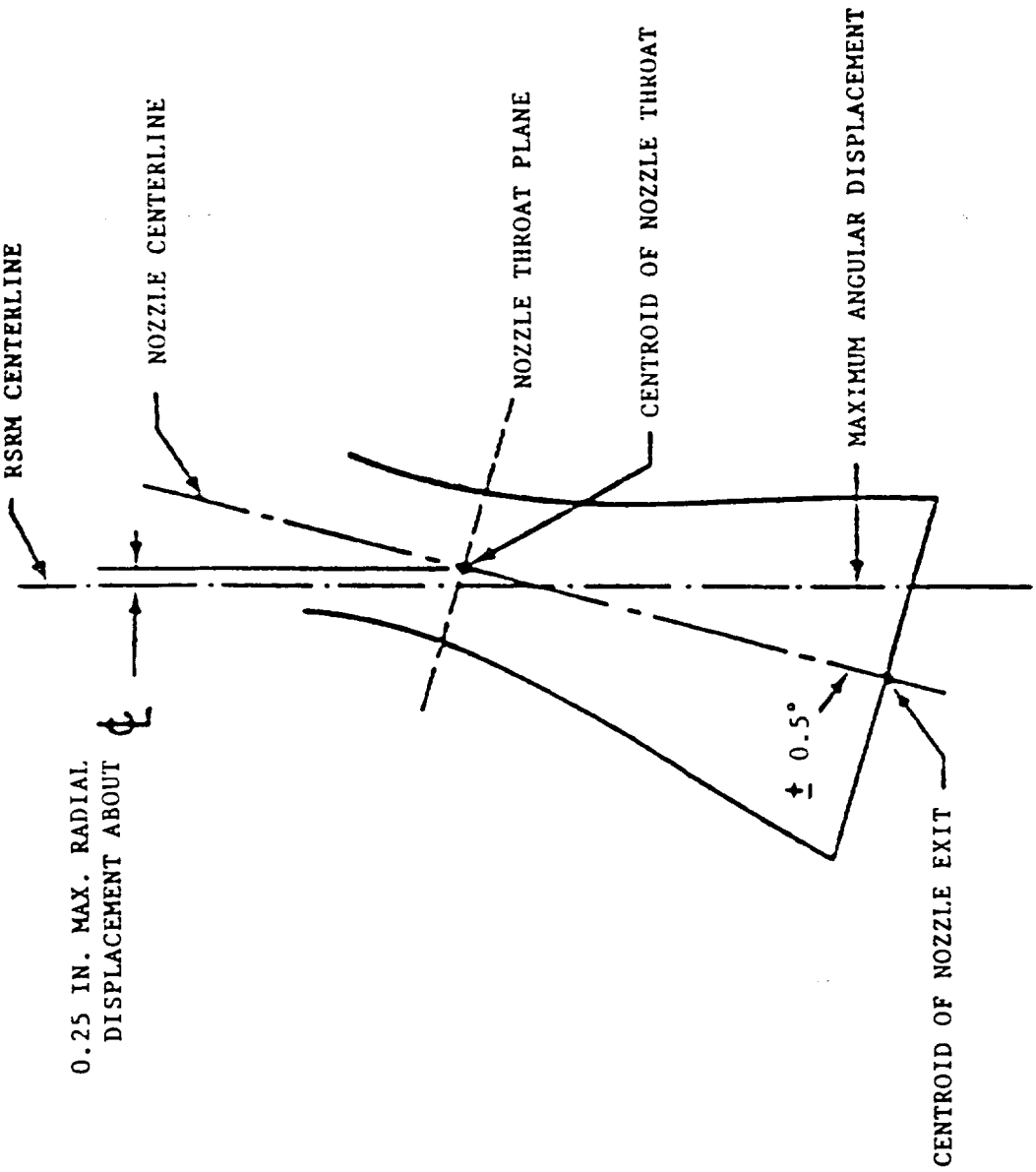

Figure 7.5-198. Geometric Thrust Vector

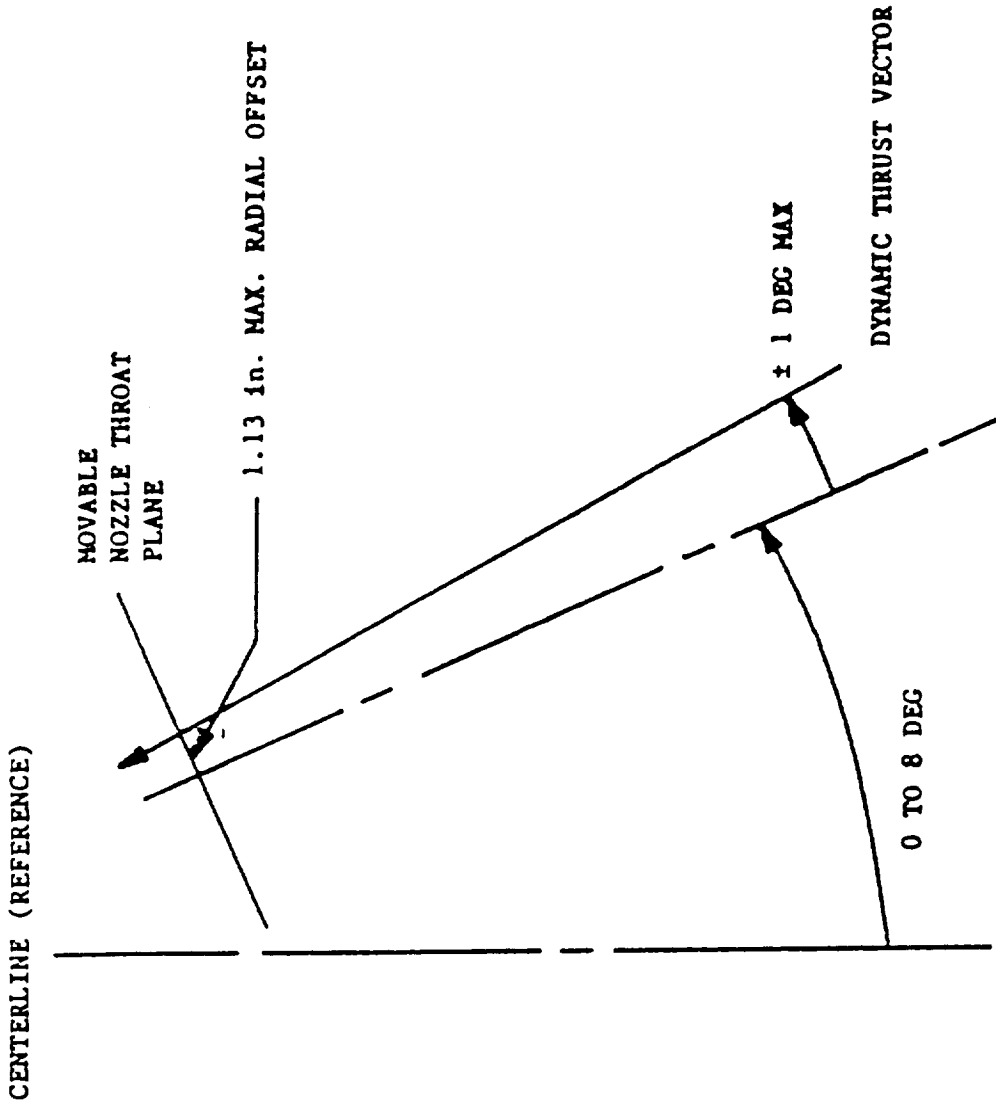

Dynamic thrust vector requirement (nozzle in any deflected position up to ± 8° and at any pressure from T +4 to T +108 seconds)

Figure 7.5-199. Dynamic Thrust Vector

c. Null Offset Angle. The nozzle null offset angle shall not exceed the following requirements at zero actuator command:

1. +0.96 deg at 0 psi nozzle stagnation pressure
2. +/-0.30 deg at 615 psi nozzle stagnation pressure
3. -0.50 deg at 915 psi nozzle stagnation pressure

During the nozzle alignment test with the nozzle centerline parallel to the motor centerline, the radial displacement of the nozzle centerline (which is the geometric thrust vector) was optically measured at the throat plane to be 0.0264 in., which is well within the 0.25 in. requirement.

The angle calculated when the centerlines were aligned were 0.019 deg which is well within the 0.5 deg requirement. With this and the previously mentioned radial offset, the requirement on the geometric thrust vector was met.

Because of the side force load train problem a comparison of yaw thrust vector angle and yaw radial offset could not be performed.

In reviewing the null offset data from DM-9, it was determined that the offset angles were as follows:

1. +0.8 deg at psi nozzle stagnation pressure
2. 0 deg at 614 psi nozzle stagnation pressure
3. -0.05 deg at 828 psi nozzle stagnation pressure

The data points for items 2 and 3 were taken when the actuators were at zero command and the nozzle stagnation pressure was not necessarily at the specified level. A linear extrapolation is used to calculate the offset angle at the specified pressure. This yielded the following results.

1. +0.8 deg at 0 psi nozzle stagnation pressure
2. 0 deg at 615 psi nozzle stagnation pressure
3. -0.055 deg at 915 psi nozzle stagnation pressure

It is apparent from the above data that DM-9 met the null offset angle requirements.

7.6 CASE

7.6.1 Introduction

The major structural concerns for the DM-9 case were the field joint rotations and growth, nozzle-to-case joint movement, and case membrane radial growth. Instrumentation was installed on the SRM to measure response to static test loading.

The DM-9 test represents the second full-scale test of the RSRM with virtually all redesign concepts incorporated. DM-9 was the first full-scale static test which incorporated the 360-deg ETA ring configuration.

Field Joints

The DM-9 capture feature field joint shown in Figure 7.6-1 incorporated the modified J-seal insulation configuration and the following hardware:

- RSRM configured capture feature tang and clevis hardware
- Long pins, pin retainer band, and custom shims

Field joints were assembled using the field joint assembly fixture (FJAF). Installation procedures for the FJAF are given in ETP-0228. Also discussed in that report is the use of the FJAF to mate the joints in full pin installation.

A 3-D finite element model was used for pretest predictions of DM-9 field joint response. The basic model represented a 1-deg cyclic symmetric slice of the case, and used friction interface elements to simulate the contact surfaces. A detailed description of the model can be found in TWR-16774.

Factory Joints

Factory joints shown in Figure 7.6-2 were configured with the following hardware:

- HPM tang and clevis hardware design width groove with increased from 0.310 in. maximum (HPM) to 0.360 in. (RSRM)
- Long pins, pin retainer band, and custom shims

The additional length of the long pins used on the field and factory joints increases the pin strength and decreases the possibility of shearing the dovetail section during testing. The nominal shim thickness used for the forward field joint was 0.045 in.; 0.034 in. for the center field joint; and 0.040 in. at the aft field joint.

A shim installation wedge was used to separate the outer clevis and tang to assist in the installation of the shims (Figure 7.6-4). The wedges considerably speed up the shimming process while protecting against damage. The wedges, made from 4130 carbon steel, do not damage the harder D6AC steel which makes up the clevis and tang.

Corrosion protection for the joints consisted of full external paint and a minimal amount of internal grease (including O-rings, sealing surfaces, and pinholes).

Nozzle-to-Case Joint

The nozzle-to-case joint shown in Figure 7.6-3 incorporated an unvented insulation configuration and the following hardware:

- RSRM fixed housing and aft dome
- 100, 0.875-in. radial and axial bolts

The nozzle-to-case joint was assembled vertically. Radial bolt hole plugs were installed in the aft dome to protect the wiper O-ring from damage during assembly. Installation clips were used to hold the secondary O-ring in place during mating.

A 3-D finite element analysis of the DM-8 nozzle-to-case joint was performed using ANSYS computer code. The model included the aft dome, fixed nozzle housing, radial and axial bolts, and phenolics. Near the joint region, a 3-D model was used, and a 2-D model was used away from the joint.

The following assumptions and/or parameters were included in the model:

- Nominal values for material properties and hardware dimensions
- A preload of 140 kip in the axial bolts and 47 kip in the radial bolts

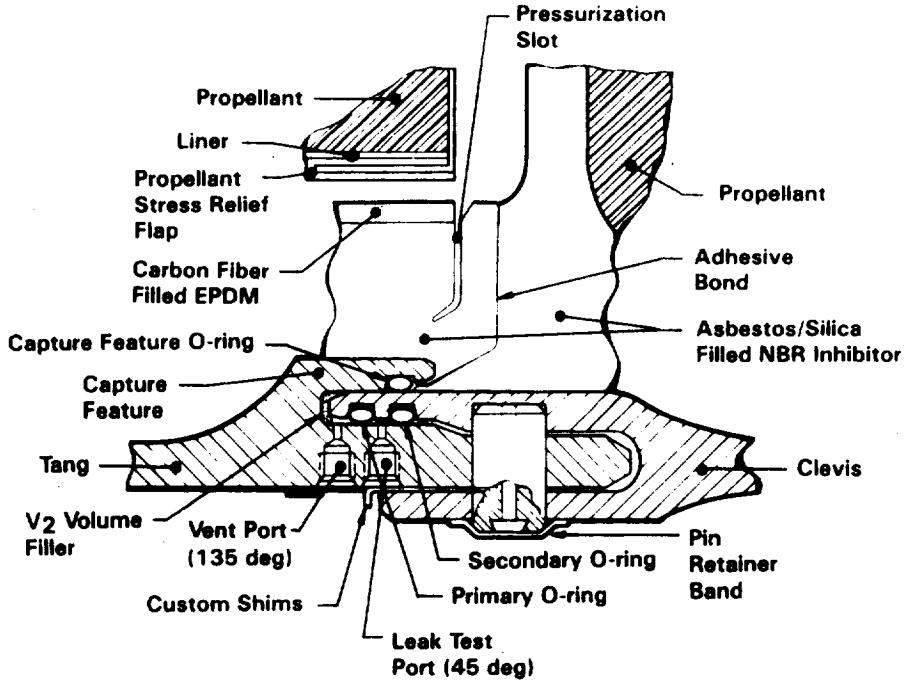

Figure 7.6-1. RSRM Case-to-Case Field Joint

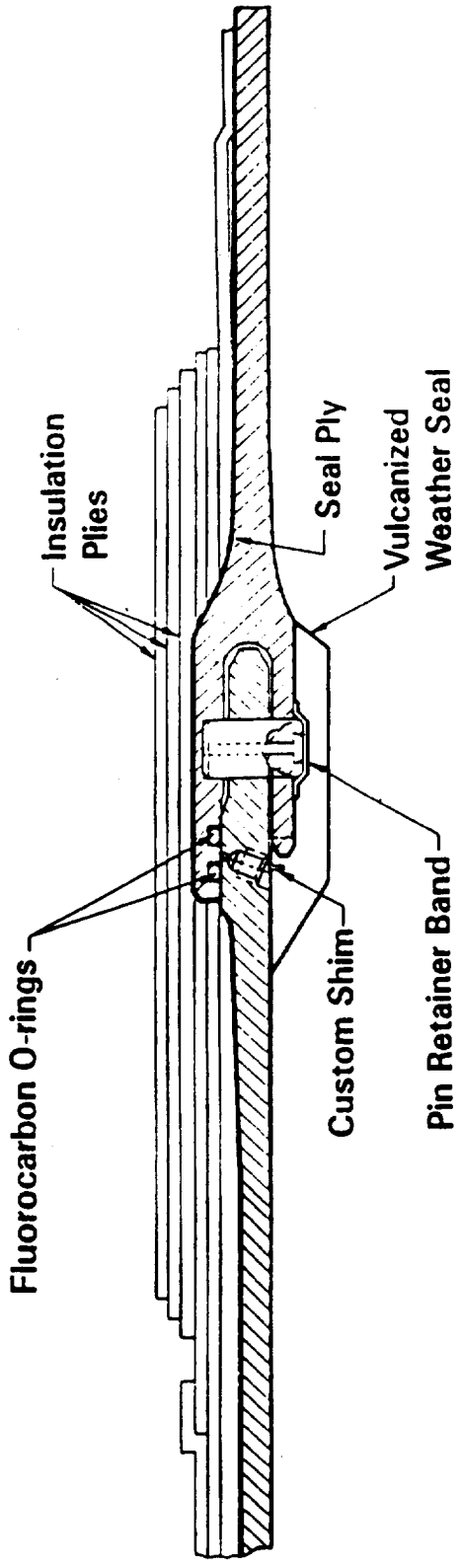

Figure 7.6-2. RSRM Case-to-Case Factory Joint

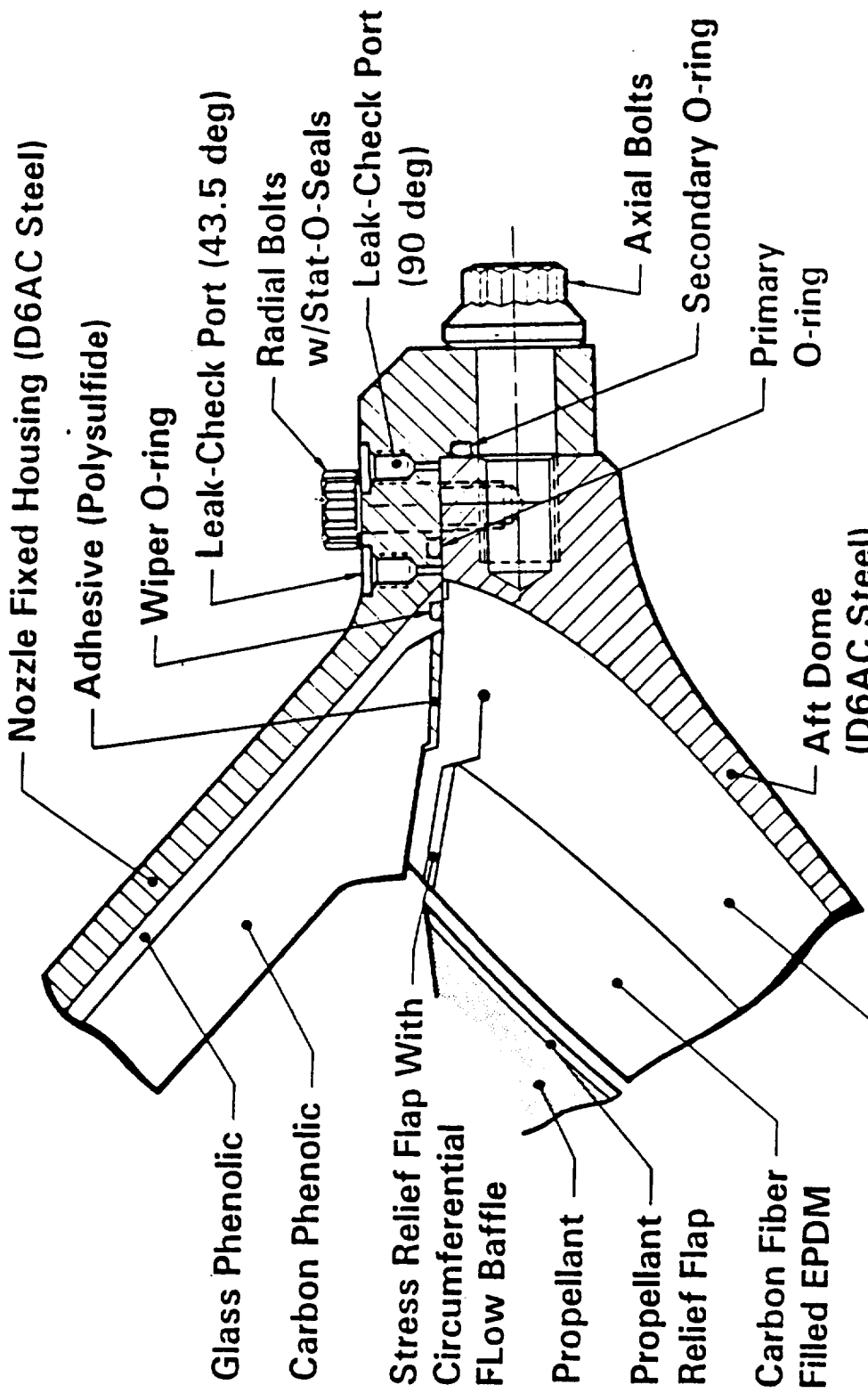

Figure 7.6-3. RSRM Nozzle-to-Case Joint

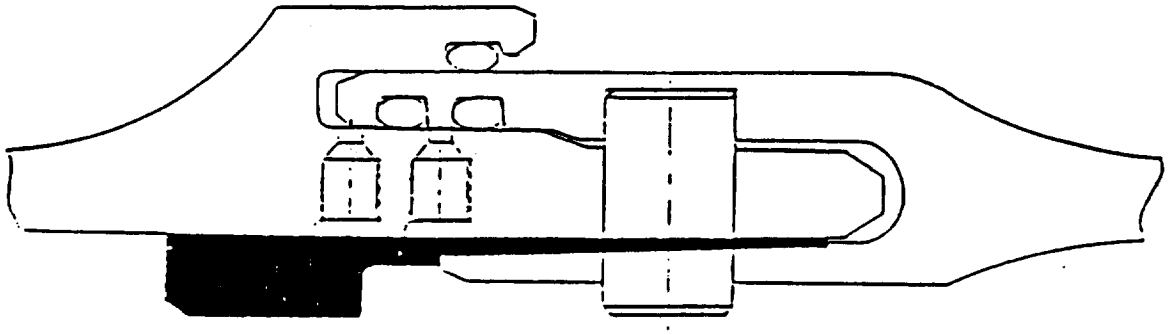

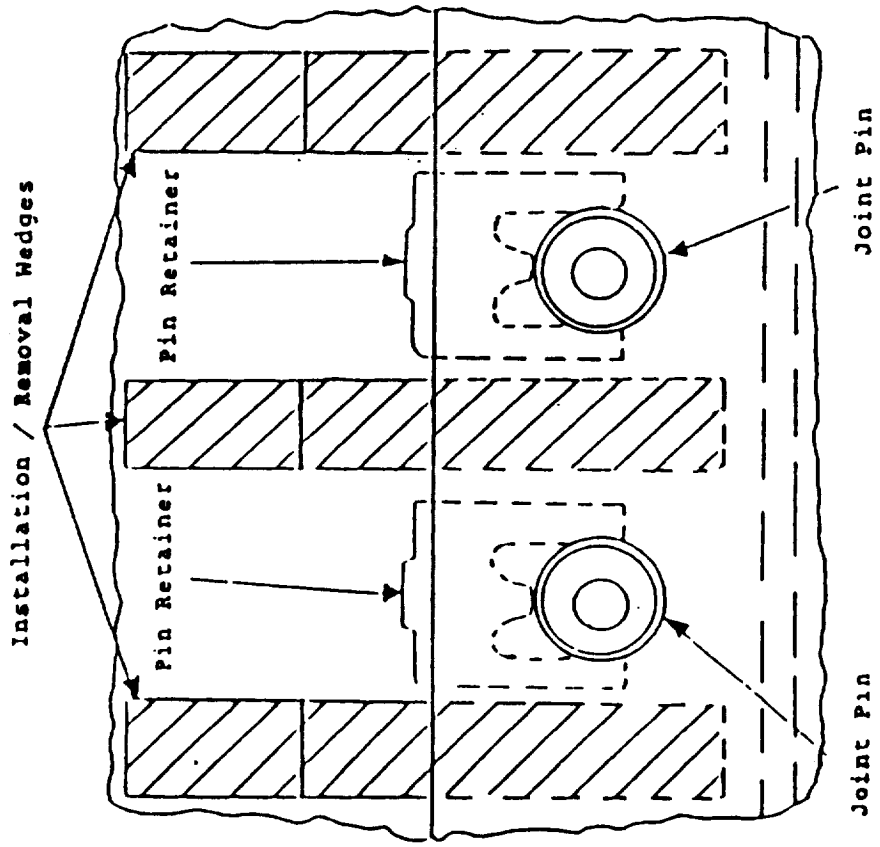

Figure 7.6-4. Shim Installation Wedge

- An internal pressure of 909 psig applied up to the backside of the primary O-ring groove
- Frictionless joint behavior
- Zero vectoring nozzle condition
- Propellant not modeled

7.6.2 Objectives

The test objectives from Section 2 with regard to case performance were:

Qualification Test Objectives

A Certify that the sealing of the case field joints is not affected by static test structural deflections.

D Certify that the case structural and sealing integrity is not degraded.

N Certify that the sealing of the nozzle-to-case joint is not affected by static test structural deflections.

AG Certify that the case is capable of containing the static test internal pressure.

AH Certify that the case segment mating joints have a pin retention device.

AJ Verify that the case segment mating joints incorporate provisions to ensure proper segment orientation and alignment to facilitate joining, stacking, disassembly, and refurbishment.

AK Verify that the RSRM segments are capable of horizontal assembly and disassembly.

Development Test Objectives

BJ Acquire engineering data for validation of joint models.

BK Obtain data to verify finite element models.

7.6.3 Conclusions/Recommendations

The DM-9 static test was conducted successfully without anomalies associated with the case or joint metal hardware. Assembly procedures proved adequate and valuable data were gathered on the structural response of the motor during testing. Chamber pressure was contained and data indicated that joint gap openings were restrained well under the maximum allowable values. No local yielding was measured.

The measured radial growth for the DM-9 field joints and nozzle-to-case joint are in close agreement with pretest predictions and radial growth data measured from subscale testing (JES-3A, JES-3B, NJES-2A, NJES-2B, and TPTA-1.1). The O-ring gap opening was not measured directly for the DM-9 field and nozzle- to-case joints. However these measurements were taken on the JES, NJES, and TPTA tests. The maximum measured O-ring gap openings, flaws, if any, to the joint, and the test pressure are listed in Table 7.6-1. The largest field joint O-ring gap measured (flawed or unflawed) was 0.006 in. (JES-3A and TPTA-1.1). Analysis predicts 0.004 inch. The maximum measured primary gap opening for the nozzle-to-case joint was 0.007 in. (NJES-2A). Analysis predicts 0.006 inch.

Since the DM-9 maximum joint pressures did not exceed the maximum subscale test pressures listed in Table 7.6-1, it is a good assumption that the DM-9 O-ring gap openings did not exceed those measured in the subscale tests.

7.6.4 Results/Discussion

7.6.4.1 Field Joints

Field Joint Radial Growth

Radial growth is determined from the product of measured girth strain and nominal hardware radii at the corresponding gage location. Test data versus predicted data are shown in Tables 7.6-2 through 7.6-4.

The results show a strong correlation between analysis and test data. All of the field joint predictions are within 9 percent of measured values. Close study of the

Table 7.6-1. Subscale Test O-ring Gap Opening

	Test	Joint	Max O-ring Gap (in.)	Defect	Chamber Pressure (psi)	ETA Ring
Field Joints	JES-3A	A	0.006	None	939	270
	JES-3A	B	0.005	J-seal Wave	939	
	JES-3B	A	0.004	Channel-to-CF O-ring	907	None
	JES-3B	B	0.005	Pressure-to-Primary O-ring	907	
	TPTA-1.1	A	0.001	None	901	360
	TPTA-1.1	B	0.006	None	901	
Nozzle-to-Case Joints	NJES-2A	Primary O-ring	0.007	Flaw to wiper O-ring (saw no pressure)	1,025	
	NJES-2A	Secondary O-ring	No data	Flaw to wiper O-ring	1,025	
	NJES-2B	Primary O-ring	0.005	Flaw to wiper O-ring (saw pressure)	847	
	NJES-2B	Secondary O-ring	0.002*	Flaw to wiper O-ring (saw pressure)	847	
	TPTA-1.1	Primary O-ring	0.006	Flaw to wiper O-ring (saw pressure)	901	
	TPTA-1.1	Secondary O-ring	0.004	Flaw to wiper O-ring (saw pressure	901	

*Maximum gap aft of secondary O-ring

Table 7.6-2. DM-9 Forward Field Joint Girth Gages

TEST NAME: DM-9 1/26/88
JOINT: FWD FIELD
DESCRIPTION: JOINT GIRTH GAGES
THE TIME RANGE IS 8.0 TO 12.0 SECONDS
CORRECTED LOCAL PRESSURE: 866 PSIG

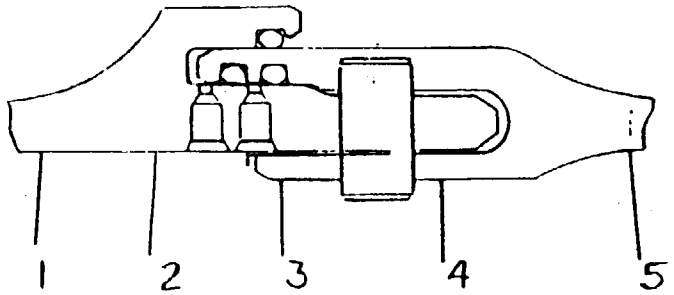

GIRTH GAGE LOCATION	GAGE NUMBER	STATION	RADIUS (IN)	RADIAL GROWTH (IN)	TEST STRAIN (UIN/IN)	ADJUSTED ANALYSIS STRAIN (UIN/IN)	ADJUSTED ANALYSIS RADIAL GROWTH (IN)	DIFF IN RADIAL GROWTH (% DIFF)
1	S615	846.8	73.1	0.172	2352	2267	0.166	-3.6
2	R303	848.5	73.1	0.160	2194	2201	0.161	0.3
3	S677	850.2	73.5	0.153	2083	2011	0.148	-3.4
4	S965	852.6	73.5	ND	ND	2054	0.151	ND
5	S621	855.0	73.1	0.174	2374	2552	0.187	7.5

Table 7.6-3. DM-9 Center Field Joint Girth Gages

TEST NAME: DM-9 1/26/88
JOINT: CTR FIELD
DESCRIPTION: JOINT GIRTH GAGES
THE TIME RANGE IS 8.0 TO 22.0 SECONDS
CORRECTED LOCAL PRESSURE: 838 PSIG

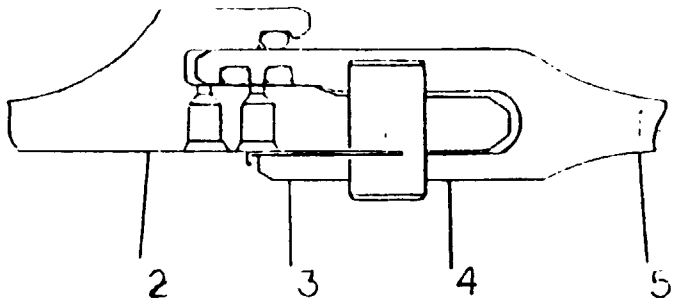

GIRTH GAGE LOCATION	GAGE NUMBER	STATION	RADIUS (IN)	RADIAL GROWTH (IN)	TEST STRAIN (UIN/IN)	ADJUSTED ANALYSIS STRAIN (UIN/IN)	ADJUSTED ANALYSIS RADIAL GROWTH (IN)	DIFF IN RADIAL GROWTH (% DIFF)
2	R304	1168.5	73.1	0.159	2181	2137	0.156	-2.0
3	S682	1170.2	73.5	0.156	2116	1946	0.143	-8.0
4	S936	1172.6	73.5	0.140	1899	1987	0.146	4.6
5	S635	1175.0	73.1	0.172	2353	2473	0.181	5.1

Table 7.6-4. DM-9 Aft Field Joint Girth Gages

TEST NAME: DM-9 1/26/88
JOINT: AFT FIELD
DESCRIPTION: JOINT GIRTH GAGES
THE TIME RANGE IS 19.0 TO 22.0 SECONDS
CORRECTED LOCAL PRESSURE: 819 PSIG

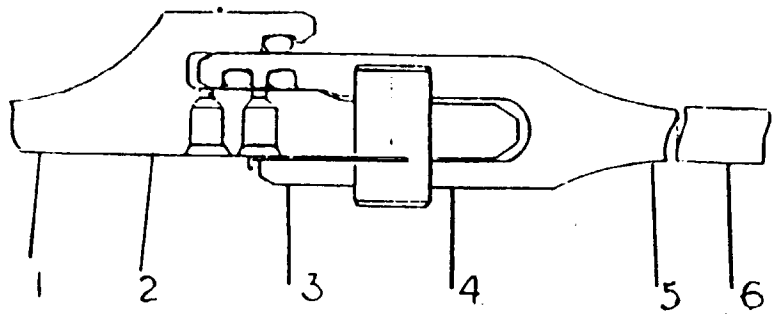

GIRTH GAGE LOCATION	GAGE NUMBER	STATION	RADIUS (IN)	RADIAL GROWTH (IN)	TEST STRAIN (UIN/IN)	ADJUSTED ANALYSIS STRAIN (UIN/IN)	ADJUSTED ANALYSIS RADIAL GROWTH (IN)	DIFF IN RADIAL GROWTH (% DIFF)
1	S690	1486.8	73.1	0.170	2320	2261	0.165	-2.6
2	R305	1488.5	73.1	0.157	2152	2052	0.150	-4.6
3	S689	1490.2	73.5	0.136	1847	1808	0.133	-2.1
4	S968	1492.6	73.5	0.145	1969	1794	0.132	-8.9
5	S686	1495.0	73.1	0.150	2048	1986	0.145	-3.0
6	S687	1497.3	73.1	0.158	2166	2140	0.156	-1.2

field joint growth behavior shows that the joint is rotating outward. This can be seen from the higher radial growth values at the forward and aft ends of each joint, and the lower values closer to the pin centerline. This trend was predicted and was seen on DM-8, TPTA-1.1, and past JES tests.

Prediction values from analysis for each gage location shown in Tables 7.6-2 through 7.6-4 were ratioed to the estimated DM-9 pressure. Analysis prediction values are calculated assuming a common pressure, which in most cases is larger than the actual pressure for the specific location. The pressure at a particular joint at time of maximum radial growth (girth strain) is found using the actual headend pressure minus the predicted pressure drop. For DM-9, the predicted pressure drops were given in TWR-16928.

The value of gage S966 on the center field joint appears to be in error and should be higher due to the joint rotation effect.

Field Joint Radial Growth Comparison to DM-8, JES-3A, JES-3B, TPTA 1.1, and Analysis

Tables 7.6-5 through 7.6-7 compare DM-9 field joint radial growth to subscale capture feature hardware testing, DM-8, and analysis. All values have been pressure-ratioed to the estimated DM-9 respective joint pressures. Radial growth values compare very well considering the differences between each test. Gage location 6 for DM-9 aft field joint illustrates that radial growth has been reduced due to the 360-deg ETA ring. This can be seen in the data from TPTA 1.1, which also had a 360-deg ETA ring.

The O-ring gap opening measured directly in JES and TPTA tests are shown in Table 7.6-8. It is a good assumption that the DM-9 O-ring gap openings did not exceed the range outlined in Table 7.6-8 because the maximum DM-9 field joint gage pressures (866 psi at forward joint) did not exceed the maximum subscale test pressures.

The largest field joint gap directly measured in subscale tests (flawed or unflawed) was 0.006 in. (JES-3A and TPTA-1.1). Analysis predicts 0.004 inch.

Table 7.6-5. DM-9 Forward Field Joint Radial Growth Comparisons

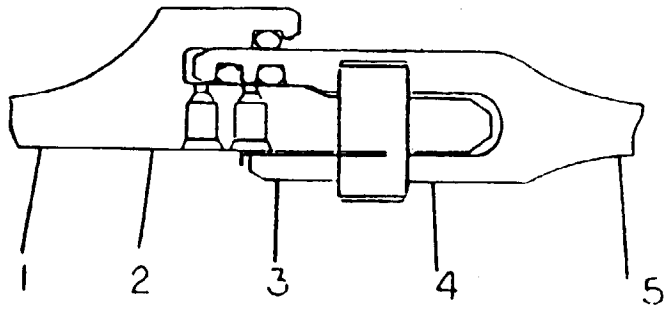

Test Pressure = 866 psig

Location	Gage	DM-9	DM-8	TPTA-1.1	JES-3A	JES-3B	ANALYSIS
1	S615	0.172	0.178	0.171	0.184	0.184	0.166
2	R303	0.160	0.165	0.162	0.166	0.167	0.161
3	S677	0.153	0.148	0.145	ND	0.149	0.148
4	S965*	ND	0.162	0.156	ND	ND	0.151
5	S621	0.174	0.185	0.169	0.185	0.184	0.187

* 1/3 Inch Aft of DM-8, JES-3A, 3B, TPTA-1.1, and Analysis Locations.

Table 7.6-6. DM-9 Center Field Joint Radial Growth Comparisons

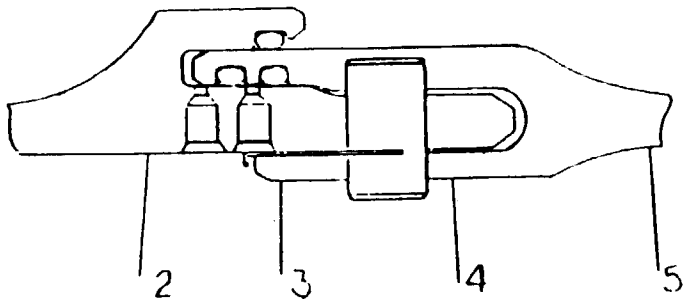

Test Pressure = 838 psig

Location	Gage	DM-9	DM-8	TPTA-1.1	JES-3A	JES-3B	ANALYSIS
2	R304	0.159	0.165	0.157	0.161	0.161	0.156
3	S682	0.155	0.146	0.140	ND	0.145	0.144
4	S966*	0.140	0.161	0.153	ND	ND	0.146
5	S635	0.171	0.183	0.163	0.179	0.178	0.181

* 1/3 Inch Aft of DM-8, JES-3A, 3B, TPTA-1.1, and Analysis Locations.

Table 7.6-7. DM-9 Aft Field Joint Radial Growth Comparisons

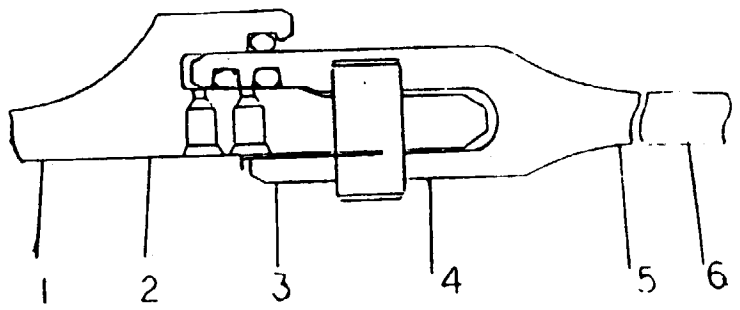

Test Pressure = 819 psig

Location	Gage	DM-9	DM-8	TPTA-1.1	JES-3A	JES-3B	ANALYSIS
1	S690	0.170	0.173	0.162	0.171	0.174	0.165
2	R305	0.157	0.163	0.153	ND	ND	0.150
3	S689	0.136	0.144	ND	ND	ND	0.133
4	S968*	0.145	0.153	0.137	0.153	0.156	0.132
5	S686	0.150	0.161	0.141	ND	0.157	0.145
6	S687	0.158	0.171	0.145	0.160	0.170	0.156
ETA Ring (Degree)		360	270	360	270	None	360

* 1/3 Inch Aft of DM-8, JES-3A, 3B, TPTA-1.1, and Analysis Locations.

Table 7.6-8. Subscale Test Field Joint O-ring Gap Opening

	Test	Joint	Max O-ring Gap (in.)	Defect	Chamber Pressure (psi)	ETA Ring
Field Joints	JES-3A	A	0.006	None	939	270
	JES-3A	B	0.005	J-seal Wave	939	
	JES-3B	A	0.004	Channel-to-CF O-ring	907	None
	JES-3B	B	0.005	Pressure-to-Primary O-ring	907	
	TPTA-1.1	A	0.001	None	901	360
	TPTA-1.1	B	0.006	None	901	

7.6.4.2 Case

Case Membrane Radial Growth

Table 7.6-9 compares the measured radial growth with predicted values. Every prediction is within 4 percent of the measured data. Analysis and data from DM-8 (Table 7.6-10) show that the pressure drop down the bore of the motor in the forward segment is illustrated by a reduction in the radial growth from Station 1 to Station 2. DM-9 and DM-8 data show that the radial growth increases from Station 2 to Station 3. This is explained by the fact that effects of the transition from a standard weight segment to a lightweight segment overpowers the effects of the pressure drop from Station 2 to 3, and a net increase in radial growth occurs. Data from DM-8 and DM-9 show that the effects of the transition are larger than that shown by analysis. Data are also shown in Table 7.6-10 from JES-3A, JES-3B, and TPTA-1.1. The values used were from a single gage location on each test and pressure ratioed to estimated DM-9 gage pressures at each location. There is no significant pressure drop in these subscale tests.

Data from gage S584 is suspected to be in error. This gage is closest to the headend and thus sees a higher pressure than gages farther aft.

Case Biaxial Growth

Table 7.6-11 lists the maximum hoop and axial stresses for the aft field joint and ETA areas along with analysis. The biaxial strain gages at Location 1 are 0.39 in. aft of the tip of the outer clevis leg.

The maximum measured stress occurred in the hoop direction of location 1. The measured value was 147.4 ksi, and occurred at location 2 is 11.2 in. aft of the tip of the outer clevis leg.

The maximum measured stress occurred in the hoop direction at 90 deg, location 2, which measured a local stress of 86.1 ksi. Given that the ultimate strength of D6AC steel is 200 ksi, a safety factor of 2.3 results. The yield strength of D6AC is 180 ksi. Therefore, no local yielding was measured in this area. Location 1 shows an

Table 7.6-9. DM-9 Case Radial Deflection Girth Gages

TEST NAME: DM-9 1/26/88
JOINT: CASE RADIAL DEFLECTION
DESCRIPTION: CASE GIRTH GAGES
THE TIME RANGE IS 7.0 TO 22.0 SECONDS

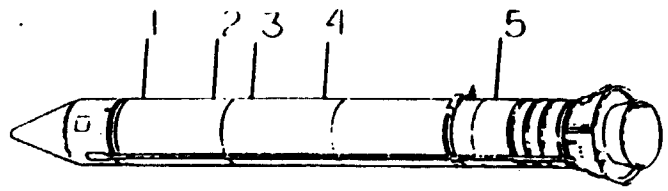

GIRTH GAGE LOCATION	GAGE NUMBER	STATION	RADIUS (IN)	RADIAL GROWTH (IN)	TEST STRAIN (UIN/IN)	ADJUSTED ANALYSIS STRAIN (UIN/IN)	ADJUSTED ANALYSIS RADIAL GROWTH (IN)	DIFF IN RADIAL GROWTH (% DIFF)	CORRECTED LOCAL PRESSURE (PSIG)
1	S584	610.0	73.0	0.268	3670	3842	0.278		884
2	S585	770.0	73.0	0.271	3714	3775	0.272		865
3	S586	930.0	73.0	0.283	3870	3738	0.273	-3.4	855
4	S587	1090.0	73.0	0.279	3826	3678	0.269	-3.9	842
5	S591	1635.0	73.0	0.253	3465	3548	0.259	2.4	812

Table 7.6-10. DM-9 Case Membrane Growth Comparisons

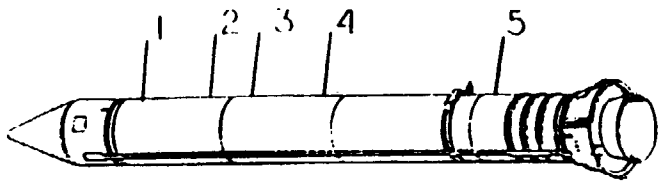

Location	Gage	DM-9	DM-8	TPTA-1.1	JES-3A	JES-3B	ANALYSIS	DM-9 Pressure psig
1	S584	0.268*	0.284*	0.270	0.286	0.287		884
2	S585	0.271*	0.282*	0.265	0.280	0.280		865
3	S586	0.283	0.291	0.261	0.277	0.277	0.273	855
4	S587	0.279	0.292	0.257	0.273	0.273	0.269	842
5	S591	0.253	0.260	ND 2	ND 1	ND 1	0.259	812

* Standard Weight Cylinders For These Gage Locations.

1 - No stiffener cylinders
2 - One stiffener cylinder (DM-9 and DM-9 had 2)

Table 7.6-11. DM-9 Aft Field/ETA Joint Biaxial Gages

TEST NAME: DM-9 1/26/88
JOINT: AFT FIELD / ET ATTACH
DESCRIPTION: JOINT BIAXIAL GAGES
MODEL PRESSURE: 913.0 PSIA
THE TIME RANGE IS 17.0 TO 22.0 SECONDS

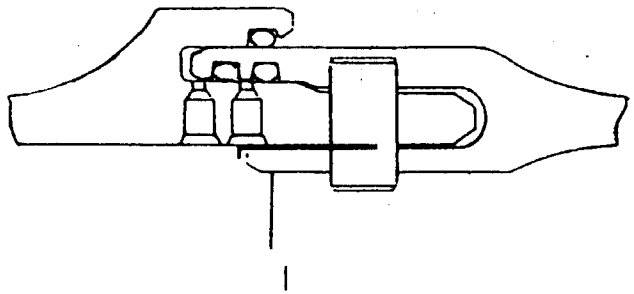

LOCAT	ANGULAR LOCATION	AXIAL GAGE	HOOP GAGE	AXIAL STRESS (KSI)	HOOP STRESS (KSI)	TEST DATA AXIAL STRAIN (UIN/IN)	TEST DATA HOOP STRAIN (UIN/IN)	ADJUSTED ANALYSIS AXIAL STRAIN (UIN/IN)	ADJUSTED ANALYSIS HOOP STRAIN (UIN/IN)	%DIFF AXIAL	%DIFF HOOP
1	0.0	R626	R625	ND	ND	-210	ND	-278	ND	32.4	ND
	90.0	R742	R741	57.7	-3.8	1962	-704	-278	861	-114.2	-222.3
	188.0	R718	R717	-2.1	61.4	-684	2067	-278	862	-59.3	-58.3
	220.0	R632	R631	0.7	67.4	-652	2239	-278	861	-57.4	-61.5
	270.0	R636	R635	-2.2	75.0	-824	2524	-278	860	-66.2	-65.9
	255.0	R638	R637	3.8	40.6	-279	1316	-879	2650	214.9	101.4
	285.0	R640	R639	2.5	55.0	-465	1807	-880	2658	89.1	47.1
	300.0	R712	R711	1.3	84.2	-798	2795	-278	860	-65.2	-69.2
	320.0	R642	R641	-0.1	82.0	-823	2734	-278	860	-66.2	-68.5
			AVERAGE:	7.7	57.7	-308	1847				

Table 7.6-11. DM-9 Aft Field/ETA Joint Biaxial Gages (cont)

TEST NAME: DM-9 1/26/88
JOINT: AFT FIELD / ET ATTACH
DESCRIPTION: JOINT BIAXIAL GAGES
MODEL PRESSURE: 913.0 PSIA
THE TIME RANGE IS 17.0 TO 22.0 SECONDS

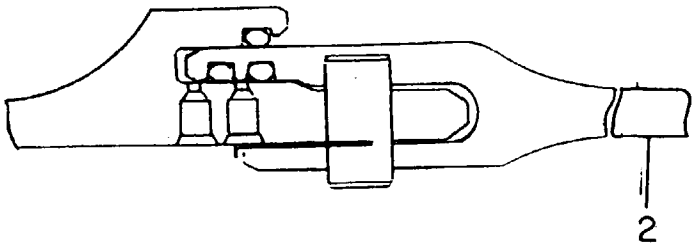

LOCAT	ANGULAR LOCATION	AXIAL GAGE	HOOP GAGE	AXIAL STRESS (KSI)	HOOP STRESS (KSI)	TEST DATA AXIAL STRAIN (UIN/IN)	TEST DATA HOOP STRAIN (UIN/IN)	ADJUSTED ANALYSIS AXIAL STRAIN (UIN/IN)	ADJUSTED ANALYSIS HOOP STRAIN (UIN/IN)	%DIFF AXIAL	%DIFF HOOP
2	0.0	R662	R661	46.3	81.7	725	2261	1188	1657	63.9	-26.7
	90.0	R746	R745	47.8	86.1	734	2391	1189	1659	62.0	-30.6
	188.0	R728	R727	55.1	82.5	1011	2199	1190	1654	17.6	-24.8
	220.0	R668	R667	51.0	82.1	880	2227	1190	1657	35.2	-25.6
	270.0	R672	R671	49.8	82.1	840	2237	1189	1654	41.4	-26.1
	255.0	R674	R673	52.8	83.7	922	2262	1188	1657	28.9	-26.7
	285.0	R676	R675	53.4	80.8	973	2160	1188	1657	22.2	-23.3
	300.0	R716	R715	51.5	81.4	903	2198	1188	1657	31.5	-24.6
	320.0	R678	R677	49.2	82.0	821	2241	1188	1658	44.7	-26.0
			AVERAGE:	50.8	82.5	868	2242				

erratic stress behavior whereas location 2 is more closely uniform. There are a number of variables which would affect stress in location 1 that are difficult to model.

a. Scalloping Effects. On the even degree locations where the pins are located, there is a shim installed which induces a stress on the outer clevis leg. In the odd degree locations where there is no shim, the stress is less. This effect is difficult to model due to slumping effects that cause the out-of-roundness condition encountered in a horizontal assembly. Also, the actual shim thickness versus the analysis shim thickness varies somewhat.

b. Stress Concentrations at and Around the Pinhole Regions. Variability in the gage placement in these areas can significantly change the strain reading.

c. Permanent Set. There was permanent set in the outer clevis leg due to the ratcheting effect (joint rotation) experienced at the time of static test.

All of these variables in combination with each other make this area hard to predict. The reason for placement of biaxial gages at this locations was to see the effect that the ETA ring has on the field joint in this area. After studying the results from DM-9 and DM-8 (which had gages located at the same location with similar results), it is felt that these gages should be removed so that other gages, such as the 3-in-1 gage (which measures pressure, temperature, and joint deflection and is used on the leak check port), can be used on future SRM static testing and flight motors.

Table 7.6-12 illustrates the case membrane biaxial stresses with the corresponding predictions. The hoop predictions compared better with the measured values than with the gages in the axial direction, especially at 0 and 188 deg. It is suspected that some of this discrepancy can be attributed to the pretest sag of the motor in the test stand, and subsequent lessening of the sag during motor pressurization.

This effect, known as column bending, would theoretically change motor stress at the 0 and 188 deg locations as follows. When the SRM chocks are removed, the motor sags. This in turn causes an induced tensile axial strain at 0 deg, and a induced compressive axial strain at 180 deg. Just before the static test, the biaxial

Table 7.6-12. DM-9 Aft/Center Segment Case Stresses

TEST NAME: DM-9 1/26/88
JOINT: AFT/CTR
DESCRIPTION: CASE STRESSES
THE TIME RANGE IS 17.0 TO 22.0 SECONDS
CORRECTED LOCAL PRESSURE: 838 PSIG

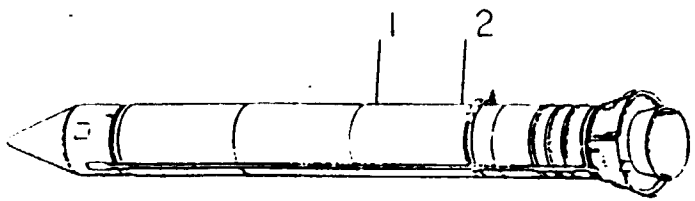

						TEST DATA		ADJUSTED ANALYSIS			
LOCAT	ANGULAR LOCATION	AXIAL GAGE	HOOP GAGE	AXIAL STRESS (KSI)	HOOP STRESS (KSI)	AXIAL STRAIN (UIN/IN)	HOOP STRAIN (UIN/IN)	AXIAL STRAIN (UIN/IN)	HOOP STRAIN (UIN/IN)	%DIFF AXIAL	%DIFF HOOP
1	0.0	R680	R679	60.7	147.4	548	4307	2031	3216	270.6	-25.3
	90.0	R740	R739	60.5	146.1	555	4266	809	3590	45.7	-15.9
	188.0	R720	R719	62.3	126.2	816	3583	-301	3914	-136.8	9.2
	270.0	R686	R685	ND	ND	440	ND	809	3589	83.8	ND
			AVERAGE:	50.8	110.5	590	4052				
2	0.0	R780	R779	55.2	134.5	494	3933	1895	3182	283.4	-19.1
	90.0	R782	R781	ND	ND	624	ND	794	3519	27.3	-31.9
	188.0	R788	R787	58.0	126.6	668	3641	-210	3821	-131.4	5.0
	270.0	R786	R785	63.5	143.7	678	4156	792	3522	16.8	-15.2
			AVERAGE:	58.9	134.9	616	3910				

gages in these areas are set to zero. Therefore, when the motor is fired and the sag is lessened, readings in both the 0- and 180-deg areas (188 deg for DM-9) are incorrect.

The maximum measured stress occurred in the hoop direction at location 1. The measured value was 147.4 ksi, and occurred at 0 deg. Using biaxial improvement increases the ultimate case strength from 200 to 214.2 ksi (i.e., 200 by 1.071 ksi = 214.2 ksi), which gives a safety factor of 1.45. No local yielding was measured.

7.6.4.3 Nozzle-to-Case Joint. Bryner girth gages were located on the DM-9 nozzle-to-case joint to obtain circumferential girth strains from which average radial deflections could be calculated. Radial deflection is an important parameter to characterize since it is proportional to joint hoop stress and bolt hole stress concentration.

Table 7.6-13 displays the locations and readings of the girth gages and their corresponding analytical prediction. Analytical results compare to test results very well, ranging from 0 to 12.1 percent difference.

The maximum strain gage readings occurred between 17 and 22 sec into the test at an estimated nozzle stagnation pressure of 837 psig. Unless otherwise stated, results presented here are at approximately 837 psig.

There are several reasons for the variation between test data and analytical data as follows:

- The analytical data was linearly scaled to the test data
- The nozzle stagnation pressure was estimated to be 837 psig, but not measured
- Nominal materials were used for the finite element model

Since the DM-9 nozzle stagnation pressure did not reach the 909 psig pressure used in the model, the analytical data for comparison to test data was obtained by linearly scaling the predictions by the estimated stagnation pressure divided by 909. There is some error involved in linearly scaling the analytical results to test pressure because the analysis is nonlinear. However, this error is on the order of 5 percent.

Table 7.6-13. DM-9 Nozzle-to-Case Joint Case Girth Gages

TEST NAME: DM-9 1/26/88
JOINT: AFT DOME, FIXED HOUSING
DESCRIPTION: NOZZLE CASE GIRTH GAGES
THE TIME RANGE IS 19.0 TO 22.0 SECONDS
CORRECTED LOCAL PRESSURE: 837 PSIG

GIRTH GAGE LOCATION	GAGE NUMBER	STATION	RADIUS (IN)	RADIAL GROWTH (IN)	TEST STRAIN (UIN/IN)	ADJUSTED ANALYSIS STRAIN (UIN/IN)	ADJUSTED ANALYSIS RADIAL GROWTH (IN)	DIFF IN RADIAL GROWTH (% DIFF)
0	S885	1861.0	40.2	-0.057	-1428	-1543	-0.062	8.7
1	S880	1873.0	50.4	0.076	1508	1566	0.079	3.9
2	S882	1875.5	50.5	0.121	2396	2381	0.121	0.0
3	S878	1876.0	50.5	0.121	2396	2543	0.128	6.6
4	S883	1877.0	54.4	0.136	2500	2464	0.134	-1.5
5	S884	1875.5	54.4	0.120	2206	2176	0.118	-0.8
6	S887	1810.0	54.8	0.091	1661	1832	0.100	12.1
7	S875	1874.0	54.8	0.107	1953	1807	0.099	7.5
8	S874	1872.5	55.2	0.090	1630	1461	0.081	-10.0

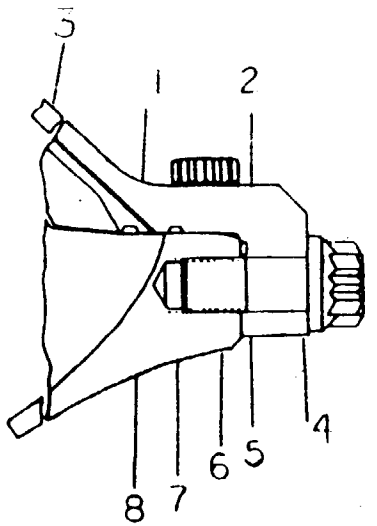

As expected, calculated radial growths indicated a prying open action and outward rotation of the joint. The maximum measured hoop strain (2,500 in./in.) and radial growth (0.136 in.) occurred at location 4.

Biaxial Strains

Biaxial strain gages were placed on the fixed housing and aft dome to measure local rather than average strains incurred in the case during pressurization (Table 7.6-14). Some of these were located at the same location as girth gages (Table 7.6-13) so that the biaxial hoop strain component could be compared to the girth strain. From the biaxial strains, case stresses were calculated. These stresses, as were the strains, were in the hoop and meridional direction.

The maximum calculated hoop stress was 78.5 ksi and occurred at location 4, at the angular location of 90 deg. The maximum calculated meridional stress was 37.2 ksi and occurred at location 3 at 270 deg. Based on the maximum calculated stress of 78.5 ksi, and an ultimate material strength of 200 ksi, the safety factor is 2.5.

Differences between predicted and measured hoop strains ranged from 5.2 to 30.7 percent. Meridional predicted and measured strain varied from 4.1 to 73.2 percent. At this time there are no available predictions for location 4. These gages were to be removed due to a cutback on engineering instrumentation to support schedule testing. However, the engineering change order which required them to be cut was released after they had already been installed. It should be noted that the gages at location 4 are between the radial bolts at each circumferential location.

Test data span 19.0 to 22.0 sec into the firing of DM-9 to avoid including vectoring effects, which were not taken into account in the analysis.

Axial Bolts

Two axial bolts were replaced with strainserts to measure tension load in the bolts. However, due to system problems the preload data were not obtained. Change in bolt load resulting from motor pressurization was monitored during the firing. One axial

Table 7.6-14. DM-9 Nozzle-to-Case Joint Biaxial Gages

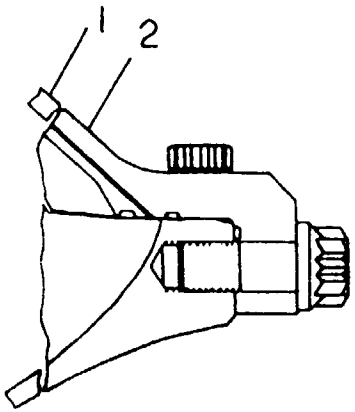

TEST NAME: DM-9 1/11/88
JOINT: FIXED HOUSING, AFT DOME
DESCRIPTION: NOZZLE / CASE BIAXIAL GAGES
THE TIME RANGE IS 19.0 TO 22.0 SECONDS
CORRECTED LOCAL PRESSURE: 837 PSIG

						TEST DATA		ADJUSTED ANALYSIS			
LOCAT	ANGULAR LOCATION	HOOP GAGE	MERID GAGE	HOOP STRESS (KSI)	MERID STRESS (KSI)	HOOP STRAIN (UIN/IN)	MERID STRAIN (UIN/IN)	HOOP STRAIN (UIN/IN)	MERID STRAIN (UIN/IN)	%DIFF HOOP	%DIFF MERID
1	0.0	R536	R535	-51.0	18.3	-1882	1121	-1543	321	-18.0	-71.4
	90.0	R538	R537	-52.7	19.8	-1955	1186	-1537	318	-21.4	-73.2
			AVERAGE:	-51.8	19.0	-1918	1153				
2	0.0	R528	R527	-33.2	8.2	-1188	604	-982	628	-17.3	4.1
	90.0	R530	R529	-30.9	7.5	-1106	559	-981	630	-11.3	12.7
	180.0	R532	R531	-29.2	9.4	-1065	604	-983	629	-7.8	4.2
	270.0	R534	R533	-31.6	7.3	-1126	560	-983	629	-12.8	12.4
			AVERAGE:	-31.2	8.1	-1121	582				

Table 7.6-14. DM-9 Nozzle-to-Case Joint Biaxial Gages (cont)

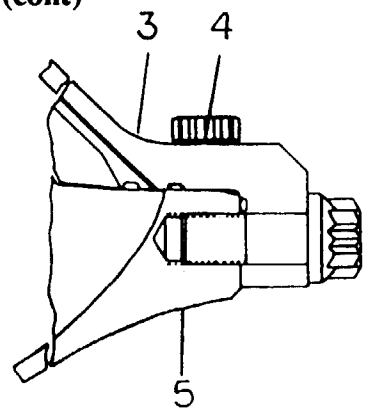

TEST NAME: DM-9 1/11/88
JOINT: FIXED HOUSING, AFT DOME
DESCRIPTION: NOZZLE / CASE BIAXIAL GAGES
THE TIME RANGE IS 19.0 TO 22.0 SECONDS
CORRECTED LOCAL PRESSURE: 837 PSIG

						TEST DATA		ADJUSTED ANALYSIS			
LOCAT	ANGULAR LOCATION	HOOP GAGE	MERID GAGE	HOOP STRESS (KSI)	MERID STRESS (KSI)	HOOP STRAIN (UIN/IN)	MERID STRAIN (UIN/IN)	HOOP STRAIN (UIN/IN)	MERID STRAIN (UIN/IN)	%DIFF HOOP	%DIFF MERID
3	0.0	R520	R519	27.3	-24.6	1156	-1094	1216	-899	5.2	-17.9
	90.0	R522	R521	34.8	-34.1	1503	-1486	1213	-896	-19.3	-39.7
	180.0	R524	R523	32.1	-24.7	1315	-1143	1217	-893	-7.5	-21.9
	270.0	R526	R525	29.3	-37.2	1350	-1533	1222	-898	-9.5	-41.4
			AVERAGE:	30.9	-30.2	1331	-1314				
4	0.0	R544	R543	59.7	-7.2	2063	-837	ND	ND	ND	ND
	90.0	R546	R545	78.5	-4.4	2660	-931	ND	ND	ND	ND
	180.0	R548	R547	67.4	-6.3	2309	-883	ND	ND	ND	ND
	270.0	R550	R549	64.8	-7.6	2236	-902	ND	ND	ND	ND
			AVERAGE:	67.6	-6.4	2317	-888				
5	0.0	R602	R601	43.8	-18.3	1643	-1047	2021	-921	23.0	-12.1
	90.0	R604	R603	ND	ND	1597	ND	2001	ND	25.3	ND
	180.0	R606	R605	43.2	-17.2	1613	-1007	2020	-921	25.2	-8.6
	270.0	R608	R607	41.5	-16.4	1546	-961	2020	-921	30.7	-4.2
			AVERAGE:	42.8	-17.3	1600	-1005				

strainsert bolt showed a slight increase in load (Table 7.6-15) of 3 kip, while other strainserts showed a 2-kip decrease.

An analysis was performed using a preload value of 140 kip in the axial bolts. The analysis predicts a load decrease of 11 kip at 920 psig. The bolt load drops off due to the thinning of the fixed housing flange. The flange thinning is attributable to Poisson's effect resulting from the flange displacing radially outward.

The reason for the strainsert bolts measured load changes of +3 kip and -2 kip is the low preload values in the axial bolts. Analysis has shown that at lower preload values the bolt loads tend to increase rather than decrease in magnitude.

Radial Bolts

The radial bolts were a main concern of the DM-9 nozzle-to-case joint because the amount of preload in these bolts governs the amount of delta gap opening of the joint. Delta gap controls the amount of dynamic O-ring squeeze and consequently the sealing of the joint.

Four radial bolts were replaced with strainsert bolts. Preload data for the strainsert bolts were not available due to system problems. However, the strainsert bolts were monitored during the firing and bolt load change resulting from case pressurization was obtained. Table 7.6-15 indicates that the radial strainsert bolts decreased in load during pressurization. The load decrease ranged between -3 and -6 kip.

The analysis, using a preload value of 47 kip, predicted the radial bolt loads would decrease by 3 kip at 920 psig. This seems to correlate well with the actual measured data. Since the initial preload data was not available, it is impossible to fully correlate test data with analytical predictions.

Nozzle-to-Case Joint Comparison, DM-8, NJES-2A, NJES-2B, TPTA-1.1, and Analysis

Table 7.6-16 compares the performance of the DM-9 nozzle-to-case joint with the same joint configuration (radial bolt design) used in DM-8, NJES-2A, NJES-2B,

Table 7.6-15. DM-9 Nozzle-to-Case Joint Strainserts

TEST NAME: DM-9 1/26/88
JOINT: FIXED HOUSING, AFT DOME (STRAINSERT)
DESCRIPTION: RADIAL, AXIAL GAGES
THE TIME RANGE IS 17.0 TO 22.0 SECONDS

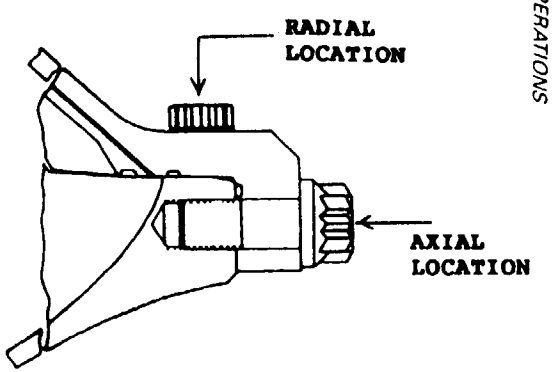

LOCAT	GAGE	ANGULAR LOCATION	PRELOAD LOAD (KIPS)	MEASURED LOAD CHANGE (KIPS)	ANALYSIS PRELOAD (KIPS)	ANALYSIS LOAD CHANGE (KIPS)	DELTA BOLT TEST vs ANAL. (KIPS)
RADIAL	R150	358.2	N/A	-6	47	-3	-3
RADIAL	R152	88.2	N/A	-4	47	-3	-1
RADIAL	R154	178.2	N/A	-3	47	-3	0
RADIAL	R156	268.2	N/A	-3	47	-3	0
AXIAL	S397	358.2	N/A	3	140	-11	14
AXIAL	S398	88.2	N/A	-2	140	-11	9

910335-15.47

Table 7.6-16. DM-9 Nozzle-to-Case Joint Radial Growth Comparisons

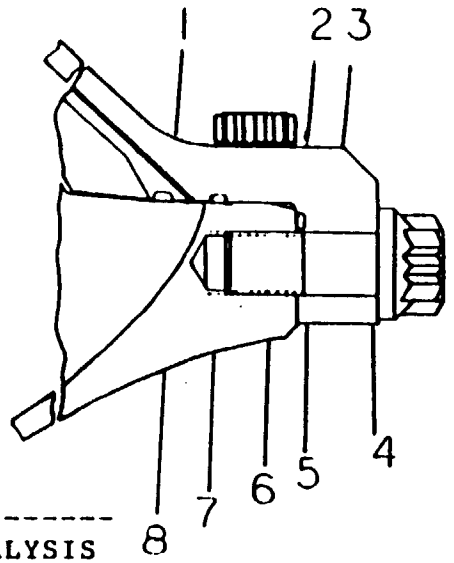

Test Pressure = 837 psig

Location	Gage	DM-9	DM-8	TPTA-1.1	NJES-2A	NJES-2B	ANALYSIS
1	S880	0.076	ND	0.092	0.072	0.081	0.079
2	S882	0.121	0.127	0.134	0.110	0.118	0.121
3	S878	0.121	ND	0.132	0.118	0.126	0.129
4	S883	0.136	ND	0.136	0.130	0.130	0.134
5	S884	0.120	ND	0.120	0.115	0.116	0.119
6	S887	0.091	0.116	0.106	ND	0.107	0.102
7	S875	0.107	0.109	0.100	ND	0.103	0.099
8	S874	0.090	0.095	0.084	0.086	0.087	0.081

TPTA-1.1, and analysis. Data from DM-9 radial growth compare very well, as expected, with the exception of gage S887. In all cases except DM-9, the reading at location 7 is lower than at location 6. This illustrates the joint rotation and prying action that occurs during the firing. Therefore, the reading of gage S887 is suspected to be in error.

The O-ring sealing surface gap growth was not directly measured for the nozzle-to-case joint. However, these measurements were taken on NJES-2A, NJES-2B, TPTA-1.1, and predicted by analysis as shown in Table 7.6-17. For DM-9 the maximum nozzle-to-case pressure was estimated at 837 psig. It is a good assumption that the DM-9 O-ring gap openings did not exceed the range outlined in Table 7.6-17 because the maximum joint pressure did not exceed the maximum subscale test pressure listed.

The maximum measured primary gap opening for the nozzle-to-case joint was 0.007 in. (NJES-2A). Analysis predicts 0.006 inch.

Data indicate that bolt skip was eliminated on DM-9. Proximity gage data on DM-9 shows a 0.001-in. displacement, but this can be accounted for in joint rotation. This was also the case for DM-8.

7.6.4.4 Headend Pressure and Joint Temperature. Table 7.6-18 lists the maximum measured headend pressures and the time at which they occurred. Table 7.6-19 gives the joint temperatures for the field and nozzle-to-case joint.

7.6.4.5 Post-Test Inspection. Structural findings of post-test inspection are discussed in Section 7.7, Seals.

7.7 SEALS

7.7.1 Introduction

O-rings

All O-rings used in the DM-9 were fluorocarbon V747-75 (Viton). Installation proceeded by cleaning and greasing the O-rings and then gently wiping off the excess grease

Table 7.6-17. Subscale Test Nozzle-to-Case Joint O-ring Gap Opening

	Test	Joint	Max O-ring Gap (in.)	Defect	Chamber Pressure (psi)	ETA Ring
Nozzle-to-Case Joints	NJES-2A	Primary O-ring	0.007	Flaw to wiper O-ring (saw no pressure)	1,025	
	NJES-2A	Secondary O-ring	No data	Flaw to wiper O-ring (saw no pressure)	1,025	
	NJES-2B	Primary O-ring	0.005	Flaw to wiper O-ring (saw pressure)	847	
	NJES-2B	Secondary O-ring	0.002*	Flaw to wiper O-ring (saw pressure)	847	
	TPTA-1.1	Primary O-ring	0.006	Flaw to wiper O-ring (saw pressure)	901	
	TPTA-1.1	Secondary O-ring	0.004	Flaw to wiper O-ring (saw pressure)	901	

*Maximum gap aft of secondary O-ring

Table 7.6-18. DM-9 Forward Dome Chamber Pressure

TEST NAME: DM-9 1/26/88
JOINT: FORWARD DOME
DESCRIPTION: CHAMBER PRESSURE
THE TIME RANGE IS 0.0 TO 1.0 SECONDS

PRESSURE LOCATION	GAGE NUMBER	CIRCUMFERENTIAL LOCATION (DEG)	MAXIMUM PRESSURE (PSIA)	TIME OF MAX PRES (SEC)
1	P001	40.0	898.7	0.634
2	P002	270.0	906.4	0.633
3	P003	180.0	905.4	0.629

Table 7.6-19. DM-9 Joint Temperatures

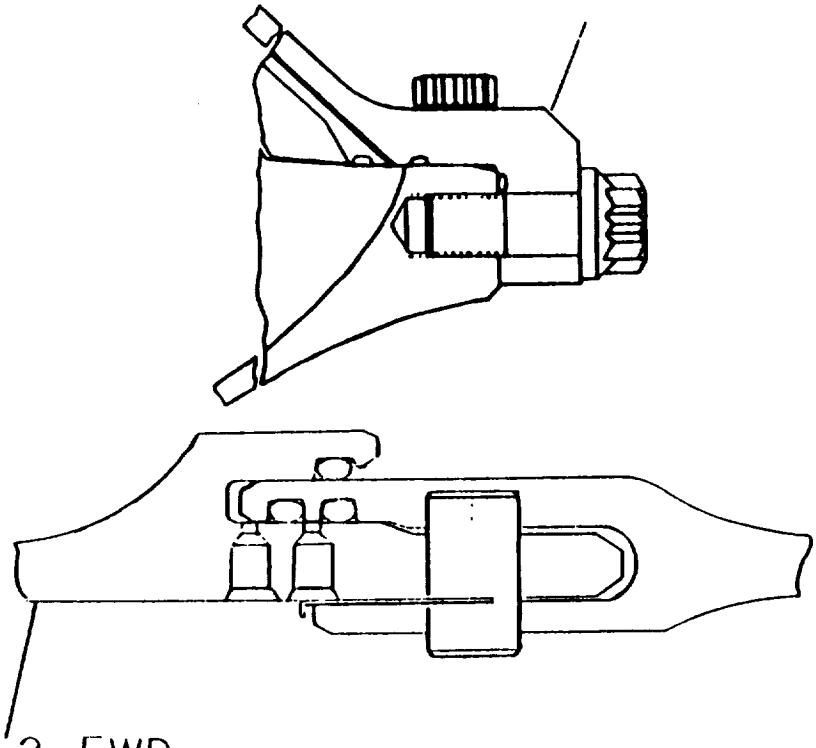

TEMPERATURE LOCAT	GAGE NUMBER	CIRCUMFERENTIAL LOCATION (DEG)	MAXIMUM TEMPERATURE (DEG F)	TIME OF MAX TEMP (SEC)
1	T142	0.0	107.9	0.000
	T143	90.0	87.8	1.296
	T144	180.0	91.0	0.688
	T145	270.0	81.6	0.624
2	T146	0.0	81.5	0.032
	T147	120.0	87.0	0.432
	T148	240.0	95.3	0.656
3	T149	0.0	90.3	1.648
	T150	120.0	117.1	1.040
	T151	240.0	94.4	1.936

with a lint-free cloth. Care was taken during all steps of the greasing and installation procedures to minimize the chances of contamination. See Figures 7.6-1 through 7.6-3 for joint configuration.

V-2 Filler

The V-2 filler, made from fluorocarbon material, consisted of eight lengths per field joint, at 54.3 in. per length. Each length was cleaned with alcohol before installation. An aluminum tool which fits the contour of the V-2 filler was used to ensure that each length was properly seated and no bubbling had occurred (Drawing 4U127153). The V-2 filler with dimensions is shown in Figure 7.7-1.

Squeeze Calculations

The case-to-case joint minimum assumed percentage squeeze set and maximum fill for the primary and secondary O-rings are listed in Table 7.7-1. Also listed is the nozzle-to-case joint minimum assumed percentage squeeze set and maximum fill. The lowest minimum percent squeezeout of the joints is 19.2 percent. This occurs on the secondary O-ring at the ETA-to-stiffener segment factory joint.

7.7.2 Objectives

The qualification test objectives from Section 2 with regard to seals performance were:

A Certify that the sealing of the case field joints is not affected by static test structural deflections.

B Certify the case field joint seal performance at ambient temperature.

D Certify that the case structural and sealing integrity is not degraded.

N Certify that the sealing of the nozzle-to-case joint is not affected by static test structural deflections.

O Certify the nozzle-to-case joint seal performance with the joint conditioned between 75° and 120°F.

A010943a

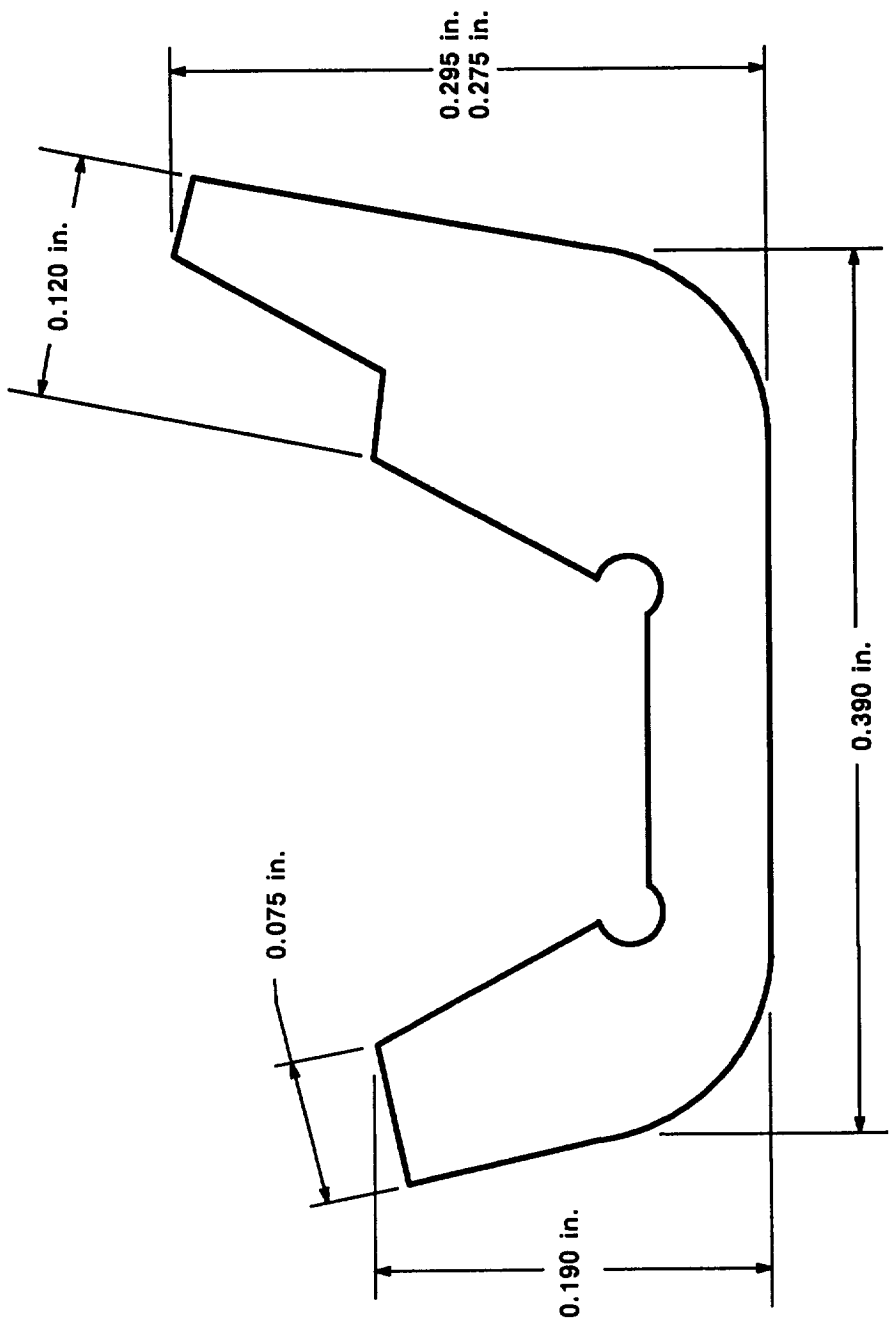

Figure 7.7-1. V_2 Volume Filler

Table 7.7-1. DM-9 O-ring Squeeze and Fill

Joint	Min Squeeze (%)		Max Fill (%)	
	Primary	Secondary	Primary	Secondary
Forward Field*	22.3	20.0	84.9	81.7
Center Field*	20.6	21.4	81.4	82.7
Aft Field*	23.2	23.2	84.1	84.0
Forward Dome	21.7	22.1	81.4	82.1
Forward Factory	20.8	22.6	80.2	83.4
Forward Center	22.4	22.6	82.1	82.5
Aft Center	22.2	21.3	81.8	81.1
ET/Stiffener	20.5	19.2	80.7	79.9
Stiffener/Stiffener	23.0	21.7	82.7	82.2
Aft Dome	21.8	21.1	81.9	81.3
Nozzle/Case	20.4	20.5	80.9	86.0

*0 percent compression set assumed

7.7.3 Conclusions/Recommendations

Field Joints

There was no evidence of gas reaching the O-rings due to the effectiveness of the J-seal insulation. Therefore, the performance of the field joint O-rings cannot be fully evaluated. No damage due to the static test assembly or disassembly occurred to the field joint O-rings.

Factory Joints

For factory joint evaluation, see TWR-18135, Rev A, Section 5.1.

Nozzle-to-Case Joint

There was no evidence of hot gas past the wiper O-ring of the nozzle-to-case joint insulation configuration. Therefore, the performance of the nozzle-to-case joint O-rings cannot be fully evaluated. There was a blowhole through the polysulfide adhesive, but no evidence of erosion, blowby, or heat damage to the wiper O-ring.

No damage due to the static test or assembly occurred to any of the O-rings. A jagged cut in the secondary O-ring is suspected to be handling damage. Gouges found in the wiper O-ring occurred during disassembly. No disassembly damage occurred to the primary O-ring.

Internal Nozzle Joints

Disassembly inspection showed that the seal components performed as expected. Gas reached the primary O-ring at four of the five nozzle internal joints where an unfilled area was found through the RTV backfill. There was no evidence of blowby, erosion, or heat effect to any of the primary/secondary O-rings.

Igniter Joints

Inner and S&A gaskets performed as expected, with no signs of erosion, heat effect, or sooting past the primary seals. A depression was found on the crown of the primary

seal of the igniter gasket. It was concluded that the depression was a manufacturing defect. All sealing surfaces were free of soot.

Anomalies

The Seals Component Program Team evaluated the observations presented in this document using Table 7.7-2 as a guide for establishing the classification of a potential anomaly.

A depression found on the crown of the primary seal at 144 deg of the igniter gasket was identified as a major anomaly (TWR-18071). No critical or minor potential anomalies were identified by the seals component team, but five observations were identified. These potential anomalies are summarized in Section 7.7.4.6.

7.7.4 Results/Discussion

7.7.4.1 Field Joints. Joint conditions were as expected; there was no O-ring damage found by inspection at the time of disassembly or by the O-ring inspection team. The V-2 filler did not obstruct the leak check port at 135 deg. Metal slivers were found during disassembly in the pinhole areas. The slivers are formed during installation after joint mating and do not present a hazard to the O-ring seals.

Aft Field Joint

Rust was found on the outer clevis leg from 357 to 0 to 60 deg from the aft edge of the chamfer to 0.375 in. aft of the chamfer. There was also rust on the forward face of the outer clevis leg from 358 to 0 to 5 deg. There did not appear to be any grease in these areas. Other areas had heavy grease. Pieces of lint, thread, and hair were found in the joint at several locations. However, it has been determined that there was no lint, thread, or hair on the sealing surface at the time of assembly.

Eighteen metal slivers were found at the pinholes. A 0.5 in. long piece of instrumentation wire was also found on the outer tang between the pinholes and tang end at 208 deg. Typical burnish marks were around the full cicumference on the inside of the inner clevis leg.

Table 7.7-2. Criteria for Classifying Potential Anomalies

Remains Observation	Anomaly		
	Minor	Major	Critical
• Requires no specific action	• Requires corrective action, but has no impact on: —Motor performance —Program schedule • Does not reduce usability of part for its intended function • Could cause damage preventing reuse of hardware in combination with other anomaly • Significant departure from the historical data base	• Could cause failure in combination with other anomaly • Could cause damage preventing reuse of hardware • Program acceptance of cause, corrective action, and risk assessment required before subsequent static test/flight	• Violates CEI spec requirements • Could cause failure and possible loss of mission/life • Mandatory resolution before subsequent static test/flight

Note: This criteria is to be applied to the specific observed potential anomaly as it relates to the observed article and as it relates to subsequent articles.

Center Field Joint

Rust was observed on the end and inner ramp on the inner clevis leg from 4 to 38 deg and 46 to 51 deg. Rust was transferred to the V-2 filler and wiped onto the capture feature O-ring in the 8 to 10 and 14 to 32 deg ranges on disassembly. Heavy grease was found in some areas and a hair was found on the aft side of the primary O-ring.

There were 16 metal slivers found on the joint, all from the pinholes. Again, burnish marks were seen on the inside of the inner clevis leg. From 110 to 119 deg, the marks were very light to nonexistent. Around the rest of the circumference the burnish marks were typical.

The leak check port at 135 deg was clear; however, the V-2 filler from 91 to 99 deg was twisted 90 deg outward. There was no deformation of the V-2 filler, indicating that it was twisted on disassembly.

Forward Field Joint

Milky-looking grease caused by moisture in the joint was observed in the clevis from the forward side of the pinholes to the bottom on the clevis, from 352 to 0 to 7 deg. Light rust was found between the 354- and 356-deg pinholes.

Hair and lint ranging from 0.125 in. to 1.0 in. in length were found in the joint area at three different locations on the clevis and at seven locations on the tang. Two of the hairs were determined to have been deposited after disassembly.

Excess grease was found on the metal surface of the joint clevis in four locations. There were eight metal slivers found on the joint, all believed to have come from the pinholes. Burnish marks were again seen on the inside of the inner clevis leg where it has interference with the capture feature leg. A piece of rubber material was found in the hole at 224 deg.

The grease on the tang was nominal and the leak check port at 135 deg was not blocked by the V-2 filler. The V-2 filler was in place, not twisted or out of position.

7.7.4.2 Factory Joints. For factory joint evaluation, see TWR-18135, Rev A, Section 5.1.

7.7.4.3 Nozzle-to-Case Joint

Fixed Housing

There was a blowhole through the polysulfide to the wiper O-ring at 46.8 deg (Figure 7.7-2). Black, greasy material extended from 0 to 63 deg. At 28.8 and 36 deg, this black material was on the aft side of the wiper. The material was not dispersed as it would have been if gas blew past the O-ring, and there was no heat effect to the O-ring. Two vent slots were directly in line with the two spots of material that were found on the aft side of the O-ring. It was determined that the greasy material squeezed through the slots at disassembly. The polysulfide was dark brown against the wiper O-ring and in the voids forward of the wiper O-ring from 63 through 180 to 0 deg. This area was wiped with a lint-free cloth to check for contamination, but nothing was removed.

A jagged cut on the secondary O-ring at 20 deg was found by the O-ring inspection team (Figure 7.7-3). It is at an angle of 45 deg measuring approximately 0.05 in. long by 0.01 in. deep. The cause of this cut is unknown, but suspected to be handling damage. This was concluded because the cut was at an angle of 45 deg and there was no raised metal in the O-ring groove or sealing surfaces.

Twenty-one gouges were found in the wiper O-ring while it was resting in the groove during the groove inspection (Figure 7.7-4). It has been determined that these gouges were caused at disassembly by the radial bolt holes located from 131.4 to 217.8 deg. Some of the gouges were still connected to the O-ring with the open slot pointing aft. Most of the severed chips were found on the polysulfide, indicating that this happened at disassembly. Another reason to substantiate this conclusion is that radial bolt hole plugs were used during the nozzle-to-case joint assembly.

A0131194a-2

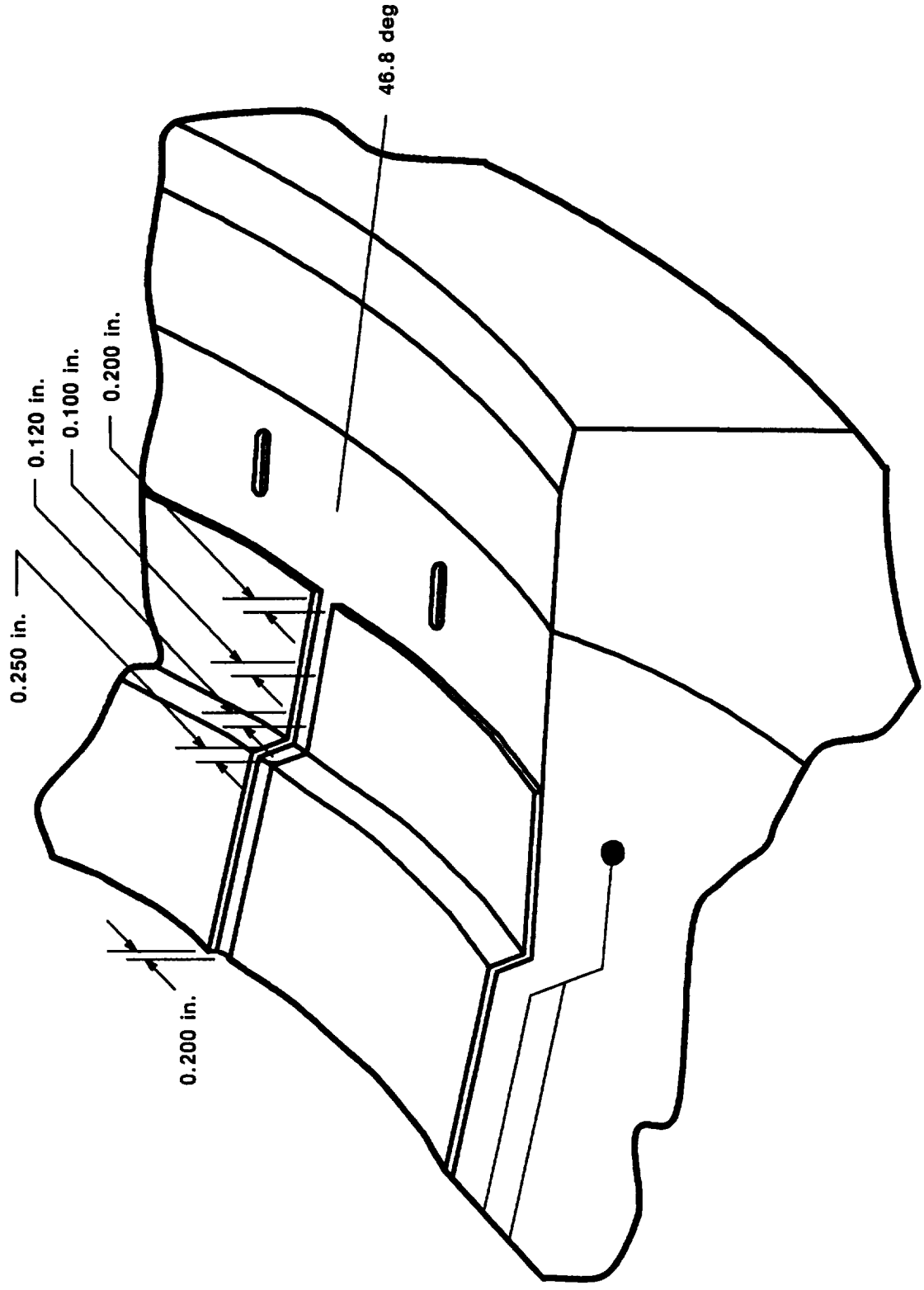

Figure 7.7-2. Nozzle-to-Case Joint Gas Path to Wiper O-ring

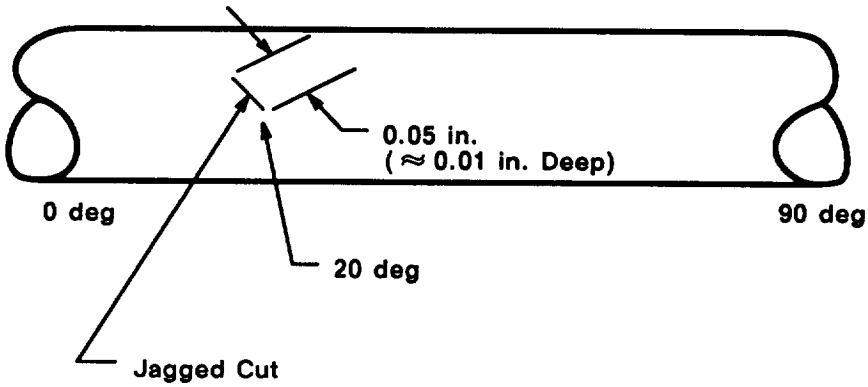

Figure 7.7-3. DM-9 Nozzle-to-Case Joint Secondary O-ring

A014316a

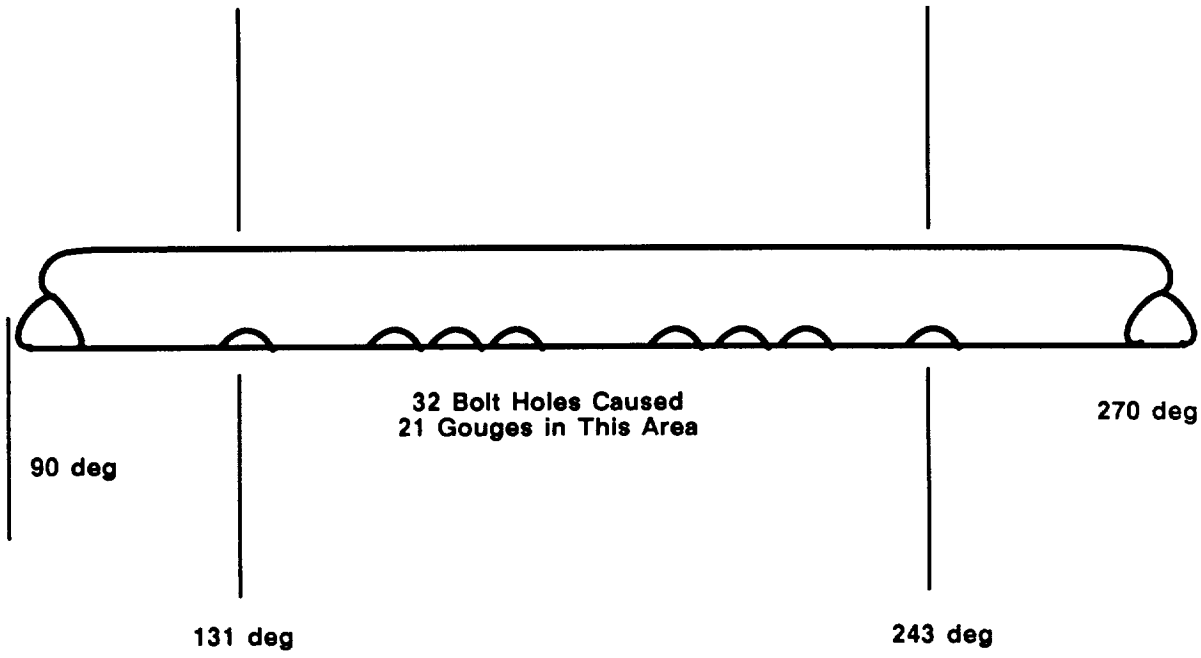

Figure 7.7-4. DM-9 Nozzle-to-Case Joint Wiper O-ring

A014317a

Aft Dome

One of the wiper O-ring chips was found in the aft side of the 149.4-deg radial bolt hole.

Excess globs of grease were found in five radial bolt holes from 30.4 to 48.4 deg. Excess grease was also found on the O-rings, believed to be due to the cold temperatures encountered during O-ring greasing at assembly. The temperature at the casting pits was approximately 40°F. At these temperatures, the grease becomes thick and sticky, making it difficult to get the proper coverage on the O-ring.

7.7.4.4 Internal Nozzle

Aft Exit Cone Field Joint (Joint No. 1)

Disassembly inspection showed that the seal components performed as expected. It is believed that gas reached the primary O-ring at 332 deg, where an unfilled area was found through the RTV backfill. No damage was found by the O-ring inspection team to either the primary, or secondary O-rings. Soot traveled on the phenolic to approximately 0.25-in. from the primary O-ring, with no signs of soot or heat on the primary O-ring or in the O-ring groove. In the blowhole region, there was no RTV present on either the forward or aft exit cones, indicating that the primary O-ring was pressurized.

RTV-to-primary RTV was pushed up against the primary O-ring around the full 360-deg circumference, except for approximately 2 in. at the 332-deg location, from 358 deg through 0 to 71 deg, and from 180 to 195 deg. This condition is expected and acceptable.

Heavy grease was observed on the secondary O-ring over the full 360 deg, except for the O-ring surface which was in contact with the forward exit cone sealing surface. A 2- to 4-mil thickness was estimated. A bead of grease ran from 64 through 0 deg to 41 deg on the outer edge of the secondary O-ring sealing surface on the forward exit cone. It was approximately 0.04 in. high by 0.03 in. wide at the base, and

came to a peak at the top. At 56 deg, grease pushed up past the vertical primary sealing surface face to within 0.1 in. of the inner side of the ramp on the forward exit cone. The grease was pushed just to the RTV. This is in the region where the RTV was not pushed up against the primary O-ring.

Forward End Ring-to-Nose Inlet Housing (Joint No. 2)

During assembly of this joint, EA 913 adhesive is used to bond the cowl to the cowl housing. This adhesive, along with RTV, is squeezed into the RTV bondline. Because the adhesive mixed with the RTV, pressure and soot reached the primary O-ring shortly after ignition. This condition is caused by the lack of bondline strength between the RTV and EA 913. Medium accumulation of soot was found at locations of 30 to 37, 186 to 204, and 276 to 282 deg. A large concentration of soot was found on the upstream side of the primary O-ring groove between 12 and 30 deg. No soot was observed downstream of the primary sealing surfaces. Light deposits of soot were found in scallop-shaped patterns between bolt holes in the circumferential direction around the entire circumference of the joint. These patterns generally extended approximately half-way between the primary seal and the inner OD of the RTV bondline except as noted previously. DM-8 showed very similar results in the amount and shape of these soot patterns. No damage was found on the primary or secondary O-rings at disassembly or by the O-ring inspection team. Sealing surfaces showed no signs of heat effects, corrosion, or disassembly damage. There was excessive buildup of grease downstream of the primary O-ring.

Nose Inlet Housing-to-Throat Support Housing (Joint No. 3)

A triangular void area in the RTV was found at 90 deg which allowed pressure to reach the primary O-ring at some time during the static test (Figure 7.7-5). The void area was not exposed to pressure until the char line degraded the strength of the RTV at the opening of the void. This decrease in strength allowed pressure to produce a cohesive failure in the RTV at the opening of the void. The base of the void was 1.0 in. wide, whereas the opening of the void was 0.16 in. wide. Excessive grease was found between the primary and secondary seals; also, a grease bead was

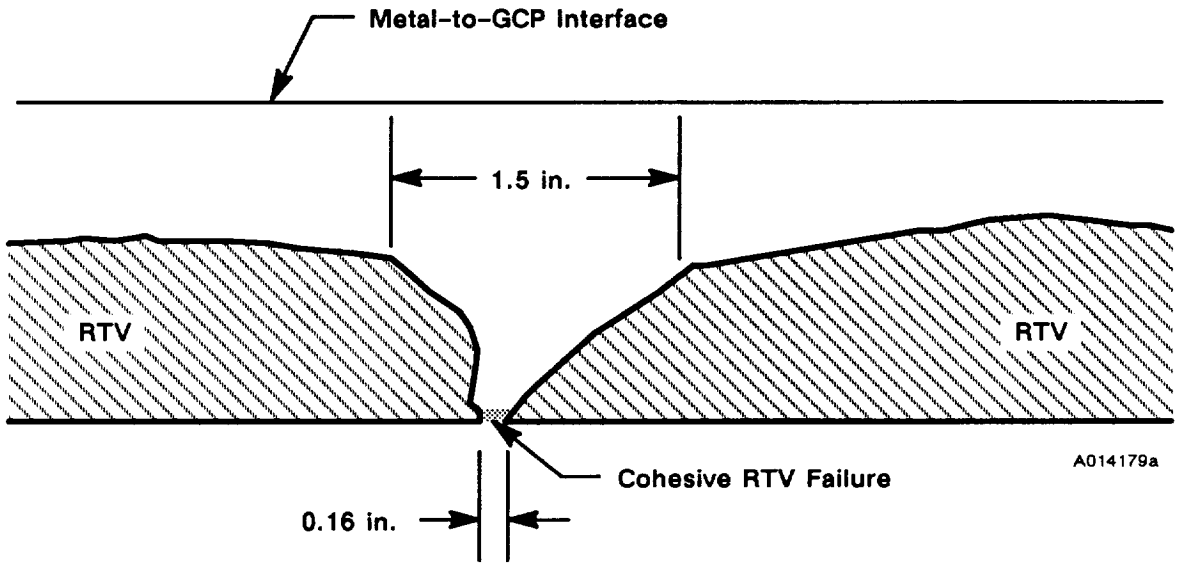

Figure 7.7-5. Void in RTV at Nose Inlet-to-Throat Support Housing Joint

formed at the metal-to-glass cloth phenolic interface. No damage to the primary or secondary O-rings was found by the inspection team. The sealing surface on the aft end of the nose inlet housing showed raised metal between 258 and 264 deg. The raised metal measured 0.050 in. wide by 0.001 to 0.005 in. high. The cause of this raised metal is under investigation.

Forward Exit Cone-to-Throat Support Housing (Joint No. 4)

There were two areas where pressure reached the primary seal at some point during the test firing. The first was a triangular void in the RTV, located between 133 and 147 deg with the center of the void located at 137.5 deg (Figure 7.7-6). The opening of this void was located at the bevel of the CCP on the forward end of the forward exit cone with a width of 0.40 inches. The base of the void measured approximately 4.5 in. in circumferential length. The second area was a triangular void in the RTV (Figure 7.7-7), located between 329 and 337.5 deg with the center of the void at 333 deg. The opening of the void was similar to the first void, located at the bevel of the CCP on the forward end of the forward exit cone with a width of 0.38 inches. The base of the void measured approximately 5.9 in. in circumferential length.

Both of the RTV voids appeared to have been caused by grease being hydraulically forced into the RTV bondline area during joint assembly. No damage to the primary or secondary O-rings was found on by the inspection team. No rust or disassembly damage was apparent to the sealing surfaces. Excessive grease buildup greater than a 4-mil thickness was evident around the entire circumference of the joint sealing surfaces.

Fixed Housing-to-Aft End Ring (Joint No. 5)

RTV completely filled the bondline between the bearing protector and inner boot ring. Thus, no voids were observed in the RTV. RTV reached the high-pressure side of the primary O-ring at 40 to 112, 150 to 170, 220 to 250, 260 to 270, 275 to 318, and 350 to 355 deg. Sealant did not extrude past the O-ring. There was no noted O-ring damage seen at the time of disassembly; however, the O-ring inspection team found a series of

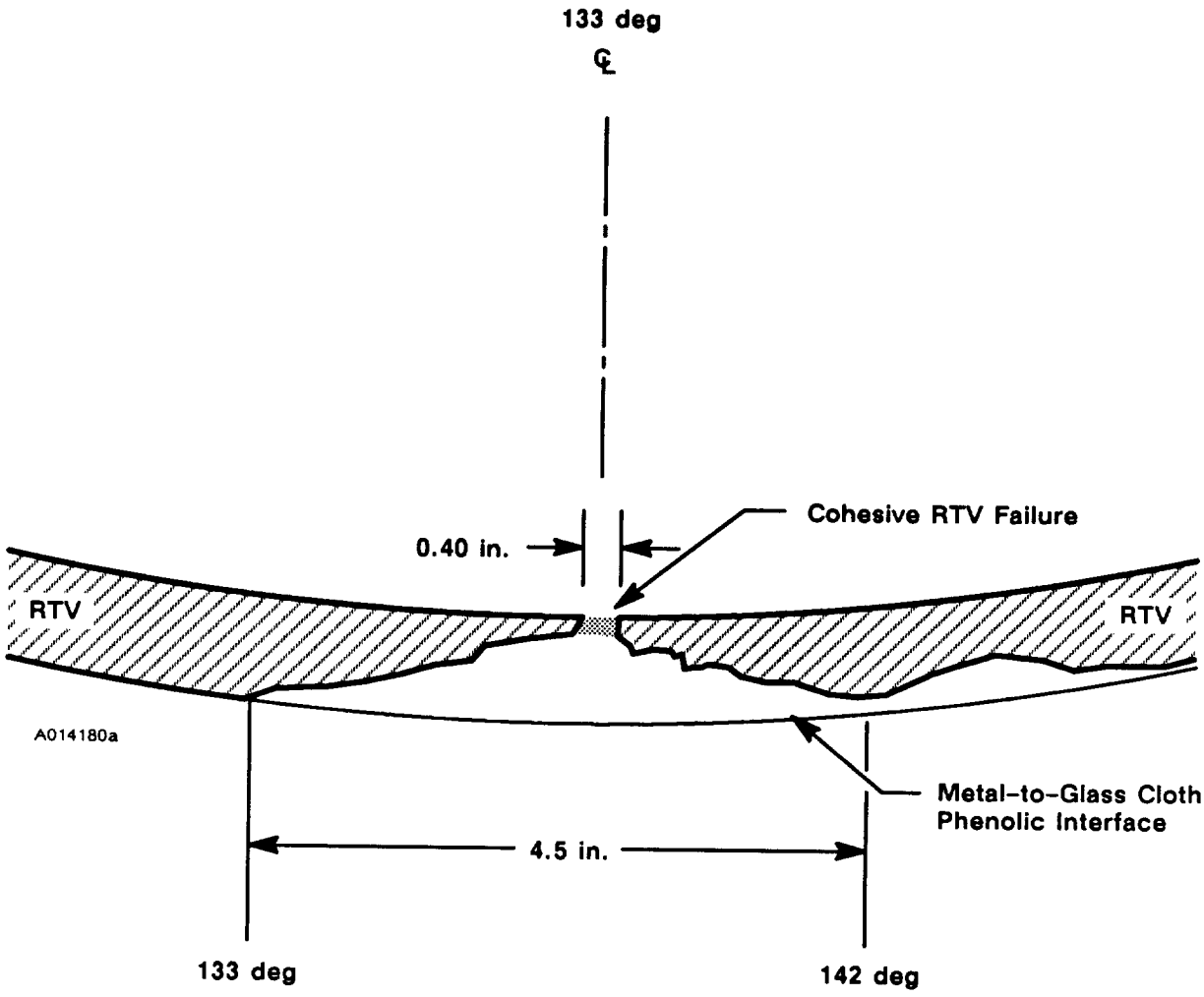

Figure 7.7-6. Void in RTV at Forward Exit Cone-to-Throat Support Housing Joint

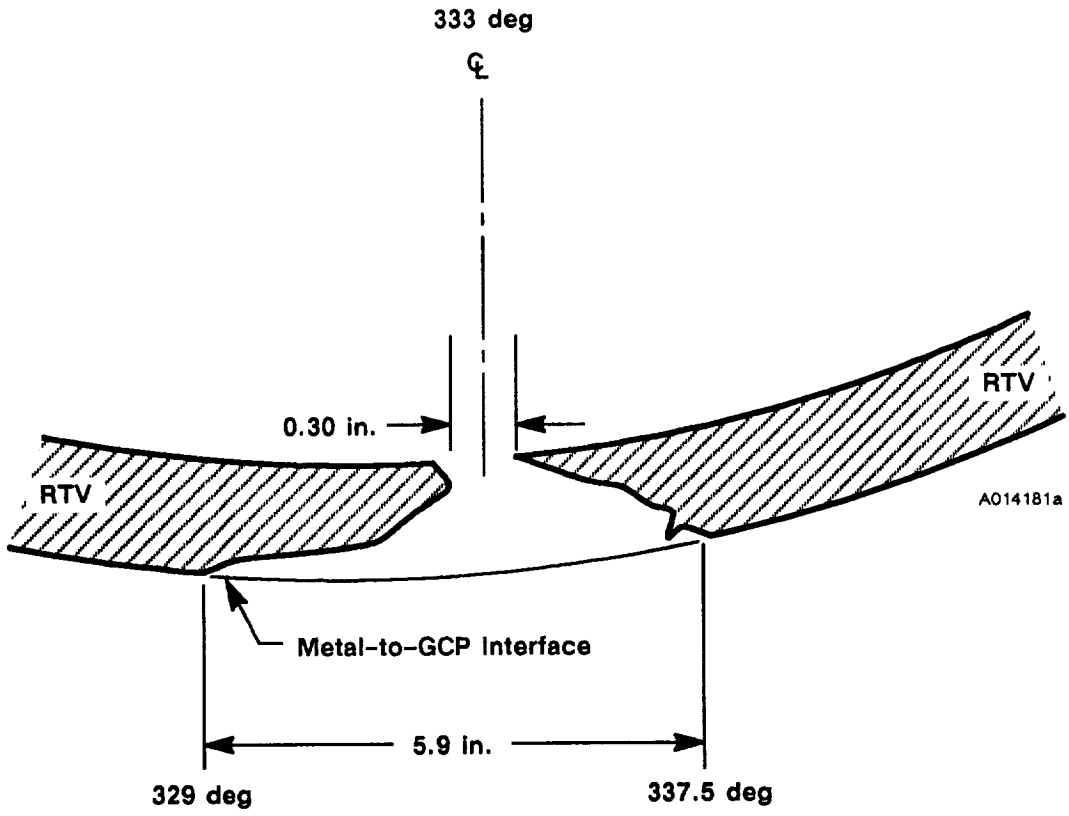

Figure 7.7-7. Void in RTV at Forward Exit Cone-to-Throat Support Housing Joint

diagonal abrasion marks (12 each) with a maximum length of 0.050 in. and maximum depth of 0.001 to 0.002 inches (Figure 7.7-8). These were found at 218 through 227 deg. It was determined that they were caused by disassembly.

Areas of vivid fluorescent green grease were observed downstream of the secondary O-ring between 355 and 0 deg. Excess grease, greater than 0.004 in. thick, was evident throughout the entire joint sealing surfaces.

7.7.4.5 Igniter Joints. Inner and S&A gaskets performed as expected, with no signs of heat effect, erosion, or sooting past the primary seals. A depression was found on the crown of the primary seal of the igniter gaskets. All sealing surfaces were free of soot.

S&A Joint (Adapter-to-B-B)

No soot was found on either side of the retainer of the S&A gasket. However, the gasket and sealing surfaces were cleaned by on-line personnel prior to the engineering inspection.

Outer Joint (Adapter-to-Forward Dome)

A blowhole of approximately 3 in. long and 0.5 in. wide was found in the putty of the igniter case exterior at the 335-deg location. There was no soot on the forward face of the outer seal, but during a thorough visual inspection a depression was found on the crown of the primary seal at the 144-deg location (Figure 7.7-9). It was concluded that this depression was due to a manufacturing defect. Laboratory analysis (Thiokol analysis) showed that there was residue of nitrile rubber particles embedded in the depression area. It is suspected that the nitrile material entered the fluorocarbon material at the time of mixing.

Sooting of approximately 0.5 in. wide, and 4 in. long was found at the 51-deg location on the retainer of the aft face of the outer seal (Figure 7.7-10).

Inner Joint (Adapter-to-Chamber)

A blowhole of approximately 1 in. wide was found in the putty of the igniter case

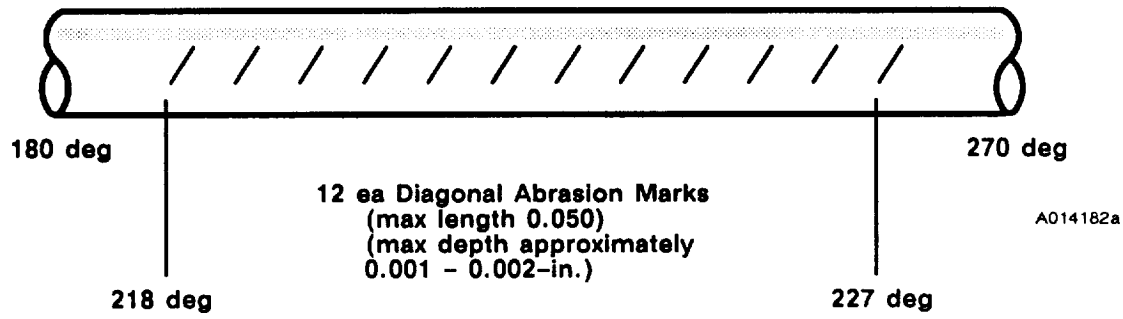

Figure 7.7-8. DM-9 Fixed Housing-to-Aft End Ring, O-ring

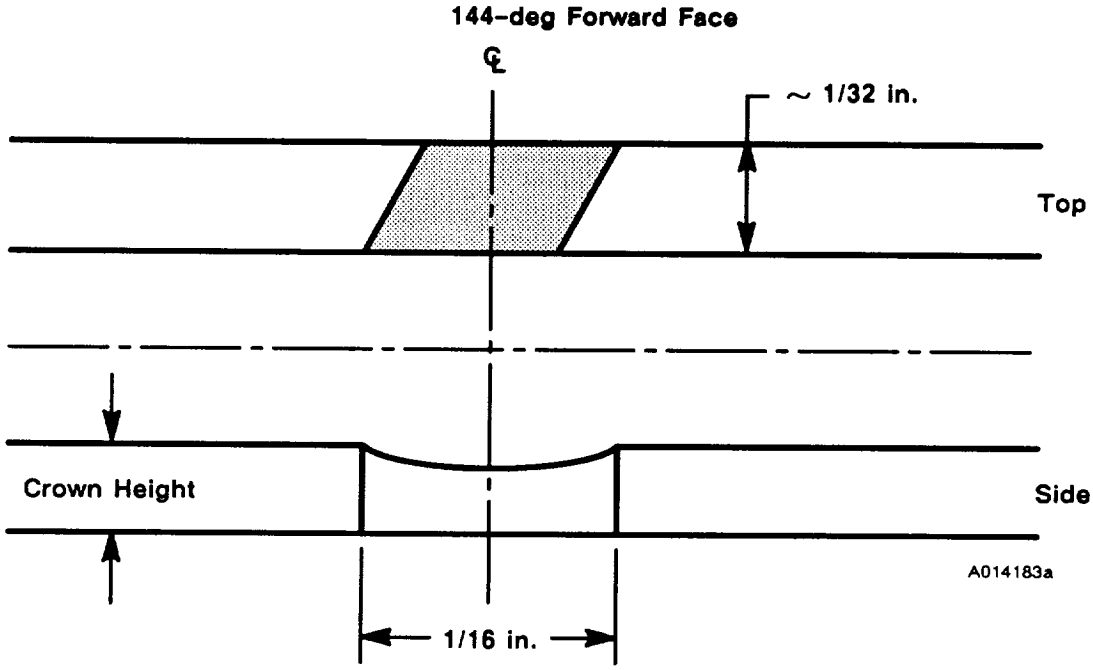

Figure 7.7-9. DM-9 Igniter Outer Gasket Primary Seal Crown

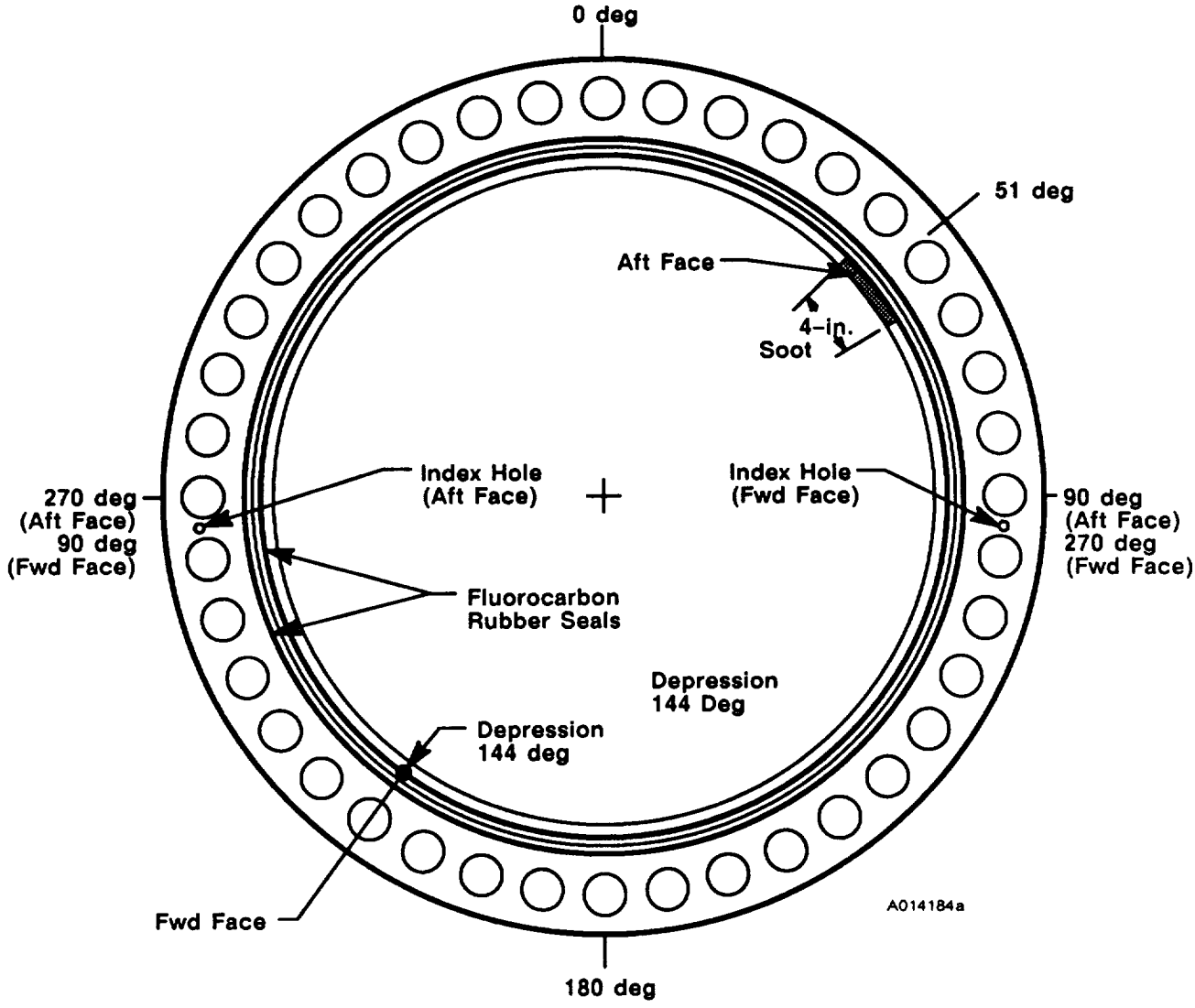

Figure 7.7-10. DM-9 Igniter Outer Gasket

interior at the 240-deg location, and soot was found on the inner edge of the forward face of the inner seal from 75 to 210 deg. No soot was found on the aft face of the inner seal.

7.7.4.6 Seals Component Program Team Recommendations. The Seals Component Program Team has reviewed all observations presented in this document and has determined that the following observations are potential anomalies, classified as critical, major, minor, or observation, as defined under Table 7.7-2 criteria.

Critical Anomalies:	None
Major Anomalies:	The depression found on the crown of the primary seal at 144 deg of the igniter gasket.
Minor Anomalies:	None
Observations:	A void at 332 deg was observed through the RTV backfill on the aft exit cone. Soot traveled on the phenolic to approximately 0.25 in. from the primary O-ring, with no signs of soot or heat on the primary O-ring or in the O-ring groove. In the blowhole region, there was no RTV present on either the forward or aft exit cones, indicating that the primary O-ring was pressurized. There was a blowhole through the polysulfide to the wiper O-ring at 46.8 deg on the nozzle-to-case joint. No blowby, erosion, or heat effects occurred to the wiper O-ring (Section 7.7.4). A jagged cut was found on the secondary O-ring of the nozzle-to-case joint at 20 deg. The cut was oriented with an angle of 45 deg and measured approximately 0.05 in. long by 0.01 in. deep. The cause of this cut is unknown, but is suspected to be handling damage. This was concluded from the nature of the cut on the face seal secondary O-ring. Joint contamination (lint and hair) was found on all three field joints. Four of the five internal\

nozzle primary seals (except Joint No. 5) saw pressure; but no erosion, heat-affected damage, or blowby occurred.

Considering that the anomaly on the primary seal of the outer igniter gasket and these case and seals observations were the most significant findings, DM-9 represents the second successful assembly and firing of a full-scale capture feature RSRM in a horizontal configuration.

7.8 IGNITER

7.8.1 Introduction

The DM-9 ignition system was the RSRM forward-mounted solid rocket-type igniter configuration modified with a CO_2 quench port. DM-9 was the first full-scale motor test of the modified ignition system. The differences in the modified igniter over the previous igniter is summarized in Table 7.8-1. Figure 7.8-1 illustrates the ignition system as it was actually assembled. The igniter was lined and cast with HARM lining/casting equipment and cast on 11 Nov 1987 from propellant mix E990005. The ignition system consisted of the following subassemblies:

a. The single nozzle, steel-chambered, internally and externally insulated, solid propellant igniter contained a case-bonded 40-point star grain. The igniter contained approximately 134 lb of TP-H1178 propellant (including 1.4 lb of propellant in the initiator). The predicted and actual igniter performance receives further discussion in Section 7.1 (Ballistics).

b. The HPM igniter adapter which provides the mounting point between the ignition system components, the motor forward segment dome, and the CO_2 quench port.

c. The headend CO_2 quench injector system which was identical to all those incorporated on previous development and qualification test motors. The system was mounted on the igniter and, when actuated, approximately 46,500 lb of liquid CO_2 was injected through the igniter adapter, out through the igniter nozzle, and into the SRM chamber.

Table 7.8-1. Major Differences in Previous Igniter Versus Modified Igniter Design

PREVIOUS IGNITER		MODIFIED IGNITER		REASON
Stepped I.D. installation		Tapered I.D. installation		Ease of Manufacturing/Inspection
STW4-2847	Putty, Vacuum Seal (Randolph)	STW4-3266	Putty and Caulking Or Glazing Compounds, Other (Inmont)	STW4-2847 Putty no longer available
STW5-2676	Liner, UF-2137, Solid Rocket Motor, Space Shuttle Project	STW5-3224	Liner, Solid Rocket Motor, Space Shuttle Project	STW5-2676 Putty no longer available
	. . .	Added metal to Igniter Chamber		Allows a positive margin of safety to the Nozzle Insert

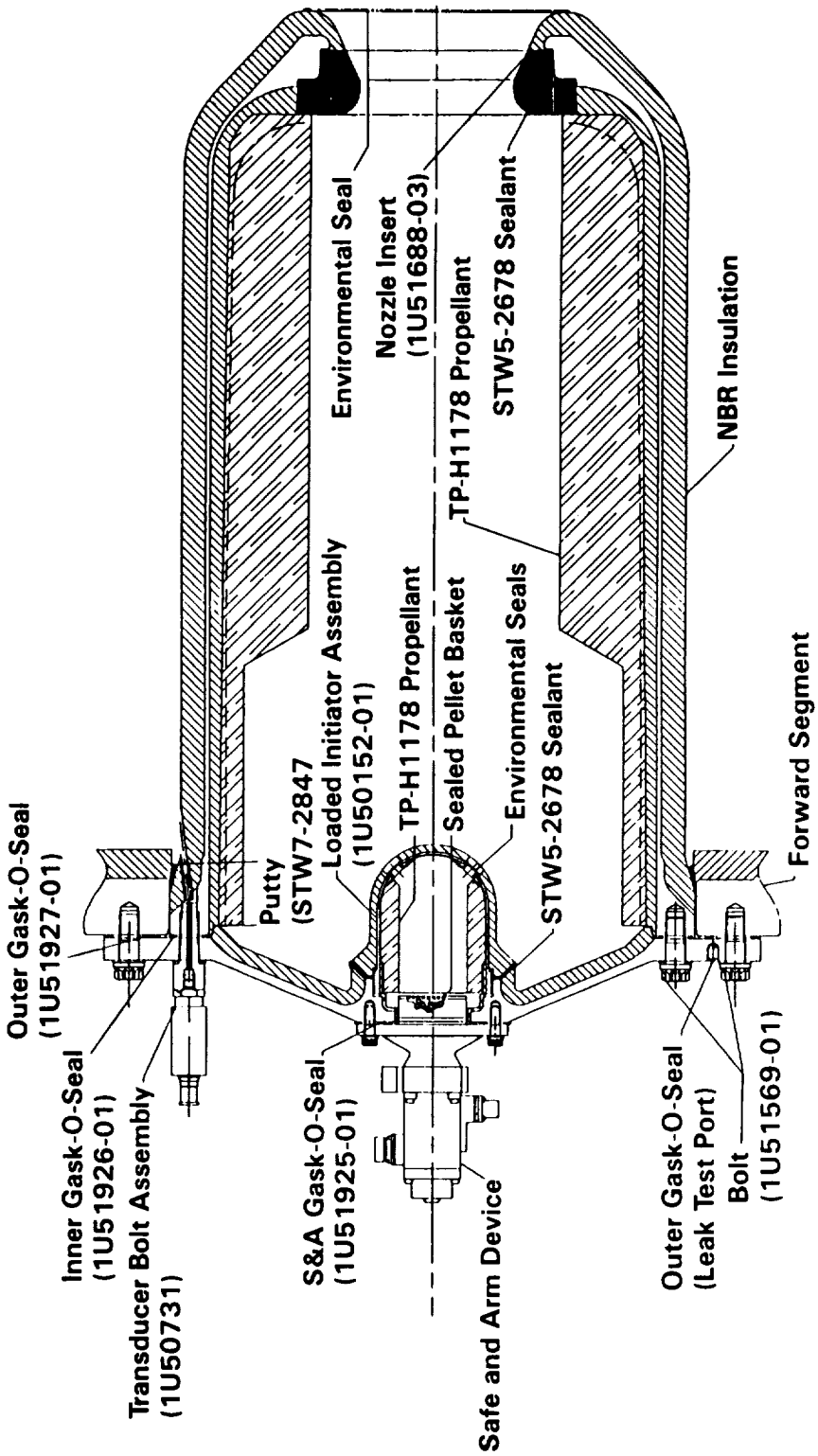

Figure 7.8-1. DM-9 Ignition System Configuration

d. The HPM S&A device shown in Figure 7.8-2 included the following major components:

   1. An electromechanical arm monitor assembly containing an electric motor, geartrain, manual safing and locking mechanism, visual position indicator, and electrical circuit switch decks.
   2. A refurbished B-B assembly containing the motor pressure seal, safety barrier, pyrotechnic booster charge, and electrical position indication switches. The B-B assembly used on the SRM static firings incorporates two of the latest SRM ignition initiators (SII) provided by NASA. The SIIs have a redundant seal design which requires a modified, wide flange. A 0.005-in. thick washer welded to the flange extends the effective sealing area and a backup ring adds structural support. The primary seal was the standard O-ring at the top of the initiator threads and the secondary seal was an O-ring under the widened flange. As in previous B-Bs, these redundant seals are 100 percent leak tested.

e. The igniter initiator, which has the HPM small, multinozzle steel-chambered, lined, externally insulated, solid propellant igniter with a 30-point star grain (Figure 7.8-3).

f. The vacuum putty used in the igniter adapter-to-chamber joint and the igniter-to-forward segment joint was manufactured by Inmont Corporation.

There was no deviation from the SRM assembly procedure.

Discrepancies, detected by Quality Control and dispositioned on discrepancy reports (DR), were all minor. Several DRs were written on the igniter chamber, igniter initiator, and adapter. Most of the other DRs involved raw materials in the insulation, propellant, sealants, and adhesives. In all instances the problems were resolved before the materials were used in the igniter assembly.

7.8.2 Objectives

A qualification test objective from Section 2 with regard to igniter performance was:

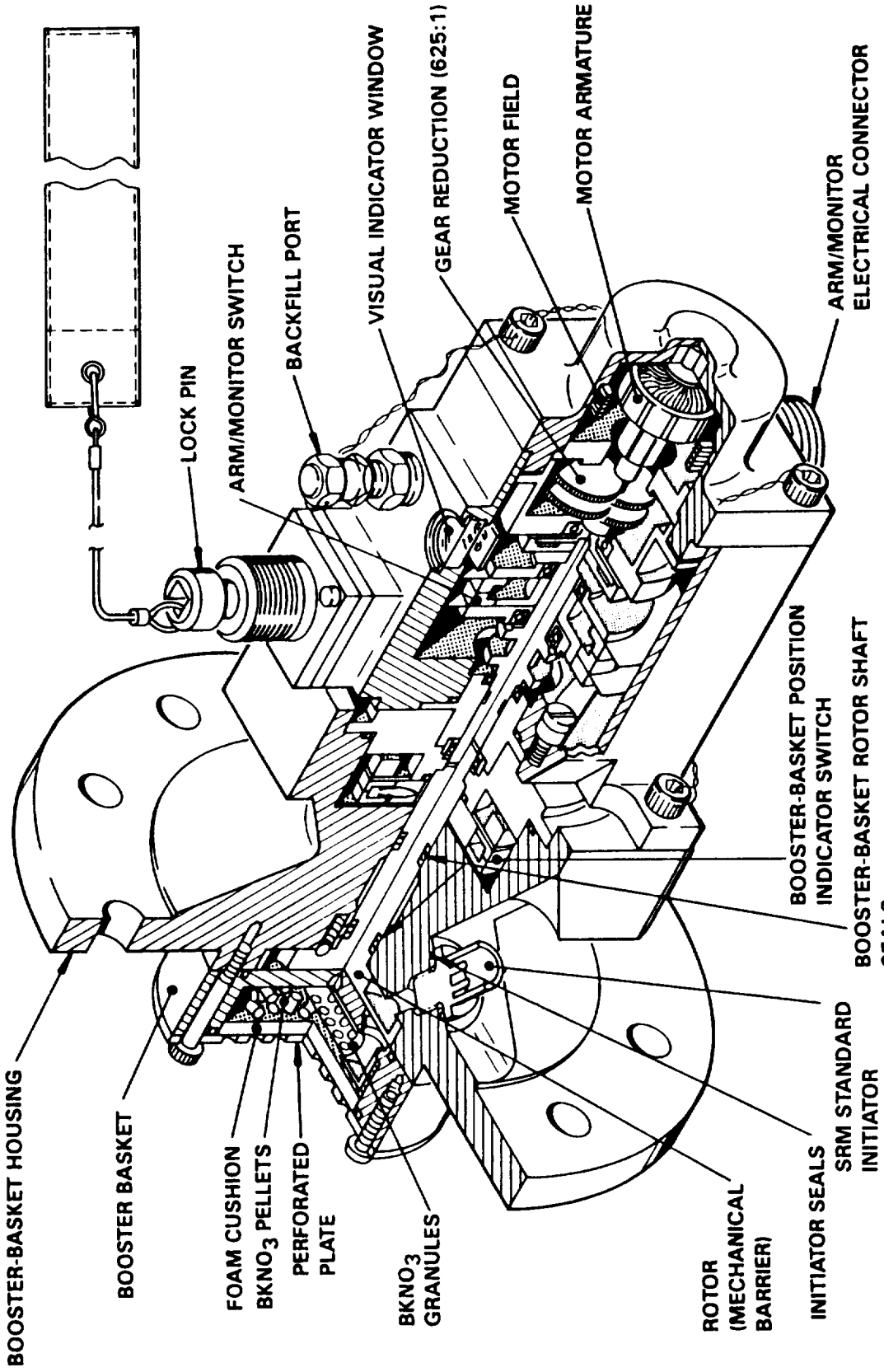

Figure 7.8-2. DM-9 S&A Device Configuration

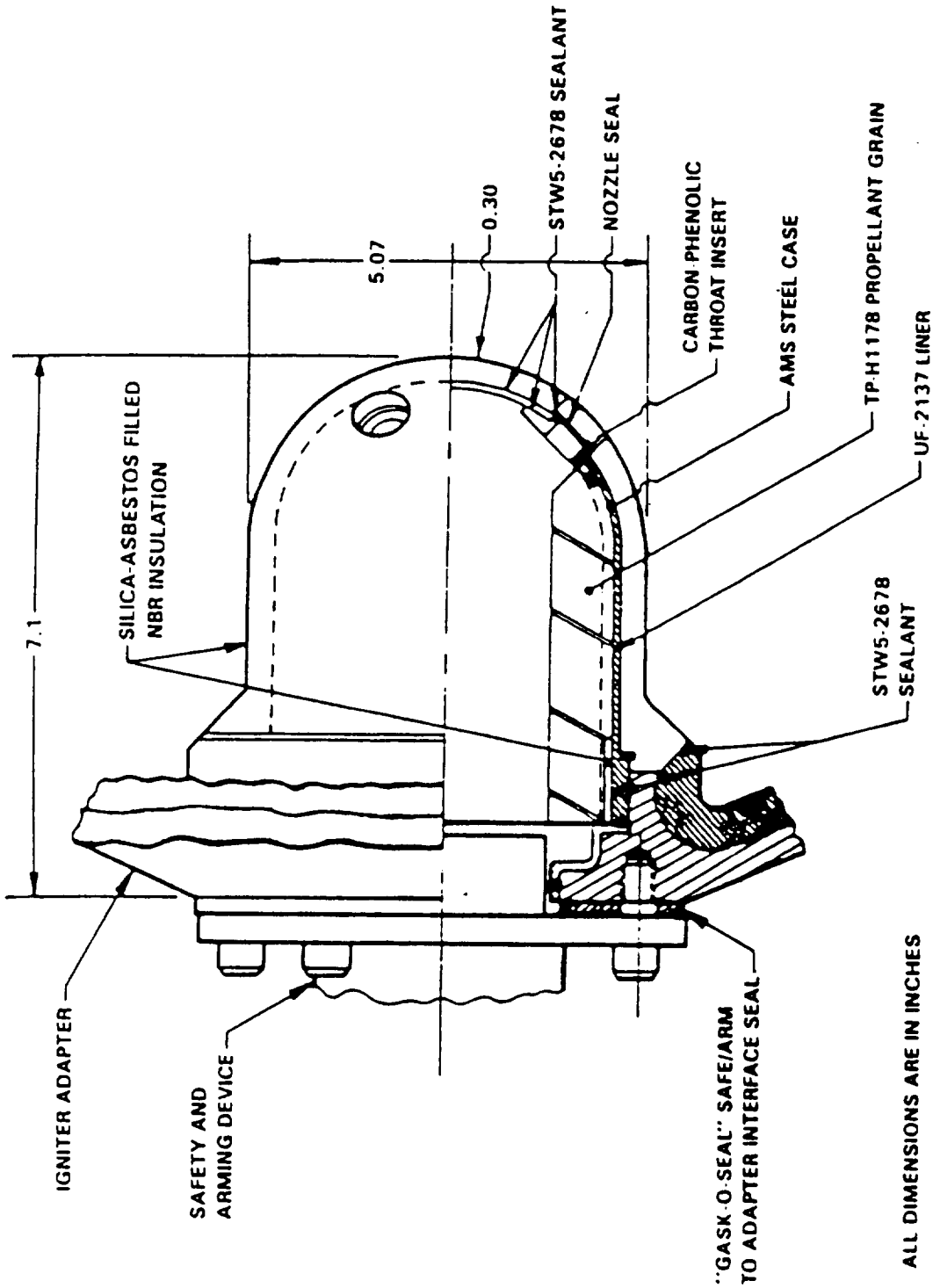

Figure 7.8-3. Igniter Initiator

AI Certify that the ignition system precludes the leakage of hot gas during and subsequent to motor ignition.

The DM-9 igniter is one of the igniters involved in the qualification of the modified ignition as specified in CTP-0011.

7.8.3 Conclusion/Recommendations

The general condition of the ignition system and CO_2 injector was good. All of the igniter hardware performed in a satisfactory manner and performance was within specification limits. The refurbishable hardware, i.e., igniter chamber, adapter gaskets, and the S&A device were adequately protected from heat damage. There was no evidence of hot gas leakage through any of the seals. The nozzle insert performed its function in a satisfactory manner. The B-B assembly experienced no anomalies in the motor firing and thus demonstrated its reuse capability.

7.8.4 Results/Discussion

7.8.4.1 Ballistics and Propellant. The ignition interval was 0.243 sec. The rate of pressure buildup was 81 psi for 10 ms. The mass flow rate of the DM-9 igniter was 337.4 lbm/sec and the maximum pressure (pmax) was 1,885 psi at a PMBT of 65°F. The motor ignition transient and propellant discussions are covered in Section 7.1 (Ballistics).

7.8.4.2 Igniter. The igniter showed no signs of any separations, joint failures, loss of parts, or any other anomalies resulting from the long exposure to the motor combustion products. There were no externally visible hot spots. The three main SRM pressure transducers (P001, P002, and P003) and the igniter pressure transducer (P005) were removed after the firing while the motor was still in the test bay. Post-test inspection revealed that P003 was loose, as discussed in Section 5.4, and no anomalies were evident for the remaining gages. The special bolts exhibited no discoloration on either the heads or the O-ring grooves. Figures 7.8-4 and 7.8-5 show external views of the igniter after removal from the forward segment.

N101478-8

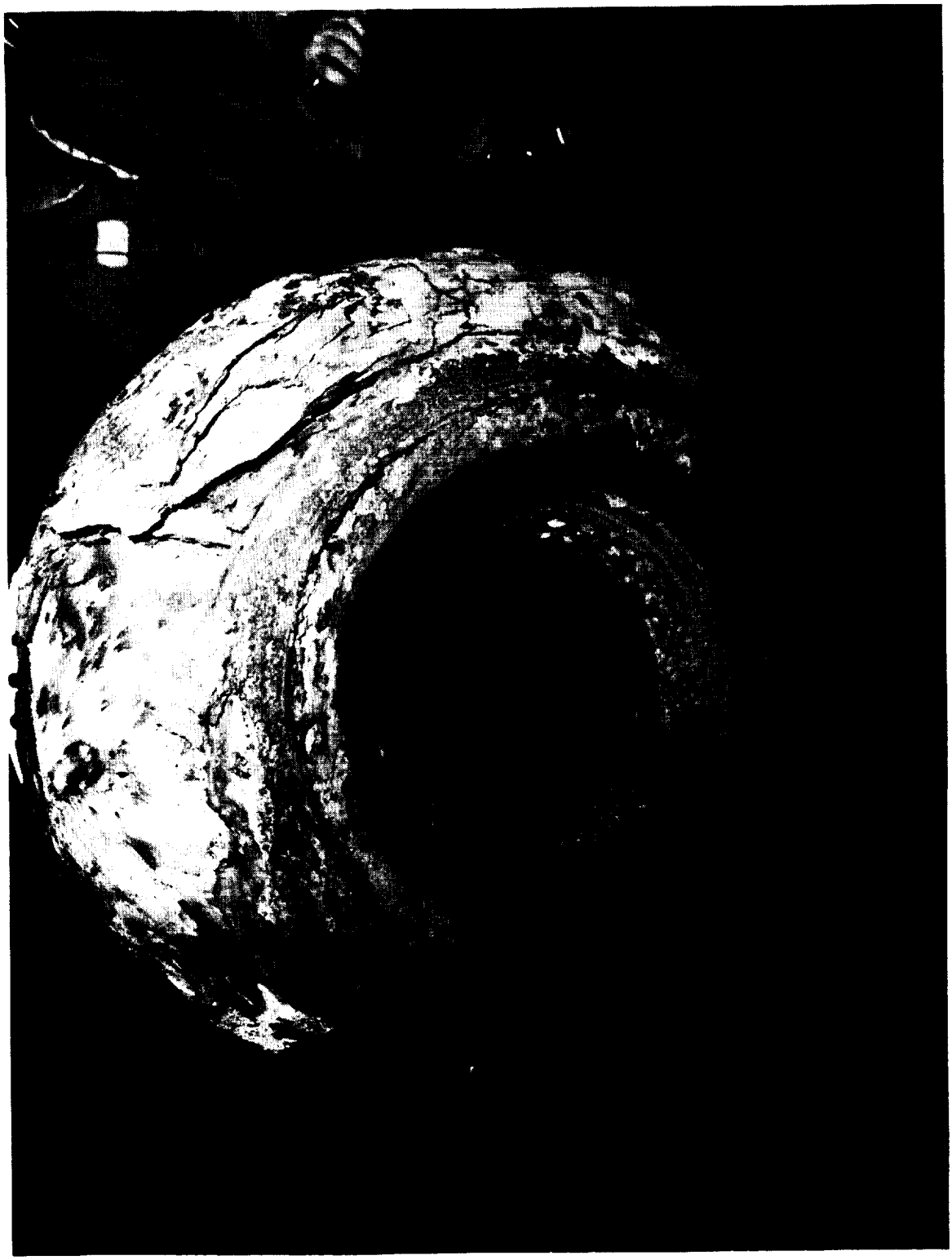

Figure 7.8-4. View of Igniter From Insert End

ORIGINAL PAGE
BLACK AND WHITE PHOTOGRAPH

N101478-7

Figure 7.8-5. DM-9 Side View of Igniter

7.8.4.3 Metal Parts. The refurbished adapter and chamber survived the firing without overheating. Combustion products were deposited on the chamber forward metal surface and on the ID of the outer gasket. The combustion products passed through the vacuum putty in the igniter-to-forward segment joint. There was evidence of combustion products passing through the vacuum putty in the igniter adapter-to-chamber joint. The only metal part that showed a sign of heating was the output end of the pyrotechnic bracket on the B-B assembly. The condition is seen on all fired B-B assemblies and is not considered a problem since the basket assembly is used only once and then discarded. Being in a protected stagnant area, this part was expected to receive some heating and a deposit of combustion products.

7.8.4.4 Seals. All seals are examined during the igniter and S&A disassembly. These included:

- O-rings on the SII surfaces and on special bolts
- Gasket between motor and igniter
- S&A and igniter
- Gasket between igniter chamber and adapter
- Igniter chamber-to-adapter
- Packing with retainer under the igniter bolt heads

All seals functioned normally. There was a deposit of combustion products on the edge of the metal retainer of the outer gasket where gas bypassed the vacuum putty at the joint (Figure 7.8-6); however, the primary seals held so that there were no deposits of combustion products between the seals (Figure 7.8-7). The chamber and adapter exhibited no indication of overheating, and there were no deposits of combustion products between the seals. The rubber seals on the DM-9 gaskets showed no evidence of overheating. There was a gas path in the adapter-to-chamber putty (Figure 7.8-8). Combustion products were deposited on the inside edge (adapter side only) of the inner gasket metal retainer (Figure 7.8-9). This anomaly has been seen on previous motor tests and has never resulted in damage to the rubber seals. No erosion or blowby of the primary seal was observed.

N101478-11

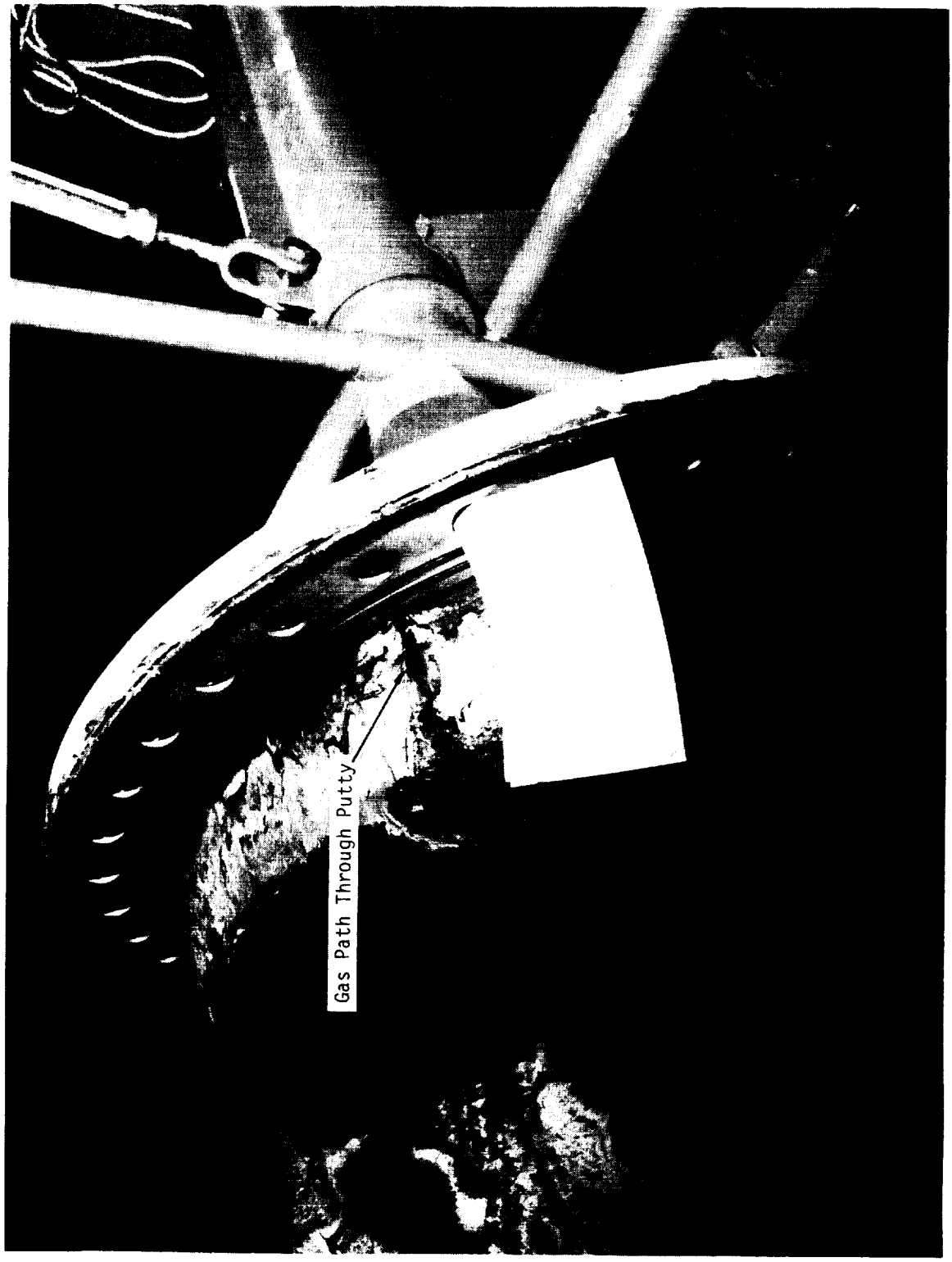

Figure 7.8-6. DM-9 Igniter-to-Forward Dome Joint

N101749-1

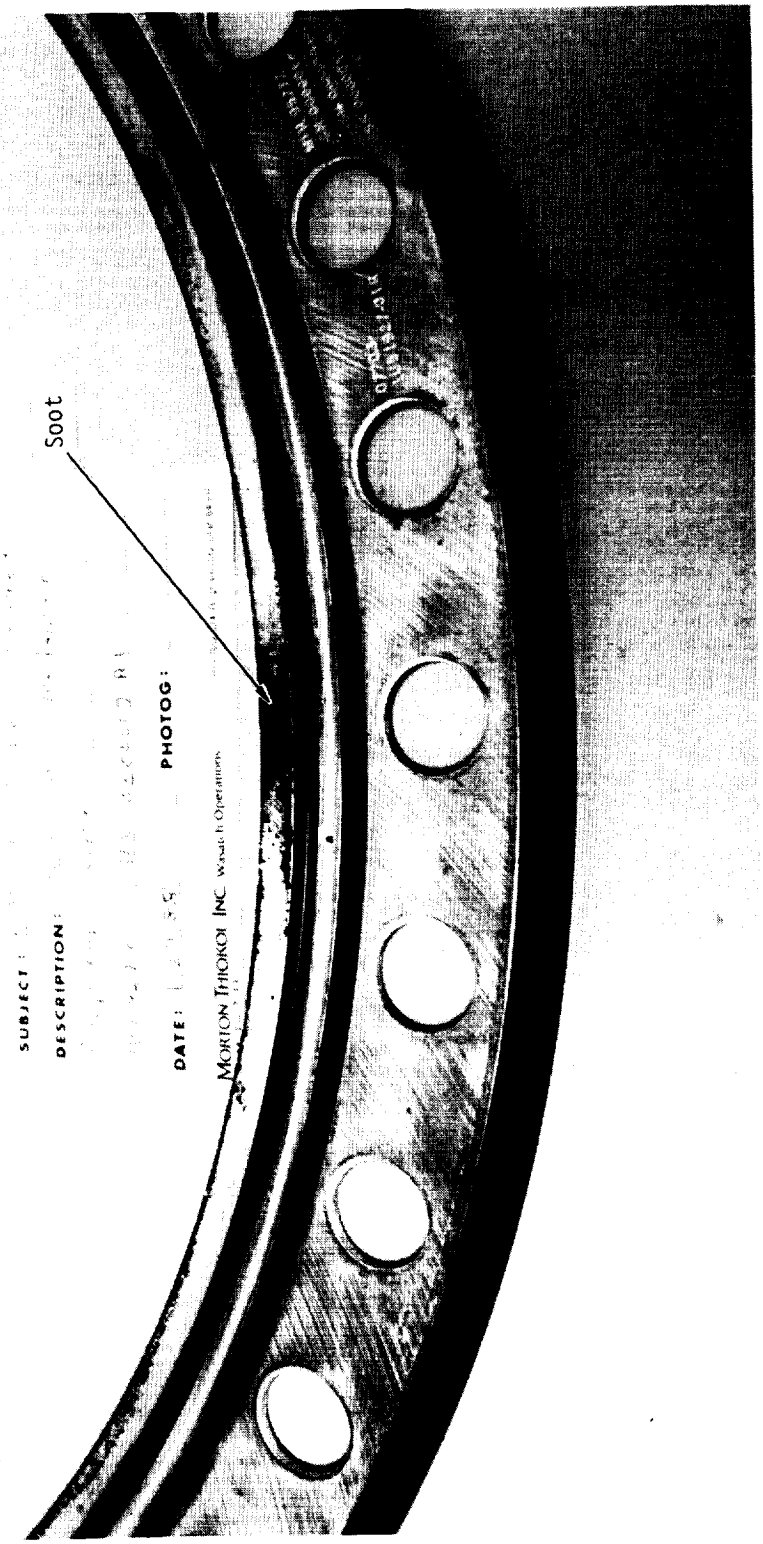

Figure 7.8-7. DM-9 Igniter Outer Gasket

N101958-4

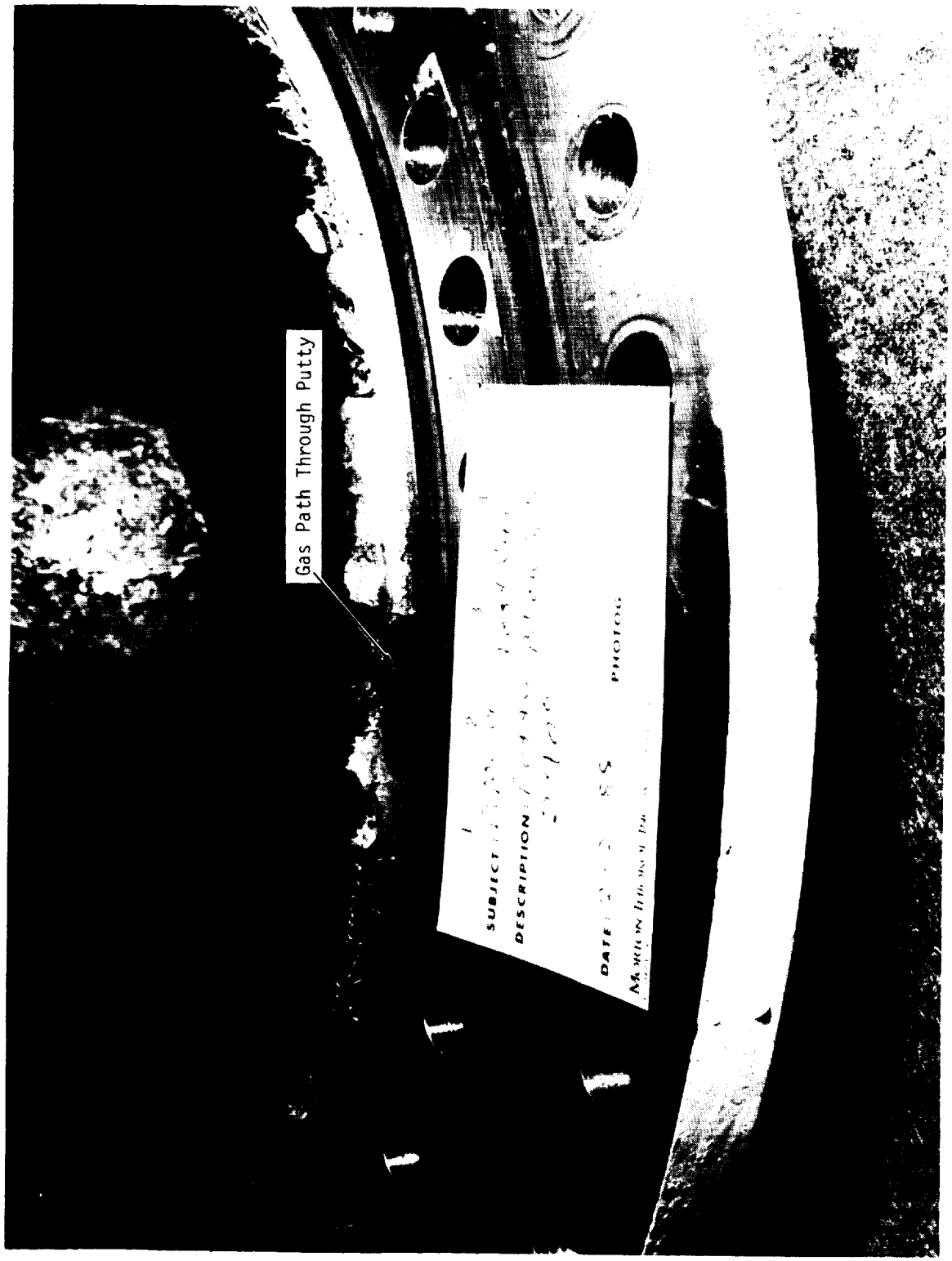

Figure 7.8-8. DM-9 Igniter Chamber-to-Adapter Joint

ORIGINAL PAGE
BLACK AND WHITE PHOTOGRAPH

N101958-5

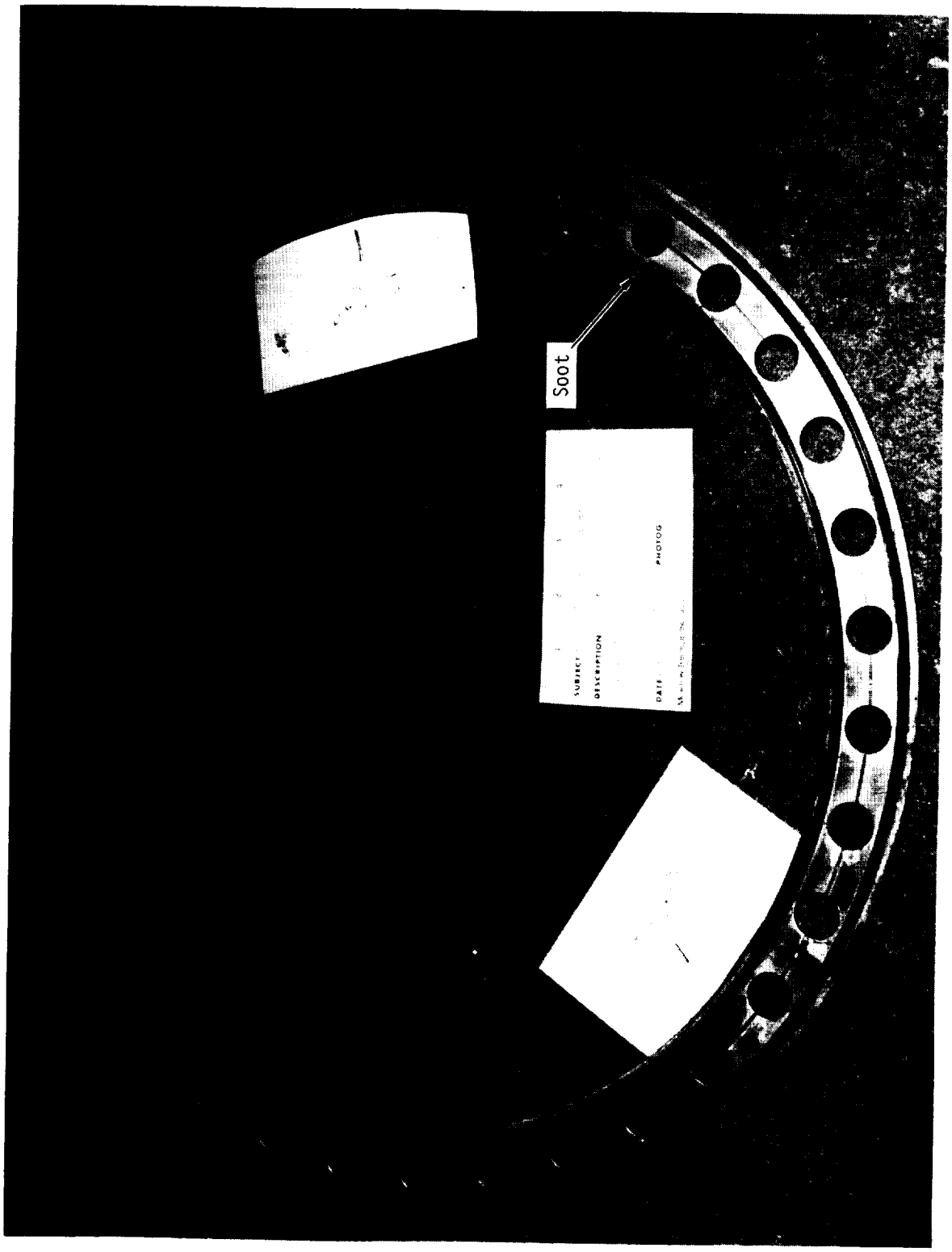

Figure 7.8-9. DM-9 Igniter Inner Gasket

7.8.4.5 Insulation. All the insulation remained strongly bonded to the adapter and chamber (Figure 7.8-5). Insulation erosion was similar to erosion seen on other igniters fired in full-scale motors. The interior chamber was relatively free of char. There was some char initially, but it was scrubbed out by the CO_2 flowing through the igniter chamber into the motor. The adapter insulator was free of char primarily due to the CO_2 flow.

7.8.4.6 Nozzle Insert. The insert remained tightly bonded to the chamber and internal and external insulation remained in place. There was no indication of any heat damage to the chamber/inset bondlines.

7.8.4.7 CO_2 Quench System. The headend CO_2 quench system on DM-9 operated as programmed. After motor burnout, a pneumatic actuator pulls the pin that retained the plug. A motor-driven valve in the CO_2 adjacent to the quench injector was then actuated and CO_2 filled the line and expelled the plug out into the motor chamber as in previous firings.

The excellent condition of the igniter adapter and injector hardware proved that the plug performed its sealing and insulating function throughout the motor firings.

All CO_2 injector parts were clean when disassembled. There have been no leaks past any of the seals and the liquid CO_2 flowing through the parts did no damage.

7.8.4.8 S&A Device. The B-B from the S&A device used to ignite DM-9 was examined to determined the condition of the O-rings and sealing surfaces. Examination of the dual seal initiators revealed nothing unusual based on experience from previous firings. The B-B housing was examined, and its clean, undamaged condition indicated that it could be refurbished.

7.8.4.9 Initiator. The initiator insulation remained firmly bonded at the headend attachment areas and insulation interface. There was no evidence of excessive heating on the inside of the initiator. The inside of the initiator is not insulated.

7.9 JPS/SYSTEMS TUNNEL

7.9.1 Introduction

JPS

a. Field Joint Heaters. The DM-9 field joint heater assemblies were flight configuration containing one primary and one redundant 3,500-W heater element. The heaters were powered with 208-Vac facility power.

The heater elements are laminated in Kapton and fluoroethylene polymer (FEP) Teflon with the redundant heater on top of the primary heater. The heating surface is 1.25 in. wide and 459.20 in. long. The heater assembly is approximately 0.062 in. thick. The underside of the heater's Kapton surface is coated with a pressure-sensitive adhesive which serves as an installation aide.

The temperature sensor assembly consists of two 1-in. wide assemblies, each containing two RTD sensors. These temperature sensors are spaced at 90 deg around the joint. The sensor and associated conductors are laminated in Kapton and FEP Teflon. The underside Kapton surface is coated with a pressure-sensitive adhesive which serves as an installation aide. The sensor assemblies are secured in place by the cork insulation which is bonded with EA 934NA over the JPS components.

The temperature of the heater at each joint is controlled by an automatic controller. Control is from the coldest of the four joint sensors.

b. Weatherseal. The field joint area, including heaters, was covered by an EPDM extruded rubber moisture seal. The moisture seal was continuous around the circumference on only one joint, and was held on by two Kevlar bands, one at each edge. A layer of cork completed the FJPS. The forward FJPS was the only one with a vent valve installed. The complete FJPS is shown in Figure 7.9-1.

A moisture seal for the factory joints consisted of 0.70-in. thick extruded rubber vulcanized over the joint (Figure 7.9-2).

A moisture seal integrity test was conducted after the static test in accordance with CTP-0042 and documented in TWR-17242.

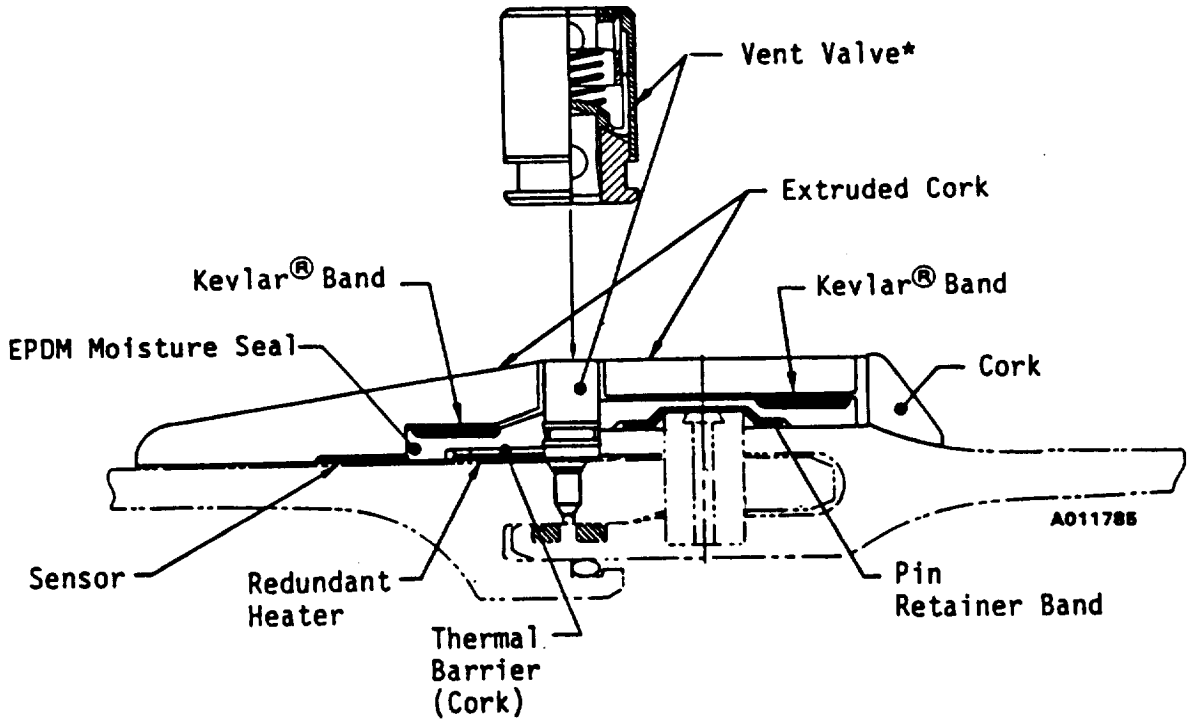

*Vent valve was installed at forward field joint only

Figure 7.9-1. FJPS

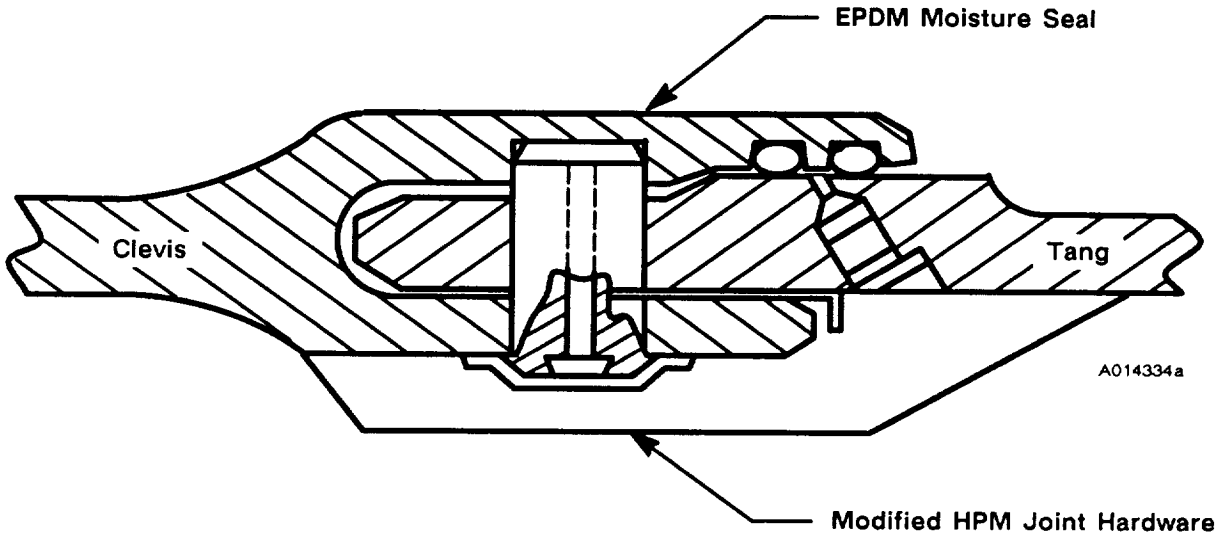

Figure 7.9-2. Factory Joint Moisture Seal

c. Systems Tunnel. Four systems tunnel floor plate sections were bonded to the DM-9 case (D6AC steel) at 180 deg on the aft center segment in accordance with Drawing 1U75426. For a flight motor the systems tunnel is bonded at 90 deg. The floor plate sections consist of an aluminum channel to which the various brackets for retaining the cables and the tunnel cover are attached. The cover and holddown straps, etc., were not attached for DM-9 testing. Two strips of EPDM shearply are vulcanized to the underside of the floor plate and then the assembly is adhered to the case (Figure 7.9-3).

A nondestructive and destructive test will be performed at the Thiokol H-7 facility at Clearfield, Utah. The tests will be performed in accordance with ETP-0231.

7.9.2 Objectives

The qualification test objectives from Section 2 with regard to JPS/systems tunnel performance were to:

S Certify aluminum systems tunnel bondline integrity after exposure to motor pressurization loads.

T Certify the ability of the field joint protection system to prevent the entry of rain.

U Certify the ability of the field joint heater assembly to maintain the joint temperature between 75° and 120°F.

V Certify the ability of the field joint protection system to prevent the accumulation of water in the joint.

W Certify the operation of the field joint heater with a power supply meeting the requirements of ICD 3-44005.

7.9.3 Conclusions/Recommendations

JPS

a. Field Joint Heaters. The heaters performed as predicted. Field joint heaters maintained the temperature at the controlling RTD at 88°F with an ambient

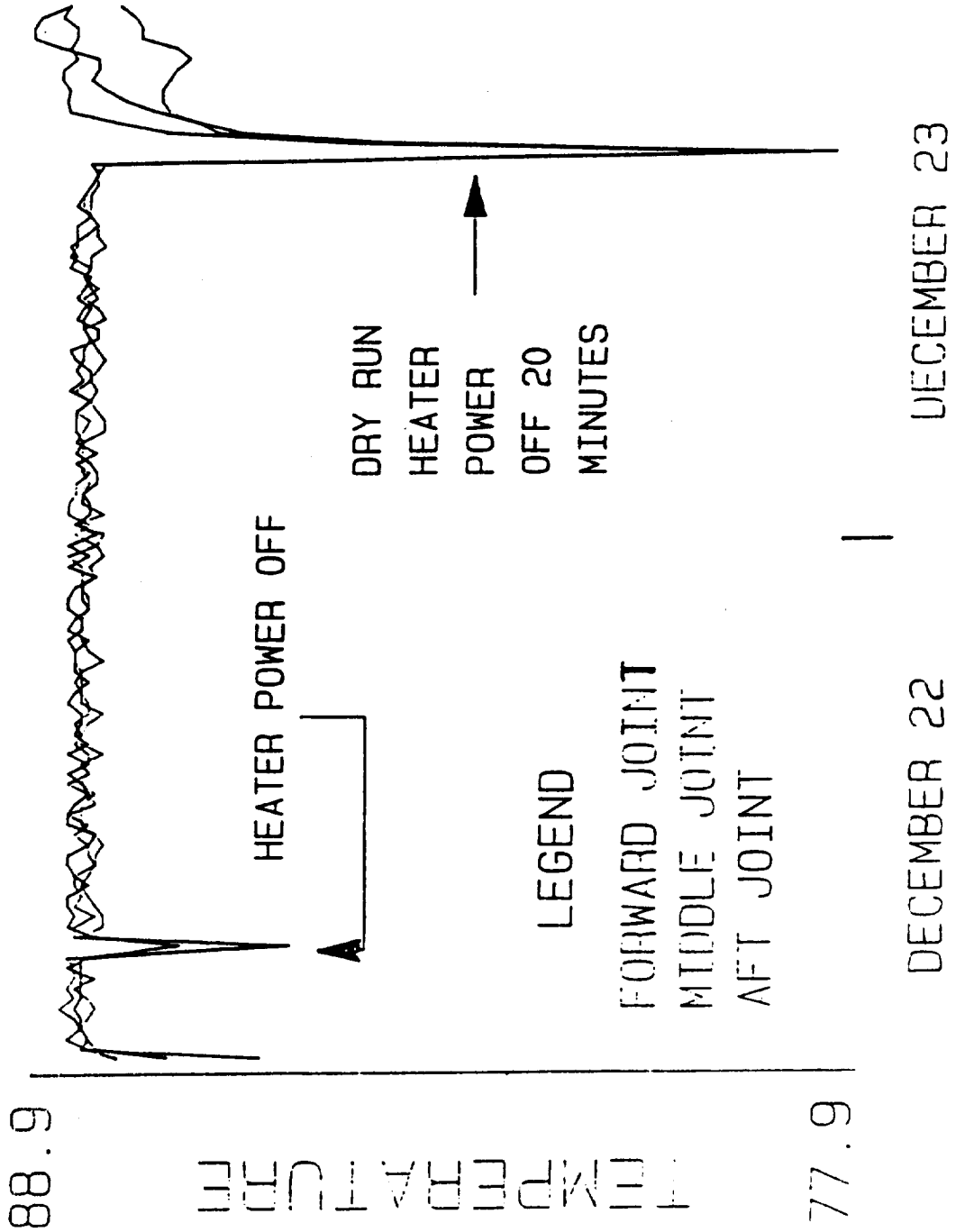

Figure 7.9-3. Field Joint Heater Temperatures at Controlling RTD

temperature of 25°F and a wind velocity of 15 to 20 mph, with gusts up to 30 mph. The heaters raised the joint to the controlled temperature of 88°F and maintained this temperature with a maximum deviation of -0.1° to +0.5°F.

The temperature data available to the test conductor at Building T-22 did not accurately provide the field joint temperature. As a result, it is recommended that the temperature of the sensor of the FJPS be made available on a real-time basis to the test conductor at Building T-22 for test commit criteria.

b. Weatherseal. The JPS performed as predicted on the DM-9 test firing with the exception of the field joint moisture seal, which permitted the entry of moisture into the joint. The source of the moisture intrusion was identified at the point where the the moisture seal passes over the pin retainer band takeup mechanism. This mechanism is approximately 0.75 in. high; it lifted the sealing edge of the moisture seal off the case.

A new, low-profile takeup mechanism has been designed for the pin retainer band. This will be installed on one of the qualification motors and the moisture seal test wil be repeated.

No moisture was found within the factory joint moisture seal.

c. Systems Tunnel. There were no test anomalies associated with the systems tunnel. Initial observations indicate no evidence of debonding of the systems tunnel and that structural integrity was maintained during the static test.

7.9.4 Results/Discussion

JPS

a. Field Joint Heaters. The set-point temperature of 88°F at the coldest resistance temperature devices (RTD) was maintained within -0.1° to +0.5°F. At the time of heater turnon, the coldest ambient temperature at any field joint was 71.1°F. After 45 min, the temperature at all three controlling RTDs was at 88°F, and remained there the balance of time that heater power was applied.

The heater power was removed for 12 min at T-2 hr for the dry run. At this time, the temperature control set-point was changed to 88.8°F.

The heater temperature controller performed with precision as the maximum temperature excursion minimum-to-maximum was 0.6°F.

Figure 7.9-3 is a plot of the temperature of the controlling RTDs at the three field joints.

The maximum differential joint temperatures of 21°F occurred in the forward joint. Figure 7.9-4 is a part of the maximum differential temperature of the three field joints.

The six field joint temperature sensors, T146 through T151, which were available to the test conductor in Building T-22 did not accurately provide the field joint temperatures. Figure 7.9-5 is a plot of these temperatures during the last 15 min prior to test. T146 data do not correlate well with data recorded from the heater-controller RTD. Heater power was removed at T-2 min. Under the extremely cold ambient temperature conditions the maximum measured temperature drop after power removal from T-2 to T-0 min was 1°F.

b. Weatherseal. Following the static firing of DM-9, a 2 by 12 ft plastic sheeting was installed over the lower portion of the forward field joint and forward segment factory joint (Figure 7.9-6). The sheeting extended circumferentially around the case far enough to allow for 1-ft head of water from the bottom of the motor and centered over the joint. Water was allowed to stand for 73 hr for the field joint and 72 hr for the factory joint. During moisture testing the joint temperature was between 60° and 70°F. No water was found within the factory joint moisture seal. Water seeped into the field joint moisture seal at the joint pin retainer band takeup mechanism. This mechanism caused the moisture seal to be locally lifted off the case. A low-profile pin retainer band takeup mechanism has been designed, and a rain test will be conducted in a vertical position to qualify the field joint moisture seal.

The vent valve installed in the forward field joint weather seal was not placed under conditions which would test its ability to vent. Venting will occur under flight conditions as the SRB ascends through the atmosphere.

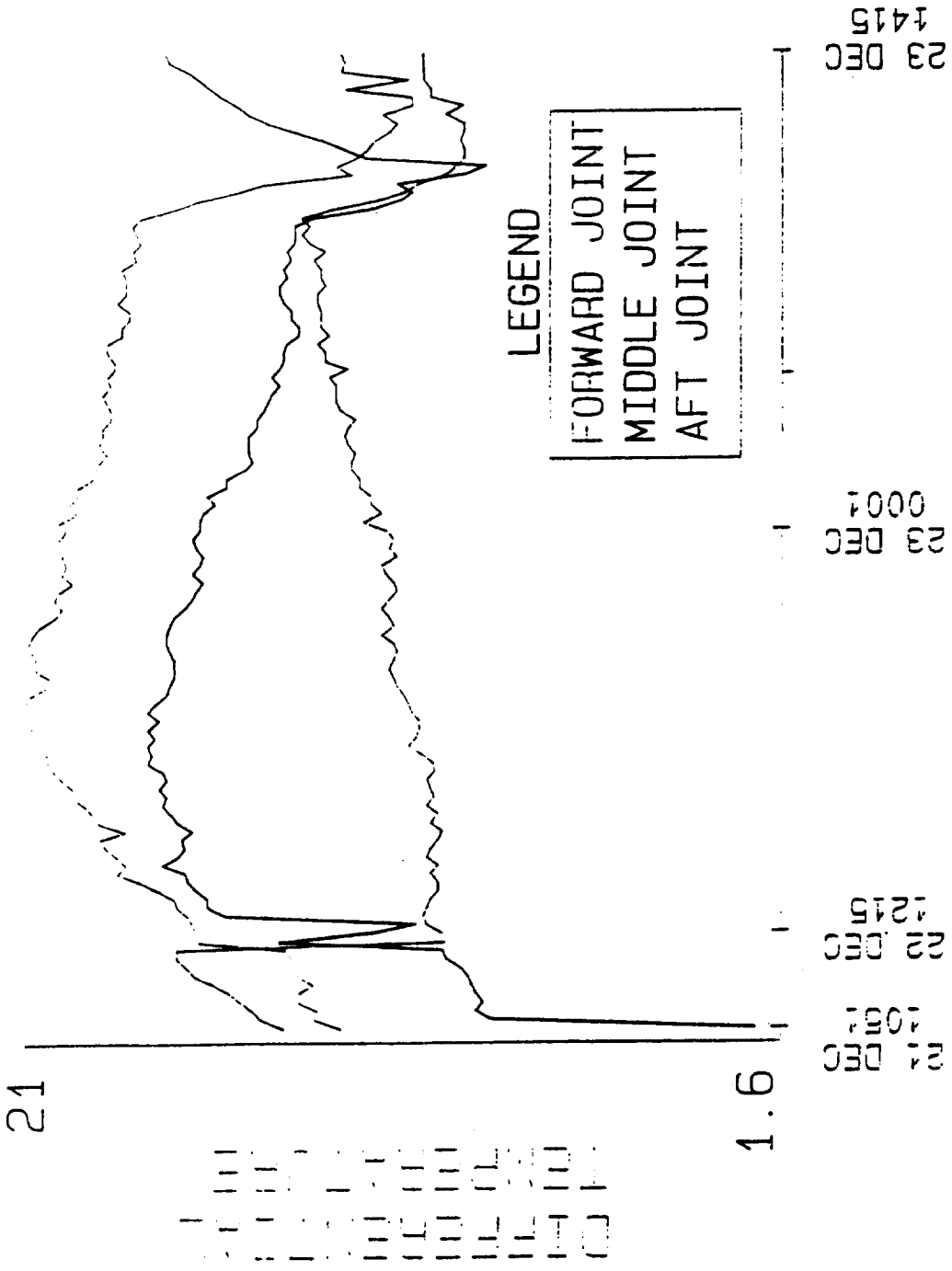

Figure 7.9-4. DM-9 Field Joint Temperature Differential

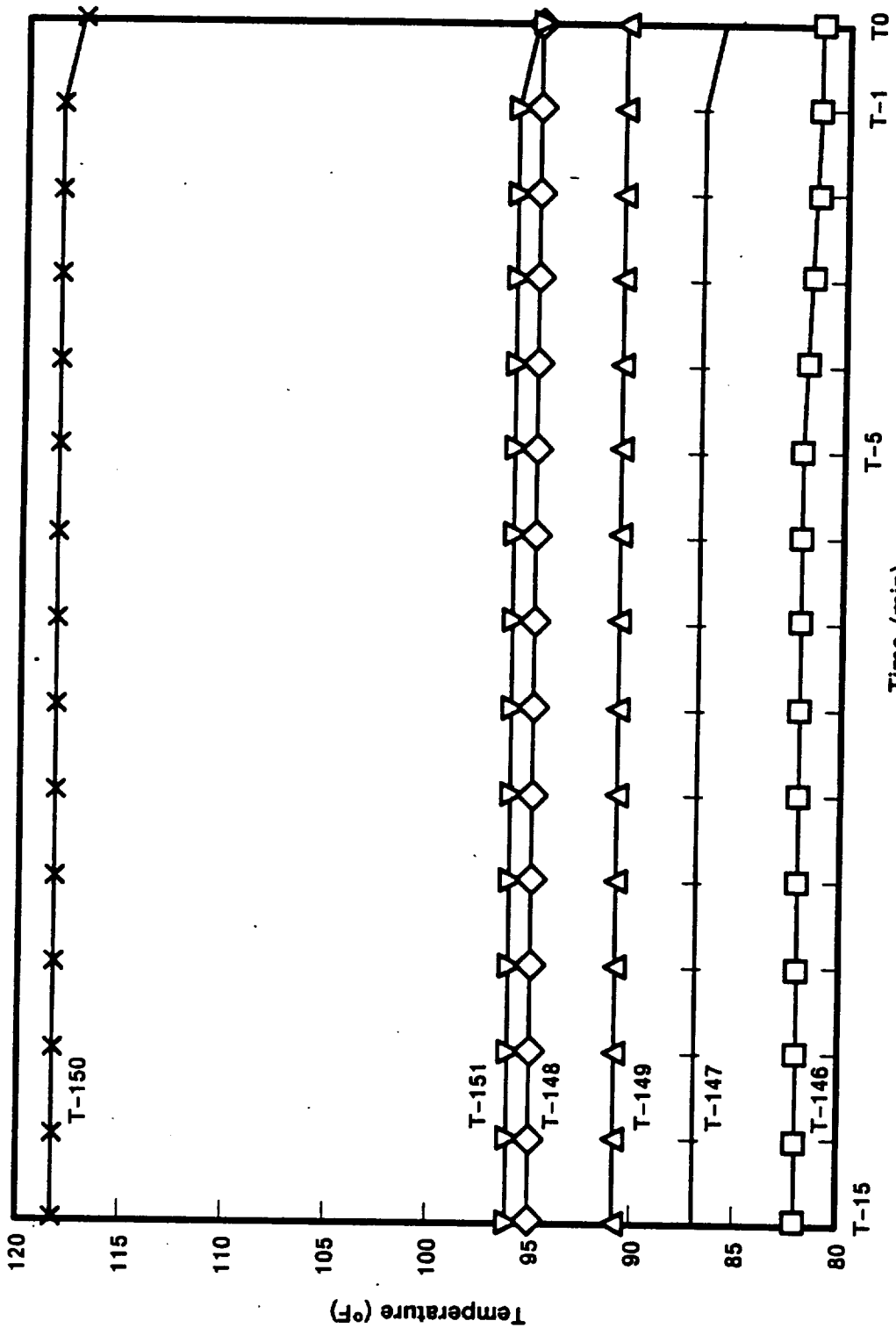

Figure 7.9-5. DM-9 Heater Auxiliary Sensors

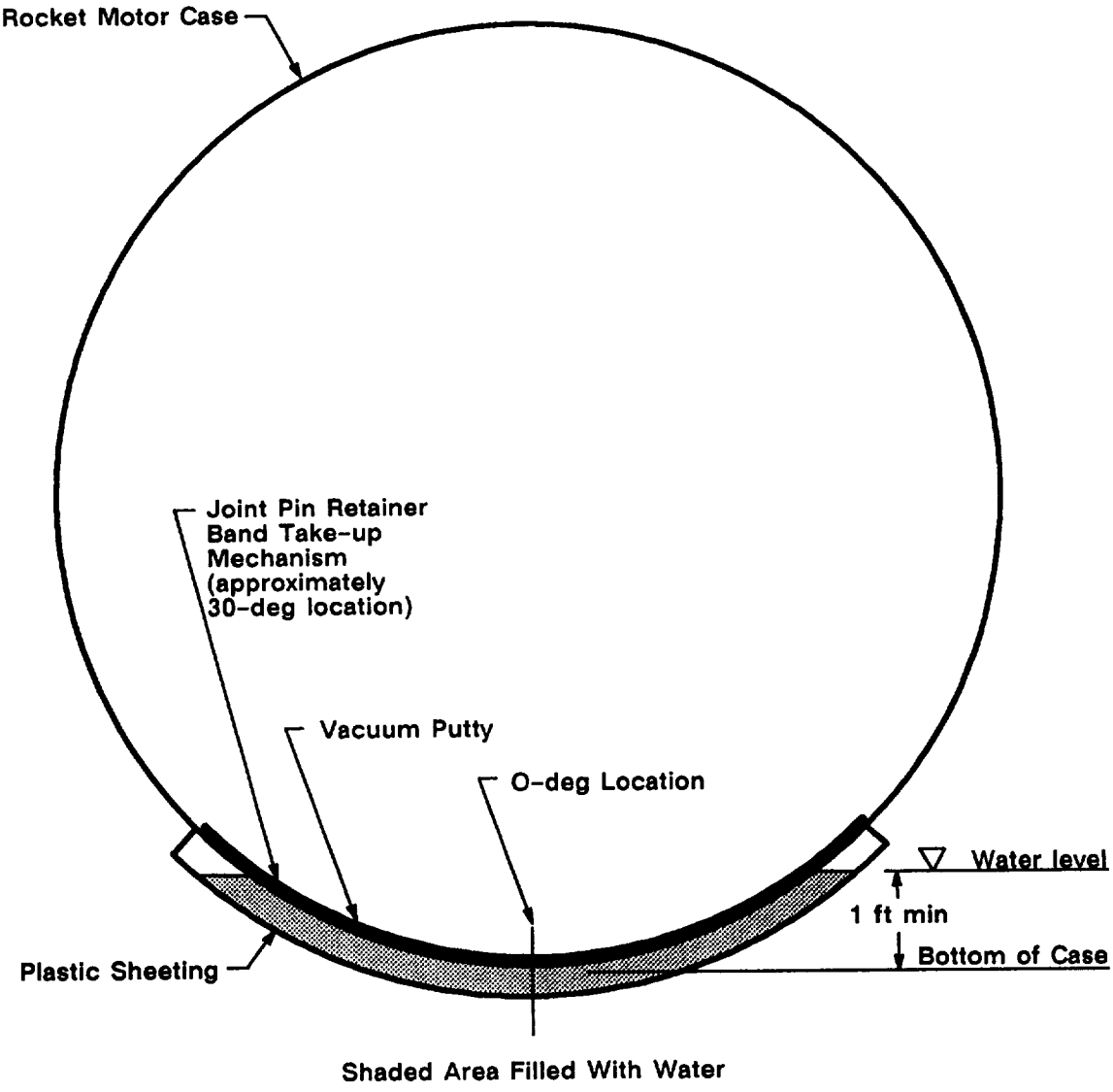

Figure 7.9-6. Moisture Seal Test Setup

c. Systems Tunnel. There were no test anomalies associated with the systems tunnel. Observations indicated no evidence of debonding of the systems tunnel and structural integrity was maintained during the static test.

7.10 LEAK CHECK

7.10.1 Introduction

Leak tests were performed on all DM-9 field and nozzle joints. This included leak testing of case field joints before and after support chock removal at the test bay. The internal nozzle joints and nozzle-to-case joint were tested using 2U129718 equipment. The case field joints and aft exit cone joint were tested using the 7U75575 prototype equipment. The 8U-GSE field joint test equipment was not available for the DM-9 field joint tests, but will be used for the QM-6 test. New 2U equipment for internal nozzle joints is not expected to be online until the QM-7 static test.

7.10.2 Objectives

The qualification test objectives from Section 2 with regard to leak test procedures were to:

C Certify that the case field joint seal verification does not degrade the performance or integrity of the joint system.

E Certify that the leak test method is compatible with the joint insulation.

P Certify that the nozzle-to-case joint seal verification does not degrade the performance or integrity of the joint system.

AL, AY Certify that the seal verification does not degrade the performance or integrity of the factory joint system.

BC Certify that the flex bearing seal verification does not degrade the performance or integrity of the system.

BF Certify that seal verification does not degrade the performance or integrity of the nozzle internal joints or the aft exit cone joint.

BG Certify that bore seals are verifiable in the proper direction.

There were no development objectives associated with the leak test procedures.

7.10.3 Conclusions/Recommendations

All leak rates were within allowable limits. Post-test disassembly inspection revealed no damage to the seals, insulation, adhesives, or the hardware attributable to the leak test procedures.

Changes to the DM-9 procedure are being discussed in order to reduce the incidence of calculated negative leak rates.

7.10.4 Results/Discussion

Each of the leak tests employs the method of pressure decay to calculate leak rates. The leak test equipment is used to pressurize and isolate each test joint. The test equipment provides real-time monitoring of pressure and temperature during the isolation period. The changes in pressure and temperature are then used to calculate a joint leak rate.

The leak test results are presented in Table 7.10-1. Test results show all joints have acceptable leak rates, and most joints have an order of magnitude less than the maximum allowable. The negative leak rates for the low-pressure tests are consistent with previous test results and represent O-ring absorption/desorption. Changes to the DM-9 procedure are being discussed in order to reduce the incidence of calculated negative leak rates.

7.11 ETA RING

7.11.1 Introduction

An ETA ring was installed on the ETA segment in accordance with Drawing 7U75416. The ETA ring as defined in USBI Drawing 10100-0047 is a redesigned, 360-deg, left-

Table 7.10-1. DM-9 Leak Test Results

Joint	Cavity	Test Pressure (psig)	Maximum Allowable (sccs)	Measured Leak Rate (scss)
End Ring-Fxd Housing	P-S P-S	920 30	0.29 0.0082	-0.008 0.000
End Ring-Nose Inlet	P-S P-S	920 30	0.29 0.0082	0.097 NA
Nose Inlet-Throat	P-S P-S	740 30	0.24 0.0082	0.12 0.000
Throat Fwd Exit	P-S P-S	144 30	0.048 0.0082	0.001 -0.001
Fwd Exit-Aft Exit	P-S P-S	80 30	0.046 0.0082	0.0005 -0.0002
Nozzle-to-Case	P-S 1 P-S 1 P-W P-S P-S 2	920 30 30 Ambient 30	0.29 0.0082 -10 psi/5 min 0.0082 0.001*	0.035 -0.012 -1.5 psi/30 min 0.000 0.000
Field Fwd (chock/no chock)	P-S P-S P-C (P-S) P-C (P-S)	1,000 30 100 Ambient 30 Ambient	0.32 0.0082 0.051 -0.051 0.0082 -0.0082	0.0067/0.0044 -0.0042/0.0062 0.0066/0.0097 -0.0005/-0.0016 -0.0036/-0.0047 -0.0006/-0.0011
Field Center (chock/no chock)	P-S P-S P-C (P-S) P-C (P-S)	1,000 30 100 Ambient 30 Ambient	0.32 0.0082 0.051 -0.051 0.0082 -0.0082	0.0036/0.0121 -0.0071/-0.0054 0.0084/0.0100 -0.0014/-0.0017 -0.0007/-0.0057 0.0000/0.0024
Field Aft (chock/no chock)	P-S P-S P-C (P-S) P-C (P-S)	1,000 30 100 Ambient 30 Ambient	0.32 0.0082 0.051 -0.051 0.0082 -0.0082	0.0060/0.0044 -0.0052/-0.0061 0.0044/-0.0149 -0.0005/-0.0017 -0.0013/-0.0016 0.0006/-0.0003

P-C = Primary O-ring to capture feature O-ring
P-S = Primary O-ring to secondary O-ring
P-W = Primary O-ring to wiper O-ring

*Equivalent of one bubble per second--test for packing with retainers only

hand ring configuration. The ETA ring is furnished to Thiokol for testing by NASA (USBI), who is responsible for analysis of the data collected.

7.11.2 Objectives

The development test objective from Section 2 with regard to ETA ring performance was:

BI Evaluate the structural integrity of ETA ring under motor pressurization loads (MSFC test objectives).

No qualification objectives were involved.

7.11.3 Results/Discussion

The ETA ring was intact and on the case after the test. No anomalous conditions of the ETA ring have been documented.

7.12 GROUND TEST SUPPORT EQUIPMENT

7.12.1 Introduction

Both the aft skirt and the igniter were conditioned for the DM-9 static test. This was the first use of the conditioning systems (Figure 7.12-1).

Aft Skirt Conditioning

Aft skirt conditioning was accomplished per Drawing 2U129774. A 600,000 Btu Model ULT-6 Ultra VI fuel oil heater was used in place of the Herman Nelson heater for the air conditioning source. Conditioned air was directed to the aft skirt through insulated ducting (Figure 7.12-2). A centrifugal blower, 2U129774-218, was installed in the ducting in order to boost the air pressure to the desired level at the outlet. Control valves were installed downstream of the blower to allow conditioned air to be vented overboard by remote control from Building T-22 during GN_2 purge. Thermocouples were installed inside the aft skirt on the nozzle-to-case joint and on the hydraulic system to monitor temperatures during the conditioning cycle.

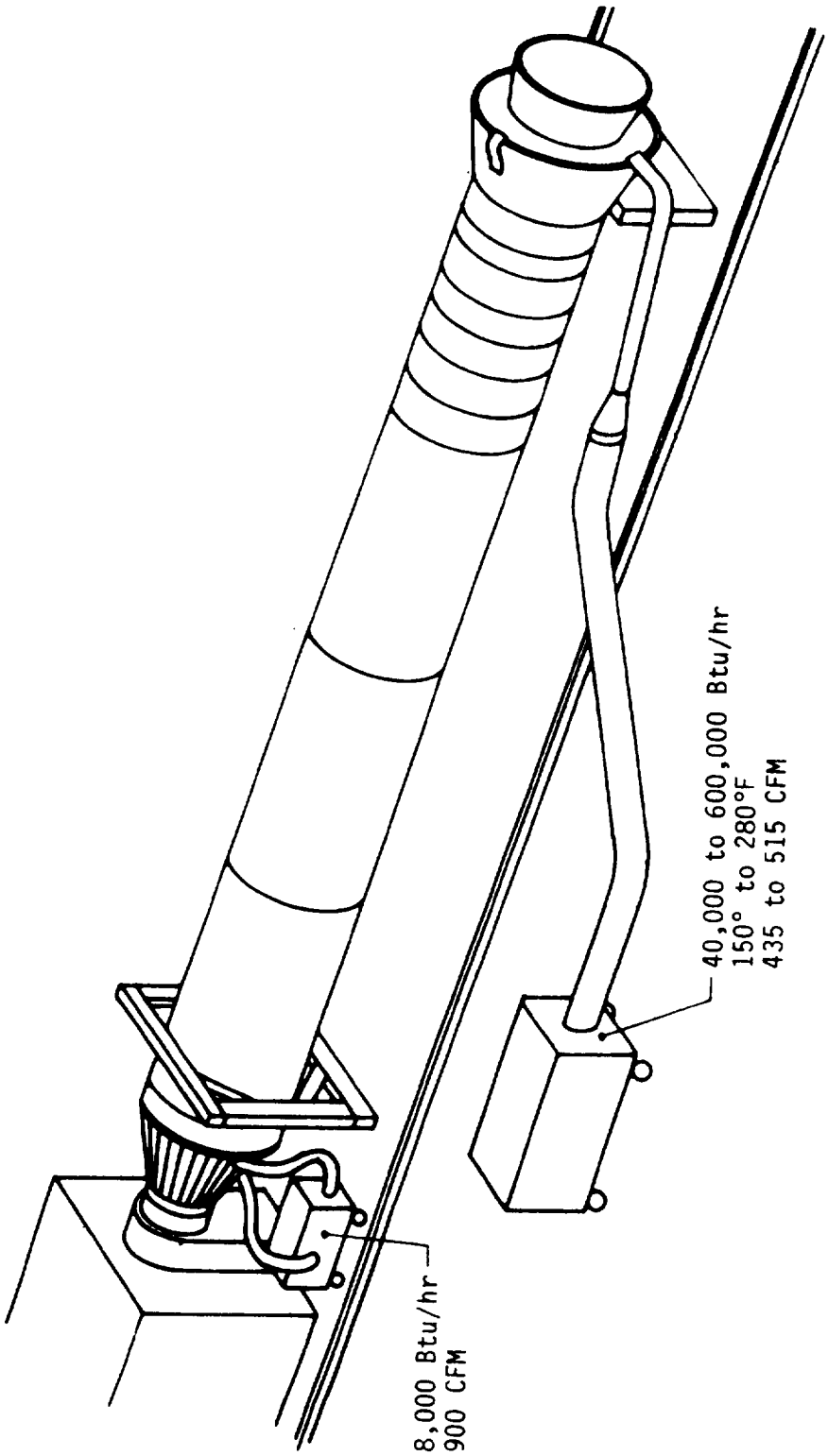

Figure 7.12-1. Aft Skirt/Igniter Conditioning

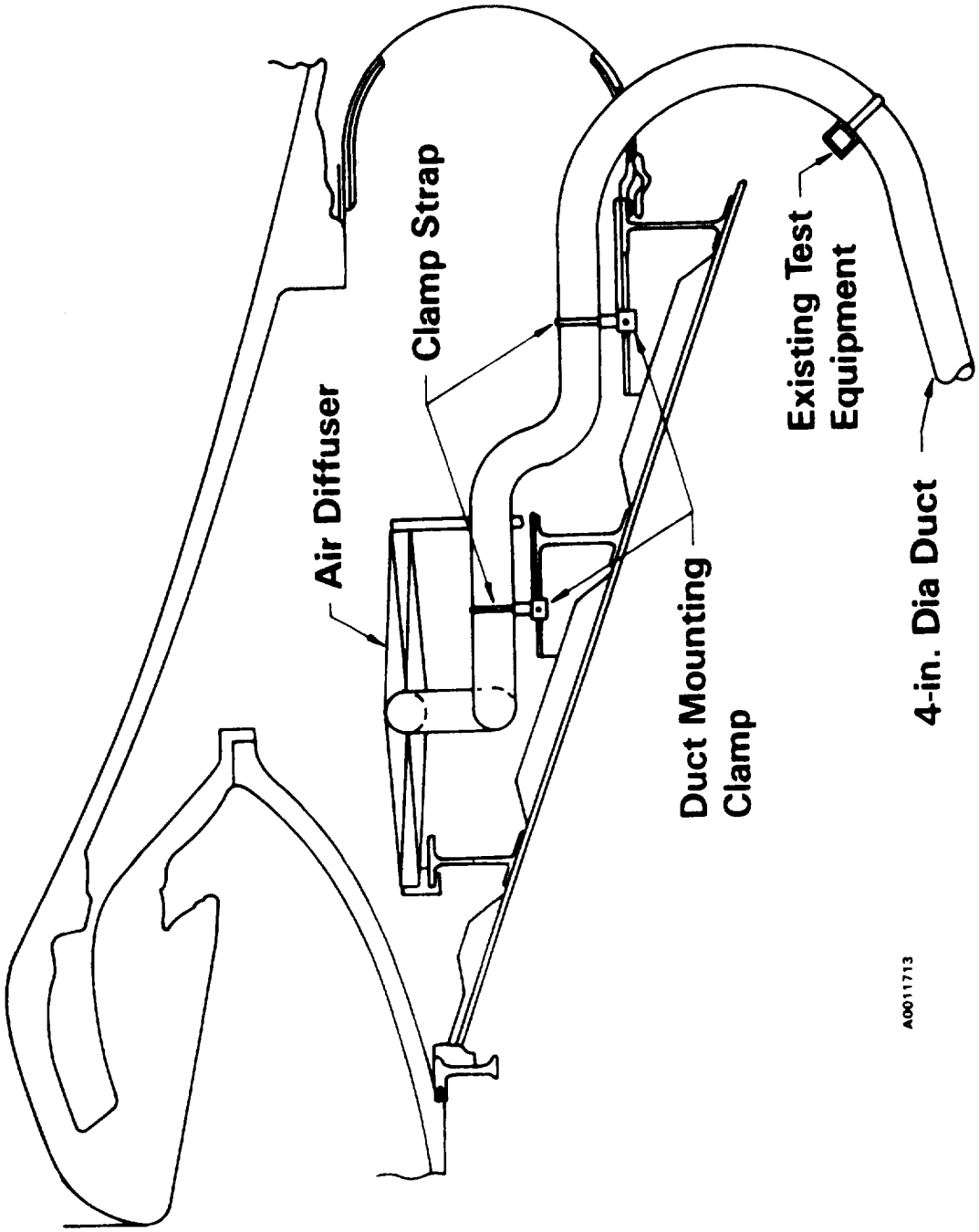

Figure 7.12-2. Aft Skirt Conditioning

Igniter Conditioning

Igniter conditioning was achieved per Drawing 2U129500. The -201 heating unit assembly was located at the forward thrust wall and connected to facility steam and electrical systems. The -01 conditioning shroud, after several modifications to allow access for arming operations, was installed inside the thrust adapter over the igniter and connected to the heater unit assembly with flexible ducting (Figure 7.12-3). Thermocouples were installed on the igniter-to-case joint to monitor temperatures during the conditioning cycle.

Water Deluge System

The redesigned water deluge system was set up per Drawing 2U129749. It was designed to supply a minimum of 2.5 gal per min per ft^2 to cool a 90- to 100-deg arc centered at the bottom of the motor (Figures 7.12-4 and 7.12-5).

7.12.2 Objectives

The objectives related to the aft skirt conditioning were to:

Qualification

Q Certify that the nozzle-to-case joint O-ring is maintained within the temperature range specified in ICD 2-0A002 (75° ±25°F). A PIRN (BI-0718) will change this to 75° to 120°F when approved.

Development

BL Determine the effects of dither/TVC performance at elevated hydraulic oil temperatures (MSFC test objective).

Igniter conditioning was performed in order to condition the igniter-to-case and S&A-to-igniter joints to 50°F minimum at the time of the static test.

The water deluge system function was to cool the SRM until temperature readings were constant below 140°F.

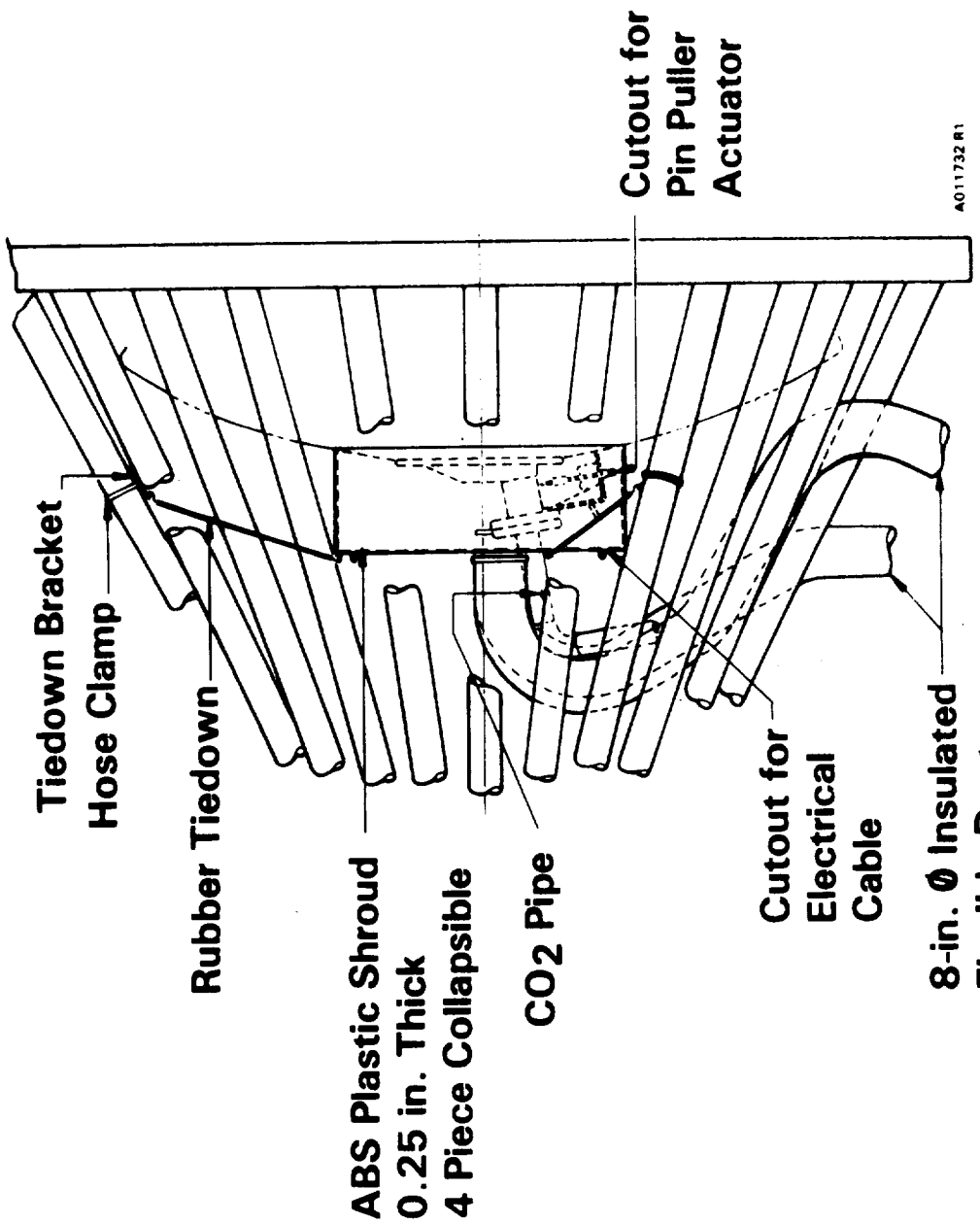

Figure 7.12-3. Igniter Conditioning

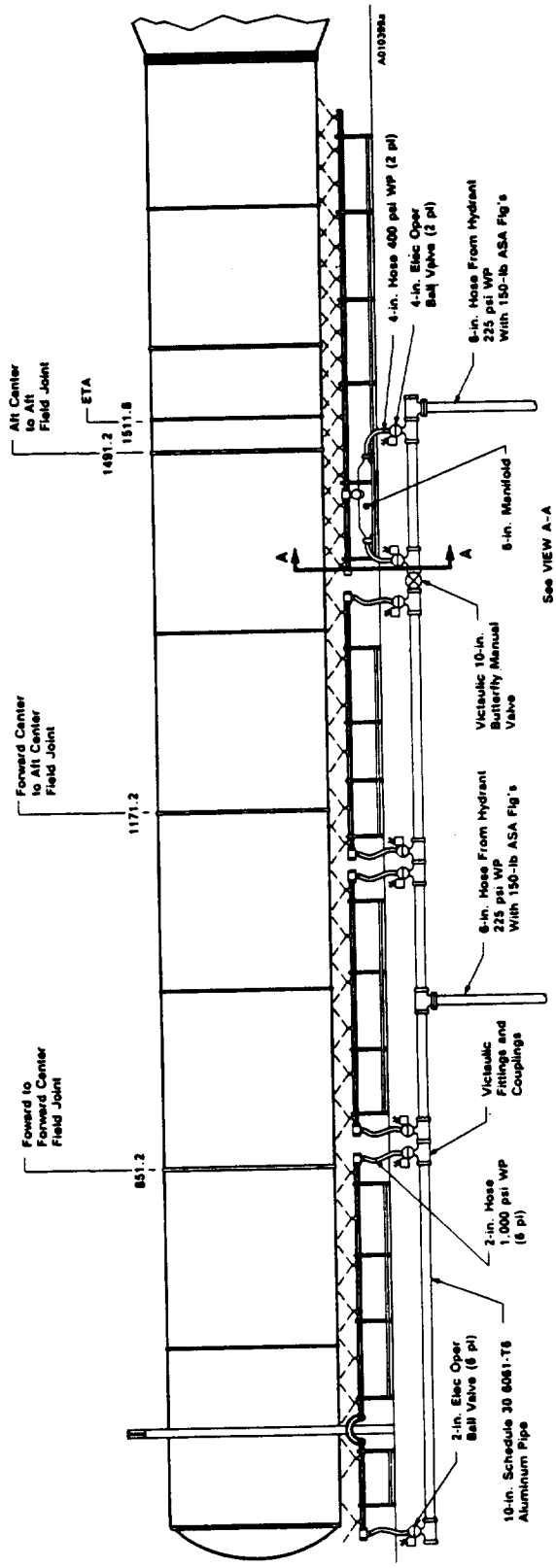

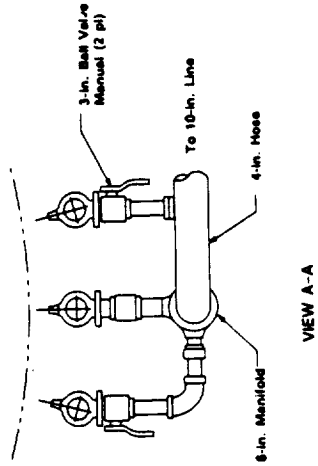

Figure 7.12-4. DM-9 Water Deluge System

ORIGINAL PAGE IS
OF POOR QUALITY

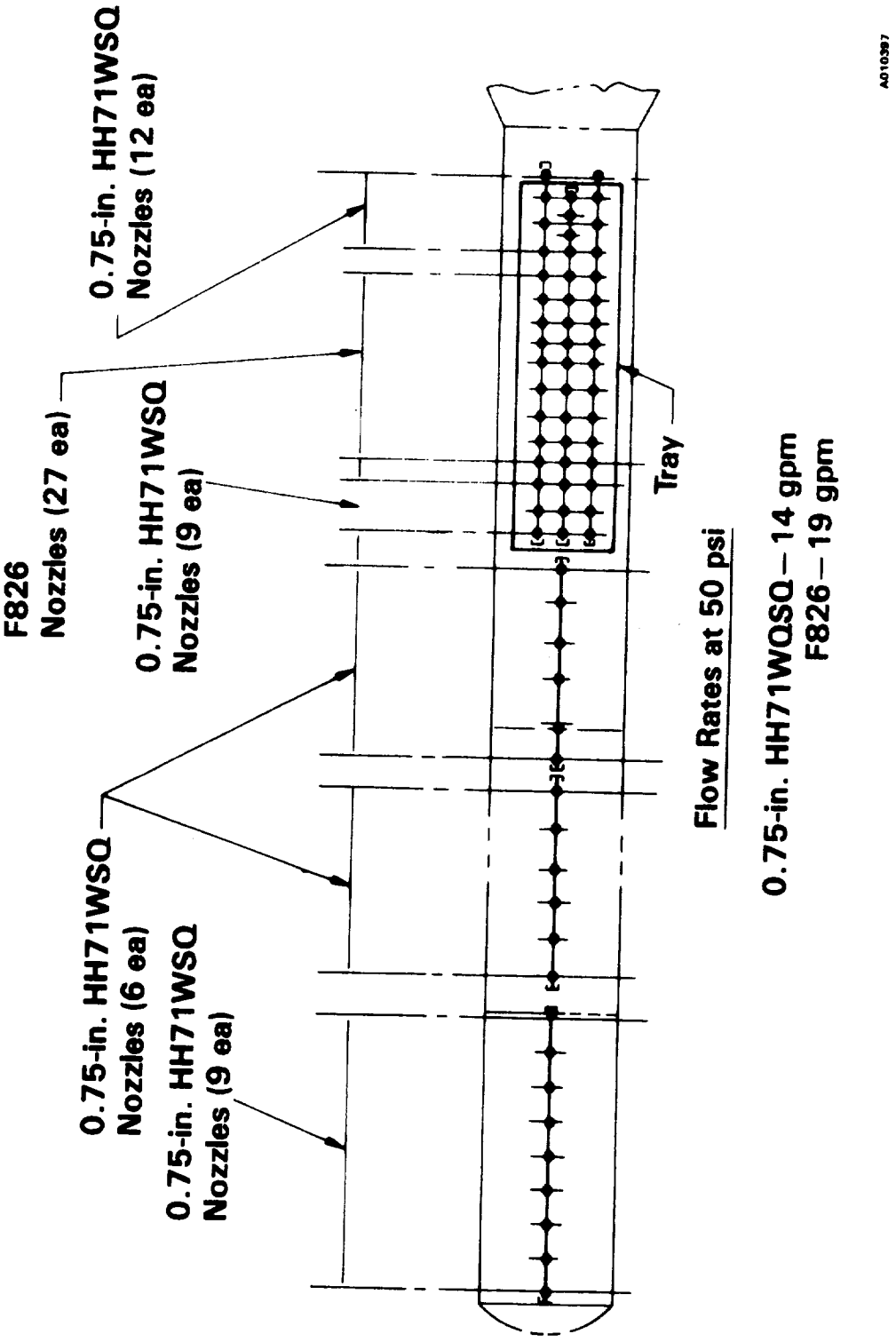

Figure 7.12-5. DM-9 Water Deluge System Nozzle Arrangement

7.12.3 Conclusions/Recommendations

Igniter/Aft Skirt Conditioning

Conditioning requirements were met; however, many problems that were encountered stem directly from ambient conditions at the test bay on the static test date. Sub-freezing temperatures, along with high winds, required maximum heat output of the aft skirt conditioning cart approximately 80 ft forward of the skirt to preclude damage during the static test. This hampered the effectiveness of that system, and the hydraulic oil temperatures were not at the expected elevated temperature at T-0.

Throughout the entire setup and static test there were numerous changes to the conditioning requirements which involved extra effort for redesign and rework of installed systems. Some of the requirements were not defined until after design had begun. Test Engineering recommends that future conditioning requirements be determined well in advance and adhered to by all parties involved. It may also be necessary to replace the aft skirt conditioning unit with a steam type in order to reach specified temperatures without requiring maximum output of the unit.

Arming operations were slightly different due to the addition of the igniter conditioning shroud, but it was a workable situation.

Water Deluge System

Severe cold temperatures also affected the water deluge system and required the use of thermal blankets and a portable conditioning unit in order to keep water lines from freezing. The forward deluge was cycled off at approximately T+20 min and then cycled on and off intermittently to prevent system freezeup. Final shutdown of the water deluge system occurred at approximately 1700 hr. Water system pressure was more than adequate for operation of the deluge system and all components operated satisfactorily.

CO_2 Quench

The CO_2 quench system functioned properly.

7.12.4 Results/Discussion

Aft Skirt Conditioning

Inclement weather severely hampered conditioning efforts throughout the static test. Beginning at 0900 hr on 23 Dec 1987 when the east rollup door was raised in order to move the house, ambient air temperatures quickly affected conditioning settings and required frequent corrections (Figures 7.12-6 through 7.12-8). Temperatures prior to the test in the aft skirt are tabulated in Table 7.12-1. At one point it was necessary to place thermal blankets around the aft skirt to prevent further heat loss due to wind velocity.

Igniter Conditioning

The igniter-to-case and S&A-to-igniter conditioning was not affected as severely as the aft skirt by the severe environment, due to the small area being conditioned and the volume of heated air being supplied. Table 7.12-2 shows the temperatures at the igniter.

Water Deluge System

Severe cold temperatures also affected the water deluge system and required the use of thermal blankets and a portable conditioning unit to keep water lines from freezing. Data from the slag temperature thermocouples are shown in Figures 7.12-9 through 7.12-11 and listed in Table 7.12-3. Aft deluge was activated at T+105 sec and forward deluge at T+110 sec. The forward deluge was cycled off approximately 20 min later and was cycled on and off intermittently to prevent system freezeup. The aft deluge was cycled off and on to monitor the temperature rise at 1510 hr and again at 1526 hr. Final shutdown of the water deluge system occurred at approximately 1700 hr. Water system pressure was more than adequate for operation of the deluge system and all components operated satisfactorily.

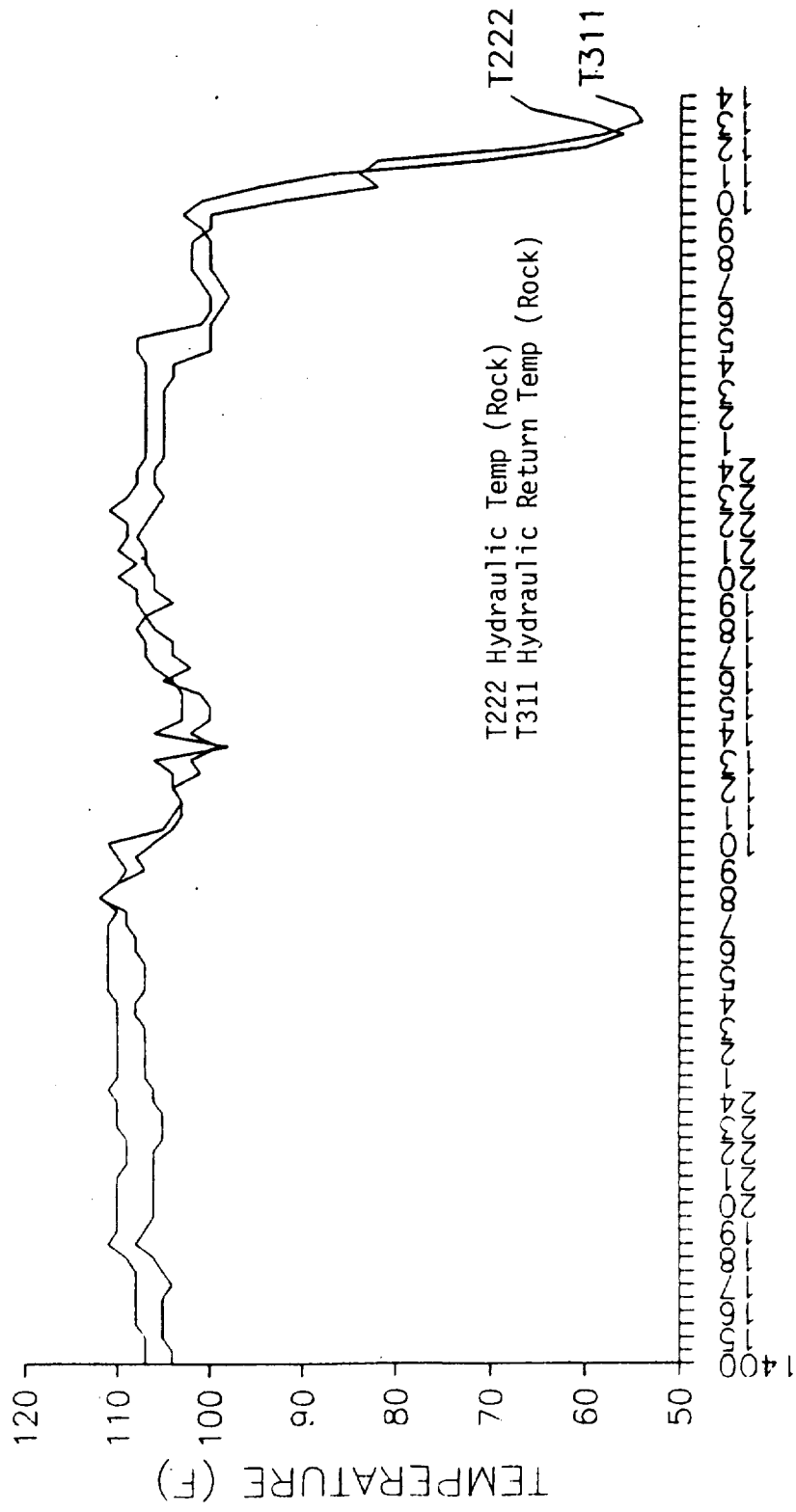

Figure 7.12-6. DM-9 Aft Skirt Conditioning (T222, T311)

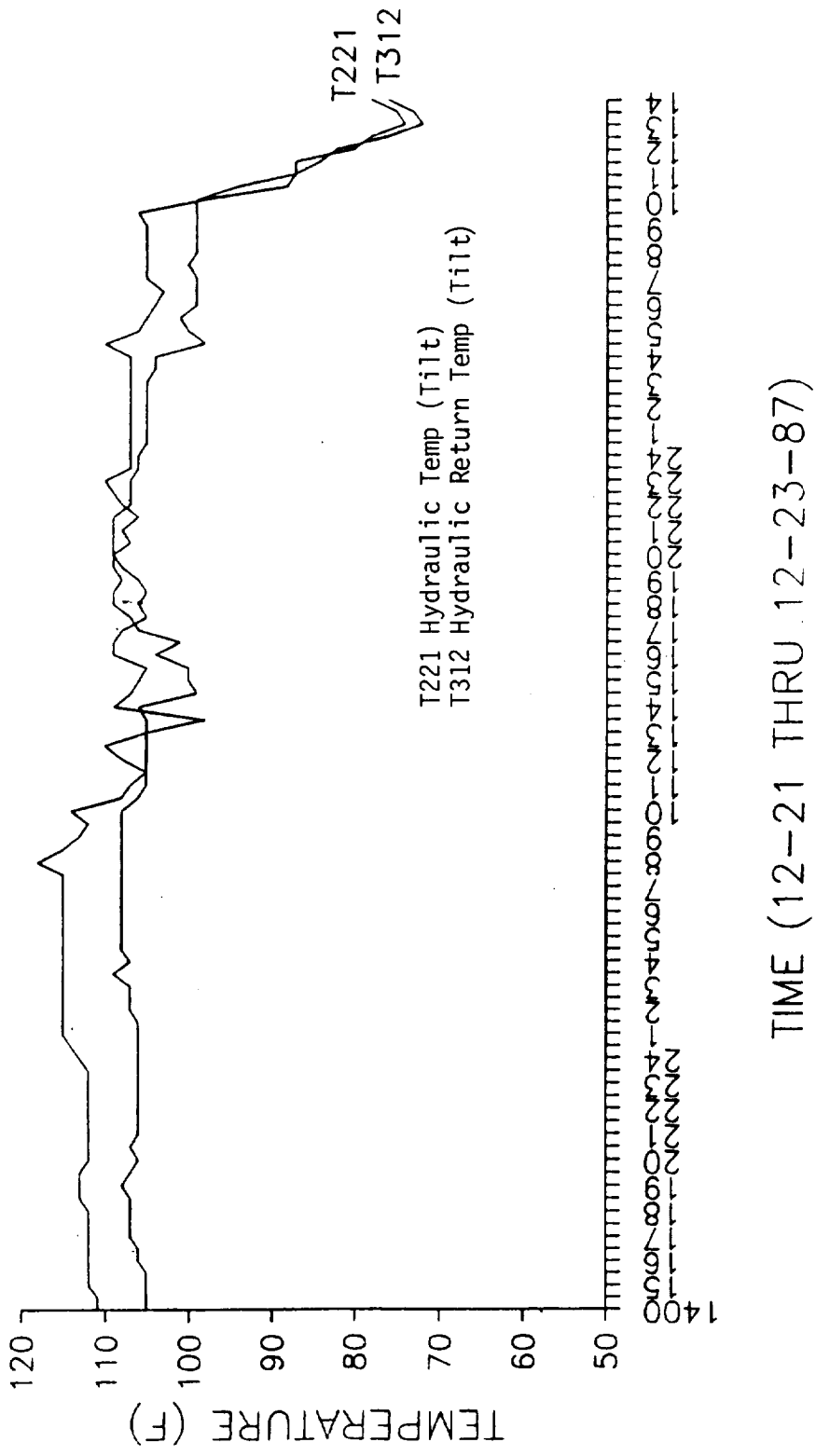

Figure 7.12-7. DM-9 Aft Skirt Conditioning (T221, T312)

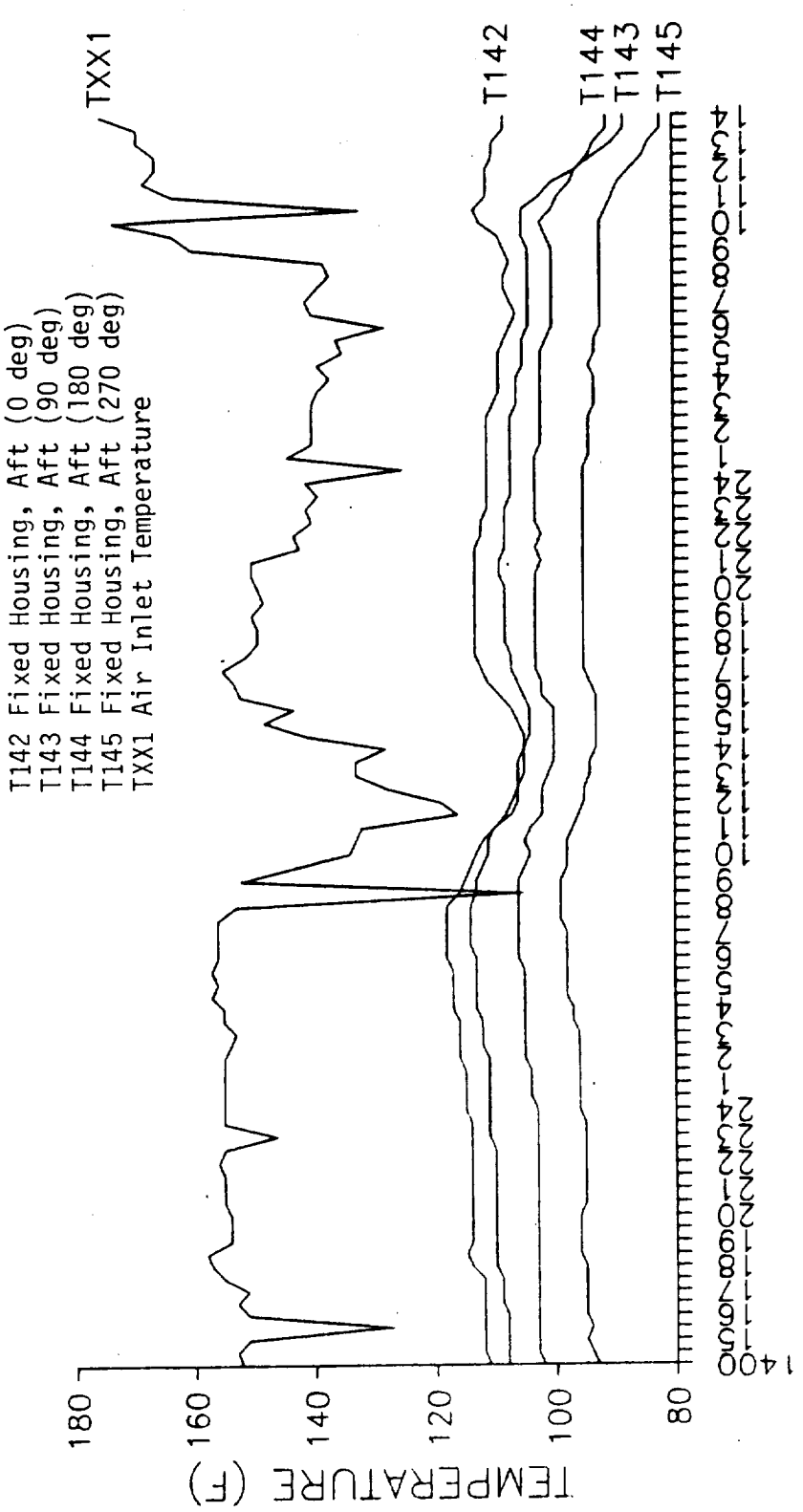

Figure 7.12-8. Nozzle-to-Case Joint Fixed Housing, Aft Temperatures

Table 7.12-1. DM-9 Aft Skirt Conditioning Temperatures

DAY	TIME	(A) T221	(B) T222	(C) T311	(D) T312	(E) T142	(F) T143	(G) T144	(H) T145	(I) TXX1
MIDNIGHT										
MONDAY	0000	106	106	110	113	115	111	103	96	155
	0015	106	106	111	114	115	111	104	96	155
	0030	106	106	111	114	115	111	104	96	155
	0045	106	107	110	115	115	111	104	96	155
	0100	106	107	110	115	115	111	104	96	155
	0115	106	107	110	115	115	111	104	96	155
	0130	106	107	110	115	115	111	104	96	155
	0145	106	107	110	115	116	111	104	96	155
	0200	107	107	110	115	116	111	105	96	155
	0215	107	107	110	115	116	111	105	96	150
	0230	107	107	110	115	116	112	105	96	154
	0245	107	107	110	115	116	112	105	96	153
	0300	107	107	110	115	116	112	105	96	153
	0315	108	107	110	115	116	112	105	97	156
	0330	109	108	110	115	116	112	105	97	155
	0345	107	107	110	115	116	112	105	97	156
	0400	107	108	110	115	117	113	105	97	155
	0415	108	108	111	115	117	113	105	97	155
	0430	108	107	111	115	117	113	105	98	157
	0445	108	107	111	115	117	113	105	98	157
	0500	108	107	111	115	117	113	105	98	156
	0515	108	107	111	115	117	113	105	98	157
	0530	108	107	111	115	117	113	105	98	157
	0545	108	107	111	115	118	113	106	98	157
	0600	108	108	111	115	118	113	106	98	156
	0615	108	108	111	115	118	113	106	98	156
	0630	108	108	111	115	118	114	106	98	156
	0645	108	109	111	115	118	114	106	98	156
	0700	108	109	111	115	118	114	106	98	156
	0715	108	108	111	115	118	114	106	98	156
	0730	108	109	110	115	118	114	106	99	156
	0745	108	112	111	118	118	114	106	99	153
	0800	108	112	112	118	118	114	106	99	153
	0815	108	112	112	118	117	114	106	99	143
	0830	108	110	110	115	116	113	106	99	105
	0845	108	108	109	114	114	113	106	99	141
	0900	108	107	109	113	115	113	106	99	152
	0915	107	105	108	111	113	112	106	98	138
	0930	108	108	110	112	114	112	105	98	143
	0945	107	105	109	111	113	114	105	98	138
	1000	108	106	111	114	113	111	104	98	134
	1015	107	105	109	112	112	111	104	98	135
	1030	106	104	105	108	112	111	105	98	133
	1045	105	104	105	107	111	110	104	98	132
	1100	105	103	104	107	110	110	104	97	132
	1115	105	107	103	102	110	110	104	97	132
	1130	DRYRUN	DRYRUN	DRYRUN	DRYRUN	107	108	102	96	116
	1145	102	99	103	103	106	108	1102	96	128

Table 7.12-1. DM-9 Aft Skirt Conditioning Temperatures (cont)

DAY	TIME	(A) T221	(B) T222	(C) T311	(D) T312	(E) T142	(F) T143	(G) T144	(H) T145	(I) TXX1
MONDAY	1400	105	104	107	111	111	108	102	93	152
	1415	105	104	107	110	112	108	103	94	153
	1430	105	104	107	111	112	108	103	94	153
	1445	105	104	107	111	112	108	103	94	154
	1500	105	105	107	112	112	108	103	95	151
	1515	105	105	108	114	113	109	103	95	152
	1530	105	105	108	112	112	108	103	94	127
	1545	105	104	107	112	113	108	103	94	139
	1600	106	105	108	112	112	108	103	95	151
	1615	106	104	108	111	112	108	103	95	152
	1630	106	105	108	112	112	109	103	95	153
	1645	107	104	108	112	112	109	103	95	150
	1700	107	104	108	112	112	109	103	95	151
	1715	107	105	108	112	113	109	103	95	151
	1730	107	105	108	112	112	109	103	95	155
	1745	107	105	108	112	114	110	103	95	157
	1800	107	106	109	112	114	110	103	95	157
	1815	107	107	112	111	115	110	103	95	158
	1830	107	108	111	113	115	110	103	96	158
	1845	108	107	110	113	115	110	103	96	155
	1900	108	107	110	113	114	110	103	96	154
	1915	108	107	110	113	114	110	103	96	153
	1930	107	106	110	113	114	110	103	96	154
	1945	106	105	109	112	114	110	103	96	154
	2000	106	106	110	112	114	110	103	96	154
	2015	106	106	110	112	114	110	103	95	154
	2030	107	106	110	112	114	110	103	95	155
	2045	107	106	110	112	114	110	103	95	155
	2100	106	106	110	112	114	110	103	95	155
	2115	106	106	110	112	114	110	102	95	155
	2130	106	106	109	112	114	110	103	95	155
	2145	106	106	109	112	114	110	103	95	155
	2200	106	106	109	112	114	110	103	95	156
	2215	106	106	109	112	114	110	103	95	156
	2230	106	105	109	112	114	110	103	95	155
	2245	106	105	109	112	114	111	103	95	154
	2300	106	105	110	112	114	111	103	95	146
	2315	106	105	110	112	114	111	103	95	153
	2330	106	105	110	112	114	111	103	95	155
	2345	106	106	110	112	115	111	103	95	155

Table 7.12-1. DM-9 Aft Skirt Conditioning Temperatures (cont)

DAY	TIME	(A) T221	(B) T222	(C) T311	(D) T312	(E) T142	(F) T143	(G) T144	(H) T145	(I) TXX1
NOON TUESDAY	1200	105	104	104	108	106	107	102	95	119
	1215	103	104	104	109	106	107	102	95	128
	1230	105	101	104	110	106	106	102	95	128
	1245	103	101	104	109	106	105	101	94	131
	1300	105	102	106	105	106	105	101	94	133
	1315	105	100	107	110	106	105	100	94	133
	1330	105	99	98	98	106	105	100	94	133
	1345	105	100	106	109	105	105	100	93	131
	1400	106	102	106	109	105	105	100	93	128
	1415	99	100	103	107	105	104	100	93	124
	1430	99	100	103	107	105	104	100	93	141
	1445	99	99	103	105	106	104	100	93	146
	1500	100	100	103	106	106	104	100	93	148
	1515	100	102	104	106	108	105	101	93	152
	1530	100	101	103	105	107	104	100	93	143
	1545	102	102	104	107	108	105	101	93	152
	1600	104	105	104	109	109	105	102	93	152
	1615	102	103	104	110	110	105	102	94	152
	1630	101	102	106	109	111	106	102	94	153
	1645	105	103	107	108	112	107	102	94	155
	1700	106	104	107	108	112	107	103	95	155
	1715	108	105	107	106	113	107	103	95	153
	1730	107	104	107	105	113	107	103	95	151
	1745	108	105	107	106	113	108	103	95	150
	1800	109	106	108	106	113	108	103	95	149
	1815	108	104	107	106	113	108	103	95	149
	1830	109	107	107	105	113	108	103	95	149
	1845	109	106	106	105	113	108	103	95	149
	1900	108	104	108	106	113	108	103	95	150
	1915	108	107	109	107	113	108	103	95	150
	1930	109	106	108	108	113	108	103	95	148
	1945	110	106	107	107	113	108	103	95	149
	2000	109	106	110	109	113	108	103	95	149
	2015	109	107	111	109	113	109	103	95	149
	2030	109	107	108	107	113	109	103	95	150
	2045	109	106	110	108	113	109	103	95	150
	2100	109	107	110	108	113	109	102	95	150
	2115	108	108	109	107	113	108	103	95	148
	2130	109	108	109	106	113	108	103	95	142
	2145	108	106	110	107	112	108	103	95	138
	2200	107	107	109	108	112	108	102	95	143
	2215	106	107	111	107	112	108	103	95	141
	2230	107	106	111	109	112	108	103	95	140
	2245	107	106	112	109	112	108	103	95	140
	2300	107	105	109	110	111	108	103	95	141
	2315	107	104	109	108	111	108	103	95	138
	2330	106	106	108	107	111	107	103	95	139
	2345	106	106	108	107	111	107	103	95	139

Table 7.12-1. DM-9 Aft Skirt Conditioning Temperatures (cont)

DAY	TIME	(A) T221	(B) T222	(C) T311	(D) T312	(E) T142	(F) T143	(G) T144	(H) T145	(I) TXX1
MIDNIGHT TUESDAY	0000	106	106	108	107	111	107	103	95	141
	0015	106	106	108	107	111	107	103	95	141
	0630	105	105	107	107	111	107	103	95	125
	0045	105	105	107	107	110	107	103	94	139
	0100	105	105	107	107	111	107	103	94	144
	0115	105	105	107	107	111	107	103	95	143
	0130	105	105	107	107	111	107	102	94	140
	0145	105	105	107	107	111	107	102	94	140
	0200	105	105	107	107	111	107	102	94	140
	0215	105	105	107	107	111	107	102	94	140
	0230	105	105	107	107	111	107	102	94	140
	0245	104	105	107	107	110	107	102	94	140
	0300	105	105	107	107	110	106	102	93	140
	0315	105	105	107	107	110	106	102	93	139
	0330	104	104	107	107	109	106	102	93	139
	0345	104	104	107	107	109	106	102	93	131
	0400	104	104	107	107	109	106	102	93	137
	0415	98	100	108	110	109	105	102	94	139
	0430	98	100	108	110	109	105	102	94	139
	0445	98	100	108	108	109	105	102	94	138
	0500	100	100	108	106	109	105	102	93	135
	0515	101	100	108	107	108	105	101	93	136
	0530	101	100	101	105	108	105	101	93	136
	0545	100	99	101	105	108	105	101	93	128
	0600	99	99	100	104	107	104	100	92	128
	0615	98	98	99	103	106	104	100	92	137
	0630	99	98	100	103	106	104	100	92	140
	0645	99	99	100	104	107	104	100	92	139
	0700	99	99	101	105	107	104	100	92	141
	0715	99	99	101	106	107	104	100	92	139
	0730	100	100	102	105	108	104	100	92	139
	0745	99	100	102	105	108	104	100	92	138
	0800	99	100	102	105	108	104	100	92	137
	0815	99	100	102	105	107	104	100	92	127
	0830	99	100	102	105	107	104	100	92	138
	0845	99	100	101	104	107	104	100	92	151
	0900	99	101	100	105	108	104	100	92	160
	0915	99	101	100	105	109	104	101	92	160
	0930	99	103	100	106	109	105	101	92	163
	0945	100	102	98	99	111	105	102	92	180
	1000	99	101	92	98	112	105	102	92	173
	1015	97	100	90	95	113	105	102	91	168
	1030	94	95	82	88	113	105	100	91	132
	1045	92	93	82	87	113	104	100	91	112
	1100	87	87	84	87	111	102	99	90	163
	1115	84	72	83	85	111	101	98	89	166
	1130	87	71	82	84	111	100	97	89	168
	1145	83	67	69	85	111	98	87	87	166

Table 7.12-1. DM-9 Aft Skirt Conditioning Temperatures (cont)

DAY	TIME	(A) T221	(B) T222	(C) T311	(D) T312	(E) T142	(F) T143	(G) T144	(H) T145	(I) TXX1
NOON										
WEDNESDAY	1200	80	60	66	82	111	96	96	87	166
	1215	80	58	61	78	111	95	95	86	166
	1230	78	56	58	76	110	93	94	85	166
	1245	75	58	55	72	110	91	94	84	168
	1300	74	60	54	72	110	90	93	84	169
	1315	73	65	55	73	109	88	92	83	119
	1330	75	66	55	73	108	88	91	82	169
	1345	75	67	57	75	108	88	91	82	174
T-0										
WEDNESDAY	1400	78	68	59	76	108	88	91	82	175

Table 7.12-2. DM-9 Igniter Conditioning

FINAL DRY RUN

DAY	TIME	T875	T876	T877	T878	TXX3
12-23-87	1245	101	99	94	84	102
	1255	100	99	95	85	99
	1259	100	99	95	84	77
	1300	100	99	94	83	75

STATIC TEST

DAY	TIME	T875	T876	T877	T878	TXX3
12-23-87	1345	89	89	87	79	68
	1355	86	87	85	78	63
	1359	83	82	84	77	61

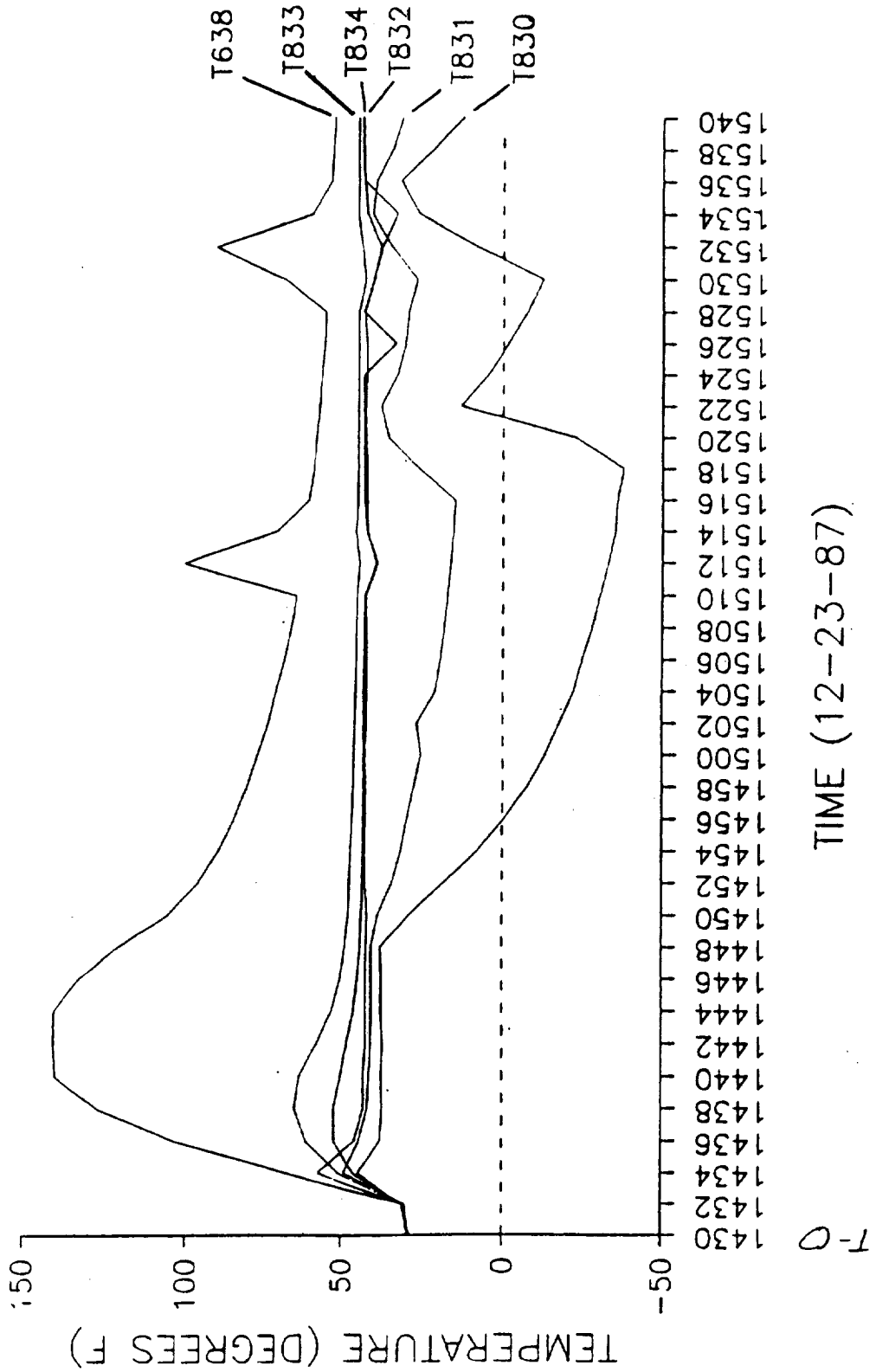

Figure 7.12-9. DM-9 Motor Case Temperatures

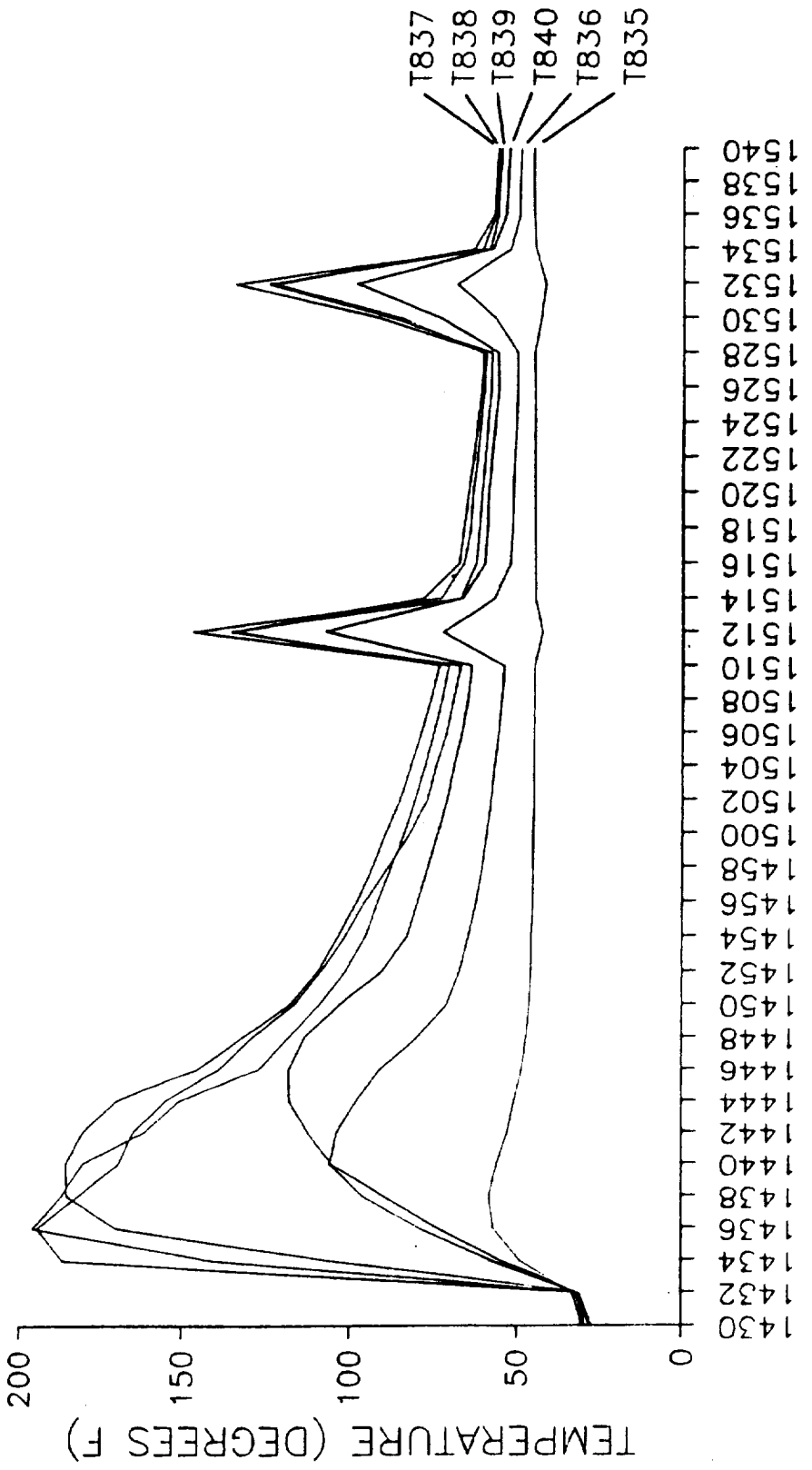

Figure 7.12-10. DM-9 Motor Case Temperatures

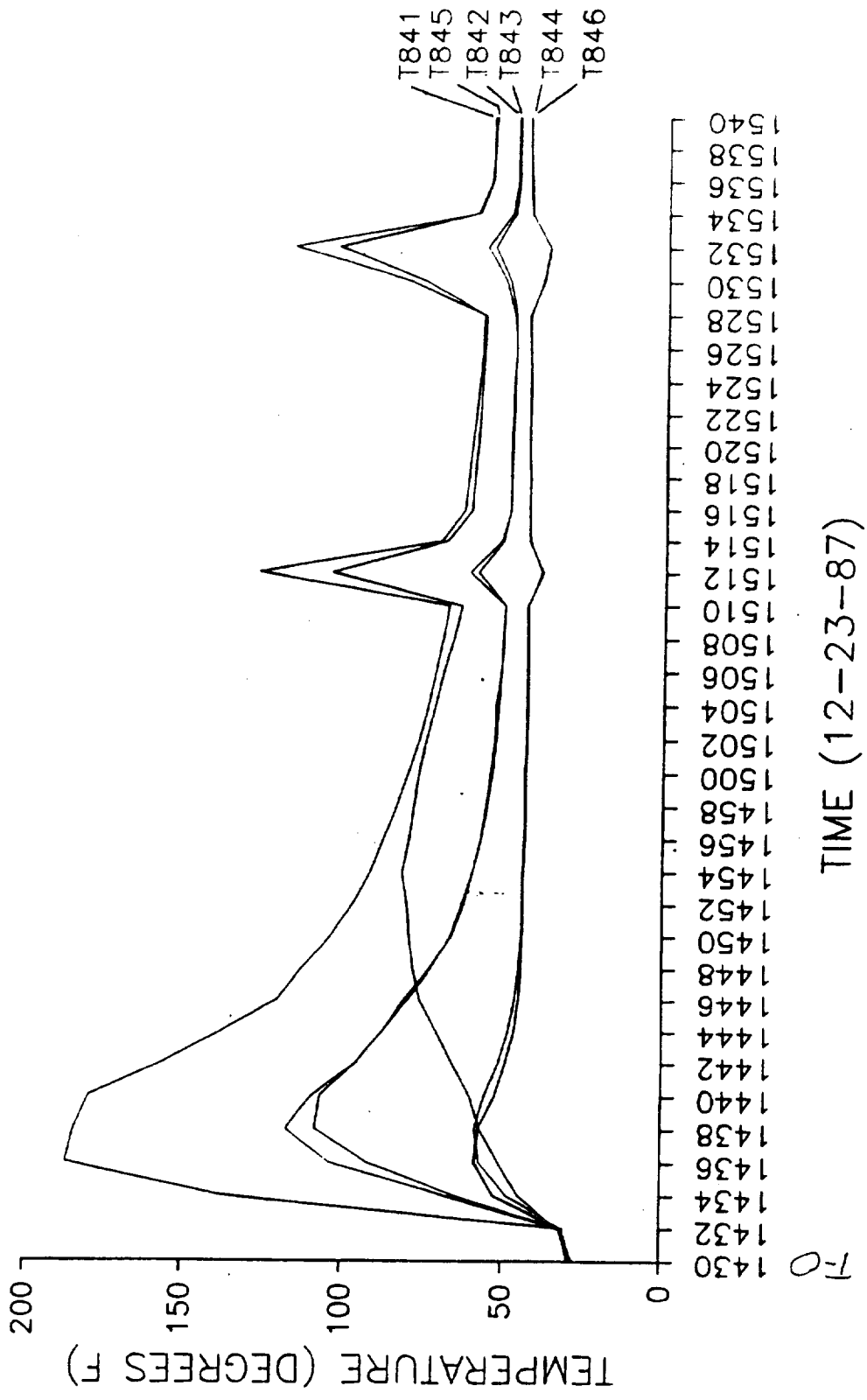

Figure 7.12-11. DM-9 Motor Case Temperatures

Table 7.12-3. DM-9 Motor Case Temperatures (23 Dec 1987)

TEMPERATURE (DEGREES F)

THERMOCOUPLE	TIME-> 1430	1432	1434	1436	1438	1440	1442	1444	1446	1448	1450
T830	28.8	30.5	44.3	37.2	36.5	36.7	36.3	36.9	36.7	37.2	28.3
T831	28.3	29.4	48.8	44.0	41.4	40.8	40.3	40.1	40.1	40.2	38.1
T832	28.0	30.5	57.3	45.5	42.7	42.7	42.0	42.0	42.0	41.9	41.6
T638	27.9	30.7	67.7	103.2	126.9	139.5	140.0	140.0	132.6	120.9	105.4
T833	27.7	30.2	50.6	61.1	64.9	63.4	57.7	52.9	50.0	48.5	47.4
T834	28.3	30.5	45.9	52.1	52.2	49.9	47.9	45.8	44.6	43.8	43.4
T836	29.1	31.5	57.9	79.1	95.9	105.6	103.7	97.9	91.0	79.8	71.1
T835	29.9	32.9	49.1	57.0	58.3	55.9	52.8	50.3	48.4	47.0	46.0
T837	26.8	30.5	106.2	169.9	185.0	185.3	180.3	169.9	145.2	131.5	117.4
T838	26.8	32.1	141.0	195.6	186.6	180.3	161.0	150.5	126.8	117.7	108.5
T839	27.6	32.1	186.3	194.2	181.6	169.0	164.5	154.7	138.8	128.6	116.0
T840	26.9	30.9	55.0	73.9	89.8	105.2	112.1	117.7	117.9	113.1	102.6
T841	27.0	31.6	44.4	50.8	56.7	59.9	65.6	70.5	76.0	78.2	79.5
T842	27.4	31.7	68.5	103.6	117.0	108.9	95.8	87.7	81.1	73.3	66.0
T843	27.3	31.1	64.8	92.0	107.8	106.4	95.5	87.5	79.8	72.5	66.5
T844	27.7	30.3	48.4	56.9	58.4	55.5	51.2	48.1	46.2	45.0	44.3
T845	26.9	30.9	138.1	186.6	183.8	179.0	155.5	137.3	119.9	112.2	103.4
T846	28.6	31.3	52.5	58.4	57.3	52.3	48.9	46.2	44.9	44.1	43.8

THERMOCOUPLE	TIME-> 1452	1454	1456	1458	1500	1502	1504	1506	1508	1510	1512
T830	17.7	7.4	-0.7	-7.8	-13.5	-18.0	-22.4	-25.1	-28.2	-30.6	-33.2
T831	33.7	31.0	29.0	26.8	24.7	25.9	20.4	18.8	17.6	16.5	15.6
T832	42.1	42.4	42.1	42.1	42.3	41.9	41.9	41.8	41.8	42.0	38.1
T638	95.9	89.4	84.3	80.0	76.7	73.2	70.7	68.1	66.0	64.3	100.5
T833	47.1	46.7	46.3	45.9	45.8	45.5	45.3	45.1	45.0	44.9	44.0
T834	43.1	43.0	42.9	42.8	42.8	42.7	42.8	42.7	42.6	42.6	38.8
T836	67.2	64.6	62.3	60.5	59.1	57.7	56.7	55.5	54.6	53.8	72.4
T835	45.6	45.3	45.0	44.9	44.9	44.7	44.7	44.6	44.6	44.6	42.3
T837	109.1	103.1	97.5	93.0	89.1	85.0	81.8	78.6	75.9	73.5	133.7
T838	100.9	95.0	91.4	87.4	83.8	80.4	77.5	75.0	72.6	70.6	146.5
T839	108.1	100.9	95.2	88.3	82.0	76.8	74.3	71.2	69.1	67.0	135.1
T840	90.2	82.8	79.6	76.6	73.8	71.0	68.9	66.6	64.9	63.8	107.0
T841	80.2	81.8	79.8	78.4	76.9	74.7	71.7	69.2	66.2	63.7	103.9
T842	62.3	59.4	57.2	55.7	54.4	53.2	52.8	51.3	50.7	50.2	61.3
T843	63.1	59.6	57.0	55.1	53.7	52.5	51.8	50.9	50.2	49.8	58.0
T844	44.1	44.1	43.5	43.4	43.6	43.1	43.2	43.1	43.0	43.2	37.9
T845	96.8	91.4	87.7	83.7	80.1	76.8	74.0	71.6	69.4	67.6	126.3
T846	43.7	43.7	43.2	43.1	43.2	42.9	42.8	42.8	42.8	43.0	38.6

Table 7.12-3. DM-9 Motor Case Temperatures (23 Dec 1987) (cont)

THERM...PLE TIME->	1514	1516	1518	1520	2	1524	1526	1528	1530	1532	534
T830	-35.5	-36.1	-38.1	-23.0	12.8	4.3	-1.8	-7.6	-12.6	8.0	25.6
T831	14.8	14.2	25.2	34.9	37.3	32.3	29.6	28.7	26.0	34.0	39.9
T832	41.5	41.6	41.7	42.0	42.1	41.9	41.9	42.5	39.6	36.8	42.2
T638	70.4	60.2	58.6	57.9	56.9	56.2	55.3	54.9	67.9	90.3	59.1
T833	45.2	44.6	44.5	44.5	44.5	44.4	44.4	44.5	42.3	43.3	44.6
T834	41.8	42.4	42.5	42.6	42.6	42.7	42.7	42.8	39.6	37.3	41.7
T836	56.9	52.0	51.4	51.2	50.7	50.3	49.9	49.8	56.6	68.3	52.[illegible]
T835	44.3	44.4	44.4	44.6	44.5	44.5	44.5	44.7	42.8	41.4	44.3
T837	78.0	67.5	66.1	64.9	63.4	62.2	60.9	60.3	84.4	121.2	63.2
T838	72.8	66.0	64.6	63.5	62.1	61.1	60.0	59.4	91.2	133.9	60.4
T839	67.0	62.5	61.5	60.7	59.7	58.9	57.9	57.6	86.9	123.8	58.2
T840	66.4	59.7	59.0	58.6	57.6	56.7	55.6	55.7	73.0	97.9	57.3
T841	68.4	60.7	60.0	59.1	58.4	57.9	57.2	56.8	75.8	102.6	59.7
T842	51.6	48.5	48.6	48.7	48.3	48.0	47.4	47.9	50.8	56.8	48.8
T843	50.8	48.5	48.3	48.1	47.8	47.5	47.2	47.2	49.3	54.3	47.8
T844	42.9	42.9	42.9	43.2	43.2	43.1	43.2	43.5	38.6	36.8	43.1
T845	70.2	63.1	62.0	61.0	59.8	58.9	58.0	57.5	81.0	116.2	58.9
T846	42.5	42.8	42.7	42.9	42.9	42.7	43.0	43.1	39.2	36.9	42.7

THERMOCOUPLE TIME->	1536	1538	1540
T830	31.0	21.0	11.8
T831	38.7	33.7	30.5
T832	42.4	43.1	42.9
T638	53.1	52.4	51.9
T833	44.4	44.6	44.5
T834	42.6	42.9	43.0
T836	49.1	49.0	48.6
T835	44.7	44.9	44.8
T837	57.0	56.5	55.6
T838	56.5	56.2	55.3
T839	55.7	55.3	54.5
T840	53.4	52.9	52.3
T841	55.4	54.8	54.7
T842	47.3	47.3	46.9
T843	46.6	46.6	46.4
T844	43.5	43.6	43.6
T845	55.0	54.7	53.9
T846	43.0	43.3	43.3

$C0_2$ Quench

The CO_2 quench system functioned properly.

S&A Operation

Arming operations were slightly different due to the addition of the shroud, but it was a workable situation.

PAGE 532 INTENTIONALLY BLANK

8

APPLICABLE DOCUMENTS

The latest revision of the following documents, unless otherwise specified, is applicable to the extent specified herein.

Specifications	Title
CPW1-3600	Prime Equipment Contract End Item Detail Specification (CEI)
Documents	
ETP-0181	DM-8 Assembly Measured Requirement for Manufacturing Plan
ETP-0231	Systems Tunnel Aluminum Floor Plate Pull Test
CTP-0011	Test Plan for Qualification of Modified Igniter
CTP-0019	Space Shuttle Development Motor No. 9 (DM-9), Static Fire Test Plan
CTP-0042	Test Plan Moisture Seal Integrity Test
TWR-12448	Space Shuttle Solid Rocket Motor Flight Evaluation of Work
TWR-15723	Development and Qualification Plan for the Redesigned Solid Rocket Motor Nozzle Assembly
TWR-16472 Vol. I to IX	DM-9 Postfire Engineering Evaluation Plan
TWR-16658	Space Shuttle Development Motor 8 (DM-8), Final Test Report
TWR-17198	Postfire Engineering Limits
TWR-17242	Moisture Seal Qualification Test, Final Test Report
TWR-17269	DM-9 Postfire Hardware Evaluation Final Report
TWR-17916	DM-9 Involute Boot Ring Material Loss (SPR No. DR 4-5/87)
TWR-17937	DM-9 Transducer Bolt Assembly Detorque (SPR No. DR 4-5/90)

TWR-18071	DM-9 Igniter Outer Gask-O-Seal® Void With Contamination (SPR No. DR 4-5/91)
TWR-18135 Rev A	DM-9 RSRM Structural Test Report

Drawings

10100-0044	ETA Ring (USBI Drawing 10399-0003), ETA Ring Installation Drawing for DM-8 (USBI Drawing)
1U51060	Bearing Assembly, Nozzle - Flexible
1U51882	Chamber Assembly, Igniter
1U75163	Chamber Assembly, Igniter - Loaded
1U75426	Tunnel Assembly, Center Segment
2U129718	Auxiliary Leak Test Equipment
2U129749	Water Deluge System
2U129774	Temperature Conditioning System, Aft Skirt
2U129774-218	Centrifuge Blower
2U65034	Three-Component Horizontal Thrust Stand-Top Assembly
7U75400	SRM Test Assembly
7U75416	Exit Cone Assembly, Segment - RSRM
7U75575	Leak Check, System Installation
7U75851	Test Assembly, SRM, DM-9

See Appendix A for complete drawing tree.

Government Documents

MIL-STD-45662	Calibration System Requirements

DISTRIBUTION

Recipient	No. of Copies	Mail Stop
J. Sutton	1	L72
T. Suatengco	1	L72
K. Speas	1	L63
C. Bown	1	L90
N. Eddy	1	L62B
K. Sperry	1	L61C
L. Nelsen	1	L61C
J. Fonnesbeck	1	L62A
J. Donat	1	L62A
E. Hale	1	L62A
J. Lavery	1	L71
M. Williams	1	L62B
K. Sanofsky	1	851B
F. Duersch	1	851
R. Papasian	38	E62A
Print Crib	5	Q51B1
Data Management	7	L72B